Effets des instabilités sédimentaires sur les microhabitats benthiques : cas du Kongsfjorden

Corentin Guilhermic

COLLEGE VEGETAL
DOCTORAL ANIMAL, ALIMENT
PAYS DE LA LOIRE MER, ENVIRONNEMENT

université angers

THESE DE DOCTORAT

DE
L'UNIVERSITÉ D'ANGERS
SOUS LE SCEAU DE
LA COMUE ANGERS – LE MANS

ECOLE DOCTORALE N° 642
Ecole doctorale Végétal, Animal, Aliment, Mer, Environnement
Spécialité : *Géosciences marines*

Par

Corentin GUILHERMIC

Effets des instabilités sédimentaires sur les microhabitats benthiques : cas du Kongsfjorden

Thèse présentée et soutenue à Angers, le 15 décembre 2023
Unité de recherche : UMR CNRS 6112 LPG – Université d'Angers

Rapporteurs avant soutenance :

Helena FILIPSSON	Professeure, University of Lund
Arthur CAPET	Chercheur, Royal Belgian Institute of Natural Sciences

Composition du Jury :

Examinateurs :

Lionel DENIS	Professeur, Université de Lille
Giuliana PANIERI	Professeure, The Arctic University of Norway

Dir. de thèse :

Hélène HOWA	Professeure, Université d'Angers

Co-encadrantes de thèse :

Maria Pia NARDELLI	Maîtresse de conférences, Université d'Angers
Aurélia MOURET	Maîtresse de conférences, Université d'Angers

Invitée :

Agnès BALTZER	Professeure, Université de Nantes

Effets des instabilités sédimentaires sur les microhabitats benthiques : cas du Kongsfjorden

Remerciements

Firstly, I thank Pr. Helena Filipsson and Dr. Arthur Capet for accepting to review my work and to provide further advice and indications on how to improve this work. I also thank Pr. Lionel Denis and Pr. Giuliana Panieri who followed my research advances during the three years. Finally, I thank Pr. Agnès Baltzer who also followed my research through sampling missions, workshops and other project meetings.

La première question qui vient à l'esprit quand on termine sa dernière année de master, c'est « Qu'est-ce que je vais faire après ? ». Quand on est en cours depuis si longtemps, se projeter dans la vie active ou même dans un métier ce n'est pas forcément évident pour tout le monde. Pour moi ce sentiment fût mitigé car d'un côté je savais que je voulais faire de la recherche depuis ma 3ème année de licence et de l'autre j'avais la peur de ne pas trouver de doctorat qui pourrait me plaire et qui m'accepterait. Un jour de rédaction de mémoire de master, je reçois une offre de thèse sur l'étude de microhabitats benthiques incluant les foraminifères benthiques et de la biogéochimie. Ça vient de l'université d'Angers et plus particulièrement de maitresses de conférences qui m'ont donné des cours en licence, qui me connaissent et que j'estime beaucoup… Evidemment, je postule à cette offre de doctorat.

Mes premiers remerciements vont bien évidemment à mes trois encadrantes Hélène, Pia et Aurélia qui m'ont laissé une chance pour mener à bien ce projet. Je n'aurais pas pu rêver meilleure équipe pour me superviser tout au long de ces 3 ans. Beaucoup d'anecdotes me viennent en tête mais je résumerais tout ça par certaines qui me semblent assez révélatrices de ces 3 dernières années. Merci Hélène pour avoir dirigé ma thèse et d'avoir toujours regardé mon travail avec une certaine distance (virtuelle bien sûr) qui a permis de mieux contraindre les questions, hypothèses et deadlines de projet. Si j'allais trop une mauvaise direction, tu rectifiais le tir à chaque fois. Je me rappelle une anecdote importante qui m'est restée dans la tête depuis le début de ma thèse et qui me suit presque au quotidien. Au cours des premiers mois, nous mangions un midi et tu as dit « Corentin, c'est un diesel. ». Sur le coup, je ne savais pas trop comment le prendre mais je pense que tu as vu le futur ce jour-là. Mon démarrage a été lent et long et puis d'un coup, c'était parti. Les raisonnements, liens entre chapitres, idées, tout était là juste en attente d'être rédigé. Je pense que cette anecdote parle d'elle-même sur ta capacité à cerner les gens et à les accompagner au long de leur parcours. Merci encore. Merci à Pia, pour ton accompagnement sans faille au cours de ma thèse. Je parle de « sans faille » parce que la question de la patience est ici pertinente. Tu as dû m'accompagner dans le plus difficile, c'est-à-dire la rédaction du premier chapitre. Ce n'était vraiment pas évident pour moi, j'ai décroché plusieurs fois mais ça avançait quand même. Comment ? Grâce à nos sessions d'écritures qui me poussaient à apprendre, me dépasser et produire un travail qualitatif. Ça s'applique à l'écriture mais aussi aux missions d'échantillonnage ou traitement de données. Je pensais savoir beaucoup de choses sur l'étude des foraminifères benthiques mais grâce à toi ce savoir a été multiplié par 10. Au moment où j'écris ces mots, tu es au terme de ta grossesse et comme tu l'as dit, on accouche en même temps. Je te souhaite le meilleur pour tes enfants et pour la suite. Merci à Aurélia pour m'avoir transmis une grande partie de son savoir de biogéochimie. Le seul savoir que j'avais je le tenais déjà de toi et Edouard pendant ma licence. J'étais tellement bon (faux) que je n'ai rien emmené en master si bien qu'en arrivant en thèse, il a fallu tout réapprendre. Au fur et à mesure de la thèse j'ai pu progresser grâce à

l'indépendance que tu me laissais, aux erreurs que je commettais et à tes corrections. Maintenant je pense être autonome dans toutes les méthodes vues ensemble. J'attends mon diplôme de master de DET maintenant. Je te remercie de m'avoir bien coaché et accompagné sur la rédaction des derniers chapitres. Ce fut effréné mais nous avons réussi.

Grâce à vous j'ai pu avancer dans ma thèse, participer à des missions d'échantillonnage incroyables, progresser dans mes raisonnements scientifiques et me conforter dans le fait que j'aimerais vraiment continuer la science dans les années à venir.

Je pense que mon encadrement est à l'image du laboratoire entier. Je remercie tous les membres du LPG plus particulièrement du site d'Angers pour les conseils, discussions et moments partagés à table le midi. Je ne pense pas que je puisse retrouver un tel esprit d'entraide et de camaraderie ailleurs dans un labo ou une entreprise. C'est impossible. J'espère vraiment pouvoir continuer à travailler avec vous dans le futur. Ne perdez jamais cet esprit, c'est vraiment ce qu'il fait l'identité cette équipe. J'aimerais également remercier l'équipe technique, Sophie S., Eric, Sophie Q., Luzia, Adeline, Aude et Damien pour leur disponibilité à participer à mes expériences, analyses et autres petits tracas techniques et administratifs du quotidien. Sans vous, c'est impossible d'avancer dans les projets scientifiques et c'est d'autant plus important pour les thésards à cause des nombreuses deadlines. On peut dire que vous ramenez une sorte d'apaisement lors du processing d'échantillons car nous pouvons progresser sur plusieurs fronts en même temps. En termes d'optimisation du temps, je remercie également tous les stagiaires de licences et master qui ont permis une accélération monumentale des analyses. Sachez que je n'aurais pas pu rencontrer des deadlines sans votre travail.

Comme nous ne sommes jamais mieux entourés que par les personnes qui ont subi, subissent et subiront le même traitement que nous, j'aimerais remercier les thésards du labo avec qui j'ai pu partager ces 3 dernières années. D'abord ceux/celles partis trop tôt. Pas de « paix à votre âme » mais plutôt un "bien joué, vous avez réussi ». Merci à Constance, Eleonora, Marie et Pauline. J'ai mis fin au combo féminin. Merci à Marie et Eleonora pour les trajets à vélo, les soirées, les restos, un certain mentoring que vous avez pu m'offrir jusqu'à votre départ et même après. Merci à Pauline, ma cobureau. Tu m'as offert des conseils vraiment précieux et j'ai pu observer ta fin de thèse avec attention. Ça m'a servi pour gérer mon temps, ma rédaction ou mon organisation pour la fin. Votre parcours a été très inspirant pour moi. Maintenant je remercie Maxime, Nour et Mohammed. J'ai adoré sortir avec vous, discuter avec vous et bosser avec vous, toutes nos interactions en fait. Je vous souhaite la meilleure réussite pour votre 3ème année et de toute façon je continuerai à vous suivre à distance. Je viendrai à votre soutenance à coup sûr (enfin peut être et uniquement si elles sont toutes le même jour, faut pas pousser). Je souhaite également le meilleur aux nouveaux Sikandar et Quentin. Je ne vous connais pas trop encore mais je vous envoie de la force pour votre doctorat et vos 3 prochaines années. En plus des thésards, j'aimerais remercier Julia qui renforce la cohésion de précaires du labo par l'organisation de soirées pour nous changer les idées. Tu es un peu la manageuse des thésards je trouve. Continue.

Maintenant je passe à l'équipe givrée d'Arctique. Premièrement je remercie Pia et Agnès pour vos projets qui m'ont permis de vivre les expériences les plus intenses et incroyables de toute ma vie. Aller en Arctique est un rêve que j'ai depuis très longtemps et pouvoir y aller tout en travaillant, c'est le rêve. Avoir vu cet endroit magnifique et fragile sur 3 missions dont une en fin d'hiver/début printemps a vraiment permis de me former dans l'échantillonnage de milieux assez extrêmes. J'ai appris que tout ne se passait pas forcément comme prévu, que l'on doit composer avec le personnel sur place et la météo du jour. Je

remercie les personnes qui ont pu m'accompagner en mission en plus de mon encadrement, Francesca, Hugues et Vincent. Nous avons passé de super moments que je n'oublierai jamais.

Je passe désormais au côté privé, je commence par remercier mes potes Thibault, Jessy, Damien et Lucas. L'avantage, quand on arrive à trouver une thèse dans sa vie natale, c'est de pouvoir échapper au travail et s'aérer l'esprit assez facilement. On a pu faire des soirées, des parties de padel récemment, et masse de parties de palet et pétanque. Si je pars en post doc à l'étranger, ça va devenir plus difficile de se voir… mais clairement pas impossible.

Je remercie ma mère, mon père et ma sœur. Vous faites partie de cette bulle d'oxygène dont j'ai pu profiter pendant 3 ans. J'ai eu beaucoup de chances de pouvoir vous voir régulièrement. Vous m'avez motivé, encouragé à poursuivre cette voie et je vous en remercie. C'est bon les études c'est terminé, je vous assure. Pour ma sœur, je te souhaite un succès sans limite après tes études. Je t'ai toujours dit que tu le méritais et maintenant c'est écrit noir sur blanc ici.

Je finis par ma Morgane. On a mis notre vie de couple un peu de côté pour me laisser gérer ma thèse plus tranquillement et pour que tu puisses faire tes armes dans ton travail également. La relation à distance c'était viable qu'un temps et a vite pesé. Je te promets qu'à partir de maintenant, c'est terminé. On a quand même avancé dans notre vie par le PACS et de très maigres vacances que j'ai pu me laisser. Je t'aime et ce texte signe le début de la suite de notre vie ensemble.

"Be curious, not judgemental"
Ted lasso (S01, Ep. 08)

© Corentin Guilhermic, Kongsfjorden

Table des matières

Experimental part

Environmental study of the Kongsfjord

Objectifs de la thèse

L'instabilité sédimentaire et surtout les évènements de dépôts intenses ont des effets significatifs sur les écosystèmes benthiques et sur la biogéochimie des sédiments dans les fjords arctiques. La fonte estivale des glaciers continentaux génère d'importants gradients environnementaux principalement dus à la décharge de sédiments avec les eaux de fonte influençant au passage les flux de matière organique vers le fond résultant d'une productivité primaire limitée. Le très étroit couplage pélagique/benthique dans ces fjords engendre donc la biozonation des faunes benthiques en fonction des conditions de stress apportées par la décharge glaciaire dans un espace limité mais également des perturbations dans les cycles biogéochimiques au sein du sédiment. La saisonnalité des dynamiques hydrologiques et sédimentaires de ces fjords est de moins en moins marquée à cause du réchauffement climatique arctique donc la nécessité de comprendre les processus liant la fonte des glaciers et la décharge de sédiments associée avec la réponse des microhabitats benthiques est primordiale pour comprendre la future évolution des autres fjords arctiques.

Afin de mieux comprendre ces processus, nous devons à la fois investiguer l'effet unique des dépôts sédimentaires et l'enfouissement des habitats benthiques mais également comprendre avec une approche holistique les liens étroits entre les gradients environnementaux et la réponse des habitats benthiques aux potentielles perturbations dans le milieu naturel.

L'intense sédimentation, seule, sur le compartiment benthique a des effets potentiellement délétères sur le fonctionnement des écosystèmes et sur la stabilité des cycles biogéochimiques car elle agit comme une barrière physique, une perturbation, à laquelle le système dans son entièreté doit s'adapter. Afin de comprendre la réaction du système, ce travail de doctorat propose d'étudier les réponses des foraminifères, choisis comme modèle biologique de l'écosystème benthique, et les effets sur les cycles biogéochimiques des évènements de dépôts dans les fjords subpolaires arctiques avec les approches complémentaires suivantes :

- Comprendre les processus impliqués dans la résilience des communautés de foraminifères benthiques et des gradients biogéochimiques dans le sédiment à des simulations de dépôts sédimentaires de fréquence et d'intensité différentes.
- Etendre le savoir sur le comportement des foraminifères dans le Kongsfjorden (Svalbard) vis-à-vis des paramètres environnementaux liés à la fonte des glaciers en incluant la sédimentation et la saisonnalité de l'hydrologie locale et des variations engendrées sur les écosystèmes benthiques.
- Comprendre les signaux biogéochimiques dans le sédiment du Kongsfjorden en relation avec le gradient de sédimentation généré par la fonte des glaciers tidaux.

Les objectifs proposés reposent sur le couplage expérimental/environnemental du projet scientifique. L'approche expérimentale proposée permet de limiter l'étude à une seule variable (perturbation sédimentaire) pour approfondir la compréhension de la réponse biogéochimique des sédiments et la réponse écologique des foraminifères à ce seul paramètre environnemental. L'expérience menée a permet d'observer avec une résolution hebdomadaire, le comportement de foraminifères intertidaux après différentes modalités d'enfouissement sous sédiment variant en intensité et en fréquence (***2ème Chapitre***). De plus elle nous permet d'observer la résilience des cycles biogéochimiques dans le sédiment vis-à-vis des dépôts de sédiment constituant une barrière physique plus ou moins épaisse entre le substrat initial et la colonne d'eau, limitant donc les échanges (***3ème Chapitre***). Les interprétations issues de cette expérience viendront

alimenter l'étude environnementale du Kongsfjorden dans lequel la fonte des glaciers apporte un volume significatif de particules détritiques tous les étés. L'étude saisonnière (Printemps et Eté) des faunes de foraminifères benthiques vivants dans ce fjord est donc menée en lien avec les variations d'apport de sédiment au cours de l'année et des gradients de stress associés. Les zonations des espèces, leur abondance ainsi que leur distribution verticale dans le sédiment sont des indicateurs de changement environnementaux dans leur habitat (***4ème chapitre***) mais aussi dans le fjord à plus grande échelle (***5ème Chapitre***). Les effets de la perturbation physique représentée par l'enfouissement des gradients redox préétablis dans le sédiment seront étudiés sur un transect partant du front du glacier tidal Kronebreen (la source de sédiment) et s'éloignant jusqu'à 10 km (***6ème Chapitre***). Les résultats obtenus pendant l'expérimentation viendront appuyer les hypothèses proposées quant à la résilience des processus observés. Finalement, la caractérisation plus fine en 2D des foraminifères vivants ainsi que des cycles biogéochimiques est effectuée grâce à des méthodes d'échantillonnage 2D (***7ème Chapitre***).

Cadre de la thèse

Ce travail de doctorat a été financé par une bourse doctorale de l'Université d'Angers (ministère de l'Enseignement supérieur, de la Recherche et de l'Innovation) pour une durée de 3 ans à partir du 1er septembre 2020 jusqu'au 1er septembre 2023. Ce doctorat a été réalisé au sein du Laboratoire de Planétologie et Géosciences (UMR CNRS 6112 LPG) sur le site d'Angers. L'environnement analytique de la thèse (missions d'échantillonnage, analyses, communication, participation à des congrès, etc…) a été amené par le projet BEGIN (PI : Dr. Maria Pia Nardelli, LPG) financé par le programme CNRS INSU LEFE CYBER (Les Enveloppes Fluides et l'Environnement) sur toute la durée du projet doctoral. Le soutien logistique des missions d'échantillonnage au Svalbard a été assuré par l'IPEV (l'Institut Polaire français Paul-Emile Victor), avec un financement du projet KONBHAS (KONBHAS (KOngsfjorden New BentHic HAbitatS ; PI Agnès Baltzer, Pr. de Nantes Université). Ce travail inclut également une collaboration avec l'Università Politecnica delle Marche (Italie), l'Università di Cagliari (Italie), Nantes Université et l'Université de la Rochelle.

Dû à la crise de la COVID-19, l'objectif initial de la thèse a été remanié à la suite de l'annulation d'une mission d'échantillonnage dans le Kongsfjord en août 2020. Un focus particulier a été mis au début de la thèse sur l'étude expérimentale qui a donc été ciblée sur les processus associés aux instabilités sédimentaires simulés dans les microcosmes utilisant du sédiment et des faunes de vasière intertidale Atlantique. De plus, les échantillons prélevés au Svalbard en Mai et Aout 2021 dans le fjord (constituant les ***chapitres 4*** à ***7***) sont arrivés à Angers avec beaucoup de retard et n'ont pu être analysés qu'à partir de Février 2022.

Organisation du manuscrit

Le ***1er chapitre*** présente le contexte scientifique de l'étude et le savoir préliminaire pour la compréhension du sujet dans son entièreté.

L'étude expérimentale sur l'effet de dépôts de sédiments sur les microhabitats benthiques est présentée en 2 volets comme suit :

Le ***2ème chapitre*** se concentre sur la réponse des foraminifères benthiques à différentes modalités de dépôts sédimentaires simulés en microcosme. L'évolution temporelle de l'abondance ainsi que de la distribution verticale des individus est étudiée avec une résolution d'échantillonnage de l'ordre d'une semaine.

Le ***3ème chapitre*** met l'accent sur les processus biogéochimiques impliqués dans la résilience des gradients redox dans le sédiment vis-à-vis de la perturbation physique représentée par les dépôts sédimentaires.

Les effets de la décharge de sédiments causée par la fonte des glaciers le Kongsfjord sur les microhabitats benthiques sont présentés dans les chapitres suivants comme suit :

Le ***4ème chapitre*** expose les paramètres environnementaux mesurés pendant les missions d'échantillonnage en Mai et Août 2021 (contenu en matière organique, mesures physico-chimiques de la colonne d'eau et granulométrie) et discute de l'évolution saisonnière des composantes marines du fjord.

Le ***5ème chapitre*** souligne l'effet des gradients environnementaux (sédimentation et flux de matière organique) sur la stabilité des fronts de diagenèse précoce dans le sédiment suivant l'éloignement à la source de sédiment dans le fjord. Les interprétations acquises par l'expérimentation sur la résilience des cycles biogéochimiques auront une implication dans ce chapitre.

Le ***6ème chapitre*** se concentre sur l'effet de la saisonnalité sur la distribution des assemblages de foraminifères vivants ainsi que sur leur distribution verticale dans le sédiment dans la partie interne du Kongsfjorden. Les stations étudiées ont été choisies sur la base de leur éloignement progressif du front du glacier tidal émettant une grande décharge de sédiments.

Le ***7ème chapitre*** propose une comparaison d'échantillonnage de sédiment (foraminifères vivants et géochimie des eaux interstitielles) sur deux stations contrastées du Kongsfjorden. La méthode de découpage de carottes d'interface (1D) sera confrontée à la caractérisation à plus grande résolution verticale et horizontale des microhabitats sédimentaires. De plus, cette haute résolution pourrait permettre d'identifier des structures sédimentaires affectant la microdistribution de composés chimiques ainsi que des faunes de foraminifères vivants.

Chapitre 1

Introduction

1 Les instabilités sédimentaires

1.1 Les instabilités naturelles dans les environnements marins côtiers

Les instabilités sédimentaires sont présentes dans beaucoup d'environnements côtiers et contribuent largement à façonner les écosystèmes. Les érosions, les remises en suspension ainsi que les dépôts sédimentaires surviennent de façon plus ou moins intense, cyclique et fréquente dans tous les écosystèmes côtiers. Les causes plus fréquentes en sont les cycles tidaux (Davies et al., 2023), les tempêtes (Bolliet et al., 2014; Budillon et al., 2006), les crues fluviatiles (Dyer, 1988; Extence et al., 2013; Hir et al., 2001; Jalón-Rojas et al., 2015; Mucci et al., 2003; Pastor et al., 2018) et la fonte des glaciers continentaux polaires (D'Angelo et al., 2018; Hodson et al., 1998; Hodgkins et al., 2003; Łepkowska and Stachnik, 2018; Meslard et al., 2018). Les enjeux spatio-temporels de ces événements sont strictement liés au type de phénomène qui les produit, à la géographie locale et à la réponse écosystémique qui en dérive.

1.2 Les perturbations sédimentaires issues des activités humaines

Les activités humaines peuvent provoquer activement ou passivement des instabilités sédimentaires en domaine côtier. L'action directe de l'humain sur son environnement entrainant des instabilités sédimentaires serait par exemple représentée par l'action de réguler les débits des rivières en construisant des barrages pour retenir l'eau en amont de fleuves. Cela a pour effet de briser l'énergie fluviale menant à des dépôts de sédiment en amont des bassins définitifs de sédimentation. De plus, l'utilisation des terres pour l'agriculture ou l'industrie peuvent également contribuer à l'augmentation des ruissellements et ainsi des apports plus importants de particules détritiques transportées par les fleuves jusqu'en milieu marin (Bussi et al., 2016; Kuhnle et al., 1996).

D'autres activités comme les dragages en fleuve ou en mer, l'extraction de granulat ou encore la pêche au chalut consistent en l'érosion de plusieurs centimètres à mètres de sédiment à un endroit très localisé et le dépôt massif du sédiment issu de la resuspension dans une autre localisation (clapage), résultant en un dépôt massif venant ensevelir la surface sédimentaire (Wolanski and Gibbs, 1992). Aussi, les installations pour la production d'énergie marine renouvelable (e.g. éoliennes off-shore) peuvent grandement contribuer aux instabilités physiques des environnements benthiques, soit durant la phase d'installation (forages, creusement de tranchées pour le passage des câbles) soit pendant la phase d'exploitation, car la présence des mâts en mer a des conséquences sur la vitesse des courants locaux et donc du transport /dépôt sédimentaire (García-García et al., 1999; Szpak et al., 2015).

De plus, des effets perturbateurs sont en train de s'observer de plus en plus en lien avec les changements climatiques affectant les enveloppes fluides superficielles de notre planète (Intergovernmental Panel on Climate Change (IPCC), 2022, 2023). Les observations actuelles ainsi que les modèles sur l'évolution future du climat montrent des changements majeurs dans les composantes atmosphériques et hydrologiques terrestres allant de régimes de pluie s'intensifiant ou diminuant drastiquement dans certaines régions jusqu'à des changements majeurs dans les régimes de courants océaniques. Ces changements sont susceptibles de changer les régimes érosifs des bassins versants de fleuves, allant de l'augmentation du transport de matériel détritique vers l'océan jusqu'à un arrêt complet de systèmes fluviatiles par manque de précipitation. La cryosphère polaire montre également des signes alarmants de diminution avec des pertes annuelles de volume de glace terrestre conséquentes engendrant une

érosion accrue des substrats rocheux et donc des décharges sédimentaires plus importantes vers les bassins océaniques.

1.3 Effets des dépôts de sédiment sur les habitats benthiques

Les habitats benthiques sont directement affectés par les événements d'instabilité sédimentaire, qui en causent une déstabilisation structurale ainsi que biogéochimique. Une phase de déséquilibre transitoire s'ensuit, éventuellement suivie d'une phase de résilience pour atteindre un nouvel état d'équilibre (Van Meerbeek et al., 2021).

Les espèces vivant dans le compartiment benthique peuvent vivre sur le fond, attachées à un substrat (algues, rochers…), sur ou dans le sédiment. Selon leur degré de mobilité (pour les faunes) ou leur vitesse de croissance (pour la flore), les effets des dépôts sédimentaires peuvent être plus ou moins néfastes. Pour le biota fixé ou à mobilité réduite, un dépôt épais de sédiment peut résulter en une asphyxie létale. En plus de l'effet d'ensevelissement provoquant un stress majeur, ce dépôt constitue une barrière physique qui limite les échanges de nourriture et d'éléments dissous comme l'oxygène entre la colonne d'eau et les écosystèmes touchés altérant les conditions biogéochimiques jusqu'alors stables. Les effets délétères de ces perturbations ont déjà été étudiés et documentés pour des environnements benthiques d'eau douce (e.g. Dudgeon, 2019; Mathers et al., 2022; Sánchez-Bayo and Wyckhuys, 2019) et pour les environnements marins (e.g., Alve, 1999; Anschutz et al., 2002; Hop and Wiencke, 2019). La résilience de la structure d'un écosystème dans le temps est une combinaison de conditions écologiques et physiques (Norkko et al., 2006; Thrush et al., 2006). Principalement, l'habilité d'une espèce à survivre à un ensevelissement va passer par ses capacités de migration au sein de la matrice sédimentaire afin de rejoindre sa niche écologique préférentielle. Toutes les espèces ne possèdent pas les mêmes traits morphologiques permettant un tel déplacement comme les individus sessiles qui ne peuvent pas suivre le rythme d'un dépôt de sédiment entrainant une perte d'abondances d'individus avec le temps (Cottrell et al., 2016; Mestdagh et al., 2018). S'ajoutant à cette migration des individus ensevelis, la recolonisation du milieu peut survenir à partir de zones refuges relativement éloignées de la perturbation. Néanmoins, cette recolonisation n'est possible que si l'environnement physique et chimique retrouve une certaine stabilité permettant le rétablissement d'une faune, similaire à celle présente avant l'évènement ou l'établissement d'une nouvelle faune pionnière.

Les pertes de faunes après des épisodes de dépôts sédimentaires ont été également prouvées par des études expérimentales dans lesquelles ont été confrontées des espèces de macrofaunes ou méiofaunes à ces perturbations (e.g. Bolam, 2011; Cottrell et al., 2016; Hendrick et al., 2016; Mestdagh et al., 2018). Ces études ont montré que la survie dans le temps des espèces étudiées, après une perturbation sédimentaire, dépendait de la résilience des conditions biogéochimiques dans le sédiment, de la survie des autres espèces préservant les liens trophiques, de l'épaisseur du dépôt de sédiment et de la qualité et quantité de la matière organique dans le système. Toutes ces variables environnementales sont donc affectées par la coupure entre le substrat initial et la colonne d'eau. Lors d'une étude en milieu naturel, il est donc impossible d'attribuer les effets d'un seul forçage sur la survie des espèces présentes et leur migration au sein du dépôt.

Les précédentes études expérimentales et environnementales expriment la nécessité d'acquérir de nouvelles informations concernant les réactions spécifiques des organismes vis-à-vis de perturbations sédimentaires. Tous les compartiments benthiques doivent être étudiés

pour comprendre l'évolution de l'écosystème dans sa globalité. Beaucoup d'études se sont focalisées sur la réponse des méga-, macrofaunes et de la méiofaune métazoaire à des dépôts de sédiment. Néanmoins peu d'études concernent la réponse de la méiofaune protozoaire telle que les foraminifères, située plus bas dans la chaine trophique.

De tous les environnements côtiers cités plus tôt sujets à des dépôts massifs de sédiments, il en est un qui présente une dynamique saisonnière, alternant entre des phases de quiescence et de décharges détritiques particulièrement importantes. Il s'agit des fjords arctiques. Ces dépôts de sédiment dépendent de la dynamique de la fonte glaciaire et par conséquent des conditions climatiques actuelles. Parmi ces fjords, ceux situés sur la côte ouest de l'archipel du Svalbard sont d'autant plus affectés par cette dynamique saisonnière, qu'ils sont également dépendants d'une hydrographie changeante au cours de l'année. De nombreuses études sur les écosystèmes marins, terrestres et glaciaires y sont menées pour comprendre les changements rapides interannuels de la faune locale afin de pouvoir comprendre le devenir à court et long terme de ces environnements dans un contexte de réchauffement global.

2 Les fjords Arctiques : zone transitoire entre domaine glaciaire et marin

2.1 Généralités sur les fjords

D'après la définition donnée par Howe et al. (2010), les fjords ont des côtes pentues et sont des vallées littorales inondées par l'océan. Ces entrées d'eau salée peuvent être trouvées à relativement hautes latitudes près des deux pôles comme en Scandinavie, au Groenland, en Islande, en Ecosse, en Nouvelle Zélande ou en Antarctique (Howe et al., 2010). La principale caractéristique d'un fjord est qu'il est le produit d'une érosion glaciaire (Howe et al., 2010; Syvitski and Shaw, 1995). De ce fait, ils sont positionnés sur des fragilités du substrat rocheux comme des failles, ou des systèmes fluviatiles localisés sur des lignes tectoniques résultant ensuite en un surcreusement d'une vallée par le passage d'un glacier (Dallmann, 2015; Howe et al., 2010). Les dernières phases conséquentes d'extension glaciaire continentale pendant le Quaternaire ont entrainé la création de ces fjords ou ont augmenté l'érosion de vallées déjà existantes. L'inondation des fjords par la mer intervient lors d'une phase de retrait des glaciers jusqu'à leur fonte, totale ou non, comme observée à toutes les latitudes où on les trouve. Du fait de leur surcreusement et du rebond isostatique post-glaciaire, ils peuvent montrer des profondeurs allant jusqu'à 1 km et des longueurs dépassant plusieurs centaines de kilomètres (Howe et al., 2010).

La géomorphologie d'un fjord, présente des caractéristiques propres (Syvitski and Shaw, 1995; Mcintyre and Howe, 2010; Paetzel and Dale, 2010). La plupart des fjords montrent une succession de bassins séparés par des seuils pouvant être des substrats rocheux plus indurés non érodés par le passage d'un glacier mais également des moraines frontales composées de sédiments déposées par la glace (Fig. 1). Ces seuils séparant des bassins sont essentiellement trouvés à l'embouchure des fjords (Howe et al., 2010) mais peuvent être trouvés dans des parties plus internes du fjord.

Howe et al. (2010) ont classé les fjords dans trois catégories distinctes :

- Les fjords tempérés sont caractérisés par l'absence de glace de mer en toute saison et de glaciers continentaux. Les sources de sédiment incluent le transport fluviatile et les

glissements de terrain. Ces fjords sont trouvés à relativement basses latitudes comme en Ecosse, en Islande, en Suède, en Norvège ou en Argentine.

- Les fjords subpolaires sont trouvés au Svalbard, à l'ouest du Groenland, et en Antarctique. Ils montrent une température atmosphérique supérieure à 0°C en été ainsi qu'une présence/absence de glace de mer saisonnière. De plus, ces fjords présentent parfois des glaciers continentaux à terminaison marine ou terrestre. Les sources de sédiment sont l'écoulement sous-glaciaire, le vêlage d'icebergs ainsi que l'érosion/transport fluviatile (cf. Fig 1).
- Les fjords polaires sont présents au nord du Groenland, du Canada ainsi que dans de larges étendues Antarctiques. Leur principale caractéristique est qu'ils sont continuellement recouverts de banquises et qu'au moins un glacier continental est présent de façon pérenne. Les sources de sédiment sont l'écoulement sous-glaciaire et le vêlage d'icebergs.

Ces fjords représentent des environnements de transition entre le domaine marin et terrestre et sont donc des zones sensibles aux changements environnementaux se produisant à grandes (saisonnalité) et plus faibles (changements interannuels, changements climatiques actuels) fréquences. L'étude de processus biologiques et géochimiques vis-à-vis de gradients environnementaux ou variations saisonnières est donc pertinente dans les fjords.

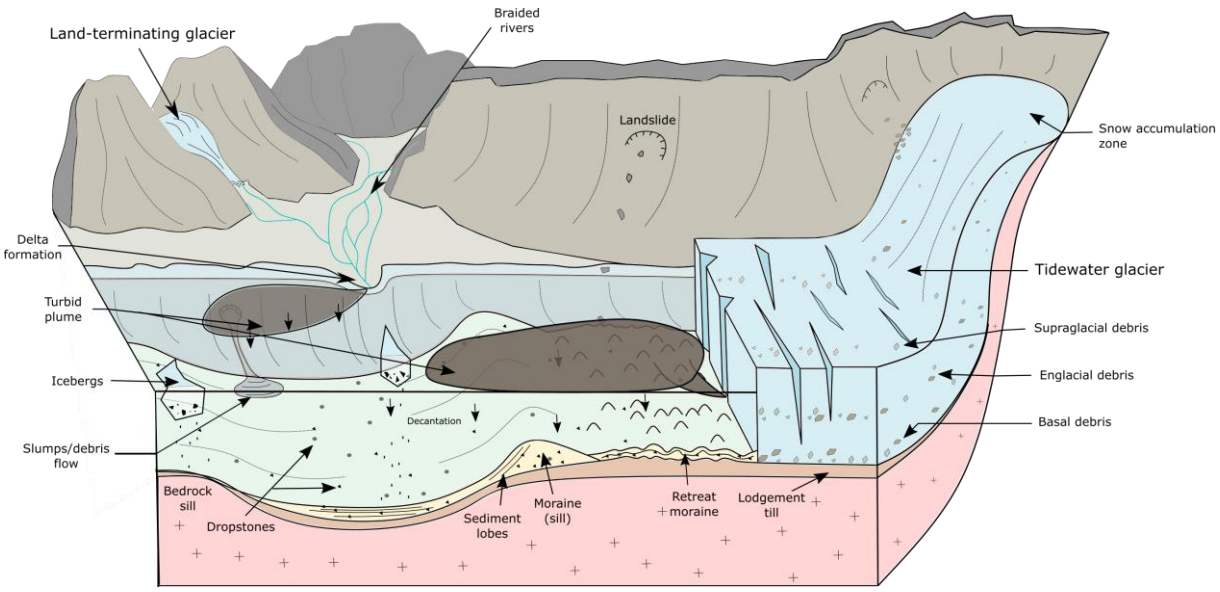

Figure 1: Représentation schématique des environnements de dépôts sédimentaires dans un fjord subpolaire ainsi que les différentes sources de sédiment. (D'après Dallman, 2015 et Elverhøy et al. (1983))

2.2 Changement climatique en Arctique

L'augmentation avérée du contenu en CO_2 dans l'atmosphère notamment mesurée par la NOAA depuis 1958 a été interprétée comme la cause principale du réchauffement climatique moderne car il agit comme gaz à effet de serre bloquant les radiations émises par la Terre dans l'atmosphère (Fig. 2). De plus, les études paléoclimatiques montrant la cyclicité du climat au cours des derniers 800.000 ans via l'étude de la composition gazeuse de bulles dans la glace

antarctique a permis d'attester du rôle des émissions en dioxyde de carbone par les activités anthropiques comme contributeur majeur aux changements climatiques globaux.

L'utilisation de combustibles fossiles depuis le début de l'industrialisation ainsi que son augmentation au fil des décennies a induit une augmentation de 0.2°C par décennie comme précisé par Allen et al. (2017).

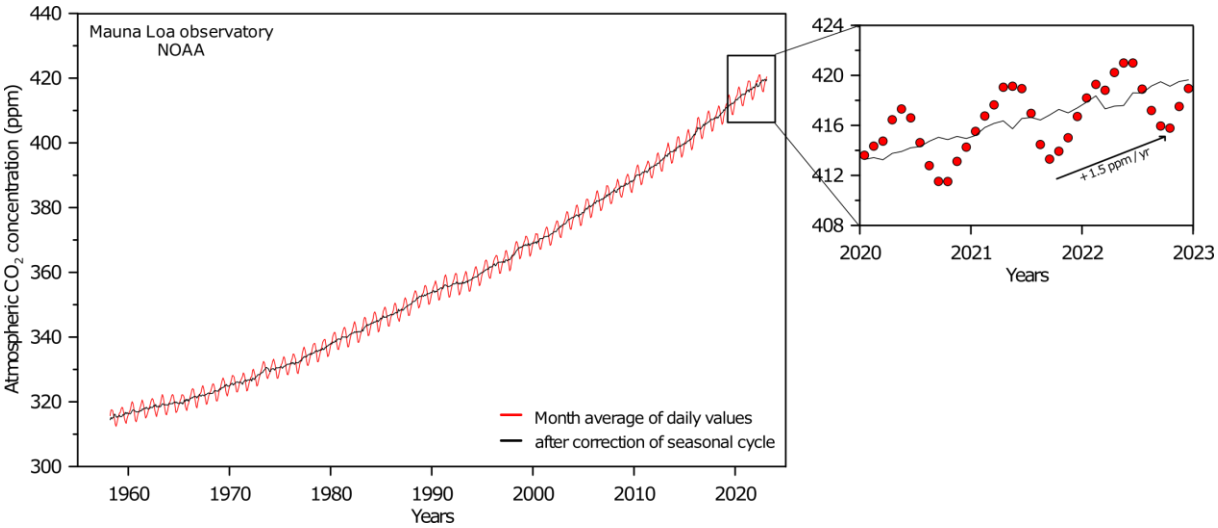

Figure 2: Concentration en dioxyde de carbone dans l'atmosphère mesurée à l'observatoire Mauna Loa (Hawaii, USA) depuis Mars 1958 (rouge, données mensuelles ; noire, avec correction des cycles saisonniers) (*Dr. Pieter Tans, NOAA/GML (gml.noaa.gov/ccgg/trends/) and Dr. Ralph Keeling, Scripps Institution of Oceanography (scrippsco2.ucsd.edu/).)*

Les effets de ce changement climatique sont visibles et mesurables dans les couches superficielles et fluides de notre planète, la cryosphère, l'atmosphère et l'hydrosphère (Intergovernmental Panel on Climate Change (IPCC), 2023). De plus, des interactions complexes sous forme de rétroactions peuvent intervenir entre ces différents composants. Des perturbations dans les océans sont déjà visibles et modélisées dans un futur relativement proche comme l'acidification de l'eau, le réchauffement, la montée des eaux, la diminution en oxygène ou encore des changements hydrographiques (Intergovernmental Panel on Climate Change (IPCC), 2023). Les cycles biologiques liés aux paramètres physico-chimiques de l'environnement s'en trouvent perturbés via des activités migratoires anormales, des cycles de vie modifiés ou encore des chaines trophiques rompues. D'après le rapport le plus récent du GIEC (IPCC), l'adaptabilité des espèces vis-à-vis de changements dans leur environnement serait déjà à la limite de ses capacités (Intergovernmental Panel on Climate Change (IPCC), 2023).

Contrairement à d'autres parties de la planète, les régions arctiques subissent un effet amplifié du réchauffement global appelé « Amplification polaire » (Intergovernmental Panel on Climate Change (IPCC), 2022). Des changements notables dans différentes composantes environnementales de ces régions sont attribuables aux émissions anthropogéniques causant un réchauffement atmosphérique deux fois plus important que la moyenne globale (Notz and Stroeve, 2016; Perovich and Richter-Menge, 2009). Les causes précises de cette amplification sont encore à l'étude mais des rétroactions locales comme la baisse d'albédo due à la diminution interannuelle de banquise ou de couverture neigeuse pourraient augmenter l'effet du réchauffement observé. De plus, l'augmentation de la température des courants de surface Atlantique (Gulf Stream) apporte de la chaleur et de l'humidité depuis les basses latitudes

équatoriales vers les régions polaires (Lind et al., 2018; Schauer et al., 2004). La saisonnalité est très marquée en Arctique notamment avec la formation de la banquise en hiver et sa fonte partielle en été ou encore avec la courantologie locale qui varie selon les fréquences observées (Lind et al., 2018). Il existe donc une dynamique naturelle à ses composantes environnementales de l'ordre du mois (saisonnalité) à l'année (Oscillation Arctique, Oscillation Nord Atlantique). Par conséquent, l'amplification arctique consiste en l'ajout de l'action anthropique sur cette dynamique naturelle. Les modèles climatiques prévoient une augmentation de température des eaux de surface marines en septembre (période estivale en générale plus chaude) de 10°C à 14°C dès 2100 avec une perte quasi-totale de la banquise d'ici là si les concentrations en gaz à effet de serre dans l'atmosphère continuent à augmenter à la même vitesse qu'aujourd'hui (Intergovernmental Panel on Climate Change (IPCC), (2022); Fig. 3). De plus, l'IPCC affirme que le retrait des glaciers à terminaison marine sur la terre (*medium evidence and high agreement*) réduira l'apport des nutriments vers la surface inhibant la productivité primaire en été dans les régions Arctiques (Hopwood et al., 2018; Meire et al., 2017). Du fait des changements de conditions physico-chimiques dans les fjords arctiques, les écosystèmes marins seront donc négativement affectés à tous les niveaux trophiques (Intergovernmental Panel on Climate Change (IPCC), 2022). Des impacts considérables sont

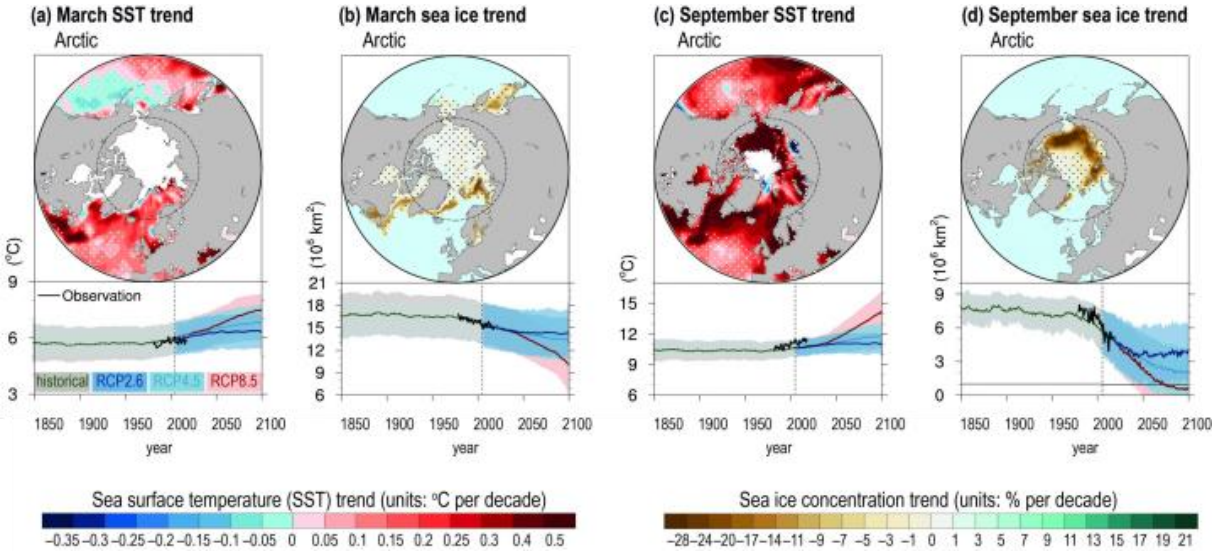

Figure 3 : Cartes des tendances linéaires (°C par décennie) de la température marine de surface (SST) en Arctique entre les années 1982 et 2017 en Mars et Septembre ainsi que les concentrations en banquise (en % par décennie). En dessous de chaque carte se trouve les mesures de concentration en banquise et de température d'eau de surface (moyennée sur la surface au-dessus de 40°N) jusqu'à 2017. Les différentes courbes allant jusqu'à 2100 font référence aux projections des différents modèles proposés par l'IPCC. Modifié d'après IPCC (2022).

donc à prévoir sur les écosystèmes, l'hydrographie et l'état de la cryosphère dans ces régions.

2.3 Hydrographie du Svalbard

L'archipel du Svalbard se situe au-dessus du cercle arctique (74-81°N et 10-35°E) entre la mer de Barents au Sud, l'Océan Arctique au Nord et le passage de Fram à l'Ouest. Ce dernier sépare le Groenland de l'archipel et est le principal point d'échange des eaux atlantiques circulant vers le nord et des eaux arctiques circulant vers le sud (Cottier et al., 2005; Schauer et al., 2004; Strzelewicz et al., 2022; Tesi et al., 2021). Ces masses d'eaux influencent le climat local car les eaux arctiques, ici représentées par le EGC (East Greenland Current) et favorisent

la formation de banquise sur le littoral groenlandais (Strzelewicz et al., 2022). Près de l'archipel du Svalbard, le WSC (West Spitsbergen Current ; Fig. 4a) est une branche du courant atlantique qui longe le Spitsberg apportant des eaux chaudes et salées vers les hautes latitudes. Ce courant circule parallèlement au talus de la plateforme continentale alors que le SPC (Spitsbergen Polar Current) circule près des côtes. Ce même courant est une extension du ESC (East Spitsbergen Current) circulant autour de l'archipel du Svalbard dans le sens horaire depuis l'Océan Arctique (Fig. 4a).

Le front Arctique est une limite qui sépare le WSC du SPC, tous deux circulant vers le nord parallèlement à la côte de l'île du Spitsberg vers le nord (Svendsen et al., 2002). Ce front présente une stabilité saisonnière (Svendsen et al., 2002). En effet, les variations de ce front au cours du temps permettent des remontées de WSC sur la plateforme et ainsi des entrées de cette masse d'eau dans les différents fjords de cette côte dépendant de la présence ou non d'un seuil à leur embouchure. L'influence grandissante de cette masse d'eau d'origine atlantique a été observée entrainant des instabilités plus fréquentes du front Arctique. Cela augmente au cours des années permettant la présence prolongée d'eau atlantique sur la plateforme et dans certains

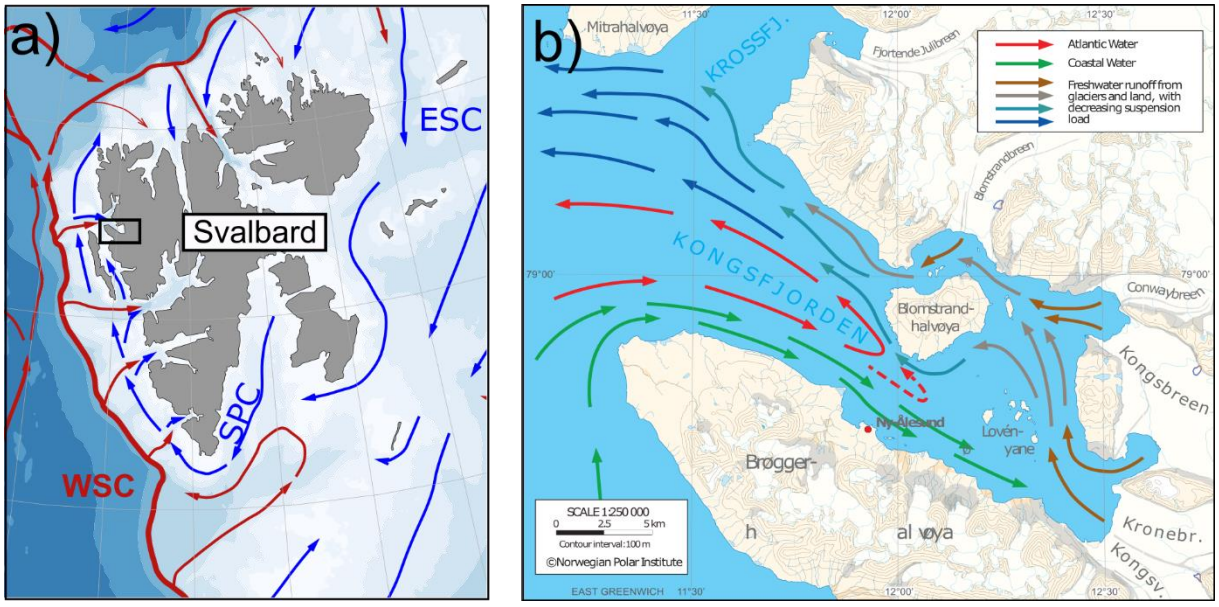

Figure 4 : a) Carte de la distribution des différents courants majeurs autour de l'archipel du Svalbard (ESC East Spitsbergen Current; SPC Spitsbergen Polar Current; WSC West Spitsbergen Current). La carte a été réalisée avec le package R PlotSvalbard (Vihtakari, 2020). b) Représentation schématique de la circulation marine horizontale dans le Kongsfjord. Les flèches rouges correspondant au courant atlantique provenant de l'océan ouvert ; la décharge turbide sous-glaciaire provenant des glaciers tidaux est symbolisée par les flèches marrons.

fjords (Lind et al., 2018; Polyakov et al., 2023; Strzelewicz et al., 2022). L'atlantification des courants locaux pourrait continuer et augmenter dans les prochaines décennies modifiant au passage les environnements terrestres et marins. Ces changements environnementaux drastiques au Svalbard au regard du réchauffement climatique se manifestent par une perte de masse des glaciers, une diminution des couvertures de banquise ainsi que par la déstabilisation du permafrost.

2.4 Le Kongsfjord : un fjord exposé au réchauffement climatique moderne

Les fjords de la côte ouest du Svalbard sont donc naturellement exposés à des changements saisonniers de courantologie introduisant des masses d'eau chaude atlantique vers l'océan Arctique en période estivale. Parmi ces fjords, le Kongsfjord possède une dynamique hydrologique saisonnière et interannuelle générée par ces intrusions marines d'un côté ainsi que par la dynamique de fonte des glaciers à terminaison marine de l'autre (Fig. 4b, 5). L'entrée de ce fjord se localise sur le passage de Fram séparant le Groenland du Svalbard (79°N, 12°E). Il mesure 20 km de long pour une largeur de 4 à 10 km et possède une orientation Ouest-Est. D'après la classification de Howe et al. (2010) exposée plus tôt, le Kongsfjord est un fjord subpolaire (Fig. 1).

Il s'agit d'un des fjords les plus étudiés d'Arctique car témoin précoce des changements climatiques actuels du fait de sa localisation. De récentes études sur l'effet des décharges de sédiment par fonte des glaciers locaux sur les écosystèmes benthiques (Fossile et al., 2022; Włodarska-Kowalczuk et al., 2016; Hop and Wiencke, 2019) ont permis de soulever des questionnements de l'effet de cette sédimentation intense sur les caractéristiques biogéochimiques des microhabitats et les populations de foraminifères benthiques dans le sédiment.

2.4.1 Géologie et géomorphologie du Kongsfjorden

Kongsfjorden est une vallée ennoyée par la mer résultant de l'érosion lors des phases glaciaires. Il présente une profondeur maximale de 350 m à son embouchure qui décroit vers la tête du fjord. Un seuil partiel est présent à son embouchure et un seuil séparant le bassin interne des parties les plus externes est présent en amont dans les îles Lovénøyane (< 30 m de profondeur ; (Halbach et al., 2019; Howe et al., 2003). La formation de ce fjord résulte de faiblesses dans le substrat rocheux dues à une série de failles et de chevauchements. En effet, le WSFB (West Spitsbergen Fold Belt) est un ensemble tectonique ayant affecté la côte ouest du Spitsberg durant l'Eocène (-52 millions d'années) déclenché par une ouverture de la mer du Labrador qui a entrainé un déplacement du Groenland vers le Svalbard. (Dallmann, 2015; Fig. 5). Cette série de failles et de chevauchements a permis la mise à l'affleurement d'une grande variété de roches. La côte nord du fjord présente des formations Mésoprotérozoïque de marbres et de mica-schistes (i.e. Blomstrandhalvøva ; Fig. 5). Depuis les îles Lovénøyane constituées de conglomérats et grès Dévonien, la tête du fjord montre des dolomites, marnes et calcaires datant du Carbonifère-Permien (Dallmann, 2015). La côte sud, plus affectée par les fronts de chevauchement consiste en des mica-schistes protérozoïques, ainsi que des phyllites et quartzites dans les formations supérieures (Fig. 5). De plus ces fronts laissent apparaitre de petites formations paléogènes de grès, conglomérats et charbon (Dallmann, 2015).

2.4.2 Cryosphère et hydrographie locale

Le fjord présente de nombreux glaciers continentaux à terminaison marine et terrestre. Les glaciers marins (ou tidaux) sont au nombre de cinq : Blomstrandbreen, Conwaybreen, Kongsbreen, Kronebreen et Kongsvegen. Les deux derniers partagent le même front entre la côte sud du fjord et la formation rocheuse de Collethøgda (Fig. 5 ; Halbach et al. 2019). Additionnellement, les glaciers à terminaison terrestre peuvent être trouvés essentiellement sur la côte sud du fjord, sur la péninsule de Brøggerhalvøya (Fig. 5).

La balance du volume des glaciers dépend à la fois du volume de fonte et de leur accrétion sur une période donnée souvent calculée sur une année. Dans les fjords subpolaires, la saison estivale correspond à une fonte accrue due à l'augmentation des températures atmosphériques, à la pluie ruisselant à la surface, et aux courants d'eau chaude pouvant faire fondre le front des glaciers tidaux. En hiver, les températures plus basses limitent cette fonte, et les précipitations sous forme de neige contribuent à l'augmentation du volume des calottes et glaciers. Une balance stable dans le temps résulte d'un équilibre entre fonte et accrétion. Avec le réchauffement actuel, la fonte est accrue pour la plupart des glaciers locaux donc le recul du front des glaciers est visible sur plusieurs années (Kohler et al., 2007; Lefauconnier et al., 1994). Néanmoins dans le cas de glaciers comme les Kongsvegen et Kronebreen, la fonte du front par l'augmentation de température des courants marins combinée à une accrétion sur les parties les plus hautes des glaciers engendrent une déstabilisation complète de l'ensemble de la structure glaciaire. Ces glaciers appelés « surge-type glaciers » sont susceptibles d'avancer à très grande vitesse après un recul trop important de leur front (Sevestre et al., 2018). Avec un manque d'appui en bas de la langue glaciaire et un volume grandissant en amont, l'ensemble peut glisser vers le fjord sur plusieurs kilomètres en quelques semaines/mois comme observés chez d'autres glaciers du Svalbard (Dowdeswell et al., 1991; Jiskoot et al., 2000). La morphologie et la texture de leur substrat sédimentaire/rocheux peuvent également favoriser ou non ces épisodes d'avancée soudaine par lubrification (Bouchayer et al., 2023; Sevestre et al., 2018; Willis et al., 2018).

La position et l'orientation du fjord vis-à-vis du passage de Fram et de la circulation océanique entre le Spitsberg et le Groenland additionnées de l'absence de seuil à l'embouchure favorisent les intrusions des courants atlantique et arctique, ponctuellement dépendant de la stabilité du front arctique positionné sur la plateforme (Fig. 4a ; Howe et al., 2003; Svendsen et al., 2002). Les instabilités du front arctique entrainent un mélange des eaux atlantique et arctique, appelé TAW (Transformed Atlantic Water), de plus en plus inégal en faveur des eaux atlantiques (Polyakov et al., 2023; Strzelewicz et al., 2022). L'intrusion de ce mélange dans le Kongsfjord se produit essentiellement en été entre fin Mai et Octobre (Cottier et al., 2005; Svendsen et al., 2002). De cette dynamique dépend la formation de glace de mer (Cottier et al., 2005) dans le Kongsfjord. La formation d'une banquise étendue dans le fjord n'a pas eu lieu depuis 2006 (Payne and Roesler, 2019). La fonte des glaciers tidaux et à terminaison terrestre intervient essentiellement pendant les mêmes périodes que les intrusions de TAW, par l'augmentation des températures atmosphériques, et fournissent au fjord des volumes considérables d'eau de fonte. Les flux principaux proviennent des glaciers tidaux en raison de leur taille et leur bassin versant plus conséquents que ceux des glaciers à terminaison terrestre. Chaque année, 1.4 km^3 d'eau sont déversés par décharge sous-glaciaire avec un maximum annuel en été (Payne and Roesler, 2019; Svendsen et al., 2002). Cela résulte en l'établissement d'une couche de surface d'eau douce froide appelée SW (Surface Water) qui peut se mélanger avec la TAW venant du large pour produire une masse d'eau intermédiaire (IW) (Cottier et al., 2005). Une stratification importante de la colonne d'eau s'installe donc en été, et disparait en hiver. La baisse des températures en hiver a pour effet de refroidir la TAW et de générer une plongée d'eau salée et froide plus dense appelée WCW (Winter Cooled Water). Cette eau se retrouve piégée dans les parties internes du fjord par le seuil des îles Lovenøyane (Payne and Roesler, 2019). Le refroidissement de ces eaux mène à la formation de glace de mer qui dépend des conditions physico-chimiques de la TAW à la fin de l'été (Payne et Roesler, 2019). Mais l'influence croissante de cette masse d'eau depuis le début des années 2000 ne permet plus la

formation de glace de mer (Schauer et al., 2004; Strzelewicz et al., 2022). En plus de l'hydrologie générale du fjord, le Kongsfjord est sujet à l'influence de la marée dont les ondes entrent en longeant la côte sud et sortent par le nord similairement à l'écoulement général des masses d'eau présenté en Fig. 4b (Svendsen et al., 2002). Les courants de marée influencent toute la colonne d'eau, malgré la présence d'une forte stratification en été et induisent un soulèvement du niveau de l'eau d'un maximum de 0.5 m (Svendsen et al., 2002).

Associée avec la distribution des masses d'eau, la fonte des glaciers génère également de forts gradients de turbidité qui influencent la productivité primaire et donc l'écosystème benthique.

Dans le Kongsfjord, les glaciers tidaux délivrent d'importants volumes de sédiments associés aux grands volumes d'eau douce de fonte (D'Angelo et al., 2018; Lydersen et al., 2014; Meslard et al., 2018; Trusel et al., 2010). Cette décharge sédimentaire est très importante près du front des glaciers Kronebreen/Kongsvegen, susceptibles de relarguer $2.48 \pm 0.36\ 10^6$ t de particules pendant les 2 mois de fonte estivale (Meslard et al., 2018) résultant en un dépôt parfois supérieur à 10 cm d'épaisseur uniquement sur cette période. Au front des glaciers tidaux, un panache turbide de surface se forme, alimenté par un upwelling qui transporte par densité les eaux de fonte sous glaciaire vers la surface, c'est-à-dire au-dessus des eaux salées du fjord, amenant aussi vers la surface les particules détritiques fines associées (Meslard et al., 2018). La forte concentration de particules fines conjuguée avec la salinité de l'eau marine permet leur floculation puis leur décantation vers les profondeurs. Cette concentration en particules fines dans la plume turbide se dilue en s'éloignant du front du glacier installant ainsi un fort gradient de turbidité entre la zone au front du glacier et la zone distale.

En plus de la sédimentation induite par la décharge glaciaire, la turbidité de surface limite la pénétration de lumière dans la colonne d'eau et ainsi inhibe la croissance phytoplanctonique dans la zone proximale, alors qu'elle est riche en nutriments. Avec une distance croissante au front des glaciers, la floculation/décantation ainsi que la dilution de la concentration en particules fines dans les eaux de surface permettent une meilleure pénétration de la lumière, ce qui favorise la productivité primaire stimulée par l'abondance de nutriments (Azzaro et al., 2021; Calleja et al., 2017; Halbach et al., 2019; Lalande et al., 2016; Piquet et al., 2014). La production phytoplanctonique augmente donc en s'éloignant du front des glaciers tidaux ainsi que l'export résultant vers les profondeurs de matière organique marine. Il existe donc deux gradients antagonistes de turbidité et de production phytoplanctonique (Lalande et al., 2016) intensifiés en été par la fonte du Kronebreen et Kongsvegen. Associés avec la distribution des masses d'eau, ces deux gradients environnementaux affectent significativement les écosystèmes benthiques (Hop and Wiencke, 2019).

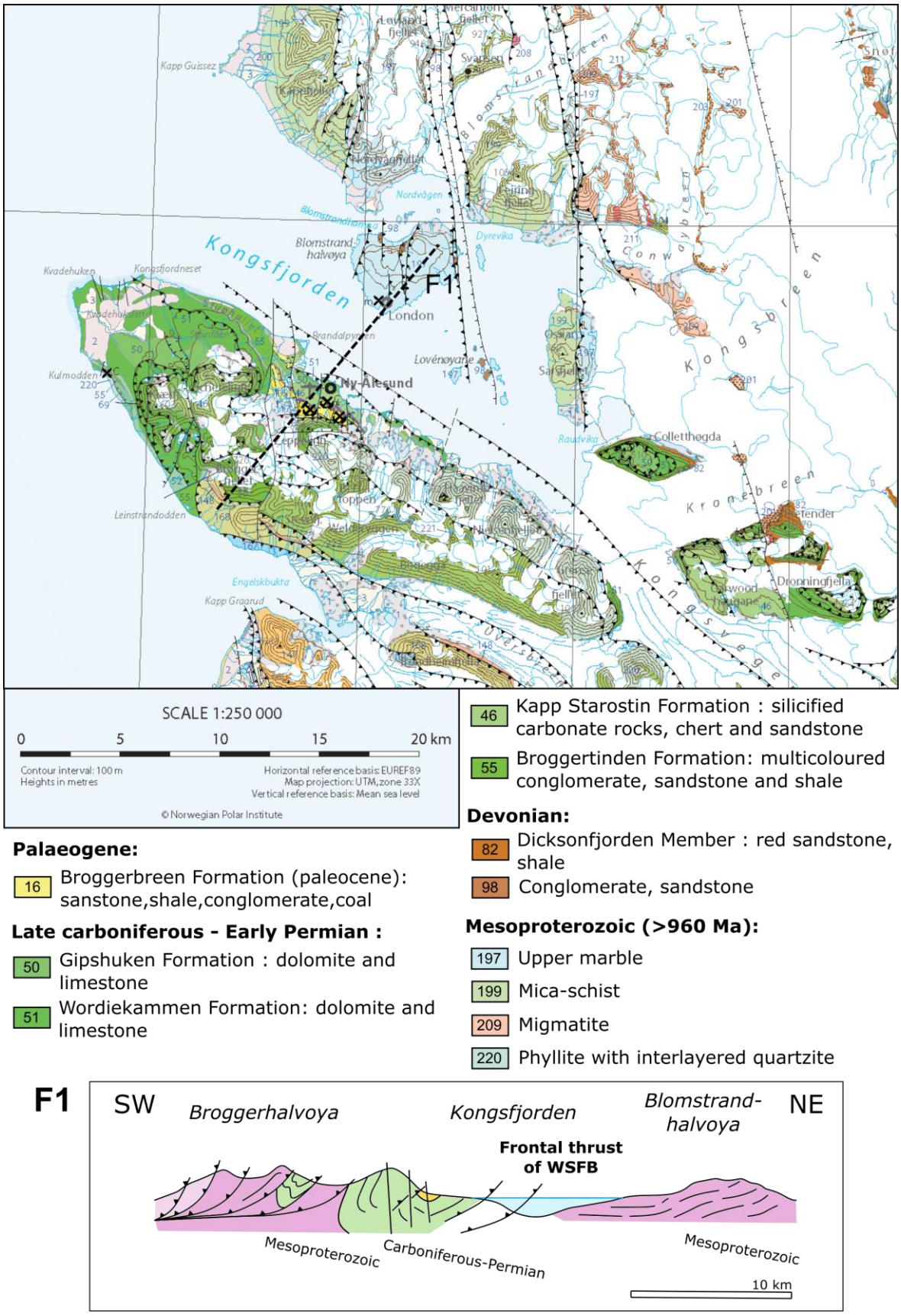

SCALE 1:250 000

0 5 10 15 20 km

Contour interval: 100 m
Heights in metres

Horizontal reference basis: EUREF89
Map projection: UTM, zone 33X
Vertical reference basis: Mean sea level

© Norwegian Polar Institute

Palaeogene:

16 Broggerbreen Formation (paleocene): sanstone,shale,conglomerate,coal

Late carboniferous - Early Permian :

50 Gipshuken Formation : dolomite and limestone

51 Wordiekammen Formation: dolomite and limestone

46 Kapp Starostin Formation : silicified carbonate rocks, chert and sandstone

55 Broggertinden Formation: multicoloured conglomerate, sandstone and shale

Devonian:

82 Dicksonfjorden Member : red sandstone, shale

98 Conglomerate, sandstone

Mesoproterozoic (>960 Ma):

197 Upper marble

199 Mica-schist

209 Migmatite

220 Phyllite with interlayered quartzite

Figure 5 : Carte géologique locale du Kongsfjorden issue de Dallman (2015). Les principales formations rocheuses environnantes sont détaillées dans la légende en dessous de la carte. La structure tectonique du fjord est représentée par la coupe structurale F1 coupant l'axe du fjord perpendiculairement.

3 Les foraminifères benthiques

Les foraminifères, spécialité du laboratoire LPG-site angevin, sont utilisés dans cette thèse comme un représentant des microorganismes benthiques. L'intérêt de l'étude des foraminifères benthiques modernes réside dans leur capacité à répondre rapidement aux changements environnementaux et à aux conditions stressantes (Murray, 2006). Avec cet objectif, ils sont désormais largement étudiés en tant que bioindicateurs de santé du milieu marin afin de déceler les pollutions, les impacts anthropiques et l'effet du changement climatique actuel sur l'environnement. Les changements de diversité, d'abondances ou de lieu de vie permettent d'établir des indices de santé d'un milieu marin, tels que Foram-AMBI ou le TSI-Med (e.g. Alve et al., 2016; Barras et al., 2014; Fouet et al., 2022; Jorissen et al., 2022).

3.1 Généralités sur les foraminifères

Les foraminifères sont des organismes unicellulaires eucaryotes appartenant au groupe des Rhizaria (Cavalier-Smith, 2003; Sierra et al., 2013). Ces protistes vivent dans les environnements aquatiques, d'habitats dulçaquicoles jusque dans tous les environnements marins. En effet, ils sont présents des zones côtières jusque dans les plaines abyssales à plusieurs milliers de mètres de profondeur où ils peuvent représenter plus de 50% de la biomasse totale (Gooday et al., 1992). Environ 50 espèces de foraminifères sont planctoniques, vivant dans la colonne d'eau tandis que plus de 10.000 espèces occupent un habitat benthique (Jones and Brady, 1994). Ils sont de petite taille (0.06 – 1.0 mm en général) et sont parfois présents en grande densité dans le sédiment avec une distribution planétaire en milieu marin et saumâtre. Cette grande distribution et le grand nombre d'espèces avec des préférences écologiques particulières, leur permet, additionnellement à une coquille (appelée « test ») hautement fossilisable, d'être des bons outils pour la reconstruction de paléoenvironnements ainsi que pour l'étude d'environnements modernes.

3.2 Les microhabitats sédimentaires

La distribution spatiale et temporelle des faunes de foraminifères dépend de forçages différents suivant l'échelle observée. En effet, sur des échelles régionales et saisonnières, les forçages influençant la distribution des foraminifères sont la nature du substrat (granulométrie du sédiment), les masses d'eau (i.e., température, salinité, turbidité), les conditions biogéochimiques dans le sédiment (i.e., contenu en matière organique, oxygène dissous, fronts redox, concentrations en éléments traces) et l'hydrodynamisme (e.g. Alve, 2001; Bouchet et al., 2009; Choquel et al., 2021; Contreras-Rosales et al., 2012; Jorissen et al., 1995; Murray, 2006; Thibault de Chanvalon et al., 2015). Leur distribution dans le sédiment peut aller de la surface jusqu'à plusieurs centimètres de profondeur dépendamment de leur préférence en termes d'oxygénation et de qualité et quantité de matière organique (Fig.6 ; Jorissen et al., 1995; Xu et al., 2021). En effet, comme montré dans la Fig. 6, toutes les espèces ne montrent pas les

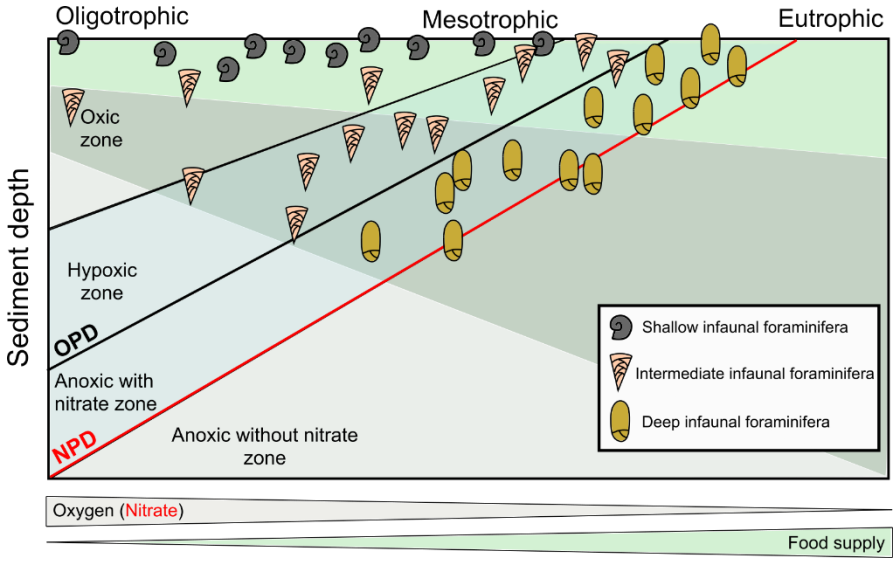

Figure 6 : Schéma du modèle TROX développé par Jorissen et al. (1995) incluant ici la concentration en nitrate et la profondeur de pénétration des nitrates (NPD) ajoutées par Xu et al. (2021)

mêmes niches écologiques en fonction de leur stratégie nutritive et tolérance à l'anoxie. Elles développent différentes stratégies suivant le milieu dans lequel elles évoluent comme herbivore, bactivore, alimentation passive par suspension, détritivore, carnivore, omnivore, mixotrophe ou parasite (Murray, 2006). Le modèle présenté en Fig. 6 inclut la possibilité pour certaines espèces à changer leur métabolisme quand le milieu devient hypoxique ou anoxique vers l'utilisation de nitrate comme accepteur terminal d'électrons.

Ce schéma ne tient pas compte des perturbations sédimentaires qui couvrent généralement des périodes plus courtes et des espaces plus restreints non généralisables à une échelle plus large. Elles interrompent l'état stationnaire de l'écosystème. En effet, lorsqu'enseveli sous un dépôt sédimentaire, le microhabitat autour des foraminifères change, en accord avec la biogéochimie locale. Il se rééquilibre vers la nouvelle interface eau-sédiment et les foraminifères doivent se déplacer pour le rejoindre. Pour cela, ils utilisent des extensions de leur cytoplasme appelées « pseudopodes » sortant par les pores du test et qui leur permet de se nourrir, se reproduire et de se déplacer activement dans la matrice sédimentaire (Sen Gupta, 1999).

3.3 Les études expérimentales

Les observations expérimentales des traits comportementaux des foraminifères, de la construction de leur test ainsi que de leur réponse métabolique et écologique vis-à-vis de changements environnementaux contribuent à donner une vision intégrative des forçages environnementaux. L'intérêt principal d'étudier l'effet d'un ou plusieurs forçages sur les faunes de foraminifères en conditions expérimentales est de limiter et contrôler les dits forçages pour réduire les effets synergiques ou antagonistes souvent difficiles à déconvoluer en milieu naturel. Dans le cas des foraminifères, les études en mésocosme (grand volume et souvent implanté en milieu naturel) et microcosme (volume restreint en laboratoire avec maitrise totale de l'environnement simulé) permettent un contrôle de forçages sur un élément biologique ou sur un autre paramètre environnemental (Lasserre, 1990). Chaque dispositif expérimental est différent car il répond à une ou plusieurs questions spécifiques. Le plan d'échantillonnage et d'observation, la durée de l'expérimentation ainsi que les espèces utilisées sont quelques-uns des aspects propres à des expériences uniques.

En ce qui concerne les instabilités sédimentaires, ou la relation entre foraminifères et microhabitat sédimentaire, les expériences de Deldicq et al. (2020, 2021, 2023) ont investigué l'effet de la bioturbation engendrée par le mouvement de certaines espèces dont *Haynesina germanica*. D'autres auteurs ont investigué les capacités motiles de plusieurs espèces (Moodley et al. 1998), ou encore le comportement après un épisode de sédimentation (e.g., Alve and Bernhard, 1995; Duijnstee et al., 2005; Ernst et al., 2002; Geslin et al., 2004) ou en cas d'enfouissement en milieu anoxique (Langlet et al., 2014; Nardelli et al., 2014).

3.4 Les foraminifères dans les fjords du Svalbard

En Arctique, les foraminifères benthiques sont sujets à de nombreuses contraintes environnementales très souvent saisonnières comme la stratification des eaux due au réchauffement estival de l'atmosphère, à l'hydrodynamique des eaux de fonte et des incursions océaniques, à des productions de saumures ou à la dispersion d'icebergs. De plus, le fort lien entre le compartiment pélagique et benthique est également soumis à cette saisonnalité avec notamment les périodes de nuit polaire affectant négativement la production phytoplanctonique pendant les périodes hivernales dans l'ensemble du fjord (e.g., Hoppe, 2022; Lalande et al., 2016). La période estivale implique de fortes turbidités qui inhibent aussi la production phytoplanctonique en zone proximale des fronts des glaciers tidaux. Le faible export de matière organique d'origine marine pendant ces périodes impacte plus ou moins localement les communautés benthiques (Hop and Wiencke, 2019; Włodarska-Kowalczuk et al., 2013, 2016). Des changements de régime nutritif peuvent donc être adoptés par les individus pour pallier à ces stress saisonniers.

Dans les fjords du Svalbard, les contraintes environnementales sont aussi très variables spatialement car elles se répartissent dans les milieux contrastés des zones de transition entre le domaine continental/glaciaire et marin. Dans les différents fjords du Svalbard, différentes faunes de foraminifères benthiques ont été documentées comme reporté dans la revue bibliographique de Jima et al. (2021) reprenant toutes les études connues sur les 4 dernières décennies sur la distribution moderne de ces individus autour de l'archipel (e.g., Fossile et al., 2022; Jernas et al., 2018; Kniazeva and Korsun, 2019; Kucharska et al., 2019; Saraswat, 2018). La distribution des assemblages est le résultat de grandes différences environnementales locales telles que la présence/absence de glace de mer ou encore des influences de courants marins arctiques ou atlantique plus ou moins marquées (Fig. 7). L'influence plus ou moins marquée des apport continentaux est aussi la cause d'un gradient entre les parties plus internes et celles plus externes du fjord qui se reflète dans la distribution spatiale des espèces (Fossile et al., 2022; Jernas et al., 2018; Jima et al., 2021).

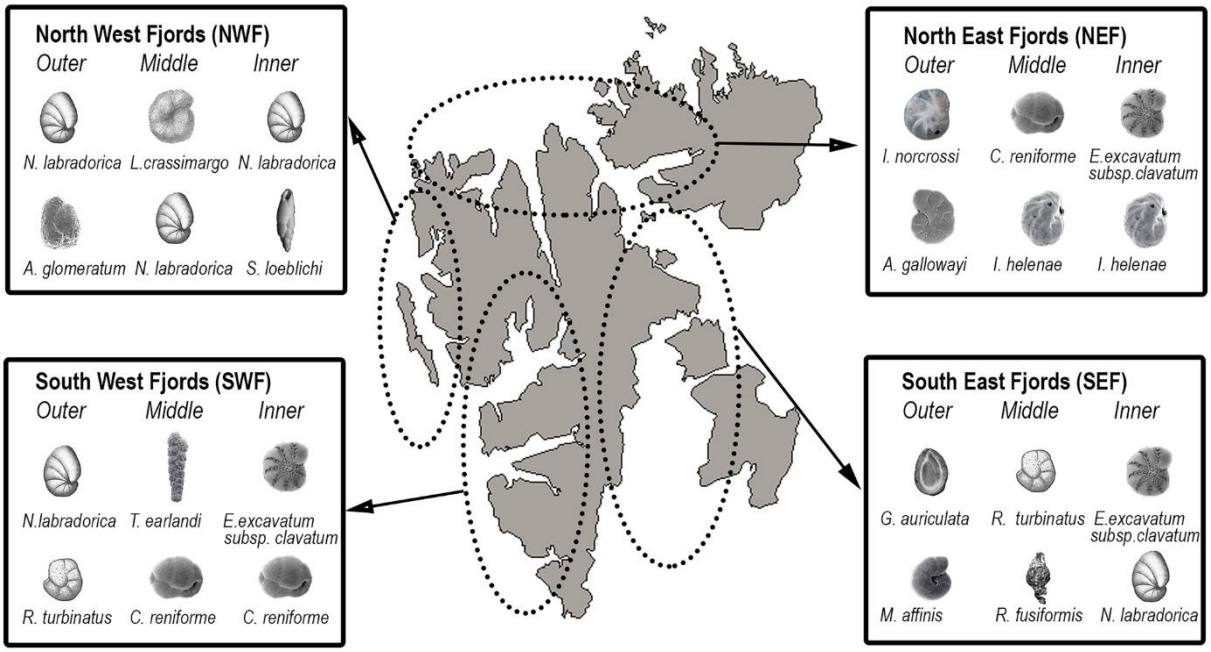

Figure 7: Carte de distribution des faunes majeures de foraminifères benthiques modernes autour de l'archipel du Svalbard. Les termes « Outer », « Middle » et « Inner » réfèrent aux différentes parties des fjords concernés entre la tête et l'embouchure du fjord. D'après Jima et al. (2021).

Par exemple, Fossile et al. (2022) et Jernas et al. (2018) ont mis en évidence, dans le Kongsfjord en période estivale, des biozonations liées à l'éloignement par rapport au front des glaciers tidaux, pouvant être expliquées par les différentes contraintes environnementales comprenant la distribution des masses d'eau, la turbidité de l'eau ainsi que les apports en matière organique (Fig. 8). La présence de *Nonionellina labradorica* et de *Adercotryma*

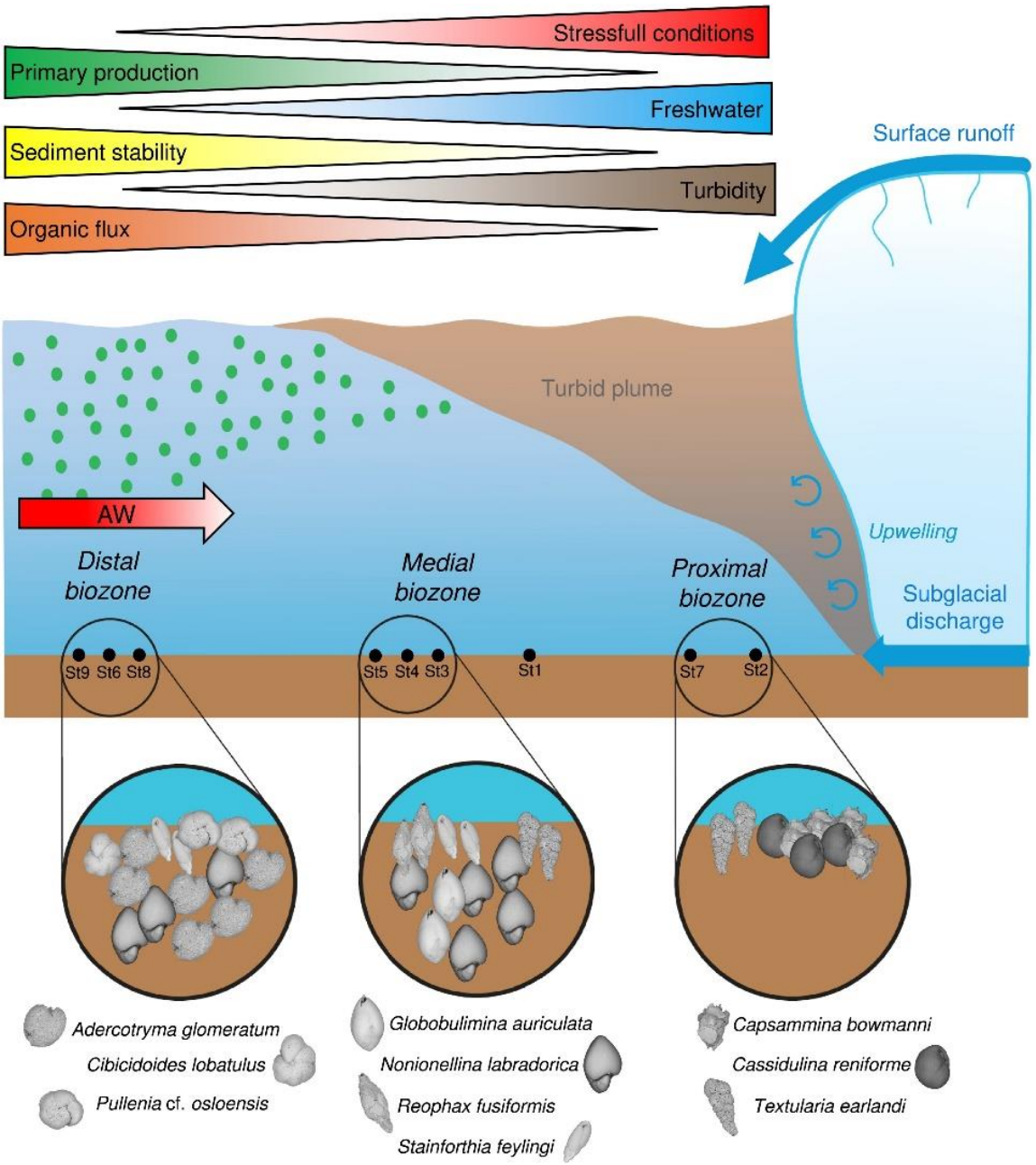

Figure 8: Modèle conceptuel de la biozonation des faunes de foraminifères benthiques ainsi que leur microhabitat en fonction des gradients environnementaux générés par la fonte des glaciers tidaux en été dans le Kongsfjord (Fossile et al., 2022)

glomeratum dans les parties externes du fjord a été associée à l'entrée des eaux d'origine Atlantique dans le fjord, et ces espèces se répartissent en fonction de la circulation intra-fjord de cette intrusion océanique. Les faunes changent en remontant vers l'amont du fjord, avec des assemblages où les espèces (sub)polaires deviennent dominantes, *Cassidulina reniforme* et *Elphidium clavatum*, étant les espèces typiques. S'ajoute à cette distribution l'influence des

gradients environnementaux locaux tels que la turbidité liée à la fonte des glaciers ou encore la productivité primaire. Ces deux gradients, fortement interdépendants, influencent l'écosystème benthique par la sédimentation intense de matériel terrigène ou encore par l'export localisé de matière organique vers le fond alimentant les faunes benthiques. Cela génère, en plus de l'influence des masses d'eaux, une hétérogénéité des zones de stress pour la vie des foraminifères répondant par des variations d'abondance ou de diversité dans les différentes parties du fjord.

4 Biogéochimie du sédiment

4.1 Etat stationnaire des gradients géochimiques

La diagenèse précoce des sédiments est induite par la transformation de la matière organique dans les premières étapes de son enfouissement (Burdige, 2007; Froelich et al., 1979). Cela implique des processus chimiques, entre des composés présents dans la phase dissoute ou la phase solide des sédiments, induits par la métabolisation de la matière organique

a)

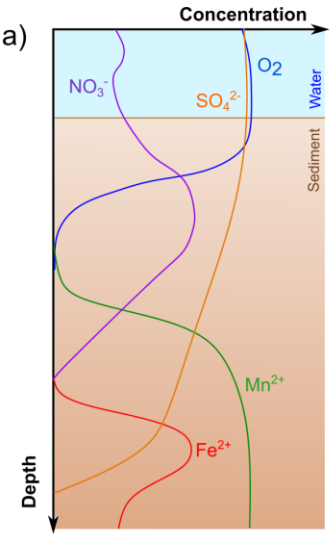

Process	Electron acceptor	Primary reactions
Aerobic respiration	O_2	(1)
Denitrification	NO_3^-	(2)
Manganese reduction	Mn^{4+} (e.g. MnO_2)	(3)
Iron reduction	Fe^{3+} (e.g. $Fe(OH)_3$)	(4)
Sulphate reduction	SO_4^{2-}	(5)
Methanogenesis	CO_2	(6)

b)

(1) $138O_2 + O.M. + 18HCO_3^- \rightarrow 124CO_2 + 16NO_3^- + HPO_4^{2-} + 140H_2O$

(2) $94.4NO_3^- + O.M. \rightarrow 13.6CO_2 + 92.4HCO_3^- + 55.2N_2 + 8\ 4.8H_2O + HPO_4^{2-}$

(3) $236MnO_2 + O.M. + 364CO_2 + 104H_2O \rightarrow 470HCO_3^- + 8N_2 + 236Mn^{2+} + HPO_4^{2-}$

(4) $424Fe(OH)_3 + O.M. + 740CO_2 \rightarrow 846HCO_3^- + 424Fe^{2+} + 16NH_3 + 320H_2O + HPO_4^{2-}$

(5) $53SO_4^{2-} + O.M. \rightarrow 39CO_2 + 67HCO_3^- + 16NH_4^+ + 53HS^- + 39H_2O + HPO_4^{2-}$

Figure 9 : a) Représentation schématique de profils dans les eaux porales des sédiments marins des concentrations des accepteurs d'électrons ou de produits de réactions et de leur succession théorique basée sur leur utilisation pour la reminéralisation de la matière organique. Ici sont représentées les réactions primaires de la diagenèse précoce. Ce modèle présente la succession des gradients dans une situation stable sans perturbation (dépôt, érosion or bioturbation). Modifié de Froelich et al. (1979) et Burdige (1993). b) Equations des réactions primaires de reminéralisation de la matière organique (O.M. = $C_{106}H_{263}O_{110}N_{16}P$; Redfield, 1963) par oxydation bactérienne dans les sédiments marins (Froelich et al., 1979). Les composés chimiques colorés représentent des oxydants ou produits réduits de ces réactions usuellement étudiées en a)

par des bactéries (oxydo-réduction, précipitation et dissolution, complexation, adsorption), ainsi que des processus physiques tels que la compaction des sédiments ou le transport des espèces chimiques par diffusion moléculaire, advection, bioturbation et bioirrigation. La matière organique agit ici en tant que donneur d'électron et sa dégradation, ou minéralisation, nécessite un accepteur d'électron. Froelich et al. (1979) ont proposé un modèle conceptuel qui repose sur le fait que l'accepteur d'électron, fournissant la plus grande quantité d'énergie libre dans l'étape du transfert terminal d'électron, est utilisé préférentiellement. Un étagement des réactions diagenétiques primaires en résulte (Fig. 9). Le métabolisme le plus efficace est donc la respiration aérobie utilisant l'oxygène dissous dans les eaux porales provenant de la diffusion depuis la colonne d'eau vers le sédiment. L'utilisation de cet oxygène est effectuée jusqu'à sa consommation totale en profondeur (Profondeur de pénétration d'Oxygène, OPD) (Aller, 2004)**.** L'étagement en dessous de l'OPD correspond aux respirations anaérobies suivantes : NO_3^- (réduction des nitrates) > MnO_2 (réduction des oxydes de manganèse réactifs) > $Fe(OH)_3$ (réduction des oxydes de fer réactifs) > SO_4^{2-} (sulfato-réduction) > CO_2 (méthanogenèse) (Burdige, 1993 ; Froelich et al., 1979). Cette succession représente un état stationnaire dans une matrice sédimentaire non perturbée (absence de bioturbation, de phénomènes non réguliers d'érosion ou de dépôt de sédiment).

4.2 Etat transitoire de sédiments perturbés

La séquence diagenétique présentée précédemment peut être interrompue ou modifiée par des perturbations extérieures comme l'érosion du substrat, la sédimentation intense via décantation, le transport de masse ou par la bioturbation. Dans les environnements de transition entre le continent et les milieux marins tels que les estuaires, deltas ou fjords, les substrats benthiques peuvent être sujets à des évènements de haute énergie induits par les cycles de marée, ou les crues ou encore du dragage ou du clapage. Cela résulte en des perturbations significatives de la biogéochimie du sédiment (Anschutz et al., 2002; Cathalot et al., 2010; Deflandre et al., 2002; Hulot et al., 2023; Mucci and Edenborn, 1992; Pastor et al., 2018; Thibault de Chanvalon et al., 2016). L'érosion des niveaux superficiels de sédiment met en contact des niveaux profonds, souvent anoxiques, avec la colonne d'eau provoquant des flux d'espèces réduites vers la colonne d'eau et un nouvel équilibrage chimique avec un nouvel étagement des gradients redox (Hulot et al., 2023). La temporalité de cet état transitoire dépend de la vitesse des réactions impliquées mais aussi de la quantité et de la qualité des accepteurs d'électrons et de la matière organique. Les effets de dépôt de sédiment sur l'état de la biogéochimie du substrat ont été documentés dans divers contextes cités précédemment comme les évènements de crue (Deflandre et al., 2002; Cathalot et al., 2010; Thibault de Chanvalon et al., 2016; Pastor et al., 2018; Hulot et al., 2023), les glissements de terrain (Mucci and Edenborn, 1992) ou les évènements turbiditiques dans les milieux marins plus profonds (Anschutz et al., 2002). Dans les cas énoncés, l'interface (SWI) est ensevelie sous plusieurs centimètres à mètres de sédiment. Ce nouveau dépôt de sédiment représente une barrière physique limitant les échanges diffusifs et advectifs alimentant les gradients redox précédemment établis. L'isolement des fronts redox, désormais instables se traduit tout d'abord par une consommation de l'oxygène emprisonné à l'ancienne SWI et parfois dans la couche de sédiment déposée, jusqu'à rendre le milieu totalement anoxique en quelques minutes à quelques heures dépendant de la quantité de matière organique et d'espèces chimiques réduites dans ces mêmes niveaux (Cathalot et al., 2010; Chaillou et al., 2007). La production ou consommation

de composés réduits peut générer des gradients susceptibles d'entrainer de la diffusion moléculaire et des flux. L'état transitoire des processus biogéochimiques après la perturbation peut durer plusieurs mois ou même plusieurs années (Anschutz et al., 2002; Deflandre et al., 2002; Thibault de Chanvalon et al., 2016).

Les premières étapes de transition des gradients géochimiques après des dépôts de sédiment variant en intensité et fréquence peuvent être révélées par une étude expérimentale. La simulation d'un environnement sédimentaire soumis à des dépôts de sédiments imitant une turbidite a déjà été réalisée en microcosme par Chaillou et al. (2007) avec des sédiments marins profonds. Les données issues de dispositifs expérimentaux sont précieuses car elles peuvent alimenter des modèles (Nmor et al., 2022; van de Velde et al., 2018; Yücel et al., 2010) en caractérisant et quantifiant l'effet de perturbations sur la biogéochimie du sédiment à des résolutions temporelles plus fines et soutenues que ce que permettent en général les observations en milieu naturel.

4.3 Biogéochimie des sédiments dans les fjords du Svalbard

Les particules sédimentaires constituant le fond des fjords du Svalbard ont pour origine l'érosion glaciaire des roches du bassin versant de ces mêmes glaciers (Herbert et al., 2021; Laufer-Meiser et al., 2021; Wehrmann et al., 2017). Ce matériel brut subit des altérations

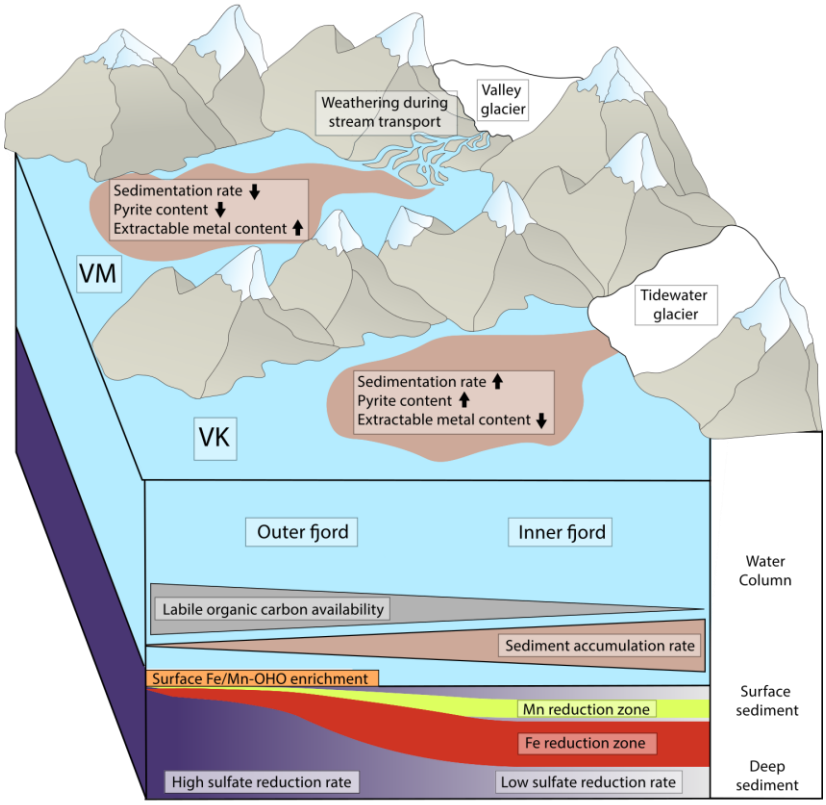

Figure 10 : Diagramme schématique illustrant les effets sur les cycles du Mn, Fe et S liés aux sources de sédiment ayant pour origine la fonte des glaciers tidaux ou des glaciers à terminaison terrestre dans le Van Mijenfjorden and Van Keulenfjorden (Svalbard). Les gradients environnementaux de la colonne d'eau comprennent la turbidité et le taux de sédimentation associé ainsi que le flux de matière organique exportée vers le sédiment ayant pour origine la productivité primaire de surface (modifié d'Herbert et al., 2020).

physiques et chimiques pendant son transport sous-glaciaire, et aussi pendant le ruissellement de surface jusqu'au fjord dans le cas d'un glacier à terminaison terrestre (Herbert et al., 2020; Hodson et al., 1998). Pendant le transport fluviatile de ces particules, des réactions d'altération interviennent telles que la dissolution de carbonates ou encore l'oxydation de sulfures avant le dépôt au fond du fjord. Dans le cas d'un glacier tidal, les particules sont directement délivrées par écoulement sous-glaciaire dans le fjord (D'Angelo et al., 2018; Meslard et al., 2018; Trusel et al., 2010) et subissent moins d'altérations pendant leur transport. En plus de délivrer ces particules terrigènes dans le fjord, contribuant à l'augmentation locale de la turbidité, ces écoulements de surface peuvent également apporter de la matière organique allochtone provenant de l'érosion de sols récents, de toundra ou de dépôts charbonneux (Fig. 5) (Jørgensen et al., 2021; Kuliński et al., 2014). Toutefois, les plus grandes quantités de matière organique influençant les systèmes benthiques proviennent de la production primaire donc du développement phytoplanctonique ayant lieu au printemps et en été lors de la période de jour polaire (Bourgeois et al., 2016; Calleja et al., 2017; Jørgensen et al., 2021; Lalande et al., 2016). Une succession de communautés d'organismes phytoplanctoniques intervient donc au cours de l'année, entretenue par les courants de surface amenant des nutriments depuis le front des glaciers résultant donc en un export important de matière organique autochtone vers le fond (Calleja et al., 2017).

Les dépôts sédimentaires situés dans les fjords du Svalbard, près des sources de sédiments ont été documentés comme en état transitoire géochimique pendant plusieurs périodes de l'année du fait de changements rapides dépendant de la fonte des glaciers mais aussi de l'export de matière organique vers le fond (Hop et al., 2002 ; Svendsen et al., 2002). Il en résulte des séquences diagenétiques en constante transition vers un état pseudo-stable. L'hétérogénéité de la turbidité ainsi que de la production phytoplanctonique a un impact considérable sur la stabilité biogéochimique, la réactivité mais également les caractéristiques physiques du sédiment (Herbert et al., 2020, 2021; Wehrmann et al., 2017). Ces gradients environnementaux ont un effet sur la distribution des communautés microbiennes et sur la pénétration de l'oxygène dissous (Jørgensen et al., 2021), la profondeur du front de dénitrification, la réduction des oxydes de manganèse et de fer puis sur la sulfato-réduction (Herbert et al., 2021; Laufer-Meiser et al., 2021; Michaud, 2020; Yang et al., 2022). Le modèle développé par Herbert et al. (2020) dans les fjords Van Keulenfjorden et Van Mildenfjorden (Svalbard) exprime cette variabilité conséquente de l'accumulation sédimentaire et de l'export de matière organique depuis la zone de productivité primaire de surface (Fig. 10). Avec l'augmentation de la distance depuis le front des glaciers tidaux, les fonds sont de moins en moins affectés par l'enfouissement sédimentaire et reçoivent une plus grande quantité de matière organique. Cela permet la migration des fronts de réduction des oxydes de manganèse et de fer vers la surface ainsi que l'enrichissement en oxydes diagenétiques dans les niveaux oxiques.

Références :

Allen, K. J., Fenwick, P., Palmer, J. G., Nichols, S. C., Cook, E. R., Buckley, B. M., and Baker, P. J.: A 1700-year Athrotaxis selaginoides tree-ring width chronology from southeastern Australia, Dendrochronologia, 45, 90–100, https://doi.org/10.1016/j.dendro.2017.07.004, 2017.

Aller, R. C.: Conceptual models of early diagenetic processes: The muddy seafloor as an unsteady, batch reactor, J Mar Res, 62, 815–835, https://doi.org/10.1357/0022240042880837, 2004.

Alve, E.: Colonization of new habitats by benthic foraminifera: a review, Earth-Science Reviews, 46, 167–185, https://doi.org/10.1016/S0012-8252(99)00016-1, 1999.

Alve, E.: Temporal variability in vertical distributions of live (stained) intertidal foraminifera, southern England, The Journal of Foraminiferal Research, 31, 12–24, https://doi.org/10.2113/0310012, 2001.

Alve, E. and Bernhard, J.: Vertical migratory response of benthic foraminifera to controlled oxygen concentrations in an experimental mesocosm, Mar. Ecol. Prog. Ser., 116, 137–151, https://doi.org/10.3354/meps116137, 1995.

Alve, E., Korsun, S., Schönfeld, J., Dijkstra, N., Golikova, E., Hess, S., Husum, K., and Panieri, G.: Foram-AMBI: A sensitivity index based on benthic foraminiferal faunas from North-East Atlantic and Arctic fjords, continental shelves and slopes, Marine Micropaleontology, 122, 1–12, https://doi.org/10.1016/j.marmicro.2015.11.001, 2016.

Anschutz, P., Jorissen, F. J., Chaillou, G., Abu-Zied, R., and Fontanier, C.: Recent turbidite deposition in the eastern Atlantic: Early diagenesis and biotic recovery, Journal of Marine Research, 60, 835–854, https://doi.org/10.1357/002224002321505156, 2002.

Azzaro, M., Aliani, S., Maimone, G., Decembrini, F., Caroppo, C., Giglio, F., Langone, L., Miserocchi, S., Cosenza, A., Azzaro, F., Rappazzo, A. C., Cabral, A. S., Paranhos, R., Mancuso, M., and La Ferla, R.: Short-term dynamics of nutrients, planktonic abundances, and microbial respiratory activity in the Arctic Kongsfjorden (Svalbard, Norway), Polar Biol, 44, 361–378, https://doi.org/10.1007/s00300-020-02798-w, 2021.

Barras, C., Jorissen, F. J., Labrune, C., Andral, B., and Boissery, P.: Live benthic foraminiferal faunas from the French Mediterranean Coast: Towards a new biotic index of environmental quality, Ecological Indicators, 36, 719–743, https://doi.org/10.1016/j.ecolind.2013.09.028, 2014.

Bolam, S. G.: Burial survival of benthic macrofauna following deposition of simulated dredged material, Environ Monit Assess, 181, 13–27, https://doi.org/10.1007/s10661-010-1809-5, 2011.

Bolliet, T., Jorissen, F. J., Schmidt, S., and Howa, H.: Benthic foraminifera from Capbreton Canyon revisited; faunal evolution after repetitive sediment disturbance, Deep Sea Research Part II: Topical Studies in Oceanography, 104, 319–334, https://doi.org/10.1016/j.dsr2.2013.09.009, 2014.

Bouchayer, C., Nanni, U., Lefeuvre, P.-M., Hulth, J., Steffensen Schmidt, L., Kohler, J., Renard, F., and Schuler, T. V.: Multi-scale variations of hydro-mechanical conditions at the base of the surge-type glacier Kongsvegen, Svalbard, https://doi.org/10.5194/egusphere-2023-618, 2023.

Bouchet, V. M. P., Sauriau, P.-G., Debenay, J.-P., Mermillod-Blondin, F., Schmidt, S., Amiard, J.-C., and Dupas, B.: Influence of the mode of macrofauna-mediated bioturbation on the vertical distribution of living benthic foraminifera: First insight from axial tomodensitometry, Journal of Experimental Marine Biology and Ecology, 14, 2009.

Bourgeois, S., Kerhervé, P., Calleja, M. L., Many, G., and Morata, N.: Glacier inputs influence organic matter composition and prokaryotic distribution in a high Arctic fjord (Kongsfjorden, Svalbard), Journal of Marine Systems, 16, 2016.

Budillon, F., Vicinanza, D., Ferrante, V., and Iorio, M.: Sediment transport and deposition during extreme sea storm events at the Salerno Bay (Tyrrhenian Sea): comparison of field data with numerical model results, Nat. Hazards Earth Syst. Sci., 6, 839–852, https://doi.org/10.5194/nhess-6-839-2006, 2006.

Burdige, D. J.: Geochemistry of Marine Sediments, in: Geochemistry of Marine Sediments, Princeton University Press, https://doi.org/10.1515/9780691216096, 2007.

Bussi, G., Dadson, S. J., Prudhomme, C., and Whitehead, P. G.: Modelling the future impacts of climate and land-use change on suspended sediment transport in the River Thames (UK), Journal of Hydrology, 542, 357–372, https://doi.org/10.1016/j.jhydrol.2016.09.010, 2016.

Calleja, M. Ll., Kerhervé, P., Bourgeois, S., Kędra, M., Leynaert, A., Devred, E., Babin, M., and Morata, N.: Effects of increase glacier discharge on phytoplankton bloom dynamics and pelagic geochemistry in a high Arctic fjord, Progress in Oceanography, 159, 195–210, https://doi.org/10.1016/j.pocean.2017.07.005, 2017.

Cathalot, C., Rabouille, C., Pastor, L., Deflandre, B., Viollier, E., Buscail, R., Gremare, A., Treignier, C., and Pruski, A.: Temporal variability of carbon recycling in coastal sediments influenced by rivers: assessing the impact of flood inputs in the Rhoˆne River prodelta, 2010.

Cavalier-Smith, T.: Protist phylogeny and the high-level classification of Protozoa, European Journal of Protistology, 39, 338–348, https://doi.org/10.1078/0932-4739-00002, 2003.

Chaillou, G., Anschutz, P., Dubrulle, C., and Lecroart, P.: Transient States in Diagenesis Following the Deposition of a Gravity Layer: Dynamics of O2, Mn, Fe and N-Species in Experimental Units, Aquat Geochem, 13, 157–172, https://doi.org/10.1007/s10498-007-9013-0, 2007.

Choquel, C., Geslin, E., Metzger, E., Filipsson, H. L., Risgaard-Petersen, N., Launeau, P., Giraud, M., Jauffrais, T., Jesus, B., and Mouret, A.: Denitrification by benthic foraminifera and their contribution to N-loss from a fjord environment, Biogeosciences, 18, 327–341, https://doi.org/10.5194/bg-18-327-2021, 2021.

Contreras-Rosales, L. A., Koho, K. A., Duijnstee, I. A. P., de Stigter, H. C., García, R., Koning, E., and Epping, E.: Living deep-sea benthic foraminifera from the Cap de Creus Canyon (western Mediterranean): Faunal–geochemical interactions, Deep Sea Research Part I: Oceanographic Research Papers, 64, 22–42, https://doi.org/10.1016/j.dsr.2012.01.010, 2012.

Cottier, F., Tverberg, V., Inall, M., Svendsen, H., Nilsen, F., and Griffiths, C.: Water mass modification in an Arctic fjord through cross-shelf exchange: The seasonal hydrography of Kongsfjorden, Svalbard, J. Geophys. Res., 110, C12005, https://doi.org/10.1029/2004JC002757, 2005.

Cottrell, R. S., Black, K. D., Hutchison, Z. L., and Last, K. S.: The Influence of Organic Material and Temperature on the Burial Tolerance of the Blue Mussel, Mytilus edulis: Considerations for the Management of Marine Aggregate Dredging, PLOS ONE, 11, e0147534, https://doi.org/10.1371/journal.pone.0147534, 2016.

Dallmann, W. K.: Geoscience Atlas of Svalbard, 2015.

D'Angelo, A., Giglio, F., Miserocchi, S., Sanchez-Vidal, A., Aliani, S., Tesi, T., Viola, A., Mazzola, M., and Langone, L.: Multi-year particle fluxes in Kongsfjorden, Svalbard, Biogeosciences, 15, 5343–5363, https://doi.org/10.5194/bg-15-5343-2018, 2018.

Davies, A. G., Robins, P. E., Austin, M., and Walker-Springett, G.: Exploring regional coastal sediment pathways using a coupled tide-wave-sediment dynamics model, Continental Shelf Research, 253, 104903, https://doi.org/10.1016/j.csr.2022.104903, 2023.

Deflandre, B., Mucci, A., Gagné, J.-P., Guignard, C., and Sundby, B. jørn: Early diagenetic processes in coastal marine sediments disturbed by a catastrophic sedimentation event, Geochimica et Cosmochimica Acta, 66, 2547–2558, https://doi.org/10.1016/S0016-7037(02)00861-X, 2002.

Dowdeswell, J. A., Hamilton, G. S., and Hagen, J. O.: The duration of the active phase on surge-type glaciers: contrasts between Svalbard and other regions, Journal of Glaciology, 37, 388–400, https://doi.org/10.3189/S0022143000005827, 1991.

Dudgeon, D.: Multiple threats imperil freshwater biodiversity in the Anthropocene, Current Biology, 29, R960–R967, https://doi.org/10.1016/j.cub.2019.08.002, 2019.

Duijnstee, I., de Nooijer, L., Ernst, S., and van der Zwaan, G.: Population dynamics of benthic shallow-water foraminifera: effects of a simulated marine snow event, Mar. Ecol. Prog. Ser., 285, 29–42, https://doi.org/10.3354/meps285029, 2005.

Dyer, K. R.: Fine Sediment Particle Transport in Estuaries, in: Physical Processes in Estuaries, edited by: Dronkers, J. and van Leussen, W., Springer Berlin Heidelberg, Berlin, Heidelberg, 295–310, https://doi.org/10.1007/978-3-642-73691-9_16, 1988.

Ernst, S., Duijnstee, I., and van der Zwaan, B.: The dynamics of the benthic foraminiferal microhabitat: recovery after experimental disturbance, Marine Micropaleontology, 46, 343–361, https://doi.org/10.1016/S0377-8398(02)00080-4, 2002.

Extence, A. C., P. Chadd, R., England, J., J. Dunbar, M., J. Wood, P., and D. Taylor, E.: The assessment of fine sediment accumulation in rivers using macro-invertebrate community response: macro-invertebrate assessment of fine sediment accumulation, River Res. Applic., 29, 17–55, https://doi.org/10.1002/rra.1569, 2013.

Fossile, E., Nardelli, M. P., Howa, H., Baltzer, A., Poprawski, Y., Baneschi, I., Doveri, M., and Mojtahid, M.: Influence of modern environmental gradients on foraminiferal faunas in the inner Kongsfjorden (Svalbard), Marine Micropaleontology, 173, 102117, https://doi.org/10.1016/j.marmicro.2022.102117, 2022.

Fouet, M. P. A., Singer, D., Coynel, A., Héliot, S., Howa, H., Lalande, J., Mouret, A., Schweizer, M., Tcherkez, G., and Jorissen, F. J.: Foraminiferal Distribution in Two Estuarine Intertidal Mudflats of the French Atlantic Coast: Testing the Marine Influence Index, Water, 14, 645, https://doi.org/10.3390/w14040645, 2022.

Froelich, P. N., Klinkhammer, G. P., Bender, M. L., Luedtke, N. A., Heath, G. R., Cullen, D., Dauphin, P., and Blaynehartman, D. Hammond.: Early oxidation of organic matter in pelagic sediments of the eastern equatorial Atlantic: suhoxic diagenesis, Geochimica et Cosmochimica Acta, 43, 1075–1090, https://doi.org/0016-7037 79,0701-1075SO?.M) 0, 1979.

García-García, A., Vilas, F., and García-Gil, S.: A seeping sea-floor in a Ria environment: Ria de Vigo (NW Spain), Environmental Geology, 38, 296–300, https://doi.org/10.1007/s002540050427, 1999.

Geslin, E., Heinz, P., Jorissen, F., and Hemleben, Ch.: Migratory responses of deep-sea benthic foraminifera to variable oxygen conditions: laboratory investigations, Marine Micropaleontology, 53, 227–243, https://doi.org/10.1016/j.marmicro.2004.05.010, 2004.

Gooday, A. J., Levin, L. A., Linke, P., and Heeger, T.: The Role of Benthic Foraminifera in Deep-Sea Food Webs and Carbon Cycling, in: Deep-Sea Food Chains and the Global Carbon Cycle, edited by: Rowe, G. T. and Pariente, V., Springer Netherlands, Dordrecht, 63–91, https://doi.org/10.1007/978-94-011-2452-2_5, 1992.

Halbach, L., Vihtakari, M., Duarte, P., Everett, A., Granskog, M. A., Hop, H., Kauko, H. M., Kristiansen, S., Myhre, P. I., Pavlov, A. K., Pramanik, A., Tatarek, A., Torsvik, T., Wiktor, J. M., Wold, A., Wulff, A., Steen, H., and Assmy, P.: Tidewater Glaciers and Bedrock Characteristics Control the Phytoplankton Growth Environment in a Fjord in the Arctic, Front. Mar. Sci., 6, 254, https://doi.org/10.3389/fmars.2019.00254, 2019.

Hendrick, V. J., Hutchison, Z. L., and Last, K. S.: Sediment Burial Intolerance of Marine Macroinvertebrates, PLOS ONE, 11, e0149114, https://doi.org/10.1371/journal.pone.0149114, 2016.

Herbert, L. C., Riedinger, N., Michaud, A. B., Laufer, K., Røy, H., Jørgensen, B. B., Heilbrun, C., Aller, R. C., Cochran, J. K., and Wehrmann, L. M.: Glacial controls on redox-sensitive trace element cycling in Arctic fjord sediments (Spitsbergen, Svalbard), Geochimica et Cosmochimica Acta, 271, 33–60, https://doi.org/10.1016/j.gca.2019.12.005, 2020.

Herbert, L. C., Zhu, Q., Michaud, A. B., Laufer-Meiser, K., Jones, C. K., Riedinger, N., Stooksbury, Z. S., Aller, R. C., Jørgensen, B. B., and Wehrmann, L. M.: Benthic iron flux influenced by climate-sensitive interplay between organic carbon availability and sedimentation rate in Arctic fjords, Limnol Oceanogr, 66, 3374–3392, https://doi.org/10.1002/lno.11885, 2021.

Hir, P. L., Ficht, A., Jacinto, R. S., Lesueur, P., Dupont, J.-P., Lafite, R., Brenon, I., Thouvenin, B., and Cugier, P.: Fine Sediment Transport and Accumulations at the Mouth of the Seine Estuary (France), Estuaries, 24, 950, https://doi.org/10.2307/1353009, 2001.

Hodgkins, R., Cooper, R., Wadham, J., and Tranter, M.: Suspended sediment fluxes in a high-Arctic glacierised catchment: implications for fluvial sediment storage, Sedimentary Geology, 162, 105–117, https://doi.org/10.1016/S0037-0738(03)00218-5, 2003.

Hodson, A., Gurnell, A., Tranter, M., Bogen, J., Hagen, J. O., and Clark, M.: Suspended sediment yield and transfer processes in a small High-Arctic glacier basin, Svalbard, Hydrol. Process., 12, 73–86, https://doi.org/10.1002/(SICI)1099-1085(199801)12:1<73::AID-HYP564>3.0.CO;2-S, 1998.

Hop, H. and Wiencke, C. (Eds.): The Ecosystem of Kongsfjorden, Svalbard, Springer International Publishing, Cham, https://doi.org/10.1007/978-3-319-46425-1, 2019.

Hoppe, C. J. M.: Always ready? Primary production of Arctic phytoplankton at the end of the polar night, Limnol Oceanogr Letters, 7, 167–174, https://doi.org/10.1002/lol2.10222, 2022.

Hopwood, M. J., Carroll, D., Browning, T. J., Meire, L., Mortensen, J., Krisch, S., and Achterberg, E. P.: Non-linear response of summertime marine productivity to increased meltwater discharge around Greenland, Nat Commun, 9, 3256, https://doi.org/10.1038/s41467-018-05488-8, 2018.

Howe, J. A., Moreton, S. G., Morri, C., and Morris, P.: Multibeam bathymetry and the depositional environments of Kongsfjorden and Krossfjorden, western Spitsbergen, Svalbard, Polar Research, 22, 301–316, https://doi.org/10.1111/j.1751-8369.2003.tb00114.x, 2003.

Howe, J. A., Austin, W. E. N., Forwick, M., Paetzel, M., Harland, R., and Cage, A. G.: Fjord systems and archives: a review, SP, 344, 5–15, https://doi.org/10.1144/SP344.2, 2010.

Hulot, V., Metzger, E., Thibault de Chanvalon, A., Mouret, A., Schmidt, S., Deflandre, B., Rigaud, S., Beneteau, E., Savoye, N., Souchu, P., Le Merrer, Y., and Maillet, G. M.: Impact of an exceptional winter flood on benthic oxygen and nutrient fluxes in a temperate macrotidal estuary: Potential consequences on summer deoxygenation, Frontiers in Marine Science, 10, 2023.

Intergovernmental Panel on Climate Change (IPCC): The Ocean and Cryosphere in a Changing Climate: Chapter 3 Polar regions, 1st ed., Cambridge University Press, https://doi.org/10.1017/9781009157964, 2022.

Intergovernmental Panel on Climate Change (IPCC): Synthesis report of the IPCC sixth assessment report (AR6), 2023.

Jalón-Rojas, I., Schmidt, S., and Sottolichio, A.: Turbidity in the fluvial Gironde Estuary (southwest France) based on 10-year continuous monitoring: sensitivity to hydrological conditions, Hydrol. Earth Syst. Sci., 19, 2805–2819, https://doi.org/10.5194/hess-19-2805-2015, 2015.

Jernas, P., Klitgaard-Kristensen, D., Husum, K., Koç, N., Tverberg, V., Loubere, P., Prins, M., Dijkstra, N., and Gluchowska, M.: Annual changes in Arctic fjord environment and modern benthic foraminiferal fauna: Evidence from Kongsfjorden, Svalbard, Global and Planetary Change, 163, 119–140, https://doi.org/10.1016/j.gloplacha.2017.11.013, 2018.

Jima, M., Jayachandran, P. R., and Bijoy Nandan, S.: Modern Benthic Foraminiferal Diversity Along the Fjords of Svalbard Archipelago: Diversity Evaluation, Thalassas, https://doi.org/10.1007/s41208-021-00356-7, 2021.

Jiskoot, H., Murray, T., and Boyle, P.: Controls on the distribution of surge-type glaciers in Svalbard, Journal of Glaciology, 46, 412–422, https://doi.org/10.3189/172756500781833115, 2000.

Jones, R. W. and Brady, H. B.: The Challenger foraminifera, Oxford University Press, Oxford ; New York, 149 pp., 1994.

Jørgensen, B. B., Laufer, K., Michaud, A. B., and Wehrmann, L. M.: Biogeochemistry and microbiology of high Arctic marine sediment ecosystems—Case study of Svalbard fjords, Limnol Oceanogr, 66, https://doi.org/10.1002/lno.11551, 2021.

Jorissen, F. J., de Stigter, H. C., and Widmark, J. G. V.: A conceptual model explaining benthic foraminiferal microhabitats, Marine Micropaleontology, 26, 3–15, https://doi.org/10.1016/0377-8398(95)00047-X, 1995.

Jorissen, F. J., Fouet, M. P. A., Singer, D., and Howa, H.: The Marine Influence Index (MII): a tool to assess estuarine intertidal mudflat environments for the purpose of foraminiferal biomonitoring, Water, 14, 676, https://doi.org/10.3390/w14040676, 2022.

Kniazeva, O. and Korsun, S.: Seasonal data on Rose Bengal stained foraminifera in the head of Kongsfjorden, Svalbard, Data in Brief, 25, 104040, https://doi.org/10.1016/j.dib.2019.104040, 2019.

Kohler, J., James, T. D., Murray, T., Nuth, C., Brandt, O., Barrand, N. E., Aas, H. F., and Luckman, A.: Acceleration in thinning rate on western Svalbard glaciers, Geophys. Res. Lett., 34, L18502, https://doi.org/10.1029/2007GL030681, 2007.

Kucharska, M., Kujawa, A., Pawłowska, J., Łącka, M., Szymańska, N., Lønne, O. J., and Zajączkowski, M.: Seasonal changes in foraminiferal assemblages along environmental gradients in Adventfjorden (West Spitsbergen), Polar Biol, 42, 569–580, https://doi.org/10.1007/s00300-018-02453-5, 2019.

Kuhnle, R. A., Bingner, R. L., Foster, G. R., and Grissinger, E. H.: Effect of land use changes on sediment transport in Goodwin Creek, Water Resour. Res., 32, 3189–3196, https://doi.org/10.1029/96WR02104, 1996.

Kuliński, K., Kędra, M., Legeżyńska, J., Gluchowska, M., and Zaborska, A.: Particulate organic matter sinks and sources in high Arctic fjord, Journal of Marine Systems, 139, 27–37, https://doi.org/10.1016/j.jmarsys.2014.04.018, 2014.

Lalande, C., Moriceau, B., Leynaert, A., and Morata, N.: Spatial and temporal variability in export fluxes of biogenic matter in Kongsfjorden, Polar Biol, 39, 1725–1738, https://doi.org/10.1007/s00300-016-1903-4, 2016.

Langlet, D., Baal, C., Geslin, E., Metzger, E., Zuschin, M., Riedel, B., Risgaard-Petersen, N., Stachowitsch, M., and Jorissen, F. J.: Foraminiferal species responses to in situ, experimentally induced anoxia in the Adriatic Sea, Biogeosciences, 11, 1775–1797, https://doi.org/10.5194/bg-11-1775-2014, 2014.

Lasserre, P.: Marine microcosms: Small-scale controlled ecosystems, in: Coastal and Estuarine Studies, vol. 37, edited by: Lalli, C. M., American Geophysical Union, Washington, D. C., 20–60, https://doi.org/10.1029/CE037p0020, 1990.

Laufer-Meiser, K., Michaud, A. B., Maisch, M., Byrne, J. M., Kappler, A., Patterson, M. O., Røy, H., and Jørgensen, B. B.: Potentially bioavailable iron produced through benthic cycling in glaciated Arctic fjords of Svalbard, Nat Commun, 12, 1349, https://doi.org/10.1038/s41467-021-21558-w, 2021.

Lefauconnier, B., Hagen, J. O., and Rudant, J. P.: Flow speed and calving rate of Kongsbreen glacier, Svalbard, using SPOT images, Polar Research, 13, 59–65, https://doi.org/10.1111/j.1751-8369.1994.tb00437.x, 1994.

Łepkowska, E. and Stachnik, Ł.: Which drivers control the suspended sediment flux in a high Arctic glacierized basin (Werenskioldbreen, Spitsbergen)?, Water, 10, 1408, https://doi.org/10.3390/w10101408, 2018.

Lind, S., Ingvaldsen, R. B., and Furevik, T.: Arctic warming hotspot in the northern Barents Sea linked to declining sea-ice import, Nature Clim Change, 8, 634–639, https://doi.org/10.1038/s41558-018-0205-y, 2018.

Lydersen, C., Assmy, P., Falk-Petersen, S., Kohler, J., Kovacs, K. M., Reigstad, M., Steen, H., Strøm, H., Sundfjord, A., Varpe, Ø., Walczowski, W., Weslawski, J. M., and Zajaczkowski, M.: The importance of tidewater glaciers for marine mammals and seabirds in Svalbard, Norway, Journal of Marine Systems, 129, 452–471, https://doi.org/10.1016/j.jmarsys.2013.09.006, 2014.

Mathers, K. L., Doretto, A., Fenoglio, S., Hill, M. J., and Wood, P. J.: Temporal effects of fine sediment deposition on benthic macroinvertebrate community structure, function and biodiversity likely reflects landscape setting, Science of The Total Environment, 829, 154612, https://doi.org/10.1016/j.scitotenv.2022.154612, 2022.

Mcintyre, K. L. and Howe, J. A.: Scottish west coast fjords since the last glaciation: a review, SP, 344, 305–329, https://doi.org/10.1144/SP344.21, 2010.

Meire, L., Mortensen, J., Meire, P., Juul-Pedersen, T., Sejr, M. K., Rysgaard, S., Nygaard, R., Huybrechts, P., and Meysman, F. J. R.: Marine-terminating glaciers sustain high productivity in Greenland fjords, Glob Change Biol, 23, 5344–5357, https://doi.org/10.1111/gcb.13801, 2017.

Meslard, F., Bourrin, F., Many, G., and Kerhervé, P.: Suspended particle dynamics and fluxes in an Arctic fjord (Kongsfjorden, Svalbard), Estuarine, Coastal and Shelf Science, 204, 212–224, https://doi.org/10.1016/j.ecss.2018.02.020, 2018.

Mestdagh, S., Bagaço, L., Braeckman, U., Ysebaert, T., De Smet, B., Moens, T., and Van Colen, C.: Functional trait responses to sediment deposition reduce macrofauna-mediated ecosystem functioning in an estuarine mudflat, Biogeosciences, 15, 2587–2599, https://doi.org/10.5194/bg-15-2587-2018, 2018.

Michaud, A. B.: Glacial influence on the iron and sulfur cycles in Arctic fjord sediments (Svalbard), Geochimica et Cosmochimica Acta, 2020.

Mucci, A. and Edenborn, H. M.: Influence of an organic-poor landslide deposit on the early diagenesis of iron and manganese in a coastal marine sediment, Geochimica et Cosmochimica Acta, 56, 3909–3921, https://doi.org/10.1016/0016-7037(92)90005-4, 1992.

Mucci, A., Boudreau, B., and Guignard, C.: Diagenetic mobility of trace elements in sediments covered by a flash flood deposit: Mn, Fe and As, Applied Geochemistry, 18, 1011–1026, https://doi.org/10.1016/S0883-2927(02)00207-X, 2003.

Murray, J. W.: Ecology and Applications of Benthic Foraminifera, Cambridge university press., 2006.

Nardelli, M. P., Barras, C., Metzger, E., Mouret, A., Filipsson, H. L., Jorissen, F., and Geslin, E.: Experimental evidence for foraminiferal calcification under anoxia, Biogeosciences, 11, 4029–4038, https://doi.org/10.5194/bg-11-4029-2014, 2014.

Nmor, S. I., Viollier, E., Pastor, L., Lansard, B., Rabouille, C., and Soetaert, K.: FESDIA (v1.0): exploring temporal variations of sediment biogeochemistry under the influence of flood events using numerical modelling, Geoscientific Model Development, 15, 7325–7351, https://doi.org/10.5194/gmd-15-7325-2022, 2022.

Norkko, A., Rosenberg, R., Thrush, S. F., and Whitlatch, R. B.: Scale- and intensity-dependent disturbance determines the magnitude of opportunistic response, Journal of Experimental Marine Biology and Ecology, 330, 195–207, https://doi.org/10.1016/j.jembe.2005.12.027, 2006.

Notz, D. and Stroeve, J.: Observed Arctic sea-ice loss directly follows anthropogenic CO_2 emission, Science, 354, 747–750, https://doi.org/10.1126/science.aag2345, 2016.

Paetzel, M. and Dale, T.: Climate proxies for recent fjord sediments in the inner Sognefjord region, western Norway, SP, 344, 271–288, https://doi.org/10.1144/SP344.19, 2010.

Pastor, L., Rabouille, C., Metzger, E., Thibault de Chanvalon, A., Viollier, E., and Deflandre, B.: Transient early diagenetic processes in Rhône prodelta sediments revealed in contrasting flood events, Continental Shelf Research, 166, 65–76, https://doi.org/10.1016/j.csr.2018.07.005, 2018.

Payne, C. M. and Roesler, C. S.: Characterizing the influence of Atlantic water intrusion on water mass formation and phytoplankton distribution in Kongsfjorden, Svalbard, Continental Shelf Research, 191, 104005, https://doi.org/10.1016/j.csr.2019.104005, 2019.

Perovich, D. K. and Richter-Menge, J. A.: Loss of Sea Ice in the Arctic, Annu. Rev. Mar. Sci., 1, 417–441, https://doi.org/10.1146/annurev.marine.010908.163805, 2009.

Piquet, A. M.-T., van de Poll, W. H., Visser, R. J. W., Wiencke, C., Bolhuis, H., and Buma, A. G. J.: Springtime phytoplankton dynamics in Arctic Krossfjorden and Kongsfjorden (Spitsbergen) as a function of glacier proximity, Biogeosciences, 11, 2263–2279, https://doi.org/10.5194/bg-11-2263-2014, 2014.

Polyakov, I. V., Ingvaldsen, R. B., Pnyushkov, A. V., Bhatt, U. S., Francis, J. A., Janout, M., Kwok, R., and Skagseth, Ø.: Fluctuating Atlantic inflows modulate Arctic atlantification, Science, 381, 972–979, https://doi.org/10.1126/science.adh5158, 2023.

Sánchez-Bayo, F. and Wyckhuys, K. A. G.: Worldwide decline of the entomofauna: A review of its drivers, Biological Conservation, 232, 8–27, https://doi.org/10.1016/j.biocon.2019.01.020, 2019.

Saraswat, R.: Assessing the environmental significance of benthic foraminiferal morpho-groups from the northern high latitudinal regions, Polar Science, 11, 2018.

Schauer, U., Fahrbach, E., Osterhus, S., and Rohardt, G.: Arctic warming through the Fram Strait: Oceanic heat transport from 3 years of measurements, Journal of Geophysical Research: Oceans, 109, https://doi.org/10.1029/2003JC001823, 2004.

Sen Gupta, B. K.: Modern Foraminifera, Springer Science & Business Media, 368 pp., 1999.

Sevestre, H., Benn, D. I., Luckman, A., Nuth, C., Kohler, J., Lindbäck, K., and Pettersson, R.: Tidewater Glacier Surges Initiated at the Terminus, Journal of Geophysical Research: Earth Surface, 123, 1035–1051, https://doi.org/10.1029/2017JF004358, 2018.

Sierra, R., Matz, M. V., Aglyamova, G., Pillet, L., Decelle, J., Not, F., de Vargas, C., and Pawlowski, J.: Deep relationships of Rhizaria revealed by phylogenomics: a farewell to Haeckel's Radiolaria, Mol Phylogenet Evol, 67, 53–59, https://doi.org/10.1016/j.ympev.2012.12.011, 2013.

Strzelewicz, A., Przyborska, A., and Walczowski, W.: Increased presence of Atlantic Water on the shelf south-west of Spitsbergen with implications for the Arctic fjord Hornsund, Progress in Oceanography, 200, 102714, https://doi.org/10.1016/j.pocean.2021.102714, 2022.

Svendsen, H., Beszczynska-Møller, A., Hagen, J. O., Lefauconnier, B., Tverberg, V., Gerland, S., Børre Ørbæk, J., Bischof, K., Papucci, C., Zajaczkowski, M., Azzolini, R., Bruland, O., and Wiencke, C.: The physical environment of Kongsfjorden–Krossfjorden, an Arctic fjord system in Svalbard, Polar Research, 21, 133–166, https://doi.org/10.3402/polar.v21i1.6479, 2002.

Syvitski, J. P. M. and Shaw, J.: Chapter 5 Sedimentology and Geomorphology of Fjords, in: Developments in Sedimentology, vol. 53, Elsevier, 113–178, https://doi.org/10.1016/S0070-4571(05)80025-1, 1995.

Szpak, M. T., Monteys, X., O'Reilly, S. S., Lilley, M. K. S., Scott, G. A., Hart, K. M., McCarron, S. G., and Kelleher, B. P.: Occurrence, characteristics and formation mechanisms of methane generated micro-pockmarks in Dunmanus Bay, Ireland, Continental Shelf Research, 103, 45–59, https://doi.org/10.1016/j.csr.2015.04.023, 2015.

Tesi, T., Muschitiello, F., Mollenhauer, G., Miserocchi, S., Langone, L., Ceccarelli, C., Panieri, G., Chiggiato, J., Nogarotto, A., Hefter, J., Ingrosso, G., Giglio, F., Giordano, P., and Capotondi, L.: Rapid Atlantification along the Fram Strait at the beginning of the 20th century, Sci. Adv., 7, eabj2946, https://doi.org/10.1126/sciadv.abj2946, 2021.

Thibault de Chanvalon, A., Metzger, E., Mouret, A., Cesbron, F., Knoery, J., Rozuel, E., Launeau, P., Nardelli, M. P., Jorissen, F. J., and Geslin, E.: Two-dimensional distribution of living benthic foraminifera in anoxic sediment layers of an estuarine mudflat (Loire estuary, France), Biogeosciences, 12, 6219–6234, https://doi.org/10.5194/bg-12-6219-2015, 2015.

Thibault de Chanvalon, A., Mouret, A., Knoery, J., Geslin, E., Péron, O., and Metzger, E.: Manganese, iron and phosphorus cycling in an estuarine mudflat, Loire, France, Journal of Sea Research, 118, 92–102, https://doi.org/10.1016/j.seares.2016.10.004, 2016.

Thrush, S. F., Gray, J. S., Hewitt, J. E., and Ugland, K. I.: Predicting the effects of habitat homogenization on marine biodiversity, Ecological Applications, 16, 1636–1642, https://doi.org/10.1890/1051-0761(2006)016[1636:PTEOHH]2.0.CO;2, 2006.

Trusel, L. D., Powell, R. D., Cumpston, R. M., and Brigham-Grette, J.: Modern glacimarine processes and potential future behaviour of Kronebreen and Kongsvegen polythermal tidewater glaciers, Kongsfjorden, Svalbard, Geological Society, London, Special Publications, 344, 89–102, https://doi.org/10.1144/SP344.9, 2010.

Van Meerbeek, K., Jucker, T., and Svenning, J.-C.: Unifying the concepts of stability and resilience in ecology, Journal of Ecology, 109, 3114–3132, https://doi.org/10.1111/1365-2745.13651, 2021.

van de Velde, S., Van Lancker, V., Hidalgo-Martinez, S., Berelson, W. M., and Meysman, F. J. R.: Anthropogenic disturbance keeps the coastal seafloor biogeochemistry in a transient state, Sci Rep, 8, 5582, https://doi.org/10.1038/s41598-018-23925-y, 2018.

Wehrmann, L. M., Riedinger, N., Brunner, B., Kamyshny, A., Hubert, C. R. J., Herbert, L. C., Brüchert, V., Jørgensen, B. B., Ferdelman, T. G., and Formolo, M. J.: Iron-controlled oxidative sulfur cycling recorded in the distribution and isotopic composition of sulfur species in glacially influenced fjord sediments of west Svalbard, Chemical Geology, 466, 678–695, https://doi.org/10.1016/j.chemgeo.2017.06.013, 2017.

Willis, M. J., Zheng, W., Durkin, W. J., Pritchard, M. E., Ramage, J. M., Dowdeswell, J. A., Benham, T. J., Bassford, R. P., Stearns, L. A., Glazovsky, A. F., Macheret, Y. Y., and Porter, C. C.: Massive destabilization of an Arctic ice cap, Earth and Planetary Science Letters, 502, 146–155, https://doi.org/10.1016/j.epsl.2018.08.049, 2018.

Włodarska-Kowalczuk, M., Pawłowska, J., and Zajączkowski, M.: Do foraminifera mirror diversity and distribution patterns of macrobenthic fauna in an Arctic glacial fjord?, Marine Micropaleontology, 103, 30–39, https://doi.org/10.1016/j.marmicro.2013.07.002, 2013.

Włodarska-Kowalczuk, M., Górska, B., Deja, K., and Morata, N.: Do benthic meiofaunal and macrofaunal communities respond to seasonality in pelagial processes in an Arctic fjord (Kongsfjorden, Spitsbergen)?, Polar Biol, 39, 2115–2129, https://doi.org/10.1007/s00300-016-1982-2, 2016.

Wolanski, E. and Gibbs, R.: Resuspension and clearing of dredge spoils after dredging, Cleveland Bay, Australia, Water Environment Research, 64, 910–914, https://doi.org/10.2175/WER.64.7.9, 1992.

Xu, Z., Liu, S., and Ning, X.: Potential foraminiferal nitrate transport in sediments in contact with oxic overlying water, Limnology and Oceanography, 66, 1510–1530, https://doi.org/10.1002/lno.11701, 2021.

Yang, Y., Ren, J., and Zhu, Z.: Distributions and Influencing Factors of Dissolved Manganese in Kongsfjorden and Ny-Ålesund, Svalbard, ACS Earth Space Chem., 6, 1259–1268, https://doi.org/10.1021/acsearthspacechem.1c00388, 2022.

Yücel, M., Luther, G. W., and Moore, W. S.: Earthquake-induced turbidite deposition as a previously unrecognized sink for hydrogen sulfide in the Black Sea sediments, Marine Chemistry, 121, 176–186, https://doi.org/10.1016/j.marchem.2010.04.006, 2010.

Experimental part

Chapter 2

Short-term response of benthic foraminifera to fine sediment depositional events simulated in microcosm

C. Guilhermic[*1], M.P. Nardelli[1], A. Mouret[1], D. Le Moigne[1], H. Howa[1]

[1] Université Angers, Nantes Univ., Le Mans Univ, CNRS, LPG, Laboratoire de planétologie et géosciences, UMR CNRS 6112, F-49000 Angers, France

Correspondence to: Corentin Guilhermic (corentin.guilhermic@etud.univ-angers.fr)

Published in Biogeosciences (Received 14 February 2023, Accepted 27 June 2023, published 11 August 2023) 10.5194/bg-20-3329-2023. Chapter's display was changed to fit with thesis unity.

Abstract:

A microcosm experiment was designed to describe how benthic foraminifera react to fine-sediment deposits varying in frequency and intensity as they may occur regularly or occasionally in coastal benthic environments, caused by discharges from (e.g.) river flooding, tidewater glacier melting in polar regions, or diverse anthropic activities linked to harbour or watershed management. The influence of seabed burial resulting from these events on the ecology of benthic ecosystems is often overlooked, and the resilience of benthic communities is poorly known. During a 51 d long experiment, a typical northeastern Atlantic intertidal foraminiferal community, mainly represented by *Ammonia confertitesta* and *Haynesina germanica* species, was subjected to two kinds of sedimentary disturbance: (1) a one-time high-volume (OHV) deposit, i.e. sediment about 3 cm thick was added at one time at the beginning of the experiment; and (2) frequent low-volume (FLV) deposits, i.e. sediment about 0.5 cm thick was added each week for 4 weeks. The geochemical environment (e.g. dissolved oxygen penetration in the sediment, salinity, temperature, and nutrient content in the supernatant water) was monitored to follow the microcosm steady state before and during the experiment. In both disturbed microcosms, *H. germanica* showed a significant linear decrease in abundance during the experiment, while the total abundance of foraminifera was significantly affected only by the OHV treatment, suggesting a stronger effect of a single thick deposit on standing stocks and biodiversity compared to frequent low-volume sediment supplies. Concerning the vertical migration of foraminifera after sedimentary disturbances, the two dominant species moved upwards to the water–sediment interface with migration speeds estimated to be 0.41 and 0.47 mm h^{-1} respectively for *A. confertitesta* and *H. germanica*. In the FLV treatment, the resilient state was already reached within 1 d following a low thickness burial, while in the OHV, it was achieved between 1 and 7 d after the 3 cm thick deposit. These results suggest that foraminifera can migrate rapidly after a sedimentary burial to recover their preferential life position under the new sediment–water interface, but in the case of an abrupt thick burial, several days are needed to reach a resilient state.

Keywords: biotic recovery, migration, oxygen penetration depth, disturbance, deposit

1 Introduction

Coastal marine environments are subject to recurrent, erratic, or rare sedimentary depositional events that abruptly bring sediment to the seafloor. Sediment depositional events in coastal marine areas occur under the influence of various drivers such as river flooding (Extence et al., 2013; Dyer, 1988; Hir et al., 2001; Jalón-Rojas et al., 2015), glacier melting in polar regions (D'Angelo et al., 2018; Fossile et al., 2022; Hodson et al., 1998; Meslard et al., 2018), storms (Bolliet et al., 2014; Budillon et al., 2006), or anthropic activi-ties such as dredging (Wolanski and Gibbs, 1992), or land use along catchment basins (Bussi et al., 2016; Kuhnle et al., 1996).

These sediment deposits, when thick and abrupt, can asphyxiate biota and provoke long-lasting destabilization of aquatic benthic ecosystems. In particular, fine-grained-sediment deposition can lead to a decline in microhabitat quality and affect benthic ecosystems in several ways (e.g. Larson and Sundbäck, 2012; Mestdagh et al., 2018; Wood, 1997): (1) by constituting a physical barrier that disrupts the connection to the water column, thereby impeding food supply and oxygen exchange; (2) by altering the substrate's geochemical composition and thus the substrate's suitability for some taxa; and (3) by providing a highly porous, water-saturated substrate whose instability can prevent recolonization from refuge areas.

The question of the impact of sediment supply to benthic realms becomes urgent in the context of the ongoing cli-mate change: among the most impressive consequences for coastal marine environments, there is the disruption of water cycles, including enhanced glacier melting at high latitudes and extreme oscillation of rainfall patterns at lower latitudes, both significantly affecting the sedimentary supply to coastal areas. Excessive deposition of fine sediment is generally recognized to have deleterious effects on aquatic biodiversity and is even considered to be one of the major threats to biodiversity in freshwater environments (Dudgeon, 2019; Mathers et al., 2022, 2022; Sánchez-Bayo and Wyckhuys, 2019) and in marine benthic environments (Alve, 1999; Anschutz et al., 2002). Biota burial and changes in substrate type can delay recovery of crucial benthic ecosystem function. The recovery rate is controlled by a complex combination of ecological and physical forcings (Norkko et al., 2006; Thrush et al., 2006). Among these, the ability of organisms to quickly migrate through the sediment is crucial to the recovery of their preferential habitat at the surface or inside the sediment column. Despite several studies focused on the response of mega- and macrobenthos to physical disturbances (Bolam et al., 2011; Cottrell et al., 2016; Hendrick et al., 2016; Mestdagh et al., 2018), little is known about meio- and microfauna, which represent lower steps of the trophic chain and therefore have the potential to control the ecosystem functioning through a bottom-up relationship.

Benthic foraminifera (Eukaryotes, Rhizaria) are unicellular organisms belonging to meiofauna and are highly sensitive to sedimentary and geochemical changes in their environment (e.g. Murray, 2006) and present several character-istics that make them powerful bio-indicators of marine environmental characteristics (Schönfeld et al., 2012): (i) high density in marine sediments; (ii) short lifecycles; (iii) occupation of specific ecological niches and microhabitats, including superficial, shallow, and deep infaunal sediment layers (up to 10–20 cm depth). Because of these characteristics, foraminifera have increasingly been used as biotic tools for assessing the quality status of coastal marine environments (Alve et al., 2016; Barras et al., 2014; Belart et al., 2018; Bouchet et al., 2018a, 2012; Fontanier et al., 2009, 2020; Frontalini and Coccioni, 2008; Jorissen et al., 2022; Laut et al., 2021; Martins et al., 2013, 2015,

2016; Murray, 2006; Nesbitt et al., 2015). Moreover, Bouchet et al. (2018b) showed that benthic foraminifera can be better bioindicators than macrofauna as they can be present on a larger spectrum of environmental gradients compared to macrofauna and are generally more sensitive to (and therefore absent in) highly stressed conditions. In Arctic fjords, foraminiferal ecological response to environmental stress has been observed to mirror the ones of macrofauna, with decreasing diversity and a dominance of opportunistic taxa (Wlodarska-Kowalczuk et al., 2013). In natural marine environments, vertical and horizontal distributions of benthic foraminiferal faunas are controlled by several parameters, noticeably organic matter and oxygen content in their habitats (e.g. Contreras-Rosales et al., 2012; Goineau et al., 2012; Gooday et al., 2000; Jorissen et al., 1995; Langezaal et al., 2006; Schumacher et al., 2007). Following the conceptual model from Jorissen et al. (1995) taken over by Van der Zwaan et al. (1999) and Koho et al. (2015), foraminiferal vertical distribution is limited in eutrophic systems by oxygen concentration in bottom and sediment porewaters and by organic matter availability in the oligotrophic realm. Beyond these two geochemical drivers, a third factor seems to affect the benthic environment, namely the physical forcing by sediment supply to the bottom. Some recent studies of naturally stressed coastal environments focused on the response of foraminiferal communities to excessive fine-sediment supply due to natural processes. Various environments were prospected: turbidites in canyon channels and terraces (Bolliet et al., 2014; Dessandier et al., 2016; Duros et al., 2017; Goineau et al., 2012; Hess and Jorissen, 2009), prodelta river flooding (Goineau et al., 2012), and river-dominated shelves (Dessandier et al., 2016). Other studies concentrated on anthropic activities that directly cause massive fine-sediment supply in coastal areas and the associated effects on benthic foraminifera faunas (e.g. oil drill cutting disposal – Mojtahid et al., 2006; exacerbated land use – Fontanier et al., 2018; industrial waste – Fontanier et al., 2020). Most of these studies mainly focus on massive and sudden or occasional deposits of sediment, and the fact that they are performed in natural environments represents a limit for the interpretations. Indeed, in natural settings, sediment supply, organic matter input, and oxygen availability often covary and synergically affect benthic communities and microhabitat distribution. Experimental studies are therefore the only way to test the effect of a single parameter in a controlled setting where environmental variability can be artificially reduced. For these reasons, we designed an experiment to test, in microcosms, the effect of different patterns of fine-grained sediment deposits on benthic foraminiferal communities without varying organic matter content and oxygen availability. Two different modes of sediment input were selected to characterize the vertical migration and survival of foraminifera under the pressure of 100 various physical disturbances, namely a single, thick sediment deposit and thin and recurrent sediment deposits, in order to test whether the ecological response is affected by the amplitude and the frequency of the sedimentary disturbance. The ecological responses we observed concerned 105 density and diversity variations at different time intervals and their vertical distribution (representing their migration ability) after the two disturbances' regimes.

Our experimental design was not intended to exactly reproduce a natural environment but rather to control a single ecological driver, i.e. the fine-grained sediment supply.

2 Material and methods

2.1 Biological model

In our experiment, we used benthic foraminifera species that inhabit the mudflats of the French Atlantic coast. Foraminifera samples were collected at low tide, in the up-per mudflat of the Bay of Bourgneuf called La Couplasse, a vast maritime bay enclosed by the island of Noirmoutier. The assemblages were largely dominated by two species, *Ammonia confertitesta* Zheng, 1978 (Hayward et al., 2021; often reported as *Ammonia tepida* in the literature) and *Haynesina germanica* (Ehrenberg, 1840). These two species live in similar shallow infaunal microhabitats, i.e. near the sediment–water interface on tidal mudflats at temperate latitudes. They are often associated and dominant in such natural coastal environments and are not expected to be in exclusive competition (Alve, 2001; Morvan et al., 2006; Murray and Alve, 2000; Thibault de Chanvalon et al., 2015). The species *Ammonia confertitesta* has already been used in microcosms and cultured in investigations focusing on growth and calcification processes (Bradshaw, 1957; Denoyelle et al., 2012; Geslin et al., 2014; Nardelli et al., 2014; Stouff et al., 1999), the effects of contaminants (Denoyelle et al., 2012; Le Cadre and Debenay, 2006; Suokhrie et al., 2017), or metabolical responses to stressed environments (Geslin et al., 2014; Heinz and Geslin, 2012; Jauffrais et al., 2016a; Koho et al., 2018; Nardelli et al., 2014). Therefore, this species was chosen here for its high ability to withstand experimental living conditions for long-lasting periods of time (up to several months). The second species, *Haynesina germanica*, has also been studied in experimental conditions for its ability to sequester chloroplasts and perform photosynthesis (Jauffrais et al., 2016b) or for its metabolic responses to stressed environments (Deldicq et al., 2021; Langlet, 2020; Seuront and Bouchet, 2015). However, previous experiments involving *H. germanica* only lasted several days. Although both species were never used in microcosms testing sediment input, we expected them to respond to sediment depositional events that would directly disturb the stability of their shallow infaunal microhabitat.

2.2 Experimental design

Two scenarios were implemented in two different aquaria to simulate simultaneously (1) a one-time high-volume (OHV) scenario in which the microcosm received one single sedimentary load, resulting in a thick deposit; and (2) a frequent low-volume (FLV) scenario with four successive (1-week period each) small supplies, each burying the microcosm under a thin sediment layer. In parallel, a control microcosm in a third aquarium received no sediment input during the experiment (Fig. 1). The three glass aquaria (50 × 15 × 26 cm; 750 cm^2 surface area) were designed to allow five consecutive samplings at 1-week intervals without disturbing the rest of the microcosm. For this purpose, in each aquarium, five compartments (10 cm long; 150 cm^2 surface area) can be successively isolated from the rest of the microcosm by inserting plexiglass plates into four pairs of small gutters attached to the aquarium walls (Fig. 1c). At each consecutive sampling time, sediment samples and geochemical measurements were collected from the newly isolated compartment. To limit evaporation, the three aquaria were covered with a large glass plate with a hole above each compartment, allowing the introduction of a continuous bubbling system to maintain good oxygenation and mixing of the water in the aquaria.

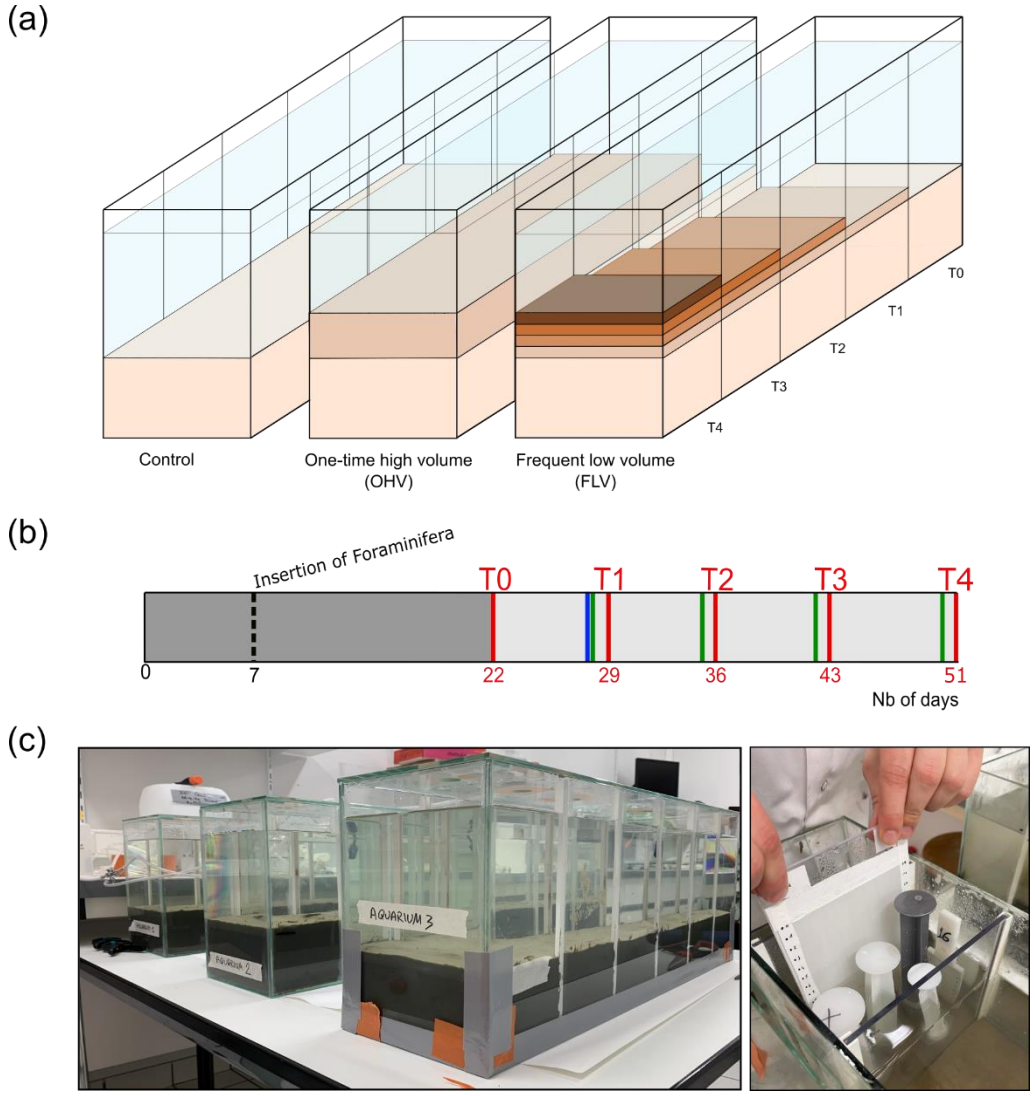

Figure 1: (a) The three aquaria correspond to the control and the two sediment deposit modes. Successive deposit layers are symbolized by darker colours. The sampling times (T0 to T4) are mentioned at the level of the associated compartment which was sampled at that time and are also linked to (b) the timeline showing sediment inputs (blue bar for OHV and green bars for FLV) and core sampling times (D + 2 after disturbances, red bars) as a function of the number of days of the experiment, starting from the introduction of the sediment into the aquaria (day 0). The insertion of foraminifera occurred on day 7, and the dark-grey area represents the period (22 d long) for geochemical and foraminifera equilibration. (c) Picture of the experimental setup after the sediment substrate addition on day 5 and in-place sampling devices (syringes) after the section closing by Plexiglas plates (right).

2.3 Experimental preparation

Natural coastal seawater, with a salinity of 33 and very low turbidity, was collected and microfiltered using paper filters with a mesh size of 0.45 µm before filling a 100 L water tank. This filtration ensured the removal of organic or mineral detritus and of macro-, meso-, and microorganisms that might have interfered with the microcosms. A closed water circuit equipped with a pump was installed to initially fill the aquaria from the water tank. On day 35, after a breakdown of the pumping system, it was decided to manually renew the water in the aquaria by replacing it completely at each sampling time and at about two-thirds of the volume twice a week with water from the tank. The sediment used to constitute the initial sediment

(Fig. 1, light beige), was collected at low tide on the Couplasse mudflat (Bourgneuf Bay – 47°0'57" N, 2°1'29" W) on 13 January 2021 and was stored in sealed plastic bags at −20 ◦C until the experiment was set up. The purpose of this freezing step was to preserve in situ organic matter content 85 and freshness and to kill present meiofauna or macrofauna that might be living in this sediment and might interfere with further treatments. In this way, we were also sure that this sediment substrate was free of the in situ foraminiferal community. Grain size analysis on sediment aliquots per-formed using a laser diffraction particle analyser, Malvern Mastersizer 3000, revealed a unimodal distribution (mode 6 µm), with a D50 of 10 µm and a D90 of 47 µm. The proportions of silt and clay were 93 % and 7 % respectively. The material used to simulate sedimentary disturbance was prepared as follows: the sediment collected at La Couplasse was unfrozen and diluted with the microfiltered seawater in or-der to obtain a highly turbid solution. This dense solution was slowly introduced into the water column of the aquaria via a small-diameter plastic tube. The particles settled down on the prior sediment surface. To seed the microcosms in a controlled manner, living foraminifera were collected on 16th February 2021 at low tide at the same location as for the sediments, i.e. the Couplasse mudflat. Surface sediment was sieved in situ to recover the 125–500 µm size fraction. This size fraction included foraminifera and possibly meiofauna or juveniles of macrofauna and some organic matter detritus. Samples were conditioned in 500 mL plastic bottles with one-fifth sediment and four-fifths in situ seawater. Then, the samples were stored in the temperature-controlled room (at 14 ◦C) where the experiment was conducted and were air-bubbled until insertion into the microcosms.

On day 0 (16 February 2021; Fig. 1b), a layer of approximately 9 cm thick was placed on the bottom of each aquarium, carefully avoiding the formation of internal voids and ensuring a flat sediment surface. The required amount of sediment was thawed and homogenized just before filling the aquaria. After a few hours, the necessary time for the settling of the fine particles, filtered seawater was gently introduced to fill the aquaria with a 10 cm high water column, avoiding any disturbance at the water–sediment interface. The three aquaria, kept oxygenated by the air-bubbling system, were left to stand for 7 d prior the insertion of foraminifera to al-low for sediment compaction and initial equilibration of the redox fronts.

On day 7 (23rd February 2021; Fig. 1b), the sediment was seeded with living foraminifera; the major challenge was to obtain a spatial distribution of living specimens that was as homogeneous as possible over the entire sediment surface in each aquarium. Each microcosm was divided into 40 rectangles (5 × 3.75 cm). For this purpose, foraminiferal samples were mixed and then split into 5 mL sub-samples. The 5 mL aliquots were carefully inserted with a small syringe into each rectangle of a grid placed just above the sediment–water interface and immediately removed after insertion of the foraminifera. Then, a 15-d rest period was observed before the first sampling (T0) to let the individuals reach their preferential microhabitats in the sediment.

2.4 Experimental procedure

The sampling period began on day 22 (Fig. 1b) after filling the aquaria with sediment and water on day 0 and inserting the foraminifera on day 7 (Fig. 1b). Five successive samplings (T0 to T4) were done every week, each in one compartment of each microcosm (Fig. 1a). On day 22, a first sample (T0) was taken from the first compartment of the three microcosms before

the application of any disturbance. After sampling, the compartment was closed using plexiglas plates carefully inserted into gutters placed on the side of the microcosms (vertical white lines on the glass; Fig. 1c) and was drained of its water. The water in the remaining part of the aquaria was renewed the next day with water from the 100 L tank. In the control microcosm (left aquarium in Fig. 1a), the next four samplings (T1 to T4) were done in successive compartments of the aquarium that were not subjected to any sedimentary disturbance throughout the whole experiment. In the one-time high-volume microcosm (middle aquarium in Fig. 1a), a 2.7 cm thick (after definitive particle settling) sediment layer was added at once on the day before sampling T1 (day 29, blue bar Fig. 1b). Afterwards, samplings T2 to T4 were done in successive compartments of the aquarium without further addition of sediment. After each sampling, the compartment was closed and emptied. In the frequent low-volume microcosm, a smaller amount of sediment was added each week (day 28, day 35, day 42, day 50; green bars in Fig. 1b) to stack layers of approximatively 0.3–0.5 cm thickness each. Samplings T1 to T4 were done in successive compartments of the aquarium on the day following each sediment addition. Therefore, T4 sampled a sedimentary column containing the four successive 0.3–0.5 cm layers in the last compartment.

2.5 Control of the stability of the microcosms

To monitor the stability of the microcosms, salinity and temperature measurements were performed daily with a WTW® Multi 3620 probe (measurement resolution of 0.1 and 0.1 ◦C for salinity and temperature respectively). Air-bubbling ensured a good oxygenation and mixing of water, thus preventing water stratification. A lateral view of each aquarium was photographed daily using a Nikon D3400 camera to monitor visual changes in the sediment column (e.g. colour, com-paction, and bioturbation).

The effect of sediment disturbance as a physical cover of the sediment surface was followed by dissolved-oxygen pro-filing in the sediment, giving the oxygen penetration depth (OPD). However, no measurements were available at T3 due to experimental failure. Measurements were done the day after each sampling time (i.e. 2 d after the sedimentary disturbance), using 50 µm tip diameter Clark-type Unisense™, microelectrodes mounted on an automated micro-manipulator (Revsbech, 1989) taking measurements with a 50 µm vertical step. Significant differences among sampling times and/or microcosms were tested by ANOVA and Tuckey post hoc tests to investigate further and more detailed relations; these tests were performed using R software.

Additionally, nutrient content (NH_4^+, NO_2^-, and NO_3^-) in the water column was monitored and displayed as total inorganic nitrogen (TIN). Indeed, fluxes from the sediment column resulting from the degradation of organic matter can lead to very high accumulations of inorganic N in the water column, which can result in the alteration of geochemical equilibria in the sediment (Hansen and Blackburn, 1992; Kristensen and Blackburn, 1987; Silverberg et al., 1995). A total of 5 mL of water was collected at least every 3 d, filtered (0.2 µm, RC25, Sartorius ©), and stored at −20 ◦C. The concentrations of all nutrients were measured using a spectrophotometric analyser (GENESYS 20, Thermo Fisher ©). Ammonium (NH_4^+) concentrations were analysed using the Berthelot method adapted for small samples and seawater samples (Metzger et al., 2019). Nitrite concentrations were measured by a colorimetric reaction with the Griess reagent (Griess, 1879). The analysis of nitrate is the second step in the

sequential determination described in García-Robledo et al. (2014) and involves the use of vanadium chloride (VCl_3) to reduce nitrate into nitrite. Nitrate concentrations [NO_3^-] can therefore be calculated from the measured NO_2^-+ NO_3^- using the following relation (García-Robledo et al., 2014):

$$[NO_3^-] = Abs^V_{NOx} - Abs^V_{reagents} - \times [NO_2^-] / S^V_{NO3^-},$$

where Abs^V_{NOx} is the final measured absorbance, i.e. combination of [NO_2^-] and [NO_3^-]; $Abs^V_{reagents}$ is the absorbance of VCl_3 without [NO_2^-] or [NO_3^-]; S^V_{NO2} and S^V_{NO3} are the slope of calibration curves after VCl_3 addition; and [NO_2^-] is the previously calculated concentration of nitrite in the sample.

2.6 Experimental sediment sampling procedure

At each sampling event (18 h after the physical disturbance), one compartment of the aquarium was physically separated from the rest of the aquarium; the overlying water was carefully pumped out to limit sediment resuspension; and four cores (2.9 cm internal diameter, ~ 8.5 cm long) were collected using adapted syringes, acting as miniature disposable piston corers. Two cores were used for foraminiferal analyses (including one replicate): one was for porosity analysis (data not shown in this paper), and one was resin embedded for further geochemical analyses (data not shown in this paper). Foraminiferal cores were immediately sliced using inox spatulas every 0.2 cm down to 4 cm depth, then every 0.5 cm from 4 to 7 cm depth. During this process, no shell debris was observed. A specifically designed push core with a screw resolution of 1 mm per turn allowed accurate sediment extrusion.

For living foraminifera analyses, sediment slices were la-belled with CellTracker Green (CTG). CTG is a dye which is hydrolysed during metabolization by living individuals, resulting in a fluorescent-green staining of the cytoplasm already in use for foraminiferal labelling (Bernhard and Bowser, 1996; Bernhard et al., 2006; Choquel et al., 2021; Geslin et al., 2014; Nardelli et al., 2014; Pucci et al., 2009; Richirt et al., 2020; Ross and Hallock, 2018). This CTG label therefore identifies foraminifera with an active metabolism and is highly reliable for detecting short temporal foraminiferal responses to disturbances. Following Bern-hard and Bowser (1996) and Bernhard et al. (2006), samples for foraminiferal analyses were incubated at experiment temperature (14°C) in a CTG solution (CellTracker™ Green, 1 mM final concentration) in microfiltered seawater for 24 h. After incubation, the solution was fixed in 70 % ethanol and sieved over 125 µm mesh screens (corresponding to the minimal size of the foraminifera introduced in the experiment). The counting process of living individuals was performed under epifluorescence stereomicroscopy (i.e. 470 nm excitation; Olympus SZX13). Only specimens presenting a clear and continuous fluorescence were picked and counted at the species level. Total foraminiferal abundances (per core) were calculated, taking into account the counting of all individuals living in the whole sediment column of 7 cm depth with a section of 6.6 cm^2, and were expressed as the number of individuals per 10 cm^2 (ind. 10 cm^{-2}), being the sum of individuals counted in each core slice. Foraminiferal densities per core slice were expressed as individuals per 10 cm^3 (ind. 10 cm^{-3}).

Additionally, one core from the second sampling time of the one-time high-volume microcosm (OHV T1) was selected to test for an eventual correlation between vertical

migration rate and foraminiferal test size. Following the procedure of Richirt et al. (2020), high-resolution pictures (6016 × 4016 pixels) of the entire assemblage picked in each core slice were taken using a camera (Nikon™ D750) set on a stereomicroscope. Each specimen of the investigated assemblage was placed on its ventral or dorsal side to obtain a picture of the maximal test length. Images were processed using ImageJ software (Schneider, 2012), with which the maximum diameter of each isolated individual was measured, and the specimen area was calculated in μm^2 (Richirt et al., 2020). In our study, data are presented by species and on a vertical scale corresponding to all slices of the investigated core (OHV T1). Statistical analysis was performed using R software. Univariate ANOVA tests were performed to compare the size of individuals in all core slices. Tuckey post hoc test was carried out when the ANOVA was significant. Displacement speeds were estimated on the same core (OHV T1). To do so, we measured the vertical distance between the initial water–sediment surface and the level within the newly deposited sediment reached by living foraminifera. This distance was therefore travelled upwards between the time of sediment addition and the sediment sampling time (i.e. 18 h). The maximum speeds (mm h^{-1}) were calculated by species using the maximum vertical distance travelled by individuals of the two species *Ammonia confertitesta* and *Haynesina germanica*. The accuracy of the distance measurement is 0.2 cm (core slice thickness). The mean speeds (mm h^{-1}) were calculated by species based on the vertical distance travelled above the initial water–sediment interface, weighted by the number of living individuals found at this level.

3 Results

3.1 Geochemical stability of the microcosms

Temperature and salinity were kept constant during the whole experiment in the three microcosms (salinity 32.9 ± 0.50; T 14.7 ± 0.18 °C). The monitoring of TIN concentrations in the water column throughout the whole experiment is presented in Fig. 2. From the filling of the aquaria (day 0) until day 15, a strong addition of 340 µmol L^{-1} of TIN was observed, with

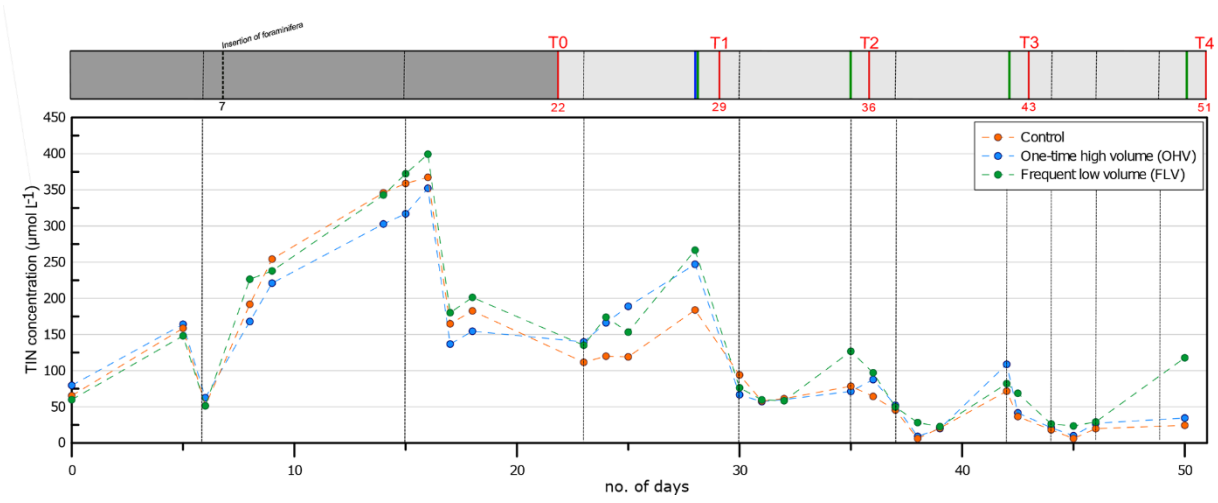

Figure 2: Total inorganic nitrogen concentration in the water column (NH_4^+, NO_2^-, and NO_3^-) in the three aquaria throughout the experiment. Vertical dotted black lines indicate water renewals (after each sampling time and more frequently after the pump breakdown at day 35). The header displays the timeline explained in Fig. 1b.

the concentration increasing from 60 µmol L^{-1} to the maximum of 400 µmol L^{-1}. This peak of approximately 3 d (day 14 to day 16) was immediately followed (day 17) by an abrupt strong decrease to a concentration of about 160 µmol L^{-1}. TIN then showed a progressive decrease with oscillations of about 100 µmol L−1 in amplitude, with the maximum of these oscillations occurring just before water renewal. From T1 until T4, the concentration remained below 100 µmol L^{-1}, except for relative peaks of about 110–150 µmol L^{-1} observed just after each sediment disturbance. Variations in TIN concentrations were relatively synchronized in all three aquaria, except just after the sediment disturbance at T4 in the FLV microcosm.

At the first sampling time T0, OPD varied between 1.3 and 1.8 mm in the three aquaria (Fig. 3). This variation has a lower range than the 2 mm resolution (size of the upper core slices) used in our foraminifera analysis. From T0 to T1, in both the control and FLV microcosms, oxygen penetration showed a significant shallowing (p values < 0.05) to a depth of 1.2 ± 0.2 mm and then remained stable until T4. At T1 and within the OHV microcosm , OPD deepened to 2.1 ± 0.1 mm after the massive deposit. After T1 and until the end of the experiment, oxygen penetration presented a shallowing trend, reaching the same depth as in the other two microcosms at T4 (1.3 ± 0.3 mm for the control microcosm, 1.2 ± 0.2 mm for the OHV microcosm, and 1.2 ± 0.2 mm for the FLV microcosm).

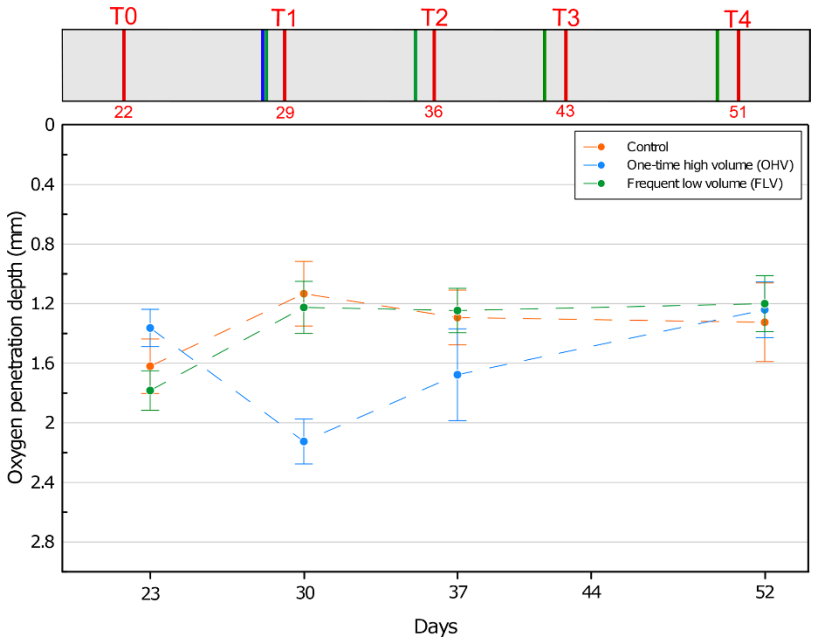

Figure 3: Mean oxygen penetration depth with associated standard deviation for each microcosm and at each sampling time. No data available for T3. On the y axis, 0 at the top represents the water–sediment interface. The header displays the timeline explained in Fig. 1b.

Lateral views of the OHV and FLV aquaria show the sedimentary column at four different moments of the experiment (Fig. 4), allowing us to track sediment compaction and colour changes during and after the sedimentary deposits. At day 14 (before any disturbance), the sediment column (i.e. the substratum of the experiment) was homogeneous in the three aquaria. It was already compacted, and no more fine sediment was visible in suspension in the overlying water column. A few millimetric black spots, scattered within the sediment matrix, were most likely microniches of organic matter anaerobic remineralization (Jørgensen, 1977; Lehto et al., 2017; Widerlund et al., 2012). At 9 cm height in the aquaria, the initial water–sediment interface was clearly visible as a doublet of yellowish and black millimetric layers (2–

3 mm), constituted by the material (foraminifera and as-sociated particulate organic matter) introduced on day 7. The upper yellowish layer corresponded to the well-oxygenated layer of this material. Its thickness was consistent with measured OPD (Fig. 3). The underlying black layer corresponded to the anaerobic degradation of the introduced organic matter.

On day 28, the first sediment addition occurred in two aquaria. A thick layer (about 4.3 cm) of beige sediment in the OHV microcosm and a thin layer (about 1 cm) in the FLV one were deposited above the former water-sediment inter-face that was still very clearly visible. On day 30, the sediment layer thickness in both aquaria was already reduced to 2.7 cm in the OHV microcosm and to 0.5 cm in the FLV one. This rapid compaction of about one-third of the newly deposited sediment occurred within 2 d. In both aquaria, the first T1 deposit was well marked between the initial surface (yellow-black doublet) and a very thin (< 1 mm) yellowish layer at the new water–sediment interface. This light colour underlined the good oxygenation of the superficial sediment less than 2 d after the deposit.

On day 50, in the FLV microcosm, it was possible to detect the four successive supplies of sediment by observing the layering of yellow–black doublets in the final 2 cm thick layer. As a final important observation, we noticed the rare development of small vertical burrows (Ø < 1 mm, a few centimetres long) in all three aquaria. In our experiment, the bioturbation was limited by the freezing of the sediment used to fill the aquaria and the initial sieving (< 500 µm) of the biological material introduced on day 7.

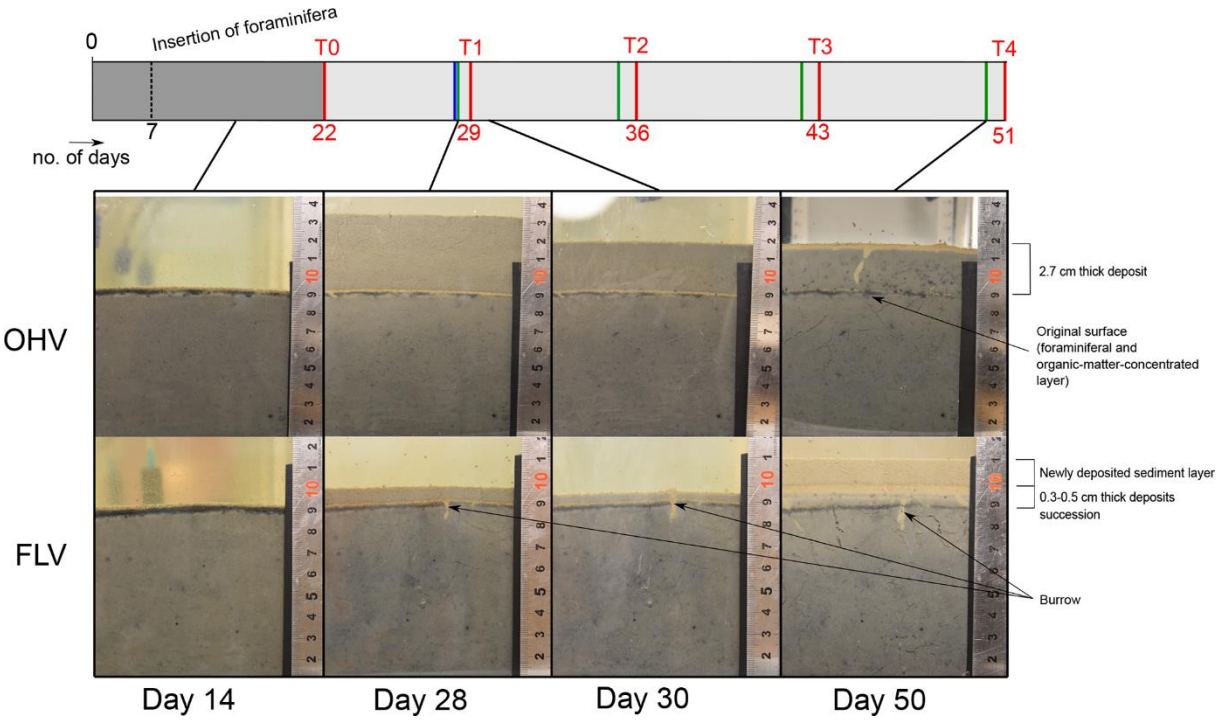

Figure 4: Lateral views of the one-time high-volume (OHV) and frequent low-volume (FLV) sedimentary disturbances at four different times during the experiment. The header displays the timeline explained in Fig. 1b.

3.2 Effects of sedimentary disturbances on total foraminiferal abundances

Variations in total foraminiferal abundances were analysed during the experiment for the three aquaria. At T0, before any sedimentary disturbance, the total foraminiferal abundances varied in the three aquaria between 790 and 1483 ind. 10 cm^{-2} (Fig. 5). In the OHV microcosm,

a linear regression demonstrates a significant (R2 = 0.55; *p* value = 0.01) decreasing trend in foraminiferal abundances over time, with an average loss of about 300 ind. 10 cm^{-2} (863 ± 73 ind. 10 cm^{-2} at T0 and 582 ± 31 ind. 10 cm^{-2} at T4).

There is no such significant trend in foraminiferal abundances with time, neither in the control microcosm (R2 = 0.15; *p* value = 0.29) nor in the FLV microcosm (R2 = 0.23; *p* value = 0.22). In the case of the control microcosm, the high variability between replicates was at its maximum at T4, ranging from 650 to 1100 ind. 10 cm^{-2}.

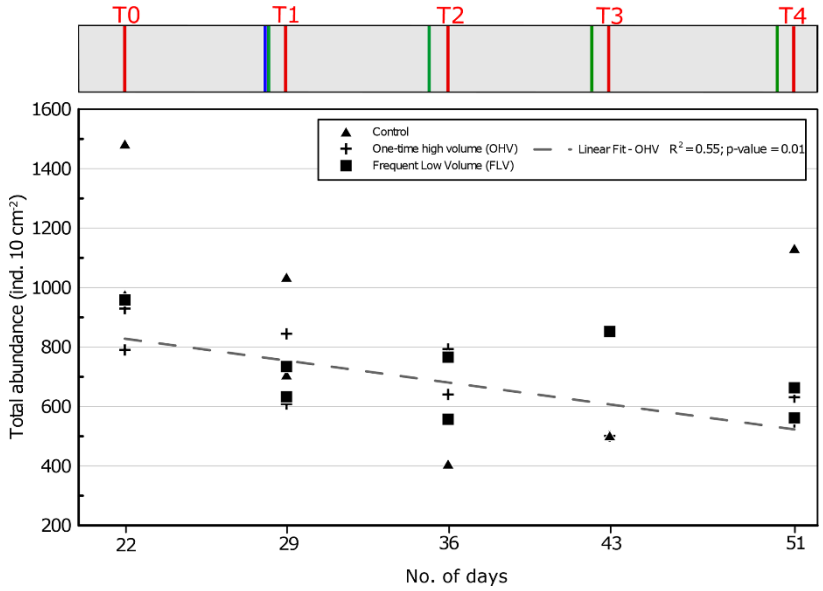

Figure 5: Total foraminiferal abundances (> 125 µm) per core sampled in each microcosm at each sampling time. The displayed values are the abundances of two replicate cores (n = 1 for control T3, FLV T0, and FLV T3). The regression line is shown for OHV with R2 and the associated p value (other regression lines are not drawn because they are not significant). Days from the start of the experiment are indicated on the x axis. The header displays the timeline explained in Fig. 1b.

3.3 Effects of sedimentary disturbances on assemblage composition

Variations in relative species abundances per core were analysed for the three microcosms over the course of the experiment (Fig. 6). The foraminiferal assemblage used in this experiment was mainly composed of *Ammonia confertitesta* and *Haynesina germanica*. At T0, in all the aquaria, H. germanica was dominant, accounting for 63 % to 79 % of the assemblage. Thereafter, the abundances of *A. confertitesta* and *H. germanica* balanced out to become equally distributed at T3. At T4, *A. confertitesta* exceeded 50 % in all aquaria and became particularly dominant in the FLV microcosm, where it accounted for 68 % of the assemblage. Relative abundances showed a clear shift from an initial domination of *H. germanica* over *A. confertitesta* to a more balanced assemblage. A few specimens of *Elphidium* spp., another species known to live in low abundances in the upper mudflat of Bourgneuf Bay in winter (Choquel, 2021), were occasionally found in the sediment samples of the three aquaria. They represented, at maximum, 6 % of the total assemblage (31 individuals counted out of 506 individuals) in only one core (FLV T2 replicate) but were mostly absent from the other cores or were present at less than 2 %.

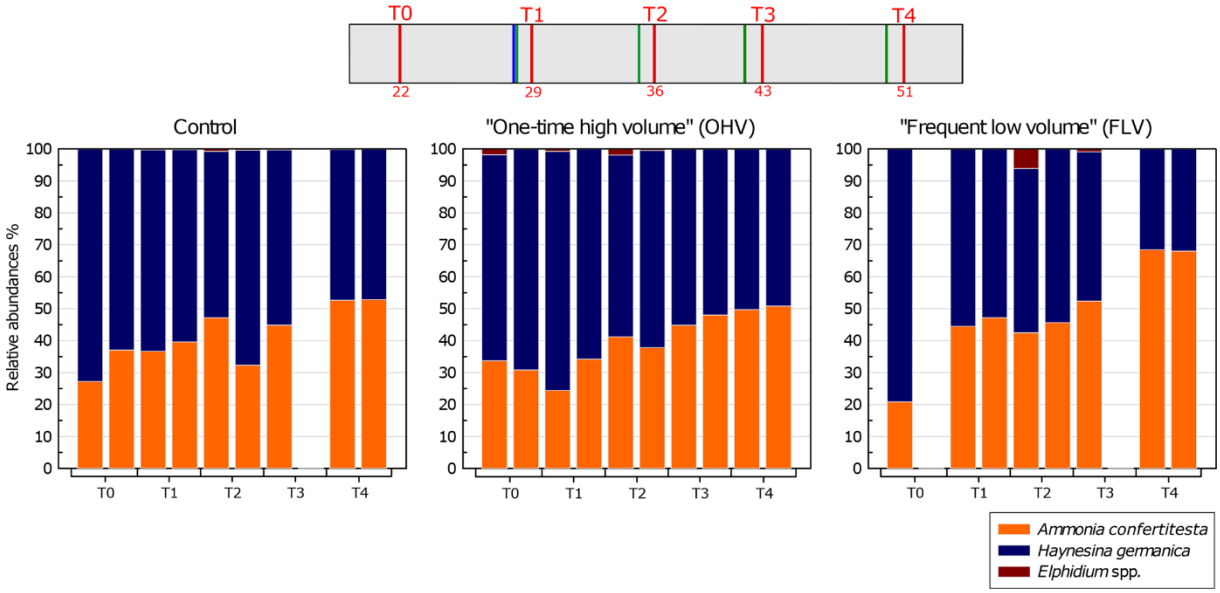

Figure 6: Relative abundances (%) of each species (> 125 µm) per core – with replicates – sampled in each microcosm at each sampling time. The displayed values are the relative abundances of two replicate cores (n = 1 for control T3, FLV T0, and FLV T3). The header displays the timeline explained in Fig. 1b. Note the absence of a second replicate in the control T3 and FLV T0 and T3 due to sampling failures.

Variations in the abundances of *A. confertitesta* and *H. germanica* per core analysed for the duration of the experiment in the three aquaria were therefore examined more specifically (Fig. 7). In the control microcosm, the total abundances of *A. confertitesta* and especially *H. germanica* were very variable between replicates throughout the experiment.

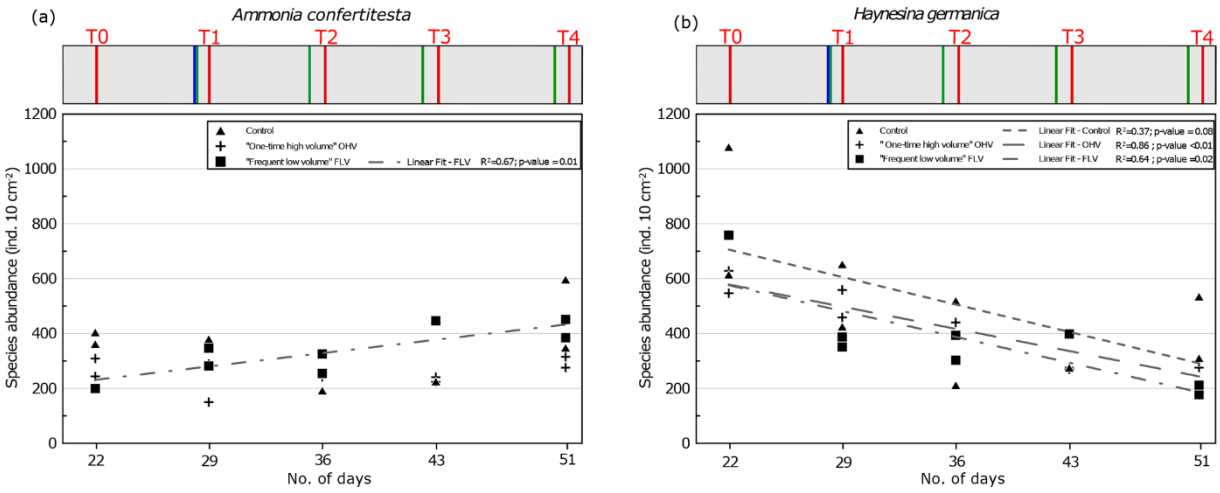

Figure 7: Foraminiferal abundances of the two main species in sampled replicates, (a) *Ammonia confertitesta* and (b) *Haynesina germanica*, at each sampling time. Replicates are missing at FLV T0 and T3 and control T3. The regression line is shown for FLV with R2 and associated p value (other regression lines are not drawn because they are not significant). The header displays the timeline explained in Fig. 1b.

Concerning *Ammonia confertitesta*, abundances in the OHV microcosm did not show any significant trend in time and were found in the narrow range of 220–300 ind. 10 cm^{-2}, except at T1 just after the single thick sedimentary disturbance, when abundances dropped to 150 ind. 10 cm^{-2}. In the FLV microcosm, a significant increasing trend occurred (p value < 0.05), doubling total abundances from T0 to T3, and then abundances remained stable between T3 and T4. However, the lack of a second replicate at T0 did not provide information on the

initial variability. Concerning *H. germanica*, total abundances significantly (p value < 0.05) decreased throughout the experiment, from ~ 600 to ~ 300 ind. 10 cm^{-2} in the OHV and from ~ 750 to ~ 200 ind. 10 cm^{-2} in the FLV. In the control microcosm, abundances decreased from 1100 ind. 10 cm^{-2} at T0 to 300 ind. 10 cm^{-2} at T4. The high variability between replicates, particularly at T0 and T4, partially concealed the decreasing trend and resulted in a relatively bad correlation, with an R2 of 0.37 and a *p* value of 0.08.

3.4 Effects of sedimentary disturbances on vertical distributions

In the control microcosm (Fig. 8a), vertical distributions of both species, *Ammonia confertitesta* and *Haynesina germanica*, showed the highest densities of individuals in the uppermost 0.2 cm of sediment throughout the whole experiment. The uppermost 0.2 cm layer contained between 58 %and 81 % of the total assemblage found in the 7 cm sediment column. For both species, a similar exponential decrease with depth occurred down to 0.8 to 1.4 cm. Below this depth, no living individuals were found. Concerning the OHV treatment, a vertical profile similar to the one of the control microcosm occurred at T0, with maximum densities in the uppermost 0.2 cm and an exponential decreasing profile with depth down to about 2 cm depth (Fig. 8b). At T1, 18 h after the addition of about 2.9 cm of sediment (before full compaction) above the initial water–sediment interface (dotted line in Fig. 8b), the foraminiferal vertical distribution displayed unimodal profiles with modes or maximum densities situated 2.3 cm below the new surface or 0.6 mm above the initial water–sediment interface. Densities then showed quite a symmetrical decrease up and down the density peak. Approximately 71 % of the fauna was found between 2 and 3 cm depth, where the specific composition of the assemblage was equally represented by *A. confertitesta* and *H. germanica*. No living foraminifera were detected above 0.2 cm depth and below 3.4–3.6 cm depth in both replicates. The few individuals that reached the upper sediment layers (from 2.2 to 0.8 cm depth) and those that remained at depth below the mode were identified as belonging to the species H. germanica. At T2, after full compaction, giving a total sediment height of 2.7 cm above the initial water–sediment interface (Fig. 4), the assemblages had shifted toward the new surface to concentrate in the upper layers of the sediment column (0 to 1.2 cm depth maximum below the new sediment surface). Vertical profiles showed exponential decreasing with depth. Only a few specimens, belonging exclusively to *H. germanica*, were found in layers deeper than 1.2 cm (Fig. 8b). This distribution remained quite similar in the successive sampling times T3 and T4, with a slight increase (30 %) of *A. confertitesta* in the topmost layer (0–0.2 cm) and a decrease in the deeper layers (below 0.4 cm depth). In Fig. 8c, assemblage profiles in the frequent low-volume (FLV) microcosm are drawn to be shifted upwards from the initial water–sediment interface. The distance between the new and former interfaces illustrates the thickness of the sediment supplied before each sampling time. On the day before each sampling time (T1 to T4), successive 0.3–0.5 cm thick sediment deposits were added, and thus the ancient surface (dotted black line in Fig. 8c) was further buried. At T0, assemblages dis-played a similar vertical distribution profile to the other microcosms (Fig. 8c). However, the assemblage was not balanced. *Ammonia confertitesta* was only present above 0.2 cm depth, with ~ 900 ind. 10 cm^{-3}, whereas *H. germanica* was present up to 1.2 cm depth and was 75 % dominant in the surface layer, with ~ 3100 ind. 10 cm^{-3}. At T1, the vertical distribution of foraminifera in both replicates was back to the original profile of T0, with a maximum foraminiferal density above 0.4 cm depth and no specimens below 1.2 cm depth. However, the assemblages showed a

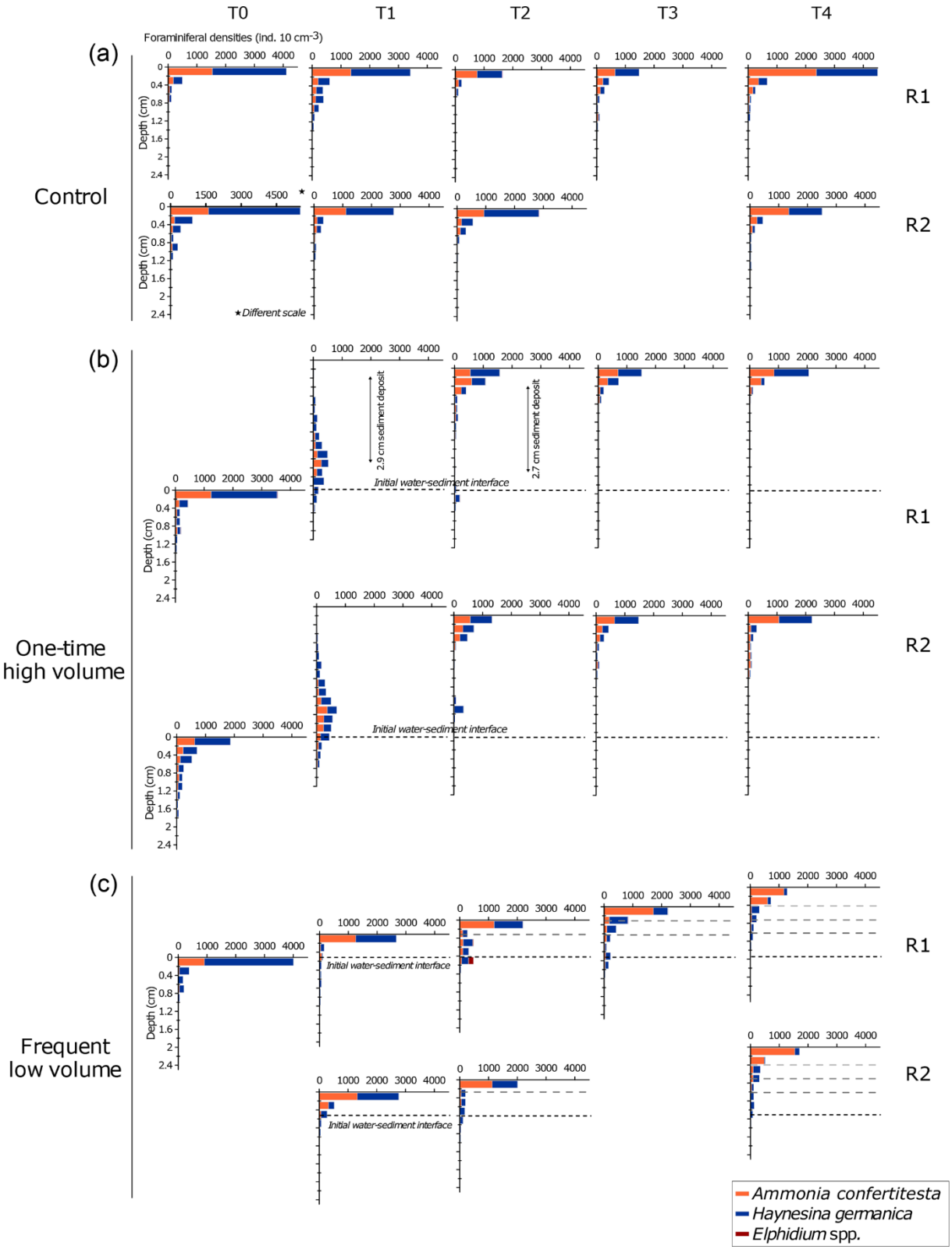

Figure 8: Vertical distribution of specific densities of living foraminifera in replicates at each sampling time displayed for each microcosm. The water–sediment interface of each plot is aligned with the previous one to illustrate the added sediment layers in the OHV and the FLV microcosms. The scale of the x axis of the control T0 replicate 2 is different to the others. Note the absence of a second replicate in the control T3 and FLV T0 and T3 due to sampling failures.

decrease in the relative density of *H. germanica* compared to T0 (70 % in the upper layer). At T2 and T3, most specimens were still concentrated in the uppermost 0.2 cm, with about 2000 ind. 10 cm^{-3}. Below the 0–0.2 cm level down to the initial water–sediment interface (0.8 cm depth at T2 and 1.1 cm depth at T3), the vertical distribution displayed persistently low densities of less than 100 ind. 10 cm^{-3} and 100–300 ind. 10 cm^{-3} for T2 and T3 respectively. From T1 to T4, *H. germanica* densities decreased in the uppermost layer in favour of *A. confertitesta*, while these remained dominant in the deeper layers (Fig. 8c). At T4, *A. confertitesta* largely dominated the 0 to 0.4 cm depth layers, with about 1900 ind. 10 cm^{-3} versus 200 ind. 10 cm^{-3} for *H. germanica*. Below 0.4 cm depth, lower densities (~ 140 to 240 ind. 10 cm^{-3}) of *A. confertitesta* were observed, whereas *H. germanica* appeared to be more abundant below 0.4 cm depth (~ 660 to 860 ind. 10 cm^{-3}).

3.5 Foraminiferal migration: relationship with test sizes and specific speed

To evaluate the migration speed of each species, data from the OHV core T1 replicate 1 (T1 R1) were used. This core was collected at T1 18 h after the disturbance that buried the initial water–sediment interface under a thick sediment layer (2.9 cm after compaction, Fig. 4). The foraminifera spread in the added sediment layer displayed a unimodal vertical distribution, where the density peak was located in the sediment slice 2.2–2.4 cm depth below the new surface and thus at 0.5–0.7 cm above the initial interface. Compared to the distribution profile displayed before the disturbance (T0), we observed an upward migration of both *Ammonia confertitesta* and *Haynesina germanica*, with a maximum vertical distance covering 2.6 cm at the time of sampling (Fig. 8b). Some individuals of the two species did not migrate at all as they were still present below the initial interface (6 % of total *A. confertitesta* individuals versus 14 % for *H. germanica*). The weighted mean speed was different between the two species (0.41 mm h^{-1} for *A. confertitesta* and 0.47 mm h^{-1} for *H. germanica*).

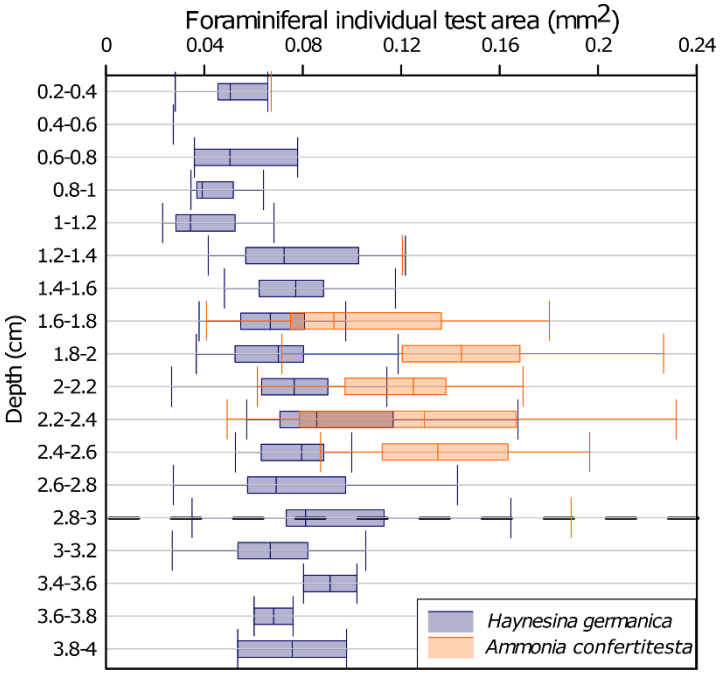

Figure 9: Vertical distribution of benthic foraminiferal test size in the one-time high-volume microcosm, core T1 R1. Values are shown as box plots (median, 25th and 75th quartiles) The depth is expressed by sediment slices. The dotted line (at the 2.8–3 level) symbolises the initial water–sediment interface before the sedimentary disturbance.

Based on the results of the T1 R1 core from the OHV microcosm, we investigated the correlation between the individuals' test sizes of each species and their location in the sediment column to find an eventual relationship between size and migration speed. To do so, a morphometric analysis was performed on the test of each specimen found at each sediment layer. The vertical distribution of the individual test area (mm^2), mean values, and standard deviations are shown by species in Fig. 9. The results showed a very high heterogeneity of test areas for *Ammonia confertitesta*, with values spreading from 0.04 to 0.2 mm^2 around median values per slice of approximately 0.1 mm^2. The statistical test did not reveal significant differences (ANOVA, p value = 0.119) in *A. confertitesta* test size between the different sediment slices. For *H. germanica*, however, statistically significant differences were found between sediment slices (ANOVA, p value = 6.17×10^{-6}). However, the Tuckey post hoc test highlighted significant differences between the 0.8 to 1.2 cm depth interval and the two similar depth intervals of 2–2.6 and 2.8–3.0 cm. Above 0.8 cm depth, the size of *H. germanica* specimens did not show significant differences compared to the other levels.

4 Discussion

4.1 Geochemical and physical stability of the experimental system

Parameters like temperature, salinity, and TIN in overlying water and O_2 penetration in the sediment were monitored throughout the experiment in order to control the geochemical stability of the microcosms. While water in the microcosms was often renewed, temperature and salinity remained constant, whereas TIN concentrations and OPD demonstrated that the geochemical stability of the microcosm was difficult to reach.

In the first part of the experiment (before day 14; Fig. 2), the high TIN concentrations could be attributed to the seeding of the microcosm, including, along with living foraminifera, high quantities of phytodetritus, meiofauna, and fecal pellets (< 500 µm). This organic matter supply was concentrated within a 0.3 cm layer at the sediment surface (organic-matter-concentrated layer; Fig. 4). The mineralization of this organic matter is an additional source of TIN in the overlying water of the microcosms. After T0, recurrent increases of TIN underlined by sharp peaks (days 16, 28, 35, and 42) occurred from the water renewals until the following sampling (Fig. 2). This testified to continuous fluxes of TIN released from the sediment to overlying waters, causing an increase of TIN concentration in the water column interrupted by water renewals in the aquaria. The peak amplitudes were gradually diminished due to the progress of organic matter mineralization and impoverishment of the system.

Even if the geochemical state of TIN in the microcosm was not perfectly stable, the regular renewals of seawater prevented excessive accumulation of organic matter degradation products in the overlying waters and sediment and were sufficiently effective to maintain TIN concentrations at a lower concentration range than that observed in the in-situ sediment of Bourgneuf Bay (Metzger et al., 2019).

The aerobic degradation of the organic matter added with the introduction of foraminifera on day 7 was probably responsible for the shallowing of the oxygen penetration depth observed between T0 and T1 in the control and frequent low-volume (FLV) microcosms. From the introduction of foraminifera, the OPD stabilization in both microcosms was reached after 22–29 d (i.e. between T0 and T1). Indeed, previous experimental studies of meso-

microcosms involving reworked sediment showed stabilization of oxygen fluxes and OPD after an equilibration period of 2–3 weeks (Ernst et al., 2002; Hansen and Blackburn, 1991, 1992; Porter et al., 2006). In the FLV microcosm, a steady state was set up from T1 until the end of the experiment despite recurrent additions of small volumes of sediment that did not affect OPD, whose values were similar to those of the control microcosm. In the OHV treatment, the addition of a large volume of sediment at once was most likely the driving factor for the deepening of the OPD at T1 (Fig. 3). Indeed, the sediment added in the microcosm settled by decantation to form a deeper oxygenated and water-enriched layer (Fig. 4). It then took up to a maximum of 3 weeks for the OPD to reach a level similar to that observed in the control and FLV microcosms during a steady state (T4, Fig. 3).

These results suggest that the large abrupt sediment supply could have a significant impact (p value < 0.05) on OPD and as such could be a driver of redox front shifts and microhabitat disturbance. In contrast, recurrent low sediment supply, resulting in the deposition of thin layers, did not show significant differences to the control and thus may be considered to have only slight or negligible impacts on benthic habitats.

4.2 Effect of sediment disturbance on benthic foraminiferal abundances

A significant decreasing trend in total foraminiferal abundance is observed in the OHV treatment (Fig. 5). The foraminiferal living faunas are therefore more affected by the arrival of a higher amount of sediment at one time than by re-current thinner inputs (FLV). This is in accordance with previous observations reported for marine areas subject to high sedimentary deposits, e.g. turbidites deposits. In fact, Tsujimoto et al. (2020) reported lower abundances of benthic foraminifera after the deposit of about 10 cm of sediment after the 2011 Tohokuoki earthquake due to burial-associated foraminiferal death. This matches with other previously reported observations after turbidite events (e.g. Bolliet et al., 2014; Hess and Jorissen, 2009). In the case of the study of Tsujimoto et al. (2020), a first recolonization of the superficial sediment by some of the species of the original assemblage (pre-turbidite) is observed within 5 months from the event, suggesting either the survival of some species in the thick sediment deposit (and migration towards the surface) or the recolonization of superficial sediment from refuge zones close to the sampling site. Since the recolonization from refuge zones was impossible in our setup, our results suggest that part of the assemblage could survive this kind of deposit, at least during a short time interval (4 weeks). The presence of pre-event faunas on the recolonized sediment could be due to the remigration of buried faunas at the surface. The survival and reproduction of this fauna on longer timescales, however, were not assessed in our experiment. It is quite possible that assemblages facing a similar event within a natural environment would receive species coming from refuge zones, as suggested by long-term observations reported by (Bolliet et al., 2014; Hess and Jorissen, 2009; Tsujimoto et al., 2020).

The two other treatments of our setup (control and FLV) did not show clear and significant trends, supporting the hypothesis that total foraminiferal abundances are not affected by frequent low-volume sediment inputs. However, the trends were significantly different when we looked at the two main species of our microcosms separately. In fact, *Ammonia confertitesta* did not suffer from a significant decline in abundance, neither in the control nor in the two treatments (Fig. 6 and 7a). The only significant linear regression was observed for the frequent low-volume microcosm where a slight increase of *A. confertitesta* abundance was observed

through time. However, we believe that this result is untrust-worthy as it was probably due to a lack of replicates for the T0 and T3. Our observations were restricted to the > 125 µm fraction of faunas, only including adult specimens, so that we could exclude the possibility that reproductions during the experiment would be the reason for this increase.

In contrast, *Haynesina germanica* showed significant linear decreasing trends in the two disturbed microcosms (OHV and FLV) with time (Fig. 7b), suggesting that this species is more sensitive to all kinds (i.e. frequency and intensity) of burial than *A. confertitesta*. However, despite insignificant *p* values (0.08) and a lower R2 (0.37) than the two disturbed microcosms, a similar decreasing trend was also visible for the control microcosm. It is therefore difficult to completely attribute the decline of *H. germanica* to the different sediment inputs. The role of the experimental conditions in the species' response should be considered. Indeed, of the two main species used in our setup, *A. confertitesta* (often reported as *Ammonia tepida* in the existing literature) was widely used as a target species in experimental studies, and it is known to tolerate laboratory conditions well and has also been used for longer time periods (i.e. days to months; e.g. Bradshaw, 1957; de Nooijer et al., 2009; Denoyelle et al., 2012; Geslin et al., 2014, 2004; Le Cadre and Debenay, 2006; Nardelli et al., 2014; Koho et al., 2018; Deldicq et al., 2020; Stouff et al., 1999), which is in agreement with our observations (Fig. 7a). *Haynesina germanica* has been rarely used in previous experimental setups and only in short-time experiments (i.e. hours to days; e.g. (Deldicq et al., 2021; Jauffrais et al., 2016b; Langlet, 2020; Seuront and Bouchet, 2015). The reason for the de-creasing trend of *H. germanica* abundance in our control microcosm can be attributed to several experimental factors. It has a more restricted diet based on specific epipelic microalgae (Choquel, 2021, unpublished; Lee et al., 1989; Pillet et al., 2011) compared to the *Ammonia* group, which can alternatively feed on organic detritus, bacteria, and meiofauna (Dupuy et al., 2010; Mojtahid et al., 2011; Pascal et al., 2009; Wukovits et al., 2018). Moreover, recent experimental results showed that *H. germanica*'s diet can switch from high-quality (low C:N values) to lower-quality organic material but that this switch often drives lowered fitness of the species (Wukovits et al., 2021). As the experiment was designed to observe the foraminiferal response to sedimentary deposits, we decided not to add extra organic matter during the experiment and to limit the tested variables. The consequent decrease of organic matter quality over time could have been unfavourable to *H. germanica* in competition with *A. confertitesta*. Moreover, it has been shown that *H. germanica* is a kleptoplastidic species that can assimilate undigested chloroplasts from specific microalgal preys (Choquel, 2021, unpublished ; Jauffrais et al., 2016b; LeKieffre et al., 2018) and perform photosynthesis as an alternative metabolism (LeKieffre et al., 2018b). However, our experiments were mostly conducted in the dark (except at the sampling times), so this metabolism was unavailable to limit starvation.

4.3 Effect of sediment disturbance on benthic foraminiferal vertical distribution

4.3.1 Foraminiferal response to sedimentary deposits

According to the specific preferences, benthic foraminifera can have epifaunal to shallow infaunal (within the first 2 cm of sediment), intermediate (1–4 cm), or deep (> 4 cm) infaunal microhabitats (Corliss, 1991). The two main species living in our microcosm are mainly epifaunal or shallow infaunal (Alve, 2001; Bouchet et al., 2009; Cesbron et al., 2016;

Murray and Alve, 2000; Papaspyrou et al., 2013; Thibault de Chanvalon et al., 2015). This preferential shallow life position is obvious when no bioturbation-induced modification of the sedimentary microhabitats occurs (e.g. Alve, 2001; Cesbron et al., 2016; Jorissen et al., 1992; McCorkle et al., 1997; Mojtahid et al., 2010; Murray, 2006). In accordance with the literature, most of living individuals of these two species were always located in the uppermost centimetre of the control microcosm (Fig. 8a). Similarly, in both OHV and FLV microcosms, at T0 before the physical disturbance, most of the foraminifera were observed in the 0–0.2 cm layer. According to Jorissen et al. (1995), this shallow habitat preference in a not-food-limited environment such as the one in our microcosms is mainly driven by oxygen availability. In our microcosms, the oxygen penetration depths varied within a range of 1.2 and 2.2 mm below the sediment surface in all the aquaria at all sampling times. This means that, despite the significant OPD variations observed between T0 and T1, the oxic layers at all core tops were always thinner than the slicing resolution of 0.2 cm used for foraminiferal analysis. Therefore, it was impossible to determine a possible effect of OPD stabilization on the vertical distribution of the living foraminifera within the topmost 0.2 cm. Nevertheless, we can assess that the near absence of fauna below 0.2 cm depth could have been limited by oxygen availability. After the disturbances, in both the one-time high-volume and frequent low-volume microcosms, an upward migration of the fauna was observed within a short time, i.e. 18 h after each sediment addition. In the FLV treatment, the migration through the added sediment (0.2–0.5 cm) was rapid and seemed to follow the recovery of the oxic front in the uppermost layer (< 0.2 cm, Figs. 8c and 3). The same dynamic was repeatedly observed at all successive sampling times (1 d after a new disturbance event) and therefore suggests that, in the FLV microcosm, the resilience of the microhabitat was achieved within 18 h after the sedimentary disturbance. This observation is in accordance with previous studies reporting rapid migration of epifaunal species after physical disturbance but largely reduces the recovery time, as previously reported (i.e. 22 d, Ernst et al., 2002). As we did not measure the dissolved oxygen evolution between the moment of each sediment supply and subsequent sampling times, we cannot assess if this migration was performed under hypoxic conditions.

A rapid upward migration was also observed in the OHV treatment following the addition of a thick (2.9 cm after 1 d of compaction) layer of sediment (Fig. 8b). In this microcosm, however, at T1, no living individuals were able to reach the sediment–water interface. The observed unimodal distribution centred within the added sediment layer suggests that the migration started rapidly after the disturbance. At T2, the vertical distribution was comparable to the two other microcosms, with a peak at the surface, and it remained the same in the following sampling periods, suggesting that the recovery was achieved within 2 weeks after the disturbance.

In the OHV microcosm, the foraminiferal fauna was positioned between 0.8 and 3 cm depth at T1, being in its migration phase before reaching the surface at T2 (Fig. 8b). During this period of migration, the OPD was measured at 2.1 ± 0.1 mm depth (Fig. 3), meaning that all the foraminifera had been moving through anoxic sediment layers. The possibility of migration of benthic foraminifera through anoxic sediment and towards oxygenated layers was already reported by Geslin et al. (2004) for deep-sea species. The shallow infaunal species we had in our microcosm, however, are generally reported as being sensitive to oxygen depletion in terms of motility. Despite several studies pointing out the ability of coastal foraminiferal species, including *Ammonia* spp., to survive days-to-months-long anoxia (e.g. Geslin et al., 2014; Nardelli et al., 2014), there is no consensus about their ability to actively move under anoxic

conditions. In some studies, the vertical migration of *Ammonia tepida* (assimilated to *Ammonia confertitesta* here) was reported as being driven by the redox fronts. For example, Thibault de Chanvalon et al. (2015) attributed the observed bimodal distribution of this species in estuarine intertidal mudflats to the combination of downward burial by bioturbation and the ability of the specimens burrowed up to 3 cm deep in the sediment to move back to the surface. These authors suggested that *A. tepida* is able to detect the oxygenated layer through geochemical gradients of other chemical species (e.g. NO_3^-, Mn^{2+}, or Fe^{2+}). Other studies, however, highlighted the reduction or cessation of motility of *A. tepida* in the absence of oxygen and attributed this to a state of reduced metabolism or dormancy induced by the anoxia (e.g. Maire et al., 2016). In accord with this hypothesis, Koho et al. (2018) reported changes in *Ammonia confertitesta* ultrastructure as a stress response to oxygen depletion and suggested that these changes could be related to dormancy (NB: in Koho et al., 2018). *Ammonia confertitesta* was mentioned as *Ammonia* sp. T6, one of the phylotypes of *Ammonia* distinguished by molecular identification (Holzmann and Pawlowski, 2000), and was renamed *Ammonia confertitesta* by Hayward et al. (2021). Additionally, in support of this theory, Le Kieffre et al. (2017) showed that *Ammonia tepida* highly reduces its metabolism and C_{org} uptake when exposed to anoxic conditions (LeKieffre et al., 2017). Our results rather support the hypothesis of Thibault de Chanvalon et al. (2015), stating that *A. tepida* would be able to follow redox fronts. The monitoring of the water column concentration of nutrients (Fig. 2) and oxygen penetration depth throughout the experiment (Fig. 3) gave us evidence of stabilization of sedimentary redox fronts 14 d after the first depositional event. Moreover, the presence of a C_{org}-enriched layer, corresponding to the original sediment surface, at 2.7 and 0.5 to 1.5 cm (respectively at T1 to T4) depth in the OHV and FLV microcosms did not seem to have influenced the upward migration, suggesting that oxygen, more than organic matter availability, was the major driving factor. Similarly, *Haynesina germanica* also showed high migration skills after the sedimentary disturbances. This species has recently been suggested to be able to move under low-oxygenated conditions and also to take advantage of the presence of existing trails to move into cohesive sediment (Deldicq et al., 2020). This agrees with our observations of rapid migration within 1 d after the FLV treatment and at a maximum of 1 week after the OHV treatment (Fig. 8c).

4.3.2 Vertical migration speeds

Only a few studies quantified the locomotion speed of benthic foraminifera in the sediment (Bornmalm et al., 1997; Deldicq et al., 2021; Gross, 2000; Hemleben and Kitazato, 1995; Kitazato, 1988; Maire et al., 2016; Severin and Erskian, 1981). Some of them and additional studies quantified foraminiferal motion speeds in petri dishes with different substrates only focusing on horizontal movement (e.g. Bornmalm et al., 1997; Jauffrais et al., 2016a; Khare and Nigam, 2000; Kitazato, 1988; Maire et al., 2016; Seuront and Bouchet, 2015). In our study, we estimated the aver-age speed of vertical migration of *Ammonia confertitesta* and *Haynesina germanica* through the added sediment in the two disturbed microcosms. We calculated the speeds based on the vertical distribution at T1 in the OHV microcosm because this was the only sampling time showing an ongoing migration, while the definitive life position was already reached in the other microcosms at this time. Our estimation assumes that the speed was constant over time (18 h from the sediment disturbance and T1) and that the locomotion started right at the moment of the sediment addition, which could have led to an underestimation of the speeds. A possible bias could also be added by the ~ 1 cm sediment compaction observed

during the 18 h (Fig. 4), which, on the other hand, could give an overestimation of the speed as a result. We calculated the specific mean speeds of *A. confertitesta* (0.41 mm h^{-1}) and *H. germanica* (0.47 mm h^{-1}) (Table 1). As none of the individuals reached the water–sediment interface 18 h after the disturbance, the calculated speeds were approximately maximum values. Recent studies from Deldicq et al. (2020) used flat aquaria to study the vertical and horizontal locomotion abilities of *A. confertitesta* and *H. germanica* in the sediment in two dimensions. Cameras tracked the migration pathways of specimens of both species over a short period of time, 48 to 72 h, in the absence of physical disturbances. Based on the distance travelled every 10 min, Deldicq et al. (2020) calculated average speeds for both species and obtained values of 0.72 ± 0.25 mm h^{-1} for *A. confertitesta* and 1.1 ± 0.4 mm h^{-1} for *H. germanica* (Table 1).

In our microcosms, the mean migration speeds of both species are on the same order of magnitude, with the speed of *H. germanica* being 2 times lower. If we retain the speeds reported by Deldicq et al. (2020), an average time of 40 and 26 h would have been needed for *A. confertitesta* and *H. germanica* respectively to go back to the water–sediment interface, which is consistent with our observations that no specimens had reached the sediment surface 18 h after the disturbance. The differences in speed values could be explained by methodological bias and/or ecological reasons. Indeed, we weighted the migration speeds on the basis of the number of specimens counted at each layer within a core, and our sampling resolution (18 h) was much lower than that (10 min) of Deldicq et al. (2020). If the migration activity is not homogeneous through time as assumed, the low resolution of our observation could have led to an underestimation of the actual speed. Additionally, as suggested by Maire et al. (2016), the presence of both anoxic conditions and potential stress induced by sediment disturbance in our OHV microcosm can be a major factor for lowering locomotion speeds. However, Kitazato (1988) and Khare and Nigam (2000) pointed out the overestimation of speed calculated from individuals presenting crawling-like movements on a glass surface as they encounter less resistance than from sediment matrix. Both this study and Maire et al. (2016) support the capacity of our species to cover a few centimetres of distance in a few hours. Differently from Maire et al. (2016), however, our results show that anoxic conditions do not induce a complete stop of the motility for *A. confertitesta*. We compared our results to the experimental study conducted by Severin and Erskian (1981) that induced physical disturbances (from 0.5 to 4 cm of sediment suddenly added to the sediment surface containing living foraminifera) on a benthic foraminiferal species other than ours (i.e. *Quinqueloculina impressa*). The authors observed that the time of first emergence of this species after burial was a function of the deposit thickness as follows: $T = 434.3\ D^2$, with T being the time of first emergence and D being the burial depth in centimetres. If we apply this relationship to the two species in the OHV microcosm, it would have taken 52.7 h, corresponding to 2.2 d, for the first individuals to reach the surface after crossing the 2.9 cm thick deposit (Table 1), corresponding to a speed of 0.55 mm h^{-1}. Despite the methodological differences (different species, sandy sediment), our findings are in accordance with the results from Severin and Erskian (1981). In their model, the migration speeds are higher when foraminifera have to cross thinner layers. If we apply this model to the FLV treatment, for which speeds were not estimated, we would assume that the speeds would be higher for specimens crossing only a 0.5 cm thick layer of added sediment. For both studied species, based on the formula of Severin and Erskian (1981), we calculated average speeds of 2.7 mm h^{-1}, which are almost 3 times higher than the ones reported by Deldicq et al. (2020). The reliability of this value should be tested in further specific studies. Nevertheless, these findings further suggest that the stress induced by physical

disturbances and the amplitude of the disturbance (in terms of the thickness of the sediment deposit) can be a controlling factor influencing foraminiferal migration speed.

4.4 General overview on benthic communities' response to depositional events

The existing literature about the effects of sediment deposition on benthic communities in experimental setups mainly concentrates on macro- and megafauna and is limited to relatively short-lasting experiments (from 4 to 32 d). Some interesting observations can be pointed out. Mestdagh et al. (2018), for example, simulated a sudden deposit of about 4 cm of sediment and observed a complete recovery of different species of molluscs and crustacean within 15 d after the disturbance. No decay of abundances of certain species was observed, indicating that some macrofaunal species can deal with 4 cm depth burial without problems. Only individuals with sessile behaviours showed a wide mortality. Similarly, Cottrell et al. (2016) observed a weak migration ability of *Mytilus edulis* through thin added-sediment layers (< 2 cm) but no migration below thicker deposits. The species mortality was also observed to be largely affected by burial duration, increased temperature, and anoxia induced by organic matter mineralization. This was attributed to a short-term tolerance of anoxia, which was not sufficient to overcome oxygen depletion on longer timescales. Whomersley et al. (2009), in a 9-month-long study focusing on the effect of different frequencies of depositional events on both macro- and meiofauna, showed different responses of the two faunal types in terms of diversity, species abundances, and turnover. Compared to Mestdagh et al. (2018), they observed a more intense impact of burial on macrofauna, with decreasing diversity under both low and high depositional intensity. Macrofauna was also generally more impacted than meiofauna (represented here by nematodes), especially by the low-frequency burial. However, a shift in communities' species composition was only noticed for meiofauna, while no effects were observed on abundances, suggesting a more rapid species turnover under stressful conditions. Similarly to our results, the high intensity of burial seems to further affect their communities com-pared to weaker deposits (Whomersley et al., 2009). However, contrary to what is reported for nematodes, in our study, we observed a significant decay in foraminiferal abundances in the one-time high-volume microcosm (OHV, Fig. 5). This difference could be related to lower motility and/or turnover rates of foraminifera compared to nematodes or to the short duration of our experiment (51 d) compared to the one of Whomersley et al. (2009) (9 months). The fact that the vertical migration of living foraminifera through newly deposited layers in the OHV treatment was way longer (1 to 7 d) than for the FLV (< 18 h) supports the hypothesis of the low motility as the main limitation to survival after burial. Compared to foraminifera, nematodes are much more mobile and possibly able to reach favourable niches faster after a physical disturbance. This lets us conclude that the response, even for the same faunal type (i.e. meiofauna), can be variable. It is therefore crucial to study the response of different components of benthic compartments for the assessment of the effects of physical disturbance in the benthic marine environments.

The knowledge about the specific responses of different faunal types is also important when considering the trophic links between the compartments. For example, Bolam et al. (2011) suggested that trophic network disruption, caused by physical instability, can affect macrofaunal response to depositional events. The study simulated the impact of dredged sediment upon macrofaunal assemblages and showed different migration abilities for different macrofaunal taxa (e.g. polychaete that are less performant than gastropods) after burial. The

authors suggested that the observed survival of successful migrating species can be overestimated in short-time observations because of the dependence on the migration of other co-existing species including prey in a long-term dynamic. In this way, it appears to be fundamental to deepen the knowledge of the response of species from lower trophic levels to similar physical disturbances to holistically interpret the experimental observation at the scale of the whole benthic community.

If we consider all these observations together, we can therefore conclude that, under a condition of physical instability, benthic communities respond in a species-specific way in terms of abundances, diversity, and migration. Less mobile and highly specialist species are negatively affected compared to highly mobile and less trophically restricted species. The main factors influencing the community resilience seem to be turnover time, organic matter and/or oxygen availability, burial depth, frequency of sediment depositions, and migration of co-existing species. The interaction of these parameters can complicate the prevision of the long-term consequences of similar physical conditions in natural settings, but a loss of more sensitive species, both from macrofauna and meiofauna, can be supposed on the basis of the existing experimental results.

5 Conclusions

Physical disturbances are often neglected as an important driving factor ecologically influencing biodiversity and standing stocks. The ongoing climate change is supposed to, at least regionally or locally, affect the natural variability of sediment input from the continent to coastal environments. The lack of information about the potential consequences for benthic faunal abundances and diversity could be a strong limit to imagining ecosystem resilience scenarios.

The results of our experimental study suggest that benthic foraminiferal assemblages respond differently to sedimentary depositional events of different intensity and thickness. On the one hand, the total foraminiferal abundances were significantly negatively affected only by the one-time high-volume treatment, suggesting that occasional and thick sediment deposits potentially have a higher impact on standing stocks compared to a frequent, lower stress (represented by the frequent low-volume treatment). On the other hand, both types of tested sedimentary disturbances appeared to negatively influence the abundances of one of the two major species of the setup, *Haynesina germanica*. This result suggests that the tolerance of this species to the physical disturbance, no matter its intensity and frequency, is lower than the one of *Ammonia confertitesta*. In a natural environment, this could mean that a lowered biodiversity can be driven by physical disturbance.

At the scale of microhabitat distribution in the sediment, while the recovery of shallow microhabitats by the tested species was very quick after the frequent low-volume deposit (< 24 h), the one-time high-volume treatment induced longer recovery times (i.e. ≤ 7 d). This difference is also reflected in the geochemical steady state of the porewater. Indeed, the recovery of oxygen penetration depth, similarly to the one at the first foraminifera sampling, was relatively quick for the FLV microcosm (< 24 h after each disturbance), while a transitory deepening of the OPD was observed later (T1) in the OHV microcosm (24 h after the disturbance), and a resilient steady state was not reached until 38 (T2) to 52 d (T4) after the disturbance.

The recovery of superficial microhabitats by buried specimens, however, does not seem to be strictly driven by the oxic front. In the OHV microcosm, foraminifera migrated through a thick anoxic sediment layer to reach the water–sediment interface. Considering that the added sediment layer was not enriched in organic matter and that the most food-enriched area of the microcosm was probably the ancient interface (see black layer in Fig. 4), we can conclude that the upward migration was not driven by food research but rather, most likely, by oxygen depletion.

Author contributions

CG, MPN, AM and HH designed the experiment; CG, MPN, AM and DLM performed the sampling procedures and measurements; CG analysed the data; CG and MPN wrote the original manuscript draft, MPN, AM and HH reviewed and edited the manuscript.

Acknowledgements

We thank “Miroiterie Nogentaise” Inc. for providing custom-made aquaria following all our requirements. Thanks to Sophie Sanchez for her technical help in the laboratory and to bachelor students who helped us collecting the foraminifera from the mudflat and sieving core slices. The first author is grateful to Edouard Metzger for his valuable advice. We also thank Dr. Robin Fentimen for reading the last version of the manuscript and improving the English language. We thank the three anonymous reviewers and the editor who helped to improve the original version of this manuscript.

Financial support

The CNRS INSU LEFE CYBER program (Fluid Envelopes and the Environment) supported our research by funding the BEGIN project (PI: M. P.Nardelli,). This research is part of a PhD project (first author) funded by the French Minister of Scientific Research and Innovation, and by Angers University.

References

Alve, E.: Colonization of new habitats by benthic foraminifera: a review, Earth-Science Reviews, 46, 167–185, https://doi.org/10.1016/S0012-8252(99)00016-1, 1999.

Alve, E.: Temporal variability in vertical distributions of live (stained) intertidal foraminifera, Southern England, The Journal of Foraminiferal Research, 31, 12–24, https://doi.org/10.2113/0310012, 2001.

Alve, E., Korsun, S., Schönfeld, J., Dijkstra, N., Golikova, E., Hess, S., Husum, K., and Panieri, G.: Foram-AMBI: A sensitivity index based on benthic foraminiferal faunas from North-East Atlantic and Arctic fjords, continental shelves and slopes, Marine Micropaleontology, 122, 1–12, https://doi.org/10.1016/j.marmicro.2015.11.001, 2016.

Anschutz, P., Jorissen, F. J., Chaillou, G., Abu-Zied, R., and Fontanier, C.: Recent turbidite deposition in the eastern Atlantic: Early diagenesis and biotic recovery, Journal of Marine Research, 60, 835–854, https://doi.org/10.1357/002224002321505156, 2002.

Barras, C., Jorissen, F. J., Labrune, C., Andral, B., and Boissery, P.: Live benthic foraminiferal faunas from the French Mediterranean Coast: Towards a new biotic index of environmental quality, Ecological Indicators, 36, 719–743, https://doi.org/10.1016/j.ecolind.2013.09.028, 2014.

Belart, P., Clemente, I., Raposo, D., Habib, R., Volino, E., Villar, A., Alves, M., Fontana, L., Lorini, M., Panigai, G., Frontalini, F., Figueiredo, M., Vasconcelos, S., and Laut, L.: Living and dead Foraminifera as bioindicators in Saquarema Lagoon System, Brazil, LAJAR, 46, 1055–1072, https://doi.org/10.3856/vol46-issue5-fulltext-18, 2018.

Bernhard, J. M. and Bowser, S. S.: Novel epifluorescence microscopy method to determine life position of foraminifera in sediments, J. Micropalaeontol., 15, 68–68, https://doi.org/10.1144/jm.15.1.68, 1996.

Bernhard, J. M., Ostermann, D. R., Williams, D. S., and Blanks, J. K.: Comparison of two methods to identify live benthic foraminifera: A test between Rose Bengal and CellTracker Green with implications for stable isotope paleoreconstructions: foraminifera viability method comparison, Paleoceanography, 21, https://doi.org/10.1029/2006PA001290, 2006.

Bolam, S. G.: Burial survival of benthic macrofauna following deposition of simulated dredged material, Environ Monit Assess, 181, 13–27, https://doi.org/10.1007/s10661-010-1809-5, 2011.

Bolliet, T., Jorissen, F. J., Schmidt, S., and Howa, H.: Benthic foraminifera from Capbreton Canyon revisited; faunal evolution after repetitive sediment disturbance, Deep Sea Research Part II: Topical Studies in Oceanography, 104, 319–334, https://doi.org/10.1016/j.dsr2.2013.09.009, 2014.

Bornmalm, L., Corliss, B. H., and Tedesco, K.: Laboratory observations of rates and patterns of movement of continental margin benthic foraminifera, Marine Micropaleontology, 29, 175–184, https://doi.org/10.1016/S0377-8398(96)00013-8, 1997.

Bouchet, V. M. P., Sauriau, P.-G., Debenay, J.-P., Mermillod-Blondin, F., Schmidt, S., Amiard, J.-C., and Dupas, B.: Influence of the mode of macrofauna-mediated bioturbation on the vertical distribution of living benthic foraminifera: First insight from axial tomodensitometry, Journal of Experimental Marine Biology and Ecology, 371, 20–33, https://doi.org/10.1016/j.jembe.2008.12.012, 2009.

Bouchet, V. M. P., Alve, E., Rygg, B., and Telford, R. J.: Benthic foraminifera provide a promising tool for ecological quality assessment of marine waters, Ecological Indicators, 23, 66–75, https://doi.org/10.1016/j.ecolind.2012.03.011, 2012.

Bouchet, V. M. P., Goberville, E., and Frontalini, F.: Benthic foraminifera to assess Ecological Quality Statuses in Italian transitional waters, Ecological Indicators, 84, 130–139, https://doi.org/10.1016/j.ecolind.2017.07.055, 2018a.

Bouchet, V. M. P., Telford, R. J., Rygg, B., Oug, E., and Alve, E.: Can benthic foraminifera serve as proxies for changes in benthic macrofaunal community structure? Implications for the definition of reference conditions, Marine Environmental Research, 137, 24–36, https://doi.org/10.1016/j.marenvres.2018.02.023, 2018b.

Bradshaw, J. S.: Laboratory studies on the rate of growth of the foraminifer, "*Streblus beccarii* (linné) var. *tepida* (Cushman)," Journal of paleontology, 31, 1138–1147, 1957.

Budillon, F., Vicinanza, D., Ferrante, V., and Iorio, M.: Sediment transport and deposition during extreme sea storm events at the Salerno Bay (Tyrrhenian Sea): comparison of field data with numerical model results, Nat. Hazards Earth Syst. Sci., 6, 839–852, https://doi.org/10.5194/nhess-6-839-2006, 2006.

Bussi, G., Dadson, S. J., Prudhomme, C., and Whitehead, P. G.: Modelling the future impacts of climate and land-use change on suspended sediment transport in the River Thames (UK), Journal of Hydrology, 542, 357–372, https://doi.org/10.1016/j.jhydrol.2016.09.010, 2016.

Cesbron, F., Geslin, E., Jorissen, F. J., Delgard, M. L., Charrieau, L., Deflandre, B., Jézéquel, D., Anschutz, P., and Metzger, E.: Vertical distribution and respiration rates of benthic foraminifera: Contribution to aerobic remineralization in intertidal mudflats covered by Zostera noltei meadows, Estuarine, Coastal and Shelf Science, 179, 23–38, https://doi.org/10.1016/j.ecss.2015.12.005, 2016.

Choquel, C., Geslin, E., Metzger, E., Filipsson, H.L., Risgaard-Petersen, N., Launeau, P., Giraud, M., Jauffrais, T., Jesus, B., Mouret, A, Denitrification by benthic foraminifera and their contribution to N-loss from a fjord environment. Biogeosciences 18, 327–341. https://doi.org/10.5194/bg-18-327-2021, 2021

Contreras-Rosales, L. A., Koho, K. A., Duijnstee, I. A. P., de Stigter, H. C., García, R., Koning, E., and Epping, E.: Living deep-sea benthic foraminifera from the Cap de Creus Canyon (western Mediterranean): Faunal–geochemical interactions, Deep Sea Research Part I: Oceanographic Research Papers, 64, 22–42, https://doi.org/10.1016/j.dsr.2012.01.010, 2012.

Corliss, B. H.: Morphology and microhabitat preferences of benthic foraminifera from the northwest Atlantic Ocean, Marine Micropaleontology, 17, 195–236, https://doi.org/10.1016/0377-8398(91)90014-W, 1991.

Cottrell, R. S., Black, K. D., Hutchison, Z. L., and Last, K. S.: The Influence of Organic Material and Temperature on the Burial Tolerance of the Blue Mussel, Mytilus edulis: Considerations for the Management of Marine Aggregate Dredging, PLOS ONE, 11, e0147534, https://doi.org/10.1371/journal.pone.0147534, 2016.

D'Angelo, A., Giglio, F., Miserocchi, S., Sanchez-Vidal, A., Aliani, S., Tesi, T., Viola, A., Mazzola, M., and Langone, L.: Multi-year particle fluxes in Kongsfjorden, Svalbard, Biogeosciences, 15, 5343–5363, https://doi.org/10.5194/bg-15-5343-2018, 2018.

Deldicq, N., Seuront, L., Langlet, D., and Bouchet, V.: Assessing behavioural traits of benthic foraminifera: implications for sediment mixing, Mar. Ecol. Prog. Ser., 643, 21–31, https://doi.org/10.3354/meps13334, 2020.

Deldicq, N., Langlet, D., Delaeter, C., Beaugrand, G., Seuront, L., and Bouchet, V. M. P.: Effects of temperature on the behaviour and metabolism of an intertidal foraminifera and consequences for benthic ecosystem functioning, Sci Rep, 11, 4013, https://doi.org/10.1038/s41598-021-83311-z, 2021.

Denoyelle, M., Jorissen, F. J., Martin, D., Galgani, F., and Miné, J.: Comparison of benthic foraminifera and macrofaunal indicators of the impact of oil-based drill mud disposal, Marine Pollution Bulletin, 60, 2007–2021, https://doi.org/10.1016/j.marpolbul.2010.07.024, 2010.

Denoyelle, M., Geslin, E., Jorissen, F. J., Cazes, L., and Galgani, F.: Innovative use of foraminifera in ecotoxicology: A marine chronic bioassay for testing potential toxicity of drilling muds, Ecological Indicators, 12, 17–25, https://doi.org/10.1016/j.ecolind.2011.05.011, 2012.

Dessandier, P.-A., Bonnin, J., Kim, J.-H., Bichon, S., Deflandre, B., Grémare, A., and Sinninghe Damsté, J. S.: Impact of organic matter source and quality on living benthic foraminiferal distribution on a river-dominated continental margin: A study of the Portuguese margin: benthic foraminifera, J. Geophys. Res. Biogeosci., 121, 1689–1714, https://doi.org/10.1002/2015JG003231, 2016.

Dudgeon, D.: Multiple threats imperil freshwater biodiversity in the Anthropocene, Current Biology, 29, R960–R967, https://doi.org/10.1016/j.cub.2019.08.002, 2019.

Dupuy, C., Rossignol, L., Geslin, E., and Pascal, P.-Y.: Predation of mudflat meio-macrofaunal metazoans by a calcareous foraminifer, *Ammonia tepida* (Cushman, 1926), The Journal of Foraminiferal Research, 40, 305–312, https://doi.org/10.2113/gsjfr.40.4.305, 2010.

Duros, P., Silva Jacinto, R., Dennielou, B., Schmidt, S., Martinez Lamas, R., Gautier, E., Roubi, A., and Gayet, N.: Benthic foraminiferal response to sedimentary disturbance in the Capbreton canyon (Bay of Biscay, NE Atlantic), Deep Sea Research Part I: Oceanographic Research Papers, 120, 61–75, https://doi.org/10.1016/j.dsr.2016.11.012, 2017.

Dyer, K. R.: Fine Sediment Particle Transport in Estuaries, in: Physical Processes in Estuaries, edited by: Dronkers, J. and van Leussen, W., Springer Berlin Heidelberg, Berlin, Heidelberg, 295–310, https://doi.org/10.1007/978-3-642-73691-9_16, 1988.

Ernst, S., Duijnstee, I., and van der Zwaan, B.: The dynamics of the benthic foraminiferal microhabitat: recovery after experimental disturbance, Marine Micropaleontology, 46, 343–361, https://doi.org/10.1016/S0377-8398(02)00080-4, 2002.

Extence, C., P. Chadd, R., England, J., J. Dunbar, M., J. Wood, P., and D. Taylor, E.: The assessment of fine sediment accumulation in rivers using macro-invertebrate community response: macro-invertebrate assessment of fine sediment accumulation, River Res. Applic., 29, 17–55, https://doi.org/10.1002/rra.1569, 2013.

Fontanier, C., Dissard, D., Ruffine, L., Mamo, B., Ponzevera, E., Pelleter, E., Baudin, F., Roubi, A., Chéron, S., Boissier, A., Gayet, N., Bermell-Fleury, S., Pitel, M., Guyader, V., Lesongeur, F., Savignac, F., 2018. Living (stained) deep-sea foraminifera from the Sea of Marmara: A preliminary study. Deep Sea Research Part II: Topical Studies in Oceanography 153, 61–78. https://doi.org/10.1016/j.dsr2.2017.12.011, 2018

Fontanier, C., Mamo, B., Mille, D., Duros, P., and Herlory, O.: Deep-sea benthic foraminifera at a bauxite industrial waste site in the Cassidaigne Canyon (NW Mediterranean): Ten months after the cessation of red mud dumping, Comptes Rendus. Géoscience, 352, 87–101, https://doi.org/10.5802/crgeos.5, 2020.

Fossile, E., Nardelli, M. P., Howa, H., Baltzer, A., Poprawski, Y., Baneschi, I., Doveri, M., and Mojtahid, M.: Influence of modern environmental gradients on foraminiferal faunas in the inner Kongsfjorden (Svalbard), Marine Micropaleontology, 173, 102117, https://doi.org/10.1016/j.marmicro.2022.102117, 2022.

Frontalini, F. and Coccioni, R.: Benthic foraminifera for heavy metal pollution monitoring: A case study from the central Adriatic Sea coast of Italy, Estuarine, Coastal and Shelf Science, 76, 404–417, https://doi.org/10.1016/j.ecss.2007.07.024, 2008.

Frontalini, F., Buosi, C., Da Pelo, S., Coccioni, R., Cherchi, A., and Bucci, C.: Benthic foraminifera as bio-indicators of trace element pollution in the heavily contaminated Santa Gilla lagoon (Cagliari, Italy), Marine Pollution Bulletin, 58, 858–877, https://doi.org/10.1016/j.marpolbul.2009.01.015, 2009.

García-Robledo, E., Corzo, A., and Papaspyrou, S.: A fast and direct spectrophotometric method for the sequential determination of nitrate and nitrite at low concentrations in small volumes, Marine Chemistry, 162, 30–36, https://doi.org/10.1016/j.marchem.2014.03.002, 2014.

Geslin, E., Heinz, P., Jorissen, F., and Hemleben, Ch.: Migratory responses of deep-sea benthic foraminifera to variable oxygen conditions: laboratory investigations, Marine Micropaleontology, 53, 227–243, https://doi.org/10.1016/j.marmicro.2004.05.010, 2004.

Geslin, E., Barras, C., Langlet, D., Nardelli, M. P., Kim, J.-H., Bonnin, J., Metzger, E., and Jorissen, F. J.: Survival, reproduction and calcification of three benthic foraminiferal species in response to experimentally induced hypoxia, in: Approaches to Study Living Foraminifera, edited by: Kitazato, H. and M. Bernhard, J., Springer Japan, Tokyo, 163–193, https://doi.org/10.1007/978-4-431-54388-6_10, 2014.

Goineau, A., Fontanier, C., Jorissen, F., Buscail, R., Kerhervé, P., Cathalot, C., Pruski, A. M., Lantoine, F., Bourgeois, S., Metzger, E., Legrand, E., and Rabouille, C.: Temporal variability of live (stained) benthic

foraminiferal faunas in a river-dominated shelf – Faunal response to rapid changes of the river influence (Rhône prodelta, NW Mediterranean), Biogeosciences, 9, 1367–1388, https://doi.org/10.5194/bg-9-1367-2012, 2012.

Gooday, A. J., Bernhard, J. M., Levin, L. A., and Suhr, S. B.: Foraminifera in the Arabian Sea oxygen minimum zone and other oxygen-deficient settings: taxonomic composition, diversity, and relation to metazoan faunas, 30, 2000.

Griess, P.: Bemerkungen zu der Abhandlung der HH. Weselsky und Benedikt „Ueber einige Azoverbindungen", Ber. Dtsch. Chem. Ges., 12, 426–428, https://doi.org/10.1002/cber.187901201117, 1879.

Gross, O.: Influence of temperature, oxygen and food availability on the migrational activity of bathyal benthic foraminifera: evidence by microcosm experiments, in: Life at Interfaces and Under Extreme Conditions, edited by: Liebezeit, G., Dittmann, S., and Kröncke, I., Springer Netherlands, Dordrecht, 123–137, https://doi.org/10.1007/978-94-011-4148-2_12, 2000.

Hansen, L. and Blackburn, T.: Aerobic and anaerobic mineralization of organic material in marine sediment microcosms, Mar. Ecol. Prog. Ser., 75, 283–291, https://doi.org/10.3354/meps075283, 1991.

Hansen, L. S. and Blackburn, T. H.: Mineralization budgets in sediment microcosms: Effect of the infauna and anoxic conditions, FEMS Microbiology Letters, 102, 33–43, https://doi.org/10.1111/j.1574-6968.1992.tb05793.x, 1992.

Hayward, B. W., Holzmann, M., Pawlowski, J., Parker, J. H., Kaushik, T., Toyofuku, M. S., and Tsuchiya, M.: Molecular and morphological taxonomy of living Ammonia and related taxa (Foraminifera) and their biogeography, mpal, 67, 109–274, https://doi.org/10.47894/mpal.67.3.01, 2021.

Heinz, P. and Geslin, E.: Ecological and Biological Response of Benthic Foraminifera Under Oxygen-Depleted Conditions: Evidence from Laboratory Approaches, in: Anoxia, vol. 21, edited by: Altenbach, A. V., Bernhard, J. M., and Seckbach, J., Springer Netherlands, Dordrecht, 287–303, https://doi.org/10.1007/978-94-007-1896-8_15, 2012.

Hemleben, C. and Kitazato, H.: Deep-sea foraminifera under long time observation in the laboratory, Deep Sea Research Part I: Oceanographic Research Papers, 42, 827–832, https://doi.org/10.1016/0967-0637(95)00024-Z, 1995.

Hess, S. and Jorissen, F. J.: Distribution patterns of living benthic foraminifera from Cap Breton canyon, Bay of Biscay: Faunal response to sediment instability, Deep Sea Research Part I: Oceanographic Research Papers, 56, 1555–1578, https://doi.org/10.1016/j.dsr.2009.04.003, 2009.

Hess, S., Alve, E., Trannum, H. C., and Norling, K.: Benthic foraminiferal responses to water-based drill cuttings and natural sediment burial: Results from a mesocosm experiment, Marine Micropaleontology, 101, 1–9, https://doi.org/10.1016/j.marmicro.2013.03.004, 2013.

Hir, P. L., Ficht, A., Jacinto, R. S., Lesueur, P., Dupont, J.-P., Lafite, R., Brenon, I., Thouvenin, B., and Cugier, P.: Fine Sediment Transport and Accumulations at the Mouth of the Seine Estuary (France), Estuaries, 24, 950, https://doi.org/10.2307/1353009, 2001.

Hodson, A., Gurnell, A., Tranter, M., Bogen, J., Hagen, J. O., and Clark, M.: Suspended sediment yield and transfer processes in a small High-Arctic glacier basin, Svalbard, Hydrol. Process., 12, 73–86, https://doi.org/10.1002/(SICI)1099-1085(199801)12:1<73::AID-HYP564>3.0.CO;2-S, 1998.

Holzmann, M. and Pawlowski, J.: Taxonomic relationships in the genus *Ammonia* (Foraminifera) based on ribosomal DNA sequences, Journal of micropaleontology, 19, 11, https://doi.org/10.1144/jm.19.1.85, 2000.

Jalón-Rojas, I., Schmidt, S., and Sottolichio, A.: Turbidity in the fluvial Gironde Estuary (southwest France) based on 10-year continuous monitoring: sensitivity to hydrological conditions, Hydrol. Earth Syst. Sci., 19, 2805–2819, https://doi.org/10.5194/hess-19-2805-2015, 2015.

Jauffrais, T., Jesus, B., Metzger, E., Mouget, J.-L., Jorissen, F., and Geslin, E.: Effect of light on photosynthetic efficiency of sequestered chloroplasts in intertidal benthic foraminifera (*Haynesina germanica* and *Ammonia tepida*), Biogeosciences, 13, 2715–2726, https://doi.org/10.5194/bg-13-2715-2016, 2016a.

Jauffrais, T., Jesus, B., Geslin, E., Briand, F., and Jézéquel, V. M.: Locomotion speed of the benthic foraminifer *Ammonia tepida* exposed to different nitrogen and carbon sources, Journal of Sea Research, 118, 52–58, https://doi.org/10.1016/j.seares.2016.07.001, 2016b.

Jørgensen, B. B.: The sulfur cycle of a coastal marine sediment (Limfjorden, Denmark)1: Sulfur cycle of marine sediment, Limnol. Oceanogr., 22, 814–832, https://doi.org/10.4319/lo.1977.22.5.0814, 1977.

Jorissen, F. J.: Benthic foraminiferal microhabitats below the sediment-water interface, in: Modern Foraminifera, Springer Netherlands, Dordrecht, 161–179, https://doi.org/10.1007/0-306-48104-9_10, 1999.

Jorissen, F. J., Barmawidjaja, D. M., Puskaric, S., and van der Zwaan, G. J.: Vertical distribution of benthic foraminifera in the northern Adriatic Sea: The relation with the organic flux, Marine Micropaleontology, 19, 131–146, https://doi.org/10.1016/0377-8398(92)90025-F, 1992.

Jorissen, F. J., de Stigter, H. C., and Widmark, J. G. V.: A conceptual model explaining benthic foraminiferal microhabitats, Marine Micropaleontology, 26, 3–15, https://doi.org/10.1016/0377-8398(95)00047-X, 1995.

Jorissen, F. J., Fouet, M. P. A., Singer, D., and Howa, H.: The Marine Influence Index (MII): a tool to assess estuarine intertidal mudflat environments for the purpose of foraminiferal biomonitoring, Water, 14, 676, https://doi.org/10.3390/w14040676, 2022.

Khare, N. and Nigam, R.: Laboratory experiment to record rate of movement of cultured benthic foraminifera, ONGC bulletin, 9, 2000.

Kitazato, H.: Locomotion of some benthic foraminifera in and on sediments, The Journal of Foraminiferal Research, 18, 344–349, https://doi.org/10.2113/gsjfr.18.4.344, 1988.

Koho, K. A., de Nooijer, L. J., and Reichart, G. J.: Combining benthic foraminiferal ecology and shell Mn/Ca to deconvolve past bottom water oxygenation and paleoproductivity, Geochimica et Cosmochimica Acta, 165, 294–306, https://doi.org/10.1016/j.gca.2015.06.003, 2015.

Koho, K. A., LeKieffre, C., Nomaki, H., Salonen, I., Geslin, E., Mabilleau, G., Søgaard Jensen, L. H., and Reichart, G.-J.: Changes in ultrastructural features of the foraminifera *Ammonia* spp. in response to anoxic conditions: Field and laboratory observations, Marine Micropaleontology, 138, 72–82, https://doi.org/10.1016/j.marmicro.2017.10.011, 2018.

Kristensen, E. and Blackburn, T. H.: The fate of organic carbon and nitrogen in experimental marine sediment systems: Influence of bioturbation and anoxia, J Mar Res, 45, 231–257, https://doi.org/10.1357/002224087788400927, 1987.

Kuhnle, R. A., Bingner, R. L., Foster, G. R., and Grissinger, E. H.: Effect of land use changes on sediment transport in Goodwin Creek, Water Resour. Res., 32, 3189–3196, https://doi.org/10.1029/96WR02104, 1996.

Langezaal, A. M., Jorissen, F. J., Braun, B., Chaillou, G., Fontanier, C., Anschutz, P., and van der Zwaan, G. J.: The influence of seasonal processes on geochemical profiles and foraminiferal assemblages on the outer shelf of the Bay of Biscay, Continental Shelf Research, 26, 1730–1755, https://doi.org/10.1016/j.csr.2006.05.005, 2006.

Langlet, D.: Motion behavior and metabolic response to microplastic leachates in the benthic foraminifera *Haynesina germanica*, Journal of Experimental Marine Biology and Ecology, 6, 2020.

Laut, L., da Matta, G., Camara, G., Belart, P., Clemente, I., Ballalai, J., Volino, E., and Couto, E. da C. G.: Living and dead foraminifera assemblages as environmental indicators in the Almada River Estuary, Ilhéus, northeastern Brazil, Journal of South American Earth Sciences, 105, 102883, https://doi.org/10.1016/j.jsames.2020.102883, 2021.

Larson, F. and Sundbäck, K.: Recovery of microphytobenthos and benthic functions after sediment deposition, Mar. Ecol. Prog. Ser., 446, 31–44, https://doi.org/10.3354/meps09488, 2012.

Le Cadre, V. and Debenay, J.-P.: Morphological and cytological responses of *Ammonia* (foraminifera) to copper contamination: Implication for the use of foraminifera as bioindicators of pollution, Environmental Pollution, 143, 304–317, https://doi.org/10.1016/j.envpol.2005.11.033, 2006.

Lee, J. J., McEnery, M. E., Kuile, B. T., Erez, J., Röttger, R., Rockwell, R. F., Jr., W. W. F., Lagziel, A., and Rottger, R.: Identification and Distribution of Endosymbiotic Diatoms in Larger Foraminifera, Micropaleontology, 35, 353, https://doi.org/10.2307/1485677, 1989.

Lehto, N. J., Larsen, M., Zhang, H., Glud, R. N., and Davison, W.: A mesocosm study of oxygen and trace metal dynamics in sediment microniches of reactive organic material, Sci Rep, 7, 11369, https://doi.org/10.1038/s41598-017-10179-3, 2017.

LeKieffre, C., Spangenberg, J. E., Mabilleau, G., Escrig, S., Meibom, A., and Geslin, E.: Surviving anoxia in marine sediments: The metabolic response of ubiquitous benthic foraminifera (*Ammonia tepida*), PLoS ONE, 12, e0177604, https://doi.org/10.1371/journal.pone.0177604, 2017.

LeKieffre, C., Bernhard, J. M., Mabilleau, G., Filipsson, H. L., Meibom, A., and Geslin, E.: An overview of cellular ultrastructure in benthic foraminifera: New observations of rotalid species in the context of existing literature, Marine Micropaleontology, 138, 12–32, https://doi.org/10.1016/j.marmicro.2017.10.005, 2018a.

LeKieffre, C., Jauffrais, T., Geslin, E., Jesus, B., Bernhard, J. M., Giovani, M.-E., and Meibom, A.: Inorganic carbon and nitrogen assimilation in cellular compartments of a benthic kleptoplastic foraminifer, Sci Rep, 8, 10140, https://doi.org/10.1038/s41598-018-28455-1, 2018b.

Maire, O., Barras, C., Gestin, T., Nardelli, M., Romero-Ramirez, A., Duchêne, J., and Geslin, E.: How does macrofaunal bioturbation influence the vertical distribution of living benthic foraminifera?, Mar. Ecol. Prog. Ser., 561, 83–97, https://doi.org/10.3354/meps11929, 2016.

Martins, V. A., Frontalini, F., Tramonte, K. M., Figueira, R. C. L., Miranda, P., Sequeira, C., Fernández-Fernández, S., Dias, J. A., Yamashita, C., Renó, R., Laut, L. L. M., Silva, F. S., Rodrigues, M. A. da C., Bernardes, C., Nagai, R., Sousa, S. H. M., Mahiques, M., Rubio, B., Bernabeu, A., Rey, D., and Rocha, F.: Assessment of the health quality of Ria de Aveiro (Portugal): Heavy metals and benthic foraminifera, Marine Pollution Bulletin, 70, 18–33, https://doi.org/10.1016/j.marpolbul.2013.02.003, 2013.

Martins, M. V. A., Silva, F., Laut, L. L. M., Frontalini, F., Clemente, I. M. M. M., Miranda, P., Figueira, R., Sousa, S. H. M., and Dias, J. M. A.: Response of Benthic Foraminifera to Organic Matter Quantity and Quality and Bioavailable Concentrations of Metals in Aveiro Lagoon (Portugal), PLoS ONE, 10, e0118077, https://doi.org/10.1371/journal.pone.0118077, 2015.

Martins, M. V. A., Pinto, A. F. S., Frontalini, F., da Fonseca, M. C. M., Terroso, D. L., Laut, L. L. M., Zaaboub, N., da Conceição Rodrigues, M. A., and Rocha, F.: Can benthic foraminifera be used as bio-indicators of pollution in areas with a wide range of physicochemical variability?, Estuarine, Coastal and Shelf Science, 182, 211–225, https://doi.org/10.1016/j.ecss.2016.10.011, 2016.

Mathers, K. L., Doretto, A., Fenoglio, S., Hill, M. J., and Wood, P. J.: Temporal effects of fine sediment deposition on benthic macroinvertebrate community structure, function and biodiversity likely reflects landscape setting, Science of The Total Environment, 829, 154612, https://doi.org/10.1016/j.scitotenv.2022.154612, 2022.

McCorkle, D. C., Corliss, B. H., and Farnham, C. A.: Vertical distributions and stable isotopic compositions of live (stained) benthic foraminifera from the North Carolina and California continental margins, Deep Sea Research Part I: Oceanographic Research Papers, 44, 983–1024, https://doi.org/10.1016/S0967-0637(97)00004-6, 1997.

Meslard, F., Bourrin, F., Many, G., and Kerhervé, P.: Suspended particle dynamics and fluxes in an Arctic fjord (Kongsfjorden, Svalbard), Estuarine, Coastal and Shelf Science, 204, 212–224, https://doi.org/10.1016/j.ecss.2018.02.020, 2018.

Mestdagh, S., Bagaço, L., Braeckman, U., Ysebaert, T., De Smet, B., Moens, T., and Van Colen, C.: Functional trait responses to sediment deposition reduce macrofauna-mediated ecosystem functioning in an estuarine mudflat, Biogeosciences, 15, 2587–2599, https://doi.org/10.5194/bg-15-2587-2018, 2018.

Metzger, E., Barbe, A., Cesbron, F., Thibault de Chanvalon, A., Jauffrais, T., Jézéquel, D., and Mouret, A.: Two-dimensional ammonium distribution in sediment pore waters using a new colorimetric diffusive equilibration in thin-film technique, Water Research X, 2, 100023, https://doi.org/10.1016/j.wroa.2018.100023, 2019.

Mojtahid, M., Griveaud, C., Fontanier, C., Anschutz, P., and Jorissen, F. J.: Live benthic foraminiferal faunas along a bathymetrical transect (140–4800m) in the Bay of Biscay (NE Atlantic), Revue de Micropaléontologie, 53, 139–162, https://doi.org/10.1016/j.revmic.2010.01.002, 2010.

Mojtahid, M., Jorissen, F., Durrieu, J., Galgani, F., Howa, H., Redois, F., Camps, R., 2006. Benthic foraminifera as bio-indicators of drill cutting disposal in tropical east Atlantic outer shelf environments. Marine Micropaleontology 61, 58–75. https://doi.org/10.1016/j.marmicro.2006.05.004, 2006

Mojtahid, M., Zubkov, M. V., Hartmann, M., and Gooday, A. J.: Grazing of intertidal benthic foraminifera on bacteria: Assessment using pulse-chase radiotracing, Journal of Experimental Marine Biology and Ecology, 399, 25–34, https://doi.org/10.1016/j.jembe.2011.01.011, 2011.

Morvan, J., Debenay, J.-P., Jorissen, F., Redois, F., Bénéteau, E., Delplancke, M., and Amato, A.-S.: Patchiness and life cycle of intertidal foraminifera: Implication for environmental and paleoenvironmental interpretation, Marine Micropaleontology, 61, 131–154, https://doi.org/10.1016/j.marmicro.2006.05.009, 2006.

Murray, J. W.: Ecology and Applications of Benthic Foraminifera, Cambridge university press., 2006.

Murray, J. W. and Alve, E.: Major aspects of foraminiferal variability (standing crop and biomass) on a monthly scale in an intertidal zone, The Journal of Foraminiferal Research, 30, 177–191, https://doi.org/10.2113/0300177, 2000.

Nardelli, M. P., Barras, C., Metzger, E., Mouret, A., Filipsson, H. L., Jorissen, F., and Geslin, E.: Experimental evidence for foraminiferal calcification under anoxia, Biogeosciences, 11, 4029–4038, https://doi.org/10.5194/bg-11-4029-2014, 2014.

Nesbitt, E. A., Martin, R. A., Martin, D. E., and Apple, J.: Rapid deterioration of sediment surface habitats in Bellingham Bay, Washington State, as indicated by benthic foraminifera, Marine Pollution Bulletin, 97, 273–284, https://doi.org/10.1016/j.marpolbul.2015.06.006, 2015.

de Nooijer, L. J., Toyofuku, T., and Kitazato, H.: Foraminifera promote calcification by elevating their intracellular pH, Proc. Natl. Acad. Sci. U.S.A., 106, 15374–15378, https://doi.org/10.1073/pnas.0904306106, 2009.

Norkko, A., Rosenberg, R., Thrush, S. F., and Whitlatch, R. B.: Scale- and intensity-dependent disturbance determines the magnitude of opportunistic response, Journal of Experimental Marine Biology and Ecology, 330, 195–207, https://doi.org/10.1016/j.jembe.2005.12.027, 2006.

Papaspyrou, S., Diz, P., García-Robledo, E., Corzo, A., and Jimenez-Arias, J.: Benthic foraminiferal community changes and their relationship to environmental dynamics in intertidal muddy sediments (Bay of Cádiz, SW Spain), Mar. Ecol. Prog. Ser., 490, 121–135, https://doi.org/10.3354/meps10447, 2013.

Pascal, P.-Y., Dupuy, C., Richard, P., Mallet, C., telet, E. A. du C., and Niquilb, N.: Seasonal variation in consumption of benthic bacteria by meio- and macrofauna in an intertidal mudflat, Limnol. Oceanogr., 54, 1048–1059, https://doi.org/10.4319/lo.2009.54.4.1048, 2009.

Pillet, L., de Vargas, C., and Pawlowski, J.: Molecular identification of sequestered diatom chloroplasts and kleptoplastidy in foraminifera, Protist, 162, 394–404, https://doi.org/10.1016/j.protis.2010.10.001, 2011.

Porter, E. T., Owens, M. S., and Cornwell, J. C.: Effect of Sediment Manipulation on the Biogeochemistry of Experimental Sediment Systems, Journal of Coastal Research, 226, 1539–1551, https://doi.org/10.2112/05-0478, 2006.

Pucci, F., Geslin, E., Barras, C., Morigi, C., Sabbatini, A., Negri, A., Jorissen, F.J. Survival of benthic foraminifera under hypoxic conditions: Results of an experimental study using the CellTracker Green method. Marine Pollution Bulletin 59, 336–351. https://doi.org/10.1016/j.marpolbul.2009.08.015, 2009

Revsbech, N. P.: An oxygen microsensor with a guard cathode, Limnology and Oceanography, 34, 474–478, https://doi.org/10.4319/lo.1989.34.2.0474, 1989.

Richirt, J., Riedel, B., Mouret, A., Schweizer, M., Langlet, D., Seitaj, D., Meysman, F. J. R., Slomp, C. P., and Jorissen, F. J.: Foraminiferal community response to seasonal anoxia in Lake Grevelingen (the Netherlands), Biogeosciences, 17, 1415–1435, https://doi.org/10.5194/bg-17-1415-2020, 2020.

Ross, B.J., Hallock, P. Challenges in using CellTracker Green on foraminifers that host algal endosymbionts. PeerJ 6, e5304. https://doi.org/10.7717/peerj.5304, 2018

Sánchez-Bayo, F. and Wyckhuys, K. A. G.: Worldwide decline of the entomofauna: A review of its drivers, Biological Conservation, 232, 8–27, https://doi.org/10.1016/j.biocon.2019.01.020, 2019.

Schneider, C. A., Rasband, W. S., and Eliceiri, K. W.: NIH Image to ImageJ: 25 years of image analysis, Nat Methods, 9, 671–675, https://doi.org/10.1038/nmeth.2089, 2012.

Schönfeld, J., Alve, E., Geslin, E., Jorissen, F., Korsun, S., and Spezzaferri, S.: The FOBIMO (FOraminiferal BIo-MOnitoring) initiative—Towards a standardised protocol for soft-bottom benthic foraminiferal monitoring studies, Marine Micropaleontology, 94–95, 1–13, https://doi.org/10.1016/j.marmicro.2012.06.001, 2012.

Schumacher, S., Jorissen, F. J., Dissard, D., Larkin, K. E., and Gooday, A. J.: Live (Rose Bengal stained) and dead benthic foraminifera from the oxygen minimum zone of the Pakistan continental margin (Arabian Sea), Marine Micropaleontology, 62, 45–73, https://doi.org/10.1016/j.marmicro.2006.07.004, 2007.

Seuront, L. and Bouchet, V. M. P.: The devil lies in details: new insights into the behavioural ecology of intertidal foraminifera, Journal of Foraminiferal Research, 45, 390–401, https://doi.org/10.2113/gsjfr.45.4.390, 2015.

Severin, K. P. and Erskian, M. G.: Laboratory experiments on the vertical movement of Quinqueloculina impressa Reuss through sand, The Journal of Foraminiferal Research, 11, 133–136, https://doi.org/10.2113/gsjfr.11.2.133, 1981.

Silverberg, N., Gagnon, J.-M., and Lee, K.: A benthic mesocosm facility for maintaining soft-bottom sediments, Netherlands Journal of Sea Research, 34, 289–302, https://doi.org/10.1016/0077-7579(95)90039-X, 1995.

Stouff, V., Geslin, E., Debenay, J.-P., and Lesourd, M.: Origin of morphological abnormalities in *Ammonia* (foraminifera): studies in laboratory and natural environments, The Journal of Foraminiferal Research, 29, 152–170, https://doi.org/10.2113/gsjfr.29.2.152, 1999.

Suokhrie, T., Saraswat, R., and Nigam, R.: Foraminifera as Bio-Indicators of pollution: A review of research over the last decade, Advanced Micropaleontology, 267–286, 2017.

Thibault de Chanvalon, A., Metzger, E., Mouret, A., Cesbron, F., Knoery, J., Rozuel, E., Launeau, P., Nardelli, M. P., Jorissen, F. J., and Geslin, E.: Two-dimensional distribution of living benthic foraminifera in anoxic sediment layers of an estuarine mudflat (Loire estuary, France), Biogeosciences, 12, 6219–6234, https://doi.org/10.5194/bg-12-6219-2015, 2015.

Thrush, S. F., Gray, J. S., Hewitt, J. E., and Ugland, K. I.: Predicting the effects of habitat homogenization on marine biodiversity, Ecological Applications, 16, 1636–1642, https://doi.org/10.1890/1051-0761(2006)016[1636:PTEOHH]2.0.CO;2, 2006.

Tsujimoto, A., Nomura, R., Arai, K., Nomaki, H., Inoue, M., and Fujikura, K.: Changes in deep-sea benthic foraminiferal fauna caused by turbidites deposited after the 2011 Tohoku-oki earthquake, Marine Geology, 419, 106045, https://doi.org/10.1016/j.margeo.2019.106045, 2020.

Van der Zwaan, G. J., Duijnstee, I. A. P., den Dulk, M., Ernst, S. R., Jannink, N. T., and Kouwenhoven, T. J.: Benthic foraminifers: proxies or problems?, Earth-Science Reviews, 46, 213–236, https://doi.org/10.1016/S0012-8252(99)00011-2, 1999.

Whomersley, P., Huxham, M., Schratzberger, M., & Bolam, S. : Differential response of meio- and macrofauna to in situ burial, Journal of the Marine Biological Association of the United Kingdom, 89, 6, 1091-1098, doi:10.1017/S0025315409000344, 2009.

Widerlund, A., Nowell, G. M., Davison, W., and Pearson, D. G.: High-resolution measurements of sulphur isotope variations in sediment pore-waters by laser ablation multicollector inductively coupled plasma mass spectrometry, Chemical Geology, 291, 278–285, https://doi.org/10.1016/j.chemgeo.2011.10.018, 2012.

Włodarska-Kowalczuk, M., Pearson, T., and Kendall, M.: Benthic response to chronic natural physical disturbance by glacial sedimentation in an Arctic fjord, Mar. Ecol. Prog. Ser., 303, 31–41, https://doi.org/10.3354/meps303031, 2005.

Włodarska-Kowalczuk, M., Pawłowska, J., and Zajączkowski, M.: Do foraminifera mirror diversity and distribution patterns of macrobenthic fauna in an Arctic glacial fjord?, Marine Micropaleontology, 103, 30–39, https://doi.org/10.1016/j.marmicro.2013.07.002, 2013.

Wolanski, E. and Gibbs, R.: Resuspension and clearing of dredge spoils after dredging, Cleveland Bay, Australia, Water Environment Research, 64, 910–914, https://doi.org/10.2175/WER.64.7.9, 1992.

Wood, P. J.: Biological effects of fine sediment in the lotic environment, Environmental Management, 21, 203–217, https://doi.org/10.1007/s002679900019, 1997.

Wukovits, J., Oberrauch, M., Enge, A. J., and Heinz, P.: The distinct roles of two intertidal foraminiferal species in phytodetrital carbon and nitrogen fluxes – results from laboratory feeding experiments, Biogeosciences, 15, 6185–6198, https://doi.org/10.5194/bg-15-6185-2018, 2018.

Wukovits, J., Enge, A., Bukenberger, P., Wanek, W., Watzka, M., and Heinz, P.: Phytodetrital quality (C:N ratio) and temperature changes affect C and N cycling of the intertidal mixotrophic foraminifer *Haynesina germanica*, Aquat. Biol., 30, 119–132, https://doi.org/10.3354/ab00746, 2021.

Chapter 3

Effects of frequent or massive sediment supplies on sediment redox stability: a microcosm simulation

C. Guilhermic[*1], A. Mouret[1], H. Howa[1] , M.P. Nardelli[1]

[1] Université Angers, Nantes Univ., Le Mans Univ, CNRS, LPG, Laboratoire de planétologie et géosciences, UMR CNRS 6112, F-49000 Angers, France

Correspondence to: Corentin Guilhermic (corentin.guilhermic@etud.univ-angers.fr)

Chapter 3: Effects of frequent or massive sediment supplies on sediment redox stability: a microcosm simulation

Abstract:

Marine coastal environments can be subjected to depositional events such as during tidal cycles, flood events or mass transport episodes. Biogeochemical stability in the substrate was already shown to be disturbed after disruption to the water column by a new sediment layer. The present study aims to understand steps of recovery of the sediment early diagenesis sequence after different modalities of sediment deposits varying in intensity and frequency simulated in microcosms using intertidal mudflat sediment. With a weekly sampling resolution and for 5 weeks, high spatial resolution methods were applied to characterise oxygen, nitrogen, manganese and iron cycles behaviour regarding i) a single 2.7 cm sediment deposit ("One-time high volume"; OHV) and ii) a 0.4 cm weekly deposit ("Frequent low volume"; FLV). It firstly appears that oxygen, ammonium and nitrites concentration showed similar distributions in the FLV and in the Control microcosms. In the OHV microcosm, oxygen penetration depth was reestablished at Control levels after 3 weeks whereas denitrification fronts in the new deposits occurred within one week after the disturbance. Regarding manganese and iron cycles, the experiment revealed that after disturbances in both OHV and FLV modalities, previously Mn/Fe-OHO enriched surface layer became anoxic therefore the source for bacterial reduction of these oxides. Unsynchronous dissolved manganese production occurred one week before dissolved iron production highlighted preferential organic matter remineralisation pathways. Biogeochemical transient state towards a new stability can therefore be appreciated through manganese and iron cycling after a sediment deposit.

Keywords : experiment, early diagenesis, sediment, deposition events, transient state

Chapter 3: Effects of frequent or massive sediment supplies on sediment redox stability: a microcosm simulation

1 Introduction

Sediment instabilities on the seabed due to abnormally high supplies can vary in frequency and intensity depending on the events that cause them. Natural seasonal events can cause abrupt transport and deposition of high amounts of particles, such as floods (Deflandre et al., 2002; Mucci et al., 2003; Thibault de Chanvalon et al., 2016; Pastor et al., 2018) or storm-generated seabed reworking (Bolliet et al., 2014; Budillon et al., 2006). Tidal cycles can also affect the coastal sea bottom stability at a daily (or following the 14 day tidal cycle) frequency with short-term intense resuspension and deposition of local or non-local sediments (Davies et al., 2023). At varying frequencies (i.e., from daily to annual), gravity flow events (Haughton et al., 2009; Mulder and Cochonat, 1996; Postma, 1986; Rodrigues et al., 2022), or glacier melting in polar regions (D'Angelo et al., 2018; Hodson et al., 1998; Hodgkins et al., 2003; Łepkowska and Stachnik, 2018; Meslard et al., 2018) can supply large amounts of recently eroded sediment that settle abruptly on the seabed. In addition to these natural events, anthropic activities such as occasional or repeated dredging and dumping can also cause sedimentary instabilities (Wolanski and Gibbs, 1992; van de Velde et al., 2018). Disturbances generated by such sediment instabilities are known to negatively affect benthic communities (Alve, 1999; Anschutz et al., 2002; Bolam, 2011; Duros et al., 2017; Fossile et al., 2022; Guilhermic et al., 2023; Mestdagh et al., 2018; Włodarska-Kowalczuk et al., 2013) and diagenetic processes in the sediment (Anschutz et al., 2002; Deflandre et al., 2002; Mucci et al., 2003; Thibault de Chanvalon et al., 2016; van de Velde et al., 2018).

Many diagenetic reactions are microbially mediated and fuelled by organic matter (OM) present in settling particles or directly produced in the sediments. These reactions consume a variety of oxidizing sediment components (Froelich et al., 1979; Berner, 1981) and change the composition of the porewater, creating concentration of what gradients, which drive fluxes of solutes and gases within the sediment and across the sediment–water interface (SWI). Sediment instabilities such as turbidites (Anschutz et al., 2002), landslide events (Mucci and Edenborn, 1992) or flood deposits (Deflandre et al., 2002; Cathalot et al., 2010; Thibault de Chanvalon et al., 2016; Pastor et al., 2018; Hulot et al., 2023) induce physical disruption of ongoing diagenetic sequence. Disturbance of established vertical redox fronts were observed, and the temporality of recovery was previously investigated (Mucci and Edenborn, 1992; Anschutz et al., 2002; Deflandre et al., 2002). Nevertheless, the temporal resolution of the observations is often limited after the main disturbance (i.e., weeks to months), making short-term response after a disturbance event scarcely described. A better understanding of involved processes towards a geochemical recovery can be achieved with modelling approaches (Yücel et al., 2010; Nmor et al., 2022; van de Velde et al., 2018). However, previous studies that described in-situ sampling cannot provide enough information to constrain models. Therefore, the modelling approach requires more data to validate the underlying assumptions. Experimental studies are a good way of acquiring adequate data on the rapid dynamics of redox gradients in response to physical and chemical disturbances generated by sediment deposition events (Chaillou et al., 2007).

We have studied biogeochemical indicators of intense depositional events and ecosystem burial using microcosms, sufficiently reliable to be applied to the understanding of natural environments subject to sedimentary disturbance.

In the perspective of studying short-term dynamics of sediment biogeochemistry in response to physical disturbance (i.e. sediment depositional events and seabed burial), we set

up an experiment testing the effects of two types of sediment deposition events over 51 days. With this aim, three microcosms were established: 1) A control microcosm in which no disturbance was induced, 2) a "One-time high volume" microcosm (OHV) in which a single abundant sedimentation event was simulated and 3) a "Frequent low volume" microcosm (FLV) in which small deposition events were induced every week.

The experimental design and procedures were widely documented by Guilhermic et al. (2023), who studied the response of living benthic foraminifera to both sediment deposition modalities, in the same set up. In this study, we examined the evolution of sediment compaction of the solid fraction (reactive oxides of Mn and Fe) and spatial distribution of dissolved chemical species in porewaters (oxygen, inorganic nitrogen, Mn and Fe) at submillimetre and millimetre spatial resolution with micro-electrodes, 1D DET and 2D DET, in order to document the physico-chemical response of sediment column to different degrees of physical instability.

2 Material and methods

2.1 Experimental design

The experiment was performed in three glass aquaria simulating different sediment disturbance modalities being i) a control microcosm in which no disturbance was induced throughout the whole experiment time, ii) a "One-time high volume" (OHV) microcosm into which only a single sediment load was inserted resulting in a thick deposit (2.7 cm after compaction), compared with iii) a "Frequent low volume" (FLV) microcosm which received small volumes of sediment once a week for 4 times (1.3 cm in total after compaction). Those sediment addition occurred 18h before each described sampling time (only once for OHV microcosm before T1).

The detailed protocol and timeline of the aquaria setting up is widely explained in Guilhermic et al. (2023). The experiment was performed at a stable temperature of 14°C and in the dark. Sediment from the Couplasse mudflat (Bourgneuf Bay, 47°0'57" N, 2°1'29" W) and natural seawater were used to fill the aquaria. The seawater was previously microfiltered (0.45 µm) and kept oxygenated throughout the experiment. Sediment was frozen and unfrozen, homogenized and diluted with the same seawater to form a highly turbid slurry, and oxygenated for one hour before its introduction. An equilibration period of 21 days between the simulation of new sedimentary inputs.

The experiment lasted 51 days from the insertion of the basal sediment, punctuated by 5 main sampling times (T0 = 22 days; T1= 29 days; T2= 36 days; T3 = 43 days and T4 = 51 days). At each time, a section of the aquaria was closed and isolated from the rest of the microcosm to avoid water and sediment transfer due to resuspension during or after sampling. Throughout the experiment, the water column was renewed to prevent experimentally induced enrichment in chemical species.

2.2 Data acquisition

Sediment compaction after disturbance was investigated using pictures taken at least once a day on the side of the "one-time high volume" and "Frequent low volume" microcosms,

with a fix Nikon D3400 camera . The pictures were cropped and decomposed into three reflectance channels with ImageJ® software. The channel showing the best sensitive response to sediment-coloured layers was the red one. Thanks to this high-resolution imagery analysis, it was possible to distinguish the different sediment layers according to greyscale profiles. Profiles of compaction were compiled with Grapher® (Golden software).

Dissolved oxygen (DO) concentration was measured in porewaters using 50 µm tip diameter Clark-type microelectrodes (Unisense^{TM}). Attached to an automated micromanipulator, microelectrodes enabled point measurements with a vertical resolution of 50 µm (Revsbech, 1989). These measurements were always performed in the same pristine sampling section of the aquaria, the other sections being closed successively after each sediment sampling. All DO measurements were made one day after each sampling event (i.e. two days after sedimentary disturbances). Diffusive oxygen flux at the sediment-water interface was assessed using the PROFILE numerical model (Berg et al., 1998).

Sediment porosity and Mn and Fe reactive oxide phase were investigated by coring the three microcosms at each sampling time (n=15) with modified syringes acting as miniature disposable piston corers. They were sliced every 0.2 cm until 4 cm depth and then every 0.5 cm from 4 to 6 cm depth. Sediment samples were sealed in pre-weighed vials and immediately frozen. All analyses of the solid sediment were carried out on freeze-dried samples and were corrected for the sea salt content using the measured salinity. The weight lost during freeze-drying was used to calculate sediment porosity. The freeze-dried samples were homogenized and ground with an agate mortar. An ascorbate reagent was used to extract the most reactive Fe(III) phases and Mn(III, IV) oxides and oxyhydroxides (Anschutz et al., 1998, 2005; Kostka and Luther, 1994). 0.1 g of dry and crushed sediment was exposed to 10 mL of sodium bicarbonate (0.6M), sodium citrate (0.17M) and ascorbic acid (0.11M) (pH=8). After centrifugation, 1 mL of the supernatant solution was diluted with 9 mL of 1% acid nitric solution for Fe_{ASC} and Mn_{ASC} analysis (Mn and Fe reactive oxide phase). The concentration determination was performed with an ICP-AES (Thermo Scientific iCAP 6300 Radial). Extracted Fe and Mn concentrations were determined with ± 3% precision.

For porewater analysis, two DET (Diffusive equilibrium in thin film) gel techniques were used in this experiment and inserted into the sediment of each aquarium at each sampling time.

First, a 1D DET probe was used, developed by Davison and Zhang (1994) and Krom et al. (1994) and adapted by Metzger et al. (2013), consisting of a Perspex support drilled with 75 compartments of 1 mm depth and all 2 mm apart. These compartments are filled with a solution of ultra-pure agarose and MilliQ water. To allow only dissolved species to be equilibrated with the gel-filled compartments, a PVDF hydrophilic membrane is attached to the probe with white PVC tape. Prior to deployment, probes were transferred into plastic bags partially filled with MilliQ water, bubbled with N_2 for at least 6 h to remove dissolved oxygen from the hydrogel (to prevent oxidation of porewater reduced compounds). 1D DET probes were inserted into sediment microcosms and left to equilibrate for 12 h. After equilibration, each probe was retrieved, and the membrane removed. Each gel piece was eluted individually with 500 µL of 5% HNO_3 (SupraPur Merck), pending a final 200-fold dilution with 0.8 % HNO_3. Fe_d and Mn_d concentrations (dissolved Mn and Fe) were then determined using the same ICP-AES as for the oxide analysis.

Secondly, 2D DET probes were used for the determination of dissolved inorganic nitrogen concentrations in porewaters. The probe consisted of a 3-mm-thick Plexiglas plate

allowing a rectangular depression of 190 mm*95 mm*1 mm on each side of the plate for two gels. On one side, a 1 mm thick 2D DET polyacrylamide hydrogel was prepared as described by Jézéquel et al. (2007) and fitted to the probe window for nitrite analysis (Metzger et al., 2016). On the other side of the plate, a 2D DET probe gel composed of ultra-pure agarose and MilliQ water prepared as described by Metzger (2019) was set up for ammonium analysis. Both gels were covered with a PVDF membrane (0.2 µm, Durapore®) and fixed with white PVC tape. As with 1D DET, probes were transferred into plastic bags partially filled with MilliQ water bubbled with N2 for at least 6 h, and then deployed into sediment microcosms around 12h. The 2D DET probes were then retrieved from the microcosms one by one. A first gel was retrieved from the probe and combined directly with one or two reagent gels (see below for the different reagent gels used). After completion of the colorimetric reaction, images were acquired using a flatbed scanner.

For nitrite concentration measurement, a reagent gel was prepared, containing Griess reagent (Griess, 1879). The polyacrylamide probe gel was laid down onto this reagent gel, inducing a colorimetric reaction with nitrite, with pink coloration appearing throughout the gel assemblage. An image was then acquired using the scanner. After this step, the images were decomposed into primary colour intensities (converted into greyscale images), and the green channel was used as it gives the most sensitive response. Conversion of images into concentrations requires calibration for both chemical species, using the same protocol as for the probe gels. Calibration curves were used to calculate concentrations from the greyscale values of each pixel as follows:

$$[NO_2^-] = (\text{slope}_{\text{nitrite}} * R_{\text{nitrite}})$$

where the $\text{slope}_{\text{nitrite}}$ is the slope of the nitrite calibration curve ; R_{nitrite} is the greyscale value in the green channel of each pixel after contact with the Griess reagent gel.

For the ammonium concentration determination, the colorimetric reaction requires two reagent gels simultaneously in contact with the gel probe, as detailed in Metzger (2019). The most sensitive colour channel of the images is the red one.

1D profiles are displayed in this study for better comparison between sampling times and microcosms. The average values and associated standard deviations of each pixel line of the ammonium and nitrite distribution images are calculated (2D images compilation in supplement material).

2.3 Production rates and oxide stocks calculations

Porewater dissolved manganese (Mn_d) and iron (Fe_d) profiles were modelled using the Savitzky Golay filter (Savitzky and Golay, 1964; Thibault de Chanvalon et al., 2016). The Savitzky-Golay filter induces a polynomial interpolation of the data. Each point in the profile is therefore replaced by a polynomial function of degree *p* that best fits each point and its *n* surrounding neighbours. Profile smoothing is accentuated as *n* increases, thus eliminating noise from the process. Parameters of the polynomial function and of the smoothing were adjusted to obtain the best compromise (here *p*=4 and *n*=5 for all profiles modelled). Then, production rates were calculated, as detailed in Thibault de Chanvalon et al. (2016), using first and second derivatives on each point, porosity profiles (Φ fitted with an exponential function) and temperature, salinity, and pressure (the last three assumed constant with depth). The entire

procedure was performed using R studio software. Apparent Production Rates (APR) were presented as the sum of all positive production rates along the profiles. They represent the total reduction of reactive oxides (ascorbate-extracted) in the sediment column. The uncertainties associated with production rates were calculated considering an uncertainty of ±1 *n* for the smoothing parameter.

Stocks of excess Fe and Mn reactive oxides were calculated after Anschutz et al. (2002) and Thibault de Chanvalon et al. (2016) in mmol m^{-2} as follows:

$$\text{Excess Mn}_{\text{ASC}} = \sum_{l_{min}}^{l_{max}} \left([Mn_{ASC}]_l - [\overline{Mn_{ASC}}]_{\text{deep}}\right)(1-\phi)\rho\, t_l$$

Where $[Mn_{ASC}]_l$ is the concentration of ascorbate-extracted Mn oxides from the layer l; $[\overline{Mn_{Asc}}]_{\text{deep}}$ is the mean of the minimal constant values of ascorbate-extracted Mn oxides in the deep layers; ϕ is the porosity of the layer; ρ is the density of dry sediment (2.65); t_l is the thickness of the sediment layer.

3 Results

3.1 Sediment compaction

Pictures taken throughout the experiment allowed us to observe changes in sediment compaction and thickness, and additionally in colour (i.e., in relation to redox reactions).

Sediment compaction after the T1 disturbance was described in Fig.1 for both “One-time high volume” (OHV) and “Frequent low volume” (FLV) microcosms. In Fig.1, the upper panel shows the sediment column at successive times after sediment deposition (newly deposited layer). The greyscale values of the different layers enabled us to distinguish the newly deposited layer from the basal initial sediment. Indeed, the newly deposited layer(s) and the initial sediment were separated by a light-yellow layer above a discontinuous dark layer in both microcosms. These levels were part of the initial sediment. Throughout time, a lighter layer appeared, at the top of the newly deposited layers. The decrease in thickness of the newly deposited sediment layer (i.e. compaction) was greater in the OHV than in the FLV, as shown by the measurement of deposit thickness over time in the second panel of Fig. 1. Initially, the

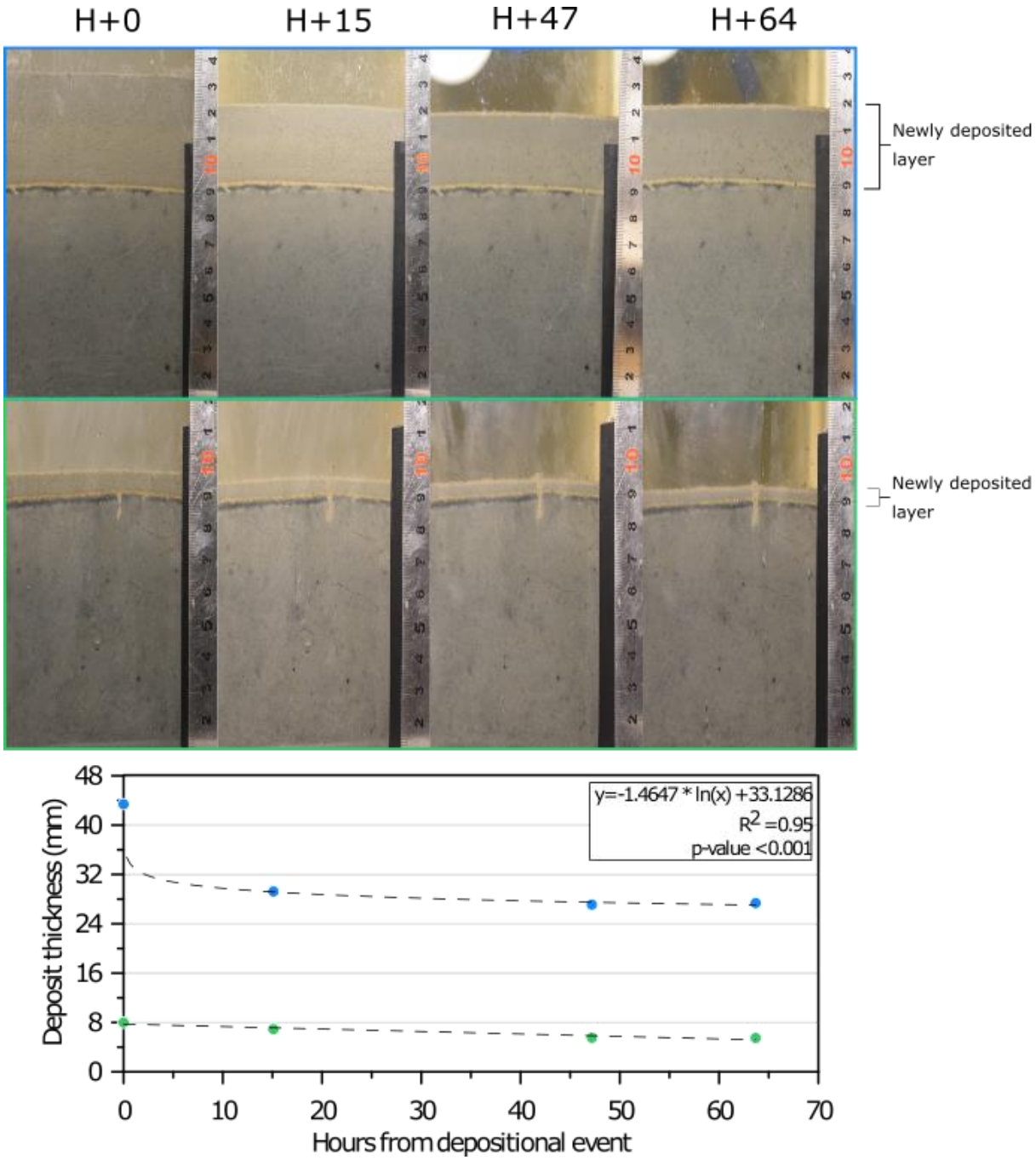

Figure 1: Compaction of the newly deposited layer over time in the "One-time high volume" (blue framed and blue dots) and in the "Frequent low volume" (green frame and green dots) microcosms. Upper panel is a compilation of pictures taken at several hours (0h, 15h, 47h and 64h) after the slurry input in the microcosms. Based on these pictures, the thickness of the new sediment layer was determined using greyscale profile analysis and plotted on the graph. The curve corresponds to the equation extracted from the OHV microcosm: deposit thickness = -1.4647 ln(h) + 33.1286.

deposit in the OHV was 43 mm thick, then thinned to 29 mm 15 h later. Then it stabilized at 27 mm 47 h after deposition. Meanwhile, the FLV presented an initial deposit of 8 mm compacted into a 5 mm layer after 64 h. After this period, the final thickness of the sediment deposits was stable.

In addition to sediment compaction analysis, porosity was also investigated using sediment cores sampled in each aquarium at each sampling time (18 h after sediment disturbance). The profiles displayed in Fig. 2 showed a relatively stable surface porosity ranging

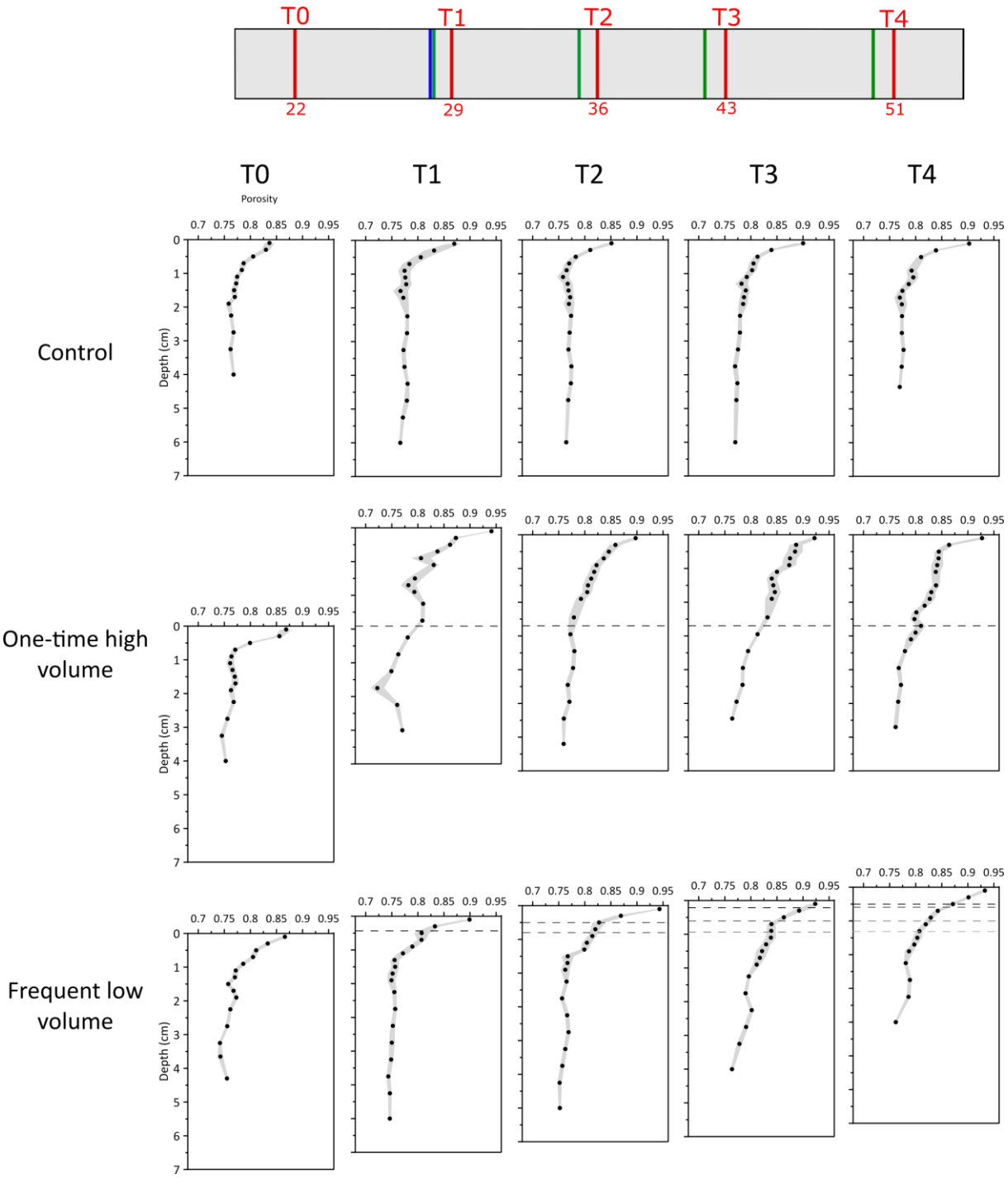

Figure 2: Porosity profiles for each sampling time and microcosm. The error associated with each porosity value is displayed by the grey colouring around the points. Depositional events are symbolized by dotted lines in the "One-time high volume" (OHV) and in the "Frequent low volume" (FLV) microcosms and are reported on the upper timescale as blue and green vertical lines respectively.

from 0.85 to 0.90. Below 2 cm depth, porosity stabilized at around 0.77 in each profile, with a similar decrease above this depth. Both disturbed microcosms, however, showed an increase in porosity in the newly deposited layers. The OHV microcosm showed an increase in surface porosity from 0.87 at T0 to 0.94, 18 h after the disturbance. All subsequent times displayed relatively stable porosity profiles with a maximum porosity of 0.92 which was higher than

stable conditions in the control microcosm. The FLV microcosm showed higher surface porosities at each sampling time after T0, always maintained by the addition of slurries 18 h before sampling. In all profiles, the uppermost 3 dots, corresponding to a 0.6 cm thick layer, were affected by unstable porosity conditions.

3.2 Oxygen sediment-water interface flux

Oxygen Penetration Depth (OPD) data were already described by Guilhermic et al. (2023). Here is presented a summary table of OPDs (Table 1) and an example of dissolved O_2 profile for the Control microcosm at T1 (Fig. 3) for which modelling was carried out. OPD for the O_2 profile presented in Fig.3 was 1 mm. A mean diffusive oxygen uptake (DOU) of 68.9 ± 4.4 mmol m^{-2} d^{-1} (n=8) was calculated based on modelled profiles.

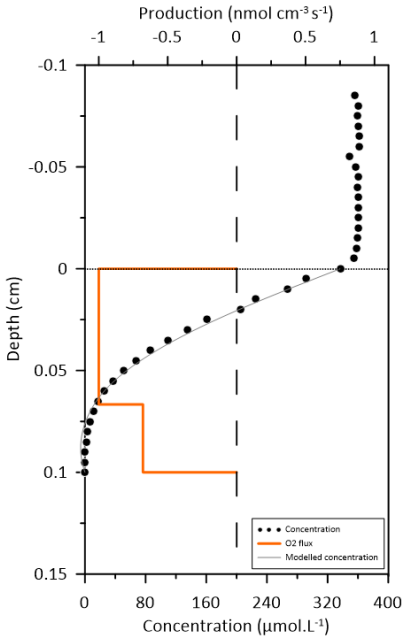

	Control			OHV			FLV		
	OPD	SD	nb of profiles	OPD	SD	nb of profiles	OPD	SD	nb of profiles
T0	1.62	0.18	10	1.36	0.13	8	1.78	0.13	6
T1	1.13	0.22	12	2.13	0.15	6	1.23	0.18	10
T2	1.29	0.18	14	1.68	0.31	13	1.25	0.15	13
T4	1.33	0.26	12	1.24	0.19	11	1.20	0.19	11

Table 1: Average oxygen penetration depth data in mm. Associated standard-deviation (SD) and number of profiles considered for mean OPD calculation.

Figure 3: Example of dissolved O_2 concentration profile in the control microcosm at T1. Black dots represent concentration data. The corresponding best-fit concentration profile, modelled with PROFILE software, is the grey line and the production/consumption zones are represented by the orange line and allowed to determine a diffusive oxygen uptake (DOU)

3.3 Inorganic nitrogen species

In the control microcosm, ammonium profiles showed concentrations below 50 µmol L^{-1} in the water column and maximum values of 800-1000 µmol L^{-1} in porewaters at 8 cm depth (Fig. 4). The observed increase in ammonium in the porewaters with depth was very similar for all the aquaria and times . The only exception was OHV T1, 18 h after the disturbance, where the ammonium profile showed the same concentrations in the water column and in the newly deposited sediment layer (~ 600 µmol L^{-1}), thus, below the previous SWI, distribution and concentrations were again similar to the other profiles of the other sampling times. The following week (OHV T2), ammonium profiles were back to the same distribution as for control.

With a few exceptions (FLV T3 and T4), nitrite profiles displayed higher concentrations in the water column than in porewaters, for all the aquaria at all sampling times. Indeed, within

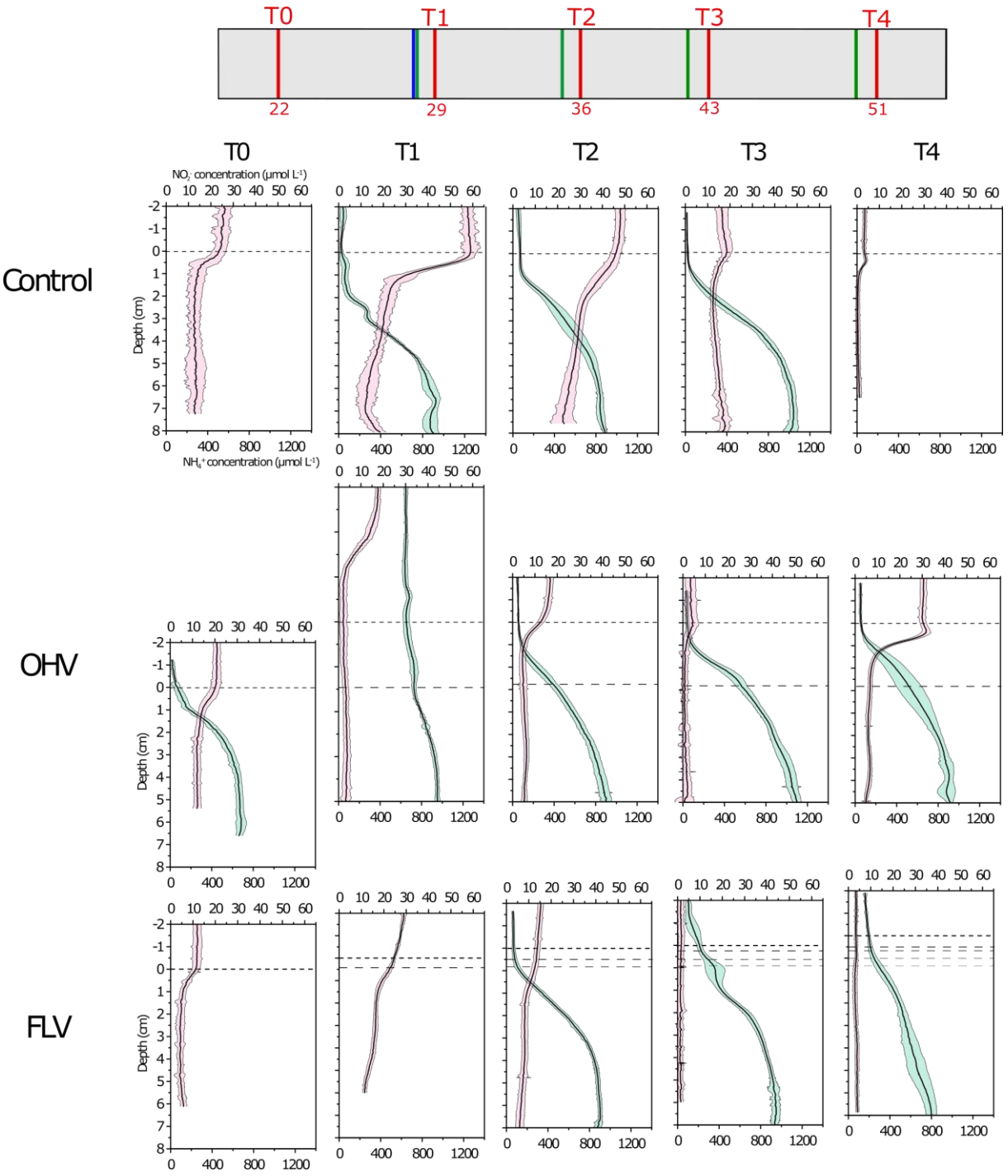

Figure 4: 1D extracted plots from 2D DET images of NO_2^- concentration (pink curve and standard deviation) and NH_4^+ concentration (green curve and standard deviation). 1D profiles were calculated using the average value of each pixel line of the nitrite and ammonium distribution images. Blue and green lines in the upper timeline correspond to "One-time high volume" microcosm (OHV) and to "Frequent low volume" microcosm (FLV) depositional events, respectively. Note the absence of data for ammonium concentrations in the control T0, T4 and FLV T0, T1.

the first centimetre of sediment, most profiles showed a decrease in concentration reaching a constant value until the deepest layers sampled. However, differences between microcosms were observed over time. In the control microcosm, at T0, the water column presented a nitrite concentration of 25 µmol L^{-1}, whereas it was 15 µmol L^{-1} below 1 cm depth in the sediment.

Between T0 and T1, the concentrations in the water column and in porewaters were more than twice as high as at T0. The depth of the decrease remained unchanged, so the gradient steepened in the upper most sediment centimetre. After this sampling time, the concentration in the water column decreased from 58 µmol L^{-1} at T1 to 4 µmol L^{-1} at T4. At this sampling time, the concentration below 1 cm depth in the sediment porewaters was close to 0 µmol L^{-1}. Within the uppermost centimetre, an increase in concentration of 5 µmol L^{-1} was observed. In the "One-time high volume" microcosm, the concentration 18 h after the sediment deposition event (T1 Fig. 4) was relatively constant in the lower water column and in the sediment, with values around 3 µmol L^{-1}. In the water column above -2.5 cm, nitrite concentration increased from 0 to 17 µmol L^{-1}. This was followed by a return to the usual profile at T2 (8 days after disturbance), with a decrease in concentration in the water column from 17 µmol L^{-1} to 6 µmol L^{-1} in the newly deposited layer and below. A decrease in concentration was also observed in the control between T2 and T3 (8 and 15 days after disturbance). However, the last sampling time showed concentrations in the water column of 30 µmol L^{-1} and an increase in nitrite concentrations in the porewater to 35 µmol L^{-1} at 0.7 cm depth. Below this zone, a decrease was observed until a constant concentration of 10 µmol L^{-1} was reached at 2 cm depth. In the "Frequent low volume" microcosm, the decrease in concentration from 28 µmol L^{-1} to 15 µmol L^{-1} occurred below the newly deposited 0.5 cm sediment layer. The same observation could be made at T2 with a lower concentration in the water column of 15 µmol L^{-1}. After this sampling time, subsequent profiles showed a constant concentration in the water column and porewaters of less than 5 µmol L^{-1}.

3.4 Manganese and iron reactive oxides

The profiles of particulate Mn and Fe extracted by ascorbate (Mn_{asc} and Fe_{asc}) showed maximum concentrations in the upper half centimetre in the control microcosm at each sampling time, with values between 10 and 16 µmol g^{-1} and 60 and 95 µmol g^{-1} for Mn_{asc} and Fe_{asc} respectively (Fig. 5). Nevertheless, before the disturbances (T0), Mn_{asc} (between 3 and 8 µmol g^{-1}) and Fe_{asc} (between 35 and 60 µmol g^{-1}) concentrations in the upper half centimetre were lower than for the following sampling times in the control microcosm. 18h after the single perturbation in the OHV microcosm (T1), the Mn_{asc} and Fe_{asc} profiles displayed no enrichment in the first half centimetre but concentrations similar to those at depth (2.5 µmol g^{-1} and 25 µmol g^{-1} for Mn_{asc} and Fe_{asc} respectively). However, Mn_{asc} and Fe_{asc} enrichments were observed within a 1 cm layer around the previous SWI (4 µmol g^{-1} for Mn_{asc} and 30 µmol g^{-1} for Fe_{asc}). In subsequent sampling times (T2 to T4), maximum Mn_{asc} and Fe_{asc} concentrations were found again at the top of the core, below the new SWI, and gradually enriched to a concentration at T4 similar to that at T0 (7.5 µmol g^{-1} and 65 µmol g^{-1} for Mn_{asc} and Fe_{asc} respectively). In the FLV microcosm, after the first perturbation in T1, the first 2 mm sediment layer sampled below the interface showed concentrations similar to those at depth (2.5 µmol g^{-1} for Mn_{asc} and 25 µmol g^{-1} for Fe_{asc}), while the underlying layers (0.2 to 0.6 cm), around the former SWI showed higher concentrations (5 µmol g^{-1} for Mn_{asc} and 40 µmol g^{-1} for Fe_{asc}). A similar enrichment around the newly buried SWI was observed for Mn_{asc} at the other sampling times, all of which followed an induced disturbance ~18 h earlier (T2 to T4). In the Mn_{asc} profiles of T3 FLV and T4 FLV, a slight decrease in concentrations was visible in both sediment layers deposited after the first two first perturbations (T1 and T2). For Fe_{asc}, enrichment at the interface between the initial sediment and the sediment layer deposited at T1 was still present at T2, and no new

enrichment was visible at the level of the newly buried SWI. At T3 and T4, Fe_{asc} enrichment moved upwards to the SWI buried a week earlier.

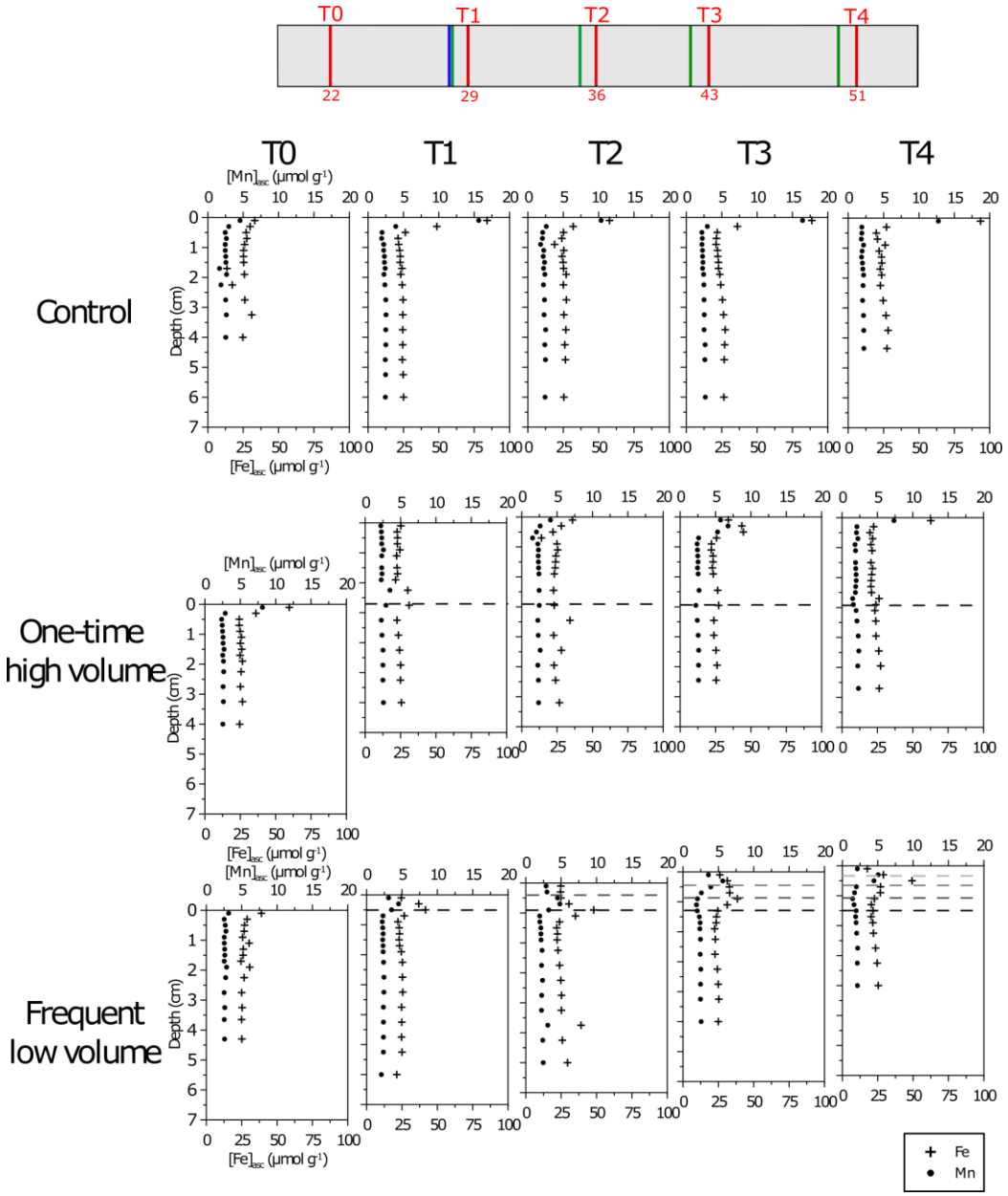

Figure 5: Manganese (Mn_{asc}) and iron (Fe_{asc}) extracted by ascorbate in each aquarium and at each sampling time. The error associated with each measurement was less than or equal to 3% for both Mn_{asc} and Fe_{asc} and is not represented here being smaller than the size of the points.

3.5 Dissolved manganese

Dissolved manganese (Mn_d) concentrations are presented in Fig. 6. At T0, before the disturbances, all aquaria showed increasing concentrations in the first centimetre of sediment and concentrations that stabilized at greater depths around 70-80 µmol L^{-1}. For T1, T2 and T3, the control microcosm displayed profiles with increasing Mn_d concentration up to a maximum of 90-110 µmol L^{-1} around 2-3 cm depth. At T1 in the OHV microcosm, 18h after disturbance,

a sharp peak (maximum concentration of 110 µmol L^{-1}) located at the former SWI was observed in the Mn_d profile. Below this peak, the profile had a similar shape to that observed in the

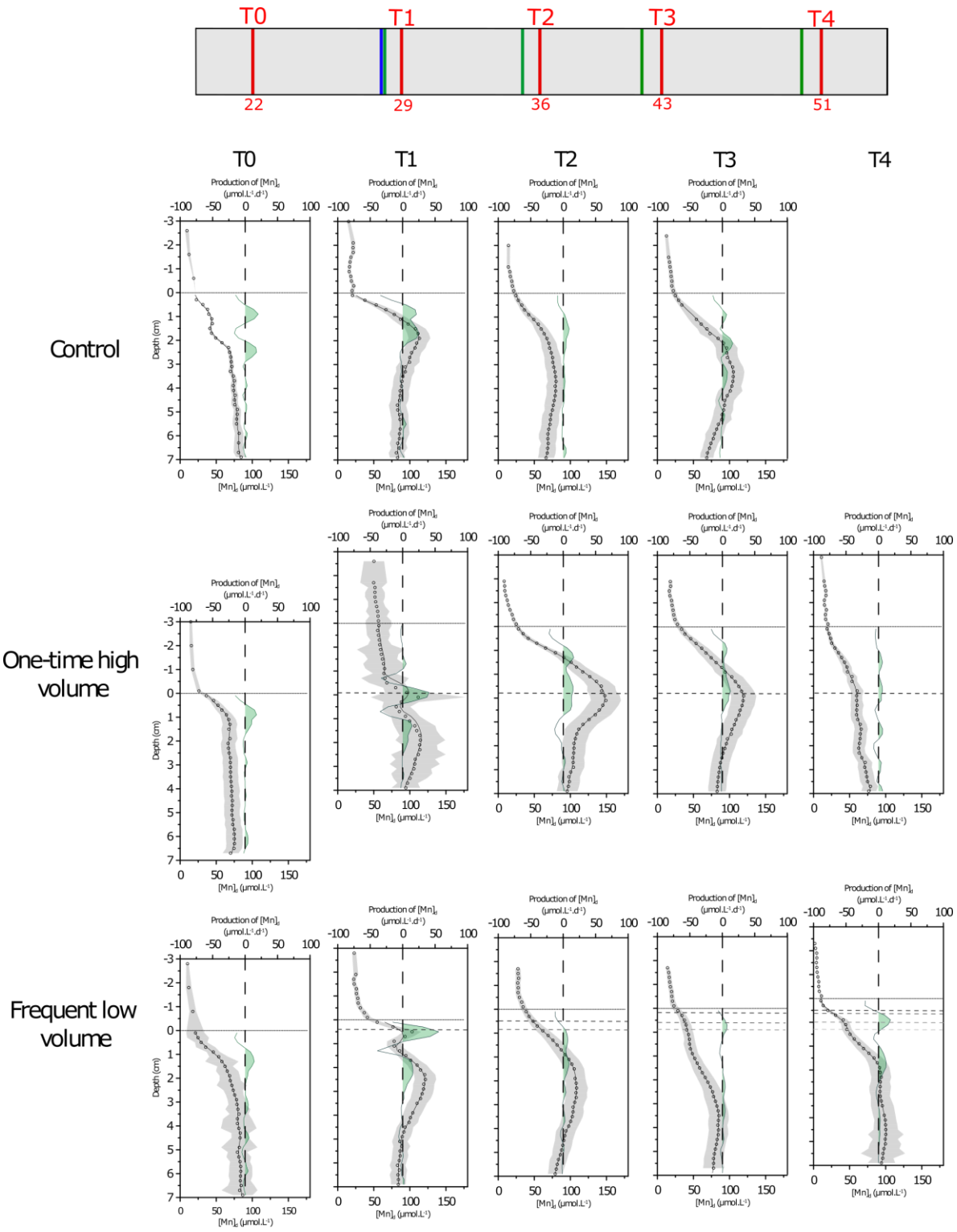

Figure 6: Dissolved Mn concentrations in the sediment porewaters and in the water column (empty circles) and associated error (grey colouring around the profile). Green profiles correspond to production rates (positive when coloured red) calculated using the modelled concentration profile (solid line). New sediment layers are symbolized by dashed lines. Each plot is aligned with the original SWI. No data is available for T4 control due to a problem with the DET 1D at the time of sampling.

control. Between 0 and 2 cm depth, porewater concentrations were constant and similar to those of the water column around 60 µmol L^{-1}. The Mn_d profile at T2 (8 days after disturbance) OHV showed a much wider peak around the previous SWI with a concentration of up to 150 µmol L^{-1} at 2.9 cm depth. Subsequent sampling times showed a profile with a decrease in the maximum peak (120 µmol L^{-1}) for T3 (15days after disturbance) and a disappearance of this peak for the last T4 profile.

A similar post-disturbance pattern was observed for the FLV microcosm (Fig. 6). Indeed, a sharp Mn_d peak (100 µmol L^{-1}) was visible at a depth of 0.5 cm, corresponding to the previous SWI. Below this depth, the profile had a similar shape to those observed in the control. A week later, the previous peak disappeared and no Mn_d enrichment was observed at the newly buried SWI. At sampling times T3 and T4, as observed for T2, no sharp peak was formed at the newly buried SWI. Concentration profiles showed a slight increase in concentrations in the sediment layer deposited at T1, and below stabilized concentrations around 90 µmol L^{-1} at depth.

3.6 Dissolved iron

At T0, dissolved Fe profiles (Fe_d) showed relatively low concentrations with an increase in the first 1-2 cm depth and stabilization at around 150 µmol L^{-1} at depth (Fig. 7). In the control microcosm, steep concentration gradients were established at T1, 18h after disturbance. From 0.7 cm to 2 cm depth, Fe_d concentrations increased to a maximum of 400 µmol L^{-1} at 2 cm depth. Below this peak, a gradual decrease with depth was observed down to 200 µmol L^{-1} at the bottom. The next two sampling times (T2 and T3, 8 and 15 days after disturbance) showed similar depths of for maximum concentrations. They were located at a depth of 2 cm at T2 and at 2.5 cm for T3, with concentrations of 300 µmol L^{-1} for T2 and 400 µmol L^{-1} for T3. In OHV T1, no Fe_d enrichment was observed at the level of the newly buried SWI, but on the contrary a slight decrease in concentrations was visible. A peak of 400 µmol L^{-1} was observed below the previous SWI at 4.5 cm depth, corresponding to the depth of the maximum observed in the control samples. Fe_d concentration was similar within the newly deposited sediment layer and in the water column with a value of 100 µmol L^{-1}. At T2 and T3, the peak concentration was located at the previous SWI with values of 600 µmol L^{-1} and became slightly wider at T3. At T4, the Fe_d profile showed a much lower peak concentration at the buried interface with a value of 320 µmol L^{-1}. For the “Frequent low volume” microcosm, the T1 and T2 Fe_d profiles displayed a maximum concentration at depths (2.5 cm and 3.5 cm respectively) corresponding to the maximum concentration values observed for the control microcosm. In the following weeks (T3 and T4), an increase in Fe_d concentration was visible just below the sediment deposits and in the first deposit (0.6 to 1.5 cm depth and 1 to 2 cm depth at T3 and T4 respectively). Deeper, the profile was relatively constant with depth.

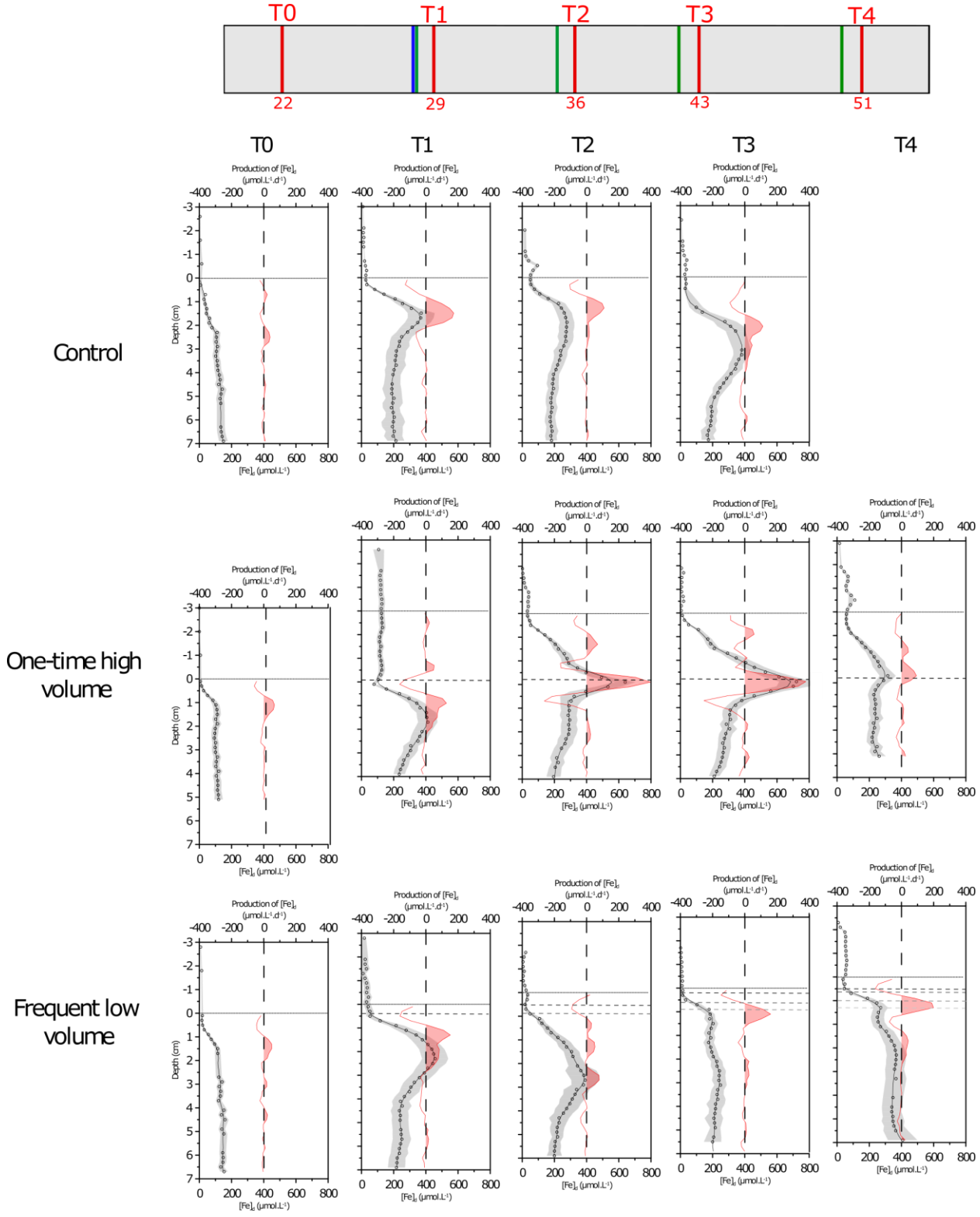

Figure 7: Dissolved Fe concentrations in sediment porewaters and in the water column (empty circles) and associated error (grey colouring around the profile). Red profiles correspond to production rates (positive when coloured red) calculated using the modelled concentration profile (solid line). New sediment layers are symbolized by dashed lines. Each plot is aligned with the original SWI. No data is available for T4 control due to a problem with the DET 1D at the time of sampling.

4 Discussion

4.1 Equilibration of redox conditions in the control

Previous experimental studies (Hansen and Blackburn, 1991, 1992; Porter et al., 2006; Chaillou et al., 2007) reported a period of 2-3 weeks for equilibration of redox gradients in sediments. Accordingly, a recovery time of 21 days was observed for our experiment to allow stabilisation of all redox layers and establishment of initial concentrations in the three microcosms. However, high densities of sieve-concentrated foraminifera were added to the sediment surface of all aquaria on day 7 in order to study the response of these faunas to depositional events in this experiment too (Guilhermic et al., 2023). This added layer is visible in the photos in Fig. 1 as a coupled light and dark grey layer at 40 mm depth in H+0h. The dark colour of this layer suggests anaerobic degradation of OM concentrated by sieving (e.g., fecal pellets) and introduced with the addition of foraminifera at day 7. At day 21 (T0) before disturbances, OPDs of all three aquaria were higher than OPDs of the control at T1 and thereafter (Table 1). As a result of the addition of OM, oxygen in the sediment was further consumed, as it is the first oxidant used in microbial oxidation of OM.

Ammonium, produced by OM remineralization, showed relatively similar profiles between T0 of all treatments and the control microcosm throughout the experiment, with a usual vertical distribution characterised by an increase of concentrations with depth as OM is mineralised through suboxic and anoxic respiration pathways (Fig. 4). The high concentration gradient below ~0.5 cm depth probably supported an ammonium efflux towards the overlaying water, explaining the relatively high concentrations in the water column despite regular water renewal. Under oxic conditions, nitrification can occur (Rysgaard et al., 1994) and ammonium is oxidized to nitrite and then to nitrate by specialized bacteria (Hsiao et al., 2014). Nitrite concentration profiles presented the same distribution pattern at T0 for all the aquaria and in the control microcosm for subsequent sampling times (T1 to T3) (Fig. 4). Thus, high nitrite concentrations measured in the water column and in the oxic part of sediments were probably due to ongoing nitrification with available oxygen. Lower concentrations in the sediment, with a sharp decrease around 1 cm depth below the oxic layer, most likely marked a denitrification zone, as this process generally occurs in sediment layers where oxygen is scarce (i.e., <5 μmol L^{-1}; Devol et al., 2008). While the distribution was similar between the different sampling times between T0 and T4, the concentrations were not. An increase in nitrite concentration in the water column and in the sediment was measured between T0 and T1 (~25 μmol L^{-1} at T0 and ~58 μmol L^{-1} at T1 in the water column, Fig. 4). Subsequently, nitrite concentration decreased between T2 and T4 (~48 μmol L^{-1} at T2, ~16 μmol L^{-1} at T3 and ~4 μmol L^{-1} at T4). Deeper, below the oxic zone, although the denitrification process lowered nitrite concentration in the first centimetre, concentrations remained relatively high at depth between T0 and T3. This can probably be explained by molecular diffusion transport from the water column, where concentrations were very high, to the sediment. At T4, 51 days after disturbance, water oxygenation and OPD were still stable in the control microcosm, but low nitrite concentrations in the water column and a weak production zone in the oxic sediments were observed. Below this zone, nitrite disappeared. Ammonium profiles and their gradients generating diffusive fluxes towards the oxic zone and the water column were relatively stable between T0 and T4 in the control microcosm, which cannot explain the variations in nitrite concentrations. Another explanation may be that the regular renewal of aquarium water was not sufficient to prevent an increase in nitrite concentrations between T0 and T1 (Guilhermic et al., 2023). Indeed, as

previously discussed, OM added to the sediment on day 7, at the same time as the foraminifera, induced sustained remineralisation, enhancing ammonium production and very possibly nitrite and then nitrate production.

At T0, vertical distributions of porewater Mn_d and Fe_d in the three aquaria were similar, whereas they differed from those subsequently observed between T1 and T3 for the control microcosm that was not subjected to sediment disturbance (Fig 3, Fig. 6 and Fig. 7). Modelling of Mn_d and Fe_d production from concentration profiles at T0 (Fig. 6 and 7) did not show well-identified and more intense production zones in the sediment, as it was the case for the control profiles between T1 and T3. At those times, Mn_d and Fe_d were produced by the dissolution of reactive Mn and Fe oxides and diffused upwards where they were re-oxidized, leading to an accumulation of reactive oxides in the surface layer (not observed at T0 where no Mn_d and Fe_d production was modelled). In that way, Mn and Fe redox equilibration in sediments appeared to be delayed by 7 days. Similar porosity profiles were observed throughout the whole experiment in the Control microcosm therefore no incidence of the physical state of the sediment column can be considered to explain those changes. This was most likely related to the addition of the foraminiferal and OM mixture at day 7. Nevertheless, thereafter, geochemical profiles in the control microcosm appeared relatively similar between T1, T2 and T3 contrary to the other treatments undergoing transient state. At T4, reactive Mn and Fe oxides remained stable with enrichment at the surface, as in previous sampling times. As described in diagenesis sequencing by Froelich et al. (1979) and Burdige (2007), this surface enrichment of diagenetically sustained Mn and Fe-oxides marks a diffusion of dissolved material towards the

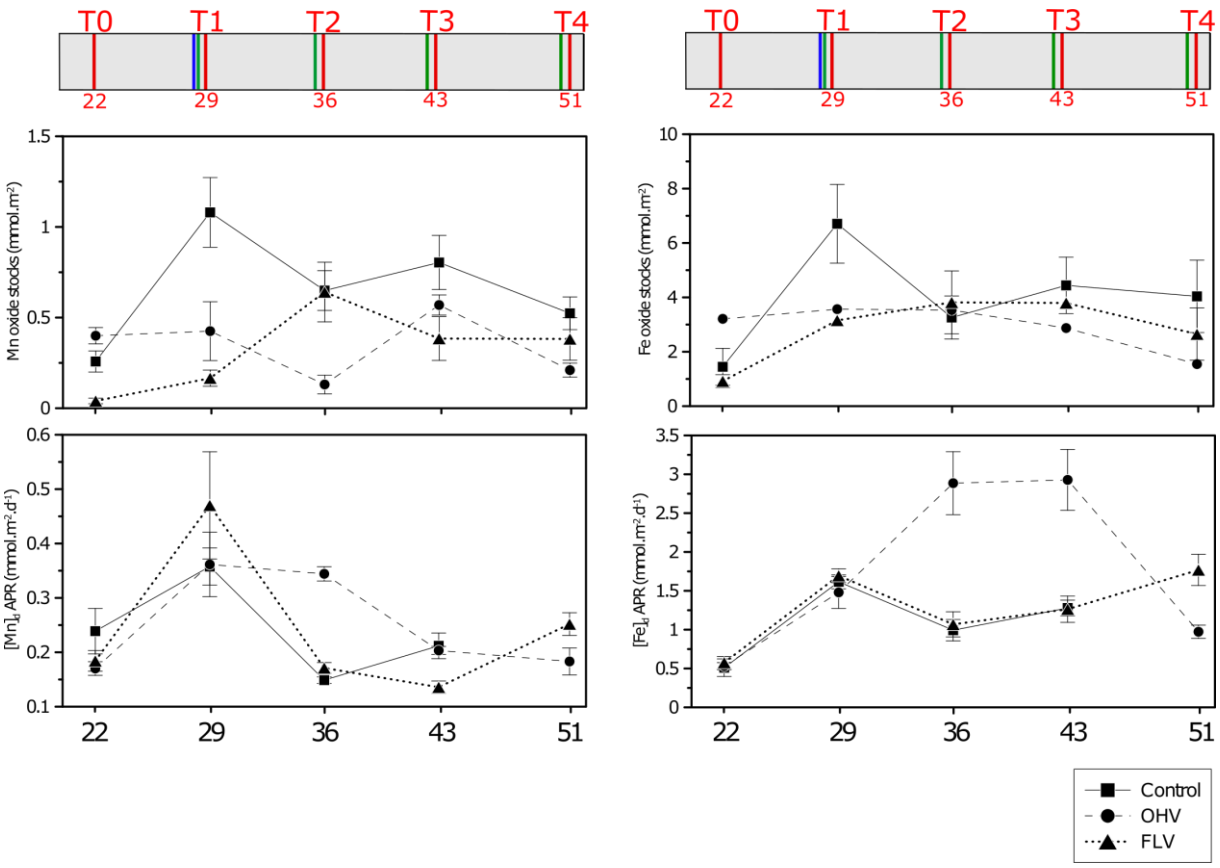

Figure 8: Temporal representation (T0 to T4) of calculated stocks of Mn_{asc} and Fe_{asc} and modelled Apparent Production Rates (APR) of dissolved Mn and Fe.

oxic layer. Thereafter, precipitation of this material occurs when no disturbance interferes with the diffusion of dissolved oxygen in the sediment also observed in the experimental study of Chaillou et al. (2007).

All redox fronts showed unsteady distributions in the sediment column and no similar states between microcosms at T0 mostly due to the late addition of surface extra organic matter and meiofauna, as demonstrated in the previous paragraphs. Therefore, T1 would be a more accurate sampling time in the Control microcosm for further comparison of disturbed conditions in the OHV et FLV microcosms.

4.2 Dynamics of sediment properties and redox conditions after the depositional events

4.2.1 Compaction rate of deposited sediments

Sediment compaction observed over the 3 days after the addition of the slurry in the "One-time high volume" microcosm followed a logarithmic relation. Therefore, compaction decreased with time and the final deposit thickness was 27 mm 47h after the addition of the slurry (Fig. 1). An experiment by Clemo et al. (2022) investigated the compaction of muddy sediment after reworking, suspension and redeposition. They reported a duration of 34h before the 5 cm-thick resuspended sediment reached the initial height. Our observations are consistent with these results, if we consider that the pictures were taken 15 and 47h after the disturbance and there were no intermediate images between these two times. After 15h, 93% of the total compaction had already occurred. Consequently, in the OHV, the newly deposited layer showed a stable compaction for the remaining of the experiment.

Porosity profiles always displayed an exponential decrease with depth in each microcosm at each sampling time (Fig. 2). Nevertheless, for all microcosms at T0 and for the control microcosm, porosity decreased strongly in the first centimetre (values between 0.83 and 0.90 in the most superficial sediment layer) due to compaction and then remained stable at depth (around 0.75). In the OHV microcosm, at T1 (18 hours after disturbance), porosity was highest at the surface (0.94) and then decreased gradually through the thickness of the deposition layer. For subsequent sampling times, the porosity profile remained stable compared to T1. The disturbance thus permanently increased sediment porosity in the 2.7 cm corresponding to the deposition layer during the experimental time. Compared to pre-disturbance conditions T0, the deposition event therefore generated a new stable state remaining during the whole experiment where the porosity in surface sediment was superior. This same observation was made by Chaillou et al. (2007) after the addition of a 7-cm thick muddy deposit. They observed that porosity within the newly deposited layer did not vary (0.90 at the surface) between one day after the disturbance to 295 days after. Moreover, Clemo et al. (2022) pointed out the importance of biological community structure in compaction and porosity of surface sediment. The addition of meiofauna at the surface of the sediment in our experiment therefore generated a different sediment physical state than the one observed after the addition of defaunated sediment explaining a sediment compaction completed, yet different porosity conditions. In the FLV microcosm, regular sediment depositions also steadily increased surface porosity the same way as in the OHV treatment. In contrast, the first 1.5 cm deposit layer (T1) showed regular compaction with a decrease in porosity up to T4. According to the compaction of the thin deposit after the addition of the sediment at T1, we can assume that the porosity stable state

was quickly achieved at each sampling time. However, the repetition of sediment additions reactivated a short transient state of this compaction and stabilisation of the porosity.

4.2.2 Oxygen dynamics at the original and new sediment-water interfaces

Prior to its insertion into the OHV and FLV microcosms, the turbid solution (slurry) was oxygenated by air bubbling. However, within the 6 to 12 h after the disturbance, DET-1D and DET-2D gels in the OHV microcosm recorded high concentrations of reduced dissolved species as Mn_d, Fe_d and ammonium in the turbid water column. For nitrite, concentrations were very low or null in the sediment and in the water column 2 cm above the new interface. The picture taken 15 h after the disturbance for the OHV microcosm showed that the water column was still turbid near the new sediment-water interface, whereas it was transparent again in the upper part where nitrite concentrations were higher (Fig. 4). Despite the oxygenation of the slurry before the insertion into the microcosms, these results suggest that an absence or very low concentrations of oxygen prevailed in the turbid water column during settling, favouring the presence of reduced chemical species and inhibiting nitrification.

Following the disturbance, the flux of dissolved O_2 from the water column towards the sediment was therefore interrupted and the oxygen initially present in the sediment was consumed, as evidenced by the absence of dissolved oxygen at the depth of the original SWI during O_2 profiling 48 h after the depositional event. A time of 103 ± 16 s to remove all oxygen was calculated on the base of the sediment O_2-demand estimated by the model on the control microcosm at T1, which was 68.9 ± 4.4 mmol m^{-2} d^{-1} (Fig. 3). During an experimental study simulating the deposition of a gravity layer, Chaillou et al. (2007) detected no dissolved O_2 at the original interface 35 minutes after the deposition. The estimated time to remove oxygen in our experiment is much shorter, but the lower sediment O_2-demand (5.5 mmol m^{-2} d^{-1}) and higher OPD (7 mm) in Chaillou et al. (2007) experiment may explain this difference.

Two days (48 h) after the deposition events, no turbidity was detected in the water and measurements showed that oxygen already diffused within the newly deposited sediment layer. In the OHV microcosm, OPD even deepened from 1.36 ± 0.13 mm at the previous SWI to 2.13 ± 0.15 mm depth (Table 1) at the new one. This observation was also made previously by Cathalot et al. (2010) and Pastor et al. (2018), who studied the impact of floods on carbon recycling at the outlet of the Rhône River. Cathalot et al. (2010) associated the OPD deepening with a decrease in dissolved oxygen uptake by the sediment most likely due to a drop in benthic community respiration, as previously reported also by Ferguson et al. (2004) in the Australian subtropical Brunswick estuary. This hypothesis is supported by the observations on benthic foraminifera carried out on our microcosm (Guilhermic et al., 2023), that highlighted the delay in upward migration induced by the 27 mm thick deposit in the OHV microcosm. OPD recovery after the disturbance in the OHV microcosm was observed at T4, which means that it took a maximum of 22 days (Fig. 3). In the FLV microcosm, where benthic foraminifera migrated rapidly following the rhythm of thin (2.7 mm) depositional events (Guilhermic et al., 2023), the OPD was similar to that of the control microcosm (Fig. 3). The difference between the treatments suggest that the disturbance induced by high loads of abrupt deposits may have a major impact on redox fronts re-equilibration and life position recovery from benthic faunas living associated to them. The penetration of oxygen in the newly deposited sediment layer is mostly due to molecular diffusion through porosity and its further stabilisation in time can be partly affected by respirating organisms. The study of foraminiferal recovery by Guilhermic et al. (2023) clearly showed that the migration of individuals through the thick deposit in the OHV

took a longer time (between one and two weeks) than in the FLV, where the individuals retrieved their life position within a few hours.

4.2.3 Nitrogen species evolution

For the "One-time high volume", ammonium profile measured 18 h after the sedimentary disturbance (T1) showed that concentration in the water column was high and equivalent to that observed in the porewaters of the new deposit (around 600 µmol L-1, Fig.4). Below the previous SWI, the ammonium profile showed an enrichment similar to the one observed in the control microcosm. One week later (T2) in OHV, the ammonium profile was re-established, similar to the control. In the flood events documented by Pastor et al. (2018), a disruption at the original SWI of the ammonium profile after sediment deposition during a flood was also observed. In this study, 26 days after flooding, the ammonium profile was similar to the pre-flooding profile, but there was no intermediate sampling to better constrain this recovery time. Our experiment results, therefore, allows to highlight that less than one week is required to reestablish stable ammonium concentration gradients within a newly deposited sediment layer. In the experimental setup with turbidite sediments of Chaillou et al. (2007), the reestablishment of stable enrichment gradients took between 33 and 75 days after the disturbance with a maximum bottom concentration of 220 µmol L^{-1}. This information further supports the different behaviour and recovery of different environments according to their concentration in OM fuelling geochemical cycling. This is furthermore supported by the observation of transient states in the Saguenay fjord and Capbreton turbidite sediments showing oligo- to mesotrophic conditions by Deflandre et al. (2002) and Anschutz et al. (2002) respectively. In our experiment, the sediment (recovered in the Bourgneuf tidal bay) was considered eutrophic after analysis of Biopolymeric Carbon concentration showing values of 39.8 mg g^{-1} (following the classification of Bianchelli et al., 2008; Fabiano et al., 1995). Therefore, high OM content measured in our three microcosms could have induced more intense biogeochemical processes leading to a faster recovery, as modelled by Nmor et al. (2022) in the case of low-thickness sediment deposit event. In the "Frequent low volume" microcosm, at T1, 18 h after sediment perturbation, ammonium concentrations in the water column and in freshly deposited sediment were still higher than in the control microcosm, but lower than in T1 OHV. Pictures taken before sampling showed that water in the FLV was less turbid than the water column in T1 OHV. Lower quantities of sediment were added in the FLV treatment than in the OHV treatment, enabling faster complete deposition of setting particle and thus faster recovery of the ammonium profile in the newly deposited layer after each event displaying a supposed consumption gradient.

At T1, 18 h after the perturbation, in the "One-time high volume", the nitrite profile showed concentrations around 17 µmol L^{-1}, in the water column, up to 5 cm above the SWI (Fig.4). Further down, nitrite decreased to reach zero at 2 cm above SWI. In the sediments, no nitrite was detected in the freshly deposited sediment layer, while in the initial sediment, nitrite was measured at an average concentration of 3 µmol L^{-1}. However, when the water column became transparent again, oxygenation was probably sufficient to allow nitrification to occur and restore nitrite concentration in the water column. At T2, 7 days after the disturbance, the nitrite profile was similar to the one at T0, with concentrations around 17 µmol L^{-1} in the water column and a denitrification zone at around 1 cm depth. At T3, 14 days later, nitrite distribution and concentrations were like the in T4 control, with less nitrite in the water column (around 4 µmol L^{-1}) and no nitrite below the denitrification zone in sediments. At T4, 21 days after the

single massive deposit, a nitrification zone in the sediment can be identified by the presence of a nitrite concentration peak at a depth of 0.75 cm, which induced a nitrite flux towards the water column, probably explaining the higher concentrations in the water, around 30 µmol L^{-1}. This observation supports a relatively stronger or more active nitrification process than denitrification which was dominant during the whole experiment. A similar balance between those two processes has already been studied in the Arcachon bay (France) (Fernandes et al., 2016). In the FLV treatment, 18h after the perturbation (T1), nitrite concentrations were lower than in the T1 control microcosm, probably because denitrification process promoted during particle settling was shorter. Nevertheless, this enhancement of denitrification was recurrent, as the perturbation was repeated weekly, and after 14 days (T3), nitrite concentration was zero.

Fast recovery of ammonium gradients after sediment deposition was rapidly achieved within a few days after the disturbance in the OHV treatment. The nitrogen cycle in the sediment is highly linked to the dissolved oxygen dynamic (Burdige, 2007; Froelich et al., 1979) which showed a shorter reestablishment of a surface oxic layer.

Fast recovery of ammonium and nitrite gradients have been observed in both treatments. Moreover, we evidenced that sediment deposition events enhanced denitrification during its transient state. However, the stability of nitrite gradients was not observed through time due to water replacement in the microcosms, and consequent lowering of sediment denitrification front position and weakening of intensity allowed the observation of the establishment of a nitrification front by the end of the experiment, 21 days after disturbance.

4.2.4 Manganese and iron remobilization

In the OHV treatment, 18 h after the disturbance (T1), Mn_{asc} and Fe_{asc}, enriched at the previous SWI were buried (Fig. 5). Mn_{asc} began to dissolve, as shown in Fig. 6 with a Mn_d peak associated with a zone of intense, localized production, separated from the production zone previously established in the pre-disturbance (initial) sediment. At that sampling time T1, no new Mn_{asc} or Fe_{asc} enrichment was visible at the new SWI (T1 OHV, Fig.5). Strong dissolution of buried Fe_{asc} was measured over the following two weeks (T2 and T3) with a sharp Fe_d concentration peak centred on the previous SWI, inducing strong Fe_d production (T2 and T3 OHV, Fig. 7). Another zone of Fe_d production was observed at around 1 cm depth, while the Mnd production zone extended into the new deposited sediment (Fig. 6). The new oxic surface layer allowed the oxidation of diffused Mn_d and Fe_d from the underlying production zones, accordingly with the results of the experiment conducted with Capbreton canyon sediments after an 8-9 cm sediment disturbance by Chaillou et al.(2007). Apparent production rates (APR) showed high values of dissolved Mn at T1 and T2 and subsequently (T3 and T4) lower values comparable to the control, while Fe_d increased at T2 and T3 and decreased at T4 (Fig.8). Furthermore, three weeks after the deposit (T4), the Mn_d production zone around the former SWI was no longer visible, indicating complete dissolution of the buried Mn_{asc} enrichment, while the Fe_d production zone was still visible (T4 OHV, Fig. 7). In natural environments, Deflandre et al. (2002) observed Mn_d and Fe_d productions at the former SWI 3 weeks after a flood generating a 10 cm-thick deposit in the Saguenay Fjord. Anschutz et al. (2002) also measured Mn_d and Mn_{asc} and Fe_{asc} enrichment at the old SWI 4 months after an 18 cm-thick turbidite deposit in the Capbreton canyon. The lower Mn and Fe reactive oxide stocks in our microcosms (~100 and 60 times lower for Mn_{asc} and Fe_{asc} compared to Anschutz et al. (2002)) may explain this difference, together with the organic carbon richness of the sediments.

In the FLV treatment, a slight enrichment in Mn_{asc} and Fe_{asc} at the base of the freshly deposited sediment was already visible 18 h after the perturbation (T1 FLV, Fig. 5) associated with strong Mn_d production located around the former SWI (Fig.6). Deeper Mn_d and Fe_d production zones were also visible, corresponding to previously established zones in the initial sediment. Subsequent samplings (T2 to T4), after the weekly disturbances, showed a similar pattern for Mn_{asc} with a maximum enrichment around 5 µmol g^{-1} observed at the base of the most recent sediment deposit (Fig. 5). Mn APR showed slightly higher values at T1 than in subsequent sampling times (Fig. 8). At T2, Mn_d production decreased whereas the production zone was located more continuously below the new sedimentary deposit compared to the profile at T1. At T3 and T4, a Mn_d production zone was established within the first layer of sediment deposited at T1, attesting to the remobilization of Mn from this first sediment deposit two and three weeks later (Fig. 6). At T2, Fe_d showed consumption zones located in the deposit of the previous week (Fig. 7), corresponding to a slight enrichment visible in Fe_{asc} (Fig. 5). Also, at T2, a Fe_d production zone was established below the first sediment deposit, showing remobilization of Fe from the former SWI one week after the first disturbance. Then, from T3, the Fe_d production zone also extended into the first sediment layer deposited at T1 (Fig. 7), testifying to the start of Fe remobilization in the first sediment layer two weeks after its deposition, as for Mn. However, Fe APR did not show higher values than the control (Fig. 8).

In the OHV treatment, a delay was observed between the remobilization of Mn and Fe at the former SWI (Fig. 6 and 7), as previously discussed in other studies with transient state diagenesis (Abril et al., 2010; Aller, 2004; Deflandre et al., 2002; Pastor et al., 2018; Thibault de Chanvalon et al., 2016; van de Velde et al., 2018). Nevertheless, high concentrations of Mn_d and Fe_d were measured in the turbid water column and freshly deposited sediment 18 h after the disturbance, whereas the Fe_d profile showed strong consumption centred on the former SWI associated with a strong production of Mn_d. Some studies showed that Fe_d can be oxidized with manganese oxides (Ehlert et al., 2014; Postma, 1986; Schaefer et al., 2017). In the FLV treatment, 18 h after the first disturbance, the same pattern was observed (Fig. 7). However, subsequent disturbances seemed to induce a less significant remobilization of Mn and Fe (Fig. 8) compared to OHV, with constant oxide stocks but a more widespread distribution at depth, within recent sediment deposits, and a shift between the Fe_{asc} peak, which was at a greater depth than the Mn_{asc} peak, compared to the control or the OHV treatment. This vertical distribution, which is classically described for electron acceptors in sediments, seems to be induced here by the more rapid remobilization of Mn relative to Fe under the effect of frequent low sedimentary disturbances.

4.3 A proxy for recent sediment deposition

The results of this experimental work on the biogeochemical response of sediments after a single or repeated sediment deposition events show that the distributions of porewater dissolved oxygen and inorganic nitrogen recover more rapidly than manganese and iron, which have particulate and dissolved redox phases. The concomitant presence of layers enriched in reactive oxides at anoxic depths and the ongoing Mn_d and Fe_d production at the same depths reveal a transient state following sediment depositions without erosion (Fig. 10). Mn and Fe cycles can therefore help to identify former SWI buried by sediment deposits with no previous erosion. The speed of Mn and Fe relaxation, and thus the recording in sediments of these instabilities, can nevertheless vary according to several parameters such as temperature, which regulates bacterial activity and kinetics of chemical reactions, OM content, which induces redox

reactions and thus metal cycles in sediments, porosity and grain-size, metal content in the sediment column and the deposition thickness (Nmor et al., 2022).

After the transient state, the re-establishment of redox fronts within the newly deposited layer includes the diagenetic enrichment layer of reactive manganese and iron oxides at the new sediment surface associated with an underlying Mn_d and Fe_d production zone. Intermediate transient states can provide insights in post-deposition temporality, particularly if dissolved manganese production is ongoing without dissolved iron production, or vice versa.

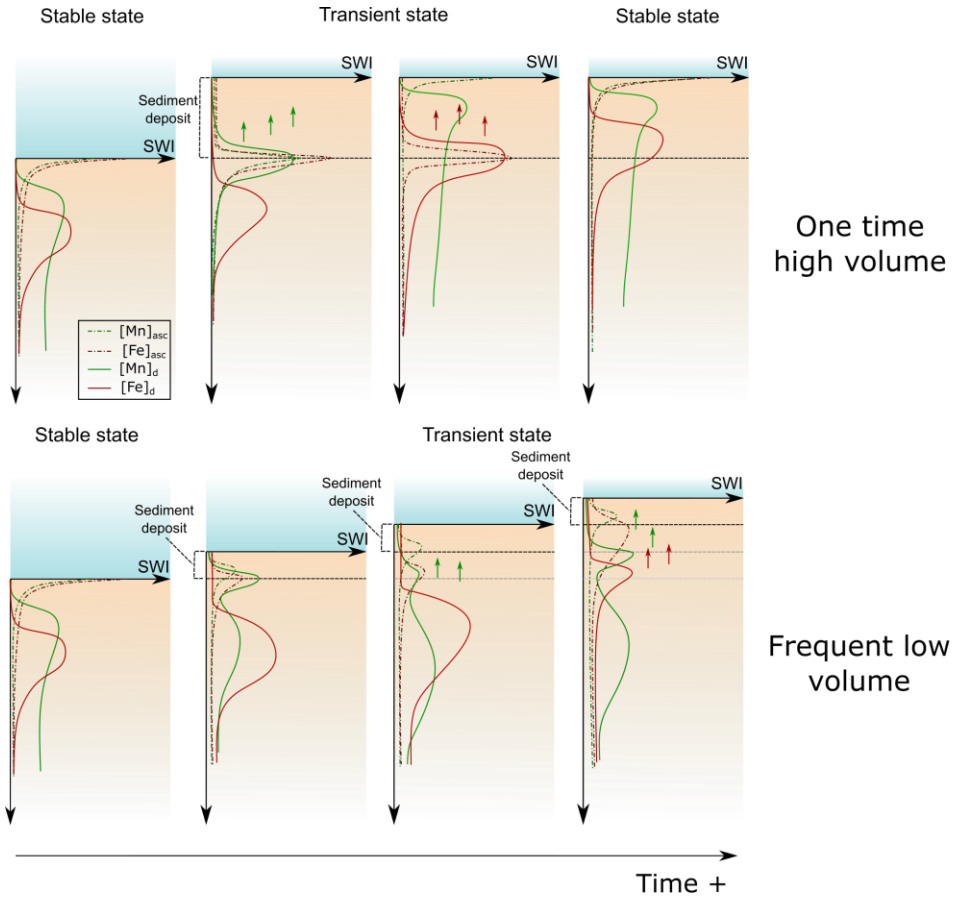

Figure 9: Schematic view of manganese and iron relaxation after an intense sedimentation deposition event and frequent thin layers of sediment.

Frequent thin sediment deposits can be detected by an enrichment in both Mn and Fe reactive oxides within the sediment column, at different depths (Fig. 9) and not at the surface. Repeated deposition events bury the previous SWI, therefore and according to all parameters ruling sediment reactivity, disconnection between Mn and Fe cycles becomes more and more important with time with accumulated successive depositions.

It is not the case for a single massive sedimentation event. Indeed, the ongoing dissolution of Mn-oxides may enrich the surface layer by precipitation while the buried Fe reactive layer provides dissolved material to be diffused. One week appeared to be enough for Mn dynamics to reach stable conditions but most likely not for Fe cycling.

5 Conclusion

This experimental work allowed to specify the short-term temporal dynamics of some redox chemical species in sediments subjected to unique or frequent sediment deposition events ranging in thickness from a few millimetres to a few centimetres. Frequent thin sediment deposits proved to have no impact on dissolved O_2 penetration depth measured two days after deposition, while OPD showed a deepening of 0.8 mm after a single but thick (2.7 cm) sediment deposition event, up to 15 days later.

The distribution of nitrite showed that during the particle settling in the water column, denitrification seemed to have been enhanced, resulting in very low nitrite concentrations in the microcosm subjected to recurrent disturbances. Ammonium gradients were observed to reestablish within a few days after the intense and unique sedimentation event.

Reactive Mn oxides enriched below the previous sediment-water interface were reduced in both sediment disturbance conditions when the environment became anoxic following burial. This fast response visible with Mn_d contrasts with the dynamics of Fe species. Indeed, the reduction of reactive Fe oxides was observed within a one-week delay compared to Mn. Recurrent sediment disturbances induced a rapid remobilization of Mn relative to Fe with a broad distribution of reactive oxides at depth, and a shift in depth between the Mn and Fe peaks. The presence of layers enriched in reactive oxides at anoxic depths associated with the production of dissolved Mn and Fe can help identify previous SWI just buried by sedimentary deposits and can therefore be used as an indicator of sedimentary instabilities.

The use of coastal sediments with a high organic matter content in the experiment fuelled redox processes and the fast relaxation of redox species, allowing to document in detail the transient state generated by sediment disturbance until a new steady state was reached. The experimentally evidenced model of geochemical transient states using Mn and Fe could be applied in natural environments to identify ecosystems stressed by high sedimentation events coupled with ecological observations. In coastal environments, further modelling using environmental parameters (OM content, T°C…) to constrain quantitative variables, may result in calculating the sediment deposition temporality. Finally, it may be a future alternative to radiochronology analysis sometimes difficult to be applied due to elemental conservation or high sediment accumulation rate areas.

Author contributions:

CG, AM, MPN and HH designed the experiment; CG, AM and MPN performed the sampling procedures and measurements; CG analysed the data; CG and AM wrote the original draft, AM, MPN, HH and EM reviewed and edited the paper.

Acknowledgments:

We thank Miroiterie Nogentaise Inc. for providing custom-made aquaria following all our requirements. We also thank Dr. Aubin Thibault de Chanvalon for providing R scripts for Mn and Fe production calculations. The first author is grateful for the valuable help of Damien Le Moigne for contributing at the daily monitoring of the experiment and for the pictures of the aquaria. The authors also thank the bachelor students whose efficiency sped up the particulate sample analysis. In addition, we thank Eric Bénéteau for ICP-AES data acquisition.

Financial support:

The CNRS INSU LEFE CYBER programme (Fluid Envelopes and the Environment) supported our research by funding the BEGIN project (PI: Maria Pia Nardelli). This research is part of a PhD project (first author) funded by the French Ministry of Scientific Research and Innovation and by Angers University.

References:

Abril, G., Commarieu, M.-V., Etcheber, H., Deborde, J., Deflandre, B., Živađinović, M. K., Chaillou, G., and Anschutz, P.: In vitro simulation of oxic/suboxic diagenesis in an estuarine fluid mud subjected to redox oscillations, Estuarine, Coastal and Shelf Science, 88, 279–291, https://doi.org/10.1016/j.ecss.2010.04.003, 2010.

Aller, R. C.: Conceptual models of early diagenetic processes: The muddy seafloor as an unsteady, batch reactor, J Mar Res, 62, 815–835, https://doi.org/10.1357/0022240042880837, 2004.

Alve, E.: Colonization of new habitats by benthic foraminifera: a review, Earth-Science Reviews, 46, 167–185, https://doi.org/10.1016/S0012-8252(99)00016-1, 1999.

Anschutz, P., Zhong, S., Sundby, B., Mucci, A., and Gobeil, C.: Burial efficiency of phosphorus and the geochemistry of iron in continental margin sediments, Limnol. Oceanogr., 43, 53–64, https://doi.org/10.4319/lo.1998.43.1.0053, 1998.

Anschutz, P., Jorissen, F. J., Chaillou, G., Abu-Zied, R., and Fontanier, C.: Recent turbidite deposition in the eastern Atlantic: Early diagenesis and biotic recovery, Journal of Marine Research, 60, 835–854, https://doi.org/10.1357/002224002321505156, 2002.

Anschutz, P., Dedieu, K., Desmazes, F., and Chaillou, G.: Speciation, oxidation state, and reactivity of particulate manganese in marine sediments, Chemical Geology, 218, 265–279, https://doi.org/10.1016/j.chemgeo.2005.01.008, 2005.

Berg, P., Risgaard-Petersen, N., and Rysgaard, S.: Interpretation of measured concentration profiles in sediment porewater, Limnology and Oceanography, 43, 1500–1510, 1998.

Berner, R. A.: Early Diagenesis: A Theoretical Approach, Geological Magazine, 118, 330–331, https://doi.org/10.1017/S0016756800035962, 1981.

Bianchelli, S., Gambi, C., Pusceddu, A., and Danovaro, R.: Trophic conditions and meiofaunal assemblages in the Bari Canyon and the adjacent open slope (Adriatic Sea), Chemistry and Ecology, 24, 101, 2008.

Bolam, S. G.: Burial survival of benthic macrofauna following deposition of simulated dredged material, Environ Monit Assess, 181, 13–27, https://doi.org/10.1007/s10661-010-1809-5, 2011.

Bolliet, T., Jorissen, F. J., Schmidt, S., and Howa, H.: Benthic foraminifera from Capbreton Canyon revisited; faunal evolution after repetitive sediment disturbance, Deep Sea Research Part II: Topical Studies in Oceanography, 104, 319–334, https://doi.org/10.1016/j.dsr2.2013.09.009, 2014.

Budillon, F., Vicinanza, D., Ferrante, V., and Iorio, M.: Sediment transport and deposition during extreme sea storm events at the Salerno Bay (Tyrrhenian Sea): comparison of field data with numerical model results, Nat. Hazards Earth Syst. Sci., 6, 839–852, https://doi.org/10.5194/nhess-6-839-2006, 2006.

Burdige, D. J.: Geochemistry of Marine Sediments, in: Geochemistry of Marine Sediments, Princeton University Press, https://doi.org/10.1515/9780691216096, 2007.

Cathalot, C., Rabouille, C., Pastor, L., Deflandre, B., Viollier, E., Buscail, R., Gremare, A., Treignier, C., and Pruski, A.: Temporal variability of carbon recycling in coastal sediments influenced by rivers: assessing the impact of flood inputs in the Rhoˆne River prodelta, 2010.

Chapter 3: Effects of frequent or massive sediment supplies on sediment redox stability: a microcosm simulation

Chaillou, G., Anschutz, P., Dubrulle, C., and Lecroart, P.: Transient States in Diagenesis Following the Deposition of a Gravity Layer: Dynamics of O2, Mn, Fe and N-Species in Experimental Units, Aquat Geochem, 13, 157–172, https://doi.org/10.1007/s10498-007-9013-0, 2007.

Clemo, W. C., Giles, K. D., and Dorgan, K. M.: Biological influences on coastal muddy sediment structure following resuspension, Limnology & Oceanography, 67, 2466–2482, https://doi.org/10.1002/lno.12213, 2022.

D'Angelo, A., Giglio, F., Miserocchi, S., Sanchez-Vidal, A., Aliani, S., Tesi, T., Viola, A., Mazzola, M., and Langone, L.: Multi-year particle fluxes in Kongsfjorden, Svalbard, Biogeosciences, 15, 5343–5363, https://doi.org/10.5194/bg-15-5343-2018, 2018.

Davies, A. G., Robins, P. E., Austin, M., and Walker-Springett, G.: Exploring regional coastal sediment pathways using a coupled tide-wave-sediment dynamics model, Continental Shelf Research, 253, 104903, https://doi.org/10.1016/j.csr.2022.104903, 2023.

Davison, W. and Zhang, H.: In situ speciation measurements of trace components in natural waters using thin-film gels, Nature, 367, 546–548, https://doi.org/10.1038/367546a0, 1994.

Deflandre, B., Mucci, A., Gagné, J.-P., Guignard, C., and Sundby, B. jørn: Early diagenetic processes in coastal marine sediments disturbed by a catastrophic sedimentation event, Geochimica et Cosmochimica Acta, 66, 2547–2558, https://doi.org/10.1016/S0016-7037(02)00861-X, 2002.

Duros, P., Silva Jacinto, R., Dennielou, B., Schmidt, S., Martinez Lamas, R., Gautier, E., Roubi, A., and Gayet, N.: Benthic foraminiferal response to sedimentary disturbance in the Capbreton canyon (Bay of Biscay, NE Atlantic), Deep Sea Research Part I: Oceanographic Research Papers, 120, 61–75, https://doi.org/10.1016/j.dsr.2016.11.012, 2017.

Ehlert, K., Mikutta, C., and Kretzschmar, R.: Impact of Birnessite on Arsenic and Iron Speciation during Microbial Reduction of Arsenic-Bearing Ferrihydrite, Environ. Sci. Technol., 48, 11320–11329, https://doi.org/10.1021/es5031323, 2014.

Fabiano, M., Danovaro, R., and Fraschetti, S.: A three-year time series of elemental and biochemical composition of organic matter in subtidal sandy sediments of the Ligurian Sea (northwestern Mediterranean), Continental Shelf Research, 15, 1453–1469, https://doi.org/10.1016/0278-4343(94)00088-5, 1995.

Ferguson, A., Eyre, B., and Gay, J.: Nutrient cycling in the sub-tropical Brunswick estuary, Australia, Estuaries, 27, 1–17, https://doi.org/10.1007/BF02803556, 2004.

Fernandes, S. O., Javanaud, C., Michotey, V. D., Guasco, S., Anschutz, P., and Bonin, P.: Coupling of bacterial nitrification with denitrification and anammox supports N removal in intertidal sediments (Arcachon Bay, France), Estuarine, Coastal and Shelf Science, 179, 39–50, https://doi.org/10.1016/j.ecss.2015.10.009, 2016.

Fossile, E., Nardelli, M. P., Howa, H., Baltzer, A., Poprawski, Y., Baneschi, I., Doveri, M., and Mojtahid, M.: Influence of modern environmental gradients on foraminiferal faunas in the inner Kongsfjorden (Svalbard), Marine Micropaleontology, 173, 102117, https://doi.org/10.1016/j.marmicro.2022.102117, 2022.

Froelich, P. N., Klinkhammer, G. P., Bender, M. L., Luedtke, N. A., Heath, G. R., Cullen, D., Dauphin, P., and Blaynehartman, D. Hammond.: Early oxidation of organic matter in pelagic sediments of the eastern equatorial Atlantic: suhoxic diagenesis, Geochimica et Cosmochimica Acta, 43, 1075–1090, https://doi.org/0016-7037 79,0701-1075SO?.M) 0, 1979.

Griess, P.: Bemerkungen zu der Abhandlung der HH. Weselsky und Benedikt „Ueber einige Azoverbindungen", Ber. Dtsch. Chem. Ges., 12, 426–428, https://doi.org/10.1002/cber.187901201117, 1879.

Guilhermic, C., Nardelli, M. P., Mouret, A., Le Moigne, D., and Howa, H.: Short-term response of benthic foraminifera to fine sediment depositional events simulated in microcosm, Biogeosciences Discussions, 1–46, https://doi.org/10.5194/bg-2023-31, 2023.

Hansen, L. and Blackburn, T.: Aerobic and anaerobic mineralization of organic material in marine sediment microcosms, Mar. Ecol. Prog. Ser., 75, 283–291, https://doi.org/10.3354/meps075283, 1991.

Chapter 3: Effects of frequent or massive sediment supplies on sediment redox stability: a microcosm simulation

Hansen, L. S. and Blackburn, T. H.: Mineralization budgets in sediment microcosms: Effect of the infauna and anoxic conditions, FEMS Microbiology Letters, 102, 33–43, https://doi.org/10.1111/j.1574-6968.1992.tb05793.x, 1992.

Haughton, P., Davis, C., McCaffrey, W., and Barker, S.: Hybrid sediment gravity flow deposits – Classification, origin and significance, Marine and Petroleum Geology, 26, 1900–1918, https://doi.org/10.1016/j.marpetgeo.2009.02.012, 2009.

Hodgkins, R., Cooper, R., Wadham, J., and Tranter, M.: Suspended sediment fluxes in a high-Arctic glacierised catchment: implications for fluvial sediment storage, Sedimentary Geology, 162, 105–117, https://doi.org/10.1016/S0037-0738(03)00218-5, 2003.

Hodson, A., Gurnell, A., Tranter, M., Bogen, J., Hagen, J. O., and Clark, M.: Suspended sediment yield and transfer processes in a small High-Arctic glacier basin, Svalbard, Hydrol. Process., 12, 73–86, https://doi.org/10.1002/(SICI)1099-1085(199801)12:1<73::AID-HYP564>3.0.CO;2-S, 1998.

Hsiao, S. S.-Y., Hsu, T.-C., Liu, J. -w., Xie, X., Zhang, Y., Lin, J., Wang, H., Yang, J.-Y. T., Hsu, S.-C., Dai, M., and Kao, S.-J.: Nitrification and its oxygen consumption along the turbid Chang Jiang River plume, Biogeosciences, 11, 2083–2098, https://doi.org/10.5194/bg-11-2083-2014, 2014.

Hulot, V., Metzger, E., Thibault de Chanvalon, A., Mouret, A., Schmidt, S., Deflandre, B., Rigaud, S., Beneteau, E., Savoye, N., Souchu, P., Le Merrer, Y., and Maillet, G. M.: Impact of an exceptional winter flood on benthic oxygen and nutrient fluxes in a temperate macrotidal estuary: Potential consequences on summer deoxygenation, Frontiers in Marine Science, 10, 2023.

Jézéquel, D., Brayner, R., Metzger, E., Viollier, E., Prévot, F., and Fiévet, F.: Two-dimensional determination of dissolved iron and sulfur species in marine sediment pore-waters by thin-film based imaging. Thau lagoon (France), Estuarine, Coastal and Shelf Science, 72, 420–431, https://doi.org/10.1016/j.ecss.2006.11.031, 2007.

Kostka, J. E. and Luther, G. W.: Partitioning and speciation of solid phase iron in saltmarsh sediments, Geochimica et Cosmochimica Acta, 58, 1701–1710, https://doi.org/10.1016/0016-7037(94)90531-2, 1994.

Krom, M. D., Davison, P., Zhang, H., and Davison, W.: High-resolution pore-water sampling with a gel sampler, Limnology and Oceanography, 39, 1967–1972, https://doi.org/10.4319/lo.1994.39.8.1967, 1994.

Łepkowska, E. and Stachnik, Ł.: Which Drivers Control the Suspended Sediment Flux in a High Arctic Glacierized Basin (Werenskioldbreen, Spitsbergen)?, Water, 10, 1408, https://doi.org/10.3390/w10101408, 2018.

Meslard, F., Bourrin, F., Many, G., and Kerhervé, P.: Suspended particle dynamics and fluxes in an Arctic fjord (Kongsfjorden, Svalbard), Estuarine, Coastal and Shelf Science, 204, 212–224, https://doi.org/10.1016/j.ecss.2018.02.020, 2018.

Mestdagh, S., Bagaço, L., Braeckman, U., Ysebaert, T., De Smet, B., Moens, T., and Van Colen, C.: Functional trait responses to sediment deposition reduce macrofauna-mediated ecosystem functioning in an estuarine mudflat, Biogeosciences, 15, 2587–2599, https://doi.org/10.5194/bg-15-2587-2018, 2018.

Metzger, E.: Two-dimensional ammonium distribution in sediment pore waters using a new colorimetric diffusive equilibration in thin-film technique, 10, 2019.

Metzger, E., Viollier, E., Simonucci, C., Prévot, F., Langlet, D., and Jézéquel, D.: Millimeter-scale alkalinity measurement in marine sediment using DET probes and colorimetric determination, Water Research, 47, 5575–5583, https://doi.org/10.1016/j.watres.2013.06.038, 2013.

Metzger, E., Thibault de Chanvalon, A., Cesbron, F., Barbe, A., Launeau, P., Jézéquel, D., and Mouret, A.: Simultaneous Nitrite/Nitrate Imagery at Millimeter Scale through the Water–Sediment Interface, Environ. Sci. Technol., 50, 8188–8195, https://doi.org/10.1021/acs.est.6b00187, 2016.

Mucci, A. and Edenborn, H. M.: Influence of an organic-poor landslide deposit on the early diagenesis of iron and manganese in a coastal marine sediment, Geochimica et Cosmochimica Acta, 56, 3909–3921, https://doi.org/10.1016/0016-7037(92)90005-4, 1992.

Mucci, A., Boudreau, B., and Guignard, C.: Diagenetic mobility of trace elements in sediments covered by a flash flood deposit: Mn, Fe and As, Applied Geochemistry, 18, 1011–1026, https://doi.org/10.1016/S0883-2927(02)00207-X, 2003.

Mulder, T. and Cochonat, P.: Classification of offshore mass movements, Journal of sedimentary research, 66, 43–57, 1996.

Nmor, S. I., Viollier, E., Pastor, L., Lansard, B., Rabouille, C., and Soetaert, K.: FESDIA (v1.0): exploring temporal variations of sediment biogeochemistry under the influence of flood events using numerical modelling, Geoscientific Model Development, 15, 7325–7351, https://doi.org/10.5194/gmd-15-7325-2022, 2022.

Pastor, L., Rabouille, C., Metzger, E., Thibault de Chanvalon, A., Viollier, E., and Deflandre, B.: Transient early diagenetic processes in Rhône prodelta sediments revealed in contrasting flood events, Continental Shelf Research, 166, 65–76, https://doi.org/10.1016/j.csr.2018.07.005, 2018.

Porter, E. T., Owens, M. S., and Cornwell, J. C.: Effect of Sediment Manipulation on the Biogeochemistry of Experimental Sediment Systems, Journal of Coastal Research, 226, 1539–1551, https://doi.org/10.2112/05-0478, 2006.

Postma, G.: Classification for sediment gravity-flow deposits based on flow conditions during sedimentation, Geol, 14, 291, https://doi.org/10.1130/0091-7613(1986)14<291:CFSGDB>2.0.CO;2, 1986.

Revsbech, N. P.: An oxygen microsensor with a guard cathode, Limnology and Oceanography, 34, 474–478, https://doi.org/10.4319/lo.1989.34.2.0474, 1989.

Rodrigues, S., Hernández-Molina, F. J., Fonnesu, M., Miramontes, E., Rebesco, M., and Campbell, D. C.: A new classification system for mixed (turbidite-contourite) depositional systems: Examples, conceptual models and diagnostic criteria for modern and ancient records, Earth-Science Reviews, 230, 104030, https://doi.org/10.1016/j.earscirev.2022.104030, 2022.

Rysgaard, S., Risgaard-Petersen, N., Niels Peter, S., Kim, J., and Lars Peter, N.: Oxygen regulation of nitrification and denitrification in sediments, Limnol. Oceanogr., 39, 1643–1652, https://doi.org/10.4319/lo.1994.39.7.1643, 1994.

Savitzky, Abraham. and Golay, M. J. E.: Smoothing and Differentiation of Data by Simplified Least Squares Procedures., Anal. Chem., 36, 1627–1639, https://doi.org/10.1021/ac60214a047, 1964.

Schaefer, M. V., Handler, R. M., and Scherer, M. M.: Fe(II) reduction of pyrolusite (β-MnO2) and secondary mineral evolution, Geochem Trans, 18, 7, https://doi.org/10.1186/s12932-017-0045-0, 2017.

Thibault de Chanvalon, A., Mouret, A., Knoery, J., Geslin, E., Péron, O., and Metzger, E.: Manganese, iron and phosphorus cycling in an estuarine mudflat, Loire, France, Journal of Sea Research, 118, 92–102, https://doi.org/10.1016/j.seares.2016.10.004, 2016.

van de Velde, S., Van Lancker, V., Hidalgo-Martinez, S., Berelson, W. M., and Meysman, F. J. R.: Anthropogenic disturbance keeps the coastal seafloor biogeochemistry in a transient state, Sci Rep, 8, 5582, https://doi.org/10.1038/s41598-018-23925-y, 2018.

Włodarska-Kowalczuk, M., Pawłowska, J., and Zajączkowski, M.: Do foraminifera mirror diversity and distribution patterns of macrobenthic fauna in an Arctic glacial fjord?, Marine Micropaleontology, 103, 30–39, https://doi.org/10.1016/j.marmicro.2013.07.002, 2013.

Wolanski, E. and Gibbs, R.: Resuspension and clearing of dredge spoils after dredging, Cleveland Bay, Australia, Water Environment Research, 64, 910–914, https://doi.org/10.2175/WER.64.7.9, 1992.

Yücel, M., Luther, G. W., and Moore, W. S.: Earthquake-induced turbidite deposition as a previously unrecognized sink for hydrogen sulfide in the Black Sea sediments, Marine Chemistry, 121, 176–186, https://doi.org/10.1016/j.marchem.2010.04.006, 2010.

Supplementary Chapter 3

Figure S1 : 2D NO_2^- concentration mapping

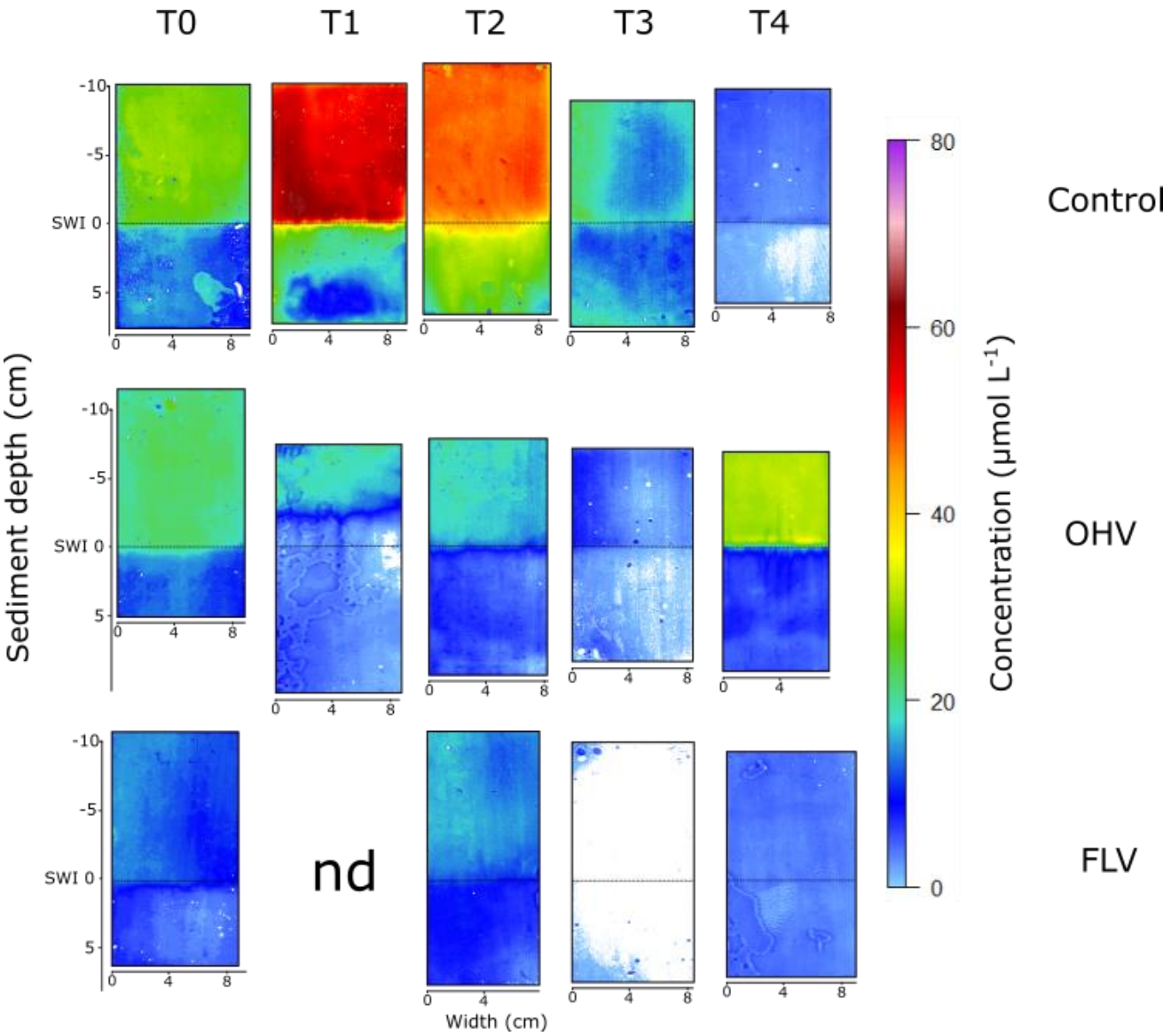

Figure S2 : 2D NH_4^+ concentration mapping

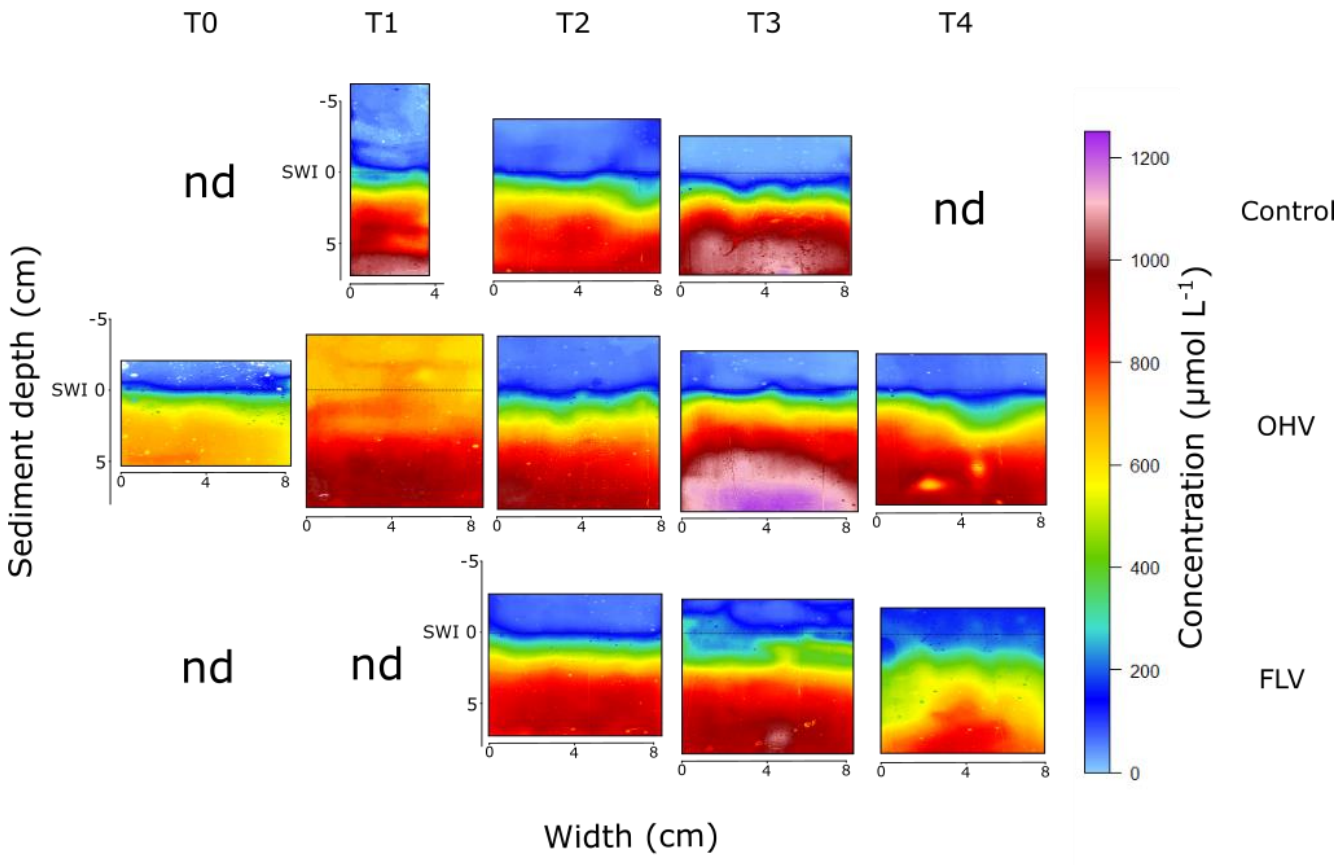

Nota bene on the experimental part:

A microcosm setup with sediment and foraminifera sampled in the Kongsfjorden in May 2021 and August 2021, respectively, was run with the same experimental conditions and protocol. It took place over two months, September to November 2021. But, after data analysis, we considered that the results obtained were not reliable enough to be presented in this manuscript, for the following reasons. The sampled foraminifera suffered from the travel conditions while they were brought back to France and stored too long before the starting of the experiment, resulting in a drastic collapse of abundance. Thus, the number of individuals injected in the microcosm was most likely too low. Unfortunately, as well, geochemical measurements were untrustful because too closed to the detection limits of our methods in addition to several sampling failures.

Environmental study of Kongsfjorden

Chapter 4

Environmental context in Kongsfjorden during May and August 2021

C. Guilhermic[*1], A. Mouret[1], H. Howa[1], A. Pusceddu[2], A. Baltzer[3], M.P. Nardelli[1]

[1] Université Angers, Nantes Univ., Le Mans Univ, CNRS, LPG, Laboratoire de planétologie et géosciences, UMR CNRS 6112, F-49000 Angers, France
[2]Department of Life and Environmental Sciences, University of Cagliari, 09126 Cagliari, Italy
[3]LETG, UMR CNRS 6554, University of Nantes, Campus du Tertre, 44312 Nantes Cedex 3, France

Preamble :

The purpose of this chapter is to display environmental parameters data collected during the two sampling missions in May and August 2021. Mainly, physicochemical measurements in the water column were performed by CTD casts and sediment grain-size and organic matter measurements were made on interface sediment cores.

Seasonal dynamic of these parameters will allow us to understand environmental variability of Kongsfjorden regarding hydrology and organic matter export from the water column to the benthic realm. In addition to a discussion of their own dynamic, these parameters will be of major importance in the understanding of processes and observations highlighted in the next chapters upon sediment redox gradient stability and foraminiferal response to seasonality.

This chapter is not destined to be published as presented. As the next chapters will use data presented here, it was chosen to present it only once here. The relevant environmental data will be included in further publications of next chapters.

1 Introduction

The aim of this chapter is to provide the holistic environmental context prevailing in May and August 2021 (referred as Spring and Summer campaigns in the manuscript) in the inner part of Kongsfjorden. After reviewing the literature on the physical conditions of the fjord, the new data acquired during this thesis are presented, including CTD measurements in the water column, grain-size analysis and organic matter content of surface sediments (0-5cm) measured at 4 stations distributed between 2 and 10 km from the Kronebreen tidewater glacier front. This information enables us to describe the environmental gradients generated seasonally by the melting of the Kronebreen glacier and the resulting sedimentary instabilities. In the next chapters, the studied ecological or biogeochemical processes will be related to these environmental gradients.

2 Study area

2.1 Geographical and geological settings

Kongsfjorden is a high latitude fjord (79°N, 12°E) located on the western coast of Spitsbergen, the largest island in the Svalbard archipelago (Fig. 1). Svalbard is located between the Arctic Ocean in the north, the Barents Sea in the south and the Fram Strait in the west. Kongsfjorden geomorphology is the result of continental glacier melting cycles through time. It is 350 m deep at the mouth and gradually shallows towards the fjord's head. Only a partial sill is present at fjord entrance, but a shallower inner sill is located near the Lovénøyane islands (Fig.1a, about 20 m water depth) (Halbach et al., 2019; Howe et al., 2003). Five tidewater glaciers flow into Kongsfjorden: Blomstrandbreen, Conwaybreen, Kongsbreen, Kronebreen and Kongsvegen (Fig.1). The last two share the same terminus between the southern coast and the Colletthøgda formation at fjord's head (Fig. 1a; Halbach et al., 2019). The Kronebreen tidewater glacier drains an ice catchment of approximately 530 km^2. Glacial erosion of the watershed bedrock remains the main supply of sediment to the fjord. Bedrock under Kronebreen glacier consists of dolomites, limestones and shale formations (Dallmann, 2015). Sediment discharge mostly originates from tidewater glacier creep and subglacial rivers that deliver erosion detrital products from different areas of the catchment to the fjord (Svendsen et al., 2002; Trusel et al., 2010; D'Angelo et al., 2018; Fig. 1a, 1b). In addition, land-terminating glaciers also erode their basal substrate. As their front is located on land, Austre and Midtre Lovénbreen glaciers develop relatively short, braided river systems passing through moraine fields and ending up in delta formations on the southern coast of the fjord (Bourriquen et al., 2016). Depending on the glacier watersheds, erosion of the various basal rocks results in the input of siliciclastic and/or carbonate particles into the fjord (***Chapter 1;*** Dallmann, 2015; D'Angelo et al., 2018).

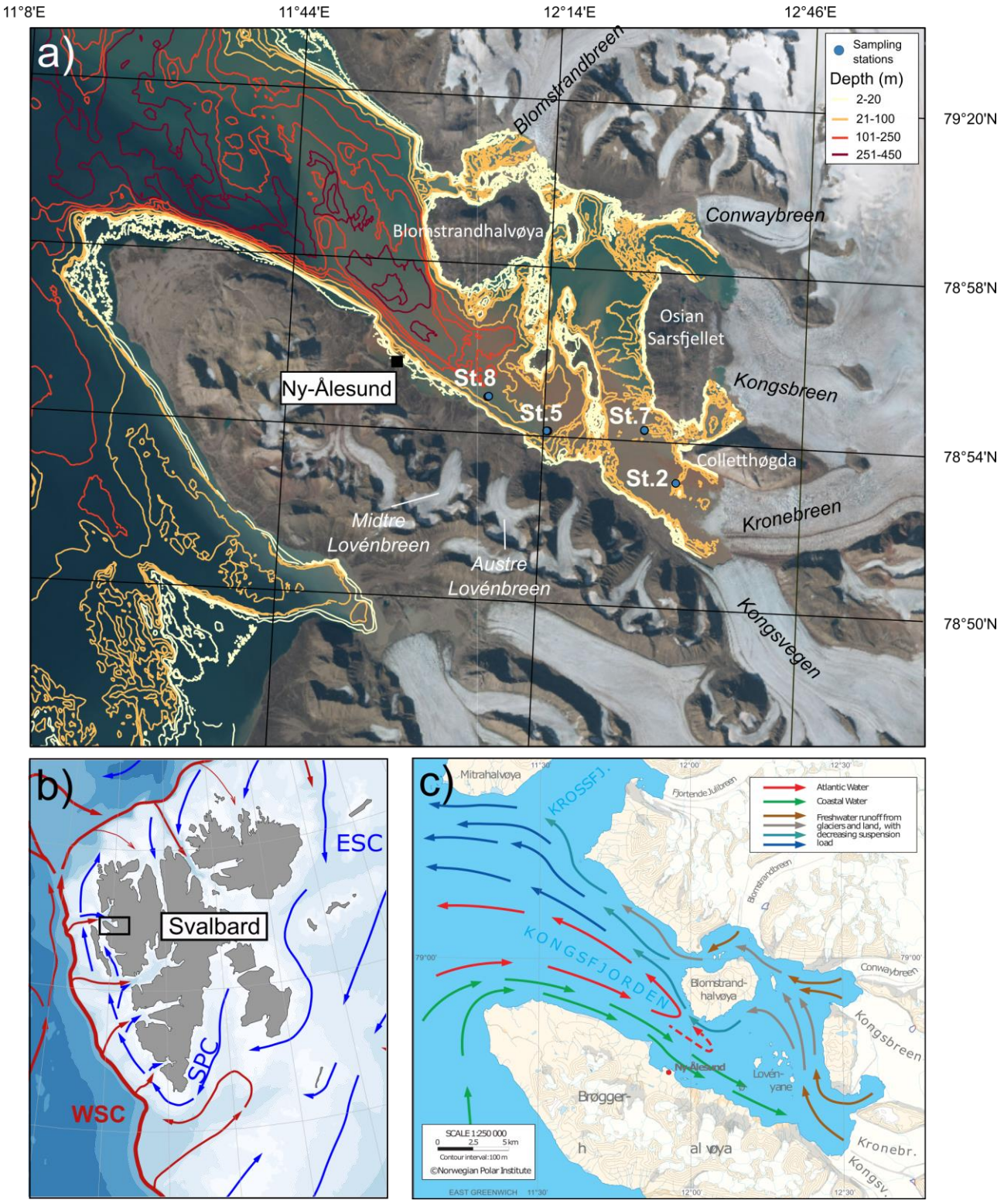

Figure 1:a) Map of Kongsfjorden displaying the locations of 4 studied stations . The five tidewater glacier fronts are located on the eastern and northern banks of the fjord (black names). The scientific station Ny-Ålesund is marked by the black square on the southern bank. Bathymetric data are symbolised by the yellow to dark red lines associated with different depth ranges (see legend); Data from the Norwegian Hydrographic Service (Karverket). Satellite image was extracted from TopoSvalbard.npolar.no (NorskPolar Institutt) and was taken in July/August 2020. b) Map of the Svalbard archipelago displaying the main local currents (ESC East Spitsbergen current; SPC Spitsbergen Polar current; WSC West Spitsbergen current). The map was performed with R package PlotSvalbard (Vihtakari, 2020). c) Schematic sketch of the horizontal circulation in the fjord. The red arrows correspond to Atlantic water originating from the open ocean displayed in map b). Turbid discharges from subglacial upwellings observed in satellite image a) are symbolized by brownish arrows.

2.2 Physical oceanography settings

Due to its geographical position, Svalbard is influenced by water mass exchanges between the Atlantic and Arctic Oceans. (Fig. 1b). The Fram Strait is the main gateway for Atlantic water (AW) inflow towards the Arctic Ocean. It is channelled on the east side of the Fram Strait along the slope of the Spitsbergen shelf as the West Spitsbergen Current (WSC) (Schauer et al., 2004). With a parallel northward inflow, the Spitsbergen Current (SPC) is a prolongation of the East Spitsbergen Current (ESC) originating from the Arctic Ocean and circulating clockwise around the Svalbard archipelago on the continental shelf. As seen on Fig. 2b, inflows of the WSC and the SPC in Kongsfjorden are observed. Due to the W-E orientation of its axis and the presence of partial sill (Howe et al., 2003), water bodies from the ocean can easily penetrate the fjord depending on the Arctic front dynamics (Svendsen et al., 2002). Whenever front instabilities occur due to geostrophic processes in the Arctic front, Atlantic water reaches the continental shelf via an upwelling and can therefore intrude into Kongsfjorden along with Arctic waters of the SPC mixing up to form Transformed Atlantic waters (TAW) (Cottier et al., 2005; Svendsen et al., 2002). Intrusion of warm and saline water of TAW, far into the fjord, is not seasonally and annually constant. This water mass dynamics is intensified by the formation of sea-ice in the fjord and associated water stratification (Payne and Roesler, 2019). However, considerable sea-ice formation did not occur in the fjord since 2006 (Payne and Roesler, 2019).

Freshwater inflows, which occur mainly in summer, arrive in the fjord via subglacial rivers and melting icebergs issued from the tidewater glacier, as well as continental outflows issued from land-terminating glaciers (Dallmann, 2015). The main freshwater input originates from tidewater glaciers which annually discharge about 1 km^3 of freshwater with a maximum activity in summer (Lefauconnier et al., 1994). This results in a strong stratification of the water column, with an upper layer of cooler and less salty water, so called Surface Water (SW). At glacier fronts, subglacial runoff rises above the intruding dense and salty TAW through a strong upwelling that feeds the SW. This upwelling amplifies the inflow of Atlantic-derived water masses towards the glacier base and further promotes its melting (Cowton et al., 2015; Sundfjord et al., 2017). In autumn-winter, due to strong winds, the SW mixes with the underlying TAW resulting in the formation of Intermediate Waters (IW) (Cottier et al., 2005).

Kronebreen glacier is the main source of meltwaters and detrital suspended particles in Kongsfjorden (Lydersen et al., 2014; Meslard et al., 2018) (Fig. 1a, c). In winter, incoming solar energy decreases and air temperature falls below the freezing point induce sea ice formation and the associated release of cold and salt-rich water bodies underlying the ice pack. This resulting Winter Cooled Water (WCW) sinks to the bottom of the Kongsfjorden inner basin, separated from the rest of the fjord by the sill of the Lovénøyane islands (Payne and Roesler, 2019). However, when large volumes of AW enter the fjord, this promotes basal melting of tidewater glaciers, increasing SW thickness and reinforcing water stratification. This hydrological context, additionally to warmer atmospheric conditions, prevents the formation of sea ice and the associated production of WCW (Payne and Roesler, 2019).

Tide waves enter the Kongsfjorden inner basin via Kelvin waves from the continental shelf, as evidenced by ADCP (Acoustic Doppler Current Profiler) measurements (Svendsen et al., 2002). The tidal range is inferior to 1 m in the fjord. Inflows are mainly restricted to the southern coast whereas outflows mainly occur along the northern coast with tidal current velocities that did not exceed 10 cm s^{-1} (Svendsen et al., 2002). Between Ny-Ålesund and

Blomstrandhalvøya (Fig. 1a), maximum water export due to tidal currents was of 12.000 m^3 s^{-1} at high tide (Svendsen et al., 2002). While the tide currents affect the whole water column even when strongly stratified, like in summer conditions, the wind-driven currents can show higher velocities but remain constrained to the surface layers (Svendsen et al., 2002).

2.3 Primary production dynamic and organic matter export

Phytoplanktonic growth in Arctic regions is mainly constrained by solar light and sea-ice extent along with nutrient availability playing also an important role. Indeed, polar night begins on October 25 each year and lasts 116 days in Svalbard. During this time, primary production is below detection levels (Berge et al., 2015; Hop et al., 2006). When the sun light comes back, the main limitation for primary production is the nutrient availability. In Kongsfjorden, sea-ice break-up, which was a key parameter for nutrient input and phytoplanktonic bloom, is nowadays limited, due to ice-free conditions of the fjord since 2006. However, some sea-ice still forms in the northern parts of Kongsfjorden (Cottier et al., 2005; Gerland et al., 2019; Payne and Roesler, 2019). The first phytoplankton bloom generally occurs in April/May followed by smaller blooms later in the summer (Calleja et al., 2017; Hegseth et al., 2019; Hodal et al., 2012). The vertical advection associated with water mass mixing brings phytoplanktonic spores at the surface where they can develop (Hegseth and Tverberg, 2013). This seasonal dynamics results in a relatively high primary productivity (120 to 180 g C m^{-2} y^{-1}) (Hegseth and Tverberg, 2013; Hop et al., 2006).

Light availability in the surface waters is also affected by freshwater inputs carrying a turbid plume originating from subglacial water upwelling to the surface and supplied by glacial erosion of the bedrock. Land-terminating glacier runoff might affect only locally the depth of the euphotic zone whereas turbid plumes originating from much larger tidewater glaciers (Kronebreen and Kongsvegen) have a negative effect on light availability in surface layers on a more extended area (Payne and Roesler, 2019). Along with this turbid plume, nutrients from depths (fjord bottom) are brought to the surface. Therefore, the SW is pushed away from the tidewater glacier fronts and is replaced by nutrient-rich AW or IW (i.e., nitrates and phosphates) bioavailable for phytoplanktonic growth (Lydersen et al., 2014).

Vertical organic matter fluxes from the surface of the water column towards the seabed show a pronounced seasonality in Arctic regions (Bourgeois et al., 2016; Juul-Pedersen et al., 2008; Moran et al., 2012). Consequently, pelagic seasonal changes are often reflected in benthos communities as observed by Morata et al. (2008) in the Beaufort Sea. Moreover, Bourgeois et al. (2016) observed that the quantity and quality of organic matter depend on the distance to the tidewater glacier front in Kongsfjorden. Consequently, the inner basin receives 4 to 6 times less organic carbon than further sites but may be composed of a higher proportion of fresh material deposited in spring (Bourgeois et al., 2016). This study postulated the existence of a persistent “food bank” in the sediment supplied by the export of products from secondary production because organic matter characteristics show only modest seasonal variations over a year. This theory was developed in Antarctica environments by Mincks et al. (2005).

3 Material and methods

3.1 Conductivity-temperature-depth profiles

During the two sampling campaigns, May and August 2021, conductivity-temperature-depth (CTD) casts were collected near the coring sites (Table 1; Fig. 1a). Water column measurements were performed, using a CTD profiler (SAIV SD204) equipped with turbidity and fluorescence (chlorophyll a concentration) sensors, from the surface until approximately 5 meters above the seafloor. Data were compiled on GRAPHER® 16.2.354 (Golden Software) to produce Temperature/Salinity and Turbidity/[chloro-a] plots. Section profiles were plotted on the Ocean Data View software 5.6.2 (Schlitzer, 2023). Spatial interpolation between profiles was performed using ODV in-built DIVA tool (Data Interpolating Variational Analysis) (Iona et al., 2018).

Station	Mission	Sampling date/hour	Depth (m)	Latitude (N)	Longitude (E)
St. 2	May-21	28/04/2021 12h36	69	78°53,331'	12°30,292'
St. 7	May-21	29/04/2021 09h49	69	78°54,219'	12°25,371'
St. 5	May-21	29/04/2021 10h43	72	78°54,366'	12°14,817'
St. 8	May-21	04/05/2021 09h29	129	78°54,970'	12°06,909'
St. 2	August-21	20/08/2021 9H45	50	78°53,046'	12°30,835'
St. 5	August-21	20/08/2021 11H10	65	78°54,229'	12°14,285'
St. 7	August-21	25/08/2021 9h30	66	78°54,382'	12°26,047'
St. 8	August-21	25/08/2021 13h40	119	78°54,963'	12°06,940'

Table 2: CTD measurement location coordinates, dates (and hours) and maximum depths. KAS 05-21 is the KONBHAS mission organised in Spring 2021 and KAS 08-21 in summer.

3.2 Sediment core sampling and treatment

The sediment samples were collected during the two missions organised in Kongsfjorden in spring, from the 26/04/2021 to 10/05/2021 (May mission), and in summer, from the 16/08/2021 to the 30/08/2021 (August mission). As a part of the KONBHAS project (KOngsfjorden New Benthic HAbitatS), the two campaigns allowed us to sample the seabed surface sediment, on the same 4 locations (Table 2) selected from the results of a previous study (Fossile et al., 2022). The selection of the studied sites was based on contrasted benthic foraminiferal content and position regarding environmental gradients including distance to Kronebreen and Kongsvegen tidewater glacier fronts. Coring was performed on the R/V Teisten (King's Bay) with a GeMAX twin corer or by subsampling inside a DayGrab (K/C Demark A/S) depending on the sediment texture. The GeMAX corer was used to recover twin cores (9 cm inner diameter) at St. 2 and 8, where the sediments are fine silts. The Day Grab was used to sample coarser sediment from silts to gravels, mostly consisting in dropstones. This device allows to sample the sediment-water interface and to subsample cores (8.2 cm inner diameter) up to 10 cm deep in the grab, through 4 windows at the top of the grab. One or two deployments were necessary to collect the required cores for all the analyses (foraminifera fauna and sediment biogeochemistry).

Station	Mission	Sampling date	Depth (m)	Latitude (N)	Longitude (E)	Coring device
St. 2	May-21	28/04/2021	55.3	78°53,078'	12°30,959'	GeMAX
St. 5	May-21	29/04/2021	63.6	78°54,228'	12°14,450'	GeMAX
St. 8	May-21	04/05/2021	126	78°54,972'	12°06,806'	DayGrab
St. 7	May-21	04/05/2021	68	78°54,336'	12°26,348'	DayGrab
St. 2	August-21	20/08/2021	50	78°53,117'	12°30,495'	GeMAX
St. 5	August-21	20/08/2021	65	78°54,229'	12°14,285'	DayGrab
St. 7	August-21	25/08/2021	65.6	78°54,349'	12°26,357'	GeMAX
St. 8	August-21	25/08/2021	125	78°54,986'	12°06,936'	GeMAX

Table 3: Sediment core location coordinates, date, depth (m) and sampling device

The collected cores were rapidly sliced on land after sampling. Sediment layers for all the analyses were recovered with the same slicing step resolution: every 0.5 cm until 2 cm depth, 1 cm thick slices from 2 to 10 cm depth.

3.2.1 Grain size analysis

For grain-size analyses, half of each layer was cool-stored at 4°C (spring mission) or freeze-dried and rehydrated before the analyses (summer mission). An aliquot (approximately 0.1 g) was extracted and inserted into a laser diffraction particle analyser Malvern Mastersizer 3000 to perform at least 3 control measurements. Particle related metrics (% of volume in each set size fraction) were then analysed using GRADISTAT 9.0 program (Blott and Pye, 2001) to obtain grain-size parameters. Grain-size plots were performed using GRAPHER® 16.2.354 (Golden Software).

3.2.2 Organic matter

For organic matter analyses, half of surface layer of sediment (0-0.5 cm) was frozen at -20 °C. Organic matter components were measured on two to three replicates each time. Phytopigment content was analysed according to Lorenzen and Jeffrey (1980) protocol to measure chlorophyll-a and additional phaeopigments concentrations in the different sediment layers. Those pigments were extracted from triplicates when available, using each time 1 g of sediment during 12h at 4°C and in the dark. Extracts were analysed by fluorometry in a first time for chlorophyll-a concentrations and in a second time for phaeopigments after acidification with 0.1 N HCl. In addition, protein, carbohydrate, and lipid contents were analysed by spectrophotometry following Danovaro (2009) protocol. For this analysis, 0.5 g of sediment were required for each measurement. Thereafter, protein, carbohydrate and lipid concentrations were converted into C equivalents using the following conversion factors 0.49, 0.40 and 0.75 mg C mg^{-1} respectively. Biopolymeric carbon is the sum of these 3 components. Degradation rates of the Leucine by extracellular enzymatic activity (aminopeptidase) were measured after the protocol of Danovaro (2009).

4 Results

4.1 Water masses

In Fig. 2a, temperature vs salinity and chlorophyll-a vs turbidity plots are given for all stations at the two sampling seasons in 2021. In May (in blue on the plot), the casts from all stations were very similar and showed a well-mixed water column with slight salinity variations (from 34.6 at the bottom of the deepest station to 34.5 at the surface) and temperature varying from 0.6°C at the bottom to a minimum of -1.5°C at the surface. The coldest surface temperatures were recorded at the two stations closest to the Kronebreen glacier front (St. 7 and St. 2, Fig. 2b). According to the observed characteristics and the limit values reported by Cottier et al. (2005), during the spring cruise we identified Local Water (LW S 34.30-34.85 and T below 1°C) at St. 5 and St. 8 and Winter Cooled Water (WCW S 34.4-35 and T below -0.5°C) at St. 2 and St. 7. In spring, the turbidity was very low (< 10 FTU) and the concentration in chlorophyll-a was always below 0.4 µg L^{-1}. This maximum pigment concentration was observed at St. 5 and St. 8, between 10 and 40 m water depth (Figure 2b).

The conditions at the end of August were very different. At all stations, and with a steeper gradient moving from St. 2 to St. 8, the water column looked stratified, with fresher (<33) and cooler (<4°C) water at the very surface (i.e., about down to 10 m, figure 2b). These characteristics are typical for superficial waters (T>1.0°C, S < 34.00, (Cottier et al., 2005; Divya and Krishnan, 2017). Near the seafloor, the salinities varied from 34.75 at St. 8 to values between 34.6 and 34.25 at St. 5, St. 2 and St. 7. Temperature was below 3°C at St. 8, while it remained between 3 and 4.5°C at St. 5, St. 2 and St. 7.

At St. 8 the bottom waters were represented by Transformed Atlantic water (TAW with salinity above 34.65 and T between 1 and 3°C) whereas St. 5, St. 2 and St. 7 displayed Intermediate water signature (IW with salinity between 34 and 34.65 and T above 1°C) (Cottier et al., 2005).

Along the transect, a steep gradient is also visible in Surface Water in terms of turbidity and chlorophyll-a concentration. Indeed, a well-defined turbidity peak marked the presence of the turbid plume between 5 and 20 m depth at St. 2, close to the glacier terminus, which rapidly decreased moving towards the distal stations. Inversely, the chlorophyll-a concentration was higher between 0 and 10 m water depth at St. 7, St. 5 and St. 8, and close to zero at St. 2. Below 20 m, both turbidity and chlorophyll-a concentration dropped to near 0 at all stations.

4.2 Sediment grain size

In spring 2021, St. 7 and St. 5 showed similar grain size curves with a unique mode in the fine silts (around 10 µm) (Fig. 3). This mode of 10 µm was also present in core from St.8 in every layer but it was associated with a second mode of very fine sand of 80 µm. The two modes were alternating as main or secondary mode all along the core, with the primary 10 µm mode mainly observed between 3 and 8 cm of depth. No data were available for St. 2 for this season.

In summer St. 8, the same alternation between the two modes of 10 and 80 µm observed in spring, was present down to 8 cm depth. Below this depth, a single mode of fine silts (10 µm) was observed. This unique 10 µm mode was also observed at St. 5. At St. 7, the main mode

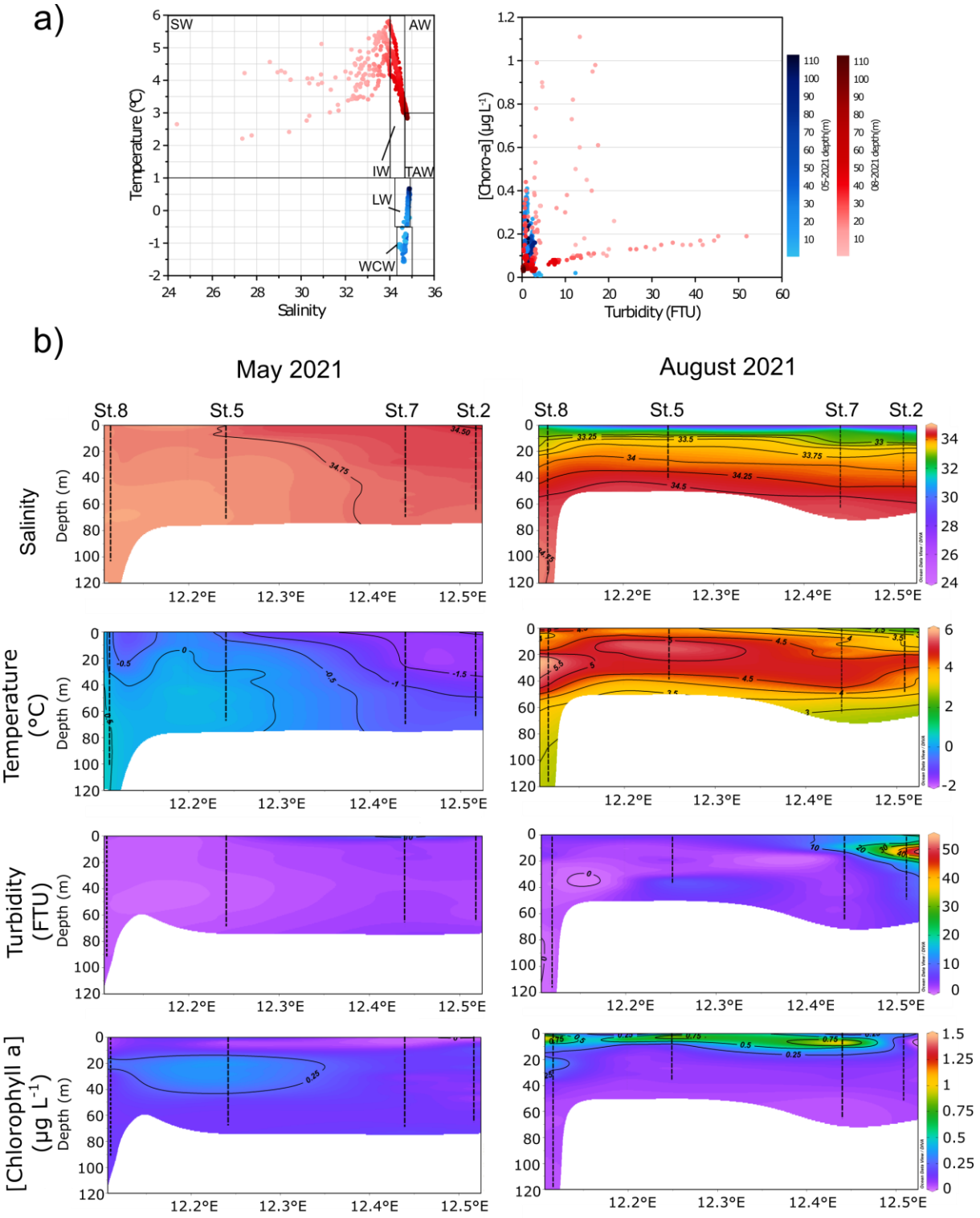

Figure 2: SE-NW CTD cast measurements. a) Salinity vs temperature and chlorophyll-a concentration vs turbidity (FTU) plots. All measurements are represented with a colour fading according to their season of acquisition and their depth (see scales on the right). Water mass limits extracted from Cottier et al. (2005) are indicated (AW Atlantic water; SW Surface water; IW Intermediate water; TAW Transformed Atlantic water; LW Local water; WCW Winter cooled water b) Sections across the deep transect (0-120m water depth) of interpolated (DIVA interpolation) profiles for salinity, temperature, concentration of chlorophyll-a and turbidity. Location of our sampling stations are marked by dotted lines. Sections on the left column are May 2021 data and the sections on the right are August 2021 data. Colour scales are different for each parameter but common for one parameter between seasons.

all along the core was still constituted of fine silts (around 10 µm). Additionally, the sediment at this station was sparsely affected by a secondary mode from 12 to 600 µm above 16 cm depth. At St. 2, the alternation between two modes was observed, characterised by slow shifts from one particle population to another as observed between 8 and 13 cm depth (Fig. 3).

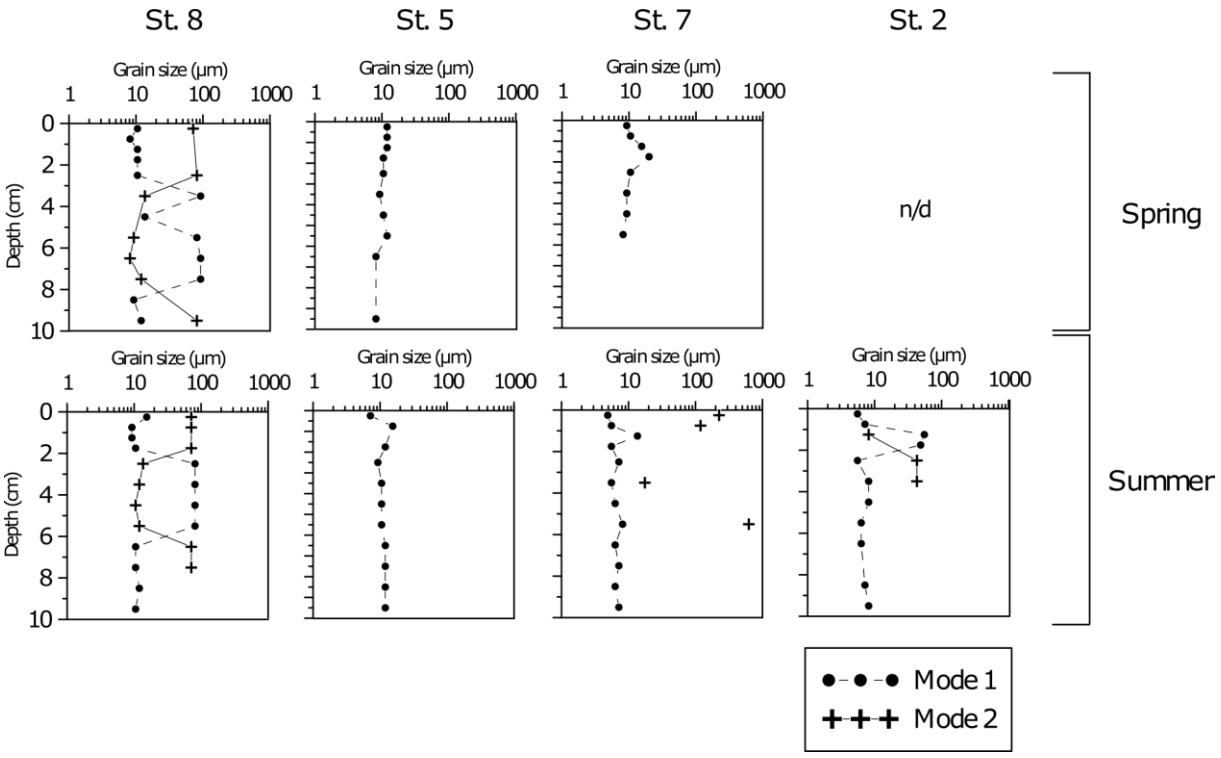

Figure 3: Profiles of primary and (when present) secondary modes (µm) of sediment grain size in May 2021 and August 2021. Grain size data were not available for St. 2 for May 2021.

4.3 Organic matter

Bioavailable organic carbon components were analysed (complete dataset in Table S1; supplementary material) and the main results are shown in Fig. 4. Biopolymeric Carbon (BPC), as the sum of proteins, lipids and carbohydrates, varied between 0.82 ± 0.02 and 1.72 ± 0.18 mg g^{-1} C in May and 0.74 ± 0.16 and 1.69 ± 0.30 mg g^{-1} C in August. The concentrations of biopolymeric carbon were higher in the two distal stations (5 and 8) with no significant differences between seasons (Supplementary material).

Phytopigment concentrations in the surface sediment ranged from 0.80 ± 0.03 and 11.63 ± 0.25 µg g^{-1} in May and 1.24 ± 0.17 and 15.92 ± 6.85 µg g^{-1} in August. Highest concentrations were found in St. 5 and St. 8 with significant differences between May and August values. The ratio of phytopigments over biopolymeric carbon showed two distinct groups in both May and August with St. 5 and St. 8 on one side and glacier proximal stations on the other side. This ratio was low in the two proximal St. 2 and St. 7 with a maximum of 0.09 ± 0.02 in St.7 in August and 0.04 ± 0.01 in May. At the opposite, St. 5 displayed a high difference between the two seasons with 0.18 ± 0.01 and 0.44 ± 0.11 in May and August respectively. St. 8 showed closest values between the two sampling times with 0.27 ± 0.04 and 0.19 ± 0.03 in May and August respectively.

Aminopeptidase enzymatic activity furthermore marked the contrast between glacier proximal and medial/distal stations (Fig. 4d). Indeed, proximal St. 2 and St. 7 showed similar aminopeptidase rates around 18.39 ± 4.83 nmol g^{-1} h^{-1} in August and lower values of 5.53 ± 0.47 nmol g^{-1} h^{-1} in St. 7 in May. Station 5 showed higher enzymatic degradation rate both in May and August without significant differences between seasons (76 ± 7.59 and 89 ± 9.17 nmol g^{-1} h^{-1} respectively) Similarly, aminopeptidase values for St. 8 were not significantly different between May and August and were around 50 ± 16.4 nmol g^{-1} h^{-1} and 61 ± 1.5 nmol g^{-1} h^{-1}.

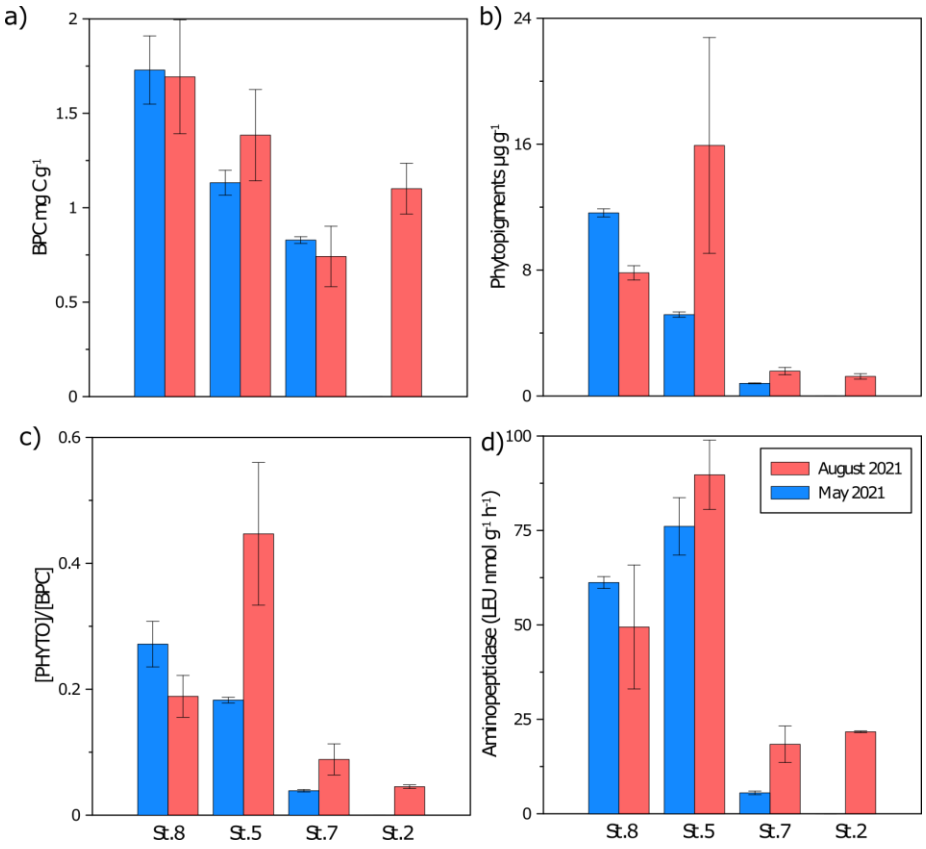

Figure 4: Organic matter component and ratios at each station for both sampling times analysed in the 0-0.5 cm sediment layer. Standard deviation was calculated from triplicates. No data were available for St.2 in May 2021. a) Biopolymeric carbon concentrations (Protein + carbohydrate + lipid concentration) (mg g^{-1}). b) Phytopigment concentration (µg g^{-1}). c) Phytopigment concentration over Biopolymeric carbon concentration ratio d) Aminopeptidase (nmol g^{-1} h^{-1}).

5 Discussion

5.1 Water masses

The water masses identified in the fjord thanks to the CTD data (Fig. 2) showed a clear seasonal contrast in water column characteristics between May and August 2021.

The two main signatures found in spring (May mission), Local water (LW) and Winter Cooled Water (WCW), corresponded to water masses originating from surface cooling during winter and eventually resulting in a convection of denser water bodies towards the bottom (Cottier et al., 2005; Svendsen et al., 2002). The convective process could also be responsible for the observed lack of stratification of the water column. Following Cottier et al. (2005),

WCW can be found in Kongsfjorden at the end of winter and can also be locally detected throughout the year as it can be trapped in semi-enclosed deep basins such as the inner part of Kongsfjorden limited by the Lovénøyane sill (Fig. 1a, c). In our case, the WCW was indeed found in this inner basin near the Kronebreen glacier front in St. 2 and St. 7, only in spring. The LW salinity range usually depends on the water present at the end of the summer season (Cottier et al., 2005). The deepest stations showed a salinity near the limit value for this water mass at 34.85 inducing an extended presence of Atlantic salty water at the end of the previous summer. Furthermore, we observe the absence of turbidity in the water column from the Kronebreen glacier front until the most distal station due to limited glacier melting and subglacial discharge. Chlorophyll-a concentrations revealed low primary production in May 2021 (Fig. 2b). However, an increase of 0.25 µg L^{-1} in concentration was observed between 20 and 40 m water depth at St. 8 and St. 5 interpretated as the start of the spring phytoplanktonic bloom (Calleja et al., 2017; Piquet et al., 2014).

In August, we found SW spread in the first 25 m of the water column at all stations, with particularly low salinities of 24 at the very surface of St. 2 and below 33 at other stations. As the sea ice production in the fjord is nowadays nearly absent, this low salinity is the result of summer melting waters flowing from all local glaciers and mostly the Kronebreen glacier whose terminus is less than 1.5 km far from St. 2. The SW, originating from the subglacial rivers, flows into the fjord, rises at the surface by upwelling (Hop et al., 2006; Trusel et al., 2010) and spreads all along the inner part of the fjord, as it is still visible at St. 8, 10 km far from the glacier terminus. At this distal station, the bottom of the water column was constituted of TAW. Reported at depths greater than 100 m (St. 8, 125 m) by Cottier et al. (2005), this water mass originates from the mixing of AW (Atlantic Water) intruding the Kongsfjorden and local ArW (Arctic water) (Fig. 2b). In our study, the recorded presence of TAW at St. 8 during summer marks the limit of the ongoing inflow of Atlantic water bodies in the inner fjord at the sampling time. Following Cottier et al. (2005), the fjord‘s bathymetry probably explains the absence of TAW water mass in the shallower, glacier proximal stations.

However, just below the SW, IW was recorded all along the transect, and until the stations close to Kronebreen glacier front. This water mass can originate from two processes: 1) the mixing of SW with TAW and/or 2) the gradual warming of LW and WCW in spring and early summer that can bring T-S signatures towards the ones of IW (Cottier et al., 2005). Between the two sampling campaigns, several processes may have been involved in the variation of water mass distribution. Firstly, the warming of the water signatures in summer is highly linked to the intrusion of AW water, only limited by the stability of the arctic front represented by the West Spitsbergen Current (Fig. 2b) and the ArW on the continental shelf break. Irregularities in the offshore northerly winds induce more regular pulses of AW onto the shelf then into Kongsfjorden following the bathymetry (Svendsen et al., 2002). This is also in accordance with water column measurements showed by Tverberg et al. (2019) that highlighted a non-regular inflow of AW inside Kongsfjorden during summer period. Usually, this cycle is inverted in autumn and winter when the atmospheric temperature decreases along with sunlight and leads to the formation of WCW and LW. This seasonal cycle was described as typical in Arctic fjords including Kongsfjorden for the past two decades (Cottier et al., 2010; Jernas et al., 2018; Nilsen et al., 2016; Payne and Roesler, 2019; Tverberg et al., 2019). Recent studies, such as Strzelewicz et al. (2022) and Jernas et al. (2018)**,** evidenced the increased presence of AW on the western Spitsbergen shelf during the last 23 years, leading to a greater inflow of AW into the Horsund fjord (south of the western Spitsbergen coast) and into Kongsfjorden. Lind et

al. (2018) suggested that the increased inflow of Atlantic water on the shelf could be due to the decreasing import of sea-ice in the Barents Sea that implies higher temperature of the ArW that feeds the SPC current (Fig. 2b). The ongoing climate change may further lower the contrasting power of ArW, resulting in a further inflow of AW into Kongsfjorden, such as suggested for the Horsund fjord by Strzelewicz et al. (2022). In Kongsfjorden, Jernas et al. (2018) reported the increased presence of both AW and TAW during summer periods between 2005 and 2008, from the outer shelf up to the middle fjord area. Their innermost station was located about 4 km far from our most glacier distal St. 8. According to our data, the presence of AW was not recorded, but the presence of TAW at St. 8 extends the geographical limits suggested by Jernas et al. (2018) towards the innermost part of the fjord. Moreover, the ubiquitous presence of IW, potentially originated from SW and TAW mixing, suggests that Atlantic water in 2021 influenced the whole fjord, up to the innermost regions close to the tidal glacier fronts at the fjord head.

Besides water masses, turbidity and chlorophyll-a concentration in the water column also varied between the two sampled seasons. In May, the turbidity was close to zero along the transect, underlying the weak glacial outflow and the associated low turbidity during the cold season, as previously suggested by D'Angelo et al. (2018) and Meslard et al. (2018). On the opposite, during the warm season, the high turbidity observed in the superficial waters of St. 2 and St. 7 highlights the massive export of sediment transported by the subglacial freshwater outflow, loaded in fine suspended particles eroded from Kronebreen and Kongsvegen glacier watersheds (Bourgeois et al., 2016; D'Angelo et al., 2018; Meslard et al., 2018; Trusel et al., 2010). The surface spreading of this turbid freshwater plume follows either tidal currents which mostly brings the plume toward the northern part of the fjord (Dallmann, 2015; Payne and Roesler, 2019) or main wind direction in the fjord axis driving the turbid plume along the southern coast. This last process should be weaker in summer than in winter (Sundfjord et al., 2017). In August 2021, the surficial high turbidity spread out to maximum at St. 2 and St. 7.

As turbidity decreased on the fringe of the turbid plume, the chlorophyll-a concentrations increased by two processes (Lydersen et al., 2014): 1) enhanced nutrient transports towards the surface by the subglacial upwelling and 2) higher light penetration that promotes photosynthesis. As a result, phytoplanktonic bloom episodes occur far from the glacier fronts (Calleja et al., 2017; Piquet et al., 2014). In May, a less intense phytoplanktonic growth occurred, with more homogenous Chl-a concentrations along the fjord and a maximum Chl-a concentrations between 20 and 40 m water depth (Fig. 3).

The differences in Chl-a concentrations between the two seasons could be explained by differences in phytoplankton communities, as evidenced by Piquet et al. (2014)**.** Spring communities are mainly composed of *Phaeocystis* spp. In May 2021, the low Chl-a concentrations suggest that this bloom was either already finished or just started. Between May and August, a shift occurs from diatom communities to nano and picophytoplankton-sized classes such as chlorophytes, dinoflagellates and cyanophytes, as documented in recent studies conducted in the area (Azzaro et al., 2021; Hegseth et al., 2019; Piquet et al., 2014; Rokkan Iversen and Seuthe, 2011; Seuthe et al., 2011).

The timing of the spring bloom depends on sea-ice and hydrographic conditions prevailing in the fjord. Inter-annual variability is high for the starting moment of the bloom, but some conditions are mandatory to trigger it. Light availability is one of the driving factors to start the spring bloom as well as water column mixing bringing diatom spores from the depths to the surface (Hegseth et al., 2019). The intrusion of AW early in the fjord can enhance water

stratification and act as a lid preventing the spores to reach the euphotic zone (Hegseth et al., 2019) and thus can explain a delay of the spring bloom. In sea-ice free waters, the phytoplanktonic bloom generally occurs in mid-April due to early light availability. But recent observations reported by Hoppe (2022) highlight the ability for phytoplankton to start growing at the very end on the polar night (17th of February) as it happened in 2018 in Kongsfjorden. Low light conditions can provide enough photons to activate photosynthesis in this period (Hoppe, 2022). The data we recorded at all stations, with the exception of St. 2 where the turbidity was too high, suggest that the phytoplankton bloom was still going on in late August 2021, like it was also observed by Hodal et al. (2012) and Piquet et al. (2014).

5.2 Sedimentation gradient

Detrital transport mass flux in the innermost fjord is evidenced by both satellite view (Fig. 1a) and *in situ* turbidity measurements (CTD casts, Fig. 2b). The sediment supply mainly originates from the melting of the two main local tidewater glaciers Kronebreen and Kongsvegen, with additional supplies from the continental glaciers of the south coast (Bourriquen et al., 2016). After D'Angelo et al. (2018) sediment inputs mostly occur between July and September. These authors reported that, between 2010 and 2016, the summer deposits represented 38% to 71% of the annual detrital mass flux. This is in accord with our CTD observations, evidencing 20x higher turbidity in August compared to May 2021 in the most glacier proximal stations. D'Angelo et al. (2018) explained that the total mass flux was highly correlated with air temperature and partially with rain. Both environmental parameters strongly induce surface glacier snowpack melting leading to water infiltration in subglacial drainage network (D'Angelo et al., 2018; Lydersen et al., 2014). Basal sediments are therefore carried out by subglacial runoff and delivered to the fjord. Whenever air temperature drops below zero, meltwater refreezes and the system switches into a slow drainage system (Lydersen et al., 2014). Our data confirmed that the drainage system was slow in May as the water column did not show melting- associated turbidity. Particle trap data described by D'Angelo et al. (2018) highlighted that in summer ~ 99% of trapped particles were terrigenous sediments, both carbonate and silicoclastic. Our grain-size data showed quite similar vertical distribution of grain sizes for each station at both seasons, with some exceptions. At St. 8 (May and August) and St. 2 (only August; no data available in May) two grain size populations were observed, constituted of fine silt (10 µm) and very fine sand (80 µm) (Fig. 4). The regular alternation of both particle sizes can be seen throughout the cores. St. 5 and St. 7, on the contrary show more homogenous grain sizes (fine silts around 10 µm) with occasional presence of coarser silt in the surficial sediment layers of St. 7 in August. The fine silt found at all stations corresponds to particles directly eroded from glacier underlying bedrocks (Meslard et al., 2018; Lund-Hansen et al., 2010). The spreading of the turbid plume away from the glacier front explains the grain size signature found at least until St. 8 (Fig. 4). Of course, this does not rule out the possibility of fine particles being transported much further towards the mouth of the fjord.

Sedimentation rates, calculated according to the model developed by Lydersen et al. (2014) on the base of data recovered in July 2003, showed a decreasing trend with increasing distance from Kronebreen front. Indeed, near the glacier front, sedimentation rates can reach 800 g m^{-2} d^{-1} whereas downfjord, beyond the Lovénøyane sill, sedimentation rates are twofold lower. On the base of Lydersen et al. (2014) model, at St. 8 and St. 5 the mean sedimentation rate could be below 25 g m^{-2} d^{-1}. Trusel et al. (2010) attributed a sedimentation rate of at least 60-90 mm y^{-1} in most glacier proximal areas due to Kronebreen subglacial runoff. According to these data,

the sediment supply to the bottom and the associated physical instability of the benthic habitats should therefore decrease with the distance from Kronebreen front.

However, the presence of coarser sediment at St. 8 also suggests that other sources of sediment can influence glacier distal areas, such as the lateral sediment supplies from the continental glaciers located on the southern coast of the fjord. Indeed, St. 8 is very close (1 km) to the prodelta constructed by the sediment discharges coming from the Midtre Lovénbreen land-terminating glacier. During summer melting, when the continental river runoff is intense, gravel and coarse sand reach the prodelta and can be transported towards the location of St. 8 by gravity flow from the prodelta. Finer particles, such as fine silts, can always reach this site by suspended transport from the turbid plumes. At St. 2, alternation between fine silt (10 µm) and fine sand (80 µm) populations observed in the sediment core reflects the changes between glacier melting intensity throughout the year with coarser particles brought by more intense subglacial runoff towards the fjord during summer.

5.3 Organic matter content

Biopolymeric C concentration in the whole area at both seasons is the same range, or lower, than BPC values reported for other coastal polar environments (e.g., Pusceddu et al., 2000; Isla et al., 2006). The increasing concentrations observed in the distal stations (Fig. 4) reflect the increase in phytopigment contents (i.e., Chl-a), especially in the summer samples, and suggest that the most labile fraction of this BCP is locally produced by primary production at the surface. At glacier proximal stations (St. 2 and St. 7) the primary production/export of phytopigments was very low both in May and in August (Fig. 4). On the opposite, the St. 5 and St. 8 displayed high accumulation of phytopigments (chlorophyll-a + phaeopigments) mostly in summer, reaching a maximum of 4 µg g^{-1} in the medial St. 5 (Fig. 4). The Phyto/BPC ratio (Fig. 4c) indicates the potential of accumulation of fresh organic matter in the sediment. When the ratio is high, the organic matter is freshly deposited (e.g. during bloom), when it is low, the organic matter reflects the residue of past accumulation (e.g., post bloom) (Pusceddu et al., 2000). Labile organic matter is represented by phytopigments and is the most bioavailable for remineralisation. Therefore, burying and accumulation of particulate organic matter mostly involve biopolymeric carbon not hydrolysable by benthic organisms (Pusceddu et al., 2000). The potential accumulation of BPC is function of both production (or export) vs consumption rates by benthic organisms and early diagenetic processes (Pusceddu et al., 2009). According to this last study, environments showing relatively high concentrations of BPC are associated with highly productive systems with low algal carbon contributions to BPC. Moreover, this same study indicates that these highly productive environments show high temporal variability of organic carbon input in the sediment due to changes in primary production essentially. In more oligotrophic areas, the organic carbon directly produced by algal bloom does not affect background concentration of organic carbon in the sediment. This dynamic can be observed in our data separating St. 5 and St. 8 from St. 7 and St. 2 where BPC and phytopigment input significantly increased in distal stations and remained near zero in glacier proximal stations.

The turbid surface water near the Kronebreen glacier front did not allow phytoplanktonic growth in the inner basin due to limited light penetration in summer when the highest primary production was observed in summer (Fig. 2b). In addition, the high detrital sedimentation down fluxes dilute the OM flux to the seafloor (Payne and Roesler, 2019). Bacterial extracellular activity brought here by the leucine aminopeptidase showed no significant differences between the two seasons of the two most distal stations (Fig. 4). Similar

OM degradation rates may support the "food bank" theory postulated by Mincks et al. (2005) in Antarctica explaining that the non-significant differences in benthic diversity and biomass between seasons are the results of high OM fluxes between the spring bloom and the end of summer and low bacterial remineralization at low temperatures. This may result in a year-round reserve in the sediment of relatively labile OM to sustain the benthic communities (Kędra et al., 2011; Wlodarska-Kowalczuk and Pearson, 2004).

6 Conclusion

Highly contrasted environmental conditions are observed between spring (May 2021) and late summer (August 2021) and between the glacier front proximal (about 1 km) and distal (10 km) sites. In summer, the strong water column stratification due to melting freshwater and warm and salty Atlantic Water entries occur along with high turbidity in the vicinity of the Kronebreen glacier and high surface primary production away from the turbid plume upwelling at the glacier front. In this summer context, glacier proximal St. 2 and St. 7 were subjected to high sediment downward flux and low fresh organic matter export (phytopigments) from the water column. The contrary can be observed on the other side of the inner sill at St. 5 and St. 8 with this last one being 10 km away from the Kronebreen glacier front. Higher organic matter export is supported both by high phytoplanktonic growth at the surface and high phytopigment extracellular bacterial OM degradation rates. Higher stability of the benthic ecosystem can be supposed in this area in spring and late summer.

Those seasonally and spatially constrained environmental gradients will be mentioned in the three next chapters investigating the geochemical response of the sediment to glacial inputs in summer (***Chapter 5***) and the seasonal response of benthic foraminiferal communities to contrasted environmental conditions (***Chapter 6***). After that, a zoom-in into sediment microhabitats and geochemical characteristics will be performed to investigate small scale heterogeneity in the two contrasted stations St. 7 and St. 8 (***Chapter 7***).

Data availability:

Surface sediment organic matter data are shown in supplementary material 1. All environmental data will be included in further publications. In this way, raw data will be available upon publication of next chapters.

Supplement:

Table S1 can be found in the Supplement section

References:

Azzaro, M., Aliani, S., Maimone, G., Decembrini, F., Caroppo, C., Giglio, F., Langone, L., Miserocchi, S., Cosenza, A., Azzaro, F., Rappazzo, A. C., Cabral, A. S., Paranhos, R., Mancuso, M., and La Ferla, R.: Short-term dynamics of nutrients, planktonic abundances, and microbial respiratory activity in the Arctic Kongsfjorden (Svalbard, Norway), Polar Biol, 44, 361–378, https://doi.org/10.1007/s00300-020-02798-w, 2021.

Berge, J., Renaud, P. E., Darnis, G., Cottier, F., Last, K., Gabrielsen, T. M., Johnsen, G., Seuthe, L., Weslawski, J. M., Leu, E., Moline, M., Nahrgang, J., Søreide, J. E., Varpe, Ø., Lønne, O. J., Daase, M., and Falk-Petersen, S.:

In the dark: A review of ecosystem processes during the Arctic polar night, Progress in Oceanography, 139, 258–271, https://doi.org/10.1016/j.pocean.2015.08.005, 2015.

Blott, S. J. and Pye, K.: GRADISTAT: a grain size distribution and statistics package for the analysis of unconsolidated sediments, Earth Surf. Process. Landforms, 26, 1237–1248, https://doi.org/10.1002/esp.261, 2001.

Bourgeois, S., Kerhervé, P., Calleja, M. L., Many, G., and Morata, N.: Glacier inputs influence organic matter composition and prokaryotic distribution in a high Arctic fjord (Kongsfjorden, Svalbard), Journal of Marine Systems, 16, 2016.

Bourriquen, M., Baltzer, A., Mercier, D., Fournier, J., Pérez, L., Haquin, S., Bernard, E., and Jensen, M.: Coastal evolution and sedimentary mobility of Brøgger Peninsula, northwest Spitsbergen, Polar Biol, 39, 1689–1698, https://doi.org/10.1007/s00300-016-1930-1, 2016.

Calleja, M. Ll., Kerhervé, P., Bourgeois, S., Kędra, M., Leynaert, A., Devred, E., Babin, M., and Morata, N.: Effects of increase glacier discharge on phytoplankton bloom dynamics and pelagic geochemistry in a high Arctic fjord, Progress in Oceanography, 159, 195–210, https://doi.org/10.1016/j.pocean.2017.07.005, 2017.

Cottier, F., Tverberg, V., Inall, M., Svendsen, H., Nilsen, F., and Griffiths, C.: Water mass modification in an Arctic fjord through cross-shelf exchange: The seasonal hydrography of Kongsfjorden, Svalbard, J. Geophys. Res., 110, C12005, https://doi.org/10.1029/2004JC002757, 2005.

Cottier, F. R., Nilsen, F., Skogseth, R., Tverberg, V., Skarðhamar, J., and Svendsen, H.: Arctic fjords: a review of the oceanographic environment and dominant physical processes, SP, 344, 35–50, https://doi.org/10.1144/SP344.4, 2010.

Cowton, T., Slater, D., Sole, A., Goldberg, D., and Nienow, P.: Modeling the impact of glacial runoff on fjord circulation and submarine melt rate using a new subgrid-scale parameterization for glacial plumes, Journal of Geophysical Research: Oceans, 120, 796–812, https://doi.org/10.1002/2014JC010324, 2015.

Dallmann, W. K.: Geoscience Atlas of Svalbard, 2015.

D'Angelo, A., Giglio, F., Miserocchi, S., Sanchez-Vidal, A., Aliani, S., Tesi, T., Viola, A., Mazzola, M., and Langone, L.: Multi-year particle fluxes in Kongsfjorden, Svalbard, Biogeosciences, 15, 5343–5363, https://doi.org/10.5194/bg-15-5343-2018, 2018.

Danovaro, R. (Ed.): Methods for the Study of Deep-Sea Sediments, Their Functioning and Biodiversity, CRC Press, Boca Raton, 458 pp., https://doi.org/10.1201/9781439811382, 2009.

Divya, D. T. and Krishnan, K. P.: Recent variability in the Atlantic water intrusion and water masses in Kongsfjorden, an Arctic fjord, Polar Science, 11, 30–41, https://doi.org/10.1016/j.polar.2016.11.004, 2017.

Fossile, E., Nardelli, M. P., Howa, H., Baltzer, A., Poprawski, Y., Baneschi, I., Doveri, M., and Mojtahid, M.: Influence of modern environmental gradients on foraminiferal faunas in the inner Kongsfjorden (Svalbard), Marine Micropaleontology, 173, 102117, https://doi.org/10.1016/j.marmicro.2022.102117, 2022.

Gerland, S., Barber, D., Meier, W., Mundy, C. J., Holland, M., Kern, S., Li, Z., Michel, C., Perovich, D. K., and Tamura, T.: Essential gaps and uncertainties in the understanding of the roles and functions of Arctic sea ice, Environ. Res. Lett., 14, 043002, https://doi.org/10.1088/1748-9326/ab09b3, 2019.

Halbach, L., Vihtakari, M., Duarte, P., Everett, A., Granskog, M. A., Hop, H., Kauko, H. M., Kristiansen, S., Myhre, P. I., Pavlov, A. K., Pramanik, A., Tatarek, A., Torsvik, T., Wiktor, J. M., Wold, A., Wulff, A., Steen, H., and Assmy, P.: Tidewater Glaciers and Bedrock Characteristics Control the Phytoplankton Growth Environment in a Fjord in the Arctic, Front. Mar. Sci., 6, 254, https://doi.org/10.3389/fmars.2019.00254, 2019.

Hegseth, E. N. and Tverberg, V.: Effect of Atlantic water inflow on timing of the phytoplankton spring bloom in a high Arctic fjord (Kongsfjorden, Svalbard), Journal of Marine Systems, 113–114, 94–105, https://doi.org/10.1016/j.jmarsys.2013.01.003, 2013.

Hegseth, E. N., Assmy, P., Wiktor, J. M., Wiktor, J., Kristiansen, S., Leu, E., Tverberg, V., Gabrielsen, T. M., Skogseth, R., and Cottier, F.: Phytoplankton Seasonal Dynamics in Kongsfjorden, Svalbard and the Adjacent Shelf, in: The Ecosystem of Kongsfjorden, Svalbard, vol. 2, edited by: Hop, H. and Wiencke, C., Springer International Publishing, Cham, 173–227, https://doi.org/10.1007/978-3-319-46425-1_6, 2019.

Hodal, H., Falk-Petersen, S., Hop, H., Kristiansen, S., and Reigstad, M.: Spring bloom dynamics in Kongsfjorden, Svalbard: nutrients, phytoplankton, protozoans and primary production, Polar Biol, 35, 191–203, https://doi.org/10.1007/s00300-011-1053-7, 2012.

Hop, H., Falk-Petersen, S., Svendsen, H., Kwasniewski, S., Pavlov, V., Pavlova, O., and Søreide, J. E.: Physical and biological characteristics of the pelagic system across Fram Strait to Kongsfjorden, Progress in Oceanography, 71, 182–231, https://doi.org/10.1016/j.pocean.2006.09.007, 2006.

Hoppe, C. J. M.: Always ready? Primary production of Arctic phytoplankton at the end of the polar night, Limnol Oceanogr Letters, 7, 167–174, https://doi.org/10.1002/lol2.10222, 2022.

Howe, J. A., Moreton, S. G., Morri, C., and Morris, P.: Multibeam bathymetry and the depositional environments of Kongsfjorden and Krossfjorden, western Spitsbergen, Svalbard, Polar Research, 22, 301–316, https://doi.org/10.1111/j.1751-8369.2003.tb00114.x, 2003.

Iona, A., Theodorou, A., Watelet, S., Troupin, C., and Beckers, J.-M.: Mediterranean Sea Hydrographic Atlas: towards optimal data analysis by including time-dependent statistical parameters, Data, Algorithms, and Models, https://doi.org/10.5194/essd-2018-9, 2018.

Isla, E., Rossi, S., Palanques, A., Gili, J.-M., Gerdes, D., and Arntz, W.: Biochemical composition of marine sediment from the eastern Weddell Sea (Antarctica): High nutritive value in a high benthic-biomass environment, Journal of Marine Systems, 60, 255–267, https://doi.org/10.1016/j.jmarsys.2006.01.006, 2006.

Jernas, P., Klitgaard-Kristensen, D., Husum, K., Koç, N., Tverberg, V., Loubere, P., Prins, M., Dijkstra, N., and Gluchowska, M.: Annual changes in Arctic fjord environment and modern benthic foraminiferal fauna: Evidence from Kongsfjorden, Svalbard, Global and Planetary Change, 163, 119–140, https://doi.org/10.1016/j.gloplacha.2017.11.013, 2018.

Juul-Pedersen, T., Michel, C., Gosselin, M., and Seuthe, L.: Seasonal changes in the sinking export of particulate material under first-year sea ice on the Mackenzie Shelf (western Canadian Arctic), Mar. Ecol. Prog. Ser., 353, 13–25, https://doi.org/10.3354/meps07165, 2008.

Kędra, M., Legeżyńska, J., and Walkusz, W.: Shallow winter and summer macrofauna in a high Arctic fjord (79° N, Spitsbergen), Mar Biodiv, 41, 425–439, https://doi.org/10.1007/s12526-010-0066-8, 2011.

Lefauconnier, B., Hagen, J. O., and Rudant, J. P.: Flow speed and calving rate of Kongsbreen glacier, Svalbard, using SPOT images, Polar Research, 13, 59–65, https://doi.org/10.1111/j.1751-8369.1994.tb00437.x, 1994.

Lind, S., Ingvaldsen, R. B., and Furevik, T.: Arctic warming hotspot in the northern Barents Sea linked to declining sea-ice import, Nature Clim Change, 8, 634–639, https://doi.org/10.1038/s41558-018-0205-y, 2018.

Lorenzen, C. J. and Jeffrey, S. W.: Determination of chlorophyll in seawater, 1980.

Lund-Hansen, L. C., Andersen, T. J., Nielsen, M. H., and Pejrup, M.: Suspended Matter, Chl-a, CDOM, Grain Sizes, and Optical Properties in the Arctic Fjord-Type Estuary, Kangerlussuaq, West Greenland During Summer, Estuaries and Coasts, 33, 1442–1451, https://doi.org/10.1007/s12237-010-9300-7, 2010.

Lydersen, C., Assmy, P., Falk-Petersen, S., Kohler, J., Kovacs, K. M., Reigstad, M., Steen, H., Strøm, H., Sundfjord, A., Varpe, Ø., Walczowski, W., Weslawski, J. M., and Zajaczkowski, M.: The importance of tidewater glaciers for marine mammals and seabirds in Svalbard, Norway, Journal of Marine Systems, 129, 452–471, https://doi.org/10.1016/j.jmarsys.2013.09.006, 2014.

Meslard, F., Bourrin, F., Many, G., and Kerhervé, P.: Suspended particle dynamics and fluxes in an Arctic fjord (Kongsfjorden, Svalbard), Estuarine, Coastal and Shelf Science, 204, 212–224, https://doi.org/10.1016/j.ecss.2018.02.020, 2018.

Mincks, S., Smith, C., and DeMaster, D.: Persistence of labile organic matter and microbial biomass in Antarctic shelf sediments: evidence of a sediment food bank, Mar. Ecol. Prog. Ser., 300, 3–19, https://doi.org/10.3354/meps300003, 2005.

Moran, S. B., Lomas, M. W., Kelly, R. P., Gradinger, R., Iken, K., and Mathis, J. T.: Seasonal succession of net primary productivity, particulate organic carbon export, and autotrophic community composition in the eastern Bering Sea, Deep Sea Research Part II: Topical Studies in Oceanography, 65–70, 84–97, https://doi.org/10.1016/j.dsr2.2012.02.011, 2012.

Morata, N., Renaud, P., Brugel, S., Hobson, K., and Johnson, B.: Spatial and seasonal variations in the pelagic–benthic coupling of the southeastern Beaufort Sea revealed by sedimentary biomarkers, Mar. Ecol. Prog. Ser., 371, 47–63, https://doi.org/10.3354/meps07677, 2008.

Nilsen, F., Skogseth, R., Vaardal-Lunde, J., and Inall, M.: A Simple Shelf Circulation Model: Intrusion of Atlantic Water on the West Spitsbergen Shelf, Journal of Physical Oceanography, 46, 1209–1230, https://doi.org/10.1175/JPO-D-15-0058.1, 2016.

Payne, C. M. and Roesler, C. S.: Characterizing the influence of Atlantic water intrusion on water mass formation and phytoplankton distribution in Kongsfjorden, Svalbard, Continental Shelf Research, 191, 104005, https://doi.org/10.1016/j.csr.2019.104005, 2019.

Piquet, A. M.-T., van de Poll, W. H., Visser, R. J. W., Wiencke, C., Bolhuis, H., and Buma, A. G. J.: Springtime phytoplankton dynamics in Arctic Krossfjorden and Kongsfjorden (Spitsbergen) as a function of glacier proximity, Biogeosciences, 11, 2263–2279, https://doi.org/10.5194/bg-11-2263-2014, 2014.

Pusceddu, A., Dell'Anno, A., and Fabiano, M.: Organic matter composition in coastal sediments at Terra Nova Bay (Ross Sea) during summer 1995, Polar Biology, 23, 288–293, https://doi.org/10.1007/s003000050446, 2000.

Pusceddu, A., Dell'Anno, A., Fabiano, M., and Danovaro, R.: Quantity and bioavailability of sediment organic matter as signatures of benthic trophic status, Mar. Ecol. Prog. Ser., 375, 41–52, https://doi.org/10.3354/meps07735, 2009.

Rokkan Iversen, K. and Seuthe, L.: Seasonal microbial processes in a high-latitude fjord (Kongsfjorden, Svalbard): I. Heterotrophic bacteria, picoplankton and nanoflagellates, Polar Biol, 34, 731–749, https://doi.org/10.1007/s00300-010-0929-2, 2011.

Schauer, U., Fahrbach, E., Osterhus, S., and Rohardt, G.: Arctic warming through the Fram Strait: Oceanic heat transport from 3 years of measurements, Journal of Geophysical Research: Oceans, 109, https://doi.org/10.1029/2003JC001823, 2004.

Schlitzer, R., 2020. Ocean Data View User's Guide Version 5.3.0, Ocean Data View. Available online at. https://odv.awi.de.

Seuthe, L., Rokkan Iversen, K., and Narcy, F.: Microbial processes in a high-latitude fjord (Kongsfjorden, Svalbard): II. Ciliates and dinoflagellates, Polar Biol, 34, 751–766, https://doi.org/10.1007/s00300-010-0930-9, 2011.

Strzelewicz, A., Przyborska, A., and Walczowski, W.: Increased presence of Atlantic Water on the shelf south-west of Spitsbergen with implications for the Arctic fjord Hornsund, Progress in Oceanography, 200, 102714, https://doi.org/10.1016/j.pocean.2021.102714, 2022.

Sundfjord, A., Albretsen, J., Kasajima, Y., Skogseth, R., Kohler, J., Nuth, C., Skarðhamar, J., Cottier, F., Nilsen, F., Asplin, L., Gerland, S., and Torsvik, T.: Effects of glacier runoff and wind on surface layer dynamics and Atlantic Water exchange in Kongsfjorden, Svalbard; a model study, Estuarine, Coastal and Shelf Science, 187, 260–272, https://doi.org/10.1016/j.ecss.2017.01.015, 2017.

Svendsen, H., Beszczynska-Møller, A., Hagen, J. O., Lefauconnier, B., Tverberg, V., Gerland, S., Børre Ørbæk, J., Bischof, K., Papucci, C., Zajaczkowski, M., Azzolini, R., Bruland, O., and Wiencke, C.: The physical environment of Kongsfjorden–Krossfjorden, an Arctic fjord system in Svalbard, Polar Research, 21, 133–166, https://doi.org/10.3402/polar.v21i1.6479, 2002.

Trusel, L. D., Powell, R. D., Cumpston, R. M., and Brigham-Grette, J.: Modern glacimarine processes and potential future behaviour of Kronebreen and Kongsvegen polythermal tidewater glaciers, Kongsfjorden, Svalbard, Geological Society, London, Special Publications, 344, 89–102, https://doi.org/10.1144/SP344.9, 2010.

Tverberg, V., Skogseth, R., Cottier, F., Sundfjord, A., Walczowski, W., Inall, M. E., Falck, E., Pavlova, O., and Nilsen, F.: The Kongsfjorden Transect: Seasonal and Inter-annual Variability in Hydrography, in: The Ecosystem of Kongsfjorden, Svalbard, vol. 2, edited by: Hop, H. and Wiencke, C., Springer International Publishing, Cham, 49–104, https://doi.org/10.1007/978-3-319-46425-1_3, 2019.

Vihtakari, M., 2020. PlotSvalbard: PlotSvalbard - Plot research data from Svalbard on maps. In: R package version 0.9.2. https://github.com/MikkoVihtakari/Plo tSvalbard.

Wlodarska-Kowalczuk, M. and Pearson, T. H.: Soft-bottom macrobenthic faunal associations and factors affecting species distributions in an Arctic glacial fjord (Kongsfjord, Spitsbergen), Polar Biol, 27, 155–167, https://doi.org/10.1007/s00300-003-0568-y, 2004.

Supplementary material 1:

- Table S1: Organic matter raw data

Station	depth	Mission	Proteins mgC/g	sd	Carbohydrates mgC/g	sd	Lipids mgC/g	sd	Biopolymeric carbon mg/g	sd	Chl-a µg/g	sd	Phaeopigments µg/g	sd	Phytopigments µg/g	sd
2	0-0.5	August 2021	0.71	0.08	0.18	0.10	0.21	0.05	1.10	0.13	0.08	0.02	1.16	0.16	1.25	0.17
7	0-0.5	August 2021	0.34	0.05	0.19	0.04	0.22	0.13	0.74	0.16	0.09	0.06	1.49	0.18	1.58	0.23
5	0-0.5	August 2021	0.86	0.06	0.25	0.15	0.28	0.12	1.38	0.24	4.07	0.83	11.85	6.04	15.92	6.86
8	0-0.5	August 2021	0.85	0.12	0.31	0.19	0.53	0.03	1.69	0.30	1.12	0.15	6.70	0.45	7.83	0.45
2																
7	0-0.5	May 2021	0.60	0.04	0.16	0.03	0.08	0.01	0.83	0.02	0.05	0.01	0.75	0.03	0.80	0.03
5	0-0.5	May 2021	0.69	0.05	0.34	0.01	0.11	0.03	1.13	0.07	0.34	0.04	4.83	0.18	5.17	0.17
8	0-0.5	May 2021	1.07	0.14	0.49	0.05	0.17	0.02	1.73	0.18	0.75	0.11	10.88	0.22	11.63	0.26

Station	depth	Mission	CPE mgC/g	sd	CCPE/BPC	sd	cPRT:BPC	sd	Protein/Carbohydrates	sd	LEU nmol/g/h	sd	LEU µgC	sd
2	0-0.5	August 2021	0.05	0.01	0.05	0.00	0.65	0.06	5.34	5.12	21.70	0.22	1.56	0.02
7	0-0.5	August 2021	0.06	0.01	0.09	0.02	0.47	0.10	1.58	0.60	18.39	4.83	1.32	0.35
5	0-0.5	August 2021	0.64	0.27	0.45	0.11	0.63	0.12	3.69	2.32	89.74	9.17	6.46	0.66
8	0-0.5	August 2021	0.31	0.02	0.19	0.03	0.51	0.04	2.69	1.10	49.44	16.40	3.56	1.18
2														
7	0-0.5	May 2021	0.03	0.00	0.04	0.00	0.72	0.04	3.21	0.79	5.53	0.47	0.40	0.03
5	0-0.5	May 2021	0.21	0.01	0.18	0.00	0.61	0.02	1.67	0.17	76.09	7.59	5.48	0.55
8	0-0.5	May 2021	0.47	0.01	0.27	0.04	0.62	0.02	1.77	0.15	61.21	1.57	4.41	0.11

Chapter 5

Sediment redox cycling instabilities generated by glacial inputs in Kongsfjorden (Svalbard)

C. Guilhermic[*1], A. Mouret[1], H. Howa[1], A. Pusceddu[2], A. Baltzer[3], M.P. Nardelli[1]

[1] Université Angers, Nantes Univ., Le Mans Univ, CNRS, LPG, Laboratoire de planétologie et géosciences, UMR CNRS 6112, F-49000 Angers, France
[2]Department of Life and Environmental Sciences, University of Cagliari, 09126 Cagliari, Italy
[3]LETG, UMR CNRS 6554, University of Nantes, Campus du Tertre, 44312 Nantes Cedex 3, France

Chapter 5: Sediment redox cycling instabilities generated by glacial inputs in Kongsfjorden (Svalbard)

Abstract :

Kongsfjorden (Svalbard) is subjected to continental glacier melting in summer. More particularly, tidal glaciers melting waters carry significant volumes of freshly eroded sediment from bedrock and deliver it through subglacial runoff into the fjord. This highly turbid water results in a high sedimentation rate near the glacier front decreasing with increasing distance from it. This decrease also generates an antagonist increase of phytoplanktonic growth leading to an organic matter export gradient along the fjord's axis. Those environmental gradients generate sediment biogeochemistry instability and resulting transient state towards an eventual recovery. The present study aims to identify unstable zones subjected to high sediment deposition and to understand the processes involved in the recovery of biogeochemical gradients. In August 2021, we sampled interface sediment cores at 4 sites with increasing distance to Kronebreen glacier front and analysed early diagenesis related chemical species, porewater oxygen, ammonium and nitrate concentrations and manganese and iron dissolved and particular phases. Oxygen penetration depth was observed to be deeper near the glacier front compared to our most distal one and interpretated in relation with respirating organism's diversity and density. The vertical distribution of Mn and Fe reactive oxides and the ongoing dissolved manganese and iron production revealed strong sediment deposition in glacier proximal areas. In this configuration where bioavailable oxides are scarce and that the main metal bearing oxide phases are more crystalline due to unprocessed freshly eroded material, it can be assumed that they previously originated from diagenetic surface enrichment now found buried, in an anoxic medium submitted to ongoing metal reduction. The duality between those two phases is an indicator of sediment deposition events in the inner basin of Kongsfjorden and of transient state. In the distal stations, the substrate was found in a stable state mostly due to decreased sedimentation rates and higher organic matter content from surface primary production catalysing all biogeochemical reactions. In this way, additional core observations and literature attest of the increasing of sulfate reduction away from the glacier and contributing to iron reduction through associated abiotic processes. Biogeochemical states heterogeneity in the fjord can be a good indicator for benthic ecosystem stress regarding high sedimentation events. Interannual glacier sediment discharge would therefore shifts upfjord or downfjord the lateral sequence of biogeochemical transient states and stable areas.

Keywords: Arctic, sediment deposition, stability, early diagenesis, transient state, glacier

1 Introduction

Seasonal melting of glaciers in high latitude fjords induces strong environmental gradients mostly induced by huge volumes of fresh meltwaters exported at their fronts on land or at sea. Glacier creeps and basal sliding induce the weathering of bedrock resulting in the transport of detrital particles by subglacial runoff through their catchment until deposition in fjord's basins (Bennett et al., 1999; Bouchayer et al., 2023; Bourriquen et al., 2016; Elverhøi et al., 1983; Streuff et al., 2015). Before particles settle on benthic substrate, a turbid plume spreads over the fjord surface (D'Angelo et al., 2018; Łepkowska and Stachnik, 2018; Meslard et al., 2018; Trusel et al., 2010). Turbid freshwater at the sea surface also create an environmental gradient of primary production inhibited by the unavailability of light to perform photosynthesis at the proximity of glacier fronts (Calleja et al., 2017; Halbach et al., 2019; Hop and Wiencke, 2019; Hopwood et al., 2020; Payne and Roesler, 2019). The resulting export of organic matter towards the seafloor therefore presents a major decrease from the mouth to the head of the fjord (Bourgeois et al., 2016; Lalande et al., 2016; Singh and Krishnan, 2019). Contrary to the organic matter export gradient, detrital sedimentation decreases from glacier fronts to the fjord's mouth (Lydersen et al., 2014; Svendsen et al., 2002). The benthic environment near glacial outlets is therefore affected by these changes in organic carbon supply and sediment accumulation rate, which induce sediment disturbance and in particular non-steady state conditions in early diagenesis processes related to organic matter mineralization.

Redox changes in sediment are mainly controlled by early diagenetic processes and the vertical sequence of organic matter remineralization by bacterial activity (Burdige, 1993; Froelich et al., 1978). Reduced metabolic products (e.g. Mn^{2+}, Fe^{2+}, $\sum NH_3$ and H_2S) are generated using dissolved oxygen, nitrate, potentially bioavailable Mn and Fe oxides, and sulfate as electron acceptors for organic matter remineralization. In an anoxic/reducing medium, these products diffuse through sediment porewaters towards less concentrated areas and can be oxidized in the oxic layer. Previous studies highlighted natural transient states generated by intense sedimentation in coastal areas caused by river flooding (Cathalot et al., 2010; Deflandre et al., 2002; Mucci et al., 2003; Mucci and Edenborn, 1992; Pastor et al., 2018; Thibault de Chanvalon et al., 2016) or gravity flow events (Anschutz et al., 2002; Wilson et al., 1985). After such disturbances, these studies described transient states caused by disruption of the diagenetic sequence by isolating the established geochemical gradients from direct diffusive exchanges with seawater. Depending on the quantity and quality of organic matter in the sediments and the thickness of the deposited sediment layer, migration of redox gradients occurs at different rates towards the surface where stable conditions can be reached after a certain time (Chaillou et al., 2007; Nmor et al., 2022; Wang and Van Cappellen, 1996).

Svalbard fjords are transitional systems between glaciated/terrestrial and marine realms and are therefore locations of significance for biogeochemical exchanges. Glacial erosion and associated seasonal melting can bring consequent amounts of freshly eroded particles enriching the fjord in micronutrients (D'Angelo et al., 2018; Halbach et al., 2019; Hegseth et al., 2019; Hoppe, 2022; Hopwood et al., 2020; Hop and Wiencke, 2019; Lalande et al., 2016; Meslard et al., 2018). From this discharge derive two major forcings ruling related pelagic and benthic biological and biogeochemical processes (Herbert et al., 2022; Hop and Wiencke, 2019). Indeed, freshwater discharge from subglacial runoff increases fjord surface turbidity on a kilometre scale inducing high sedimentation rates in the vicinity of the glacier front (D'Angelo et al., 2018; Lydersen et al., 2014; Meslard et al., 2018; Svendsen et al., 2002; Trusel et al.,

2010). On the fringe of this turbid plume, nutrient supply allows phytoplanktonic blooms in spring and summer resulting in important export of organic matter to the seafloor (Hegseth et al., 2019; Hopwood et al., 2020). These two antagonistic environmental gradients were proven to have a real impact on the geochemical state of fjord sediment through the dynamics of redox gradients such as manganese and iron cycles (Herbert et al., 2020). In Svalbard fjords, Kongsfjorden in particular, geochemical studies were carried out over the past few decades in order to investigate the role of high-latitude fjords in the overall geochemical dynamics of the Arctic (Gihring et al., 2010; Herbert et al., 2020, 2021, 2022; Jørgensen et al., 2021; Laufer-Meiser et al., 2021; Michaud, 2020; Yang et al., 2022; Wehrmann et al., 2014).

The stress induced by glacier discharge and concomitant primary production zonation not only affect the sediment biogeochemistry state, but also benthic life (Hop and Wiencke, 2019; Koziorowska et al., 2017; Wlodarska-Kowalczuk et al., 2005). Ecosystem functioning and structure depend on the pelagic/benthic link. Therefore, more precise identification of disturbed areas through sediment geochemistry state could help to understand and constrain the forcings affecting the benthic realm from a holistic point of view.

The aim of this study is to investigate the transient states of sedimentary redox gradients caused by the intense detrital sedimentation and localized organic matter export generated by summer melting in Kongsfjorden on a kilometre scale. As this fjord is an early witness of ongoing warming amplification in Arctic systems, the study of the relation between local glacial inputs and benthic geochemical processes could provide additional information for understanding the dynamics of similar fjords in the future. To this end, dissolved porewater species (oxygen, ammonium, nitrate, manganese, iron, sulfate) and parameter (alkalinity) were investigated along with Mn and Fe solid phases in order to characterize the dynamics of geochemical processes in the sediment column. We expect different stages of transient state generated by the gradients in detrital sedimentation and organic matter export along the fjord axis.

2 Study area

Kongsfjorden is a subpolar fjord located on the West-Spitsbergen coast (79°N) in the Svalbard archipelago. It is a glaciated fjord with five marine-terminating glacier fronts in its inner parts (Kongsvegen, Kronebreen, Kongsbreen, Conwaybreen and Blomstrandbreen) and land terminating glaciers located on the southern coast (Lovénbreen glaciers) (Dallmann, 2015). As it is open on the Fram Strait separating Svalbard from Greenland along a West-East transect and the Atlantic Ocean from the Arctic Ocean along a South-North transect and lacks an entrance sill like many fjords (Dallmann, 2015; Howe et al., 2010), it is subject to seasonal intrusions of warm, salty and nutrient-rich Atlantic waters (Cottier et al., 2005; Hop et al., 2006; Svendsen et al., 2002; Payne and Roesler, 2019). Primary production bloom in the water column usually occurs in April-May followed by irregular phytoplanktonic blooms in summer (Azzaro et al., 2021; Calleja et al., 2017; Hegseth et al., 2019; Piquet et al., 2014; van de Poll et al., 2018) resulting in a high export of organic matter of marine origin to the seafloor (Hop and Wiencke, 2019; Koziorowska et al., 2017; Lalande et al., 2016). However, organic matter export is not homogeneous within the fjord due to local hydrodynamic conditions (Bourgeois et al., 2016; Koziorowska et al., 2017). The incursions of Atlantic warm water, combined with summer rise in air temperature, generate melting of local glaciers resulting in calving and freshwater runoff into the fjord (Cowton et al., 2015; Howe et al., 2010; Kohler et al., 2007).

Glacial discharge produces surface turbid plumes spreading in the fjord (D'Angelo et al., 2018; Elverhøi et al., 1983; Meslard et al., 2018). This surface water loaded with fine detrital particles induces high sedimentation rates near the Kronebreen front, the glacier generating most of the suspended material in the fjord, and which decrease with distance from the glacier front (Lydersen et al., 2014). The bedrock eroded by this glacier consists of sedimentary formations mostly composed of sandstones, conglomerates, limestones or shales formed during the Carboniferous and Devonian periods (Dallmann, 2015; Meslard et al., 2018). In the inner part of the fjord where turbidity is highest, primary production is inhibited resulting in low organic matter export (Payne and Roesler, 2019; Piquet et al., 2014). In summer, high sedimentation rates of 60-90 mm y^{-1} occur in the inner basin (Trusel et al., 2010) and further dilute this low organic matter export occurring at the fjord head. More details on the study area and environmental parameter analysis are presented in ***Chapter 1*** and ***Chapter 4***.

3 Material and methods

A sampling campaign was carried out between 16/08/2021 and 30/08/2021 in Kongsfjorden (Svalbard) to recover interface sediment cores. The four chosen stations were aligned along the fjord axis with increasing distance from the Kronebreen glacier front. Geochemical analyses were performed on sediment cores sampled with a GeMAX corer or a DayGrab (K/C Demark A/S). Only St. 5 was sampled with the latter device. At each station, in addition to the core used for geochemical analyses, two other cores were reserved for organic matter measurements and for dissolved oxygen microprofiling. Before processing, the cores were stored for a maximum of one day in a cold room set to the fjord bottom water temperature, which was 3°C, with air-bulled bottom water.

Sample processing and measurements

To calculate sediment porosity, empty tubes were weighted before the slicing of the cores. After the core slicing, the tubes filled with wet sediment from each layer were also weighted before centrifugation to recover the porewater. The sediment fraction was then frozen at -20°C and freeze-dried to remove the remaining porewater from the sample. Finally, dried sediment was weighted for the final porosity calculation. Easily reducible metals (potentially bioavailable for bacterial reduction) associated with amorphous oxides were extracted from crushed freeze-dried samples following the ascorbate extraction protocol by Kostka and Luther (1994) and Anschutz et al. (1998, 2005). Samples (0.1g) were individually mixed with 10 mL of sodium bicarbonate (0.6 M), sodium citrate (0.17 M) and ascorbic acid (0.11 M) at a pH of 8. All samples were gently stirred for 24h and then centrifugated. A 10-fold dilution was thereafter performed using 1 mL of supernatant solution and 9 mL of 1% nitric acid solution for $[Mn]_{asc}$, $[Fe]_{asc}$ measurements by ICP-AES (Thermo scientific iCAP 6300 Radial). Additional sequential extractions for particulate Mn and Fe were performed on sediment of two sites following the protocol detailed by Lenstra et al. (2021). The second step after ascorbate extraction used hydrochloric acid (HCl) to extract reducible crystalline Fe oxides and Mn and Fe carbonates (Claff et al., 2010), the third step used citrate-buffered dithionite (CDB) to extract crystalline oxides (Poulton and Canfield, 2005). Recalcitrant crystallized oxides were extracted using oxalic acid (Poulton and Canfield, 2005) and pyrite and bound metal were extracted using nitric acid (Claff et al., 2010). These measurements were also performed by ICP-AES analysis.

Grain size measurements were performed on humidified freeze-dried sediment using a laser diffraction particle analyser (Malvern Mastersizer 3000).

Dissolved oxygen microprofiling was performed using 50µm tip diameter Clark-type microelectrodes (Unisense^{TM}). These microelectrodes can measure oxygen concentration in porewaters with a vertical step resolution of 50 µm. They are attached to an automated micro-manipulator connected to a motor allowing a controlled descent into the sediment (Revsbech, 1989). Several descents were made at different points in the core in order to cover spatial variability.

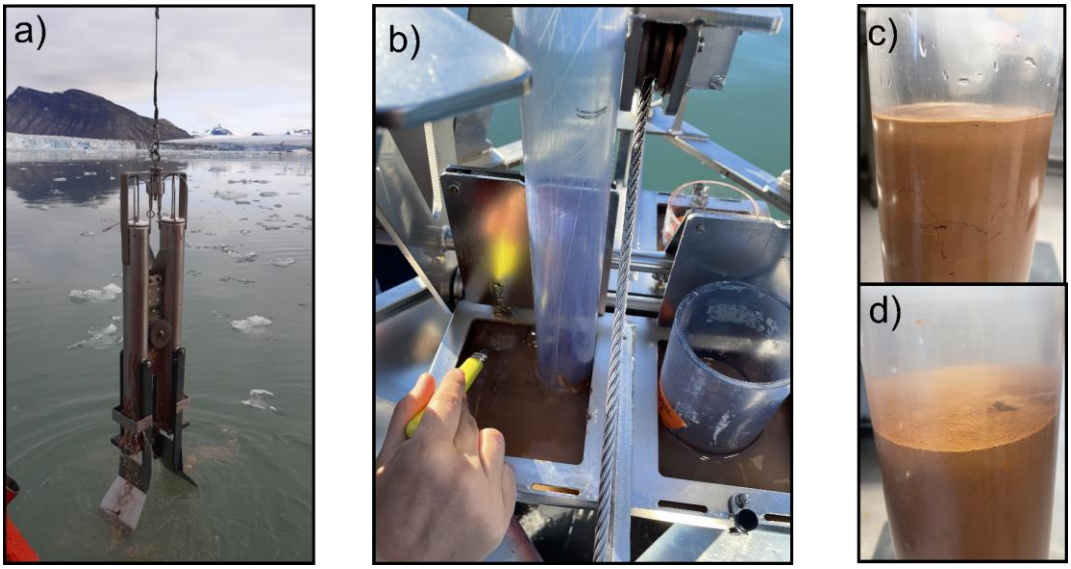

Figure 1: a) GeMAX corer at St. 2 after sediment recovery. b) Surface sediment coring through open hatches at the top of the DayGrab after sediment recovery. c) Sediment-water interface of the core sampled at St. 7. d) Sediment-water interface of the core sampled at St. 2

Porewater alkalinity, nitrite and nitrate concentrations were measured in each core within the 24 hours after recovery. The cores were set up in a N_2-filled bag for the slicing process to avoid oxidation of reduced chemical species. Under these conditions, sediment layers were sliced with the following resolution: 0.5 cm thick from surface to 2 cm depth, 1 cm thick from 2 cm to 20 cm depth and 1 cm thick every 5 cm to the end of the core. Each sample was then centrifuged (3000 rpm for 15 min) to separate the porewater from the sediment matrix. Still under anoxic atmosphere, each water sample (including bottom water) was filtered through 0.2 µm Minisart® RC25 cellulose syringe filters and separated into three subsamples for either nutrient and alkalinity analyses, or for subsequent ICP-AES measurements. This latter aliquot was acidified with a 1% volume equivalent of concentrated nitric acid (HNO_3). Nitrite (NO_2^-) and nitrate (NO_3^-) concentrations were measured sequentially, immediately after sampling, according to the Griess method (Griess, 1879) and using vanadium chloride (VCl_3) as nitrate reducer (García-Robledo et al., 2014; Schnetger and Lehners, 2014). The spectrophotometer (Thermo scientific® genesis 20) was set at the wavelength 543 nm for absorbance measurement. The resulting measurement is therefore the concentration in NO_x ($[NO_2^- + NO_3^-]$). Nitrate concentration was calculated from this value using the following relation (Garcia-Robledo et al., 2014):

$$[NO_3^-] = (Abs^V_{NOx} - Abs^V reagents - S^V NO_2^- * [NO_2^-]) / S^V NO_3^-$$

Where: Abs^{V}_{NOx} is the final measured absorbance i.e., the combination of $[NO_2^-]$ and $[NO_3^-]$; Abs^{V}reagents is the absorbance of VCl_3 without $[NO_2^-]$ or $[NO_3^-]$, $S^{V}NO_2^-$ and $S^{V}NO_3^-$ are the slopes of the calibration curves after VCl_3 addition; $[NO_2^-]$ is the nitrite concentration previously calculated in the sample. The remaining water sample from this analysis was stored frozen at -20°C for subsequent ammonium analysis. The last filtered aliquot of each sample was also used immediately after core processing for porewater alkalinity measurements performed following the colorimetric method of (Sarazin et al., 1999). This method consists in a titration with a solution containing known concentrations of formic acid, bromophenol blue and NaCl. Absorbance values were measured at 590 nm.

Porewater $\sum NH_3$ ($NH_3 + NH_4^+$) was analysed on frozen preserved samples according to the Berthelot method recently adapted for small saline samples (Metzger et al., 2019). The colorimetric reaction involves two reagents, the one containing sodium hydroxide, etidronic acid and sodium hypochlorite and the other a solution of sodium nitroprussiate and thymol. Absorbance analysis was made at 690 nm wavelength with a spectrophotometer. ICP-AES (Thermo scientific iCAP 6300 Radial) analysis was performed on previously acidified samples after a 10-fold dilution with 1% HNO_3. After a calibration step, $[Mn_d]$, $[Fe_d]$ and [S] were measured. Due to sample acidification, [S] measurements were interpreted as $[SO_4^{2-}]$ since sulfide is volatile and was removed from the sample solution under acidic conditions.

All graphs were designed on GRAPHER (golden software), and artworks were modified and finalized with Inkscape software.

4 Results

4.1 Sediment characteristics

4.1.1 Porosity and grain-size analysis

Grain size analysis was performed for all stations and the particle populations are represented in Fig. 2 by primary and secondary modes). All analysed sediment showed a fine silt mode of around 10 µm. At St. 5, this mode was unique. At St. 7, where a bimodal distribution was found in the upper 20cm of the core, coarser secondary modes were found, ranging from 12 to 600 µm. At the other two stations 8 and 2, the 10 µm mode was also present throughout the sediment column as a primary mode. However, the increasing presence of a second 80 µm mode at both stations generated an alternation of the two particle populations as primary and secondary modes. At St. 8, this shift can be observed twice in the uppermost 10 cm of sediment. At St. 2, changes in primary modes can be observed deeper in the core with the layers between 10 and 20 cm depth showing the primary mode of 80 µm.

Vertical porosity was investigated in all sediment cores and the results are shown in Fig. 2. Different porosity patterns were observed in the stations. At St. 2, the surface porosity was 0.81 with a rapid decrease in the first 5 cm to 0.64. This was followed by an increase within the next 4 cm to reach 0.70. Below, a decrease until 0.51 at 20 cm depth was followed by an increase to 0.60 at the bottom of the core. At St. 7, a decrease from 0.87 at the surface to 0.60 at 12 cm depth was observed. This was followed by an increase to 0.69 at 16 cm depth. Below, porosity stabilized around 0.62 until the bottom of the core. The short core at St. 5 displayed a decreasing porosity from 0.78 at the surface to 0.58 at 10 cm depth. Finally, St. 8 core showed a surface

porosity of 0.72 followed by a strong decrease to 4 cm depth reaching the value of 0.56. Below, porosity stabilized around 0.56.

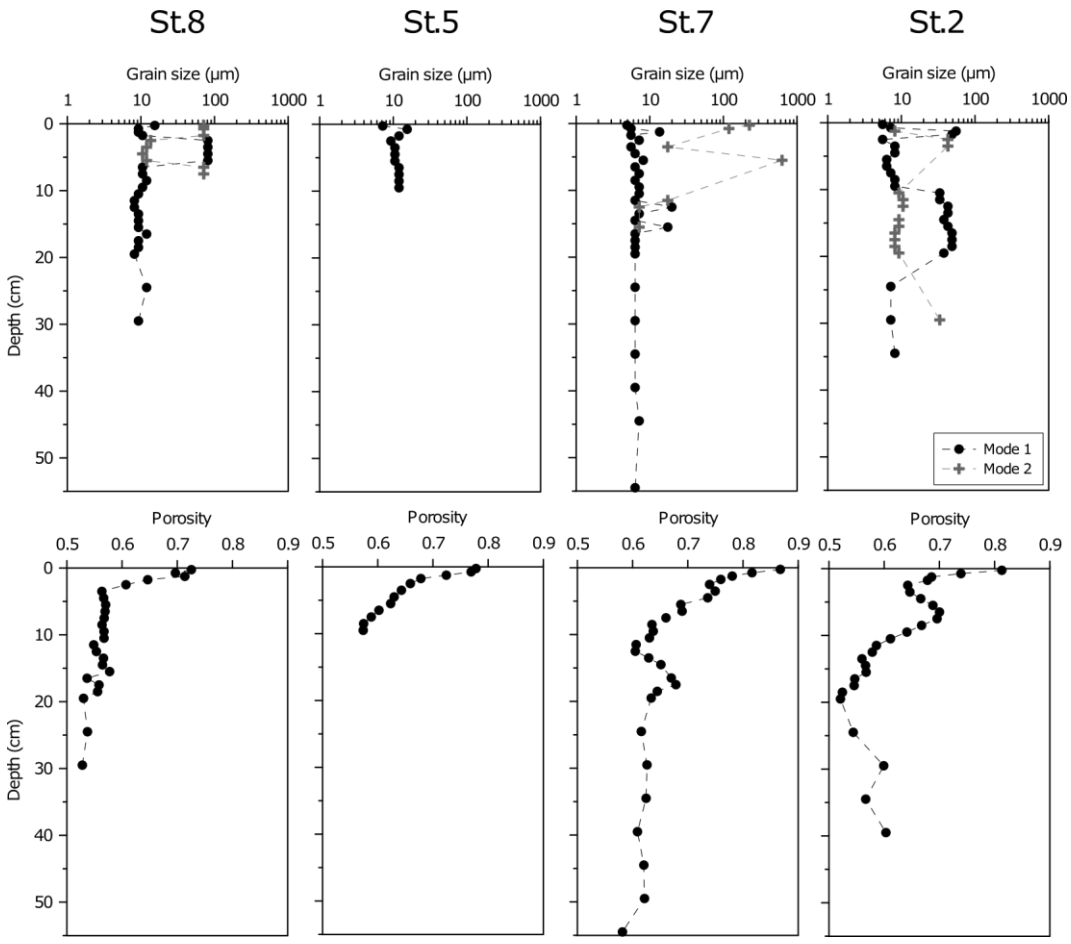

Figure 2: Vertical profiles of sediment grain size mode values and porosity. Note that main mode (mode 1) is represented in black in the upper panel and secondary mode is in grey when present in the sample. More detailed grain-size data are shown in Chapter 4.

4.1.2 Solid phase Mn and Fe

Chemical extractions were carried out sequentially along the sediment cores from St. 7 and St. 8 and displayed in Fig. 3. The most abundant Mn solid phase was the one extracted by hydrochloric acid (HCl; grey area in Fig. 3) at both stations. Indeed, this phase showed concentrations of 4 to 5 µmol g^{-1} at St. 7 and 3.2 to 4.6 µmol g^{-1} at St. 8. Surface enrichment was visible in all ascorbate- and HCl-extracted phases at St. 8 (9 µmol g^{-1}). The CDB-extracted phase showed similar concentrations to the ascorbate-extracted one at both stations but with lower surface enrichment at St. 8. On the opposite, crystalline Fe-oxides were mostly measured by CDB extraction with concentrations between 150 and 200 µmol g^{-1} at St. 7 and 120 and 180 µmol g^{-1} at St. 8, with notable enrichment above 4 cm depth. The HCl-extracted phase showed less variability with depth at both stations with values around 120 µmol g^{-1}. The most abundant phases (HCl for Mn and CDB for Fe) were higher at St. 7 than at St. 8.

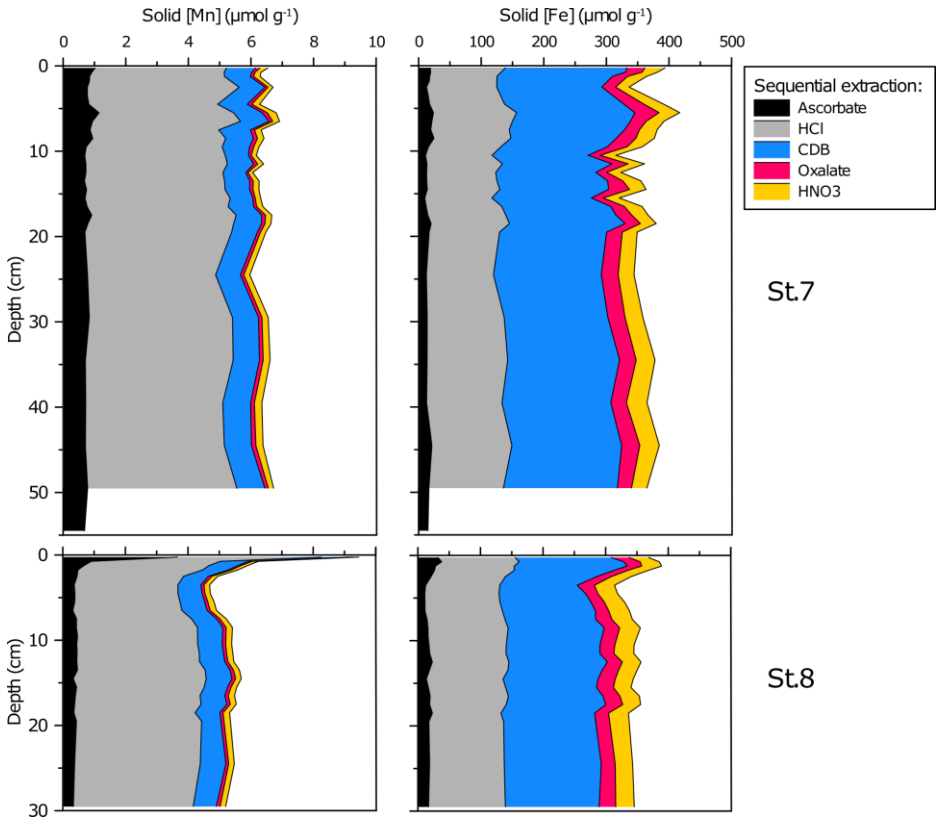

Figure 3: Depth profiles of solid Mn and Fe concentrations extracted following the ascorbate (black), HCl (grey), CDB (blue), oxalate (pink red) and HNO_3 extraction sequence for the two contrasted stations 7 and 8, in the inner and outer basins, respectively.

4.2 Redox-sensitive species in the sediment

4.2.1 Oxygen penetration depth

Dissolved oxygen concentrations in bottom water and porewater were investigated at St. 7 and 8, both located in different basins of the fjord. Station 7, located near the Kronebreen glacier front, showed an oxygen penetration depth (OPD) of 10.3 ± 0.5 mm (n=9; n being the number of O_2 measured profile), while St. 8 displayed an OPD of 8.5 ± 0.8 mm (n=4). The surface oxic layer is displayed as a grey stripe in Fig. 4 for both stations.

4.2.2 Inorganic nitrogen species

Fig. 4 (first column) displays the vertical distribution of nitrite, nitrate and ammonium concentrations in bottom water and sediment porewaters. At St. 2, a downward increase in [$\sum NH_3$] from 70 µmol L^{-1} in the uppermost sediment layer to 350 µmol L^{-1} at 20 cm sediment depth was observed. Similarly, to the St. 2, the profile of [$\sum NH_3$] of St. 7, displayed a downward increase of concentration to reach 550 µmol L^{-1} at 45 cm depth. At St. 5, ammonium concentration increased from 30 to 120 µmol L^{-1} within the sampled upper sediment column of 10 cm thick. At St. 8 the sediment showed an enrichment between 2 and 5 cm depth, from 30 µmol L^{-1} in the oxic layer to 100 µmol L^{-1}. Below, no increase as seen in the St. 2 and St. 7 was observed.

At St. 2, a nitrate concentration of 2.5 µmol L^{-1} was measured in bottom water. A decrease to 1 µmol L^{-1} was observed below 0.5 cm and before 2 cm depth in the sediment. Downcore, a noticeable concentration peak reached 4 µmol L^{-1} at 11 cm depth. Below, nitrate

concentration stabilized at around 1 µmol L^{-1}. At St. 7, a decreasing gradient of nitrate in porewater from the highest concentration in the oxic layer was evidenced. Within the uppermost 3 cm of sediment, [NO_3^-] dropped from 3.7 to 1 µmol L^{-1}. Below, the concentration remained stable around 1 µmol L^{-1}. At this station, porewater ammonium concentration increased from 20 µmol L^{-1} in surface sediment to 350 µmol L^{-1} at 25 cm depth. Below, a high variability can be observed from 550 µmol L^{-1} at 45 cm depth to 170 µmol L^{-1} at the bottom of the core. The short core (10 cm) recovered from St. 5 allowed the observation of a [NO_3^-] decrease within the uppermost 1 cm below the SWI to a stable value of 1 µmol L^{-1} down to 10 cm depth. At St. 8, surface porewater [NO_3^-] displayed a concentration of 9.6 µmol L^{-1} , higher than in bottom water with 6 µmol L^{-1}. Concentration rapidly dropped from 9.6 µmol L^{-1} in surface porewater to 1 µmol L^{-1} between 2-3 cm depth. A slight increase in [$\sum NH_3$] was observed from the surface to 5 cm depth with 80 µmol L^{-1}. Below, a variation between 20 µmol L^{-1} and 90 µmol L^{-1} was observed.

4.2.3 Manganese vertical distribution

Vertical distribution of manganese reactive oxides was not similar between stations (Fig. 3 and Fig 4. second column). Indeed, at St. 2 a slight peak of [Mn_{asc}] was observed at 8 cm depth with 1.1 µmol g^{-1} whereas the deeper and upper levels only showed concentrations of 0.6–0.8 µmol g^{-1} (Fig. 4). At St. 7, a similar increase of [Mn_{asc}] was identified between 4-5 cm depth. While the rest of the sediment column remained below 0.7 µmol g^{-1}, a smaller increase was observed around 17 cm depth, reaching 0.9 µmol g^{-1}. The more distal stations displayed a different vertical distribution of manganese reactive oxides with surface enrichments reaching 2 and 3.6 µmol g^{-1} at St. 5 and St. 8, respectively. Below these higher surface concentrations, a rapid decrease was observed within the first centimetres. At St. 5, the short core showed a decrease until 0.5 µmol g^{-1} in the underlying 10 cm without reaching a stable value. At St. 8, concentration decreased within the first 3 cm to reach the relatively constant value of 0.4 µmol g^{-1} down to 30 cm depth.

In addition to [Mn_{asc}] profiles, associated porewater [Mn_d] showed different distributions according to sampling sites (Fig. 4). St. 2 displayed two [Mn_d] peaks of 27 and 50 µmol L^{-1} around 3 and 10 cm depth, respectively. Below the deepest peak, [Mn_d] decreased to reach concentrations around 10 µmol L^{-1}. A single peaked vertical distribution was identified in St. 7 core at the same depth as the peak of manganese oxyhydroxides (5-6 cm depth). The maximum concentration was 65 µmol L^{-1}. Above, concentration reached 10 µmol L^{-1} in the oxic layer and was at 0 10 µmol L^{-1} in the bottom water. Below the peak, the concentration rapidly decreased down to 25 cm depth, followed by a slow decrease to reach 8 µmol L^{-1} at the bottom of the core. The concentration maximum was located between 1-1.5 cm depth at St. 5 and between 0.5-1 cm depth at St. 8. However, the peak at St. 5 reached 85 µmol L^{-1} whereas the one at St.8 showed a concentration of 25 µmol L^{-1}. Due to the small length of the St. 5 core, the decrease observed only reached 10 µmol L^{-1} at 10 cm depth without stabilisation. At St. 8, a small decrease of concentration reached 4 µmol L^{-1} at 15 cm depth. In the surface sediment sample and in bottom water, no [Mn_d] was detected.

4.2.4 Iron vertical distribution

Concentration and vertical distribution of ascorbate-extracted iron differed along the studied transect (Fig. 3 and 4. third column). At St.2, a [Fe_{asc}] peak between 5-10 cm depth

reached 21 µmol g^{-1} with concentrations around 10 µmol g^{-1} between the SWI and 5 cm depth and 5 µmol g^{-1} at 20 cm depth.

At St. 7, a two peak vertical distribution was observed with increasing concentrations between 5-10 cm depth and 15-21 cm depth reaching values of 25 and 21 µmol g^{-1}, respectively. Throughout the sediment column, [Fe_{asc}] minimal values reached 10 µmol g^{-1}. In contrast, at St. 5 and St. 8, the main [Fe_{asc}] enrichment was located in the uppermost sediment sample, reaching 27 µmol g^{-1} and 39 µmol g^{-1}, respectively. The decrease observed at St. 5 occurred all the way to the bottom of the core, with a concentration of 12 µmol g^{-1} at 10 cm depth. Within the uppermost 5 cm of sediment at St. 8, concentration in reactive iron oxides decreased to 12 µmol g^{-1}. Below, an increase of concentration reached 24 µmol g^{-1} at 12 cm depth. Underlying samples displayed relatively constant concentrations around 17 µmol g^{-1}.

Different vertical patterns of dissolved iron were also observed at the four studied sites (Fig. 4). At St. 2, no [Fe_d] was detected down to 6 cm depth below SWI. A small peak of [Fe_d] reaching 40 µmol L^{-1} was observed between 6 and 10 cm depth followed by a large increase of concentration downwards to 210 µmol L^{-1} at the bottom of the core. This large increase occurred at the same depth as the decrease of [Fe_{asc}] down the sediment core. A similar vertical distribution of [Fe_d] was identified at St. 7 with an increase in [Fe_d] from 0 µmol L^{-1} at 6 cm depth to 320 µmol L^{-1} at 20 cm depth. This sharp increase was followed by a decrease downward to values between 100 and 220 µmol L^{-1}. At this station, the maximum [Fe_d] occurred at the same depth as the second [Fe_{asc}] peak. No [Fe_d] was detected in the uppermost porewaters at St. 5. Between 1-1.5 cm depth, a maximum of 300 µmol L^{-1} was observed, followed by a decrease to 60 µmol L^{-1} at 10 cm depth. At St. 8, a more limited increase of concentration was observed within the uppermost 2 cm of sediment with a maximum value of 120 µmol L^{-1}. This was immediately followed by a relatively constant decrease to reach 0 µmol L^{-1} at the depth of 30 cm.

4.2.5 Sulfate vertical distribution

In all studied stations, [SO_4^{2-}] showed values between 25 and 30 mmol L^{-1}.(Fig.4. fourth column) Moreover, a slight downward decrease was observed at St. 2 and St. 7. At St. 2, concentration of sulfate varied from 27 mmol L^{-1} in the uppermost sediment layer to 25 mmol L^{-1} at 40 cm depth. From the same concentration in the oxic layer, the sulfate concentration at St. 7 decreased to 23 mmol L^{-1} at 55 cm depth.

4.2.6 Alkalinity

Fig. 4 (fifth column) displays vertical profiles of alkalinity in sediment porewaters. At all stations, bottom water concentration was close to 2.5 mmol L^{-1}. At St. 2, the concentration profiles showed inner variations starting with an increase to 5 mmol L^{-1} at 10 cm depth followed by a decrease to 3.5 mmol L^{-1} at 15 cm depth and another increase back to 5 mmol L^{-1} at 30 cm depth. At St. 7, slight and brief increase of concentration was observed as the concentration variates from 4.5 to 5 mmol L^{-1} around 12 cm depth to stabilize around this value until the bottom of the core. At St. 5, the profile differed with a decreasing trend downcore to 3.7 µmol L^{-1} within the 10 cm core. At St. 8, within the first 5 cm of sediment, an increase in alkalinity to around 5 mmol L^{-1} was observed followed by downward stability around this value.

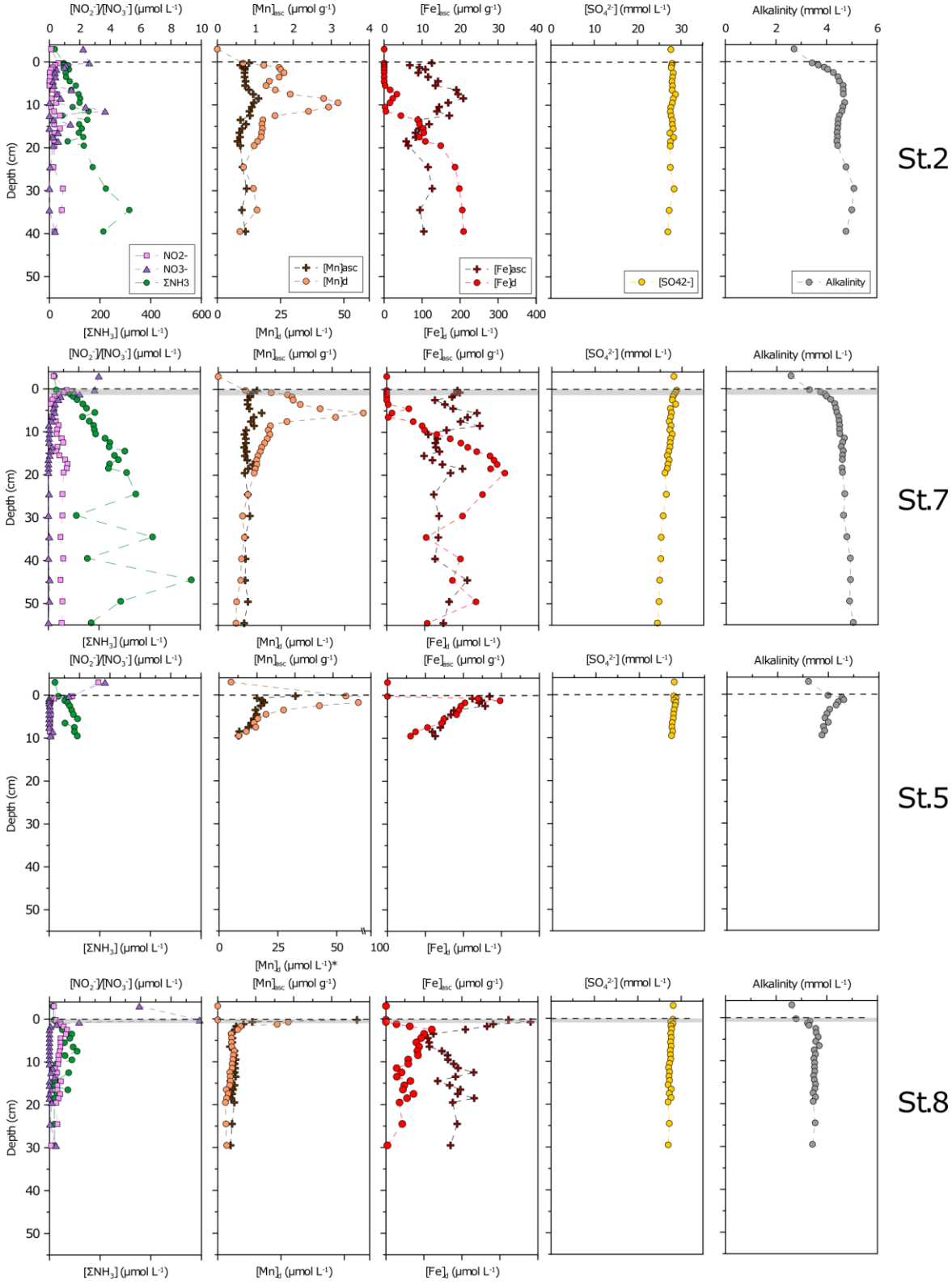

Figure 4: Depth profiles of some dissolved chemical species and Mn and Fe ascorbate-extracted oxides at the four studied stations. First column) Depth profiles of porewater nitrite [NO_2^-] (squares), nitrate [NO_3^-] (triangles) and ammonium [$\sum NH_3$] (circles). Second column) Depth profiles of reactive manganese oxides [Mn_{asc}] (crosses) and dissolved manganese [Mn_d] (circles). Note that concentration scale of the [Mn_d] of St. 5 presents an axis break. Third column) Depth profiles of reactive iron oxides [Fe_{asc}] (crosses) and dissolved iron [Fe_d] (circles). Fourth column) Depth profiles of sulfate [SO_4^{2-}] (circles). Fifth column) Alkalinity concentration profiles (grey circles). The dotted line corresponds to the Sediment-Water Interface (SWI). Bottom water concentrations were measured in supernatant water of the cores. Oxygen penetration depth is symbolized by grey areas in St. 7 and St. 8.

5 Discussion

5.1 Sediment characteristics in the fjord

5.1.1 Sedimentation gradient in the fjord

As discussed in the ***Chapter 4***, the main grain-size population (around 10 µm), observed at all four studied stations (Fig. 2), most likely originated from the turbid plume generated by the Kronebreen sub-glacial discharge. The extent and influence of the sediment plume, traceable by the fine silt mode, can be asserted to affect areas up to 10 km from the head of the fjord. Consequently, sedimentation rates strongly increase as the distance from the Kronebreen glacier front decreases. The effect of low sedimentation rates on benthic sediment stability at distal stations is attested by porosity profiles showing a decrease of surface porosity with increasing distance from the glacier front. This indicates relatively higher sediment compaction at distal stations, where sedimentation rates are lower, in contrast to proximal stations receiving high sediment supplies. Furthermore, grain-size changes in the profiles of glacier-proximal stations probably induced observed porosity variations within the sediment cores. For example, at St. 2, grain-size population drastically changed from 80 to 10 µm dominant mode inducing a decrease of porosity then another abrupt change from 10 µm to 80 µm around 10 cm depth resulting in a disruption of the porosity profile. These coarser particles were carried by a higher energy current mainly resulting from higher sub-glacial discharge, noticeable during melting seasons. Therefore, their sedimentation and further compaction after settling, is not similar to the compaction of silts (10 µm). This alternation results in disturbed porosity profiles.

5.1.2 Geochemistry of the glacial inputs

The results brought by the sequential chemical extractions of manganese and iron revealed that the most abundant phases were the most crystalline phases and not the easily reducible ones (Fig. 5). Indeed, particulate manganese was mostly found as carbonates and iron was mostly found as crystalline oxides. These results are in line with the findings of previous studies in Kongsfjorden and in other Svalbard fjords (Herbert et al., 2020, 2021; Laufer-Meiser et al., 2021; Wehrmann et al., 2014). Stations with a major sedimentary influence from tidewater glacier showed a higher content in crystalline material due to its early settling after erosion. According to Laufer-Meiser et al. (2021), ascorbate-extracted Fe only constitutes 0.6-12% of the total particulate Fe arriving in the fjord from glacial discharge. Their observation showed that the flux of ascorbate-extracted material from glacial input was more important after longer weathering in river systems formed by land-terminating glacier melting.

This raw and unprocessed material is a direct product of bedrock erosion by Kronebreen and Kongsvegen creeps, basal slidings and subglacial runoff (D'Angelo et al., 2018; Lydersen et al., 2014; Meslard et al., 2018). Geological studies of Kronebreen catchment outcrops showed that bedrocks are composed of various sedimentary rocks such as red sandstones, limestones, shales, conglomerates or dolomites formed between the late Carboniferous and the Devonian (***Chapter 1***) (Dallmann, 2015). The reddish colour of the sampled sediment corroborates the relationship with the red rock formations of the Colletthøgda mountain (***Chapter 4***; Fig. 1a). In addition, Laufer-Meiser et al. (2021) highlighted the importance of the eroded bedrock geology as a factor explaining differences of phase concentration in the turbid plume. Indeed, they found 1.3 times higher concentration of ascorbate-extracted Fe in the plume originated from subglacial discharge of Kongsvegen compared the one issued from the Kronebreen.

Moreover, the high occurrence of crystalline material compared to the ascorbate-extracted phase in our stations highlights the low or absent remineralization of organic matter in the water column and ice before settling. However, oxidation and weathering of crystallized phases such as pyrite in ice-trapped sediment can occur and contribute to a highly reactive Fe input (Raiswell et al., 2016, 2018). Another source of production of potentially bio-available Fe-oxides is the abiotic reduction (followed by reoxidation) of glacially derived crystalline Fe-oxides with hydrogen sulfide (H_2S) produced by sulfate reduction (Herbert et al., 2021, 2022) which is considered a major organic matter (OM) remineralisation pathway in sediments of western Svalbard fjords (Herbert et al., 2020).

5.2 Benthic biogeochemical functioning gradient

5.2.1 Oxygen and inorganic nitrogen dynamics in Kongsfjorden sediments

The studies from Glud et al. (1998) and Jørgensen et al. (2005) in Svalbard fjords evidenced a range of OPDs between 3 to 11 mm which is in accordance with our results. Oxygen microprofiling measurements revealed a lower OPD at St. 8 which is the most distal station than at St. 7 which is closer to the glacier front. In the inner basin, St. 7 receives more glacial input probably resulting in constant or frequent burial of Sediment-Water Interface (SWI) by newly deposited sediment and OM dilution (Koziorowska et al., 2017). As evidenced by our experimental study (***Chapter 3***), more frequent and low sediment deposition events would allow OPD to keep pace with disturbance through constant equilibration with the water column and newly deposited sediments. Diffusion of oxygen from the water column into the sediment therefore occurs continuously but stabilisation of its penetration is highly dependent on the inhabiting respirating fauna (Jørgensen et al., 2005). In the case of low sediment deposition, fauna consuming oxygen as an electron acceptor can rather easily and rapidly migrate through the new thin sediment layer and continue to consume porewater oxygen (Guilhermic et al., 2023). Ecological studies pointed out the effects of high sedimentation rates at the head of the fjord as a stressful factor for ecosystem structuring limiting the area to only a few macro- meiofaunal species with high motility features (Hop and Wiencke, 2019; Wlodarska-Kowalczuk et al., 2005). Since the OPD near the glacier front was deeper than is the distal station, we can hypothesize that less OM was deposited in this area or was highly diluted by high detrital deposition (***Chapter 4***). In this way, only a few organisms can use porewater oxygen due to weaker ecosystem functioning provoked by stressful conditions compared to the distal station. Although our oxygen profiles did not show any sign of bio-irrigation, our results tend to be interpreted as indicating the presence of a higher fauna density such as polychaete or tube dwelling species observed during core slicing process and as already described by Hop and Wiencke (2019) in the St. 8 area.

Oxygen consumption in surface sediments can also be induced by the reoxidation of reduced chemical species. Thus, ammonium depletion within the uppermost sediment levels was concomitant with nitrate increase, suggesting an oxic nitrification process (Fig. 4). According to Gihring et al. (2010), in Kongsfjorden, nitrate production in oxic layer outpaces the demand for denitrification and anammox. This is supported by Thamdrup and Fleischer, (1998) who observed extensive nitrification in Svalbard coastal sediment in relation with nitrifier organisms well-adapted to cold temperatures. In our transect, varying degrees of downcore ammonium enrichment were observed with higher concentrations at the glacier proximal station compared to the most distal one showing less than 100 µmol L^{-1} at 30 cm

depth. As ammonium is a product of OM remineralization, an inverse production gradient might be expected, as OM inputs are globally higher in the distal part of the fjord. As said previously, our observations during core slicing highlighted a higher fauna density such as polychaetes or tube dwelling species at the distal stations (St. 5 and 8) than at the proximal stations (St. 2 and 7) (***Chapter 7***). Biogeochemical processes are enhanced by infaunal activities, as burrows increase the surface of the SWI, and the ventilation of some infauna induces bioirrigation. Nitrification would be enhanced, as would denitrification and/or anammox (Braeckman et al., 2010; Kristensen et al., 2013; Pelegri et al., 1994), contributing to higher ammonium consumption in sediments at the distal stations and possibly to a nitrogen loss for the ecosystem.

5.2.2 Manganese and iron cycling

Dissolved Mn and Fe profiles are mainly distributed according to biotic and abiotic reductive dissolution of manganese and iron oxides in the sediment column. In the upper oxic layer of sediment, upward diffusion of dissolved Mn and Fe through porewater from production zones related to reductive dissolution of reactive oxides can result in a reoxidation into diagenetic oxides (Aller, 1980; Burdige, 1993). A gradient can be observed from the glacier most proximal St. 2 to the most distal St. 8 in the production depth of dissolved manganese and iron. The main layers of dissolved manganese production were observed at 10, 6, 1 and 1 cm depth from St. 2 to St. 8 and below 20, 20, 1 and 2 cm depth respectively for dissolved iron (Fig. 4). Moreover, it was found that in glacier proximal stations, dissolved manganese production occurred at the same depth as a peak of reactive Mn and Fe oxides, while dissolved Fe production was observed deeper. Considering an OPD of 10.3 ± 0.5 mm at St. 7, this reactive oxide enriched layer was located in an anoxic medium which induced reducing processes. Similar observations were also made by Herbert et al. (2020) in other Svalbard glaciated fjords. They showed a shallowing of the reduced manganese and iron production zones from deep levels in high glacial input areas near tidewater glacier fronts to uppermost layers away from the sediment source. They explained this dynamics by an overall higher reducing potential sustained by higher labile organic matter content due to enhanced primary production not limited by turbidity in areas further from the glaciers. Herbert et al. (2022) also demonstrated, in Kongsfjorden, that dissolved iron in the sediment can originate from either dissimilatory iron oxide reduction and/or iron oxide reduction by H_2S produced by sulfate reduction occurring in superficial sediments. In periods or areas showing low organic matter inputs and increased iron oxide delivery by glacial inputs, such as at our stations 2 and 7, dissimilatory iron reduction prevails. However, with an increase of OM content and/or decrease of sedimentation rate, iron oxides are reduced by both processes. In both scenarios, upward dissolved iron fluxes allow the enrichment of superficial sediment with potentially bio-available iron oxides. A gradient of involved iron and manganese reduction processes can be considered from dominant dissimilatory reduction near the glacier front and additional reductive processes related to sulfate reduction by-products downfjord. In this last case, iron is highly sequestrated by precipitation with sulfide as pyrite (Herbert et al., 2020). These interpretations by Herbert et al. (2022) are supported by our observations of localized black spots during core processing (Supplementary material 1). Indeed, in proximal areas small and scarce pyrite precipitation markers were seen at the bottom of the cores (below 20 cm depth) whereas numerous large black spots were present near 3 cm depth. Except in St. 7, the sulfate profile did not demonstrate clear evidence of sulfate reduction that could be linked with Fe_d concentration decrease implying precipitation of FeS species. However, Michaud et al. (2020) determined

experimentally that sulfide produced from biotic sulfate reduction is regenerated to sulfate with highly reactive Fe oxides which are constantly present in our studied sediments.

Manganese and iron are also likely to be affected by authigenic carbonate precipitation as evidenced by some studies (Herbert et al., 2020, 2021, 2022). Sequential chemical extractions revealed higher HCl-extracted Mn concentrations, assumed to be representative of Mn carbonates, at the proximal station (St. 7) than at the distal station (St. 8) (Fig. 3). By calculating saturation state using DIC, Herbert et al. (2020) also found than at stations close to glaciers, porewater was supersaturated with siderite and rhodochrosite. Alkalinity profiles at our proximal stations showed higher values than at distal stations (Fig. 4). Consumption of sulfate, followed by precipitation of FeS can contribute to this increase in alkalinity, as evidenced at St. 7 by the observation of black spots during core processing and the slight decrease in sulfate concentration below 20 cm depth (Fig. 4). Recently, the study of Thibault de Chanvalon et al. (2023) also highlighted the potential strong impact of manganese cycle on alkalinity with Mn-oxides oxidizing H_2S produced by sulfate reduction and leading to the production of $MnCO_3$.

In the end, biogeochemical gradients along the fjord can therefore be linked to environmental disturbance induced by summer melting of the Kronebreen tidewater glacier. Indeed, meltwater originating from subglacial discharge is loaded with freshly eroded detrital particles reaching 484.84 ± 118.10 kg m^3 at the surface near the Kronebreen glacier front (Meslard et al., 2018). The surface spreading of this highly turbid plume results in a decrease in sedimentation with increasing distance from the glacier front (D'Angelo et al., 2018; Lydersen et al., 2014; Meslard et al., 2018; Svendsen et al., 2002). This weakening of the plume leads to an increase of primary production on its edge, enhanced by micronutrient supply in surface water (***Chapter 4***). More labile OM can therefore be exported towards the seabed in summer at our most distal stations. Nevertheless, our data document a summer situation, but previous studies in the Kongsfjorden showed higher OM export in this season compared to the winter period (Lalande et al., 2016), leading to a higher reducing potential (Herbert et al., 2021, 2022; Laufer-Meiser et al., 2021).

5.3 Evidence of sedimentary deposit events inducing biogeochemical transient states

More than one peak of ascorbate-extracted Mn and Fe oxides associated with the production of either dissolved manganese or iron occurred at different depths in cores from St. 2 and St. 7. In addition, the inner basin clearly shows evidence of high sedimentation decreasing with increasing distance from the Kronebreen glacier (Meslard et al., 2018; Svendsen et al., 2002) and evidence of sediment deposition events, burying former SWIs with diagenetic oxide enrichments in past oxic layers, are suggested by porosity data (Fig. 4) showing profile disruptions at several depths downcore.

Results provided by the experimental work regarding the effect of sediment deposits on redox fronts generating a transient state generated and recovering with time (***Chapter 3***) are easily transposable to our environmental study in Kongsfjorden. St. 2 and St. 7 showed evidence of intense sedimentation with buried former SWIs enriched in reactive oxides with ongoing oxide reduction (***Chapter 3***). Disturbance here caused by high sedimentation rates in the proximal stations allows us to point out the delayed iron reduction by ongoing manganese reduction in deep ascorbate-extracted enriched layers (at 9 cm depth for St. 2 and 6 cm depth

for St. 7) already highlighted in ***Chapter 3*** after the addition of the massive sediment deposit. These enriched layers most likely correspond to the diagenetic precipitation of Mn and Fe oxides in a previous oxic surface layer, induced by upward diffusion of dissolved Mn and Fe. Our experimental results after the addition of a unique sediment deposit in the OHV microcosm in ***Chapter 3*** showed a first stage with Mn oxide reduction releasing dissolved Mn, which could correspond to the dissolved Mn peak at 6 cm depth in St. 7. This first stage was followed by a second stage when Fe oxide reduction began with Mn dissolution still ongoing, which could correspond to the situation of the Mn and Fe peaks at 9 cm depth in St. 2. The final stage corresponded to the impoverishment of Mn oxide and the most important release of dissolved Fe, which could correspond to the dissolved Fe peak at 20 cm depth in St. 7.

Herbert et al. (2021) evidenced a "sweet spot" characterized by a sufficiently low sedimentation rate (estimations of 0.9–1.6 cm yr^{-1}, based on their data) to allow primary production and OM export to the seabed and generate a high Fe flux towards the water column through a more dynamic cycling. Following Herbert's definition, our St. 5 is located within the "sweet spot" of the Kongsfjorden. Closer to the glacier (St. 7) high sediment depositions generate continuous or frequent burial. At St. 5, located just downstream the sill that physically marks the boundary between the inner basin and outer parts of the fjord (***Chapter 1***), displayed an ongoing subsurface precipitation of Mn and Fe-oxides with upward dissolved Mn and Fe fluxes towards the water column. In deeper environments in outer parts of the fjord (St. 8), precipitation of reactive Fe oxides in the surface oxic layer and less sediment escape are favoured. The higher surface gradients of dissolved Mn and Fe in St. 5 than in St. 8, probably supporting higher upward fluxes of both dissolved Mn and Fe, support the location of the "sweet spot" on the inner sill. Similarly to the study of Herbert et al. (2021), downfjord areas, represented here by St. 8, display a clear diagenetic enrichment in reactive oxide in the surface oxic layer, associated with zones of reduced Mn and Fe production in subsurface. This enrichment in potentially bioavailable oxide at the surface is the result of higher precipitation rates compared to the transport of dissolved species towards the water column. Similar interpretation was made by Herbert et al. (2021) explaining that lower OM export to the seafloor due to greater depth, combined with lower delivery of oxides due to lower sedimentation rates would be the reason of lower Mn and Fe production downstream from the sweet spot. Bacterial extracellular activity revealed by aminopeptidase analysis (***Chapter 4***), clearly supports this idea of a "sweet spot" near St. 5 as it showed the highest Leucine degradation rate of the four stations. Higher bacterial activity in this zone would therefore imply higher OM remineralisation and stimulated redox reactions.

Finally, redox state of the sediments was considered to achieve an optimal remineralization near the inner sill where a balance of relatively low turbidity could trigger primary production and OM export towards the seafloor generating higher bacterial activity. Transient states in the fjord from inner basin to outer parts would therefore be distributed as follows (Fig. 5): (1) Burial of previous SWIs due to high detrital sedimentation near the Kronebreen glacier front, (2) an optimal remineralisation area characterised by high microbial activity, high dissolved Mn and Fe fluxes towards the water column as a result of low sedimentation rates and high organic matter content in the sediment and (3) more stable sediment redox structure characterized by Mn and Fe oxide diagenetic precipitation in the oxic surface layer and low or absence of upward fluxes through the SWI.

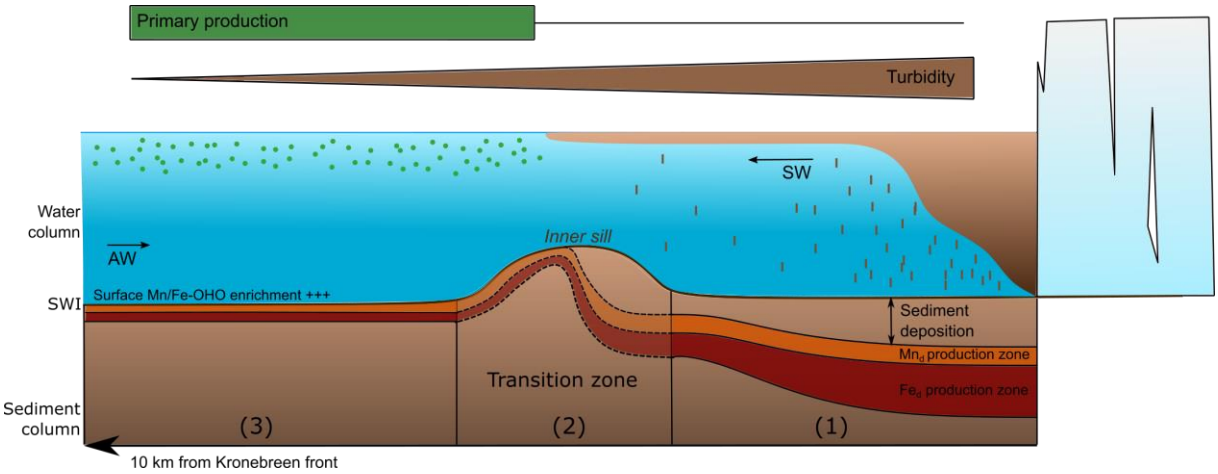

Figure 5: Conceptual model showing the spatial variation of geochemical stability within Kongsfjorden. Sediment deposition is highlighted by the depth of dissolved manganese production. The term transition zone corresponds to the "sweet spot", proposed by Herbert et al. (2021), and refers to upward fluxes of Mn and Fe towards the water column.

In the near future, with the Kronebreen front still at sea, our data support the hypothesis that the acceleration and intensity of the melting of tidewater glaciers generating stronger subglacial runoff might extend downfjord the unstable zone driven by high sedimentation rates, here localized only in the inner basin in late-summer 2021. This would have an effect on all biological and biogeochemical components from primary production to redox processes in the sediment and chemical fluxes, as stated in the previous parts. On a longer timescale, if global warming goes on, the melting of the glacier will shift the glacial front onto land that would drastically decrease the influence of turbidity on the hydrographic components of the fjord. A decrease of glacial erosion material supply into the fjord might highly affect phytoplanktonic growth and the resulting export on the seabed. In that way, the succession of the three states previously defined (Fig. 5) may be constrained to a much smaller spatial scale near the coastline, as expected from the restricted extend of turbid plumes from land-terminating glacier systems of the Kongsfjorden south coast. Reactivity of deposited oxides would also be higher as weathering in river systems is documented to be higher than during direct subglacial supply into the fjord by tidewater glaciers (Laufer-Meiser et al., 2021). The "sweet spot" defined by Herbert et al. (2021) releasing dissolved manganese and iron into the water column would be spatially reduced but still active in response to relatively high organic matter fluxes and lower sedimentary input but enriched in reactive oxides (Herbert et al., 2020, 2021; Laufer-Meiser et al., 2021; Wehrmann et al., 2014). Sediment biogeochemical dynamics under land-terminating glaciers influence was already studied in Dicksonfjorden by Laufer-Meiser et al. (2021) and in Van Mijenfjorden by Herbert et al. (2020). One way of understanding this scenario in Kongsfjorden, would be to study the shallow environments near the mouths of small river systems on the southern coast of Kongsfjorden originating from the melting of the Lovénbreen land-terminating glaciers.

6 Conclusion

Glacial inputs highly affect sediment biogeochemistry in inner Kongsfjorden at a kilometre scale. Gradients in turbidity and organic matter export as a function of distance from the Kronebreen glacier front have a real effect on redox gradient distribution in the sediment

column. In the light of our results, it is possible to define an unstable area in the inner basin receiving high sediment discharge and low fresh organic matter. This area is characterised by buried sediment-water interfaces highlighted by Mn and Fe reactive oxide enriched layers with ongoing Mn_d production at the same depth. This indicator of intense sediment burial described in microcosms (***Chapter 3***) proved to be applicable in Arctic environments subjected to high glacial inputs. The stress of high sedimentation rate on aerobic organisms can be observed by a deeper penetration of dissolved oxygen compared to outer fjord areas as a response to lower abundances and diversity of inhabiting species.

With increasing distance downfjord the inner sill, and better transparency of the surface waters, phytoplanktonic growth is favoured, inducing higher OM export to the sea floor. The consequent enhanced OM concentrations in the sediment catalyse the metal cycling that is supposed to result in enhanced Mn and Fe fluxes from the sediment towards the water column. A more stable redox state compared to the inner basin with enrichment of diagenetic reactive oxides at the surface was observed away from the inner sill. The rate of OM remineralisation was assumed to be faster due to less glacial induced sediment burial and higher bacterial activity.

For summer 2021, the inner sill proved to be a tipping point for balancing environmental gradient impact on benthic substrate stability and restrain “unstable” sediment geochemical state in the inner basin. Glacial inputs originating from tidewater glacier movements and subglacial runoff directly to the fjord, showed a relatively high concentration of crystalline oxide within the deposited particles. Oxide reduction processes also appear to present a gradient from dissimilatory oxide reduction by anaerobic respiration at fjord head under the effect of high terrigenous supplies and low OM inputs, to an additional contribution from abiotic oxide dissolution by sulfide produced by enhanced sulfate reduction in response to higher OM input downfjord. With the expected total retreat on land in a next future, weathering of particles through meltwater streams towards the fjord may induce a more intense cycling followed by increased organic matter export from land and sea due to less turbidity as observed on the southern coast of Kongsfjorden. In that way, the unstable area might decrease in favour of more stable substrates.

Data availability:

Raw data are presented in supplementary material 2 and 3. It will be made available upon publication of this manuscript on an online repository.

Author contributions:

CG: conceptualisation, data curation, formal analysis, investigation, methodology, visualisation, writing-original draft, writing-review and editing. AM: conceptualisation, methodology, data curation, investigation, validation, writing-review and editing. MPN: conceptualisation, funding acquisition, investigation, resources, supervision, validation, writing-review and editing. HH and: conceptualisation, investigation, supervision, validation, writing-review and editing. AP: methodology, investigation, data curation, formal analysis. AB: funding acquisition.

References:

Aller, R. C.: Diagenetic processes near the Long Island Sound. II. Fe and Mn sediment-water interface, Advances in Geophysics, 22, 351–414, 1980.

Anschutz, P., Zhong, S., Sundby, B., Mucci, A., and Gobeil, C.: Burial efficiency of phosphorus and the geochemistry of iron in continental margin sediments, Limnol. Oceanogr., 43, 53–64, https://doi.org/10.4319/lo.1998.43.1.0053, 1998.

Anschutz, P., Jorissen, F. J., Chaillou, G., Abu-Zied, R., and Fontanier, C.: Recent turbidite deposition in the eastern Atlantic: Early diagenesis and biotic recovery, Journal of Marine Research, 60, 835–854, https://doi.org/10.1357/002224002321505156, 2002.

Anschutz, P., Dedieu, K., Desmazes, F., and Chaillou, G.: Speciation, oxidation state, and reactivity of particulate manganese in marine sediments, Chemical Geology, 218, 265–279, https://doi.org/10.1016/j.chemgeo.2005.01.008, 2005.

Azzaro, M., Aliani, S., Maimone, G., Decembrini, F., Caroppo, C., Giglio, F., Langone, L., Miserocchi, S., Cosenza, A., Azzaro, F., Rappazzo, A. C., Cabral, A. S., Paranhos, R., Mancuso, M., and La Ferla, R.: Short-term dynamics of nutrients, planktonic abundances, and microbial respiratory activity in the Arctic Kongsfjorden (Svalbard, Norway), Polar Biol, 44, 361–378, https://doi.org/10.1007/s00300-020-02798-w, 2021.

Bennett, M. R., Hambrey, M. J., Huddart, D., Glasser, N. F., and Crawford, K.: The landform and sediment assemblage produced by a tidewater glacier surge in Kongsfjorden, Svalbard, Quaternary Science Reviews, 18, 1213–1246, https://doi.org/10.1016/S0277-3791(98)90041-5, 1999.

Bouchayer, C., Nanni, U., Lefeuvre, P.-M., Hulth, J., Steffensen Schmidt, L., Kohler, J., Renard, F., and Schuler, T. V.: Multi-scale variations of hydro-mechanical conditions at the base of the surge-type glacier Kongsvegen, Svalbard, https://doi.org/10.5194/egusphere-2023-618, 2023.

Bourgeois, S., Kerhervé, P., Calleja, M. L., Many, G., and Morata, N.: Glacier inputs influence organic matter composition and prokaryotic distribution in a high Arctic fjord (Kongsfjorden, Svalbard), Journal of Marine Systems, 16, 2016.

Bourriquen, M., Baltzer, A., Mercier, D., Fournier, J., Pérez, L., Haquin, S., Bernard, E., and Jensen, M.: Coastal evolution and sedimentary mobility of Brøgger Peninsula, northwest Spitsbergen, Polar Biol, 39, 1689–1698, https://doi.org/10.1007/s00300-016-1930-1, 2016.

Braeckman, U., Provoost, P., Gribsholt, B., Gansbeke, D. V., Middelburg, J. J., Soetaert, K., Vincx, M., and Vanaverbeke, J.: Role of macrofauna functional traits and density in biogeochemical fluxes and bioturbation, Marine Ecology Progress Series, 399, 173–186, https://doi.org/10.3354/meps08336, 2010.

Calleja, M. Ll., Kerhervé, P., Bourgeois, S., Kędra, M., Leynaert, A., Devred, E., Babin, M., and Morata, N.: Effects of increase glacier discharge on phytoplankton bloom dynamics and pelagic geochemistry in a high Arctic fjord, Progress in Oceanography, 159, 195–210, https://doi.org/10.1016/j.pocean.2017.07.005, 2017.

Cathalot, C., Rabouille, C., Pastor, L., Deflandre, B., Viollier, E., Buscail, R., Gremare, A., Treignier, C., and Pruski, A.: Temporal variability of carbon recycling in coastal sediments influenced by rivers: assessing the impact of flood inputs in the Rhoˆne River prodelta, 2010.

Chaillou, G., Anschutz, P., Dubrulle, C., and Lecroart, P.: Transient States in Diagenesis Following the Deposition of a Gravity Layer: Dynamics of O2, Mn, Fe and N-Species in Experimental Units, Aquat Geochem, 13, 157–172, https://doi.org/10.1007/s10498-007-9013-0, 2007.

Claff, S. R., Sullivan, L. A., Burton, E. D., and Bush, R. T.: A sequential extraction procedure for acid sulfate soils: Partitioning of iron, Geoderma, 155, 224–230, https://doi.org/10.1016/j.geoderma.2009.12.002, 2010.

Cottier, F., Tverberg, V., Inall, M., Svendsen, H., Nilsen, F., and Griffiths, C.: Water mass modification in an Arctic fjord through cross-shelf exchange: The seasonal hydrography of Kongsfjorden, Svalbard, J. Geophys. Res., 110, C12005, https://doi.org/10.1029/2004JC002757, 2005.

Cowton, T., Slater, D., Sole, A., Goldberg, D., and Nienow, P.: Modeling the impact of glacial runoff on fjord circulation and submarine melt rate using a new subgrid-scale parameterization for glacial plumes, Journal of Geophysical Research: Oceans, 120, 796–812, https://doi.org/10.1002/2014JC010324, 2015.

Dallmann, W. K.: Geoscience Atlas of Svalbard, 2015.

D'Angelo, A., Giglio, F., Miserocchi, S., Sanchez-Vidal, A., Aliani, S., Tesi, T., Viola, A., Mazzola, M., and Langone, L.: Multi-year particle fluxes in Kongsfjorden, Svalbard, Biogeosciences, 15, 5343–5363, https://doi.org/10.5194/bg-15-5343-2018, 2018.

Deflandre, B., Mucci, A., Gagné, J.-P., Guignard, C., and Sundby, B. jørn: Early diagenetic processes in coastal marine sediments disturbed by a catastrophic sedimentation event, Geochimica et Cosmochimica Acta, 66, 2547–2558, https://doi.org/10.1016/S0016-7037(02)00861-X, 2002.

Elverhøi, A., Lønne, Ø., and Seland, R.: Glaciomarine sedimentation in a modern fjord environment, Spitsbergen, Polar Research, 1, 127–149, https://doi.org/10.3402/polar.v1i2.6978, 1983.

Froelich, P. N., Klinkhammer, G. P., Bender, M. L., Luedtke, N. A., Heath, G. R., Cullen, D., Dauphin, P., and Blaynehartman, D. Hammond.: Early oxidation of organic matter in pelagic sediments of the eastern equatorial Atlantic: suhoxic diagenesis, Geochimica et Cosmochimica Acta, 43, 1075–1090, https://doi.org/0016-7037 79,0701-1075SO?.M) 0, 1979.

García-Robledo, E., Corzo, A., and Papaspyrou, S.: A fast and direct spectrophotometric method for the sequential determination of nitrate and nitrite at low concentrations in small volumes, Marine Chemistry, 162, 30–36, https://doi.org/10.1016/j.marchem.2014.03.002, 2014.

Gihring, T. M., Lavik, G., Kuypers, M. M. M., and Kostka, J. E.: Direct determination of nitrogen cycling rates and pathways in Arctic fjord sediments (Svalbard, Norway), Limnol. Oceanogr., 55, 740–752, https://doi.org/10.4319/lo.2010.55.2.0740, 2010.

Glud, R., Holby, O., Hoffmann, F., and Canfield, D.: Benthic mineralization and exchange in Arctic sediments (Svalbard, Norway), Mar. Ecol. Prog. Ser., 173, 237–251, https://doi.org/10.3354/meps173237, 1998.

Griess, P.: Bemerkungen zu der Abhandlung der HH. Weselsky und Benedikt „Ueber einige Azoverbindungen", Ber. Dtsch. Chem. Ges., 12, 426–428, https://doi.org/10.1002/cber.187901201117, 1879.

Halbach, L., Vihtakari, M., Duarte, P., Everett, A., Granskog, M. A., Hop, H., Kauko, H. M., Kristiansen, S., Myhre, P. I., Pavlov, A. K., Pramanik, A., Tatarek, A., Torsvik, T., Wiktor, J. M., Wold, A., Wulff, A., Steen, H., and Assmy, P.: Tidewater Glaciers and Bedrock Characteristics Control the Phytoplankton Growth Environment in a Fjord in the Arctic, Front. Mar. Sci., 6, 254, https://doi.org/10.3389/fmars.2019.00254, 2019.

Hegseth, E. N., Assmy, P., Wiktor, J. M., Wiktor, J., Kristiansen, S., Leu, E., Tverberg, V., Gabrielsen, T. M., Skogseth, R., and Cottier, F.: Phytoplankton Seasonal Dynamics in Kongsfjorden, Svalbard and the Adjacent Shelf, in: The Ecosystem of Kongsfjorden, Svalbard, vol. 2, edited by: Hop, H. and Wiencke, C., Springer International Publishing, Cham, 173–227, https://doi.org/10.1007/978-3-319-46425-1_6, 2019.

Herbert, L. C., Riedinger, N., Michaud, A. B., Laufer, K., Røy, H., Jørgensen, B. B., Heilbrun, C., Aller, R. C., Cochran, J. K., and Wehrmann, L. M.: Glacial controls on redox-sensitive trace element cycling in Arctic fjord sediments (Spitsbergen, Svalbard), Geochimica et Cosmochimica Acta, 271, 33–60, https://doi.org/10.1016/j.gca.2019.12.005, 2020.

Herbert, L. C., Zhu, Q., Michaud, A. B., Laufer-Meiser, K., Jones, C. K., Riedinger, N., Stooksbury, Z. S., Aller, R. C., Jørgensen, B. B., and Wehrmann, L. M.: Benthic iron flux influenced by climate-sensitive interplay between organic carbon availability and sedimentation rate in Arctic fjords, Limnol Oceanogr, 66, 3374–3392, https://doi.org/10.1002/lno.11885, 2021.

Herbert, L. C., Michaud, A. B., Laufer-Meiser, K., Hoppe, C. J. M., Zhu, Q., Aller, R. C., Jørgensen, B. B., and Wehrmann, L. M.: Tight benthic-pelagic coupling drives seasonal and interannual changes in iron-sulfur cycling in Arctic fjord sediments (Kongsfjorden, Svalbard), Journal of Marine Systems, 225, 103645, https://doi.org/10.1016/j.jmarsys.2021.103645, 2022.

Hop, H. and Wiencke, C. (Eds.): The Ecosystem of Kongsfjorden, Svalbard, Springer International Publishing, Cham, https://doi.org/10.1007/978-3-319-46425-1, 2019.

Hop, H., Falk-Petersen, S., Svendsen, H., Kwasniewski, S., Pavlov, V., Pavlova, O., and Søreide, J. E.: Physical and biological characteristics of the pelagic system across Fram Strait to Kongsfjorden, Progress in Oceanography, 71, 182–231, https://doi.org/10.1016/j.pocean.2006.09.007, 2006.

Hoppe, C. J. M.: Always ready? Primary production of Arctic phytoplankton at the end of the polar night, Limnol Oceanogr Letters, 7, 167–174, https://doi.org/10.1002/lol2.10222, 2022.

Hopwood, M. J., Carroll, D., Dunse, T., Hodson, A., Holding, J. M., Iriarte, J. L., Ribeiro, S., Achterberg, E. P., Cantoni, C., Carlson, D. F., Chierici, M., Clarke, J. S., Cozzi, S., Fransson, A., Juul-Pedersen, T., Winding, M. H. S., and Meire, L.: Review article: How does glacier discharge affect marine biogeochemistry and primary production in the Arctic?, The Cryosphere, 14, 1347–1383, https://doi.org/10.5194/tc-14-1347-2020, 2020.

Howe, J. A., Austin, W. E. N., Forwick, M., Paetzel, M., Harland, R., and Cage, A. G.: Fjord systems and archives: a review, SP, 344, 5–15, https://doi.org/10.1144/SP344.2, 2010.

Jørgensen, B., Glud, R., and Holby, O.: Oxygen distribution and bioirrigation in Arctic fjord sediments (Svalbard, Barents Sea), Mar. Ecol. Prog. Ser., 292, 85–95, https://doi.org/10.3354/meps292085, 2005.

Jørgensen, B. B., Laufer, K., Michaud, A. B., and Wehrmann, L. M.: Biogeochemistry and microbiology of high Arctic marine sediment ecosystems—Case study of Svalbard fjords, Limnol Oceanogr, 66, https://doi.org/10.1002/lno.11551, 2021.

Kohler, J., James, T. D., Murray, T., Nuth, C., Brandt, O., Barrand, N. E., Aas, H. F., and Luckman, A.: Acceleration in thinning rate on western Svalbard glaciers, Geophys. Res. Lett., 34, L18502, https://doi.org/10.1029/2007GL030681, 2007.

Kostka, J. E. and Luther, G. W.: Partitioning and speciation of solid phase iron in saltmarsh sediments, Geochimica et Cosmochimica Acta, 58, 1701–1710, https://doi.org/10.1016/0016-7037(94)90531-2, 1994.

Koziorowska, K., Kuliński, K., and Pempkowiak, J.: Distribution and origin of inorganic and organic carbon in the sediments of Kongsfjorden, Northwest Spitsbergen, European Arctic, Continental Shelf Research, 150, 27–35, https://doi.org/10.1016/j.csr.2017.08.023, 2017.

Kristensen, E., Haese, R., and Kostka, J. E.: Interactions Between Macro- and Microorganisms in Marine Sediments, 1 pp., https://doi.org/10.1029/CE060, 2013.

Lalande, C., Moriceau, B., Leynaert, A., and Morata, N.: Spatial and temporal variability in export fluxes of biogenic matter in Kongsfjorden, Polar Biol, 39, 1725–1738, https://doi.org/10.1007/s00300-016-1903-4, 2016.

Laufer-Meiser, K., Michaud, A. B., Maisch, M., Byrne, J. M., Kappler, A., Patterson, M. O., Røy, H., and Jørgensen, B. B.: Potentially bioavailable iron produced through benthic cycling in glaciated Arctic fjords of Svalbard, Nat Commun, 12, 1349, https://doi.org/10.1038/s41467-021-21558-w, 2021.

Lenstra, W. K., Klomp, R., Molema, F., Behrends, T., and Slomp, C. P.: A sequential extraction procedure for particulate manganese and its application to coastal marine sediments, Chemical Geology, 584, 120538, https://doi.org/10.1016/j.chemgeo.2021.120538, 2021.

Łepkowska, E. and Stachnik, Ł.: Which Drivers Control the Suspended Sediment Flux in a High Arctic Glacierized Basin (Werenskioldbreen, Spitsbergen)?, Water, 10, 1408, https://doi.org/10.3390/w10101408, 2018.

Lydersen, C., Assmy, P., Falk-Petersen, S., Kohler, J., Kovacs, K. M., Reigstad, M., Steen, H., Strøm, H., Sundfjord, A., Varpe, Ø., Walczowski, W., Weslawski, J. M., and Zajaczkowski, M.: The importance of tidewater glaciers for marine mammals and seabirds in Svalbard, Norway, Journal of Marine Systems, 129, 452–471, https://doi.org/10.1016/j.jmarsys.2013.09.006, 2014.

Meslard, F., Bourrin, F., Many, G., and Kerhervé, P.: Suspended particle dynamics and fluxes in an Arctic fjord (Kongsfjorden, Svalbard), Estuarine, Coastal and Shelf Science, 204, 212–224, https://doi.org/10.1016/j.ecss.2018.02.020, 2018.

Metzger, E., Barbe, A., Cesbron, F., Thibault de Chanvalon, A., Jauffrais, T., Jézéquel, D., and Mouret, A.: Two-dimensional ammonium distribution in sediment pore waters using a new colorimetric diffusive equilibration in thin-film technique, Water Research X, 2, 100023, https://doi.org/10.1016/j.wroa.2018.100023, 2019.

Michaud, A. B.: Glacial influence on the iron and sulfur cycles in Arctic fjord sediments (Svalbard), Geochimica et Cosmochimica Acta, 2020.

Mucci, A. and Edenborn, H. M.: Influence of an organic-poor landslide deposit on the early diagenesis of iron and manganese in a coastal marine sediment, Geochimica et Cosmochimica Acta, 56, 3909–3921, https://doi.org/10.1016/0016-7037(92)90005-4, 1992.

Mucci, A., Boudreau, B., and Guignard, C.: Diagenetic mobility of trace elements in sediments covered by a flash flood deposit: Mn, Fe and As, Applied Geochemistry, 18, 1011–1026, https://doi.org/10.1016/S0883-2927(02)00207-X, 2003.

Nmor, S. I., Viollier, E., Pastor, L., Lansard, B., Rabouille, C., and Soetaert, K.: FESDIA (v1.0): exploring temporal variations of sediment biogeochemistry under the influence of flood events using numerical modelling, Geoscientific Model Development, 15, 7325–7351, https://doi.org/10.5194/gmd-15-7325-2022, 2022.

Pastor, L., Rabouille, C., Metzger, E., Thibault de Chanvalon, A., Viollier, E., and Deflandre, B.: Transient early diagenetic processes in Rhône prodelta sediments revealed in contrasting flood events, Continental Shelf Research, 166, 65–76, https://doi.org/10.1016/j.csr.2018.07.005, 2018.

Payne, C. M. and Roesler, C. S.: Characterizing the influence of Atlantic water intrusion on water mass formation and phytoplankton distribution in Kongsfjorden, Svalbard, Continental Shelf Research, 191, 104005, https://doi.org/10.1016/j.csr.2019.104005, 2019.

Pelegri, S. P., Nielsen, L. P., and Blackburn, T. H.: Denitrification in estuarine sediment stimulated by the irrigation activity of the amphipod Corophium volutator, Marine Ecology Progress Series, 105, 285–290, 1994.

Piquet, A. M.-T., van de Poll, W. H., Visser, R. J. W., Wiencke, C., Bolhuis, H., and Buma, A. G. J.: Springtime phytoplankton dynamics in Arctic Krossfjorden and Kongsfjorden (Spitsbergen) as a function of glacier proximity, Biogeosciences, 11, 2263–2279, https://doi.org/10.5194/bg-11-2263-2014, 2014.

van de Poll, W. H., Kulk, G., Rozema, P. D., Brussaard, C. P. D., Visser, R. J. W., and Buma, A. G. J.: Contrasting glacial meltwater effects on post-bloom phytoplankton on temporal and spatial scales in Kongsfjorden, Spitsbergen, Elementa: Science of the Anthropocene, 6, 50, https://doi.org/10.1525/elementa.307, 2018.

Poulton, S. W. and Canfield, D. E.: Development of a sequential extraction procedure for iron: implications for iron partitioning in continentally derived particulates, Chemical Geology, 214, 209–221, https://doi.org/10.1016/j.chemgeo.2004.09.003, 2005.

Raiswell, R., Hawkings, J. R., Benning, L. G., Baker, A. R., Death, R., Albani, S., Mahowald, N., Krom, M. D., Poulton, S. W., Wadham, J., and Tranter, M.: Potentially bioavailable iron delivery by iceberg-hosted sediments and atmospheric dust to the polar oceans, Biogeosciences, 13, 3887–3900, https://doi.org/10.5194/bg-13-3887-2016, 2016.

Raiswell, R., Hawkings, J., Elsenousy, A., Death, R., Tranter, M., and Wadham, J.: Iron in Glacial Systems: Speciation, Reactivity, Freezing Behavior, and Alteration During Transport, Frontiers in Earth Science, 6, 2018.

Revsbech, N. P.: An oxygen microsensor with a guard cathode, Limnology and Oceanography, 34, 474–478, https://doi.org/10.4319/lo.1989.34.2.0474, 1989.

Sarazin, G., Michard, G., and Prevot, F.: A rapid and accurate spectroscopic method for alkalinity measurements in sea water samples, Water Research, 33, 290–294, https://doi.org/10.1016/S0043-1354(98)00168-7, 1999.

Schnetger, B. and Lehners, C.: Determination of nitrate plus nitrite in small volume marine water samples using vanadium(III)chloride as a reduction agent, Marine Chemistry, 160, 91–98, https://doi.org/10.1016/j.marchem.2014.01.010, 2014.

Singh, A. and Krishnan, K. P.: The spatial distribution of phytoplankton pigments in the surface sediments of the Kongsfjorden and Krossfjorden ecosystem of Svalbard, Arctic, Regional Studies in Marine Science, 31, 100815, https://doi.org/10.1016/j.rsma.2019.100815, 2019.

Streuff, K., Forwick, M., Szczuciński, W., Andreassen, K., and Ó Cofaigh, C.: Submarine landform assemblages and sedimentary processes related to glacier surging in Kongsfjorden, Svalbard, Arktos, 1, 14, https://doi.org/10.1007/s41063-015-0003-y, 2015.

Svendsen, H., Beszczynska-Møller, A., Hagen, J. O., Lefauconnier, B., Tverberg, V., Gerland, S., Børre Ørbæk, J., Bischof, K., Papucci, C., Zajaczkowski, M., Azzolini, R., Bruland, O., and Wiencke, C.: The physical environment of Kongsfjorden–Krossfjorden, an Arctic fjord system in Svalbard, Polar Research, 21, 133–166, https://doi.org/10.3402/polar.v21i1.6479, 2002.

Thamdrup, B. and Fleischer, S.: Temperature dependence of oxygen respiration, nitrogen mineralization, and nitrification in Arctic sediments, Aquat. Microb. Ecol., 15, 191–199, https://doi.org/10.3354/ame015191, 1998.

Thibault de Chanvalon, A., Mouret, A., Knoery, J., Geslin, E., Péron, O., and Metzger, E.: Manganese, iron and phosphorus cycling in an estuarine mudflat, Loire, France, Journal of Sea Research, 118, 92–102, https://doi.org/10.1016/j.seares.2016.10.004, 2016.

Trusel, L. D., Powell, R. D., Cumpston, R. M., and Brigham-Grette, J.: Modern glacimarine processes and potential future behaviour of Kronebreen and Kongsvegen polythermal tidewater glaciers, Kongsfjorden, Svalbard, Geological Society, London, Special Publications, 344, 89–102, https://doi.org/10.1144/SP344.9, 2010.

Wang, Y. and Van Cappellen, P.: A multicomponent reactive transport model of early diagenesis: Application to redox cycling in coastal marine sediments, Geochimica et Cosmochimica Acta, 60, 2993–3014, https://doi.org/10.1016/0016-7037(96)00140-8, 1996.

Wehrmann, L. M., Formolo, M. J., Owens, J. D., Raiswell, R., Ferdelman, T. G., Riedinger, N., and Lyons, T. W.: Iron and manganese speciation and cycling in glacially influenced high-latitude fjord sediments (West Spitsbergen, Svalbard): Evidence for a benthic recycling-transport mechanism, Geochimica et Cosmochimica Acta, 141, 628–655, https://doi.org/10.1016/j.gca.2014.06.007, 2014.

Wilson, T. R. S., Thomson, J., Colley, S., Hydes, D. J., Higgs, N. C., and Sørensen, J.: Early organic diagenesis: The significance of progressive subsurface oxidation fronts in pelagic sediments, Geochimica et Cosmochimica Acta, 49, 811–822, https://doi.org/10.1016/0016-7037(85)90174-7, 1985.

Wlodarska-Kowalczuk, M., Pearson, T., and Kendall, M.: Benthic response to chronic natural physical disturbance by glacial sedimentation in an Arctic fjord, Mar. Ecol. Prog. Ser., 303, 31–41, https://doi.org/10.3354/meps303031, 2005.

Yang, Y., Ren, J., and Zhu, Z.: Distributions and Influencing Factors of Dissolved Manganese in Kongsfjorden and Ny-Ålesund, Svalbard, ACS Earth Space Chem., 6, 1259–1268, https://doi.org/10.1021/acsearthspacechem.1c00388, 2022.

Chapter 5: Sediment redox cycling instabilities generated by glacial inputs in Kongsfjorden (Svalbard)

Supplementary material 1: Core pictures

From right to left : St. 2, St. 7, St. 5, St. 8

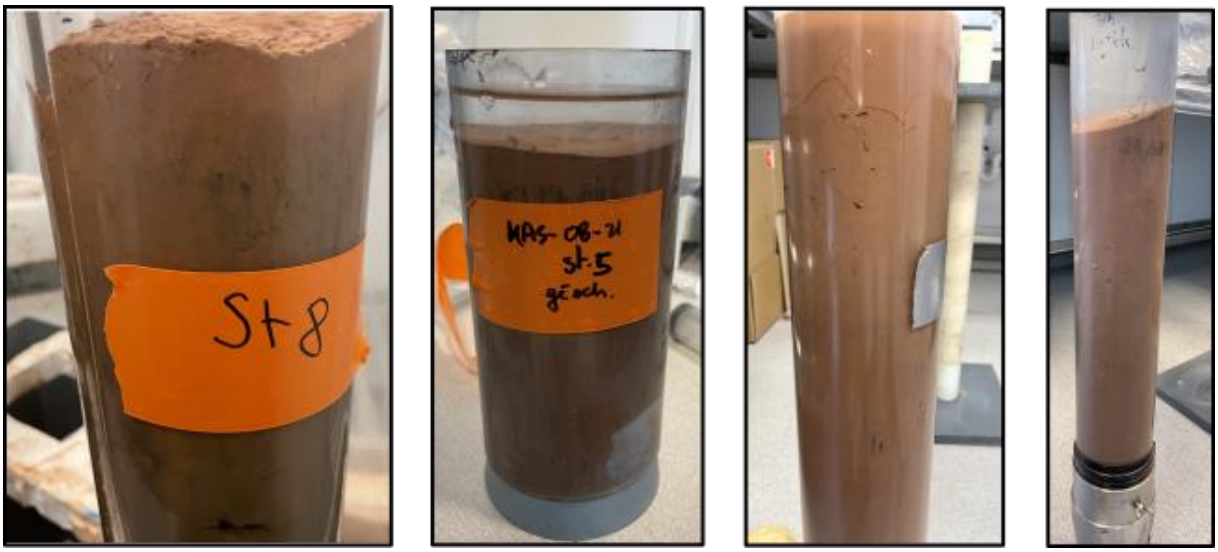

Supplementary material 2: Sediment grain-size and porosity

Depth	St2	Porosity	MODE 1	MODE 2	St7	Porosity	MODE 1	MODE 2	St5	Porosity	MODE 1	MODE 2	St8	Porosity	MODE 1	MODE 2
cm			µm	µm			µm	µm			µm	µm			µm	µm
0.25		0.81	5.56			0.87	4.90	225.41		0.78	7.18			0.73	15.44	71.45
0.75		0.74	7.18			0.82	5.56	119.06		0.77	15.44			0.70	9.27	71.45
1.25		0.69	55.35	8.16		0.78	13.59			0.72				0.71	9.27	
1.75		0.68	48.72			0.76	5.56			0.68	11.96			0.65	10.53	71.45
2.5		0.64	5.56	42.88		0.74	7.18			0.66	9.27			0.61	81.18	13.59
3.5		0.65	8.16	42.88		0.75	5.56	17.55		0.64	10.53			0.56	81.18	11.96
4.5		0.67	8.16			0.74	6.32			0.63	10.53			0.57	81.18	10.53
5.5		0.69	6.32			0.69	8.16	625.90		0.62	10.53			0.57	81.18	11.96
6.5		0.70	6.32			0.69	6.32			0.60	11.96			0.57	10.53	71.45
7.5		0.70	7.18			0.66	7.18			0.59	11.96			0.57	10.53	71.45
8.5		0.67	8.16			0.64	6.32			0.57	11.96			0.56	11.96	
9.5		0.64	8.16			0.64	7.18			0.57	11.96			0.57	10.53	
10.5		0.61	33.22	9.27		0.63	7.18							0.57	9.27	
11.5		0.59	33.22	10.53		0.61	6.32	17.55						0.55	8.16	
12.5		0.58	42.88	10.53		0.60	19.93	7.18						0.55	8.16	
13.5		0.56	42.88			0.63	7.18							0.57	9.27	
14.5		0.57	37.74	9.27		0.65	6.32							0.56	9.27	
15.5		0.57	42.88	9.27			17.55	7.18						0.58	9.27	
16.5		0.55	48.72	8.16		0.67	6.32							0.54	11.96	
17.5		0.55	48.72	8.16		0.68	6.32							0.56	9.27	
18.5		0.52	48.72	8.16		0.64	6.32							0.56	9.27	
19.5		0.52	37.74	9.27		0.63	6.32							0.53	8.16	
24.5		0.54	7.18			0.62	6.32							0.54	11.96	
29.5		0.60	7.18	33.22		0.63	6.32							0.53	9.27	
34.5		0.57	8.16			0.62	6.32									
39.5		0.60				0.61	6.32									
44.5						0.62	7.18									
49.5						0.62										
54.5						0.58	6.32									

Supplementary material 3: Biogeochemical raw data

Table 1: Sequential extraction of oxides (colours corresponding to Fig. 3)

Depth (cm)	St.7	Asc	Mn	Fe	HCl	Mn	Fe	CDB	Mn	Fe	oxalate	Mn	Fe	HNO_3	Mn	Fe
			µmol/g	µmol/g		µmol/g	µmol/g		µmol/g	µmol/g		µmol/g	µmol/g		µmol/g	µmol/g
0.25			1.02	18.62		4.19	120.02		0.94	193.94		0.14	28.90		0.25	32.20
0.75			0.92	19.23		4.23	112.51		0.88	199.01		0.10	26.60		0.19	24.60
1.25			0.84	17.79		4.31	107.30		0.82	184.55		0.11	24.30		0.21	30.30
1.75			0.84	17.20												
2.5			0.77	12.68		4.85	112.13		0.83	167.86		0.10	22.00		0.16	21.60
3.5			0.77	15.30												
4.5			0.82	17.48		4.11	119.80		0.95	190.57		0.14	32.10		0.25	31.40
5.5			1.15	23.76		4.30	132.84		0.91	188.87		0.17	38.70		0.28	33.10
6.5			0.94	21.28		4.73	128.70		0.91	188.47		0.12	25.40		0.22	28.40
7.5			0.86	19.43		4.11	125.35		1.01	184.36		0.13	23.80		0.21	28.10
8.5			0.95	24.53		4.25	122.83		0.89	168.46		0.13	31.40		0.21	29.50
9.5			0.74	15.75		4.35	115.64		0.87	170.21		0.13	31.60		0.17	24.30
10.5			0.69	10.95		4.49	106.34		0.74	153.42		0.09	19.30		0.16	25.10
11.5			0.73	13.33		4.52	120.49		0.84	175.01		0.13	25.90		0.19	26.20
12.5			0.73	12.79		4.38	110.40		0.73	159.89		0.07	17.40		0.15	22.70
13.5			0.68	12.94		4.47	112.19		0.81	176.98		0.11	24.10		0.19	29.00
14.5			0.75	13.89		4.43	115.80		0.78	173.75		0.11	33.40		0.19	26.60
15.5			0.70	9.83		4.63	107.16		0.72	158.85		0.08	19.00		0.17	25.60
16.5			0.77	12.05		4.51	120.96		0.81	174.04		0.10	21.80		0.20	28.20
17.5			0.91	14.67		4.62	124.47		0.82	175.79		0.12	25.50		0.20	26.00
18.5			0.79	19.96		4.66	125.21		0.89	184.69		0.11	24.40		0.19	25.40
19.5			0.70	16.79		4.69	112.51		0.82	170.99		0.10	25.10		0.17	23.80
24.5			0.78	12.40		4.09	107.24		0.79	172.14		0.11	27.10		0.19	25.30
29.5			0.84	13.77		4.58	122.96		0.83	165.63		0.11	27.40		0.20	28.60
34.5			0.71	13.58		4.72	128.71		0.84	178.73		0.12	26.60		0.22	30.10
39.5			0.72	12.73		4.38	120.49		0.89	173.82		0.12	25.00		0.24	32.90
44.5			0.71	21.21		4.44	127.76		0.87	175.45		0.14	29.00		0.23	31.10
49.5			0.78	16.43		4.77	119.10		0.89	182.05		0.11	22.60		0.17	24.60
54.5			0.68	14.92												

Depth (cm)	St8	Asc	Mn	Fe	HCl	Mn	Fe	CDB	Mn	Fe	oxalate	Mn	Fe	HNO_3	Mn	Fe
			µmol/g	µmol/g		µmol/g	µmol/g		µmol/g	µmol/g		µmol/g	µmol/g		µmol/g	µmol/g
0.25			3.67	32.28		4.59	123.16		0.90	153.26		0.11	29.00		0.19	31.00
0.75			0.91	38.08		4.12	123.62		0.90	167.35		0.12	26.30		0.20	30.30
1.25			0.68	28.23		3.99	125.82		0.91	180.09		0.11	23.50		0.21	31.80
1.75			0.49	26.62		3.99	127.35		0.82	159.57		0.11	22.20		0.20	32.80
2.5			0.46	20.93		3.40	118.71		0.79	145.43		0.11	23.60		0.19	31.50
3.5			0.37	12.49		3.31	118.38		0.73	123.63		0.10	27.50		0.18	32.20
4.5			0.39	11.01		3.29	118.59		0.77	138.60		0.09	19.60		0.17	31.30
5.5			0.38	11.36		3.36	119.78		0.79	145.51		0.10	21.50		0.20	32.40
6.5			0.32	11.45		3.48	123.74		0.81	148.68		0.10	21.10		0.20	33.10
7.5			0.44	14.73		3.68	124.44		0.80	144.90		0.11	25.90		0.20	32.70
8.5			0.44	16.24		3.87	128.05		0.81	153.54		0.11	24.60		0.20	33.10
9.5			0.47	16.32		6.00	161.74		1.09	187.47		0.19	49.70		0.29	46.30
10.5			0.45	17.83		3.86	123.40		0.79	149.68		0.11	23.90		0.19	30.70
11.5			0.46	19.00		3.90	121.77		0.77	149.97		0.10	22.30		0.20	31.90
12.5			0.45	23.11		3.92	122.32		0.81	157.43		0.10	23.80		0.19	29.90
13.5			0.47	18.33		4.08	125.49		0.80	150.35		0.11	26.30		0.19	29.70
14.5			0.33	13.63		4.25	122.45		0.82	151.64		0.12	27.70		0.18	28.60
15.5			0.44	16.79		4.08	123.50		0.75	145.08		0.11	27.20		0.18	27.90
16.5			0.40	19.61		3.98	125.00		0.79	151.09		0.11	27.10		0.20	31.20
17.5			0.38	18.90		4.04	122.33		0.82	158.89		0.11	27.20		0.19	28.50
18.5			0.36	23.23		3.87	109.46		0.79	149.59		0.10	22.40		0.21	31.80
19.5			0.44	17.58		4.00	119.54					0.10	20.60		0.17	27.90
24.5			0.38	18.75		4.02	119.31		0.82	154.98		0.09	22.40		0.18	27.70
29.5			0.34	17.00		3.83	122.81		0.74	149.74		0.12	26.60		0.18	29.60

Table 2: Dissolved species and ascorbate-extracted oxides displayed in Fig. 4 (colour code respected)

Depth (cm)	ST2	NO_2^-	NO_3^-	NH_4^+	∑DIN	Mn_{asc}	Fe_{asc}	Mnd	Fed	SO_4^{2-}	Alkalinity
		µmol/L	µmol/L	µmol/L	µmol/L	µmol/g	µmol/g	µmol/L	µmol/L	mmol/L	mmol/L
SW		0.11	2.22	21.61	24.35			0.00	0.00	27.65	2.71
0.25		0.60	2.62	56.82	60.32	0.84	12.56	10.22	0.00	27.95	3.43
0.75		0.38	1.07	74.62	76.72	0.60	6.75	18.35	0.00	27.82	3.67
1.25		0.21	0.98	56.42	58.29	0.72	9.28	24.39	0.00	27.73	3.91
1.75		0.11	0.46	77.42	78.80	0.72	10.87	25.06	0.00	32.22	4.04
2.5		0.02	0.37	63.62	64.84	0.72	8.97	26.37	0.00	28.20	4.26
3.5		0.04	0.40	65.62	66.88	0.72	11.58	24.45	0.00	28.04	4.45
4.5		0.00	0.23	80.22	81.32	0.75	14.19	20.53	0.00	27.88	4.51
5.5		0.00	0.29	104.63	105.76	0.73	13.50	19.26	2.58	28.03	4.65
6.5		0.21	1.45	86.42	88.65	0.83	19.01	22.90	15.73	27.94	4.66
7.5		0.50	0.51	115.43	117.21	0.95	19.47	28.83	33.51	28.71	4.66
8.5		0.16	0.75	121.63	123.27	1.09	20.85	42.00	22.65	28.19	
9.5		0.45	0.02	119.03	120.38	0.96	16.86	47.68	15.29	27.98	4.71
10.5		0.11	2.38	91.42	94.28	0.91	14.48	43.98	2.39	27.63	4.64
11.5		0.31	3.67	155.03	159.06	0.84	13.90	36.03	4.48	27.53	4.61
12.5		0.69	0.00	51.02	52.43	0.86	17.17	22.81	44.12	27.71	4.51
13.5		0.28	0.26	149.83	151.22	0.61	8.98	18.01	88.37	27.98	4.46
14.5		0.31	1.38	117.63	119.90	0.76	11.85	17.65	92.90	27.99	4.45
15.5		0.69	0.00	128.23	129.72	0.65	9.24	17.82	103.18	28.17	4.44
16.5		0.31	0.58	116.03	117.67	0.58	8.25	17.47	104.44	27.41	4.41
17.5		0.23	0.23	133.63	134.94	0.60	8.30	17.31	92.92	28.29	4.43
18.5		0.31	0.58	72.02	73.67	0.53	5.82	15.90	108.36	27.55	4.40
19.5		0.33	0.24	135.83	137.24	0.61	6.35	14.54	148.92	27.52	4.44
24.5		0.26	0.05	170.84	172.03	0.67	11.56	10.35	186.66	27.53	4.77
29.5		0.89	0.00	222.84	224.39	0.77	12.65	14.29	197.89	28.40	5.08
34.5		0.82	0.00	315.86	317.37	0.65	9.43	15.69	205.73	27.26	5.00
39.5		0.33	0.37	213.04	214.55	0.74	10.43	8.95	209.00	26.96	4.77

Depth (cm)	ST7	NO_2^-	NO_3^-	NH_4^+	∑DIN	Mn_{asc}	Fe_{asc}	Mnd	Fed	SO_4^{2-}	Alkalinity
		µmol/L	µmol/L	µmol/L	µmol/L	µmol/g	µmol/g	µmol/L	µmol/L	mmol/L	mmol/L
SW		0.34	3.32	23.21	27.33			0.00	0.00	28.13	2.56
0.25		1.21	3.04	31.41	36.11	1.02	18.62	10.77	0.00	28.77	3.29
0.75		1.00	1.70	67.62	70.94	0.92	19.23	20.94	0.00	28.49	3.72
1.25		0.72	2.06	87.42	90.80	0.84	17.79	27.38	0.00	28.15	3.90
1.75		0.39	0.80	98.22	100.17	0.84	17.20	29.16	0.00	27.89	3.96
2.5		0.26	0.65	113.43	115.13	0.77	12.68	29.60	0.00	27.78	4.12
3.5		0.16	0.43	136.03	137.44	0.77	15.30	32.43	3.79	28.55	4.29
4.5		0.39	0.34	150.43	151.97	0.82	17.48	40.26	58.24	27.34	4.32
5.5		0.34	0.42	183.24	184.80	1.15	23.76	57.34	13.88	27.57	4.37
6.5		0.21	0.27	134.83	136.14	0.94	21.28	46.37	3.70	27.38	4.44
7.5		0.49	0.21	161.43	162.96	0.86	19.43	27.15	69.73	27.05	4.46
8.5		0.67	0.03	178.64	180.17	0.95	24.53	20.60	93.22	27.47	4.48
9.5		0.57	0.08	181.44	182.92	0.74	15.75	19.75	99.56	27.20	4.47
10.5		0.54	0.07	186.24	187.69	0.69	10.95	20.41	131.70	27.74	4.49
11.5		0.87	0.04	223.64	225.38	0.73	13.33	19.38	167.07	27.40	4.66
12.5		0.98	0.05	242.65	244.48	0.73	12.79	18.35	195.18	27.26	4.60
13.5		0.60	0.24	239.85	241.49	0.68	12.94	17.15	213.20	27.21	4.54
14.5		0.52	0.13	301.85	303.33	0.75	13.89	16.60	236.92	26.94	4.62
15.5		0.72	0.08	260.85	262.48	0.70	9.83	15.68	271.92	26.61	4.59
16.5		1.10	0.00	276.25	278.02	0.77	12.05	15.18	282.66	27.03	4.59
17.5		1.26	0.00	241.65	243.57	0.91	14.67	15.21	290.72	26.74	
18.5		1.21	0.00	237.05	238.99	0.79	19.96	14.64	273.45	26.60	4.57
19.5		1.00	0.00	308.86	310.62	0.70	16.79	14.21	310.81	26.08	4.59
24.5		0.93	0.04	345.06	346.85	0.78	12.40	11.72	252.17	26.38	4.68
29.5		0.93	0.00	110.23	111.82	0.84	13.77	9.65	199.58	25.66	4.63
34.5		0.80	0.06	411.27	412.95	0.71	13.58	10.35	103.82	25.20	4.76
39.5		0.98	0.00	153.83	155.57	0.72	12.73	9.24	194.13	25.11	4.90
44.5		0.80	0.09	564.49	566.20	0.71	21.21	8.90	173.02	24.85	4.90
49.5		0.93	0.07	285.45	287.26	0.78	16.43	7.27	234.98	24.71	4.87
54.5		0.87	0.00	169.04	170.63	0.68	14.92	7.03	106.64	24.34	5.02

Depth (cm)	St.5	NO_2^-	NO_3^-	NH_4^+	∑DIN	Mn_{asc}	Fe_{asc}	Mnd	Fed	SO_4^{2-}	Alkalinity
		µmol/L	µmol/L	µmol/L	µmol/L	µmol/g	µmol/g	µmol/L	µmol/L	mmol/L	mmol/L
SW		3.24	3.67	22.81	29.63			5.09	0.00	28.02	3.21
0.25		1.52	1.31	36.42	39.83	2.01	26.88	53.90	0.00	27.93	3.99
0.75		0.33	0.00	66.82	67.83	1.00	22.35	82.41	238.52	28.44	4.54
1.25		0.11	0.00	61.82	62.79	1.14	24.72	74.19	296.58	27.97	4.61
1.75		0.09	0.00	73.22	74.23	1.19	24.15	59.19	204.04	28.38	4.39
2.5		0.02	0.04	81.42	82.38	1.10	25.72	42.66	193.22	28.22	4.31
3.5		0.06	0.00	89.02	89.91	0.96	17.50	27.43	187.72	27.98	4.05
4.5		0.11	0.00	95.82	96.80	0.99	16.70	19.97	182.05	27.87	3.95
5.5		0.06	0.00	112.43	113.37	0.91	15.02	16.46	148.64	27.80	3.87
6.5		0.06	0.00	62.42	63.30	0.85	14.37	14.81	142.75	27.56	4.00
7.5		0.04	0.00	99.62	100.57	0.77	13.93	15.57	105.40	27.48	3.80
8.5		0.04	0.24	99.62	100.75	0.53	11.82	11.59	74.03	27.67	3.86
9.5		0.14	0.09	111.23	112.34	0.51	12.57	8.38	60.69	27.40	3.75

Depth (cm)	St.8	NO_2^-	NO_3^-	NH_4^+	∑DIN	Mn_{asc}	Fe_{asc}	Mnd	Fed	SO_4^{2-}	Alkalinity
		µmol/L	µmol/L	µmol/L	µmol/L	µmol/g	µmol/g	µmol/L	µmol/L	mmol/L	mmol/L
SW		0.29	5.91	13.81	20.32			0.00	0.00	28.14	2.62
0.25		0.42	9.88	18.01	28.14	3.67	32.28	0.00	0.00	28.07	2.79
0.75		0.70	1.95	32.61	36.01	0.91	38.08	27.81	0.00	27.58	3.33
1.25		0.75	0.47	31.81	33.95	0.68	28.23	23.50	27.73	28.07	3.24
1.75		0.93	0.07	49.22	51.17	0.49	26.62	9.05	62.74	27.63	3.30
2.5		1.15	0.00	51.02	53.13	0.46	20.93	7.90	120.91	27.78	3.57
3.5		1.08	0.00	88.02	90.01	0.37	12.49	5.31	100.28	27.58	3.58
4.5		0.72	0.00	80.22	81.92	0.39	11.01	5.45	92.43	27.69	3.66
5.5		0.72	0.00	58.82	60.43	0.38	11.36	5.39	79.96	27.54	3.56
6.5		0.72	0.00	93.22	94.83	0.32	11.45	5.54	87.25	27.67	3.70
7.5		0.67	0.00	109.23	110.76	0.44	14.73	6.52	82.57	27.46	3.50
8.5		0.60	0.00	61.02	62.59	0.44	16.24	6.16	84.37	27.50	3.55
9.5		0.60	0.00	88.62	90.13	0.47	16.32	5.96	58.63	27.58	3.49
10.5		0.57	0.00	26.41	27.92	0.45	17.83	5.69	58.69	27.27	3.52
11.5		0.37	0.20	15.61	17.15	0.46	19.00	5.67	28.30	27.07	3.51
12.5		0.49	0.10	75.82	77.39	0.45	23.11	4.76	41.17	27.32	3.52
13.5		0.39	0.34			0.47	18.33	4.93	28.70	27.15	3.48
14.5		0.75	0.00	21.21	22.94	0.33	13.63	5.01	64.30	27.30	3.51
15.5		0.52	0.00	16.81	18.29	0.44	16.79	4.73	48.27	26.95	3.56
16.5		0.52	0.10	72.42	74.02	0.40	19.61	3.38	44.68	27.68	3.53
17.5		0.70	0.00	29.61	31.20	0.38	18.90	4.08	72.73	27.23	3.46
18.5		0.60	0.00	19.21	20.74	0.36	23.23	3.51	55.57	27.64	3.55
19.5		0.44	0.15			0.44	17.58	3.03	35.89	26.95	3.46
24.5		0.52	0.05	19.01	20.56	0.38	18.75	3.25	42.99	27.23	3.54
29.5		0.11	0.43	19.61	21.11	0.34	17.00	3.54	3.82	26.98	3.43

Chapter 6

Interseasonal responses of benthic foraminifera close to the Kronebreen glacier front (Kongsfjorden, Svalbard)

C. Guilhermic[*1], H. Howa[1], A. Mouret[1], A. Pusceddu[2], A. Baltzer[3], M.P. Nardelli[1]

[1] Université Angers, Nantes Univ., Le Mans Univ, CNRS, LPG, Laboratoire de planétologie et géosciences, UMR CNRS 6112, F-49000 Angers, France
[2]Department of Life and Environmental Sciences, University of Cagliari, 09126 Cagliari, Italy
[3]LETG, UMR CNRS 6554, University of Nantes, Campus du Tertre, 44312 Nantes Cedex 3, France

Abstract:

Arctic fjords are transitional areas between glacier-covered land and the ocean, characterised by strong environmental gradients. In addition to global changes affecting Arctic coastal environments, spatial and seasonal variabilities of physical and geochemical conditions in fjords affect benthic ecosystem, particularly living foraminiferal microhabitats. It is urgent to understand the functioning of these complex environments, to better monitor their modifications under the current global warming conditions. Two sampling campaigns were carried out in Kongsfjorden in May and August 2021 to characterize seasonal environmental changes along a longitudinal transect from the Kronebreen glacier front to around 10 km far from it. Our research focused on the seasonal effect of physico-chemical gradients on foraminiferal communities, their spatial distribution, and microhabitats. Organic matter quantity and quality, sediment grain size, and physical parameters of the water masses were investigated as possible driving parameters for benthic ecosystem responses. In the proximal area, foraminiferal assemblages were characterised by the dominance of the pioneer species *Capsammina bowmanni* in the top sediment layers in August, and very low abundances to total absence of foraminifera in May. Food limitation and substrate instability induced by the turbid plume seem to be the major factors driving the summer foraminiferal distribution. In the distal area, foraminiferal assemblages were mainly represented by *Nonionellina labradorica* and *Adercotryma glomeratum* associated with a higher diversity in both seasons. However, in May, foraminiferal abundances were generally lower, due to food limitation. Interestingly, despite the occurrence of different bottom water masses at the two seasons, similar species compositions were observed, suggesting that the water masses do not directly influence the presence or absence of a species. However, a change in main microhabitat distribution was observed for both species, with a peak in superficial layers in summer and more infaunal behaviour in May. This change could be the response to different feeding regimes in the two seasons and/or possibly to enhanced downward transport of foraminifera by macrofaunal bioturbation in spring. Our results clearly show that physical and geochemical gradients induced by melting waters and sediment discharges originating from the tidewater glacier during summer are the main factors that drive foraminiferal distribution at the local (10 km) scale. This finding induces that foraminifera can be used to monitor the effects of ongoing climate change on the benthic ecosystems of Arctic fjords and have the potential to be proxies for reconstructing glacier front positions in the recent past.

Keywords: Arctic, fjord, seasonality, benthic foraminifera, glacier, stability

1 Introduction

Arctic regions are undergoing changes in all their environmental components such as the ocean, the cryosphere and the atmosphere due to global warming and ecosystems have reached hard adaptation limits (Intergovernmental Panel on Climate Change (IPCC), 2023). Between 1979 and 2018, global sea surface temperature increased up to 0.5°C per decade and the sea ice concentration decreased of 12% per decade in summer (Intergovernmental Panel on Climate Change (IPCC), 2022; Perovich and Richter-Menge, 2009). Differently from other parts of the world, Arctic regions are subjected to polar amplification, responsible for the two-fold higher increase of surface air temperature compared to the global average during the past two decades (Notz and Stroeve, 2016; Richter et al., 2012). The exact causes of this amplification are still debated but it probably results from a combination of reduced summer albedo, increased water vapour in the atmosphere due to increased northward heat transport and moisture (Goosse et al., 2018; Stuecker et al., 2018). The northward rise in temperature is favoured by the delayed freeze-up of sea-ice and progressive warming of Arctic water masses (Lind et al., 2018). This dynamic can be particularly observed on the western continental shelf of Svalbard (74-81°N and 10-35°E) where warm Atlantic water (AW) becomes more present over the year since the early 2000's due to weakened southward advection of cold Arctic Water (ArW) (Lind et al., 2018; Strzelewicz et al., 2022). The change of the equilibrium between cold and warm water masses affects the local hydrography of the fjords located on the western coast of Spitsbergen and influences their temporal (seasonal and interannual) variabilities (Cottier et al., 2005; Payne and Roesler, 2019; Svendsen et al., 2002). As the ecosystems of the fjords, from the pelagic to the benthic realms, follow the hydrographic variations on a seasonal scale (Hegseth and Sundfjord, 2008; Hop and Wiencke, 2019; Lydersen et al., 2014; Morata et al., 2008), strong consequences of these hydrological and climatic changes are expected on marine systems.

Western Svalbard fjords are located near the Arctic front separating the northward Atlantic Water current and the southward Arctic Water current (Svendsen et al., 2002). Intrusion of open sea currents inside the fjords depends on a combination of parameters such as the presence of a bottom sill at the entrance of the fjord (Howe et al., 2010; Syvitski and Shaw, 1995), the seasonal stability of the Arctic front (Svendsen et al., 2002), or the interannual variation of local presence of both Atlantic and Arctic currents (Dallmann, 2015; Divya and Krishnan, 2017; Strzelewicz et al., 2022; Svendsen et al., 2002). The seasonal dynamic of these intrusions generates extreme environmental gradients. In winter, the Atlantic Water is not present inside West Spitsbergen fjords (Horsund, Isfjorden, Krossfjorden, Kongsfjorden), therefore, as atmospheric temperatures drop, the water column cools and in subpolar fjords, sea-ice can form (Cottier et al., 2005). In late spring/ early summer, the shift between a mixed to a stratified water column occurs whenever the Atlantic Water flows into these fjords and fresh Surface Water is produced by continental ice melting (Divya and Krishnan, 2017; Hegseth and Sundfjord, 2008; Hopwood et al., 2020; Payne and Roesler, 2019; Svendsen et al., 2002). Before summer water stratification sets in, a spring phytoplanktonic bloom occurs, promoted by the increase in the daily duration of sunlight and the higher concentration of nutrients coming from ice melting and Atlantic waters (Hodal et al., 2012; Hopwood et al., 2020; Payne and Roesler, 2019).

The installation of a strong water stratification during summer and the concomitant turbidity excess originated by melting glaciers represent a limit for local primary production

(e.g., Hegseth et al., 2019; van De Poll et al., 2016), turbidity (D'Angelo et al., 2018; Lydersen et al., 2014) and promote environmental stress (e.g., Fossile et al., 2022; Włodarska-Kowalczuk et al., 2013).

The same oceanographic dynamics is also observed in Kongsfjorden, a fjord located on the north-west of Spitsbergen. Kongsfjorden opens onto the Fram Strait separating the Arctic Ocean to the north, the Atlantic Ocean to the south and Greenland to the west (Dallmann, 2015). Differently from typical fjords, this over-deepened valley only presents a partial sill separating the mouth from the inner area. This implies a higher influence of oceanic circulation in the outer area, mitigated by land driven forcings in the innermost area (Cottier et al., 2010; Svendsen et al., 2002). Indeed, this fjord presents both land-terminating glaciers and marine terminating glaciers (or tidewater glaciers) at its head (Dallmann, 2015). As a subpolar fjord (Howe et al., 2010), Kongsfjorden used to be considerably covered by sea-ice in winter before 2006 (Cottier et al., 2007; Payne and Roesler, 2019; Tverberg et al., 2019) but sea-ice extension rapidly decreased over the last decade and only patchy sea-ice cover is observed at present day, mostly near the northern coast of the fjord. This phenomenon was linked to the warmer water masses present during the warm season (Divya and Krishnan, 2017; Cottier et al., 2007; Payne and Roesler, 2019) and the progressive atlantification of the Fram strait (Cottier et al., 2010; Lind et al., 2018; Strzelewicz et al., 2022). Also, tidewater glaciers are subjected to enhanced frontal ablation through calving and melting due to increased heat transport inside fjords. Warmer atmospheric temperatures also promote the production of superficial glacier meltwaters whose infiltration feeds subglacial runoff. This results in a higher discharge of sediment-rich freshwater in the fjord (D'Angelo et al., 2018; Lydersen et al., 2014; Meslard et al., 2018).

Due to the high seasonality of these environmental drivers (i.e., water mass circulation, stratification, sediment discharges, primary production), important variations in the benthic community structure are expected between seasons. Indeed, several studies reported seasonal phytoplanktonic dynamics (Hegseth et al., 2019; Hodal et al., 2012; Hop and Wiencke, 2019; Hoppe, 2022; Moran et al., 2012) in Kongsfjorden, but little is known about benthic ecosystems. Włodarska-Kowalczuk et al. (2016) studied the macrofaunal and meiofaunal communities' seasonality in the fjord and reported inconsistent signals of seasonal variability. However, living benthic foraminiferal communities showed a much clearer seasonal response, suggesting their usefulness as bio-indicators of fjord benthic ecosystem dynamics. Indeed, foraminifera are particularly useful to monitor rapid environmental changes thanks to their short life cycle and specific ecological requirements (e.g. Bouchet et al., 2018; Duchemin et al., 2008; Fouet et al., 2022; Jorissen et al., 1995, 2022; Richirt et al., 2020). In the middle to outer Kongsfjorden, Jernas et al. (2018) already reported the clear response of benthic foraminiferal communities to the progressive atlantification of the fjord by comparing summer samples from 2005 to 2008. Previous studies investigated foraminifera in different Svalbard regions to characterize modern or past environments (Fossile et al., 2020; Husum et al., 2019; Jernas et al., 2018; Jima et al., 2022; Pawłowska et al., 2017; Saraswat, 2018). Their distribution regarding environmental gradients were investigated in Kongsfjorden by Jernas et al. (2018) and by Fossile et al. (2022). This last study highlighted a spatial zonation of assemblages and densities of individuals driven in summer 2018 by the distance from the Kronebreen glacier front, where the main freshwater input to the fjord comes from.

The present study focuses on seasonal changes in foraminiferal faunal distribution and composition during two contrasted periods of a same year: spring (May) and late summer (August) 2021. Foraminiferal vertical distribution in the sediment column was investigated

along with surrounding environmental parameters such as organic matter quantity and quality, sediment grain size and water column physical parameters (***Chapter 4***). As the duration of the warm season is currently changing due to global warming (Calleja et al., 2017; Divya and Krishnan, 2017; Hop and Wiencke, 2019; Wiencke and Hop, 2016), interseasonal response of benthic foraminifera to variation in environmental gradients in Kongsfjorden was studied with the aim of understanding the present-day functioning of this kind of ecosystems and foreseeing the consequences of drastic changes in seasonality, expected in the context of climate change, on benthic biodiversity and ecosystem functioning.

2 Material and methods

2.1 Environmental parameters

To understand the seasonal variations in living foraminiferal populations, various environmental parameters were considered. Indeed, during the two sampling missions, the water column was investigated using CTD casts (Temperature and Salinity) along with turbidity and [chlorophyll-a] as well as microhabitat characteristics (sediment grain-size and surface organic matter content). These parameters were already presented in ***Chapter 4*** and will be discussed with foraminiferal community from a holistic point of view.

2.2 Foraminifera analysis

The seasonal analysis of foraminiferal fauna is based on the study of short interface cores (10 cm) sampled in May and August 2021. Description of the coring devices is given in ***Chapter 4*** along with a map displaying core locations and a table giving sampling date, core location and depth.

2.2.1 Sample processing

After sampling, cores were sliced in 0.5 cm thick layers from SWI to 2 cm depth and 1 cm thick to 10 cm depth for foraminiferal analyses and stored in plastic bottles filled with a solution of 2 g L^{-1} of Rose Bengal stain in 95 % ethanol (Schönfeld et al., 2012), in order to distinguish living from dead benthic foraminifera. Back in laboratory, samples were sieved through 63 µm and 125 µm meshes and stored in 95 % ethanol. All Rose Bengal-stained benthic foraminifera, considered as living, were handpicked in the > 125 µm size fraction under stereomicroscope. All specimens were identified and assigned to a species (or at least a genus). Abundances of individuals were standardised for a surface of 50 cm^2. Densities of specimens for each single layer were standardized to 50 cm^3 (ind. 50 cm^{-3}). Normalized data are presented in supplementary material 1 in addition to figures in the chapter. The large tubular agglutinated species *Archimerismus subnodosus* was only included in species richness calculations but not included in abundance calculations because of its important fragmentation in the samples. All graphical representations were performed using GRAPHER® 16.2.354 (Golden Software).

2.2.2 Diversity metrics and multivariate analysis

Diversity indices were calculated on species composition of the assemblage in each slice of the studied cores. The species richness (S) was determined as the number of species identified in the assemblages. The Shannon index (H') gave the specific diversity calculated as follows:

$$H' = -\sum_{i=1}^{S} pi * \ln(pi)$$

Where pi is the proportion of each species *i* in the assemblage. Complementary to the Shannon index, Piélou evenness (J) highlights the dominance of one or more species in the assemblage. It was calculated as follows:

$$J = \frac{H'}{\ln(S)}$$

Graphical representation of the diversity metrics was performed using GRAPHER® 16.2.354 (Golden Software).

A clustering analysis was performed on with PAST software using normalized abundances (ind. 50 cm^{-2}) of living foraminifera for the upper 0-5 cm layer on the > 125 µm fraction (Bray-Curtis dissimilarity). Species considered were those with a relative abundance of more than 5% in at least one sample. The clustering analysis included all stations sampled during the two sampling campaigns of May 2021 and August 2021. Moreover, differences between seasons were investigated with a non-metric multidimensional scaling analysis (nMDS) performed with R software (2022.02.0 version, R core team). The function *metaMDS* was used, which applied a square root transformation and Wisconsin double standardisation (Bray-Curtis dissimilarity). This function was available in the R package *vegan* (Oksanen, 2015). Normalized abundances of living foraminifera were used for this analysis. In addition, a similarity of percentage analysis was performed with the simper function also present in the R package vegan (Oksanen, 2015) to investigate specific contribution to differences between stations and seasons. Species showing a contribution > 5% to the differences were indicated on the ordinal plot.

A transformation-based redundancy analysis (tb-RDA) was performed on foraminiferal abundances (0-5 cm and >125 µm) and on environmental parameters. Significant environmental parameters retained by the function *anova.cca* from the R package *vegan* (Oksanen, 2015) were surface turbidity (0-20 m), water depth of the station (m), sea bottom water salinity and temperature, phytopigment content (µg g^{-1}) and Leucine-aminopeptidase (nmol g^{-1} h^{-1}) at the sediment surface (methods given in ***Chapter 4***). Hellinger transformation was applied to foraminiferal abundances and environmental parameters that were centred and scaled using the *decostand* function (Oksanen, 2015).

3 Results

3.1 Foraminiferal diversities and abundances

Foraminiferal abundances and diversity metrics for the 0-5 cm surficial sediment interval are presented in Fig. 1 for both spring and summer sampling times. Foraminiferal abundances showed values increasing from the glacier front (St. 2) to the distal zone (St. 8), both in spring and summer, and were much lower in spring than in summer at all stations (0 and 463 ind. 50 cm^{-2} for St.2, 13 and 803 ind. 50 cm^{-2} for St. 7, 1155 and 1963 ind. 50 cm^{-2} for

St.5 and 1727 and 2196 ind. 50 cm^{-2} for St.8, in May and August respectively). It should be noted that St.2 was barren in May 2021. The specific richness (S) (Fig. 1b) was much lower at the proximal stations St. 2 and St. 7 (between 0 and 7 species respectively) than at the medial station St.5 (between 30 and 33 species) and distal station St. 8 (between 23 and 35 species). The highest diversity values were observed at the medial station St. 5 both in spring and summer. The number of species present at each station in spring and summer was similar, with a maximum difference of 5 species at St. 8.

The lowest Shannon index (H') was measured at St. 2, 0.1 during summer 2021. St. 7 displayed values of 1.1 in spring and 0.5 in summer. The Shannon index was higher than 2 in both seasons at St. 8 and St. 5 with a difference of less than 0.5 between seasons (Fig. 1c).

A much higher seasonal difference was observed for St. 7, with values of 0.79 in spring and 0.28 in summer. Equitability values for St. 2 were below 0.1 in summer 2021. Equitability indices (J) at St. 8 and St. 5 were also similar in both seasons and ranged between 0.59 and 0.71 (Fig. 1d).

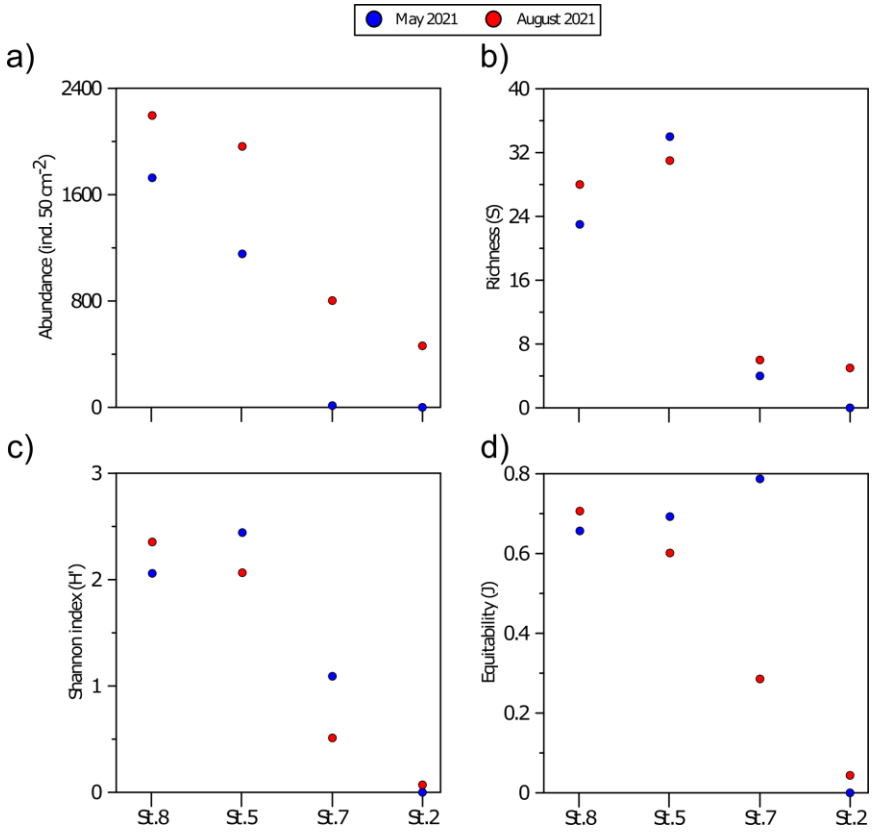

Figure 1: Biodiversity metrics for the two sampling campaigns of May and August 2021, for the upper 5 cm of sediment: a) Normalized total foraminiferal abundances (ind. 50 cm^{-2}), b) specific richness (S), c) Shannon index (H') and d) equitability index (J).

Relationship between specific richness (S) (Fig. 1b) and aminopeptidase (***Chapter 4***; Fig. 4c) was investigated (Fig. 2) as a proxy of ecosystem functioning. Pusceddu et al. (2014) evidenced a higher specific richness of benthic meiofaunal community associated with higher aminopeptidase (extracellular OM degradation proxy) values in stable areas compared to trawled zones in the Mediterranean Sea. A significant linear relationship (R^2 = 0.88; *p*-value <0.01) between the two parameters was observed. Indeed, the low specific diversities observed at the proximal St. 2 and St. 7 were associated with low aminopeptidase. Higher

aminopeptidases measured at the medial St. 5 and at the distal St. 8 were associated to higher specific diversities, both in May and August.

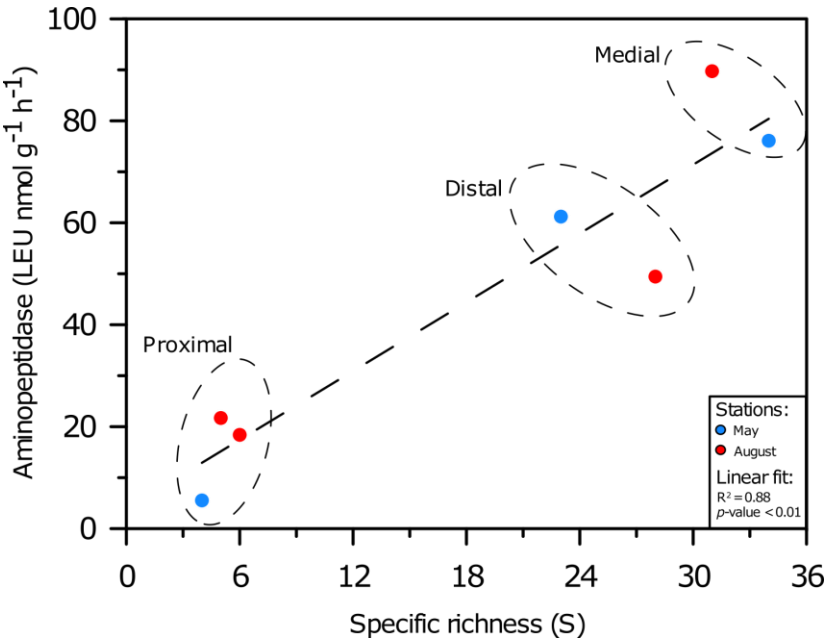

Figure 2: Relationship between specific richness(S) and associated aminopeptidase (nmol g^{-1} h^{-1}) in the upper 0-0.5 cm of sediment at all stations, and both sampling times. No data were available for the proximal St. 2 in May

3.1.1 Specific abundances

In spring, the proximal St. 2 (located at 2 km from the glacier front) was barren. At St. 7 (4 km from the front), *Elphidium clavatum* dominated the low-abundance assemblage (50%, out of 13 ind. 50 cm^{-2}) (Fig. 3). In summer, both St. 2 and St. 7 were largely dominated (99 and 86 % respectively) by *Capsammina bowmanni* with a minor contribution of *Cassidulina reniforme* (< 20 %).

At the medial St. 5, the assemblage was mainly composed of the species *Nonionellina labradorica* in both seasons, with 34 and 50 % of the assemblages in May and August, respectively, accompanied by *Labrospira crassimargo* (3.5%), *Reophax fusiformis* (3.4%)and *Siphonaperta agglutinata* (5.1%).

At the distal St. 8, the assemblage was mainly composed of *Adercotryma glomeratum* and *N. labradorica* in both seasons, with 49 and 38 % and 10 and 21 % in spring and in summer respectively. Moreover, minor species such as *Reophax scorpiurus* and *Reophax fusiformis* were present at 9 and 3 % in May and at 1 and 6 % in August, respectively. Species present at less than 5% in each sample represented 13 and 12 % in May and August, respectively (Fig. 3). Scanning electron micrographs (SEM) of the main observed species are presented in Plate 1.

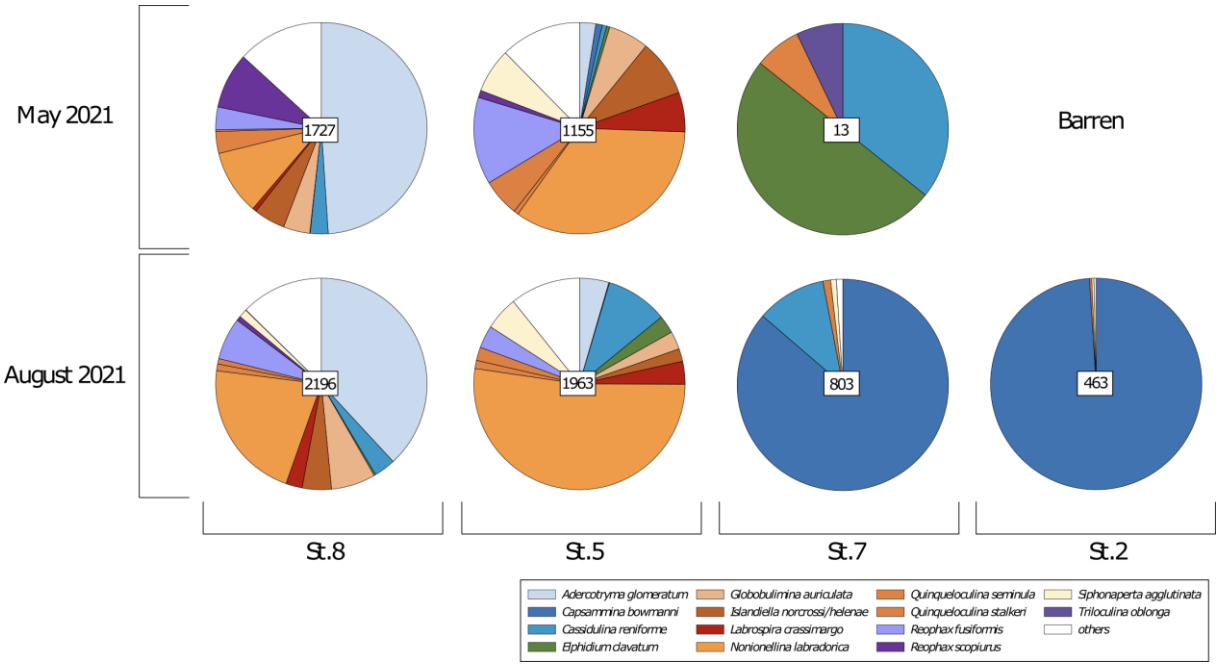

Figure 3: Relative abundances of the major living foraminiferal species within the upper 0-5 cm sediment. Total abundances (ind cm^{-2}) are displayed in the centre of the pie charts.

3.1.2 Multivariate statistical analysis

Statistical dissimilarities were investigated between stations and seasons (Fig. 8), using clustering and nMDS (non-metric multidimensional scaling) analyses. These analyses were based on normalized abundances (ind. 50 cm^{-2}) of each species observed in the upper 0-5 cm sediment at each station. The St. 2 in May was removed from the nMDS analysis for a practical reason as it was barren and therefore completely dissimilar from all the others. Cluster analysis (Fig. 3) showed that St. 7 in May was also highly dissimilar to the other stations (> 95%). In August, however, proximal St. 2 and 7 were both found in the same cluster with a dissimilarity of 25%. Similar observations can be made from the ordination plot (Fig. 4b). SIMPER analysis showed that both stations were driven by the species *Capsammina bowmanni* (20%) on the nMDS1 axis. St. 8 and St. 5 were 55% dissimilar (Fig. 4a). This cluster included both seasons of each station. The ordination plot confirmed this cluster as both stations were separated by the nMDS1 and nMDS2 axes. The species *Nonionellina labradorica* and *Adercotryma glomeratum* contributed respectively at 19 and 18% to the differences between these stations. The species presented were the only ones identified by the SIMPER analysis as having a contribution over 5% influencing the differences between sites.

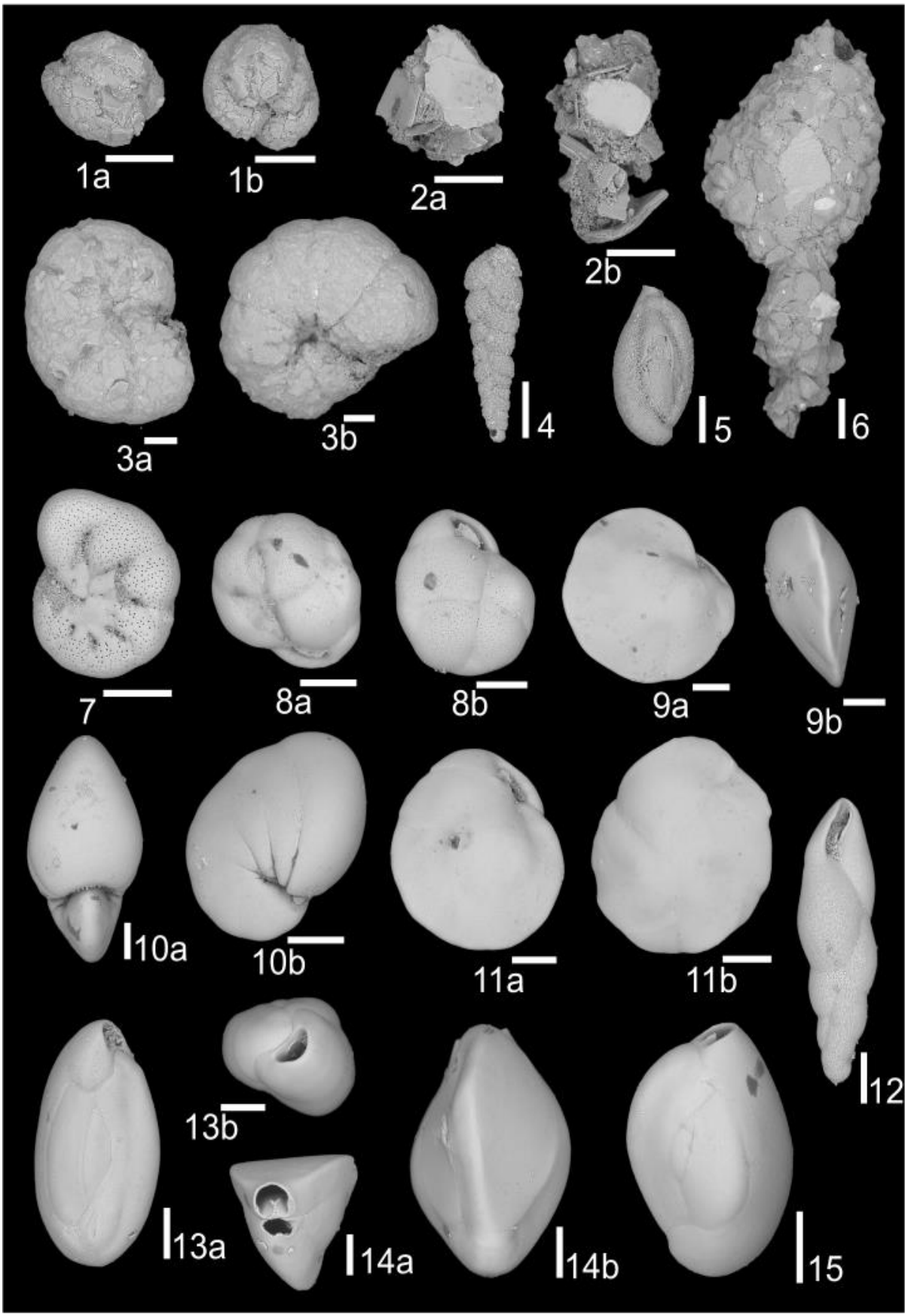

Plate 1: see caption on next page.

Plate 2: Scanning electron micrographs (SEM) of the most relevant benthic foraminifera species at the sampled stations (scale bars = 100 µm). **1a. 1b.** *Adercotryma glomeratum* (Brady, 1878). **2a. 2b** *Capsammina bowmanni* (Heron-Allen and Earland, 1912). **3a. 3b.** *Labrospira crassimargo* (Norman, 1892). **4.** *Textularia earlandi* (Parker, 1952). **5.** *Quinqueloculina stalkeri* (Loeblich and Tappan, 1953). **6.** Reophax scorpiurus (Montfort, 1808). **7.** *Astrononion gallowayi* (Loeblich and Tappan, 1953). **8a. 8b.** *Cassidulina reniforme* (Nørvang, 1945). **9a. 9b.** *Islandiella norcrossi* (Nørvang, 1958). **10a. 10b.** *Nonionellina labradorica* (Dawson, 1860). **11a. 11b**. *Cassidulina teretis* (Tappan, 1951). **12.** Stainforthia feylingi (Knudsen and Seidenkrantz, 1994). **13a. 13b**. *Quinqueloculina seminula* (Linnaeus, 1758). **14a. 14b.** *Triloculina tricarinata* (d'Orbigny, 1832) **15.** *Quinqueloculina arctica* (Cushman, 1933)

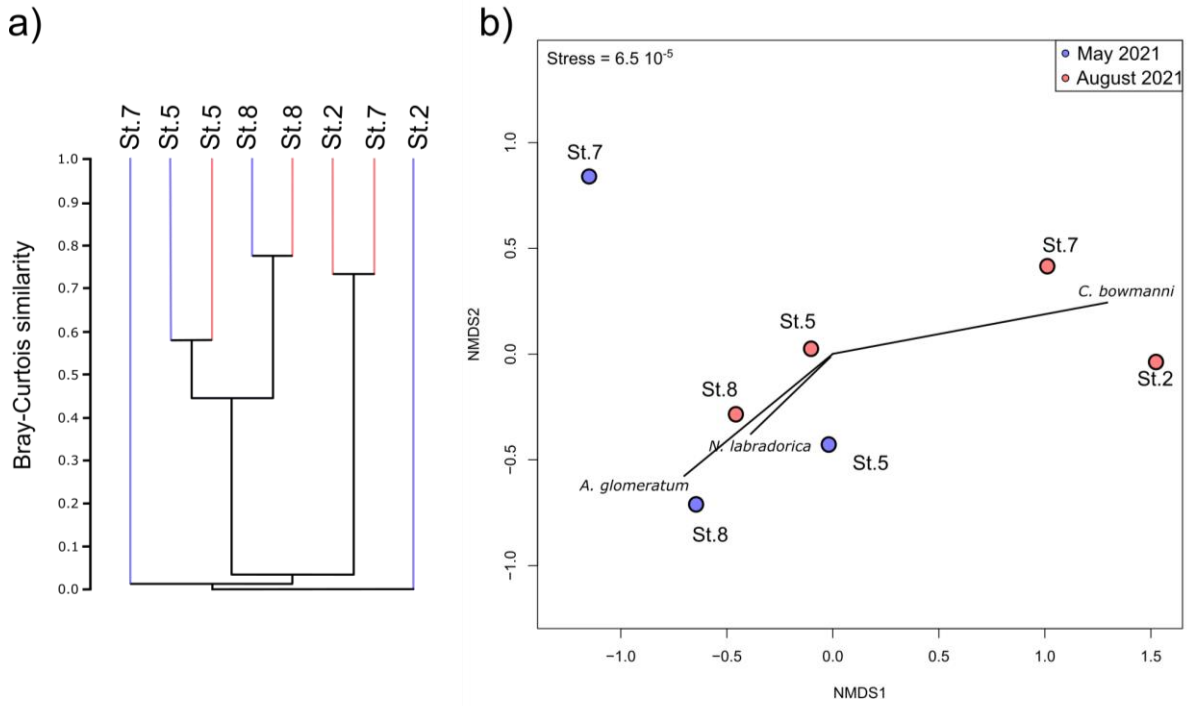

Figure 4: Dissimilarity analysis between the deep transect stations of May and August 2021. a) Clustering based on Bray-Curtis dissimilarity, b) Non-metric multidimensional scaling analysis (Bray-Curtis dissimilarity) on normalized foraminiferal abundances (stress of 6.5 10^{-5}). The colour of the two panels is based on the two missions (blue for May 2021 and red for August 2021). The displayed vectors are the species contributing more than 5% to dissimilarity based on SIMPER analysis.

3.2 Microhabitat distribution

Figure 5 displays the vertical distribution of major species of living benthic foraminifera at the four stations along the fjord axis, both in spring and summer. Specific diversities and densities can be seen here according to species microhabitat (i.e., depth in sediment).

At the proximal St. 2 and St. 7, assemblages and microhabitat distribution were noteworthy. In spring, no individuals were living in the sediment at the proximal St. 2. At the next proximal station, St. 7, only 25 ind. 50 cm^{-3} were found in the surface layers (0-1.5 cm) where the assemblage contained individuals of *Elphidium clavatum, Cassidulina reniforme, Triloculina oblonga* and *Quinqueloculina seminula*. In summer, at the proximal St.2 and St.7, all living individuals were found in the upper 1.5 cm sediment, with a maximum at the topmost layer (0-0.5cm). Below this depth, no living specimen were recovered. Densities of living individuals reached 800 and 1400 ind. 50 cm^{-3} at St. 2 and St. 7, respectively. The summer assemblages at both stations were dominated by *Capsammina bowmanni* accompanied by a few *C. reniforme* individuals.

At the medial St. 5, in spring, the surface layer (0-0.5 cm) contained 480 ind. 50 cm^{-3} of living foraminifera. The surface assemblage was dominated by *Siphonaperta agglutinata, Labrospira crassimargo, Reophax fusiformis and Islandiella norcrossi/helenae*. The species *Nonionellina labradorica* showed a relatively uniform vertical distribution down to 3 cm, followed by a clear decrease in density from 158 ind 50 cm^{-3} at 3 cm depth to 42 ind 50 cm^{-3} in the layer below. In summer, densities of living individuals decreased with depth with a maximum at the surface of 1600 ind. 50 cm^{-3} down to 130 ind. 50 cm^{-3} at 5 cm depth. The dominant species *N. labradorica* showed a maximum density within the first cm of sediment and decreased until disappearing below 3 cm depth. Associated species *C. reniforme, Spiroplectamina biformis, L. crassimargo and E. clavatum* also decreased rapidly with depth. Between 4 and 5 cm, a small increase of *Adercotryma glomeratum* was observed, whereas it was absent in the upper layers.

At the distal St. 8, in May 2021, foraminiferal density was maximum in the surface layer, with 650 ind. 50 cm^{-3}, with the dominant species *A.glomeratum*. Below, a decrease in abundance was observed, with *A. glomeratum* showing a relatively constant density of 200 ind. 50 cm^{-3} down to 5 cm depth, while all other species decreased with depth. Summer assemblages showed a bimodal vertical distribution of abundances. Indeed, the first maximum of density was observed in the 0-0.5 cm layer reaching 1600 ind. 50 cm^{-3}. The assemblage was then mainly composed of *A. glomeratum, I. norcrossi/helenae, R.fusiformis* and *N. labradorica*. The second peak in abundance (700 ind. 50 cm^{-3}) was found between 1.5-2 cm depth, and contained mostly *A. glomeratum* and *N. labradorica* specimens.

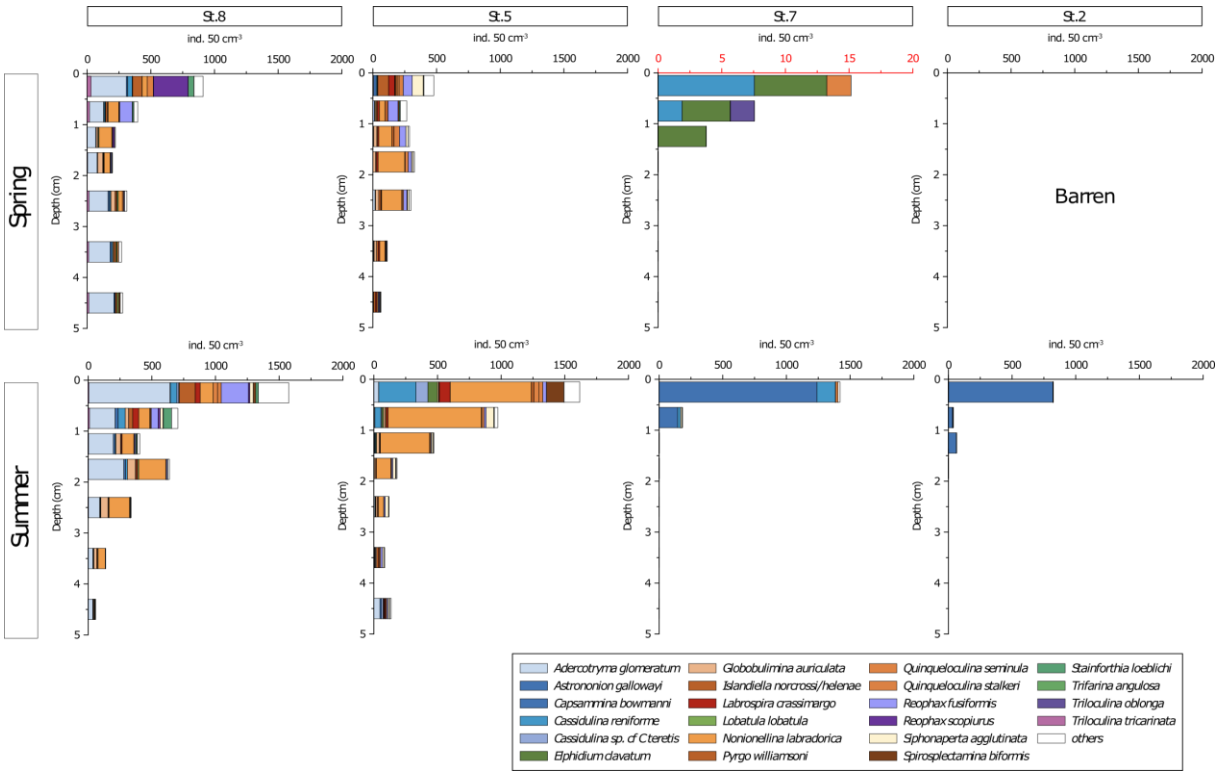

Figure 5: Vertical distribution of the most relevant foraminifera species (more than 5% in at least one sample) from the sediment surface down to 5 cm depth, at the 4 studied stations. The size fraction represented here is > 125 µm. The upper panel presents data from the spring campaign (May 2021) and the lower one is for the summer campaign (August 2021). Note that the density scale for St. 7 in spring (in red) is 100x lower than the others.

3.3 Redundancy analysis

In addition to the foraminiferal vertical distribution, a redundancy analysis was performed to highlight eventual link between environmental factors and the spatial foraminiferal distribution along the fjord axis (Fig. 6).

Five parameters were identified as non-colinear and significant predictors of variations in species abundances at each site for both seasons: mean turbidity values in the upper 20 m of the water column, water depth of the sampling site, concentration in phytopigments in the uppermost first centimetre of sediment along with aminopeptidase values and salinity and temperature of the bottom water (Fig. 6).

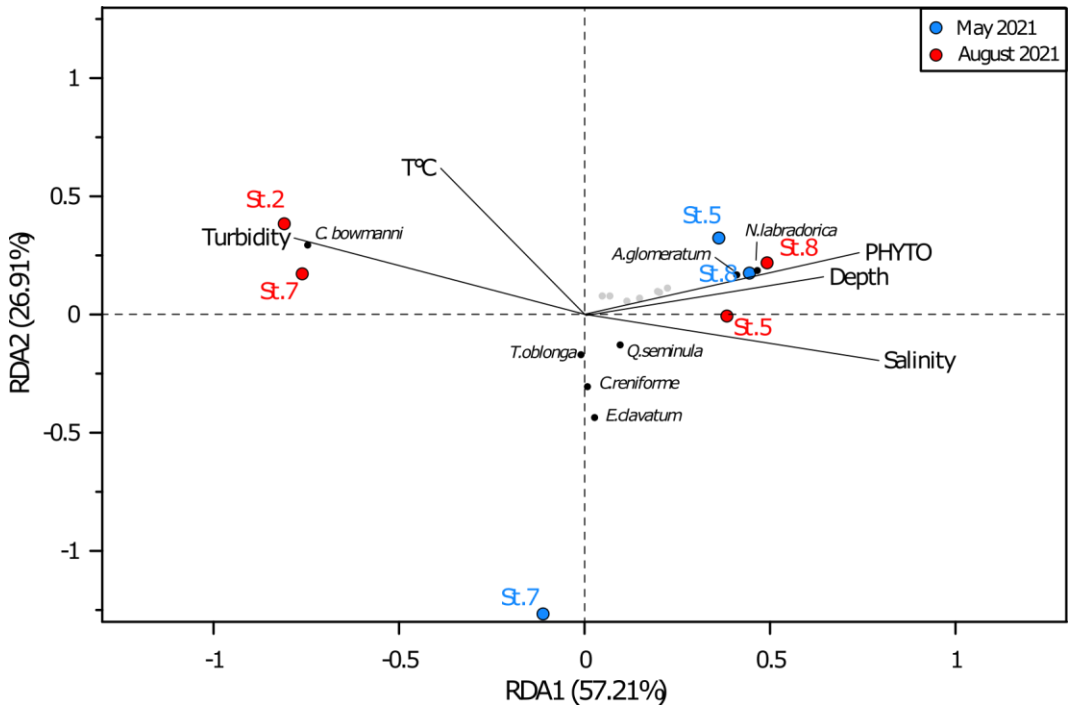

Figure 6: Transformed-based redundancy analysis (tb-RDA) performed on the specific abundances of living foraminifera within the first 0-5 cm of sediment at each sampling site both in May and August, considering the > 125 µm size fraction. Significative environmental parameters are displayed by the continuous black lines and their length correspond to the importance of the variable to explain the variance in the abundance matrix. The mean turbidity value was calculated from measurements taken in the upper 20 m of the water column, PHYTO is the sum of chlorophyll-a and phaeopigments concentrations in the first 0-0.5 cm of sediment (µg g^{-1}), Depth is the sampling water depth (m), salinity, T°C are the bottom water values measured by CTD probes at each site and LEU is the leucine-aminopeptidase (nmol g^{-1} h^{-1}) in the first 0-0.5 cm of sediment. Data from St. 2 in May were not included in this analysis. Raw environmental data are presented in ***Chapter 4***.

Both RDA1 and RDA2 axes explain 84.1% of the total variance (r^2 = 0.64). The first axis is positively correlated with depth, phytopigments, aminopeptidase and salinity and negatively correlated with turbidity and temperature. This RDA1 axis also clearly separates the proximal St. 2 and St. 7 from the distal St. 8 and medial St. 5, in Spring, with the proximal stations highly correlated with turbidity, and slightly less with temperature, whereas the medial/distal stations are highly correlated with phytopigments, aminopeptidase and depth. The foraminiferal composition at St. 5 in August was negatively correlated with the second component and no environmental variable seemed to be correlated with this axis. The species with the highest scores for correlation were *Capsammina bowmanni* (St. 2 and 7), *Nonionellina labradorica* and *Adercotryma glomeratum* (St. 8 and 5).

4 Discussion

4.1 Benthic community responses to seasonality

Spatial distribution of assemblages was investigated in relation with environmental gradients and their seasonal variations. Previous studies conducted in Kongsfjorden highlighted a summer high spatial variability in terms of biodiversity and abundance of benthic foraminifera (e.g. Jernas et al., 2018; Fossile et al., 2022). This variability was attributed to different drivers, mainly bottom water masses (e.g., Atlantic vs Arctic water bodies, Jernas et al., 2018) or to physical disturbance induced by glacier fronts in the inner basin (Fossile et al., 2022).

Our research investigated the seasonal variability of these drivers and the associated response of benthic foraminiferal faunas. In addition to the previously investigated parameters, we also focused on the availability of organic matter, as benthic foraminifera are largely known to primarily respond to trophic conditions (e.g. Jorissen, (1999)). The data we collected at the two seasons showed an existing gradient of decreasing abundances and diversity moving towards the glacier front (Fig. 4). This same gradient was reported by Fossile et al. (2022) and attributed to the environmental stress induced by the glacier melting during summer.

Similarly, to Fossile et al. (2022) we found few species only at the very surface of the sediment at the glacier proximal St. 2 and 7 (*Capsammina bowmanni*, *Cassidulina reniforme* and *Quinqueloculina stalkeri*). The RDA analysis showed a high correlation between these assemblages and high turbidity and low phytopigment contents in August (Fig. 6). The presence of the agglutinated species *C. bowmanni* in the uppermost centimetre of the sediment has already been reported in Kongsfjorden and in other Arctic fjords by previous studies (Fossile et al., 2022; Gooday et al., 2010). This species was suggested by Gooday et al. (2010) to be opportunistic in this kind of stressful environments. In accordance with this, the high abundances we observed and the strong dominance in the assemblages where it appeared support the hypothesis of an opportunistic or pioneer behaviour of the species. Also, the limitation of the nearly monospecific faunas at the uppermost layers of the sediment at the proximal stations further indicates that habitat restrictions were induced by environmental stress, possibly related both to physical disturbance induced by glacier melting inducing high sedimentation and food limitations (see Trox model, Jorissen, (1999)). However, our data also show that in May, when conditions in terms of sediment supply and physical instability were less stressful (Chapter 4; Fig. 2), assemblages at the proximal stations were not more diverse. On the contrary, St. 2 was barren and St. 7 only presented few living specimens (13) of glacier proximal opportunistic species in Svalbard fjords (*C. reniforme* and *E. clavatum*; (Hald and Korsun, 1997; Fossile et al., 2020, 2022)). The absence of *C. bowmanni* and other opportunistic species present in summer could be a combination of different factors : (i) food limitation, suggested by low concentrations of labile organic matter at the seabed (BPC and chlorophyll-a concentrations; ***Chapter 4***; Fig. 4) during spring, (2) reproduction events occurring in summer, which may occur in response to BPC accumulation after the bloom events (= low Phyto/BPC, ***Chapter 4***; Fig. 4c). In addition, the high supply of micas, delivered during summer to the fjord by the subglacial particle discharge, and freshly eroded from Proterozoic bedrocks of Kronebreen ice shed (Dallmann, 2015) could represent a further advantage for the summer development of *C. bowmanni*, as this species builds its test exclusively with mica minerals (Gooday et al., 2010).

Farther from the Kronebreen glacier front and beyond the Lovenøyane shallows, at medial St. 5 abundances over the total depth of the sampled cores and biodiversity were much higher than at the proximal stations. In accordance with Fossile et al. (2022), the overall increase of diversity and abundance of living benthic foraminifera is associated with lower stress induced by glacier proximity and induced environmental gradients. However, important differences were observed between the two sampled seasons. Indeed, abundances were twice as high in summer than in spring, further suggesting the role of food limitation (Fig. 4) as the main cause of low abundances in May. Despite this, the assemblage was substantially represented by *Nonionellina labradorica* both in May (35%) and August (60%), accompanied by numerous minor species (*Labrospira crassimargo*, *Reophax fusiformis* and *Siphonaperta agglutinata*). *Nonionellina labradorica* was previously described as feeding on fresh phytodetritus and associated to OM-enriched AW intrusions during summer (Bernhard and Bowser, 1996; Fossile et al., 2022; Hald and Korsun, 1997; Jernas et al., 2018). In these previous studies and in our samples from the August campaign, the species is largely represented in the upper centimetre of sediment. Organic matter data we obtained at the same period showed the highest chlorophyll-a concentration, [Phyto]/[BPC] values and aminopeptidase rates in August at St. 5 compared to the other stations (Chapter 4; Fig. 4c), indicating higher fresh phytodetritus export to the seabed and increased extracellular bacterial activity in the sediment. The maximum presence of *N. labradorica* in the uppermost layers of sediment further corresponds to its food requirements and the supply of organic matter (Fig. 5). However, despite completely different water masses recorded at the seabed (WCW in May, instead of IW in August; Chapter 4; Fig. 2) and a trophic regime largely poorer than in summertime, *N. labradorica* was still largely present in the May assemblages. This suggests, that its presence is not systematically related to the presence of Atlantic Water (as previously hypothesized by Hald and Korsun, (1997) and Kucharska et al., (2019) and that this species has the capacity to adapt to very changing environmental conditions. One possible strategy could be a change in preferential microhabitat. Indeed, in spring the species was poorly represented in surface layers and showed its maximum density at 1.5-2 cm depth in sediment. This infaunal microhabitat preference in spring suggests the possibility for this species to be able to exploit other food sources when fresh phytodetritus is not available, such as older and buried organic matter evidenced by lower values of the [PRT]/[CHO] ratio (***Chapter 4***). This interpretation further supports the validity of the "food bank" theory (Mincks et al., 2005) in this environment. The ability to switch from shallow to intermediate infaunal preferential microhabitats could also be due to the possibility for this species to use denitrification as an alternative metabolism, as suggested by previous studies (*Nonionellina* sp. T1; Jauffrais et al., 2019). Other hypotheses for the different vertical distribution of *N. labradorica* and associated species, between May and August, can be proposed, reflecting different conditions in physical stability, driven, for example, by higher bioturbation or that the surface peak of the species in summer is due to a recent reproductive event (which generally occurs near the sediment surface). This last hypothesis does not seem to be supported by the sizes of the picked specimens (125>x>63 µm fraction investigated for confirmation), which are not noticeably different from the ones of May and do not show a presence of juveniles. A significant change in the seasonal influence of bioturbation on the stability of macro- meiofaunal communities (except foraminifera) in the fjord was not observed in previous studies in shallow or deep benthic environments (Hop and Wiencke, 2019; Kędra et al., 2011; Włodarska-Kowalczuk et al., 2016), as no seasonal changes in standing stocks and diversity were observed.

At St. 8, the most distal station from the Kronebreen glacier front, the species composition of foraminiferal assemblages was highly correlated with phytopigment content and water depth, at both seasons (Fig. 6). Indeed, despite relatively lower abundances and biodiversity in spring compared to summer, the major species present at the two seasons were the same, *Adercotryma glomeratum* and *Nonionellina labradorica*. The first species is always more abundant, particularly during summer. Its presence was previously observed during summer and linked to Atlantic Water influence and presented as having the ability of the species to profit of high quantity of low quality organic matter (e.g., Fossile et al., 2022; Hald and Korsun, 1997; Jernas et al., 2018). As in our dataset TAW was only present in summer, while the species was recorded in both seasons, this direct link with Atlantic Water does not seem to be confirmed. On the opposite, the ability to feed on low quality organic matter seems to be an advantage in competition with the second major species, *N. labradorica,*, as previously suggested by Fossile et al. (2022). Indeed, at this station, in both seasons, Phyto/BCP ratios are similar to each other and lower than at St. 5 (***Chapter 4***; Fig.4c). Differently to the latter, at St. 8, *A. glomeratum* was dominant in the superficial layers, and *Nonionellina labradorica* was only present in more infaunal microhabitats (0.5 to 3 cm depth). This vertical distribution could be due to a weaker performance of *N. labradorica* in competition with *A. glomeratum* under low quality food regimes. The effect was stronger in summer, when Phyto/BCP ratios at St. 8 were noticeably lower than in spring.

4.2 Conclusions : implications on ecosystem functioning

Previous studies suggested that sediment stability and organic matter export to seabed represent the main local components for ecosystem structuring in Kongsfjorden (Fossile et al., 2022; Hop and Wiencke, 2019; Kędra et al., 2011; Wlodarska-Kowalczuk et al., 2005). In soft bottom environments, the spatial succession of communities from highly disturbed to physically undisturbed habitats was already observed both for meiofauna and macrofauna. For example, pioneer taxa of cumacean or polychaete class can recolonize ice-scoured soft-bottoms in Kongsfjorden (Conlan and Kvitek, 2005) with a progressive increase of faunal abundances after disturbance and associated extermination, without exceeding the abundances observed in unscoured areas. A similar behaviour can be assumed for the benthic foraminifera group, as shown by the behaviour of *Capsammina bowmanni* in the stressed proximal stations. Indeed, after low abundances in spring when the sediment discharge from meltwater is lower, this opportunistic species increases in abundance in the warm season, without exceeding total foraminiferal abundances recorded at the distal stations, considered physically less disturbed.

Indeed, with reduced turbidity and sedimentation, an increase of complexity in community structure and functional diversity was reported for macrofauna (Elverhøi et al., 1983; Wlodarska-Kowalczuk and Pearson, 2004; Kędra et al., 2010) and foraminifera (Fossile et al., 2022). In Kongsfjorden, the bathymetric sill clearly marks a break in the turbidity spreading, the settling of which has an impact on the colonization of the benthic environment with increasing sea bottom stability downfjord (Hop and Wiencke, 2019). At St. 5, downstream of the sill in the outer part of the fjord, the highest specific richness and aminopeptidase (extracellular OM degradation) were observed suggesting higher ecological functioning (Fig. 2). This result could be either the effect of the shallower depth at St. 5 than at St. 8 and a more efficient fresh organic matter export to the seabed or the result of intermediate disturbance conditions (Connell, 1978), as St. 5 is located in the middle zone of the turbidity gradient. In

the distal area, the lower abundances observed in spring were attributed to lower organic matter contents (i.e. before bloom condition), and the similar diversity between seasons was interpreted as the effect of an enhanced storage of organic matter, accumulated during the high productivity periods (summertime). This hypothesis is consistent with the "food bank theory" of Mincks et al. (2005) and would be promoted by the fact that at this distal area turbidity is reduced, and primary production enhanced during summer.

However, interannual variations of Kronebreen subglacial discharge might change the effects of spatial and temporal amplitude of turbidity and physical instability on benthic communities in this area. The available data (Fossile et al., 2022 and the present study) do not show evidences of a strong interannual variability, but in the near future, seasonality in hydrography, primary production and glacier melting yearly dynamics are supposed to become less and less marked (Hop and Wiencke, 2019; Payne and Roesler, 2019). On a short time scale (10 years) (Intergovernmental Panel on Climate Change (IPCC), 2022), the entrance of AW could occur earlier in the year and be prolonged during the warm season in the fjord, resulting in a potential increase in tidewater glacier melting and water stratification, limited spring blooms (Payne and Roesler, 2019; Piquet et al., 2014) and increased turbidity due to higher sediment discharges. This would push downfjord the conditions we observe today in the proximal stations, with a decrease in ecological functioning in the innermost basin. In a longer-term scenario, the Kronebreen will retreat on land and the consequent sediment discharge will drastically decrease, reducing turbidity and also nutrient inputs into the fjord, resulting in larger, but possibly poorer, stable areas at the fjord head. Another possible future scenario regarding glacier dynamics is the imminent surge of the Kongsvegen glacier which shares the front with the Kronebreen assumed by Bouchayer et al. (2023), who observed an acceleration of the glacier downstream velocity from 6 m yr^{-1} in 2014 to nearly 40 m yr^{-1} in 2022. A surge event would move the glacier front downfjord on a kilometric scale within several weeks/months with the potential effect to catastrophically shift the sediment unstable area downfjord.

Data availability:

Normalised counting of individuals are presented in supplementary material 1. Raw data will be available in online repository upon publication on this manuscript.

Author contributions:

CG: conceptualisation, data curation, formal analysis, investigation, methodology, visualisation, writing-original draft, writing-review and editing. MPN: conceptualisation, funding acquisition, investigation, resources, supervision, validation, writing-review and editing. HH and AM: conceptualisation, investigation, supervision, validation, writing-review and editing. AP: methodology, investigation, data curation, formal analysis. AB: funding acquisition.

References:

Bernhard, J. M. and Bowser, S. S.: Novel epifluorescence microscopy method to determine life position of foraminifera in sediments, J. Micropalaeontol., 15, 68–68, https://doi.org/10.1144/jm.15.1.68, 1996.

Bouchayer, C., Nanni, U., Lefeuvre, P.-M., Hulth, J., Steffensen Schmidt, L., Kohler, J., Renard, F., and Schuler, T. V.: Multi-scale variations of hydro-mechanical conditions at the base of the surge-type glacier Kongsvegen, Svalbard, https://doi.org/10.5194/egusphere-2023-618, 2023.

Bouchet, V. M. P., Goberville, E., and Frontalini, F.: Benthic foraminifera to assess Ecological Quality Statuses in Italian transitional waters, Ecological Indicators, 84, 130–139, https://doi.org/10.1016/j.ecolind.2017.07.055, 2018.

Calleja, M. Ll., Kerhervé, P., Bourgeois, S., Kędra, M., Leynaert, A., Devred, E., Babin, M., and Morata, N.: Effects of increase glacier discharge on phytoplankton bloom dynamics and pelagic geochemistry in a high Arctic fjord, Progress in Oceanography, 159, 195–210, https://doi.org/10.1016/j.pocean.2017.07.005, 2017.

Conlan, K. and Kvitek, R.: Recolonization of soft-sediment ice scours on an exposed Arctic coast, Mar. Ecol. Prog. Ser., 286, 21–42, https://doi.org/10.3354/meps286021, 2005.

Connell, J. H.: Diversity in Tropical Rain Forests and Coral Reefs: High diversity of trees and corals is maintained only in a nonequilibrium state., Science, 199, 1302–1310, https://doi.org/10.1126/science.199.4335.1302, 1978.

Cottier, F., Tverberg, V., Inall, M., Svendsen, H., Nilsen, F., and Griffiths, C.: Water mass modification in an Arctic fjord through cross-shelf exchange: The seasonal hydrography of Kongsfjorden, Svalbard, J. Geophys. Res., 110, C12005, https://doi.org/10.1029/2004JC002757, 2005.

Cottier, F. R., Nilsen, F., Inall, M. E., Gerland, S., Tverberg, V., and Svendsen, H.: Wintertime warming of an Arctic shelf in response to large-scale atmospheric circulation, Geophysical Research Letters, 34, https://doi.org/10.1029/2007GL029948, 2007.

Cottier, F. R., Nilsen, F., Skogseth, R., Tverberg, V., Skarðhamar, J., and Svendsen, H.: Arctic fjords: a review of the oceanographic environment and dominant physical processes, SP, 344, 35–50, https://doi.org/10.1144/SP344.4, 2010.

Dallmann, W. K.: Geoscience Atlas of Svalbard, 2015.

D'Angelo, A., Giglio, F., Miserocchi, S., Sanchez-Vidal, A., Aliani, S., Tesi, T., Viola, A., Mazzola, M., and Langone, L.: Multi-year particle fluxes in Kongsfjorden, Svalbard, Biogeosciences, 15, 5343–5363, https://doi.org/10.5194/bg-15-5343-2018, 2018.

van De Poll, W. H., Maat, D. S., Fischer, P., Rozema, P. D., Daly, O. B., Koppelle, S., Visser, R. J. W., and Buma, A. G. J.: Atlantic Advection Driven Changes in Glacial Meltwater: Effects on Phytoplankton Chlorophyll-a and Taxonomic Composition in Kongsfjorden, Spitsbergen, Front. Mar. Sci., 3, https://doi.org/10.3389/fmars.2016.00200, 2016.

Divya, D. T. and Krishnan, K. P.: Recent variability in the Atlantic water intrusion and water masses in Kongsfjorden, an Arctic fjord, Polar Science, 11, 30–41, https://doi.org/10.1016/j.polar.2016.11.004, 2017.

Duchemin, G., Jorissen, F. J., Le Loc'h, F., Andrieux-Loyer, F., Hily, C., and Thouzeau, G.: Seasonal variability of living benthic foraminifera from the outer continental shelf of the Bay of Biscay, Journal of Sea Research, 59, 297–319, https://doi.org/10.1016/j.seares.2008.03.006, 2008.

Elverhøi, A., Lønne, Ø., and Seland, R.: Glaciomarine sedimentation in a modern fjord environment, Spitsbergen, Polar Research, 1, 127–149, https://doi.org/10.3402/polar.v1i2.6978, 1983.

Fossile, E., Nardelli, M. P., Jouini, A., Lansard, B., Pusceddu, A., Moccia, D., Michel, E., Péron, O., Howa, H., and Mojtahid, M.: Benthic foraminifera as tracers of brine production in the Storfjorden "sea ice factory," Biogeosciences, 17, 1933–1953, https://doi.org/10.5194/bg-17-1933-2020, 2020.

Fossile, E., Nardelli, M. P., Howa, H., Baltzer, A., Poprawski, Y., Baneschi, I., Doveri, M., and Mojtahid, M.: Influence of modern environmental gradients on foraminiferal faunas in the inner Kongsfjorden (Svalbard), Marine Micropaleontology, 173, 102117, https://doi.org/10.1016/j.marmicro.2022.102117, 2022.

Fouet, M. P. A., Singer, D., Coynel, A., Héliot, S., Howa, H., Lalande, J., Mouret, A., Schweizer, M., Tcherkez, G., and Jorissen, F. J.: Foraminiferal Distribution in Two Estuarine Intertidal Mudflats of the French Atlantic Coast: Testing the Marine Influence Index, Water, 14, 645, https://doi.org/10.3390/w14040645, 2022.

Gooday, A. J., Lecroq, B., and Pearce, R. B.: The “mica sandwich”; a remarkable new genus of Foraminifera (Protista, Rhizaria) from the Nazaré Canyon (Portuguese margin, NE Atlantic), Micropaleontology, 56, 345–357, 2010.

Goosse, H., Kay, J. E., Armour, K. C., Bodas-Salcedo, A., Chepfer, H., Docquier, D., Jonko, A., Kushner, P. J., Lecomte, O., Massonnet, F., Park, H.-S., Pithan, F., Svensson, G., and Vancoppenolle, M.: Quantifying climate feedbacks in polar regions, Nat Commun, 9, 1919, https://doi.org/10.1038/s41467-018-04173-0, 2018.

Hald, M. and Korsun, S.: Distribution of modern benthic foraminifera from fjords of Svalbard, European Arctic, The Journal of Foraminiferal Research, 27, 101–122, https://doi.org/10.2113/gsjfr.27.2.101, 1997.

Hegseth, E. N. and Sundfjord, A.: Intrusion and blooming of Atlantic phytoplankton species in the high Arctic, Journal of Marine Systems, 74, 108–119, https://doi.org/10.1016/j.jmarsys.2007.11.011, 2008.

Hegseth, E. N., Assmy, P., Wiktor, J. M., Wiktor, J., Kristiansen, S., Leu, E., Tverberg, V., Gabrielsen, T. M., Skogseth, R., and Cottier, F.: Phytoplankton Seasonal Dynamics in Kongsfjorden, Svalbard and the Adjacent Shelf, in: The Ecosystem of Kongsfjorden, Svalbard, vol. 2, edited by: Hop, H. and Wiencke, C., Springer International Publishing, Cham, 173–227, https://doi.org/10.1007/978-3-319-46425-1_6, 2019.

Hodal, H., Falk-Petersen, S., Hop, H., Kristiansen, S., and Reigstad, M.: Spring bloom dynamics in Kongsfjorden, Svalbard: nutrients, phytoplankton, protozoans and primary production, Polar Biol, 35, 191–203, https://doi.org/10.1007/s00300-011-1053-7, 2012.

Hop, H. and Wiencke, C. (Eds.): The Ecosystem of Kongsfjorden, Svalbard, Springer International Publishing, Cham, https://doi.org/10.1007/978-3-319-46425-1, 2019.

Hoppe, C. J. M.: Always ready? Primary production of Arctic phytoplankton at the end of the polar night, Limnol Oceanogr Letters, 7, 167–174, https://doi.org/10.1002/lol2.10222, 2022.

Hopwood, M. J., Carroll, D., Dunse, T., Hodson, A., Holding, J. M., Iriarte, J. L., Ribeiro, S., Achterberg, E. P., Cantoni, C., Carlson, D. F., Chierici, M., Clarke, J. S., Cozzi, S., Fransson, A., Juul-Pedersen, T., Winding, M. H. S., and Meire, L.: Review article: How does glacier discharge affect marine biogeochemistry and primary production in the Arctic?, The Cryosphere, 14, 1347–1383, https://doi.org/10.5194/tc-14-1347-2020, 2020.

Howe, J. A., Austin, W. E. N., Forwick, M., Paetzel, M., Harland, R., and Cage, A. G.: Fjord systems and archives: a review, SP, 344, 5–15, https://doi.org/10.1144/SP344.2, 2010.

Husum, K., Howe, J. A., Baltzer, A., Forwick, M., Jensen, M., Jernas, P., Korsun, S., Miettinen, A., Mohan, R., Morigi, C., Myhre, P. I., Prins, M. A., Skirbekk, K., Sternal, B., Boos, M., Dijkstra, N., and Troelstra, S.: The marine sedimentary environments of Kongsfjorden, Svalbard: an archive of polar environmental change, Polar Research, 38, https://doi.org/10.33265/polar.v38.3380, 2019.

Intergovernmental Panel on Climate Change (IPCC): The Ocean and Cryosphere in a Changing Climate: Special Report of the Intergovernmental Panel on Climate Change, 1st ed., Cambridge University Press, https://doi.org/10.1017/9781009157964, 2022.

Intergovernmental Panel on Climate Change (IPCC): SYNTHESIS REPORT OF THE IPCC SIXTH ASSESSMENT REPORT (AR6), 2023.

Jauffrais, T., LeKieffre, C., Schweizer, M., Geslin, E., Metzger, E., Bernhard, J. M., Jesus, B., Filipsson, H. L., Maire, O., and Meibom, A.: Kleptoplastidic benthic foraminifera from aphotic habitats: insights into assimilation of inorganic C, N and S studied with sub-cellular resolution, Environmental Microbiology, 21, 125–141, https://doi.org/10.1111/1462-2920.14433, 2019.

Jernas, P., Klitgaard-Kristensen, D., Husum, K., Koç, N., Tverberg, V., Loubere, P., Prins, M., Dijkstra, N., and Gluchowska, M.: Annual changes in Arctic fjord environment and modern benthic foraminiferal fauna: Evidence from Kongsfjorden, Svalbard, Global and Planetary Change, 163, 119–140, https://doi.org/10.1016/j.gloplacha.2017.11.013, 2018.

Jima, M., Jayachandran, P. R., and Bijoy Nandan, S.: Modern Benthic Foraminiferal Diversity Along the Fjords of Svalbard Archipelago: Diversity Evaluation, Thalassas, 38, 647–664, https://doi.org/10.1007/s41208-021-00356-7, 2022.

Jorissen, F. J.: Benthic foraminiferal microhabitats below the sediment-water interface, in: Modern Foraminifera, Springer Netherlands, Dordrecht, 161–179, https://doi.org/10.1007/0-306-48104-9_10, 1999.

Jorissen, F. J., de Stigter, H. C., and Widmark, J. G. V.: A conceptual model explaining benthic foraminiferal microhabitats, Marine Micropaleontology, 26, 3–15, https://doi.org/10.1016/0377-8398(95)00047-X, 1995.

Jorissen, F. J., Fouet, M. P. A., Singer, D., and Howa, H.: The Marine Influence Index (MII): A Tool to Assess Estuarine Intertidal Mudflat Environments for the Purpose of Foraminiferal Biomonitoring, Water, 14, 676, https://doi.org/10.3390/w14040676, 2022.

Kędra, M., Włodarska-Kowalczuk, M., and Węsławski, J. M.: Decadal change in macrobenthic soft-bottom community structure in a high Arctic fjord (Kongsfjorden, Svalbard), Polar Biol, 33, 1–11, https://doi.org/10.1007/s00300-009-0679-1, 2010.

Kędra, M., Legeżyńska, J., and Walkusz, W.: Shallow winter and summer macrofauna in a high Arctic fjord (79° N, Spitsbergen), Mar Biodiv, 41, 425–439, https://doi.org/10.1007/s12526-010-0066-8, 2011.

Kucharska, M., Kujawa, A., Pawłowska, J., Łącka, M., Szymańska, N., Lønne, O. J., and Zajączkowski, M.: Seasonal changes in foraminiferal assemblages along environmental gradients in Adventfjorden (West Spitsbergen), Polar Biol, 42, 569–580, https://doi.org/10.1007/s00300-018-02453-5, 2019.

Lind, S., Ingvaldsen, R. B., and Furevik, T.: Arctic warming hotspot in the northern Barents Sea linked to declining sea-ice import, Nature Clim Change, 8, 634–639, https://doi.org/10.1038/s41558-018-0205-y, 2018.

Lydersen, C., Assmy, P., Falk-Petersen, S., Kohler, J., Kovacs, K. M., Reigstad, M., Steen, H., Strøm, H., Sundfjord, A., Varpe, Ø., Walczowski, W., Weslawski, J. M., and Zajaczkowski, M.: The importance of tidewater glaciers for marine mammals and seabirds in Svalbard, Norway, Journal of Marine Systems, 129, 452–471, https://doi.org/10.1016/j.jmarsys.2013.09.006, 2014.

Meslard, F., Bourrin, F., Many, G., and Kerhervé, P.: Suspended particle dynamics and fluxes in an Arctic fjord (Kongsfjorden, Svalbard), Estuarine, Coastal and Shelf Science, 204, 212–224, https://doi.org/10.1016/j.ecss.2018.02.020, 2018.

Mincks, S., Smith, C., and DeMaster, D.: Persistence of labile organic matter and microbial biomass in Antarctic shelf sediments: evidence of a sediment food bank, Mar. Ecol. Prog. Ser., 300, 3–19, https://doi.org/10.3354/meps300003, 2005.

Moran, S. B., Lomas, M. W., Kelly, R. P., Gradinger, R., Iken, K., and Mathis, J. T.: Seasonal succession of net primary productivity, particulate organic carbon export, and autotrophic community composition in the eastern Bering Sea, Deep Sea Research Part II: Topical Studies in Oceanography, 65–70, 84–97, https://doi.org/10.1016/j.dsr2.2012.02.011, 2012.

Morata, N., Renaud, P., Brugel, S., Hobson, K., and Johnson, B.: Spatial and seasonal variations in the pelagic–benthic coupling of the southeastern Beaufort Sea revealed by sedimentary biomarkers, Mar. Ecol. Prog. Ser., 371, 47–63, https://doi.org/10.3354/meps07677, 2008.

Notz, D. and Stroeve, J.: Observed Arctic sea-ice loss directly follows anthropogenic CO_2 emission, Science, 354, 747–750, https://doi.org/10.1126/science.aag2345, 2016.

Oksanen, J.: Community Ecology Package, 2015.

Pawłowska, J., Łącka, M., Kucharska, M., Szymańska, N., Koziorowska, K., Kuliński, K., and Zajączkowski, M.: Benthic foraminifera contribution to fjord modern carbon pools: A seasonal study in Adventfjorden, Spitsbergen, Geobiology, 15, 704–714, https://doi.org/10.1111/gbi.12242, 2017.

Payne, C. M. and Roesler, C. S.: Characterizing the influence of Atlantic water intrusion on water mass formation and phytoplankton distribution in Kongsfjorden, Svalbard, Continental Shelf Research, 191, 104005, https://doi.org/10.1016/j.csr.2019.104005, 2019.

Perovich, D. K. and Richter-Menge, J. A.: Loss of Sea Ice in the Arctic, Annu. Rev. Mar. Sci., 1, 417–441, https://doi.org/10.1146/annurev.marine.010908.163805, 2009.

Piquet, A. M.-T., van de Poll, W. H., Visser, R. J. W., Wiencke, C., Bolhuis, H., and Buma, A. G. J.: Springtime phytoplankton dynamics in Arctic Krossfjorden and Kongsfjorden (Spitsbergen) as a function of glacier proximity, Biogeosciences, 11, 2263–2279, https://doi.org/10.5194/bg-11-2263-2014, 2014.

Pusceddu, A., Bianchelli, S., Martín, J., Puig, P., Palanques, A., Masqué, P., and Danovaro, R.: Chronic and intensive bottom trawling impairs deep-sea biodiversity and ecosystem functioning, Proc. Natl. Acad. Sci. U.S.A., 111, 8861–8866, https://doi.org/10.1073/pnas.1405454111, 2014.

Richirt, J., Riedel, B., Mouret, A., Schweizer, M., Langlet, D., Seitaj, D., Meysman, F. J. R., Slomp, C. P., and Jorissen, F. J.: Foraminiferal community response to seasonal anoxia in Lake Grevelingen (the Netherlands), Biogeosciences, 17, 1415–1435, https://doi.org/10.5194/bg-17-1415-2020, 2020.

Richter, A., Groh, A., and Dietrich, R.: Geodetic observation of sea-level change and crustal deformation in the Baltic Sea region, Physics and Chemistry of the Earth, Parts A/B/C, 53–54, 43–53, https://doi.org/10.1016/j.pce.2011.04.011, 2012.

Saraswat, R.: Assessing the environmental significance of benthic foraminiferal morpho-groups from the northern high latitudinal regions, Polar Science, 11, 2018.

Schönfeld, J., Alve, E., Geslin, E., Jorissen, F., Korsun, S., and Spezzaferri, S.: The FOBIMO (FOraminiferal BIo-MOnitoring) initiative—Towards a standardised protocol for soft-bottom benthic foraminiferal monitoring studies, Marine Micropaleontology, 94–95, 1–13, https://doi.org/10.1016/j.marmicro.2012.06.001, 2012.

Strzelewicz, A., Przyborska, A., and Walczowski, W.: Increased presence of Atlantic Water on the shelf south-west of Spitsbergen with implications for the Arctic fjord Hornsund, Progress in Oceanography, 200, 102714, https://doi.org/10.1016/j.pocean.2021.102714, 2022.

Stuecker, M. F., Bitz, C. M., Armour, K. C., Proistosescu, C., Kang, S. M., Xie, S.-P., Kim, D., McGregor, S., Zhang, W., Zhao, S., Cai, W., Dong, Y., and Jin, F.-F.: Polar amplification dominated by local forcing and feedbacks, Nature Clim Change, 8, 1076–1081, https://doi.org/10.1038/s41558-018-0339-y, 2018.

Svendsen, H., Beszczynska-Møller, A., Hagen, J. O., Lefauconnier, B., Tverberg, V., Gerland, S., Børre Ørbæk, J., Bischof, K., Papucci, C., Zajaczkowski, M., Azzolini, R., Bruland, O., and Wiencke, C.: The physical environment of Kongsfjorden–Krossfjorden, an Arctic fjord system in Svalbard, Polar Research, 21, 133–166, https://doi.org/10.3402/polar.v21i1.6479, 2002.

Syvitski, J. P. M. and Shaw, J.: Chapter 5 Sedimentology and Geomorphology of Fjords, in: Developments in Sedimentology, vol. 53, Elsevier, 113–178, https://doi.org/10.1016/S0070-4571(05)80025-1, 1995.

Tverberg, V., Skogseth, R., Cottier, F., Sundfjord, A., Walczowski, W., Inall, M. E., Falck, E., Pavlova, O., and Nilsen, F.: The Kongsfjorden Transect: Seasonal and Inter-annual Variability in Hydrography, in: The Ecosystem of Kongsfjorden, Svalbard, vol. 2, edited by: Hop, H. and Wiencke, C., Springer International Publishing, Cham, 49–104, https://doi.org/10.1007/978-3-319-46425-1_3, 2019.

Wiencke, C. and Hop, H.: Ecosystem Kongsfjorden: new views after more than a decade of research, Polar Biol, 39, 1679–1687, https://doi.org/10.1007/s00300-016-2032-9, 2016.

Wlodarska-Kowalczuk, M. and Pearson, T. H.: Soft-bottom macrobenthic faunal associations and factors affecting species distributions in an Arctic glacial fjord (Kongsfjord, Spitsbergen), Polar Biol, 27, 155–167, https://doi.org/10.1007/s00300-003-0568-y, 2004.

Chapter 6: Interseasonal responses of benthic foraminifera close to the Kronebreen glacier front (Kongsfjorden, Svalbard)

Wlodarska-Kowalczuk, M., Pearson, T., and Kendall, M.: Benthic response to chronic natural physical disturbance by glacial sedimentation in an Arctic fjord, Mar. Ecol. Prog. Ser., 303, 31–41, https://doi.org/10.3354/meps303031, 2005.

Włodarska-Kowalczuk, M., Pawłowska, J., and Zajączkowski, M.: Do foraminifera mirror diversity and distribution patterns of macrobenthic fauna in an Arctic glacial fjord?, Marine Micropaleontology, 103, 30–39, https://doi.org/10.1016/j.marmicro.2013.07.002, 2013.

Włodarska-Kowalczuk, M., Górska, B., Deja, K., and Morata, N.: Do benthic meiofaunal and macrofaunal communities respond to seasonality in pelagial processes in an Arctic fjord (Kongsfjorden, Spitsbergen)?, Polar Biol, 39, 2115–2129, https://doi.org/10.1007/s00300-016-1982-2, 2016.

Supplementary material 1: Foraminifera counting (ind. 50 cm^{-3}) 3 pages

	Adercotryma glomeratum	Ammodiscus sp.	Archimerismus subnobdosus (fragments)	Astronion galloway	Bolivina sp.	Bulimina sp.	Buccella frigida	Capsammina bowmanni	Cassidulina reniforme	Cassidulina sp. cf. C. teretis	Cornupsira involvens	Elphidium clavatum	Elphidium incertum	Epistominella vitrea	Globobulimina auriculata
ST8 08/21															
0-0.5	644	0	89	2	0	0	0	0	51	15	2	4	13	0	0
0.5-1	212	0	144	25	0	0	11	0	55	0	0	0	0	0	27
1-1.5	199	0	13	11	0	0	0	0	8	0	0	0	0	0	38
1.5-2	280	0	9	15	0	0	4	0	13	0	0	0	0	0	62
2-3	91	0	3	3	0	0	1	0	4	0	0	3	0	0	57
3-4	38	0	0	3	1	0	1	0	3	1	0	1	0	0	22
4-5	37	0	2	2	0	0	1	0	2	0	0	0	0	0	7
5-6	230	0	1	2	0	0	1	0	5	0	0	12	0	0	3
6-7	103	0	0	4	0	0	1	0	1	0	0	0	0	0	0
7-8	55	0	0	0	0	0	0	0	2	1	0	0	0	0	0
8-9	198	0	0	20	0	0	9	0	19	0	0	0	0	0	0
ST8 05/21															
0-0.5	307	0	53	11	0	0	0	0	36	0	0	0	0	0	4
0.5-1	129	0	6	6	0	0	0	0	9	0	0	0	0	0	2
1-1.5	68	0	13	4	0	0	0	0	0	0	0	0	0	0	13
1.5-2	78	0	2	4	0	0	0	0	2	0	0	0	0	0	40
2-3	165	0	0	12	0	0	0	0	9	0	0	0	0	0	33
3-4	181	0	0	12	0	0	4	0	9	0	0	1	0	0	8
4-5	209	0	0	9	0	1	1	0	6	0	0	0	0	0	0
5-6	252	0	0	0	0	0	7	0	5	0	0	0	0	0	0
6-7	291	0	0	9	0	0	9	0	6	0	0	0	0	0	0
7-8	111	0	0	7	0	0	1	0	0	0	0	0	0	0	3
8-9	37	0	0	0	0	0	0	0	0	0	0	0	0	0	0
9-10	76	0	0	7	0	0	2	0	1	0	0	0	0	0	0
St5 08/21															
0-0.5	38	0	0	0	0	0	0	0	294	93	0	76	0	2	9
0.5-1	8	0	0	0	2	0	0	0	47	8	0	13	0	0	15
1-1.5	4	0	0	0	0	0	0	4	8	0	0	6	0	0	23
1.5-2	2	0	0	0	0	0	0	0	2	0	0	0	0	0	9
2-3	9	0	0	0	0	0	0	0	4	2	0	2	0	0	11
3-4	3	0	0	3	0	0	0	0	1	5	0	3	0	0	9
4-5	48	0	0	11	0	0	0	0	0	13	0	0	0	1	4
St5 05/21															
0-0.5	6	2	0	0	0	0	0	20	8	3	0	2	0	0	0
0.5-1	0	0	0	0	0	0	0	0	0	13	5	6	0	0	8
1-1.5	2	0	0	0	0	0	0	2	3	0	2	0	0	0	25
1.5-2	2	0	0	0	0	0	0	0	0	0	0	0	0	0	20
2-3	17	0	0	0	0	0	2	0	1	1	2	2	0	0	25
3-4	6	0	0	0	0	0	0	0	0	5	0	0	0	0	18
4-5	1	0	0	2	0	0	1	0	2	2	0	0	0	0	0
St7 08/21															
0-0.5	0	0	0	0	0	0	0	1240	146	0	0	0	0	0	0
0.5-1	0	0	0	0	0	0	0	146	24	0	0	0	0	0	0
1-1.5	0	0	0	0	0	0	0	0	2	0	0	0	0	0	0
St7 05/21															
0-0.5	0	0	0	0	0	0	0	0	8	0	0	6	0	0	0
0.5-1	0	0	0	0	0	0	0	0	2	0	0	4	0	0	0
1-1.5	0	0	0	0	0	0	0	0	0	0	0	4	0	0	0
St2 08/21															
0-0.5	0	0	0	2	0	0	0	821	0	0	0	0	0	0	0
0.5-1	0	0	0	0	0	0	0	35	0	0	0	0	0	0	0
1-1.5	0	0	0	0	0	0	0	61	0	0	0	0	0	0	0

	Islandiella norcrossi/helenae	Lagenammina atlantica	Labrospira crassimargo	Lobatula lobatula	Moliolids juvenils	Miliolinella circularis	Miliolinella sp.	Nonionellina labradorica	Psammosphaera fusca	Pullenia sp. Cf. P. osloensis	Pyrgo williamsoni	Quinqueloculina arctica	Quinqueloculina seminula	Quinqueloculina stalkeri	Quinqueloculina sp.
ST8 08/21															
0-0.5	125	11	40	0	0	0	2	102	2	0	0	11	34	28	0
0.5-1	32	0	47	0	0	0	0	87	0	0	0	0	4	8	0
1-1.5	4	0	8	0	0	0	0	93	0	0	0	0	4	0	0
1.5-2	8	0	9	9	0	0	0	214	0	0	0	2	2	0	0
2-3	3	0	3	2	0	0	0	163	0	0	0	0	0	0	0
3-4	9	0	0	2	0	0	0	57	0	0	0	0	1	0	0
4-5	2	0	0	4	0	0	0	4	0	0	0	0	0	0	0
5-6	16	0	4	12	0	0	0	1	0	0	0	0	29	0	0
6-7	11	0	0	6	0	0	0	0	0	0	0	0	0	0	0
7-8	3	0	0	5	0	0	0	0	0	0	0	0	0	0	0
8-9	25	0	3	12	0	0	0	0	0	0	0	1	1	1	0
ST8 05/21															
0-0.5	74	0	0	0	0	15	0	40	0	0	0	8	47	2	0
0.5-1	15	0	0	4	0	2	0	83	0	0	0	2	6	2	0
1-1.5	0	0	2	6	0	2	0	102	0	0	2	0	0	4	0
1.5-2	4	0	4	4	0	0	0	45	0	0	0	0	4	0	0
2-3	10	0	5	10	0	1	0	31	0	0	0	2	10	0	0
3-4	15	0	2	9	0	0	0	2	0	0	0	2	9	1	0
4-5	11	0	1	10	0	0	0	3	0	0	0	0	9	0	0
5-6	19	0	0	6	0	0	0	3	0	0	0	0	2	0	0
6-7	15	0	1	16	0	0	0	2	0	0	0	0	4	1	0
7-8	11	0	1	3	0	0	0	0	0	0	0	0	2	0	0
8-9	0	0	0	0	0	0	0	0	0	0	0	0	0	0	0
9-10	3	0	2	3	0	1	0	0	0	0	0	0	0	0	0
St5 08/21															
0-0.5	6	0	85	0	0	0	28	636	2	17	21	6	40	30	0
0.5-1	8	0	11	2	0	0	4	733	0	2	0	2	4	19	0
1-1.5	4	0	4	0	0	0	2	388	0	0	0	0	0	8	0
1.5-2	8	0	0	0	0	0	0	114	0	0	0	0	0	6	0
2-3	7	0	2	0	0	0	0	42	0	1	0	0	2	0	0
3-4	14	0	6	0	0	0	0	9	0	2	1	2	0	0	0
4-5	4	1	9	0	0	0	0	3	0	2	2	5	0	8	0
St5 05/21															
0-0.5	85	6	47	3	0	0	2	3	2	14	14	19	14	33	0
0.5-1	9	0	14	2	5	0	0	44	8	13	22	2	2	0	0
1-1.5	6	0	9	0	0	0	0	101	0	0	19	2	0	42	0
1.5-2	6	0	13	0	0	0	8	209	0	0	3	0	0	25	0
2-3	17	0	5	2	0	0	0	158	0	0	3	7	0	10	0
3-4	14	0	11	0	0	0	0	42	0	0	2	0	0	2	0
4-5	14	0	11	0	0	0	0	9	0	0	0	2	0	3	0
St7 08/21															
0-0.5	0	0	0	0	0	0	0	0	0	0	0	0	0	19	6
0.5-1	0	0	0	0	0	0	0	0	0	0	0	0	0	0	0
1-1.5	0	0	0	0	0	0	0	0	0	0	0	0	0	0	0
St7 05/21															
0-0.5	0	0	0	0	0	0	0	0	0	0	0	0	2	0	0
0.5-1	0	0	0	0	0	0	0	0	0	0	0	0	0	0	0
1-1.5	0	0	0	0	0	0	0	0	0	0	0	0	0	0	0
St2 08/21															
0-0.5	0	0	0	0	0	0	0	0	0	0	0	0	0	2	0
0.5-1	0	0	0	0	0	0	0	0	0	0	0	0	0	0	0
1-1.5	0	0	0	0	0	0	0	0	0	0	0	0	0	2	0

	Recurvoides turbinatus	Reophax catella	Reophax fusiformis	Reophax scopiurus	Reophax sp.	Robertina arctica	Stelligerum	Siphonaperta agglutinata	Spirosplectamina biformis	Stainforthia feylingi	Stainforthia loeblichi	Textularia earlandi	Trifarina angulosa	Triloculina oblonga	Triloculina tricarinata	Total
ST8 08/21																
0-0.5	68	0	214	11	0	28	0	27	19	34	21	61	0	0	6	1575
0.5-1	0	0	53	17	0	2	0	23	2	0	64	25	0	0	11	704
1-1.5	6	0	8	0	0	6	0	4	2	0	8	4	0	2	4	405
1.5-2	4	0	8	0	0	0	0	0	0	0	0	2	4	0	2	638
2-3	0	0	0	1	0	0	0	2	2	0	2	0	0	0	3	338
3-4	0	0	0	0	0	0	0	0	0	0	0	0	0	0	0	137
4-5	0	0	0	0	0	0	0	0	0	0	0	0	1	0	0	59
5-6	0	0	1	4	0	0	2	0	0	0	1	0	9	0	3	334
6-7	0	0	0	1	0	0	0	1	1	0	0	0	5	0	0	133
7-8	0	0	0	0	0	0	0	0	0	0	0	0	7	0	0	72
8-9	0	0	1	25	0	0	0	2	0	0	0	3	3	0	6	327
ST8 05/21																
0-0.5	13	0	0	273	0	4	0	0	0	0	45	2	0	0	30	911
0.5-1	6	0	100	0	0	2	0	0	0	0	9	0	2	0	19	398
1-1.5	4	0	0	15	0	0	0	0	0	0	0	0	0	0	0	222
1.5-2	0	0	8	2	0	0	0	0	0	0	0	0	2	0	4	199
2-3	0	0	6	2	0	0	0	0	0	0	0	0	0	0	15	312
3-4	1	0	0	0	0	0	0	0	0	0	0	4	0	0	12	271
4-5	0	0	0	1	0	0	0	0	0	0	0	5	0	0	13	279
5-6	0	0	0	0	1	0	0	0	0	0	0	1	0	0	6	300
6-7	0	0	0	6	0	0	0	0	0	0	0	1	3	0	8	371
7-8	0	0	0	2	0	0	0	1	0	0	0	0	2	0	3	146
8-9	0	0	0	0	0	0	0	1	0	0	0	0	2	0	0	40
9-10	0	0	0	4	0	0	0	0	0	0	0	0	3	0	0	100
St5 08/21																
0-0.5	0	0	28	0	0	27	0	0	138	34	0	8	0	0	0	1617
0.5-1	4	0	15	0	0	8	0	61	0	6	4	0	0	0	0	973
1-1.5	2	0	6	0	0	0	0	13	0	0	2	0	0	0	0	472
1.5-2	6	0	9	0	0	0	0	23	0	0	4	0	0	0	0	182
2-3	0	0	10	0	0	1	0	26	0	0	0	0	1	0	1	119
3-4	0	0	16	0	0	0	0	12	0	0	0	0	0	0	0	85
4-5	3	0	9	0	0	0	0	11	3	0	0	0	0	0	0	136
St5 05/21																
0-0.5	9	2	71	0	0	22	0	86	3	0	0	0	2	0	0	478
0.5-1	0	0	79	0	0	9	0	0	9	0	8	9	0	0	0	266
1-1.5	2	0	50	0	0	3	0	16	0	2	0	3	0	0	0	288
1.5-2	2	0	25	2	0	0	0	13	0	0	0	0	0	0	0	327
2-3	3	0	27	5	0	0	0	12	1	0	0	2	0	0	0	300
3-4	2	0	4	4	0	0	0	2	0	0	0	1	0	0	0	112
4-5	0	0	8	3	0	0	0	6	0	0	0	0	0	0	0	63
St7 08/21																
0-0.5	0	0	0	0	0	0	0	0	0	0	0	9	0	0	0	1421
0.5-1	0	0	0	0	0	0	0	13	0	0	0	0	0	0	0	182
1-1.5	0	0	0	0	0	0	0	2	0	0	0	0	0	0	0	3
St7 05/21																
0-0.5	0	0	0	0	0	0	0	0	0	0	0	0	0	0	0	15
0.5-1	0	0	0	0	0	0	0	0	0	0	0	0	0	2	0	8
1-1.5	0	0	0	0	0	0	0	0	0	0	0	0	0	0	0	4
St2 08/21																
0-0.5	0	0	0	0	0	0	0	0	0	0	0	0	0	0	0	824
0.5-1	0	0	0	0	0	0	0	3	0	0	0	0	0	0	0	38
1-1.5	0	0	0	0	0	0	0	0	0	0	0	2	0	0	0	64

Chapter 6: Interseasonal responses of benthic foraminifera close to the Kronebreen glacier front (Kongsfjorden, Svalbard)

Chapter 7

Two-dimensional foraminiferal sedimentary microhabitat distribution in two contrasted stations in Kongsfjorden (Svalbard)

C. Guilhermic[*1], A. Mouret[1],H. Howa[1], A. Baltzer[2], M.P. Nardelli[1]

[1] Université Angers, Nantes Univ., Le Mans Univ, CNRS, LPG, Laboratoire de planétologie et géosciences, UMR CNRS 6112, F-49000 Angers, France
[2]LETG, UMR CNRS 6554, University of Nantes, Campus du Tertre, 44312 Nantes Cedex 3, France

Chapter 7: Two-dimensional foraminiferal sedimentary microhabitat distribution in two contrasted stations in Kongsfjorden (Svalbard)

Abstract:

Biozonations of benthic foraminiferal communities et sediment redox transient states were observed on a 10 km scale in Kongsfjorden in response to summer melting of the Kronebreen glacier generating gradients of sedimentation organic matter export towards the seabed. With an increase of ecosystem structure and stability in biogeochemical gradients away from the glacier front, foraminiferal distribution and biogeochemical gradients may be disturbed by small scale biogenic features such as bioturbation and bioirrigation. The small-scale study of two contrasted stations regarding the larger scale environmental gradients in the fjord may add further knowledge to already observed processes. To do so, a 2D sediment sampling device called the "jaw device" allowed the submillimetre mapping of porewater dissolved species by DET methods and also the horizontal and vertical sampling of living benthic foraminifera. This procedure allows the visualisation of the effects of potential sediment structures on nitrates, dissolved manganese and iron and phosphates concentration distribution in an interface sediment core whereas horizontal centimetric distribution of foraminiferal density may reveal patchiness in response to sediment heterogeneity. Depleted concentrations of dissolved manganese and iron revealed vertical sediment features in the DET probes most likely interpreted as active bioirrigation occurred thanks to burrows created by macrofauna in our distal station. Low effects of bioturbation can be seen near the glacier but lateral heterogeneity in dissolved metal production may be a result of organic matter patchiness derived from fecal pellets or macrofauna decomposition in the sediment on the buried sediment-water interface. Foraminiferal vertical distribution showed similar vertical distribution of densities compared to regular core slicing method. However, patchiness of *Capsammina bowmanni* in the glacier proximal area did not allow its sampling in our 2D sampling device. Community structure being higher in the distal area, lateral distribution of the main species *Adercotryma glomeratum*, *Globobulimina auriculata* and *Nonionellina labradorica* revealed a maximum patchiness of 4 cm. However, their distribution could not be linked with biogeochemical highlighted features such as burrows. This additional analysis of lateral small-scale sediment features effect on biochemistry and foraminiferal distribution provides further knowledge of sediment structure in response to environmental parameters.

Key words: bioturbation, small-scale, sediment, heterogeinity, patchiness, fjord, Arctic

Chapter 7: Two-dimensional foraminiferal sedimentary microhabitat distribution in two contrasted stations in Kongsfjorden (Svalbard)

1 Introduction

Arctic fjords are transitional areas between continental ice domain and sea. As such, they are highly affected by strong environmental gradients linked to local hydrography with inflows of Atlantic water bodies and inflows of freshwater issued from glacier melting. Gradients of turbidity, sedimentation rates and primary production have a significant effect on the lateral zonation and heterogeneity of the benthic ecosystem at meter to kilometre scale. This thesis was able to define and characterize biogeochemically unstable areas in Kongsfjorden (Svalbard) (***Chapter 5***) and succession of different foraminiferal fauna (***Chapter 6***) regarding the distance from the Kronebreen tidewater glacier front during summer melting period. Recent studies similarly pointed out the effect of environmental gradients on macrofaunal activities and biozonation (Hop and Wiencke, 2019; Kędra et al., 2011; Petrowski et al., 2016; Włodarska-Kowalczuk et al., 2013; Wlodarska-Kowalczuk et al., 2005). They showed that ecosystem structure was higher further away from Kronebreen glacier front, mostly due to higher export of marine-derived organic matter and higher substrate stability. As a result, the numerous macroorganisms living in the outer fjord are likely to rework the sediment substrate enhancing bioturbation and bioirrigation. This biological activity would generate small-scale sedimentary disturbances affecting microhabitat distribution.

Vertical benthic foraminiferal distribution was conceptualized by Jorissen et al. (1995) which stated that the vertical sequence of microhabitats is driven by a combination of oxygen availability and organic matter quantity and quality. Disturbances in microhabitats may lead to a patchy distribution of individuals at centimetre or millimetre scales. Vertical and horizontal centimetric distribution of foraminifera was only investigated in a few studies such as Buzas (1968), Olsson and Erisksson (1974), and more recently Thibault de Chanvalon et al. (2015). With a focus on foraminiferal distribution around burrows enhancing oxygenation at depth and organic matter displacement by bioturbation, additional studies proposed that oxic microenvironments would be an important factor explaining small-scale heterogeneity. For example, Koller et al. (2006) showed a significant foraminiferal density enrichment on the walls of a macrofauna burrow. Furthermore, certain foraminiferal species can therefore be found deeper in the sediment due to the presence of active burrows (Thibault de Chanvalon et al., 2015).

Sampling methods were recently developed to better visualize small scale 2D location of microhabitats by coupling DET (Diffusive Equilibrium in Thin film) analysis and associated foraminiferal fauna sampling (Choquel et al., 2021; Thibault de Chanvalon et al., 2015). Porewater concentration mapping through DET gels allows a vertical and horizontal visualisation of geochemical species at millimetre to sub-millimetre resolution (Bennett et al., 2015; Cesbron et al., 2014; Jézéquel et al., 2007; Kankanamge et al., 2020; Metzger et al., 2016, 2019; Pagès et al., 2011; Thibault de Chanvalon et al., 2017). With this method, it is possible to visualise microenvironments generated by organic matter uneven lateral distribution (faunal decay or fecal pellets) inducing foraminiferal patchiness and/or localized bacterial remineralisation spots. 2D DETs were already used to identify active burrows. This method allows to map the reduced geochemical species such as dissolved manganese, iron or ammonium, that can be oxidized by oxygen supplied by bioirrigation. Resulting precipitation of oxidized species causes a depletion of dissolved reduced species at the burrow location, creating geochemical fingerprints (Thibault de Chanvalon et al., 2015, 2017; Choquel, 2021).

In addition to the kilometre-scale heterogeneity in foraminiferal assemblages and in biogeochemical transient states previously investigated, this present chapter aims to identify potential heterogeneities in sedimentary microhabitats on a smaller scale. With this objective, this study combines high-resolution vertical and horizontal characterization of living foraminifera density and porewater dissolved geochemical species to highlight small-scale microhabitats at two contrasted stations in Kongsfjorden: one located close to the Kronebreen glacier front and influenced by high sedimentation rates and characterize by a poor fauna, and the other one far from the glacier front characterize by a good ecological structure. Small-scale analysis of sedimentary microhabitats would allow us to further understand the different processes affecting these two contrasted stations located on the observed benthic stability gradient.

2 Material and methods

2.1 Site description

Kongsfjorden is a subpolar Arctic fjord located on the Western coast of Spitsbergen (79°N). It is a glaciated fjord with tidewater glaciers and land-terminating glaciers (Dallmann, 2015). With a E-W orientation, this fjord opens onto the Fram Strait separating the Arctic Ocean in the north and the Atlantic Ocean in the south. Like other fjords, it does not present an entrance sill (Dallmann, 2015; Howe et al., 2010) and is therefore subjected to seasonal intrusions of warm and salty Atlantic Water flowing towards the head of the fjord (Cottier et al., 2005; Hop et al., 2006; Svendsen et al., 2002; Payne and Roesler, 2019). In summer, when this Atlantic water body is present, melting of local glaciers results in subglacial freshwater runoff and iceberg calving from marine-terminating glaciers. This freshwater spreads at the surface of the fjord over Atlantic-derived water bodies and enhances water stratification. The freshwater discharge further transports turbid plume resulting from bedrock glacial erosion mostly originating from the Kronebreen tidewater glacier located at the head of the fjord. Stressful environmental gradients along the fjord axis originate from this surface turbid water, i.e. sedimentation rate (Lydersen et al., 2014; Meslard et al., 2018; Svendsen et al., 2002) and sediment instability (Hop and Wiencke, 2019), primary production and organic matter flux towards the seabed or benthic ecosystem structuring (Hop and Wiencke, 2019). More detailed data about environmental parameters and their consequences on benthic ecosystems in the fjord are discussed in previous chapters.

Studied sites were located at two different stations along the fjord axis and thus along environmental gradients generated by the melting of the Kronebreen glacier. Samples were taken in August 2021 when glacial runoff was at its yearly maximum. These stations are the St. 7 and St. 8 which locations and dynamics were presented in the previous chapters. Moreover, ***chapters 4,5*** and ***6*** described the spatial variability of geochemical stability and foraminiferal content in summer 2021 regarding the already developed influence of glacier melting in the fjord.

2.2 1D core sampling and processing

Two cylindrical cores were recovered at each station for 1D living foraminifera analysis and for 1D geochemical analysis using a GeMAX corer. This coring device allows the sampling of two twin cores at each deployment in soft-bottom environments. Cores were sliced quickly after recovery. Each core underwent a slicing process with similar resolution but with different processing explained afterwards. Slices were 0.5 cm thick between the surface and 2 cm depth, then 1 cm thick continuously between 2 cm to 20 cm depth (foraminiferal treatment was applied down to 10 cm depth only) and 1 cm thick every 5 cm below 20 cm depth.

In order to distinguish living from dead foraminifera, we stained living individuals with a rose Bengal solution consisting in 2 g of Rose Bengal stain in 1 L of 70% ethanol. Following the protocol established by Schönfeld et al. (2012) for living foraminifera analyses, sediment slices were stored in plastic containers and covered with Rose Bengal solution of 2 times the volume of sampled sediment. After transportation to the laboratory in France, each sample was sieved through > 125 µm and > 63 µm mesh sieves to separate two fractions. Only the > 125 µm fraction was analysed for this study due to time constraints (the smaller fraction will be analysed in the next future). All samples were examined under a stereomicroscope. Each stained individual was handpicked and identified (species or genus).

The slicing process described earlier was followed also for the geochemical cores in a N_2 atmosphere. In each sediment slice, porewater was separated from the particulate matrix by centrifugation. After a filtration (0.2 µm Minisart® RC25 syringe filters), all samples were divided between two aliquots for nitrite and nitrate and further ICP-AES measurements. Porewater nitrite and nitrate concentrations were immediately analysed by colorimetry according to the Griess method (Griess, 1879) and using vanadium chloride (VCl_3) as nitrate reducer (García-Robledo et al., 2014). The spectrophotometer used was a Thermo scientific® genesis 20. The resulting measurement is therefore the concentration in NO_x ($[NO_2^- + NO_3^-]$). Nitrate concentration is calculated from this value using the following relation (García-Robledo et al., 2014):

$$[NO_3^-] = (Abs^V_{NOx} - Abs^V reagents - S^V NO_2^- * [NO_2^-]) / S^V NO_3^- \quad (1)$$

Where: Abs^V_{NOx} is the final measured absorbance i.e., combination of $[NO_2^-]$ and $[NO_3^-]$, Abs^Vreagents is the absorbance of VCl_3 without $[NO_2^-]$ or $[NO_3^-]$, $S^V NO_2^-$ and $S^V NO_3^-$ are the slopes of calibration curves after VCl_3 addition, $[NO_2^-]$ is the calculated concentration of nitrite in the sample. The second porewater aliquot was acidified with concentrated nitric acid and stored until further analyses. ICP-AES (Thermo scientific iCAP 6300 Radial) analysis was done after a 10-fold dilution with 1% HNO_3. After a calibration step, $[Mn_d]$ and $[Fe_d]$ were measured. All graphics were designed on GRAPHER (golden software), and artworks were modified and finalized in Inkscape software.

2.3 2D sampling and processing

For two-dimensional sampling, one interface sediment core per site was recovered with the GEMAX gravity corer. After sampling, we inserted a “jaw device” (developed at the LPG Laboratory; 180*83*19 mm; Fig. 1) allowing the sampling of a 130*80*15 mm sediment slab and 2D characterisation of sediment porewater chemistry at high resolution using DET

(Diffusive Equilibrium in Thin Film) gel probes. This "jaw device" was already used in other studies (Choquel et al., 2021; Thibault de Chanvalon et al., 2015) and was adapted for this work.

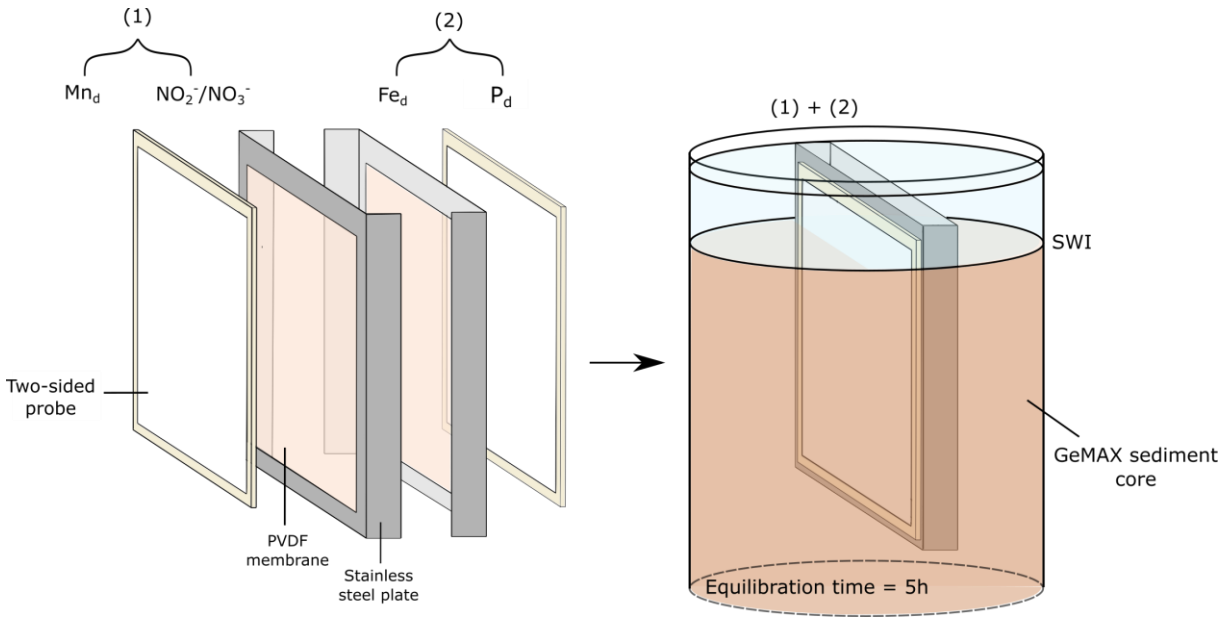

Figure 1: Schematic view of the 2D device deployment for 2D DET and sediment slab samplings. Note the position of the 2D DET probes on plates (1) and (2) placed on the exterior of each "jaw". (1) Mn_d (exterior) and NO_2^-/NO_3^- (interior), (2) Fe_d (interior) and P_d (exterior). After the assembly of all parts, the complete "jaw device" was inserted into a GEMAX core with the uppermost part of the device above the SWI. It was left for equilibration with sediment porewater during 5 h.

With the design of the "Jaw device", four simultaneous samplings of dissolved species were possible. The first pair of 2D DET probes was for dissolved manganese (exterior of the plate) and nitrite/ nitrate (interior of the plate) (dimensions pf all probes: 6.3 cm x 16 cm). [Mn_d] was revealed by the addition on the gel probe of a reagent gel equilibrated with a solution containing imidazole and a cadmium-porphyrin complex via the substitution of Cd by Mn leading to the formation of a Mn-TCPP complex (Mouret et al, in prep). Nitrite and nitrate concentration analysis required a sequential processing starting with nitrite with the addition of a reagent gel previously equilibrated with "Griess reagent", followed by a first image acquisition with a flatbed scanner and then the addition of another reagent gel equilibrated with a vanadium chloride solution and a second image acquisition. After this treatment, the first image is indicative of nitrite only and the second image corresponds to initial nitrite plus reduced nitrate. The image acquisition protocol differs from Metzger et al. (2016) who used a hyperspectral camera. Here, the quantification of nitrate in the second image required the use of the formula (1) to remove the previously measured nitrite concentration in each image pixel.

The second pair of 2D DET was used to obtain the concentration of dissolved iron (interior of the plate) and dissolved reactive phosphate (exterior of the plate). [P_d] was mapped by covering the gel probe with a reagent gel containing sulfuric acid, potassium antimony(III) tartrate hydrate, ammonium molybdate tetrahydrate and ascorbic acid (Cesbron et al., 2014; Pagès et al., 2011) A reagent gel equilibrated with a ferrozine and ascorbic acid solution was applied on the other gel probe to reveal [Fe_d] with pink shades (Cesbron et al., 2014; Jézéquel et al., 2007; Thibault de Chanvalon et al., 2017).

All image treatments were carried out using ImageJ® software and R® software. Image sizing and cropping for nitrite/nitrate treatment were performed on Adobe photoshop® for

precise wedging. Further artworks were designed on the Inkscape® software. All concentration images were cropped at their edges to remove boundary effects such as lateral diffusion from the porewater during the equilibration process or partial desiccation of the gel during handling (Thibault de Chanvalon et al., 2017). Sediment-water interface was estimated for each probe using pictures of the probes set in the cores during equilibration process.

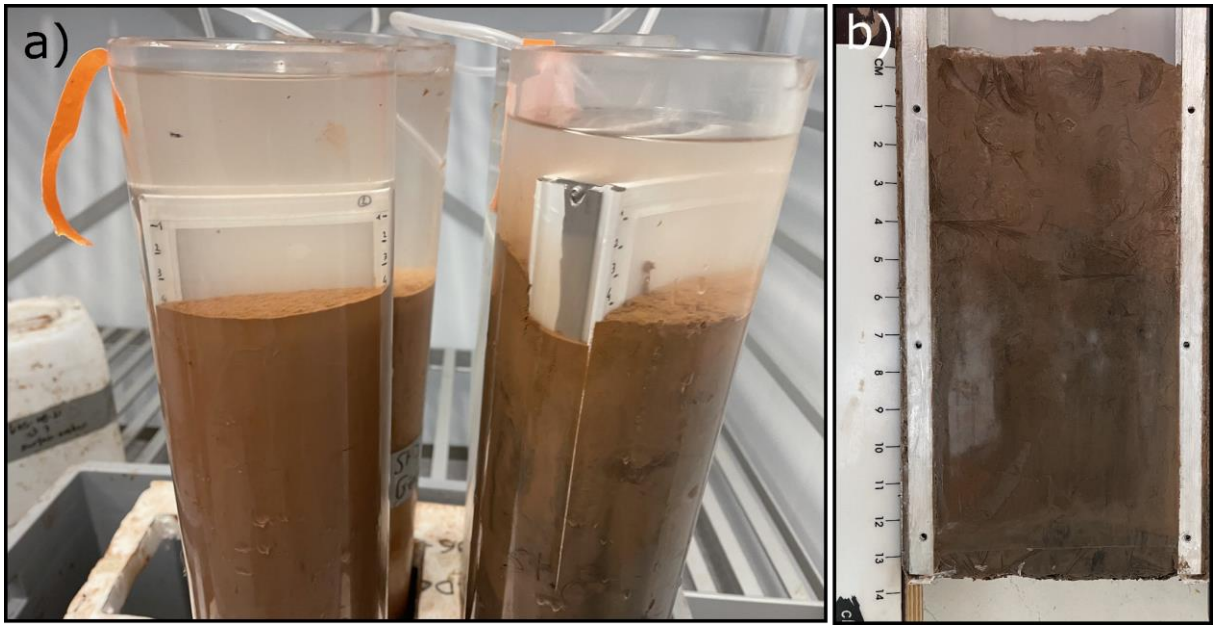

Figure 2: a) "Jaw device" inserted in St.7 (left) and St. 8 (right) cores after their sampling in the fjord. b) Sediment slab extracted from the "jaw device" inserted in St. 8 core before slicing process.

After the removal of the "jaw device", the sediment slab was manually sliced into small volumes of 1.5 cm^3 for a total surface of 130 x 80 mm. As the sediment had a very liquid texture, the sediment slab was frozen to harden it in order to ensure a good and reliable slicing of the sediment (Fig. 2b). A total of 104 samples were then recovered for each plate and labelled according to horizontal (A to H) and vertical (1 to 13) position in a virtual grid (example: C6). All samples were stored in tubes with Rose Bengal staining solution in order to colour the living individuals. Further processing of foraminiferal samples was similar to the 1D methodology (***Chapter 6***).

Additional patchiness effect (or autocorrelation) of foraminifera distribution in the sediment slab was assessed through Moran's index (*I*) computation using the method described by Thibault de Chanvalon et al. (2015). From this model, positive significant values of the Moran's index correspond to grouped organisation (depending on the tested numbers of neighbours) and negative correspond to contrasted organisation. Near 0 values attest of random organisation on the tested scale. Each sample was compared with its nearest vertical or lateral neighbour. Therefore, to constrain our analysis for the lateral heterogeneity of fauna and not overestimate the vertical distribution which decreases with depth (***chapter 6***), we framed our analysis to the uppermost 4 cm of sediment.

3 Results

3.1 Sediment porewater geochemistry

3.1.1 2D dissolved species distribution

High resolution vertical and horizontal concentration mapping of porewater dissolved chemical species is displayed in Fig. 3.

The first pair of probes was dedicated to sample dissolved manganese and nitrite and nitrate in porewaters. [Mn_d] showed values below 70 µmol L^{-1} for both stations. Concentration distribution in sediment porewaters differed between the two stations. In St. 7, a maximum concentration was reached at around 6.5 cm depth with a layer showing values between 50 and 65 µmol L^{-1}. Horizontal heterogeneity was observed with this maximum concentration on the right of the probe associated with an upward and downward decrease. Below this layer, the concentration in the porewaters reached around 45 µmol L^{-1}. The St. 8 probe showed a maximum concentration spot localized on the left edge at 5 cm depth with a value of 50 µmol L^{-1}. A central and vertical depression down to 10 cm depth was present with minimum concentrations around 20 µmol L^{-1} surrounded by concentrations between 30 and 40 µmol L^{-1}. On the other side of this probe was the one treated for nitrite and nitrate mapping. No nitrite was revealed on the gels, only nitrate was detected. The St. 7 probe showed very low enrichment below the sediment water interface and until 2 cm depth, with concentrations around 5 µmol L^{-1}. Concentrations in the supernatant water of the St. 8 probe were around 5 µmol L^{-1}. Large more concentrated patches (~15 µmol L^{-1}) were present below the sediment water interface (SWI) down to 2 cm depth. Deeper, several small and enriched spots were visible, including a very concentrated one at 6 cm depth showing a concentration of 50 µmol L^{-1}.

On the other side of the "jaw device", the second pair of probes was dedicated to sample [Fe_d] and [P_d]. For dissolved Fe, the water column at both stations had a concentration close to 0 µmol L^{-1}. In St. 7, porewater also showed concentrations close to 0 µmol L^{-1} down to 6 cm depth where a 1 cm thick layer showed a concentration of 60 µmol L^{-1}. At 12 cm depth, a localized enrichment at the same concentration can be observed on the left side of the probe. Contrary to St. 7, the distal station displayed a concentration near 0 µmol L^{-1} within the uppermost 2 cm of sediment and below, an overall higher concentration, always above 80 µmol L^{-1}. Two centimetres below the SWI, the enrichment gradient was underlined by a lateral heterogeneous distribution of the increasing concentration front. Moreover, below the SWI, a slight increase of 25 µmol L^{-1} with a vertical structure about 1 cm high and widening at its extremity in a plume-like shape above the SWI was observed. A steep increasing gradient was present with depth, up to a maximum of 140 µmol L^{-1} between 3 and 4.5 cm depth. Below, strong horizontal heterogeneity was observed down to 10 cm depth, where the concentration became uniform with 80 µmol L^{-1}. On the left side of the probe, at a depth of 7-9 cm, a small, elongated feature presented concentrations between 150 and 250 µmol L^{-1} at its centre.

The last probe was used for phosphate concentration mapping. In St. 7, low concentrations were observed in the water column and in the sediment. Most of the probe displayed concentrations below 10 µmol L^{-1} but several patches reached concentrations of 15 µmol L^{-1}. Contrarily to St. 7, St. 8 showed a higher overall concentration of at least 15 µmol L^{-1} in the sediment. At 3.5 cm depth, a 2 cm-thick horizontal patch with high enrichment appeared with maximum concentrations of 30-35 µmol L^{-1}. And above this patch, a vertical figure about

1 cm high was observed between 2 and 3.5 cm depth with a maximum concentration of 25 µmol L^{-1}.

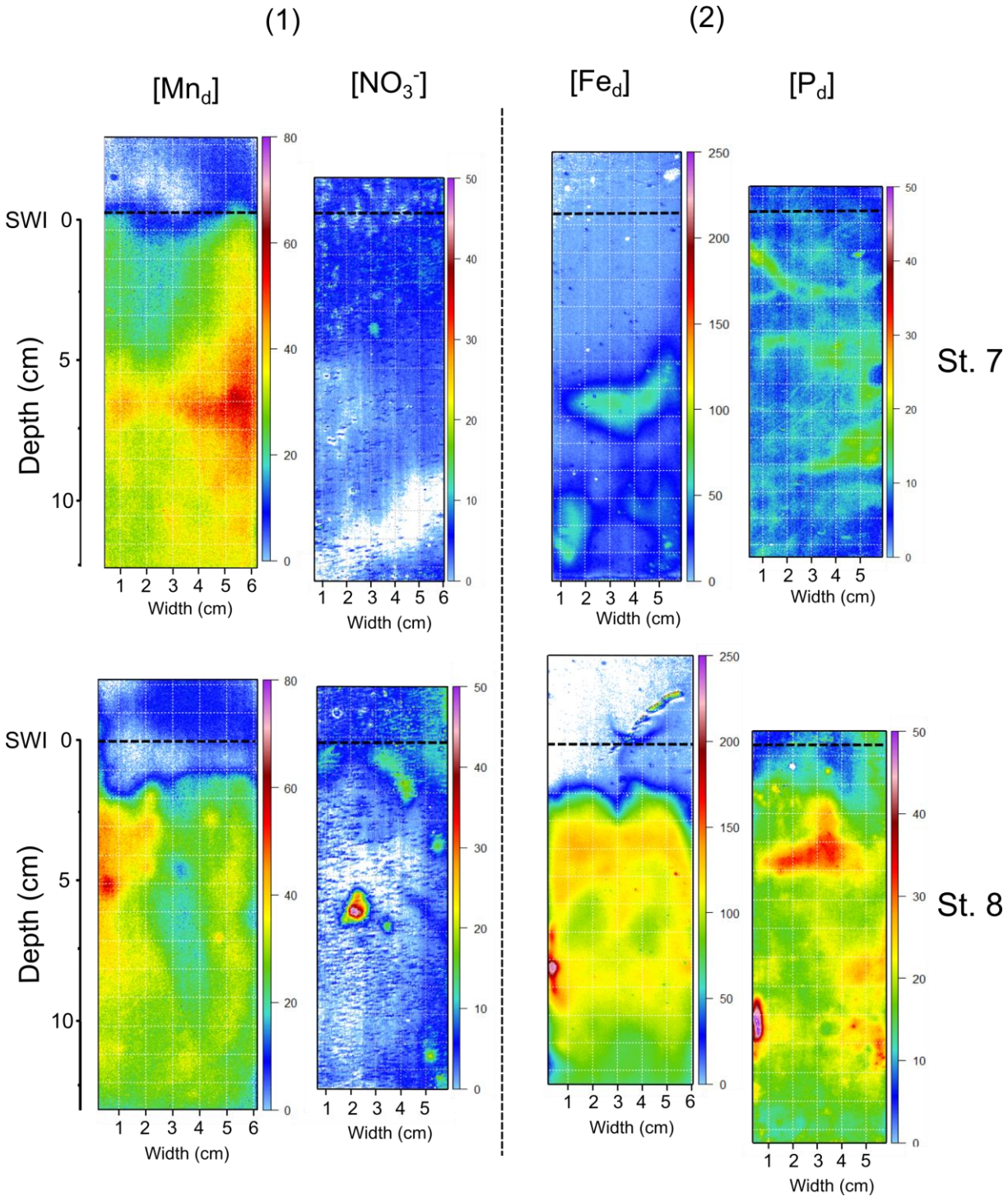

Figure 3: 2D mapping of concentration of different dissolved species in false colour. The upper panel refers to probes retrieved at St. 7 and the lower one concerns the ones from St. 8. Both sides of the "jaw device" are represented by pair of probes symbolized by (1) and (2) as shown in Fig. 1. The horizontal dotted line corresponds to the sediment-water interface with sediment depth downward increase (scale on the left). Horizontal scale shows the width of the probe from the left edge . Presented images were cropped to avoid edge associated artefacts and consequently do not display the 0 cm. Concentration of all dissolved species are specific to each chemistry but common between the two sites (scale on the right of each image). All concentrations are expressed in µmol L^{-1}.

Other enrichment zones can be seen in the sediment, including a strong enrichment at 9-10 cm depth on the left side of the image. In this elongated spot, a maximum concentration of 50 µmol L^{-1} was observed.

3.1.2 Comparison of 1D and 2D data

The two stations St. 7 and St. 8 were sampled for porewater chemical analysis following two methods, 1D profile and 2D mapping. Sediment core slicing, porewater extraction and analysis with ICP-AES and colorimetry resulted in 1D profiles shown in ***Chapter 5***. To compare the results obtained with the two different sampling and analysis technics, high spatial resolution concentration 2D mapping obtained by the DET method (Fig. 3) can be transformed into 1D profiles computed by averadging the values measured at each pixel line of the images (i.e. the same level in the sediment), with an associated standard deviation. The comparison of these two different sampling and analysis technics is displayed in Fig. 4.

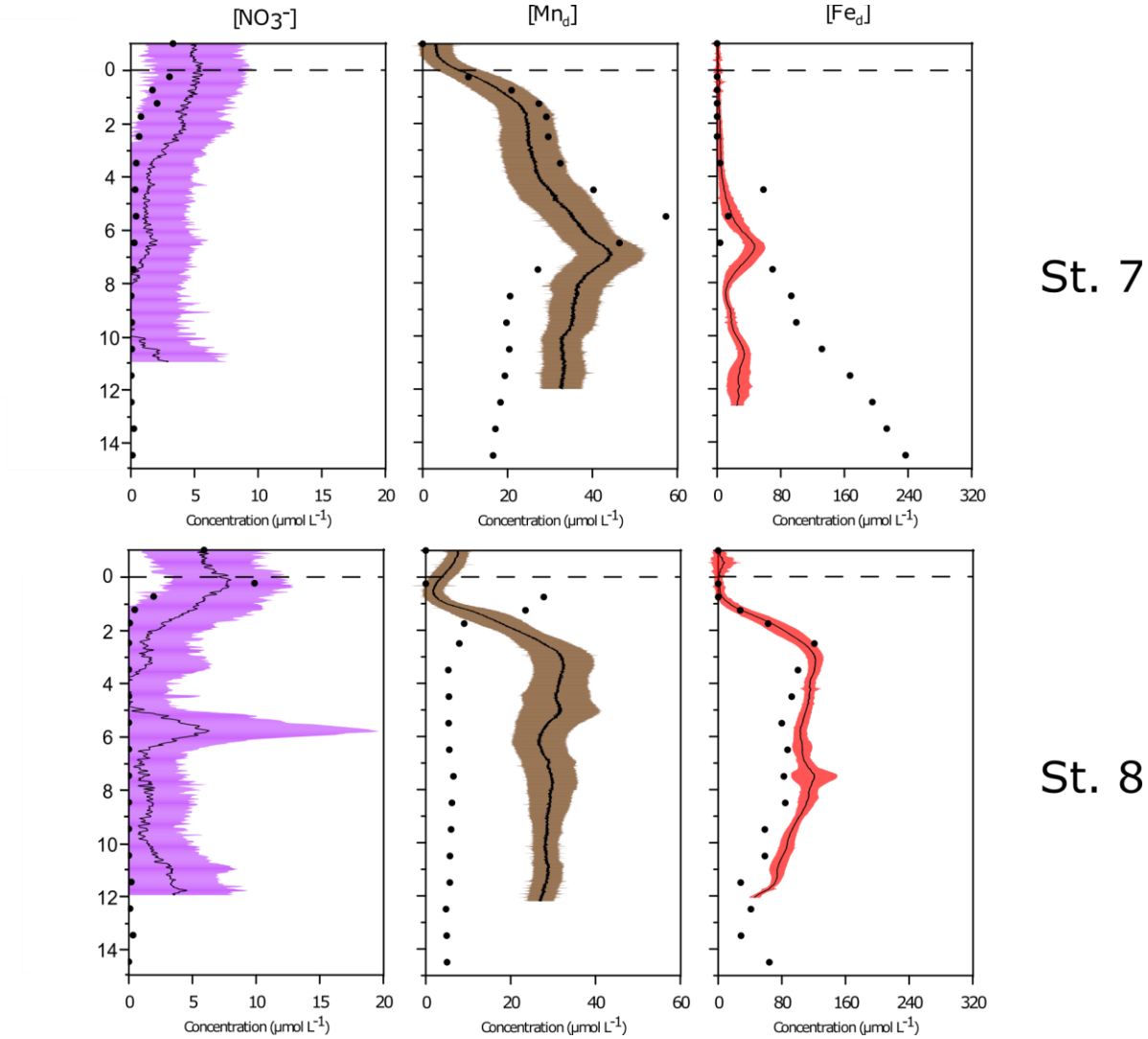

Figure 4: Concentration profiles of nitrate, dissolved manganese, and iron from porewater analysis of 1D sediment cores (Chapter 5; black dots) and averaged profiles (continuous line) with SC (coloured area) extracted from the 2D measurements at the two sampled stations in Kongsfjorden. Note the absence of dissolved phosphorus due to lack of data in 1D sediment cores.

The 1D nitrate concentration profiles averaged from 2D mapping showed relatively similar distribution compared to the ones of the 1D profiles (***Chapter 5***). Indeed, the 1D data displayed slightly higher concentrations in the uppermost sediment layers reaching 3 µmol L^{-1} at St. 7 and 10 µmol L^{-1} at St. 8, and a downward decrease below the first 2 cm to reach 0 µmol L^{-1}. Similar trends were observed in the averaged profiles extracted from the 2D mapping (Fig. 4) with concentrations below the SWI of 5 µmol L^{-1} at St. 7 and 8 µmol L^{-1} at St. 8, and concentrations around 0 µmol L^{-1} below 2 cm depth. One discrepancy appeared at St. 8 profile displaying a concentration of 7 µmol L^{-1} with a high standard deviation induced by the enriched spot described previously around 5 cm depth.At St. 7, manganese averaged profile displayed similar ranges of concentration compared to the 1D data. An increase in concentration with depth following the same gradient within the uppermost 2 cm was observed. A concentration peak of around 60 µmol L^{-1} was observed at 6 cm depth for the 1D profile and a peak at 7 cm depth with a mean concentration of 40 µmol L^{-1} for the averaged profile. Deeper, the averaged profile presented higher concentrations than the 1D profile by around 20 µmol L^{-1}. At St. 8, the averaged profile differed from the 1D data. Indeed, the 1D data showed an increasing concentration gradient within the first centimetre below SWI reaching 30 µmol L^{1} for the1D profile. Below, a sharp decrease was observed down to 3 cm depth reaching 9 µmol L^{1} followed by a slight decrease downwards. The averaged profile showed a concentration peak around 3 cm depth reaching 35 µmol L^{-1} which was similar in concentration value to the 1D profile. The major difference between both profiles was that the downward concentration of dissolved manganese from the peak only reached 25 µmol L^{-1} at the bottom of the 2D image (12 cm depth). Therefore, at the same depth, there was a difference of 20 µmol L^{-1} between the two sampling and analysis methods.

Porewater iron profiles extracted from 2D mapping looked similar to 1D profiles. At St. 7, a concentration peak of 70 µmol L^{-1} was displayed at 4.5 cm depth with the 1D profile and at 5.5 cm depth with the averaged profile. The averaged profile differed below the peak from the 1D profile which showed a high increasing concentration gradient. At St. 8, the enrichment gradient in dissolved iron observed below the SWI was similar in both profiles. Their maximum concentration was 120 µmol L^{-1} at 5 cm depth. A downward decreasing trend was observed in both profiles after this maximum concentration.

3.2 Living foraminifera distribution

The 2D grids of the two studied stations for rose-Bengal-stained foraminiferal analysis are displayed in Fig. 5a allowing vertical and horizontal representation of total densities (main species distribution shown in supplementary material 1). Major differences were observed between the two sampled stations. The counting of individuals was usually performed until the total absence of individuals was observed in one level as displayed in St. 7 distribution with only a few individuals concentrated in the uppermost first centimetre (based on counting in the 1D core). The glacier distal St. 8 however presented living individuals down to the bottom of the sediment slab. Yet, 69% of total individuals were identified in the uppermost 3 cm. At St. 7, foraminiferal density varied from 0 to 13 ind. cm^{-3} and from 0 to 43 ind. cm^{-3} at St. 8. The glacier proximal St. 7 showed a clear dominancy of *Cassidulina reniforme* individuals explaining 67% of the total assemblage. At St.8, the major species were *Adercotryma glomeratum* with a relative abundance of 46%, *Nonionellina labradorica* with 20% and

Globobulimina auriculata with 7%. Within the uppermost 3 cm, an important variability can be observed in the total densities.

At St. 8, the 1D vertical distribution of foraminiferal fauna obtained from the sediment core slicing was similar to the distribution obtained from the 2D sampling of the sediment slab (i.e. with the "jaw device" sampler; Fig. 5b; ***Chapter 6***). The variability of integrated densities computed at each row of the 2D grid, displayed by horizontal box plots, decreased exponentially with depth as observed in the sediment core. At St. 7, results from the two sampling methods showed a major difference of density in the uppermost level (Fig. 5b). A maximum of 420 ind. 50 cm^{-3} was observed in the sediment slab whereas the sediment core displayed a total density for this level of 1600 ind. 50 cm^{-3}. The main reason for this difference is the absence of *Capsammina bowmanni* specimens in the sediment slab, representing more than 90% of the total density in the sediment core (***Chapter 6***).

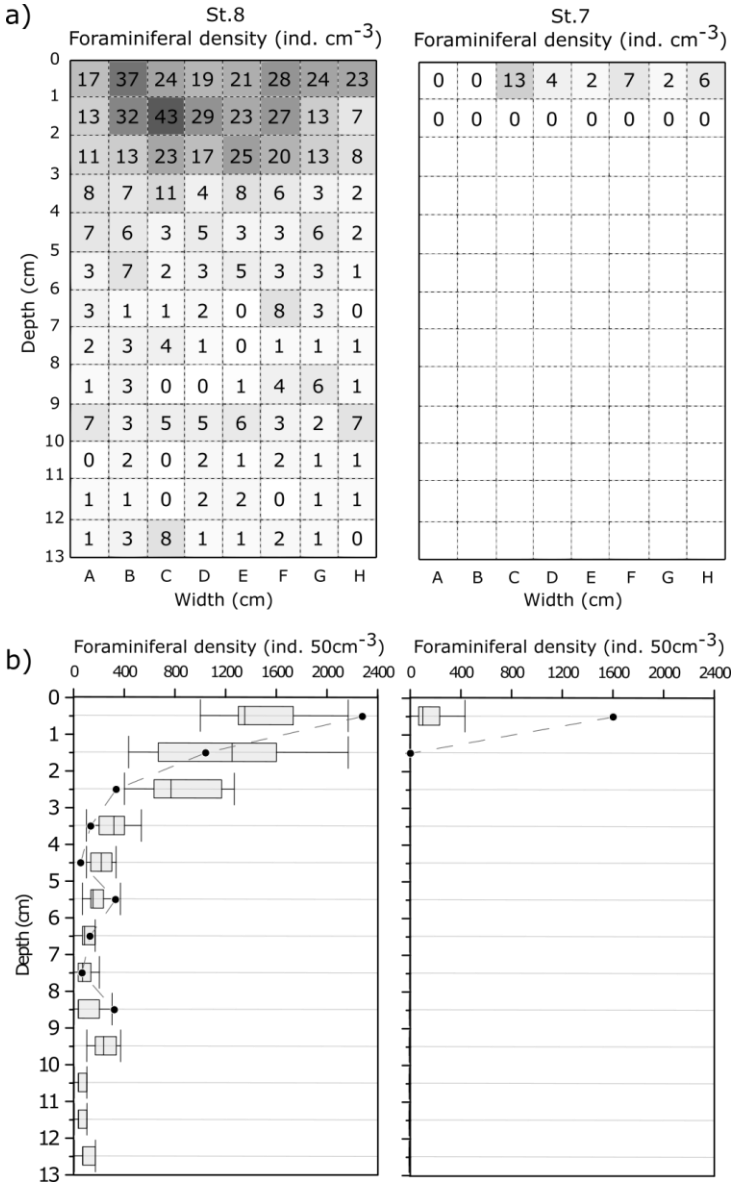

Figure 5: a) 2D distribution of total foraminiferal densities in each sample from the sediment slab for the two considered stations. b) Vertical comparison of total foraminiferal densities from the sediment slab (each box plot integrates the 8 samples of each raw) and from 1D cores (black dots).

4 Discussion

4.1 Consistency between 1D and 2D results

Nitrate showed close concentrations and similar gradients with both methods (Fig. 4). At St. 8, the average 2D nitrate profile displayed a centimetric highly concentrated nitrate spot at 6 cm depth, in the anoxic zone. In 1D sediment cores, this type of nitrate concentration spot is barely visible in the 1D profiles, where nitrate concentrations remained low to zero. The reason could be that nitrate is diluted over the large volume of sediment sampled within a core slice.

For dissolved Mn, the averaged 2D profile in St. 7 showed a similar distribution compared to the 1D core, with the peak maximum observed at slightly different depths (1 cm offset) (Fig. 4). Concentrations obtained by the two methods are close but show more difference at depth with higher concentrations for the 2D method. At St. 8, the two profiles were very different both in terms of distribution and concentration below the surface and at depth. Again, higher concentrations were observed with the 2D method at depth. This could be due to Mn reversibly adsorbed on sediment particles, generating a flux across the 2D gel. A similar hypothesis was proposed by Herbert at al. (2021) for 2D Fe sensors. The difference between the two methods in surface sediment, with higher dissolved Mn measured by ICP AES, might be induced by Mn^{3+} complexed with strong ligands which could not have substituted Cd in the Cd-porphyrin complex used for the colorimetric technics employed for 2D Mn gels. Mn^{3+} might be more present in suboxic conditions observed here down to 2 cm depth, as showed by nitrate profile (Madison et al., 2013). Moreover, the high OM input at this station could favour the production of organic ligands.

Dissolved Fe profiles from St. 8 were highly consistent between the two methods (Fig. 4). Differently, St. 7 displayed pluricentimetric patches of dissolved Fe with a heterogeneous distribution that may not have been sampled with the 2D gel considering its width (6.5 cm). The average profile may therefore have been affected. The 2D DET method should be considered as a complementary approach to characterize, with high details, microhabitats and heterogeneities at a millimetre scale. Moreover, a close method with planar optical Fe^{2+} sensors was recently used in Kongsfjorden by Herbert et al. (2021) to model SWI fluxes.

As regards to foraminiferal analysis results, at St. 8, away from the Kronebreen glacier front, foraminiferal densities obtained by both methods were similar (Fig. 5). At St. 7, the sediment slab did not sample any *Capsammina bowmanni* individuals although this species was highly dominant in the 1D sediment core sampled during the same mission in August 2021 (***Chapter 6***) and also in August 2018 (according to the study of (Fossile et al., 2022)) (Fig. 2). Preliminary results from an additional core sampled for softshell foraminifera analysis from the 2021 sampling campaign confirmed the presence of *C. bowmanni* in the area. No shell debris or broken individuals were found in the uppermost samples of the sediment slab. In addition, secondary species mostly represented by *Cassidulina reniforme* displayed similar densities within the first centimetre of sediment compared to the core studied in the ***Chapter 6***. Based on this observation, we can afford that no dilution of the assemblage by high sedimentation deposits expected in the area close to the glacier front (St. 7) can therefore explain the total absence of *C. bowmanni* in the 2D sampling. We suggest that this discrepancy in *C. bowmanni* abundance could be explained by the fact that this species has a low spatial dispersion and a patchy distribution. This patchiness may not have been sampled either because of the limited

surface sampled by the "jaw device" (12 cm^2 against 52 cm^2 in a sediment core), or because the 1D sediment core was not sampled within the same cast as the core for the 2D device.

4.2 Evidence of bioirrigation, microniches as a consequence of high densities of benthic macrofauna

Chemical heterogeneities on a small spatial scale are generally imputable to biological activity of plant roots or benthic macrofauna or meiofauna (Bouchet et al., 2009; Braeckman et al., 2010; Petrowski et al., 2016). *Sediment bio*reworking due to burrowing and associated ventilation, can contribute to transfer oxidants such as oxygen, nitrate, metal oxides into the anoxic part of the sediment column. This generates enhanced oxidation of organic matter and oxidation of reduced chemical species or promoting effluents of these reduced chemical species directly into the water column. Fauna also generate localized enrichments of OM in sediments in the form of decaying organisms or fecal pellets enhancing local remineralization (Cesbron et al., 2014; Thibault de Chanvalon et al. 2015) and create additional microhabitats for meio- or microorganisms. In Kongsfjorden, several ecological studies reported higher ecosystem structure and functioning with increasing distance from glacial sedimentary inputs of the Kronebreen glacier which represent a benthic stress source (Hop and Wiencke, 2019; Kędra et al., 2011; Wlodarska-Kowalczuk and Pearson, 2004; Wlodarska-Kowalczuk et al., 2005; Włodarska-Kowalczuk et al., 2016). Consequently, a succession of macrofaunal assemblages was observed along the fjord axis in response to gradients in sedimentation rates and organic matter fluxes also documented with living foraminiferal species (***Chapter 6***). According to Wlodarska-Kowalczuk et al. (2005), macrofaunal species located in the inner basin, where the St. 7 of our study is located, were represented by small bivalves and polychaetes living near the sediment surface with active motility behaviour in response to high sedimentation rates and consequent burying. In central parts of the fjord, from the inner sill to Ny-Alesund area, they found large burrowing and sediment structuring polychaetes species such as *Spiochaetopterus typicus* or *Maldane sarsi*. These tube-dwelling species were associated with other mobile species digging in the sediment or crawling at the sediment surface (Wlodarska-Kowalczuk and Pearson, 2004). As they are assumed to be the main cause of biogeochemical heterogeneity, these species (individuals from 0.01 to 50 cm have the ability to reorganize or homogenize the sediment structure (Thibault de Chanvalon et al., 2015; Wlodarska-Kowalczuk et al., 2005). They were observed inside the cores or the day grabs during sampling in May and August 2021 (Fig. 6b). Nevertheless, macrofauna species identification was not done during this study.

Chemical heterogeneities on a small spatial scale can be observed through all chemical mapping performed here. At St. 7, a potential buried SWI was identified at 6 cm depth where reactive oxides had previously accumulated (***Chapter 5***). On 2D concentration maps, pluricentimetric patches enriched in dissolved Mn and Fe were visible at a depth around 6 cm (Fig. 3). No visual evidence of burrows was observed at this station which is consistent with the low densities of bioturbating organisms observed by Wlodarska-Kowalczuk et al. (2005). In addition, the highly fluid sediment matrix (see porosity data; ***chapter 5***) may be an indicator of a relatively recent deposit that may not yet have been recolonized by faunas. These heterogenous dissolved Mn and Fe production zones might thus be the consequence of a heterogeneous deposition of OM at small scale, enhancing local anaerobic remineralisation through reactive oxide reduction. P_d mapping with several patches of similar size supports this hypothesis (Fig. 3).

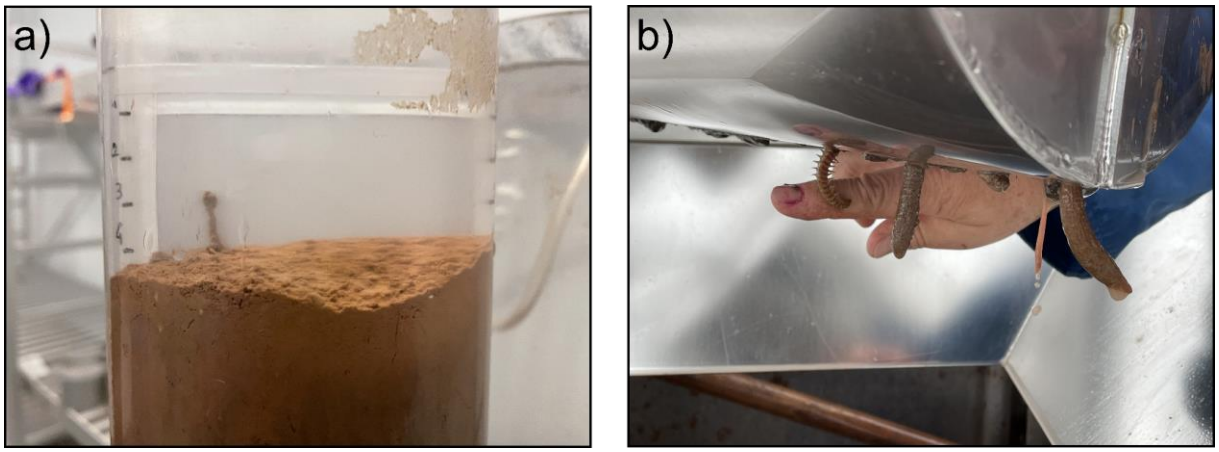

Figure 6: a) "jaw device" inserted in a sediment core from St.8 with the presence of a biological construction above the SWI on the side (2) of the sampling device. b) Macrofaunal individuals sampled with the day grab around St. 8.

St. 8 was located in a part of the fjord with higher densities of macrofauna (Wlodarska-Kowalczuk et al., 2005). Therefore, in this area, it is likely to observe fauna-induced features in the sediment structure (Fig. 6). In the [Mn_d] image, a vertical structure about 10 cm long with Mn_d depletion can be observed in the center of the probe (Fig. 3). The Fe_d image also showed a shorter vertical structure with Fe depletion around 2 cm depth and slight enrichment towards the SWI (localized at 3 cm gel width, Fig. 3). These depletions may be the result of bioirrigation induced by a ventilated burrow, bringing dissolved oxygen into deeper, anoxic levels (OPD of 8.5 ± 0.8 mm; ***Chapter 5***). Active movement of individuals can create such features in the sediment column (Braeckman et al., 2014; Meysman et al., 2010; Thibault de Chanvalon et al., 2015). Similar observations were made by other authors studying estuaries or coastal environments for dissolved Fe (Robertson et al., 2009; Stockdale et al., 2010; Thibault de Chanvalon et al., 2015) and for dissolved Mn (Choquel et al., 2021). This oxygen supply can induce diagenetic precipitation of oxides along burrow walls but also contributes to effluents of dissolved Mn and Fe into the water column (Choquel, 2021, Thibault de Chanvalon et al, 2017), as suggested by the concentrations of Mn (~15 µmol L^{-1}, Fig. 3) and Fe (~25 µmol L^{-1}, Fig. 3) in the putative burrows and the Fe plume feature observed near the SWI. The influence of this last identified burrow was also visible on the [P_d] image where a vertical enrichment in [P_d] was observed at the same location as the Fe_d depletion (at around 2 cm depth, Fig. 3). Deeper, a high enrichment in P_d was present between 3 and 4.5 cm depth, which could be partially induced by the release of phosphate previously adsorbed on Fe oxides undergoing dissolution (as this zone was also enriched in dissolved Fe) and contribute to a P_d release towards the water column via the putative burrow. An elongated structure was also observed between 7 to 11 cm depth on the left side of the images with high enrichments in Fe_d and P_d (Fig. 3) and could also be linked to an abandoned burrow where Fe oxide reduction was very efficient (Thibault de Chanvalon et al., 2015). Nitrate concentration map could also illustrate the small-scale heterogeneity in sediments with the presence of centimetric patches and also smaller nitrate-enriched spots in the anoxic part of sediment as already observed in estuarine sediments (Metzger et al., 2016), constituting potential microhabitats for meio- or microfauna such as denitrifying foraminifera. This high nitrate production could be sustained by oxygen supply of oxygen induced by burrow ventilation which enables ammonium oxidation, but it could also be the result of anaerobic oxidation of ammonium by Mn or Fe oxides (Hulth et al., 1999; Luther et al., 1997; Mortimer et al., 2004).

Finally, the study of Herbert et al. (2021) used 2D sensors to highlight Fe heterogeneity but they did not find clear evidence of bioirrigation. However, they hypothesized that if bioirrigation were to play a role in Kongsfjorden sediment, it would probably increase the Fe release into the water column (Elrod et al., 2004). Our data from St. 8 show strong evidence of bioirrigation influence, particularly with the Fe plume in the water column. A 2D modelling of the production/consumption of chemical species measured with 2D gel techniques and an estimate of fluxes based on this modelling (Thibault de Chanvalon et al., 2017) would undoubtedly allow to verify these hypotheses.

4.3 Potential effect of benthic macrofaunal activity on foraminiferal distribution

In our study, we deployed for the first time a 2D sampling method coupling 2D biogeochemical and foraminiferal analyses in Kongsfjorden environments. Using this sampling method, centimetric heterogeinity can be assessed in addition to the already demonstrated kilometric heterogeneity (Fossile et al., 2022; Herbert et al., 2022; Jernas et al., 2018; ***Chapter 5***; ***Chapter 6***) as a response to the forcing of environmental gradients generated by tidewater glacier melting and Atlantic water bodies intrusion into the fjord. The two studied stations were primarlily chosen according to their respective locations regarding the stressing parameters which are the terrigeneous sedimentation and the organic matter supply. As shown in the previous ***chapter 6*** with the study of the 1D cores, a abundant and diverse foraminiferal community was observed at the distal St. 8, with a deeper community distribution compared to St. 7, close to the tidal glacier front. With the 2D sampling, the effect of lateral heterogeneity in the distribution of microenvironments on benthic foraminiferal densities at both stations can be discussed.

A statistical analysis of foraminiferal distribution was investigated by calculating the Moran's Index (Thibault de Chanvalon et al., 2015) to estimate the size of potential niches (Fig. 7) in St. 8, which showed higher specific richness and densities down to 13 cm depth compared to St. 7 where this analysis was not applicable or even justifiable because of too low densities and resulting insignificant calculations. However, as more than 75% of the whole assemblage was found in the uppermost 4 cm in St. 8, we decided to constrain the Moran's I calculation to these levels to limit the influence of the vertical distribution of fauna on the statistical analysis. Indeed, an additional Moran's I calculation on levels below 4 cm depth revealed a totally random distribution of fauna (not shown here) because of too low abundances. In this way, the characteristic sizes of foraminiferal niches were assessed for the total foraminiferal fauna (total densities counted in each sample displayed in Fig. 5a) and for the major species *Adercotryma glomeratum* (relative abundance of 37%), *Globobulimina auriculata* (8%) and *Nonionellina labradorica* (25%) (densities shown in supplementary material). The total assemblage revealed a significant patchiness of 1 cm wide niches only (Fig. 7). This distribution seems to be driven by the major species *A. glomeratum* and *N. labradorica*, whose Moran analysis showed the same result (Fig. 7). On larger spatial scales, the Moran's index tends towards 0 describing a random distribution and does not show significant results. A similar analysis by Thibault de Chanvalon et al. (2015) revealed that the small centimetric niches of *Ammonia tepida* in a Loire river mudflat did not match with lateral distribution of dissolved iron features. Similarly to our results, they evidenced biologically induced burrows and bioirrigation highlighted by dissolved

iron distribution. According to foraminiferal distribution models (Jorissen et al., 1995; Langezaal et al., 2006; Langlet et al., 2014; Van der Zwaan et al., 1999), we expect individuals to be distributed in accordance to microhabitat distribution here affected by bioirrigation and potentially deeper dissolved oxygen supply. Therefore, it is most likely that small 1-2 cm wide niches of foraminifera individuals respond to microenvironments generated by the uneven distribution of organic matter caused by heterogeneous export and deposit (organism decay, fecal pellets) and biomixing.

Finally, a further effect of foraminiferal metabolisms may locally affect biogeochemical patterns. Indeed, some species such as *N. labradorica* might be able to alternate between oxic respiration and denitrification as is was demonstrated for two species of the foraminiferal genus *Nonionellina* (Choquel et al., 2021; Risgaard-Petersen et al., 2006; Schmidt et al., 2022). Nitrate spots shown in Fig. 3 (NO_3^-) may be beneficent microhabitats for these species.

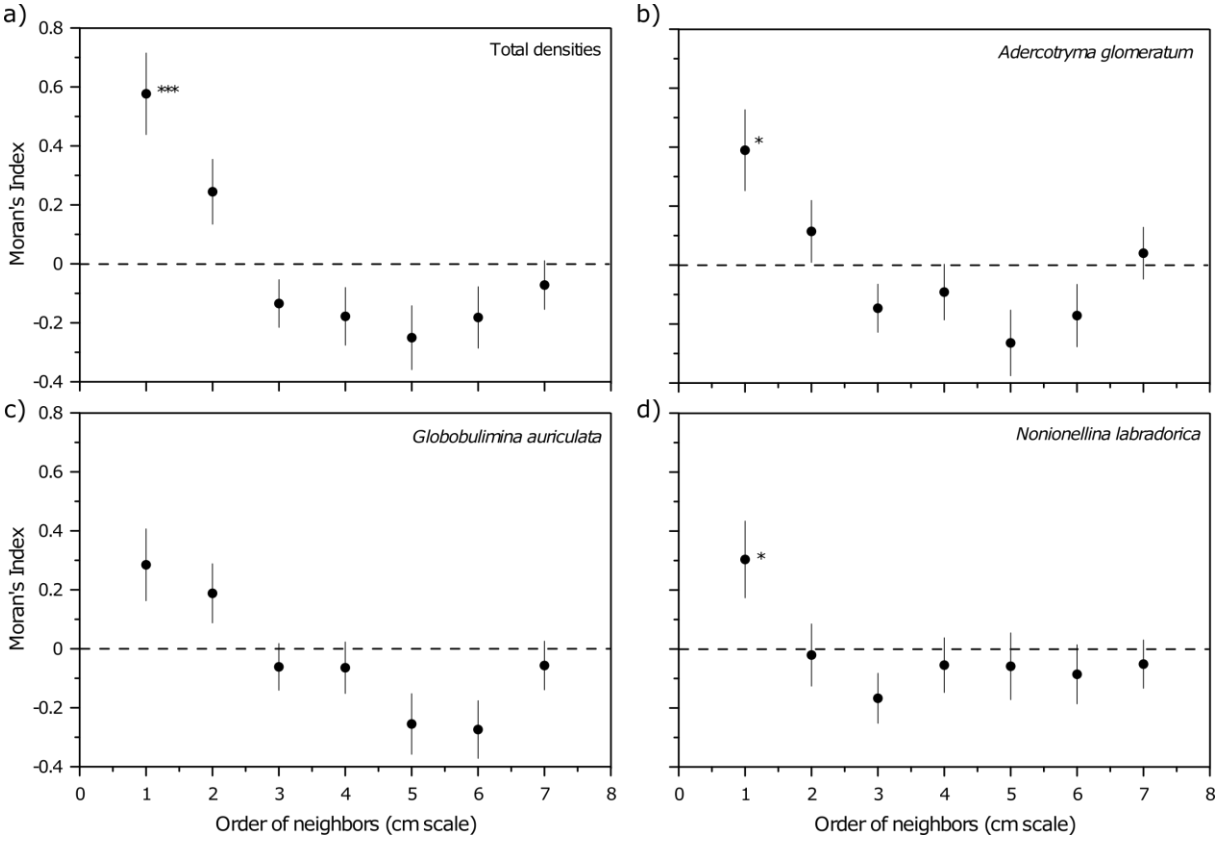

Figure 7: Moran's index correlograms for living foraminiferal densities sampled between 0 and 4 cm depth at St. 8. Moran's Index was calculated for a) total foraminiferal densities, b) *Adercotryma glomeratum*, c) *Globobulimina auriculata* and d) *Nonionellina labradorica*. Error bars correspond to the standard deviation. Asterisks next to points correspond to significance of the Moran's Index value (p-value : ***<0.0001, **<0.001, *<0.01).

5 Conclusion

The application of the 2D sediment sampling method in two contrasted areas of Kongsfjorden, subjected to different sediment discharge from the Kronebreen glacier, revealed a small-scale effect of the kilometric gradient of sediment stability on microhabitat distribution. The additional observations provided by the 2D foraminiferal and biogeochemical sampling technics reinforce the knowledge brought by vertical core slicing process.

As observed near the glacier front, where bioreworking is much less intense (no bioturbation features) due to fewer bioturbating organisms, the chemical heterogeneity could be explained by glacial sedimentation-derived burial of previous SWIs where heterogeneous decay of centimeter-sized fauna occurred and resulted in remineralization spots. Following the results from ***Chapter 5***, such spots can also occur within the freshly deposited sediment layer. These spots result from localized accumulations of labile organic matter that are remineralised through anaerobic pathways increasing the concentration of nitrate, dissolved manganese, iron and phosphates that create attractive microniches. 2D sampling of benthic foraminifera was revealed to be irrelevant for this area as the main species *Capsammina bowmanni* was absent in samples while being dominant in 1D cores (***Chapter 6***). It may express a high patchiness of this species that can be properly sampled with regular coring devices such as used in the previous chapters. By this way, the potential effect of microhabitat small-scale distribution on foraminiferal densities could not be assessed in the inner basin.

Ten kilometres away from Kronebreen glacier front submitted to less glacial sedimentation, active burrows, highlighted by sediment spots and features depleted in dissolved manganese and iron, may structure the biophysical architecture of the benthic ecosystem (spatial distribution of biotope and associated biocenose). The 2D method is adequate to sample benthic foraminifera in the distal station as the diversity and densities were similar to 1D cores. Further analysis of their distribution in the sediment slab showed a small centimetric patchiness of the main species distribution that cannot be attributed to burrow patterns being larger but most likely to heterogeneous deposits of organic matter, generating attractive microenvironments.

The high-resolution concentration mapping of the different chemical species would further be useful in recently developed numerical modelling of fluxes through SWI and dissolved species production rates. These calculations, able to take into account the implication of bioturbation and bioirrigation in interface processes, will quantify the biogeochemical fluxes that we deduced from our observations and measurements.

References:

Bennett, W. W., Welsh, D. T., Serriere, A., Panther, J. G., and Teasdale, P. R.: A colorimetric DET technique for the high-resolution measurement of two-dimensional alkalinity distributions in sediment porewaters, Chemosphere, 119, 547–552, https://doi.org/10.1016/j.chemosphere.2014.07.042, 2015.

Bouchet, V. M. P., Sauriau, P.-G., Debenay, J.-P., Mermillod-Blondin, F., Schmidt, S., Amiard, J.-C., and Dupas, B.: Influence of the mode of macrofauna-mediated bioturbation on the vertical distribution of living benthic foraminifera: First insight from axial tomodensitometry, Journal of Experimental Marine Biology and Ecology, 371, 20–33, https://doi.org/10.1016/j.jembe.2008.12.012, 2009.

Braeckman, U., Provoost, P., Gribsholt, B., Gansbeke, D. V., Middelburg, J. J., Soetaert, K., Vincx, M., and Vanaverbeke, J.: Role of macrofauna functional traits and density in biogeochemical fluxes and bioturbation, Marine Ecology Progress Series, 399, 173–186, https://doi.org/10.3354/meps08336, 2010.

Braeckman, U., Foshtomi, M. Y., Van Gansbeke, D., Meysman, F., Soetaert, K., Vincx, M., and Vanaverbeke, J.: Variable Importance of Macrofaunal Functional Biodiversity for Biogeochemical Cycling in Temperate Coastal Sediments, Ecosystems, 17, 720–737, https://doi.org/10.1007/s10021-014-9755-7, 2014.

Buzas, M. A.: Foraminifera from the Hadley Harbor Complex, Massachusetts, 1968.

Cesbron, F., Metzger, E., Launeau, P., Deflandre, B., Delgard, M.-L., Thibault de Chanvalon, A., Geslin, E., Anschutz, P., and Jézéquel, D.: Simultaneous 2D Imaging of Dissolved Iron and Reactive Phosphorus in Sediment Porewaters by Thin-Film and Hyperspectral Methods, Environ. Sci. Technol., 48, 2816–2826, https://doi.org/10.1021/es404724r, 2014.

Choquel, C., Geslin, E., Metzger, E., Filipsson, H. L., Risgaard-Petersen, N., Launeau, P., Giraud, M., Jauffrais, T., Jesus, B., and Mouret, A.: Denitrification by benthic foraminifera and their contribution to N-loss from a fjord environment, Biogeosciences, 18, 327–341, https://doi.org/10.5194/bg-18-327-2021, 2021.

Cottier, F., Tverberg, V., Inall, M., Svendsen, H., Nilsen, F., and Griffiths, C.: Water mass modification in an Arctic fjord through cross-shelf exchange: The seasonal hydrography of Kongsfjorden, Svalbard, J. Geophys. Res., 110, C12005, https://doi.org/10.1029/2004JC002757, 2005.

Dallmann, W. K.: Geoscience Atlas of Svalbard, 2015.

Elrod, V. A., Berelson, W. M., Coale, K. H., and Johnson, K. S.: The flux of iron from continental shelf sediments: A missing source for global budgets, Geophysical Research Letters, 31, https://doi.org/10.1029/2004GL020216, 2004.

Fossile, E., Nardelli, M. P., Howa, H., Baltzer, A., Poprawski, Y., Baneschi, I., Doveri, M., and Mojtahid, M.: Influence of modern environmental gradients on foraminiferal faunas in the inner Kongsfjorden (Svalbard), Marine Micropaleontology, 173, 102117, https://doi.org/10.1016/j.marmicro.2022.102117, 2022.

García-Robledo, E., Corzo, A., and Papaspyrou, S.: A fast and direct spectrophotometric method for the sequential determination of nitrate and nitrite at low concentrations in small volumes, Marine Chemistry, 162, 30–36, https://doi.org/10.1016/j.marchem.2014.03.002, 2014.

Griess, P.: Bemerkungen zu der Abhandlung der HH. Weselsky und Benedikt „Ueber einige Azoverbindungen", Ber. Dtsch. Chem. Ges., 12, 426–428, https://doi.org/10.1002/cber.187901201117, 1879.

Herbert, L. C., Zhu, Q., Michaud, A. B., Laufer-Meiser, K., Jones, C. K., Riedinger, N., Stooksbury, Z. S., Aller, R. C., Jørgensen, B. B., and Wehrmann, L. M.: Benthic iron flux influenced by climate-sensitive interplay between organic carbon availability and sedimentation rate in Arctic fjords, Limnol Oceanogr, 66, 3374–3392, https://doi.org/10.1002/lno.11885, 2021.

Herbert, L. C., Michaud, A. B., Laufer-Meiser, K., Hoppe, C. J. M., Zhu, Q., Aller, R. C., Jørgensen, B. B., and Wehrmann, L. M.: Tight benthic-pelagic coupling drives seasonal and interannual changes in iron-sulfur cycling in Arctic fjord sediments (Kongsfjorden, Svalbard), Journal of Marine Systems, 225, 103645, https://doi.org/10.1016/j.jmarsys.2021.103645, 2022.

Hop, H. and Wiencke, C. (Eds.): The Ecosystem of Kongsfjorden, Svalbard, Springer International Publishing, Cham, https://doi.org/10.1007/978-3-319-46425-1, 2019.

Hop, H., Falk-Petersen, S., Svendsen, H., Kwasniewski, S., Pavlov, V., Pavlova, O., and Søreide, J. E.: Physical and biological characteristics of the pelagic system across Fram Strait to Kongsfjorden, Progress in Oceanography, 71, 182–231, https://doi.org/10.1016/j.pocean.2006.09.007, 2006.

Howe, J. A., Austin, W. E. N., Forwick, M., Paetzel, M., Harland, R., and Cage, A. G.: Fjord systems and archives: a review, SP, 344, 5–15, https://doi.org/10.1144/SP344.2, 2010.

Hulth, S., Aller, R. C., and Gilbert, F.: Coupled anoxic nitrification/manganese reduction in marine sediments, Geochimica et Cosmochimica Acta, 63, 49–66, https://doi.org/10.1016/S0016-7037(98)00285-3, 1999.

Jernas, P., Klitgaard-Kristensen, D., Husum, K., Koç, N., Tverberg, V., Loubere, P., Prins, M., Dijkstra, N., and Gluchowska, M.: Annual changes in Arctic fjord environment and modern benthic foraminiferal fauna: Evidence from Kongsfjorden, Svalbard, Global and Planetary Change, 163, 119–140, https://doi.org/10.1016/j.gloplacha.2017.11.013, 2018.

Jézéquel, D., Brayner, R., Metzger, E., Viollier, E., Prévot, F., and Fiévet, F.: Two-dimensional determination of dissolved iron and sulfur species in marine sediment pore-waters by thin-film based imaging. Thau lagoon (France), Estuarine, Coastal and Shelf Science, 72, 420–431, https://doi.org/10.1016/j.ecss.2006.11.031, 2007.

Jorissen, F. J., de Stigter, H. C., and Widmark, J. G. V.: A conceptual model explaining benthic foraminiferal microhabitats, Marine Micropaleontology, 26, 3–15, https://doi.org/10.1016/0377-8398(95)00047-X, 1995.

Kankanamge, N. R., Bennett, W. W., Teasdale, P. R., Huang, J., and Welsh, D. T.: A new colorimetric DET technique for determining mm-resolution sulfide porewater distributions and allowing improved interpretation of iron(II) co-distributions, Chemosphere, 244, 125388, https://doi.org/10.1016/j.chemosphere.2019.125388, 2020.

Kędra, M., Legeżyńska, J., and Walkusz, W.: Shallow winter and summer macrofauna in a high Arctic fjord (79° N, Spitsbergen), Mar Biodiv, 41, 425–439, https://doi.org/10.1007/s12526-010-0066-8, 2011.

Koller, H., Dworschak, P. C., and Abed-Navandi, D.: Burrows of Pestarella tyrrhena (Decapoda: Thalassinidea): hot spots for Nematoda, Foraminifera and bacterial densities, Journal of the Marine Biological Association of the United Kingdom, 86, 1113–1122, https://doi.org/10.1017/S0025315406014093, 2006.

Langezaal, A. M., Jorissen, F. J., Braun, B., Chaillou, G., Fontanier, C., Anschutz, P., and van der Zwaan, G. J.: The influence of seasonal processes on geochemical profiles and foraminiferal assemblages on the outer shelf of the Bay of Biscay, Continental Shelf Research, 26, 1730–1755, https://doi.org/10.1016/j.csr.2006.05.005, 2006.

Langlet, D., Baal, C., Geslin, E., Metzger, E., Zuschin, M., Riedel, B., Risgaard-Petersen, N., Stachowitsch, M., and Jorissen, F. J.: Foraminiferal species responses to in situ, experimentally induced anoxia in the Adriatic Sea, Biogeosciences, 11, 1775–1797, https://doi.org/10.5194/bg-11-1775-2014, 2014.

Luther, G. W., Sundby, B., Lewis, B. L., Brendel, P. J., and Silverberg, N.: Interactions of manganese with the nitrogen cycle: Alternative pathways to dinitrogen, Geochimica et Cosmochimica Acta, 61, 4043–4052, https://doi.org/10.1016/S0016-7037(97)00239-1, 1997.

Lydersen, C., Assmy, P., Falk-Petersen, S., Kohler, J., Kovacs, K. M., Reigstad, M., Steen, H., Strøm, H., Sundfjord, A., Varpe, Ø., Walczowski, W., Weslawski, J. M., and Zajaczkowski, M.: The importance of tidewater glaciers for marine mammals and seabirds in Svalbard, Norway, Journal of Marine Systems, 129, 452–471, https://doi.org/10.1016/j.jmarsys.2013.09.006, 2014.

Madison, A. S., Tebo, B. M., Mucci, A., Sundby, B., and Luther, G. W.: Abundant Porewater Mn(III) Is a Major Component of the Sedimentary Redox System, Science, 341, 875–878, https://doi.org/10.1126/science.1241396, 2013.

Meslard, F., Bourrin, F., Many, G., and Kerhervé, P.: Suspended particle dynamics and fluxes in an Arctic fjord (Kongsfjorden, Svalbard), Estuarine, Coastal and Shelf Science, 204, 212–224, https://doi.org/10.1016/j.ecss.2018.02.020, 2018.

Metzger, E., Thibault de Chanvalon, A., Cesbron, F., Barbe, A., Launeau, P., Jézéquel, D., and Mouret, A.: Simultaneous Nitrite/Nitrate Imagery at Millimeter Scale through the Water–Sediment Interface, Environ. Sci. Technol., 50, 8188–8195, https://doi.org/10.1021/acs.est.6b00187, 2016.

Metzger, E., Barbe, A., Cesbron, F., Thibault de Chanvalon, A., Jauffrais, T., Jézéquel, D., and Mouret, A.: Two-dimensional ammonium distribution in sediment pore waters using a new colorimetric diffusive equilibration in thin-film technique, Water Research X, 2, 100023, https://doi.org/10.1016/j.wroa.2018.100023, 2019.

Meysman, F. J. R., Galaktionov, O. S., Glud, R. N., and Middelburg, J. J.: Oxygen penetration around burrows and roots in aquatic sediments, J Mar Res, 68, 309–336, https://doi.org/10.1357/002224010793721406, 2010.

Mortimer, R., Harris, S., Krom, M., Freitag, T., Prosser, J., Barnes, J., Anschutz, P., Hayes, P., and Davies, I.: Anoxic nitrification in marine sediments, Mar. Ecol. Prog. Ser., 276, 37–52, https://doi.org/10.3354/meps276037, 2004.

Pagès, A., Teasdale, P. R., Robertson, D., Bennett, W. W., Schäfer, J., and Welsh, D. T.: Representative measurement of two-dimensional reactive phosphate distributions and co-distributed iron(II) and sulfide in

seagrass sediment porewaters, Chemosphere, 85, 1256–1261, https://doi.org/10.1016/j.chemosphere.2011.07.020, 2011.

Payne, C. M. and Roesler, C. S.: Characterizing the influence of Atlantic water intrusion on water mass formation and phytoplankton distribution in Kongsfjorden, Svalbard, Continental Shelf Research, 191, 104005, https://doi.org/10.1016/j.csr.2019.104005, 2019.

Petrowski, S., Molis, M., Schachtl, K., and Buschbaum, C.: Do bioturbation and consumption affect coastal Arctic marine soft-bottom communities? Polar Biol, 39, 2141–2153, https://doi.org/10.1007/s00300-015-1654-7, 2016.

Risgaard-Petersen, N., Langezaal, A. M., Ingvardsen, S., Schmid, M. C., Jetten, M. S. M., Op den Camp, H. J. M., Derksen, J. W. M., Piña-Ochoa, E., Eriksson, S. P., Nielsen, L. P., Revsbech, N. P., Cedhagen, T., and van der Zwaan, G. J.: Evidence for complete denitrification in a benthic foraminifer, Nature, 443, 93–96, https://doi.org/10.1038/nature05070, 2006.

Robertson, D., Welsh, D. T., and Teasdale, P. R.: Investigating biogenic heterogeneity in coastal sediments with two-dimensional measurements of iron(II) and sulfide, Environ. Chem., 6, 60, https://doi.org/10.1071/EN08059, 2009.

Schmidt, C., Geslin, E., Bernhard, J. M., LeKieffre, C., Svenning, M. M., Roberge, H., Schweizer, M., and Panieri, G.: Deposit-feeding of *Nonionellina labradorica* (foraminifera) from an Arctic methane seep site and possible association with a methanotroph, Biogeosciences, 19, 3897–3909, https://doi.org/10.5194/bg-19-3897-2022, 2022.

Schönfeld, J., Alve, E., Geslin, E., Jorissen, F., Korsun, S., and Spezzaferri, S.: The FOBIMO (FOraminiferal BIo-MOnitoring) initiative—Towards a standardised protocol for soft-bottom benthic foraminiferal monitoring studies, Marine Micropaleontology, 94–95, 1–13, https://doi.org/10.1016/j.marmicro.2012.06.001, 2012.

Stockdale, A., Davison, W., and Zhang, H.: Formation of iron sulfide at faecal pellets and other microniches within suboxic surface sediment, Geochimica et Cosmochimica Acta, 74, 2665–2676, https://doi.org/10.1016/j.gca.2010.02.005, 2010.

Svendsen, H., Beszczynska-Møller, A., Hagen, J. O., Lefauconnier, B., Tverberg, V., Gerland, S., Børre Ørbæk, J., Bischof, K., Papucci, C., Zajaczkowski, M., Azzolini, R., Bruland, O., and Wiencke, C.: The physical environment of Kongsfjorden–Krossfjorden, an Arctic fjord system in Svalbard, Polar Research, 21, 133–166, https://doi.org/10.3402/polar.v21i1.6479, 2002.

Thibault de Chanvalon, A., Metzger, E., Mouret, A., Cesbron, F., Knoery, J., Rozuel, E., Launeau, P., Nardelli, M. P., Jorissen, F. J., and Geslin, E.: Two-dimensional distribution of living benthic foraminifera in anoxic sediment layers of an estuarine mudflat (Loire estuary, France), Biogeosciences, 12, 6219–6234, https://doi.org/10.5194/bg-12-6219-2015, 2015.

Thibault de Chanvalon, A., Metzger, E., Mouret, A., Knoery, J., Geslin, E., and Meysman, F. J. R.: Two-dimensional mapping of iron release in marine sediments at submillimetre scale, Marine Chemistry, 191, 34–49, https://doi.org/10.1016/j.marchem.2016.04.003, 2017.

Van der Zwaan, G. J., Duijnstee, I. A. P., den Dulk, M., Ernst, S. R., Jannink, N. T., and Kouwenhoven, T. J.: Benthic foraminifers: proxies or problems? Earth-Science Reviews, 46, 213–236, https://doi.org/10.1016/S0012-8252(99)00011-2, 1999.

Wlodarska-Kowalczuk, M. and Pearson, T. H.: Soft-bottom macrobenthic faunal associations and factors affecting species distributions in an Arctic glacial fjord (Kongsfjord, Spitsbergen), Polar Biol, 27, 155–167, https://doi.org/10.1007/s00300-003-0568-y, 2004.

Wlodarska-Kowalczuk, M., Pearson, T., and Kendall, M.: Benthic response to chronic natural physical disturbance by glacial sedimentation in an Arctic fjord, Mar. Ecol. Prog. Ser., 303, 31–41, https://doi.org/10.3354/meps303031, 2005.

Chapter 7: Two-dimensional foraminiferal sedimentary microhabitat distribution in two contrasted stations in Kongsfjorden (Svalbard)

Włodarska-Kowalczuk, M., Pawłowska, J., and Zajączkowski, M.: Do foraminifera mirror diversity and distribution patterns of macrobenthic fauna in an Arctic glacial fjord? Marine Micropaleontology, 103, 30–39, https://doi.org/10.1016/j.marmicro.2013.07.002, 2013.

Włodarska-Kowalczuk, M., Górska, B., Deja, K., and Morata, N.: Do benthic meiofaunal and macrofaunal communities respond to seasonality in pelagial processes in an Arctic fjord (Kongsfjorden, Spitsbergen)? Polar Biol, 39, 2115–2129, https://doi.org/10.1007/s00300-016-1982-2, 2016.

Supplementary material 1: Distribution grid of the three main species in St. 8 (ind. cm^{-3}). Vertical scale is in centimetre.

Globobulimina auriculata

0.5	1	1	1	0	1	0	0	0
1.5	1	3	9	1	2	1	1	1
2.5	3	5	3	6	3	3	0	0
3.5	2	1	3	1	0	0	0	0
4.5	0	0	0	0	0	0	0	0
5.5	0	0	0	0	0	0	0	0
6.5	0	0	0	0	0	0	0	0
7.5	0	0	0	0	0	0	0	0
8.5	0	0	0	0	0	0	0	0
9.5	0	0	0	0	0	0	0	0
10.5	0	0	0	0	0	0	0	0
11.5	0	0	0	0	0	0	0	0
12.5	0	0	0	0	0	0	0	0
	A	B	C	D	E	F	G	H

Nonionellina labradorica

0.5	0	2	3	3	4	5	7	3
1.5	6	11	10	13	10	9	7	1
2.5	1	3	3	3	4	5	11	5
3.5	3	3	1	0	1	1	1	0
4.5	1	0	1	0	0	0	0	1
5.5	0	1	0	0	0	0	0	1
6.5	1	0	0	0	0	0	0	0
7.5	0	0	0	0	0	0	0	0
8.5	0	0	0	0	0	0	0	0
9.5	0	0	0	0	0	0	0	0
10.5	0	0	0	0	0	0	0	0
11.5	0	0	0	0	0	0	0	0
12.5	0	0	0	0	0	0	0	0
	A	B	C	D	E	F	G	H

Adercotryma glomeratum

0.5	8	11	7	7	8	5	5	7
1.5	5	12	18	11	7	14	3	3
2.5	5	4	10	6	15	9	0	2
3.5	2	3	5	3	7	5	2	1
4.5	4	3	2	5	2	3	5	1
5.5	0	5	2	3	4	3	3	0
6.5	1	1	1	1	0	8	2	0
7.5	1	3	3	1	0	1	1	1
8.5	1	2	0	0	1	4	5	1
9.5	4	1	4	4	4	3	2	7
10.5	0	2	0	2	1	2	1	1
11.5	0	1	0	2	2	0	1	0
12.5	0	3	1	1	1	1	1	0
	A	B	C	D	E	F	G	H

Synthèse et perspectives

Préambule

L'objectif principal de ce travail de thèse était de comprendre les effets d'intenses sédimentations (sans érosion) sur les communautés de foraminifères benthiques ainsi que sur la biogéochimie du sédiment dans le Kongsfjord (Svalbard). Pour cela, les processus associés aux états transitoires de l'écosystème ont été étudiés par le biais expérimental, en microcosme, puis ces connaissances ont été utilisées pour comprendre l'environnement naturel du Kongsfjorden avec des échantillonnages dans le fjord en Mai et Août 2021. La complémentarité entre ces deux approches a permis de mettre en lumière des comportements biologiques et des dynamiques biogéochimiques exclusivement liés à l'enfouissement durant une période de décantation importante de matériel terrigène d'origine glaciaire. L'étude expérimentale a permis de définir des zonations ou des stades de résilience des écosystèmes benthiques en fonction de leur état biogéochimique transitoire et au contenu et distribution des foraminifères benthiques dans le sédiment liées à la distance au front du glacier tidal Kronebreen générant un gradient estival de turbidité et de sédimentation.

Le but de cette synthèse est de retranscrire les résultats majeurs de ce travail de thèse et lier les différents chapitres entre eux dans une approche holistique et logique.

1 Effets de dépôts de sédiment sur la stabilité biogéochimique du sédiment.

Dans la nature, il a déjà été observé que l'érosion, le transport et le dépôt sédimentaire perturbent la stabilité des gradients redox dans le sédiment (e.g. Anschutz et al., 2002; Deflandre et al., 2002; Hulot et al., 2023). Les états biogéochimiques transitoires liés à ces processus ont été décrits dans des environnements variés tels que des fleuves (Cathalot et al., 2010; Pastor et al., 2018), des canyons sous-marins (Anschutz et al., 2002) ou encore des fjords sujets à des transports de masse (Deflandre et al., 2002) ou à une sédimentation intense (Herbert et al., 2020, 2022). Néanmoins, ces études environnementales manquent parfois de résolution temporelle et spatiale pour contraindre les processus de résilience biogéochimique car les échantillonnages dans de tels environnements sont uniques ou peu fréquents. Le besoin de comprendre avec une bonne échelle spatiale et temporelle les stades de transition vers un nouvel état stable de systèmes biogéochimiques vis à vis de la sédimentation seule variant en fréquence et intensité peut être assouvi par une approche expérimentale.

L'observation d'une intense sédimentation en été dans le Kongsfjord (Svalbard) ayant pour source l'érosion de l'encaissant puis l'écoulement sous-glaciaire provenant du glacier tidal Kronebreen (D'Angelo et al., 2018; Lydersen et al., 2014; Meslard et al., 2018; Trusel et al., 2010) a soulevé l'hypothèse d'un gradient de stabilité du substrat benthique au sein du fjord sur une échelle kilométrique. Un impact de ce gradient de turbidité/sédimentation sur les équilibres redox dans le sédiment a déjà été documenté par plusieurs études (Herbert et al., 2021, 2022; Laufer-Meiser et al., 2021; Michaud, 2020; Wehrmann et al., 2014), toutes apportant des éléments dans la compréhension de la nature des dépôts et des différents cycles diagenétiques et processus intervenant dans la reminéralisation de la matière organique. Les différentes dynamiques biogéochimiques à l'échelle kilométrique dans le fjord déterminent/délimitent des zones plus ou moins stressées potentiellement sujettes à des dépôts massifs de sédiments et à des variations d'apport en matière organique.

De nombreux forçages environnementaux peuvent affecter la biogéochimie benthique dans un fjord tels que la sédimentation détritique qui est l'objet de notre travail, ou encore les gradients de productivité primaire (Lalande et al., 2016), la distribution des faunes benthiques (Fossile et al., 2022; Hop and Wiencke, 2019; Wlodarska-Kowalczuk et al., 2005) ou la répartition des masses d'eau (Cottier et al., 2005; Payne and Roesler, 2019; Svendsen et al., 2002). Afin de documenter l'effet de la sédimentation seule sur la biogéochimie du sédiment dans le Kongsfjord, les processus associés à la transition des gradients redox ont dans un premier temps été étudiés par une expérimentation en microcosme ***Chapitre 3*** (setup présenté par Guilhermic et al. (2023)). L'utilisation de sédiments provenant d'une vasière intertidale de la côte Atlantique française nous a permis de mieux contraindre dans le temps l'état transitoire du système grâce à une plus grande concentration de matière organique ainsi que de plus hautes températures catalysant les activités microbiennes de reminéralisation comparées aux conditions polaires du Kongsfjorden (Froelich et al., 1979). Deux modalités de sédimentation ont été testées variant en intensité et fréquence, avec d'un côté un microcosme « One-time high volume » recevant un seul dépôt de sédiment (environ 2.7 cm après compaction) et d'un autre coté un microcosme appelé « Frequent low volume » qui a reçu 4 dépôts hebdomadaires de sédiment de plus faible épaisseur (entre 0.1 et 0.5 cm). Avec des méthodes d'analyse à haute résolution spatiale, les réponses des différents gradients redox de la diagenèse précoce ont pu être investiguées chaque semaine. Les états transitoires de l'oxygène dissous, des composés azotés, du cycle du manganèse et du fer ainsi que des sulfates ont donc été documentés dans le ***chapitre 3***. L'impact de la sédimentation sur l'oxygène dissous dans le sédiment a été significatif dans le « One-time high volume » (OHV) avec une diffusion depuis la colonne d'eau immédiate après l'ajout du dépôt mais comprenant une période de 3 semaines pour se rééquilibrer à hauteur de conditions « contrôle ». Ce retard de rétablissement peut être imputé à la migration de la faune respirant de l'oxygène qui a pris plus de temps dans le dépôt plus épais (***Chapitre 2***). Un état transitoire relativement court a ensuite été observé dans le microcosme OHV concernant la distribution des nitrites et de l'ammonium dans le sédiment. Un profil stationnaire de ces deux espèces azotées comprend une diminution de concentration entre la colonne d'eau et les premiers centimètres de sédiment indiquant une dénitrification et l'utilisation des nitrates, nitrites comme accepteur d'électrons de la reminéralisation anaérobie de la matière organique par les bactéries. L'effet des dépôts de sédiment est peu perceptible dans le microcosme « Frequent-low volume » (FLV) alors qu'un arrêt conséquent de la dénitrification dans le sédiment et de la production d'ammonium sont observés dans le OHV. Le court temps de 18h écoulé entre la perturbation et l'échantillonnage n'a pas permis le rééquilibrage des gradients de dénitrification et d'enrichissement en ammonium dans le nouveau dépôt du OHV. Néanmoins, une distribution stable de ces gradients a été observée la semaine suivante dans le dépôt récent.

Les cycles du manganèse et du fer ont présenté une réponse différente des précédents gradients redox dans les 2 microcosmes perturbés. Contrairement aux précédentes espèces traitées ici, le manganèse et le fer sont présents sous deux formes, particulaires et dissoutes, dans le sédiment (Burdige, 2007; Froelich et al., 1979). Une séquence stable de leur cycle serait représentée par un enrichissement en oxydes réactifs de Mn et Fe sous la SWI (sediment-water interface) lorsque le milieu est oxique (Burdige, 2007). Cette phase d'oxydes réactifs, qui est utilisée par les bactéries comme accepteurs d'électrons lors de la reminéralisation anaérobie de la matière organique, peut avoir une origine par dépôt depuis la colonne d'eau ou par précipitation du flux diffusif des phases dissoutes depuis des niveaux de production plus

profonds vers la surface. Dans les niveaux anoxiques, ces excès en oxydes sont réduits par voie bactérienne en Mn et Fe dissous diffusant autour des niveaux de production y compris vers la surface. L'état transitoire mis en lumière dans les deux modalités de dépôts OHV et FLV montre une dynamique de rétablissement non synchronisée entre le cycle du manganèse et celui du fer (***Chapitre 3***). En effet, l'enfouissement des précédentes interfaces (SWI) enrichies en oxydes réactifs a mené à une production de Mn dissous sur ces mêmes niveaux quelques heures après les dépôts. La réduction des oxydes de manganèse, qui présente un meilleur rendement que la réduction des oxydes de fer pour les métabolismes bactériens, est donc privilégiée sur ces niveaux. La semaine suivante, quand la réduction des oxydes de manganèse est moins intense, la réduction des oxydes de Fe intervient sur ce même niveau enrichi en oxydes. La diffusion de ces espèces dissoutes vers la nouvelle surface entraine une précipitation d'oxydes diagenétiques dans la nouvelle couche oxique. Lorsque l'enrichissement se stabilise alors le nouvel état stationnaire est atteint. Néanmoins dans la modalité FLV dans laquelle le dépôt est peu épais et répété une fois par semaine, l'état stable n'est jamais atteint au cours de l'expérience et l'écart spatial entre la zone de production de Mn et Fe dissous s'agrandit car le cycle du manganèse peut s'effectuer entièrement en une semaine à l'inverse de celui du fer. En effet, l'alternance des dynamiques oxiques/anoxiques des SWI successives permet la précipitation des oxydes réactifs de manganèse chaque semaine mais pas celle des oxydes de fer. Le déphasage de précipitation des oxydes est donc également bien observé dans cette modalité FLV.

2 Indicateurs d'enfouissement sédimentaire dans le Kongsfjord

L'approche expérimentale nous a permis de définir la réponse des gradients redox à des épisodes de sédimentation variant en fréquence et en intensité. Parmi ces réponses, l'état transitoire du cycle du manganèse et du fer permettent d'identifier des interfaces eau-sédiment antérieures ensevelies après des périodes de sédimentation induisant l'enfouissement de niveaux riches en oxydes biodisponibles. La production de manganèse additionnée à celle du fer sur ce niveau, résultant en un excès d'oxydes réactifs biodisponibles, marque une précédente couche oxygénée de surface (***Chapitre 3***).

Il a été précédemment documenté puis observé par des mesures de turbidité que le Kongsfjord était sujet à un relargage conséquent de sédiment par le glacier tidal Kronebreen en saison estivale (Calleja et al., 2017; D'Angelo et al., 2018; Dallmann, 2015; Hodgkins et al., 2003; Lydersen et al., 2014; Meslard et al., 2018; Trusel et al., 2010; Zajączkowski, 2008). Les particules issues de l'érosion des roches surtout carbonatées et marneuses du bassin versant sont donc transportées par les rivières sous-glaciaires pendant les périodes de fonte et se déposent dans le fjord avec un taux de sédimentation pouvant dépasser 10 cm an^{-1} essentiellement concentré pendant les périodes estivales, dans les zones les plus proximales du front du glacier (Lydersen et al., 2014; Meslard et al., 2018; Trusel et al., 2010). Cette intense sédimentation de particules impacte la stabilité physique et chimique des habitats benthiques (Fossile et al., 2022; Hop and Wiencke, 2019; Włodarska-Kowalczuk et al., 2013). De plus, cette charge sédimentaire fine d'origine glaciaire provoque une forte turbidité au front du glacier qui inhibe la productivité primaire marine empêchant la photosynthèse et donc le développement phytoplanctonique dans cette zone proximale. En s'éloignant du front glaciaire, la diminution de la sédimentation terrigène glaciaire est associée au gradient décroissant de turbidité qui s'installe vers le fjord aval (Calleja et al., 2017; Hegseth et al., 2019; Hodal et al., 2012)

(***Chapitre 4***). Antagoniste à ce gradient sédimentaire, un gradient croissant vers l'aval de production phytoplanctonique, et sa conséquence en terme d'export de matière organique labile, s'installe également en période estivale (Lalande et al., 2016).

Les différentes mesures biogéochimiques des cycles du manganèse et du fer dans la zone proximale du front du glacier ont donc permis d'attester de plusieurs états transitoires dans le fjord sur une distance de 10 km au front du glacier. Ces cycles montrent une réponse plus claire à la dynamique des gradients de turbidité/matière organique labile, que les cycles de l'oxygène ou de l'azote réagissant plus rapidement aux perturbations (***Chapitre 3*** et ***5***). La présence d'un niveau montrant à la fois un enrichissement en oxydes réactifs de Mn et Fe ainsi qu'une production de manganèse dissous atteste de la pertinence du modèle expérimental développé précédemment (***Chapitre 3***). De plus, avec l'éloignement au glacier la profondeur dans le sédiment de ce niveau d'enrichissement diminue (***Chapitre 5***). Il serait donc possible d'utiliser ce niveau d'enrichissement en oxydes de Mn et Fe comme indicateur de précédentes interfaces (SWI), et donc d'enfouissement sédimentaire dans le Kongsfjord.

En effet, ces oxydes réactifs sont plus vraisemblablement d'origine diagénétique que détritique sachant que les phases particulaires porteuses dominantes de manganèse et de fer sont plus cristallisées dérivées des carbonates, comme l'ont attesté les extractions séquentielles des oxydes. Le matériel déposé rapidement dans le bassin interne du fjord est très immature provenant directement de l'érosion de l'encaissant rocheux du glacier (Herbert et al., 2020; Laufer-Meiser et al., 2021; Wehrmann et al., 2014). Du fait de son transport relativement court, dans la glace et dans la colonne d'eau, tous deux pauvres en matière organique, son recyclage par reminéralisation bactérienne reste faible. De ce fait, la fraction d'oxydes biodisponibles déposés au fond du fjord est limitée. Les enrichissements observés à certains niveaux (enfouis ou superficiels) ont donc une origine diagenétique. Il est donc vraisemblable que ce niveau supposé enfoui fut précédemment oxique et donc à la surface de la colonne sédimentaire.

Contrairement aux stations du bassin interne (St. 2 et St. 7) qui présentent la marque d'importants dépôts de sédiment provenant de la fonte du Kronebreen décroissant avec l'éloignement au front du glacier (zone 1 dans Fig. 1), les stations situées au-delà au seuil interne (St. 5 et St. 8, proches des Iles Lovénøyane ; ***Chapitre 1***) présentent deux états également différents (Zones 2 et 3 indiquées en Fig.1). L'étude de Herbert et al. (2021) a théorisé la présence d'une zone d'optimum de reminéralisation de la matière organique sujette à une sédimentation détritique suffisamment faible avec la turbidité associée pour permettre une production primaire de surface importante et donc un export de matière organique vers le fond. A la marge de l'instabilité sédimentaire, ce « sweet spot » se manifesterait par de forts flux sortants de Mn et Fe dissous catalysés par une forte activité bactérienne. La mesure d'une activité extracellulaire microbienne la plus haute de notre zone d'étude (***Chapitre 4***), d'un potentiel flux de manganèse dissous vers la colonne d'eau et d'un début d'enrichissement superficiel en oxydes diagenétiques (***Chapitre 5***) à 8 km du front du Kronebreen, en St. 5 proche du « sweet spot » défini par Herbert et al. (2021), corroborent l'hypothèse de l'existence d'une telle zone d'optimum de reminéralisation de la matière organique. Il est donc plus que probable que ce « sweet spot » soit localisé vers le seuil interne du Kongsfjorden, au niveau des îles Lovénøyane. Aux stations distales, à l'aval du seuil, l'enrichissement de surface en oxydes diagenétiques de Mn et Fe est plus important, associé à des flux nuls à l'interface, car la perturbation physique par enfouissement moins importante conjuguée à un plus grand apport en matière organique labile permet une plus grande reminéralisation microbienne. De plus, nos données et observations renforcent les interprétations de Herbert et al. (2021) pointant une

augmentation de la réduction des oxydes de fer par les sulfures produit par sulfato-réduction, elle-même catalysée par un apport plus important de matière organique pouvant atteindre ce processus en profondeur. Vers l'aval, la diminution de la turbidité ainsi que des taux de sédimentation associés permet la structuration d'un écosystème plus diversifié avec une riche macrofaune influençant la structure de la colonne sédimentaire, notamment par bioturbation (Kędra et al., 2011; Wlodarska-Kowalczuk et al., 2005). En effet, grâce à la visualisation haute-résolution des concentrations en espèces dissoutes dans les eaux porales, des preuves de bioirrigation, terriers et hétérogénéité latérale de la répartition de la matière organique ont pu être décelées à 10km du front glaciaire (St.8, ***Chapitre 7***). Cela résulte en l'établissement de microhabitats pouvant générer des hétrogénéités centimétriques chez les méio- et microorganismes comme les foraminifères benthiques

Cette succession du front du glacier vers le fjord aval de différents états transitoires biogéochimiques au regard de la perturbation que représente la décharge détritique fine d'origine glaciaire nous permet donc d'attester de gradients kilométriques de stabilité (Fig. 1). Un paramètre majeur observé dans le fjord et non simulé en approche expérimentale est la variation en contenu en matière organique entre zone proximale et distale, qui rend obligatoire sa quantification pour comprendre la dynamique biogéochimique locale. Les états mis en évidence par l'approche expérimentale ont permis d'identifier les marqueurs d'enfouissement ainsi que le rétablissement des phases stables des cycles du manganèse et du fer. L'ajout de la composante biologique avec la stimulation de l'activité microbienne a permis d'appuyer l'existence d'une zone d'état transitoire supplémentaire dans le fjord, ou « sweet spot ».

3 Impact de la sédimentation sur les communautés de foraminifères benthiques

L'impact direct de la sédimentation sur les foraminifères a été étudié dans l'étude expérimentale en microcosme présentée en ***Chapitre 2***. Dans ce setup expérimental, deux espèces de foraminifères provenant d'une vasière intertidale de la côte Atlantique ont été soumises à des dépôts de sédiments variant en intensité et en fréquence. Le but de cette expérience était d'observer les variations dans le temps des abondances de foraminifères vivants ainsi que la capacité de migration d'individus à la suite de ces perturbations. Des expérimentations supplémentaires plus poussées et contraintes seraient nécessaires pour caractériser la réponse spécifique des foraminifères du Kongsfjorden vis-à-vis de dépôts sédimentaires (NB page 99).

L'expérimentation sur les espèces *Ammonia confertitesta* et *Haynesina germanica* a permis de révéler un effet différent des dépôts de sédiment sur les abondances spécifiques ainsi que des migrations actives des individus. Chez *A. confertitesta* une résistance à la perturbation a été décelée car cette espèce n'a montré aucune variation d'abondance au cours du temps après les différents ajouts de sédiment. Cependant, d'après les réplicas prélevés dans les différents microcosmes, les enfouissements uniques ou successifs ont déclenché une migration des individus vers la nouvelle surface (***Chapitre 2***). Chez *H. germanica*, cette migration s'est également vue avec une vitesse supérieure de 0.06 mm h^{-1} à *A. confertitesta*., et par un effet négatif des perturbations sédimentaires avec le temps sur son abondance.

Les différents traitements ont donc montré que les foraminifères pouvaient se mouvoir dans un dépôt plus ou moins épais et fréquent caractérisé comme rapidement anoxique. En effet, la rapide consommation de l'oxygène dissous à l'ancienne surface eau-sédiment par

reminéralisation aérobie de la matière organique, présente en grande quantité dans les sédiments intertidaux utilisés dans les microcosmes, rend rapidement l'environnement anoxique. La déstabilisation du microhabitat des foraminifères benthiques déclenche donc une migration vers la surface pour retrouver un environnement de vie adéquat et stable. Dans un milieu eutrophe comme celui étudié ici, la perte d'oxygène est donc le paramètre motivant le déplacement des foraminifères.

Les différentes réponses des deux espèces de foraminifères étudiées en microcosmes ont permis de mettre en lumière le caractère spécifique de la résistance des individus à la perturbation. Les différents compartiments benthiques ne répondent pas de la même manière à une perturbation, et l'étude de tous les niveaux benthiques est nécessaire afin de bien comprendre la résilience de l'entièreté de la faune suite à des dépôts de sédiment ou autre perturbation du milieu. Cette recolonisation des dépôts récents de sédiment par les foraminifères peut donc être un indicateur de rétablissement du fonctionnement de l'écosystème et une stratégie d'adaptation à un stress, à relier avec la résilience des fronts redox exprimée plus tôt et plus spécialement la stabilisation de la pénétration en oxygène alors en accord avec la demande des organismes aérobies.

L'impact de la sédimentation sur les faunes benthiques a déjà été documenté dans les fjords du Svalbard et particulièrement dans le Kongsfjord (Hop and Wiencke, 2019; Kędra et al., 2011; Wlodarska-Kowalczuk et al., 2005; Włodarska-Kowalczuk et al., 2016). Elle a montré un effet délétère sur les écosystèmes y compris sur les foraminifères comme étudié précédemment par Fossile et al. (2022). Des biozonations comprenant des assemblages particuliers d'espèces et des abondances différentes se mettent alors en place au regard du stress causé par l'intense sédimentation glaciaire mais aussi à l'apport de matière organique et à la distribution des masses d'eau.

Afin d'augmenter notre compréhension de l'impact de la fonte des glaciers et de la décharge sédimentaire associée sur les faunes de foraminifères benthiques, nous avons étudié 4 stations dans l'axe du fjord, sur 10 km en partant du front du glacier tidal Kronebreen, en Mai et Août 2021. Les conditions hydrographiques se sont révélées très contrastées entre les deux saisons, avec au printemps une colonne d'eau bien mélangée, sans turbidité et avec une productivité primaire très limitée contrairement à la fin de l'été présentant une forte stratification de la colonne d'eau (***Chapitre 4***). La présence d'eau Atlantique a été détectée au fond de de la colonne d'eau tandis que les eaux de surface résultant de la fonte des glaciers ont été trouvées riches en particules détritiques près du front du Kronebreen. Un second gradient environnemental, antagoniste à celui de la turbidité est la productivité primaire qui apparait lorsque la turbidité atteint des niveaux assez faibles autorisant la photosynthèse du phytoplancton (***Chapitre 4***).

Les biozonations de populations de foraminifères ont été déterminées et comparées pour les deux saisons, printemps et fin d'été 2021.

Pour les stations proches du front du glacier, les assemblages ont montré de très faibles abondances (voire nulles) à mi-printemps (NB : échantillonnage fait début Mai, au tout début de la période de bloom phytoplanctonique) tandis que la saison estivale était caractérisée notamment par l'apparition et la large dominance de l'espèce agglutinée *Capsammina bowmanni* (> 90%) cantonnée dans cette zone proximale (***Chapitre 6***). Cette grande différence entre les deux saisons peut être expliquée par deux hypothèses non exclusives. D'une part, le faible export en matière organique en zone proximale pendant les blooms phytoplanctoniques printaniers et estivaux ne permettrait pas un stockage de nourriture suffisant pour entretenir des

faunes benthiques tout au long d'une année (Food Bank theory, Mincks et al., 2005, ***Chapitre 4***). D'autre part, les taux de sédimentation estivaux excessivement élevés en zone proximale, engendreraient une dilution du matériel biologique labile au profit du terrigène d'origine glaciaire. L'apparition de *C. bowmanni* (espèce agglutinée) en été pourrait être concomitante avec la décharge de sédiment apportant les particules nécessaires à la formation de leur test (Gooday et al., 2010). De plus, la forte densité estivale de *C. bowmanni* est concentrée en surface pour pouvoir capter les faibles apports de matière organique produite dans la zone et dilué avec l'apport terrigène. Une migration active de cette espèce peut donc être envisagée pour expliquer sa distribution verticale superficielle.

En aval du seuil interne, les stations éloignées au glacier présentent un contenu spécifique similaire au cours des 2 saisons étudiées, et les assemblages de foraminifères vivants y sont plus abondants et plus diversifiés qu'en zone proximale (***Chapitre 6*** et ***7***). Ils sont dominés par deux espèces inféodées à différentes variables environnementales telles que le contenu en matière organique et la distribution des masses d'eau. *Nonionellina labradorica* témoigne d'un contenu en matière organique labile important observé grâce aux analyses de concentrations en phytopigments dans les sédiments de surface (St. 5 ; 8 km du front du glacier), et *Adercotryma glomeratum* corrobore la présence de la masse d'eau Atlantique à 125 m de profondeur (St. 8 ; 10 km du front du glacier). La différence majeure entre les deux saisons dans ces deux stations est la distribution verticale des individus dans la colonne sédimentaire. Au printemps, juste à l'aval du seuil (St. 5), les individus montraient un maximum de densité autour de 2 cm de profondeur avec une décroissance vers la surface et en profondeur, tandis qu'en fin d'été, ils étaient essentiellement concentrés dans le premier centimètre de sédiment suivi d'une diminution exponentielle avec la profondeur. Cette même dynamique saisonnière est également visible en St. 8 concernant l'assemblage dominé par *A. glomeratum*. De plus, l'étude de la distribution 2D des foraminifères, notamment des deux espèces sus-citées, en été 2021 a révélé une distribution groupée (patchiness) sur 1-2 cm de largeur dans les premiers 4 cm de profondeur (***Chapitre 7***). Cette hétérogénéité latérale ne peut être imputée à la présence de bioturbation et de terriers car présente de plus grandes structures. L'explication de cette distribution réside plutôt dans la création de microenvironnements générés par une hétérogénéité dans la distribution de la matière organique créant ainsi des spots de reminéralisation.

L'hypothèse permettant d'expliquer, en zone distale, les richesses spécifiques similaires au cours des deux saisons ainsi que l'étalement vertical des microhabitats au printemps, est la présence d'une réserve de nourriture annuelle suffisamment entretenue en été par les blooms phytoplanctoniques et l'export important de matière organique associé (« food bank » ; Mincks et al., 2005). Cette hypothèse avait déjà été formulée pour expliquer la persistance des macrofaunes benthiques dans la zone de nos stations distales (Hop and Wiencke, 2019; Włodarska-Kowalczuk et al., 2016). Les mesures des paramètres physico-chimiques dans la colonne d'eau (CTD) ainsi que de matière organique (concentration en phytopigments) appuient fortement cette hypothèse. De plus, les taux de dégradation extracellulaire représentée par la mesure d'aminopeptidase dans les sédiments de surface révèlent des valeurs similaires entre les deux saisons et une forte relation linéaire avec le nombre d'espèces de foraminifères présents dans les sédiments. Cet indicateur d'activité de reminéralisation bactérienne de la matière organique supporte également la théorie de la « food bank » car son activité est plus haute aux deux saisons en aval du seuil interne avec un pic d'activité au printemps en St. 5. Cette dernière observation peut être reliée avec une zone de transition biogéochimique où est

observé un optimum de reminéralisation de la matière organique par les processus redox (« sweet spot » (***Chapitre 5***), et des flux de manganèse ou fer dissous vers la colonne d'eau comme décrit précédemment. Toutes ces dernières observations autour de la St. 5 impliquent donc un optimum de développement biologique au point de transition entre la diminution de la turbidité de surface et l'augmentation de la productivité primaire.

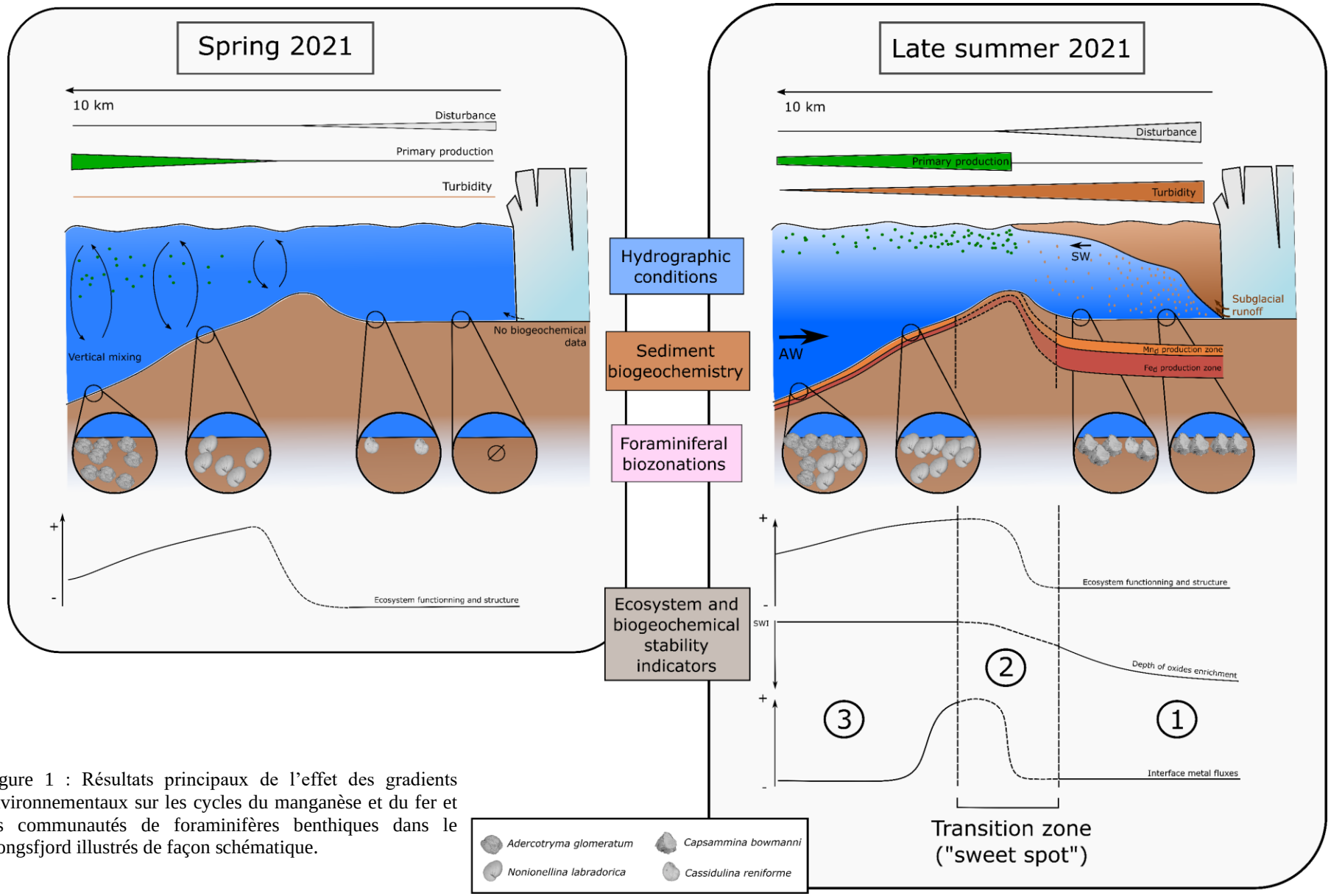

Figure 1 : Résultats principaux de l'effet des gradients environnementaux sur les cycles du manganèse et du fer et les communautés de foraminifères benthiques dans le Kongsfjord illustrés de façon schématique.

4 Perspectives

4.1 Suivi interannuel de l'effet de la fonte des glaciers sur les microhabitats benthiques

Un des objectifs initiaux de ce travail de doctorat était le suivi interannuel de l'effet de la fonte des glaciers sur les microhabitats benthiques commençant en été 2020. Pour cause de pandémie de Covid-19 et confinement associé, la mission d'échantillonnage 2020 a été annulée. Dans un second temps, les projets BEGIN (CNRS INSU ; PI : Maria Pia Nardelli, Univ. Angers) et KONBHAS (IPEV ; PI : Agnès Baltzer, Nantes Univ.) ont permis d'effectuer deux campagnes d'échantillonnage en 2021, dont les données sont présentées dans cette thèse. Dans le cadre du suivi interannuel, deux missions additionnelles ont pu être effectuées en Août 2022 et Août 2023. Du fait de la durée du doctorat et du temps alloué au transport des échantillons depuis Ny-Ålesund, je n'ai pas pu travailler sur ces données pluriannuelles. En effet, si les échantillons de 2023 ne nous sont pas encore parvenus, ceux de 2022 ont pu faire l'objet de plusieurs stages de master 1 et 2 (printemps 2023) que j'ai activement encadré, notamment au niveau de l'étude sédimentologique, l'analyse des données environnementales (traitement des données de CTD) et traitement des mesures biogéochimiques.

Nous avons pu montrer dans cette thèse l'intérêt de l'étude des biozonations de foraminifères vivants et leur microhabitats sédimentaires ainsi que des gradients redox en lien avec la fonte des glaciers locaux. Dans un contexte d'amplification du réchauffement climatique en région Arctique, la dynamique de cet environnement est donc intimement liée à la cryosphère locale. Des variations interannuelles du lien pélagique/benthique peuvent donc intervenir à l'échelle du fjord. Les zones de stabilité et d'instabilité benthiques peuvent donc migrer dans l'axe du fjord suivant l'intensité du relargage de sédiment par les glaciers.

Bien que ces données puissent faire l'objet de futures publications, la compilation des résultats préliminaires de la fin d'été 2022 a permis de tester les hypothèses émises sur la dynamique du fjord dans les différents chapitres de cette thèse pour 2021. Les descriptions et interprétations associées aux résultats préliminaires de 2022 peuvent être retrouvées en ANNEXE 1 des perspectives. Dans un premier temps, les foraminifères benthiques ainsi que les états transitoires de la diagenèse précoce étudiés sur les mêmes stations montrent une extension de la zone d'effet de la sédimentation intense sur les microhabitats. Cela est supporté par la mesure d'un panache turbide étendu et une productivité primaire plus limitée et contrainte en aval de nos stations. Le contenu en carbone organique est par conséquent plus faible dans toutes les stations résultant en des activités de reminéralisation plus faibles. De plus amples discussions sont nécessaires pour pleinement comprendre la dynamique de la fin d'été 2022, néanmoins ces données révèlent clairement une variabilité interannuelle qui pourra être vérifiée ou infirmée avec l'analyse des assemblages de foraminifères benthiques vivants en 2023.

4.2 Modélisations biogéochimiques

Ici, je présente des pistes d'amélioration ou d'utilisation du modèle biogéochimique développé dans cette thèse.

4.2.1 Améliorations de l'identification d'évènements de dépôts par les cycles du manganèse et du fer

L'état transitoire du cycle du manganèse et du fer simulé dans le ***Chapitre 3*** et utilisé dans le ***Chapitre 5*** a permis de déceler des zones soumises à de fortes sédimentations dans le Kongsfjord. Néanmoins, l'utilisation des cycles du manganèse et du fer pour identifier les zones de dépôts massifs a montré des faiblesses inhérentes aux processus dont elle dépend telle que la température, la concentration en métaux biodisponibles, l'oxygénation de l'environnement ou encore la quantité et qualité de la matière organique reminéralisée. A cause de toutes ces limitations, des tests ou applications dans d'autres environnements pourraient conforter l'utilisation du cycle du manganèse et du fer dans l'étude des dépôts de sédiment sans érosion.

Afin d'améliorer ce modèle, la temporalité des évènements de dépôt pourrait être atteinte en ajoutant des analyses isotopiques. Des analyses de ^{210}Pb, permettrait de discriminer un substrat sédimentaire en place avant un dépôt massif de sédiment frais. La temporalité de ces évènements dans la nature permettrait de contraindre la période de décharge sédimentaire et son influence sur le substrat benthique. De plus, en ayant mesuré les variables environnementales et la distribution verticale des fronts redox dans le sédiment, il pourrait être pertinent de modéliser des flux qui nous permettraient de dater ces dépôts depuis le moment où les reminéralisations aérobie et anaérobie n'auraient pas pu suivre le rythme de la sédimentation.

4.2.2 Utilisation des données expérimentales pour contraindre la modélisation de perturbations sédimentaires

Les données récoltées dans le ***Chapitre 3*** sur l'évolution des états transitoires des différents gradients redox après les deux modalités de dépôt sédimentaires pourraient aider à la calibration de certains modèles comme celui développé par Nmor et al. (2022), FESDIA (v1.0). Après une discussion avec l'auteur, nous savons que la modalité OHV peut déjà être bien modélisée par ce modèle. Un seul dépôt est déjà considéré par FESDIA et permet de modéliser l'évolution de gradients redox jusqu'à la méthanogenèse dans le temps après une telle perturbation. Le réel intérêt des données expérimentales réside dans la modalité FLV présentant l'évolution du système biogéochimique avec une succession de petits dépôts sédimentaires. Nous avons vu que plus les processus métaboliques primaires se trouvaient en profondeur dans la séquence diagenétique, plus un décalage temporel de leur état transitoire était observé car dépendant de l'état des processus sus-jacents et de leur état transitoire respectif. Par exemple, le cycle de l'azote se rééquilibre plus rapidement que celui du manganèse, lui-même plus rapide que celui du fer. Une publication à paraître prochainement de Stanley Nmor met en exergue l'évolution des gradients biogéochimiques dans le cas de dépôts successifs en prenant en compte l'état diagenétique précédent s'il présente toujours un état transitoire. Pour l'étude des cycles du manganèse et du fer, l'emphase doit être mise sur la dynamique de réoxydation du matériel diffusif dans les niveaux oxiques. La non-synchronicité entre les cycles du manganèse et du fer pourrait donc être plus finement modélisée grâce aux données expérimentales décrites dans cette thèse. Une collaboration avec Stanley Nmor est déjà envisagée.

4.2.3 Modélisation de flux à partir des images 2D DET dans le Kongsfjord (Chapitre 7)

La description de la distribution des composés dissous dans les eaux porales de deux stations du Kongsfjorden a permis de mettre en évidence des figures de bioirrigation et d'hétérogénéité latérale de contenu en matière organique. Nous pensons que ces données

pourraient affiner notre compréhension de la dynamique biogéochimique du fjord, présentée en ***chapitre 5***, en ajoutant de la modélisation de flux sur les images à l'instar des études de Herbert et al. (2021) et Thibault de Chanvalon et al. (2017). Les structures biogéniques peuvent participer à l'hétérogénéité des flux de matériel dissous à l'interface. De ce fait, les sondes DET sont de parfaits supports pour prendre en compte la variabilité latérale à petite échelle révélant des constructions d'origine biologique perturbant la séquence verticale de diagenèse précoce. Une collaboration entre Thibault de Chanvalon et l'équipe de géochimistes du LPG est déjà effective.

4.3 Régime trophique des foraminifères dans le Kongsfjord

L'étude saisonnière et pluriannuelle des biozonations et microhabitats des foraminifères a permis d'hypothétiser des régimes trophiques différents en fonction des espèces mais également au sein d'une même espèce telles que *Nonionellina labradorica* ou *Adercotryma glomeratum* (***Chapitre 6***). Leur zonation en fonction des gradients environnementaux et donc de la concentration en matière organique fraiche dans le sédiment influence leur régime trophique de façon saisonnière. Une espèce montre-t-elle des régimes trophiques différents à un instant t dans des sites différents du fjord ?

Au sein du projet BEGIN, un volet est dédié à l'étude isotopique du contenu cytoplasmique en ^{15}N et ^{13}C des foraminifères benthiques du fjord afin de les comparer à différents niveaux de la chaine trophique locale allant de la méiofaune métazoaire benthique (Nématodes…) aux espèces planctoniques présentes dans la colonne d'eau (collaboration Dr. Christine Dupuy, Université de la Rochelle, LIENSs). Ces analyses, non encore finalisées, permettraient de valider ou réfuter les hypothèses énoncées dans cette thèse concernant la distribution des faunes de foraminifères au sein du fjord mais aussi dans la colonne sédimentaire comme la présence annuelle de la « food bank » entretenant les faunes benthiques pendant les périodes de faibles apports de matière organique.

4.4 Investiguer l'impact de l'éloignement à la côte sur l'écosystème benthique

La côte sud du Kongsfjorden présente des glaciers à terminaison terrestre générant des systèmes fluviatiles courts (jusqu'à 4 km) transportant des sédiments fins et grossiers par les eaux de fonte. Les sédiments grossiers s'accumulent sur le littoral sous forme de deltas et prodeltas très mobiles, accompagnés ou non d'un léger panache turbide se repandant sur le fjord. Le ruissellement des eaux de fonte sur le substratum à l'affleurement augmente la part d'oxydes biodisponibles déposée sur le littoral du fait d'une activité bactérienne plus importante que dans un contexte de rivière sous-glaciaire déversant directement les sédiments érodés au sein des eaux du fjord. L'incidence de quoi ?? d'apport augmenté d'oxydes ?? sur la reminéralisation de la matière organique est donc importante dans ces environnements côtiers de fjord (Herbert et al., 2020).

En lien avec l'étude de progradation ou aggradation sédimentaire des deltas et prodeltas de cette côte par le projet KONBHAS (Bourriquen et al., 2016), l'investigation biogéochimique et biologique pourrait permettre de mettre en lumière des conditions de stabilité des écosystèmes benthiques en lien avec l'éloignement à la côte. Ces zones restreintes aux

embouchures changeantes des systèmes fluviatiles périglaciaires présentent des dynamiques biologiques différentes par rapport aux milieux plus profonds étudiés dans cette thèse, influençant plus amplement la macrofaune, la méiofaune et potentiellement les foraminifères du fait de leur plus faible profondeur. En comparaison avec les systèmes profonds, l'activité de reminéralisation de la matière organique et la structure de l'écosystème seraient-ils plus importants ? Comment varient-ils avec l'éloignement à la côte ? Comment les conditions biogéochimiques du sédiment évoluent-elles avec l'éloignement d'une côte alimentée par un système fluviatile périglaciaire ?

4.5 L'IA pour étudier la distribution verticale des faunes

En marge de cette thèse, une méthode d'identification de foraminifères dans le sédiment est en cours de développement au laboratoire LPG, utilisant des carottes enrésinées provenant des expériences décrites en ***Chapitre 2*** et ***3***. L'analyse par micro-tomographie par rayon X permet la cartographie 3D à haute résolution (13µm), de l'intérieur d'un solide. Les différences de densité de la matière et donc d'impédance mettent en lumière des formes et par conséquent les coquilles de foraminifères. Grâce à cette méthode puis un traitement d'images poussé développé au cours d'un stage de Master 2 par Maryline Moller (encadrement M.P.Nardelli et A. Mouret (LPG), collaboration avec N. Vanderesse (PACEA UMR 5199, Université de Bordeaux) il est possible de donner des coordonnées 3D à chaque individu et de pouvoir ainsi établir leur profondeur d'habitat, et d'étudier finement la variabilité spatiale de densité (patchiness). Cette méthode manuelle peut maintenant être enrichie par l'identification automatique des faunes en utilisant un réseau de neurone virtuel alimenté par une banque d'images préalablement acquises afin de distinguer les particules terrigènes des tests de foraminifères (Master 2 de Yaqian Zhao ; encadrement M. P. Nardelli, N. Vanderesse, A. Mouret). De plus amples développements par cette équipe sont envisagés pour améliorer la méthode d'analyse.

Références :

Anschutz, P., Jorissen, F. J., Chaillou, G., Abu-Zied, R., and Fontanier, C.: Recent turbidite deposition in the eastern Atlantic: Early diagenesis and biotic recovery, Journal of Marine Research, 60, 835–854, https://doi.org/10.1357/002224002321505156, 2002.

Bourriquen, M., Baltzer, A., Mercier, D., Fournier, J., Pérez, L., Haquin, S., Bernard, E., and Jensen, M.: Coastal evolution and sedimentary mobility of Brøgger Peninsula, northwest Spitsbergen, Polar Biol, 39, 1689–1698, https://doi.org/10.1007/s00300-016-1930-1, 2016.

Burdige, D. J.: Geochemistry of Marine Sediments, in: Geochemistry of Marine Sediments, Princeton University Press, https://doi.org/10.1515/9780691216096, 2007.

Calleja, M. Ll., Kerhervé, P., Bourgeois, S., Kędra, M., Leynaert, A., Devred, E., Babin, M., and Morata, N.: Effects of increase glacier discharge on phytoplankton bloom dynamics and pelagic geochemistry in a high Arctic fjord, Progress in Oceanography, 159, 195–210, https://doi.org/10.1016/j.pocean.2017.07.005, 2017.

Cathalot, C., Rabouille, C., Pastor, L., Deflandre, B., Viollier, E., Buscail, R., Gremare, A., Treignier, C., and Pruski, A.: Temporal variability of carbon recycling in coastal sediments influenced by rivers: assessing the impact of flood inputs in the Rhoˆne River prodelta, 2010.

Cottier, F., Tverberg, V., Inall, M., Svendsen, H., Nilsen, F., and Griffiths, C.: Water mass modification in an Arctic fjord through cross-shelf exchange: The seasonal hydrography of Kongsfjorden, Svalbard, J. Geophys. Res., 110, C12005, https://doi.org/10.1029/2004JC002757, 2005.

Dallmann, W. K.: Geoscience Atlas of Svalbard, 2015.

D'Angelo, A., Giglio, F., Miserocchi, S., Sanchez-Vidal, A., Aliani, S., Tesi, T., Viola, A., Mazzola, M., and Langone, L.: Multi-year particle fluxes in Kongsfjorden, Svalbard, Biogeosciences, 15, 5343–5363, https://doi.org/10.5194/bg-15-5343-2018, 2018.

Deflandre, B., Mucci, A., Gagné, J.-P., Guignard, C., and Sundby, B. jørn: Early diagenetic processes in coastal marine sediments disturbed by a catastrophic sedimentation event, Geochimica et Cosmochimica Acta, 66, 2547–2558, https://doi.org/10.1016/S0016-7037(02)00861-X, 2002.

Fossile, E., Nardelli, M. P., Howa, H., Baltzer, A., Poprawski, Y., Baneschi, I., Doveri, M., and Mojtahid, M.: Influence of modern environmental gradients on foraminiferal faunas in the inner Kongsfjorden (Svalbard), Marine Micropaleontology, 173, 102117, https://doi.org/10.1016/j.marmicro.2022.102117, 2022.

Froelich, P. N., Klinkhammer, G. P., Bender, M. L., Luedtke, N. A., Heath, G. R., Cullen, D., Dauphin, P., and Blaynehartman, D. Hammond.: Early oxidation of organic matter in pelagic sediments of the eastern equatorial Atlantic: suhoxic diagenesis, Geochimica et Cosmochimica Acta, 43, 1075–1090, https://doi.org/0016-7037 79,0701-1075SO?.M) 0, 1979.

Gooday, A. J., Lecroq, B., and Pearce, R. B.: The "mica sandwich"; a remarkable new genus of Foraminifera (Protista, Rhizaria) from the Nazaré Canyon (Portuguese margin, NE Atlantic), Micropaleontology, 56, 345–357, 2010.

Guilhermic, C., Nardelli, M. P., Mouret, A., Le Moigne, D., and Howa, H.: Short-term response of benthic foraminifera to fine-sediment depositional events simulated in microcosm, Biogeosciences, 20, 3329–3351, https://doi.org/10.5194/bg-20-3329-2023, 2023.

Hegseth, E. N., Assmy, P., Wiktor, J. M., Wiktor, J., Kristiansen, S., Leu, E., Tverberg, V., Gabrielsen, T. M., Skogseth, R., and Cottier, F.: Phytoplankton seasonal dynamics in Kongsfjorden, Svalbard and the adjacent shelf, in: the ecosystem of Kongsfjorden, Svalbard, vol. 2, edited by: Hop, H. and Wiencke, C., Springer International Publishing, Cham, 173–227, https://doi.org/10.1007/978-3-319-46425-1_6, 2019.

Herbert, L. C., Riedinger, N., Michaud, A. B., Laufer, K., Røy, H., Jørgensen, B. B., Heilbrun, C., Aller, R. C., Cochran, J. K., and Wehrmann, L. M.: Glacial controls on redox-sensitive trace element cycling in Arctic fjord sediments (Spitsbergen, Svalbard), Geochimica et Cosmochimica Acta, 271, 33–60, https://doi.org/10.1016/j.gca.2019.12.005, 2020.

Herbert, L. C., Zhu, Q., Michaud, A. B., Laufer-Meiser, K., Jones, C. K., Riedinger, N., Stooksbury, Z. S., Aller, R. C., Jørgensen, B. B., and Wehrmann, L. M.: Benthic iron flux influenced by climate-sensitive interplay between organic carbon availability and sedimentation rate in Arctic fjords, Limnol Oceanogr, 66, 3374–3392, https://doi.org/10.1002/lno.11885, 2021.

Herbert, L. C., Michaud, A. B., Laufer-Meiser, K., Hoppe, C. J. M., Zhu, Q., Aller, R. C., Jørgensen, B. B., and Wehrmann, L. M.: Tight benthic-pelagic coupling drives seasonal and interannual changes in iron-sulfur cycling in Arctic fjord sediments (Kongsfjorden, Svalbard), Journal of Marine Systems, 225, 103645, https://doi.org/10.1016/j.jmarsys.2021.103645, 2022.

Hodal, H., Falk-Petersen, S., Hop, H., Kristiansen, S., and Reigstad, M.: Spring bloom dynamics in Kongsfjorden, Svalbard: nutrients, phytoplankton, protozoans and primary production, Polar Biol, 35, 191–203, https://doi.org/10.1007/s00300-011-1053-7, 2012.

Hodgkins, R., Cooper, R., Wadham, J., and Tranter, M.: Suspended sediment fluxes in a high-Arctic glacierised catchment: implications for fluvial sediment storage, Sedimentary Geology, 162, 105–117, https://doi.org/10.1016/S0037-0738(03)00218-5, 2003.

Hop, H. and Wiencke, C. (Eds.): The Ecosystem of Kongsfjorden, Svalbard, Springer International Publishing, Cham, https://doi.org/10.1007/978-3-319-46425-1, 2019.

Hulot, V., Metzger, E., Thibault de Chanvalon, A., Mouret, A., Schmidt, S., Deflandre, B., Rigaud, S., Beneteau, E., Savoye, N., Souchu, P., Le Merrer, Y., and Maillet, G. M.: Impact of an exceptional winter flood on benthic oxygen and nutrient fluxes in a temperate macrotidal estuary: Potential consequences on summer deoxygenation, Frontiers in Marine Science, 10, 2023.

Kędra, M., Legeżyńska, J., and Walkusz, W.: Shallow winter and summer macrofauna in a high Arctic fjord (79° N, Spitsbergen), Mar Biodiv, 41, 425–439, https://doi.org/10.1007/s12526-010-0066-8, 2011.

Lalande, C., Moriceau, B., Leynaert, A., and Morata, N.: Spatial and temporal variability in export fluxes of biogenic matter in Kongsfjorden, Polar Biol, 39, 1725–1738, https://doi.org/10.1007/s00300-016-1903-4, 2016.

Laufer-Meiser, K., Michaud, A. B., Maisch, M., Byrne, J. M., Kappler, A., Patterson, M. O., Røy, H., and Jørgensen, B. B.: Potentially bioavailable iron produced through benthic cycling in glaciated Arctic fjords of Svalbard, Nat Commun, 12, 1349, https://doi.org/10.1038/s41467-021-21558-w, 2021.

Lydersen, C., Assmy, P., Falk-Petersen, S., Kohler, J., Kovacs, K. M., Reigstad, M., Steen, H., Strøm, H., Sundfjord, A., Varpe, Ø., Walczowski, W., Weslawski, J. M., and Zajaczkowski, M.: The importance of tidewater glaciers for marine mammals and seabirds in Svalbard, Norway, Journal of Marine Systems, 129, 452–471, https://doi.org/10.1016/j.jmarsys.2013.09.006, 2014.

Meslard, F., Bourrin, F., Many, G., and Kerhervé, P.: Suspended particle dynamics and fluxes in an Arctic fjord (Kongsfjorden, Svalbard), Estuarine, Coastal and Shelf Science, 204, 212–224, https://doi.org/10.1016/j.ecss.2018.02.020, 2018.

Michaud, A. B.: Glacial influence on the iron and sulfur cycles in Arctic fjord sediments (Svalbard), Geochimica et Cosmochimica Acta, 2020.

Mincks, S., Smith, C., and DeMaster, D.: Persistence of labile organic matter and microbial biomass in Antarctic shelf sediments: evidence of a sediment food bank, Mar. Ecol. Prog. Ser., 300, 3–19, https://doi.org/10.3354/meps300003, 2005.

Pastor, L., Rabouille, C., Metzger, E., Thibault de Chanvalon, A., Viollier, E., and Deflandre, B.: Transient early diagenetic processes in Rhône prodelta sediments revealed in contrasting flood events, Continental Shelf Research, 166, 65–76, https://doi.org/10.1016/j.csr.2018.07.005, 2018.

Payne, C. M. and Roesler, C. S.: Characterizing the influence of Atlantic water intrusion on water mass formation and phytoplankton distribution in Kongsfjorden, Svalbard, Continental Shelf Research, 191, 104005, https://doi.org/10.1016/j.csr.2019.104005, 2019.

Svendsen, H., Beszczynska-Møller, A., Hagen, J. O., Lefauconnier, B., Tverberg, V., Gerland, S., Børre Ørbæk, J., Bischof, K., Papucci, C., Zajaczkowski, M., Azzolini, R., Bruland, O., and Wiencke, C.: The physical environment of Kongsfjorden–Krossfjorden, an Arctic fjord system in Svalbard, Polar Research, 21, 133–166, https://doi.org/10.3402/polar.v21i1.6479, 2002.

Thibault de Chanvalon, A., Metzger, E., Mouret, A., Knoery, J., Geslin, E., and Meysman, F. J. R.: Two dimensional mapping of iron release in marine sediments at submillimetre scale, Marine Chemistry, 191, 34–49, https://doi.org/10.1016/j.marchem.2016.04.003, 2017.

Trusel, L. D., Powell, R. D., Cumpston, R. M., and Brigham-Grette, J.: Modern glacimarine processes and potential future behaviour of Kronebreen and Kongsvegen polythermal tidewater glaciers, Kongsfjorden, Svalbard, Geological Society, London, Special Publications, 344, 89–102, https://doi.org/10.1144/SP344.9, 2010.

Wehrmann, L. M., Formolo, M. J., Owens, J. D., Raiswell, R., Ferdelman, T. G., Riedinger, N., and Lyons, T. W.: Iron and manganese speciation and cycling in glacially influenced high-latitude fjord sediments (West Spitsbergen, Svalbard): Evidence for a benthic recycling-transport mechanism, Geochimica et Cosmochimica Acta, 141, 628–655, https://doi.org/10.1016/j.gca.2014.06.007, 2014.

Wlodarska-Kowalczuk, M., Pearson, T., and Kendall, M.: Benthic response to chronic natural physical disturbance by glacial sedimentation in an Arctic fjord, Mar. Ecol. Prog. Ser., 303, 31–41, https://doi.org/10.3354/meps303031, 2005.

Włodarska-Kowalczuk, M., Pawłowska, J., and Zajączkowski, M.: Do foraminifera mirror diversity and distribution patterns of macrobenthic fauna in an Arctic glacial fjord?, Marine Micropaleontology, 103, 30–39, https://doi.org/10.1016/j.marmicro.2013.07.002, 2013.

Włodarska-Kowalczuk, M., Górska, B., Deja, K., and Morata, N.: Do benthic meiofaunal and macrofaunal communities respond to seasonality in pelagial processes in an Arctic fjord (Kongsfjorden, Spitsbergen)?, Polar Biol, 39, 2115–2129, https://doi.org/10.1007/s00300-016-1982-2, 2016.

Zajączkowski, M.: Sediment supply and fluxes in glacial and outwash fjords, Kongsfjorden and Adventfjorden, Svalbard, Polish Polar Research, 29, 59–72, 2008.

ANNEXE 1

Ici, sont présentées des pistes de réflexion, incluant les données partielles concernant l'échantillonnage d'Août 2022, qui viendront soutenir les interprétations qui seront développées lors de futures valorisations scientifiques.

Variation pluriannuelle de la distribution des foraminifères dans le Kongsfjord

L'analyse de la distribution des foraminifères benthiques ainsi que celle des paramètres environnementaux en Mai et Août 2021 nous a permis de révéler une saisonnalité des réponses des faunes avec une perte totale d'individu aux stations proches du front du Kronebreen au printemps, alors que les assemblages restaient similaires entre les deux saisons en partie distale. De plus, la biozonation estivale révélée par notre étude de 2021 semble similaire à celles d'Août 2018, documentés par Fossile et al. (2022). Les conditions environnementales estivales sont donc supposées être similaires en Août 2018 et Août 2021.

Dans un futur proche (avant retrait sur terre du front glaciaire du Kronebreen) une fonte glaciaire accrue provoquerait une augmentation des décharges sédimentaires au front du glacier, avec des taux de sédimentation en zone proximale plus importants ainsi qu'un éloignement vers l'aval du fjord du développement phytoplanctonique. L'évolution des habitats benthiques en réponse à ces changements environnementaux pourrait provoquer le déplacement de la zone d'instabilité benthique au-delà du seuil interne vers les stations distales.

Présentation des résultats préliminaires de l'échantillonnage 2022 et comparaison avec les données 2021

Gradients environnementaux dans le Kongsfjorden

Contrairement à Août 2021, les données CTD d'Août 2022 montrent un panache turbide s'étalant dans le fjord sur deux profondeurs distinctes (Fig. 1), en surface et autour de 40 m de profondeur. De plus, les valeurs de turbidité sont bien plus importantes en Août 2022 pouvant indiquer une décharge d'eau de fonte sous-glaciaire plus importante. Un étalement du panache sur une plus grande distance supporte également cette hypothèse d'une fonte plus conséquente

Similairement à 2021, la biomasse phytoplanctonique (concentration en chlorophylle-a) augmente à la limite avec le panache turbide. Toutefois, les zonations de cette augmentation en chlorophylle-a est bien différente en 2022. En effet, le panache turbide n'est pas exactement localisé près du front du glacier laissant la place à une croissance phytoplanctonique dans le bassin interne. La seconde zone de croissance phytoplanctonique se situe à l'aval du panache turbide comme observé en 2021. Néanmoins, le front de productivité primaire semble poussé vers l'aval du fjord par ce panache turbide bien plus étalé qu'en 2021.

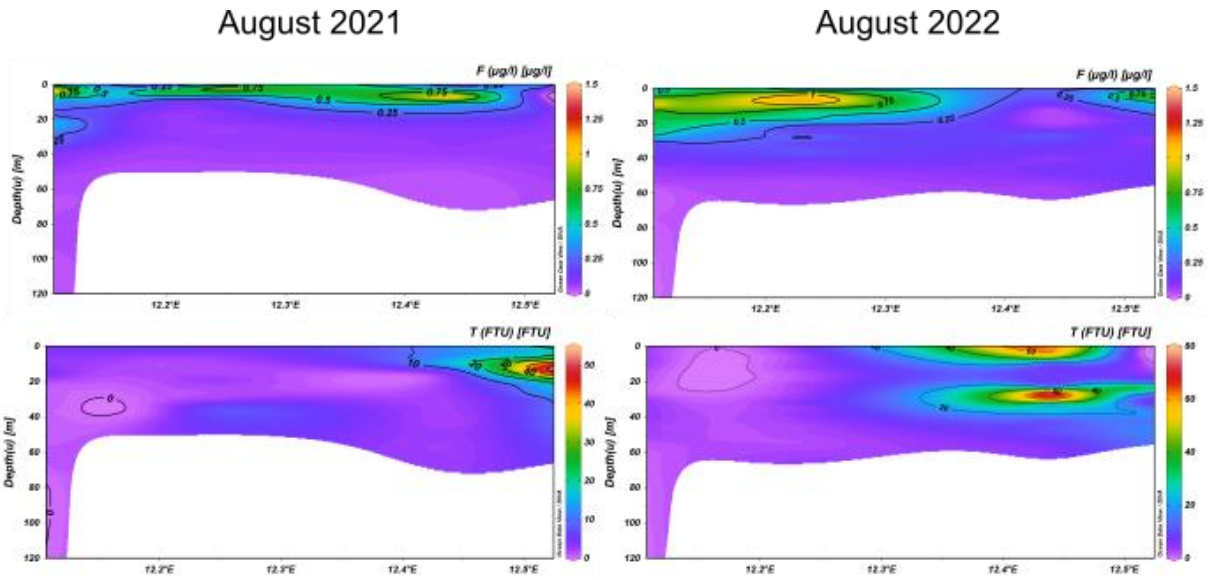

Figure 1 : Sections de mesures CTD de concentration en chlorophylle-a (panel supérieur) et turbidité (panel inférieur) dans le Kongsfjord pour les mois d'Aout 2021 et 2022 (Front du Kronebreen à droite de chaque section). La partie blanche de chaque secotion correspond à une zone sans modélisation et à la bathymétrie réelle

Matière organique dans les sédiments de surface

La comparaison entre les données saisonnières de 2021 déjà discutées et les analyses d'été 2022 est présentée en Fig. 2. La concentration en carbone biopolymérique à l'été 2022 est inférieur à toutes les stations comparées à l'été précédent. Les concentrations estivales de 2022 en phytopigments montrent des valeurs en St. 7, St. 2 et St. 8 similaires à celles des deux saisons 2021. Néanmoins, la St. 5 montre une très faible concentration en phytopigments ce qui est également visible dans le ratio PHYTO/BPC qui met également en lumière une haute valeur de ce ratio pour la St. 8. Les sections de concentration en chlorophylle-a et de turbidité (Fig. 1) nous ont montré qu'un décalage vers l'aval de la productivité primaire était présent. Par conséquent, l'hypothèse d'un export plus faible ainsi qu'une sédimentation détritique plus forte en St. 5 est envisageable et soutenue par les concentrations en phytopigments observées à cette station. De plus, toutes les stations montrent une activité extracellulaire de reminéralisation bien plus basses en 2022 qu'en 2021, notamment en Mai. La St. 5 précédemment qualifiée comme la station montrant une efficacité de reminéralisation la plus haute (92 nmol g^{-1} h^{-1}) en été 2021 n'atteint ici que 20 nmol g^{-1} h^{-1} ce qui correspond aux taux mesurés dans le bassin interne pendant l'été précédent.

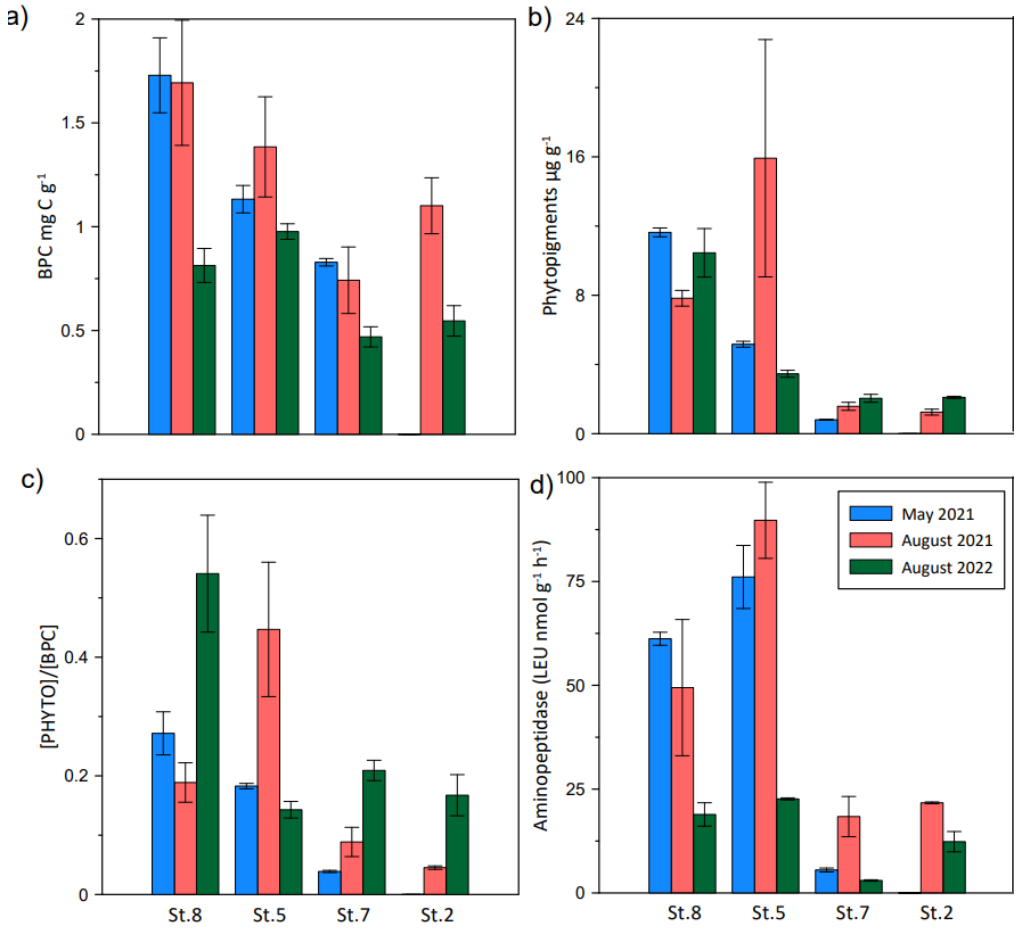

Figure 2 : Contenu en matière organique particulaire dans le sédiment de surface pour Mai et Août 2021 et Août 2022 (vert). a) concentration en Biopolymeric carbon, b) concentration en phytopigments (chlorophylle a et phaeopigments), c) ratio entre les concentrations en phytopigments et biopolymeric carbon, d) Aminopeptidase (Taux de dégradation extracellulaire de la matière organique)

Réponse des foraminifères benthiques aux conditions environnementales d'Août 2022 (données stage de master 2 de Nais Ferrié)

La distribution des foraminifères vivants dans la colonne sédimentaire jusqu'à 5 cm de profondeur pour Août 2022 est comparée aux données saisonnières précédemment discutées dans le ***Chapitre 6***. Différentes biozonations ainsi que les distributions verticales des faunes de foraminifères sont observables. En effet, les stations proximales présentent des densités d'individus bien inférieures à l'été précédent. La composition spécifique reste similaire en St.2 avec la dominance de *Capsammina bowmanni*. En St. 7, un assemblage totalement différent est trouvé avec une domination de *Textularia earlandi* et une absence totale de *C. bowmanni*.

La St. 5, qui se situe à l'aval du seuil interne présente une domination de *Nonionellina labradorica* avec de plus faibles densités que pendant l'été précédent. Toutefois, cet assemblage semble présenter une distribution assez similaire au printemps 2021 avec un maximum d'individus vers 2 cm de profondeur. Il est donc probable que le faible apport en phytopigments provenant d'une faible productivité primaire au-dessus de la St. 5 ne suffise pas à motiver les individus à rejoindre la surface du sédiment comme postulé pour la fin d'été 2021. Les conditions environnementales moins propices au bon fonctionnement écologique de cette

station influencent négativement les densités en individus et contraignent les foraminifères à adopter un microhabitat plus profond qu'en présence de fortes concentrations en phytopigments. Les faibles densités pourraient également s'expliquer par un épuisement de la « food bank », postulée pour entretenir les faunes benthiques en hiver et printemps en attendant les blooms phytoplanctoniques. La St. 8 quant à elle présente des densités bien plus importantes en *Adercotryma glomeratum* et *Labrospira crassimargo* qu'en 2021. Cette espèce montre un maximum de densité entre 1.5 et 2 cm de profondeur tandis que des espèces moins denses occupent majoritairement les niveaux de subsurface comme *Labrospira crassimargo* ou encore *Reophax fusiformis*. Bien que la St. 8 reçoive la plus grande quantité en phytopigments, la majeure partie des individus se trouve plus profondément, comparé à l'été précédent. Se nourrissant de matière organique plus réfractaire, cette espèce de foraminifère est également associée à l'advection d'eau Atlantique dans le fjord (***Chapitre 6***).

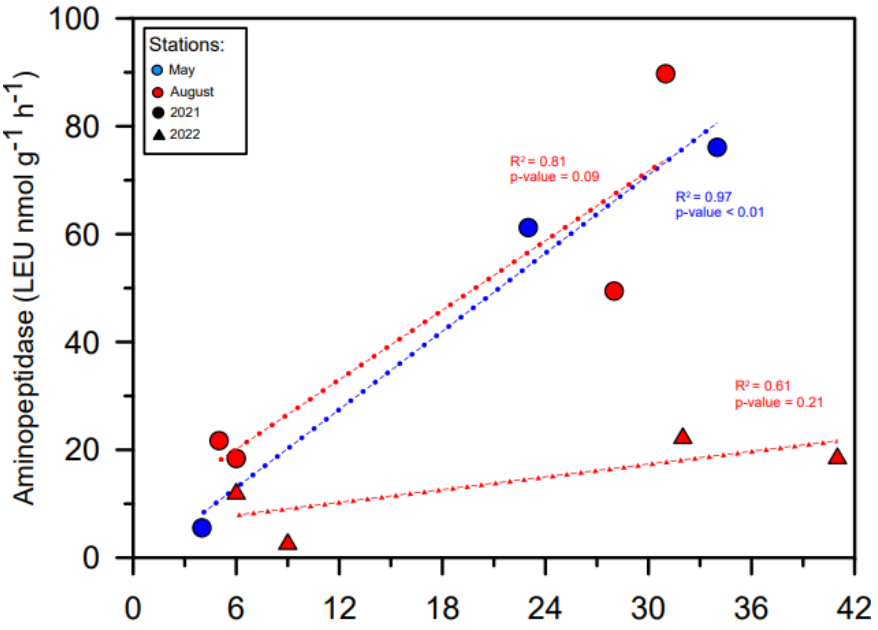

Figure 4 : Relation entre aminopeptidase et richesse spécifiques des 3 périodes échantillonnage

La relation définie dans le ***Chapitre 6*** entre le taux de dégradation de la leucine et la richesse spécifique en foraminifères benthiques vivants (> 125 µm) aux différentes stations a également été investiguée pour l'année 2022. Ici, les échantillonnages de printemps et fin d'été 2021 ont été séparés et montrent une pente similaire. En intégrant les mesures et richesses spécifiques de l'été 2022, on se rend compte que les stations proximales suivent une dynamique similaire aux précédentes mesures avec de faibles richesses spécifiques et de faibles aminopeptidases. Les différences majeures sont ici attribuées aux stations situées à l'aval du seuil interne. Elles présentent un nombre similaire d'espèces mais des valeurs d'aminopeptidase bien inférieures. Bien que la relation soit encore présente en 2022 (non significative), la plus faible pente révèle bien une différence de fonctionnement écosystémique et une performance microbienne affaiblie pour dégrader la matière organique en surface.

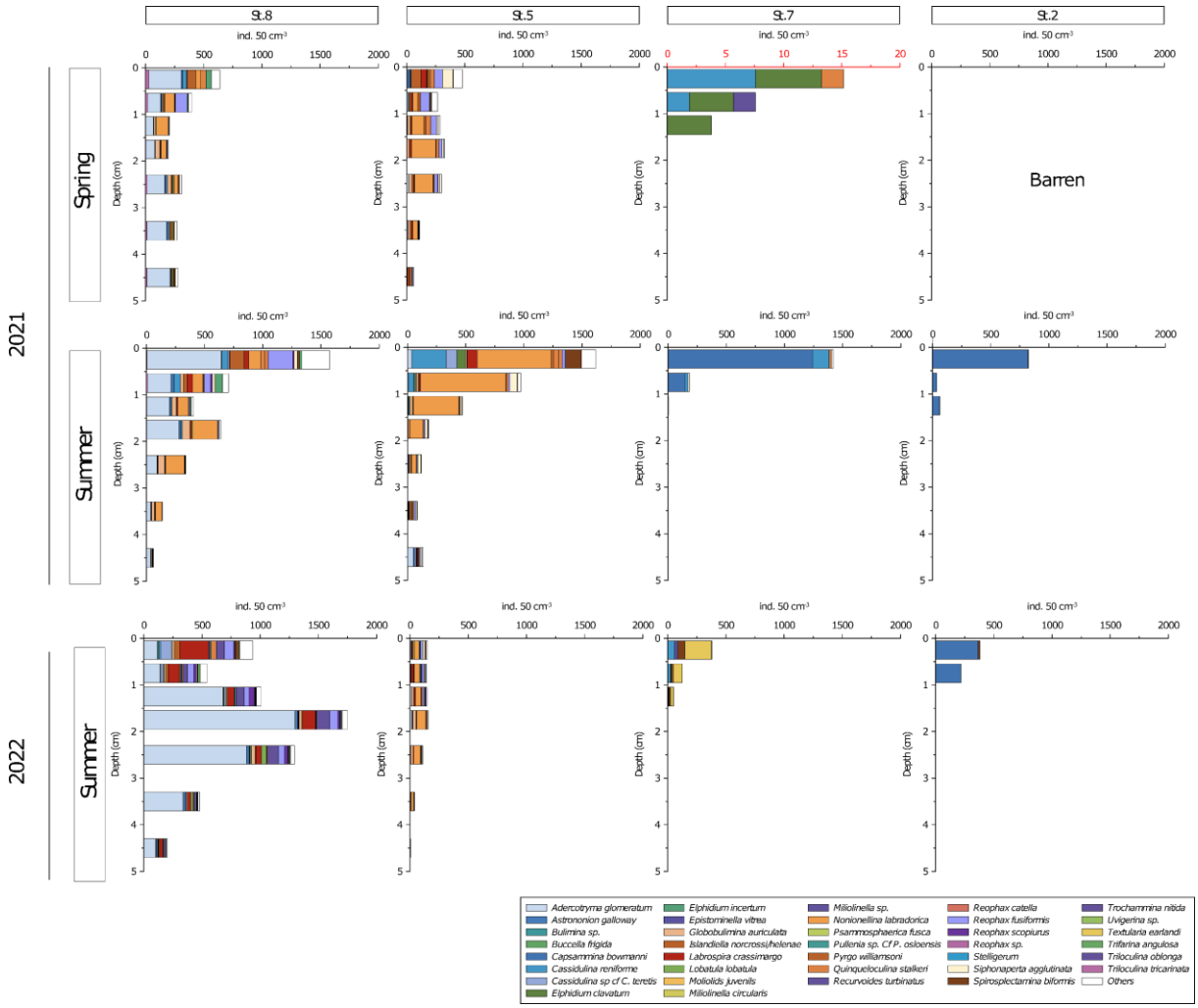

Figure 3 : Distribution vertical des densités spécifiques des foraminifères benthiques vivants échantillonnés en Mai et Août 2021 ainsi qu'en Août 2022.

Conclusions préliminaires

L'extension de l'étude pluriannuelle des faunes de foraminifères benthiques vivants permet de mettre en lumière les changements environnementaux liés à la fonte accrue des glaciers délivrant une plus grande quantité de particules détritiques dans le fjord. Comme hypothétisée dans le ***Chapitre 6***, une fonte plus conséquente du Kronebreen a pour conséquence immédiate l'extension de la zone d'instabilité benthique au-delà du seuil interne par le biais des gradients environnementaux dans la colonne d'eau décalant le front de productivité primaire et ainsi les écosystèmes benthiques, ici tracés par les foraminifères vers l'aval du fjord. Les intrusions d'eaux atlantiques semblent se produire de façon plus intense chaque année, marquées par une augmentation de la température du fjord et une fonte accrue du glacier libérant de plus grands volumes d'eau de fonte.

A la lumière des biozonations des assemblages de foraminifères benthiques se déplaçant en aval du fjord et de l'affaiblissement de la relation entre le taux de dégradation extracellulaire et la richesse spécifique (Fig. 4), nous pouvons hypothétiser un déplacement de l'état transitoire des gradients redox et plus particulièrement des cycles du Mn et Fe dans le sédiment. En effet, la supposée plus faible activité bactérienne de reminéralisation de la matière organique

additionnée d'une décharge sédimentaire d'origine glaciaire plus lointaine dans le fjord pourrait faire apparaitre de plus profondes interfaces par enrichissement en oxydes biodisponibles dans le bassin interne ainsi que dans les sites distaux contrairement à la situation en 2021 attestant d'une intense reminéralisation juste à l'aval du seuil (St. 5) et d'un état stable en partie distale (St. 8).

Etats transitoires des cycles du manganèse et fer en 2022 comparés à 2021

Ici, nous nous intéresserons uniquement aux données concernant le cycle du manganèse et du fer. Les données présentées dans le ***Chapitre 5*** ont déjà mis en lumière une zone d'instabilité sujette à une sédimentation estivale intense s'étendant du front du Kronebreen jusqu'au seuil interne. A l'aval du seuil (St. 8 et St. 5), un enrichissement en oxydes diagenétiques en surface est observé. De plus, la présence d'une zone présentant des flux à l'interface de Mn et Fe dissous appelée « sweet spot » par Herbert et al. (2021) étant le résultat d'une plus grande reminéralisation a été hypothétisée à l'aval du seuil (St. 5). Cette zone correspondrait à la limite entre le panache turbide et le pic de production primaire dans la colonne d'eau permettant un export plus important de matière organique. La Fig. 4 montre une comparaison des profils de concentration de Mn et Fe dissous et oxydes biodisponibles pour 2021 (***Chapitre 5***) et 2022 analysés dans le cadre d'un stage de master 1 en 2023 (Enzo Huet). En zone proximale (St. 2 et St. 7), l'enfouissement des SWI situées respectivement à 9 et 6 cm de profondeur en 2021, est plus profond en 2022, située à 18 et 9 cm respectivement pour les St. 2 et 7. La sédimentation par décharge glaciaire a donc été accrue soit en intensité, durée ou les deux. Les données de turbidité ont montré une plus forte concentration en particules ainsi qu'un plus grand étalement du panache vers l'aval du fjord. Un front profond de turbidité a été observé en 2022 donc il est probable qu'un export plus important de particules ait pu survenir. Ce changement de distribution de la turbidité et de ses conséquences sur le milieu benthique est visible dans les profils de concentration des stations distales. En effet, un enrichissement en oxydes réactifs est visible à 4 cm de profondeur en St.5 en 2022 ainsi qu'une production de manganèse sur ce même niveau. Le déphasage observé entre le cycle du manganèse et celui du fer peut être observé entre la St. 5 et 8 puisque cette dernière montre un profil stable du cycle du manganèse avec un enrichissement en oxydes en surface alors qu'un pic d'oxydes de fer réactifs et une production de fer dissous concomitante se trouvent à 3 cm de profondeur. Ici, on retrouve l'écart de précipitation d'oxydes de manganèse et de fer observés dans la modalité FLV du ***chapitre 3***.

D'après ces profils biogéochimiques, il est clair qu'aucune de nos stations ne présente un état stable des cycles du manganèse et du fer en 2022 contrairement à 2021. Le rétablissement du niveau de subsurface enrichi en oxydes réactifs semble se produire pour la station la plus distale avec des fronts de production supposés de Mn et Fe dissous près de l'interface. Néanmoins les profils d'oxydes de fer réactifs montrent clairement des niveaux enrichis en subsurface attestant d'un dépôt de sédiment dont le rétablissement redox n'est pas parvenu à se rétablir. Cela pourrait s'expliquer par une efficacité de reminéralisation de la matière organique plus faible qu'en 2021.

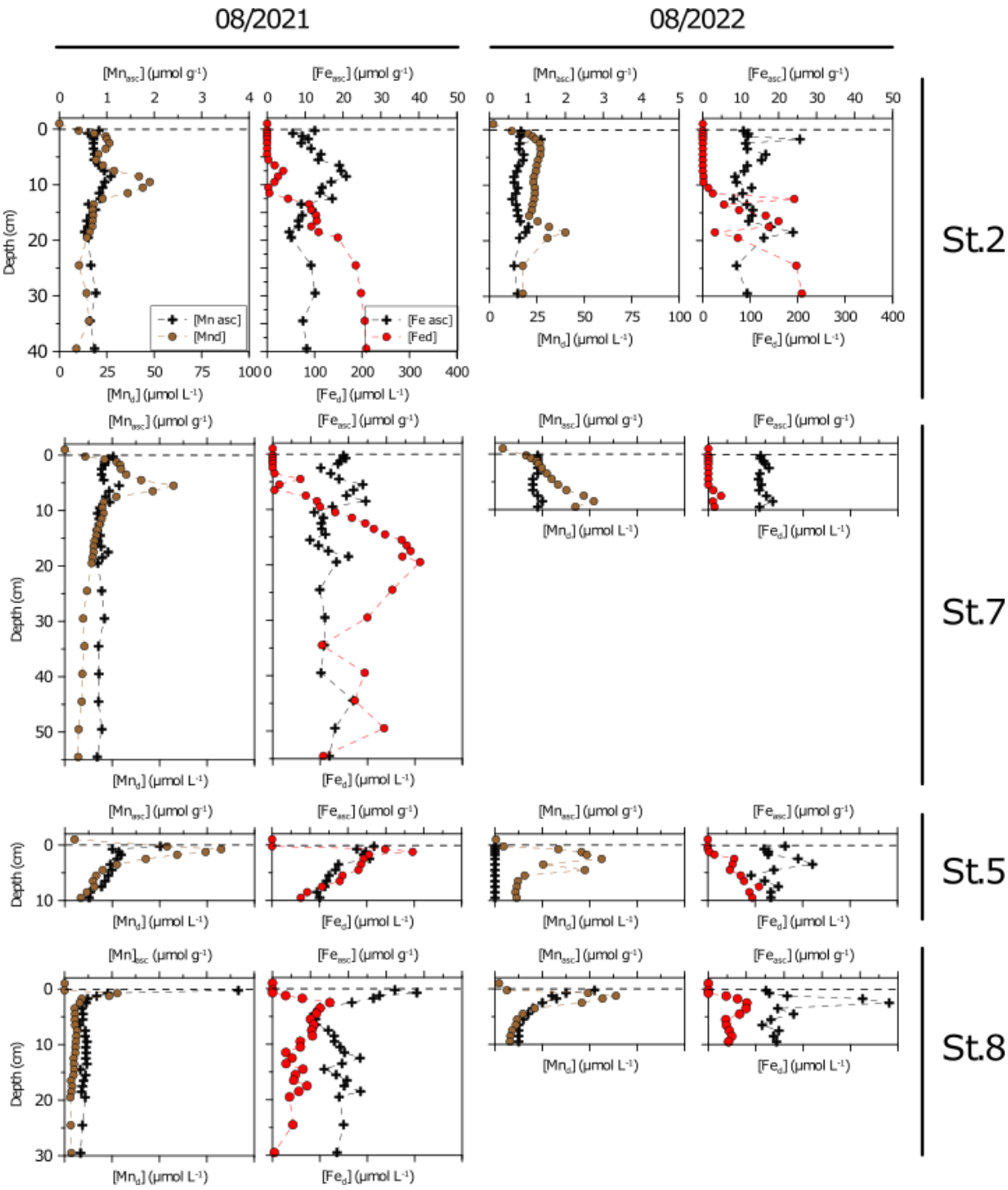

Figure 4 : Profiles de concentration des phases dissoutes et particulaires réactives du manganèse et du fer aux 4 stations profondes du transect pour les étés 2021 (***Chapitre 5***) et 2022

Conclusions préliminaires

Il existe bien une variabilité interannuelle dans la stabilité du substrat benthique dans le Kongsfjorden observable avec les cycles du manganèse et du fer ainsi qu'avec la dynamique de population des foraminifères. Les décharges sédimentaires provenant de la fonte du Kronebreen

ne sont pas similaires entre les années et influencent la taille des zones de stabilité, différente chaque année avec des taux de sédimentation différents.

Les observations faites ici rejoignent donc les interprétations sur les distributions des foraminifères benthiques montrant un étalement de la zone soumise à la sédimentation intense par conséquent instable. Également les concentrations en matière organique étant plus faibles qu'en 2021, il est tout à fait possible que sa reminéralisation par les différents stades de la diagenèse précoce soit plus lente et donc enregistre sur un plus long terme l'état transitoire des gradients redox.

Activités supplémentaires

Missions d'échantillonnages

01/02/2021 – 13/02/2021 : Mission REBELRED (PI : Edouard Metzger)

Participants (équipe à terre) : Aurélia Mouret, Eric Bénéteau, Lisa Nauton, Vivien Hulot, Corentin Guilhermic

Ma participation à cette mission d'échantillonnage a pour but de me former aux méthodes d'analyse et de traitement géochimiques de carottes sédimentaires pour la mesure d'éléments dissous. J'ai fait partie de l'équipe réceptionnant les carottes prélevées dans la Loire et s'occupant de leur traitement à terre.

Mes différentes missions étaient les suivantes :

- Découpe de carottes sédimentaires en atmosphère anoxique contrôlée.
- Conditionnement des échantillons de sédiment et d'eau interstitielle sous atmosphère contrôlée pour de futures analyses d'espèces dissoutes et particulaires
- Mesures par colorimétrie au spectrophotomètre de l'alcalinité des eaux porales

10/04/2021 - 26/04/2021 : Mission KONBHAS (Institut Polaire français) à Ny-Alesund, Kongsfjorden (Svalbard) (PI : Pr. Agnès Baltzer)

Participants : Agnès Baltzer, Hélène Howa, Corentin Guilhermic (et Maria Pia Nardelli qui a organisé le plan d'échantillonnage, absente par cause de COVID).

Cette mission avait pour but d'échantillonner des carottes de sédiment d'interface afin d'en étudier le contenu en foraminifères vivants ainsi que la granulométrie du sédiment et la concentration en matière organique particulaire (***chapitre 4*** et ***6***).

L'échantillonnage des carottes a eu lieu à bord du R/V Teisten (King's Bay) et le traitement des carottes à lieu à terre, dans les locaux de l'AWIPEV à Ny-Alesund.
Mes différentes missions étaient les suivantes :

- Participation à la préparation du matériel pour la mission.
- Manipulation et déploiement d'une sonde CTD pour mesures de température, salinité, concentration en chlorophylle-a et turbidité dans la colonne d'eau aux différentes stations échantillonnées (***chapitre 4***).

- Déploiement d'un carottier GEMax et d'une benne Day pour échantillonner des carottes sédimentaires d'interface à 8 stations différentes.
- Découpage des carottes sédimentaires et conditionnement pour analyse future de foraminifères vivants (avec coloration des individus vivants au rose-bengal), de granulométrie et du contenu en matière organique (chapitre 6).
- Echantillonnage de particules planctoniques à l'aide d'un filet à plancton (étude du réseau trophique avec couplage pélagique/benthique)

Additionnellement aux échantillonnages dans le cadre de ma thèse, j'ai participé à l'acquisition d'images sonar à bord du R/V Jean-Floch (AWIPEV) dans l'objectif d'un suivi de la progradation des prodeltas littoraux sous l'influence de la fonte des glaciers à terminaison terrestre de la côte sud du Kongsfjorden.

De plus, j'ai été invité à participer à une mission de ravitaillement de matériel sur le glacier Kongsvegen par Pr. Thomas Schuler and Coline Bouchayer (Norsk Polarinstittut).

15/08/2021 – 29-08/2021 : Mission KONBHAS (Institut Polaire français) à Ny-Alesund, Kongsfjorden (Svalbard) (PI : Pr. Agnès Baltzer)

Participants : Agnès Baltzer, Aurélia Mouret, Maria Pia Nardelli, Hugues de Lauzon, Corentin Guilhermic

Cette mission avait pour but d'échantillonner des carottes de sédiment d'interfaces afin de faire un suivi saisonnier des faunes de foraminifères vivants (***chapitre 6***) et de leur microhabitat (granulométrie et contenu en Matière organique, ***chapitre 4***). Mes missions ont été les mêmes que pour la mission précédente d'avril 2021, avec un volet supplémentaire dédié à la biogéochimie du sédiment. L'échantillonnage des carottes à lieu à bord du R/V Teisten (King's Bay) et le traitement des carottes a lieu à terre, dans les locaux de l'AWIPEV à Ny-Alesund.

Mes missions supplémentaires par rapport à la mission précédente d'avril 2021 étaient les suivantes :

- Découpage et conditionnement d'échantillons de sédiments à destination de mesures d'éléments géochimiques caractérisant la distribution des gradients redox (***chapitre 5***)
    - Mesures sur place par colorimétrie des concentrations d'alcalinité, nitrite et nitrates.
- Utilisation de dispositifs d'échantillonnage 2D pour quantifier les densités de foraminifères vivants et les concentrations en certains éléments dissous dans les eaux porales (***Chapitre 7***).

16/08/2022 – 30/08/2022 : Mission KONBHAS (Institut Polaire français) à Ny-Alesund, Kongsfjorden (Svalbard) (PI : Pr. Agnès Baltzer)

Participants : Agnès Baltzer, Hugues de Lauzon, Vincent Lacombe, Maria Pia Nardelli, Hélène Howa, Corentin Guilhermic

Cette mission avait pour but d'échantillonner des carottes de sédiment d'interface afin de faire un suivi interannuel des faunes de foraminifères vivants et de leur microhabitat (granulométrie, contenu en Matière organique, géochimie et fronts redox). L'échantillonnage des carottes a lieu à bord du R/V Teisten (King's Bay) et le traitement des carottes a lieu à terre, dans les locaux de l'AWIPEV à Ny-Alesund. Mes missions ont été les mêmes que pour la mission précédente d'Août 2021, le volet « géochimie » ayant été effectué en totale autonomie.

Formations

Afin de valider mon diplôme de doctorat, un minimum de 100h de formation est demandé (professionnel et/ou disciplinaire). Avec les différentes formations suivies et les équivalences apportées par les participations aux congrès scientifiques et différentes vulgarisations scientifiques, je cumule 129 heures de formation.

1ère année :

- Accéder aux données du SHOM pour developer votre activité (Webinaire, 2h)
- Ethnique et intégrité scientifique (Formation présentiel, 2h)
- Atelier pédagogique (Formation visio, 14h)
- MOOC Doctorat et développement de carrière (Formation en ligne, 12h)
- Participation to REBELRED mission on the Loire River (10 days in February 2021).
- Formation au traitement biogéochimique de carottes sédimentaires (découpage et conditionnement des échantillons) en vue des missions d'échantillonnage en Arctique
- Participation à une mission du projet REBELRED, échantillonnage de vasière. Formation en laboratoire pour la manipulation de sondes et réactifs 2D DET en vue des expériences en microcosme (Chapitre 3) et des échantillonnages dans le Kongsfjord

2ème année :

- How to write and publish your paper (10h)
- English class for PhDs (20h)
- Ma thèse en 180s (14h)

- Réunion annuelle de l'école doctorale
- How to pitch ? (3h)
- Réseaux professionnels – Comprendre les fondamentaux (4h)
- Safety course in Ny-Alesund (bear behaviour and shooting courses)

3ème année :

- Les violences sexistes et sexuelles dans l'enseignement supérieur (4h)
- Membre élu du conseil de laboratoire (non-permanent) (2022-2023) (équivalence : 5h)

Supervisions d'étudiants

07/12/2021 – 17/12/2021 Supervision de Youn Besse, Florie Bossin-Petiteau, Paul Brichard, Valentin Challier et Flavie Koch (Licence 3) pour un stage volontaire (encadrement de Hélène Howa). Lavage d'échantillons pour piquage de foraminifères et conditionnement d'échantillons de sédiment pour analyses d'oxydes (broyage et pesée)

15/01/2022 – 15/06/2022 Co-encadrement de Maryline Moller (Master 2) (Encadrement avec Maria Pia Nardelli et Aurélia Mouret) « Simulation expérimentale de dépôts sédimentaires massifs : Evolution des microenvironnements géochimiques et mise en place d'une méthode de repérage automatique des foraminifères benthiques dans le sédiment. »

03/10/2022 – 04/11/2022 Supervision de Brieg Nedelec (2ème année école d'ingénieur) (Encadrement par Maria Pia Nardelli) « Préparation et analyse d'échantillons de sédiments et microfaunes Arctiques »

02/04/2023 – 03/06/2023 Encadrement de Luc Mouline (Master 1) (co-encadrement de Hélène Howa) « Etude granulométrique des sédiments du Kongsfjorden, Svalbard »

- **Supervision de Enzo Huet et Océane Garandel** (Master 1) sur la même période pour faire le lien entre les différents stages du projet BEGIN concernant les échantillons de 2022 dans le Kongsfjorden (biogéochimie et foraminifères benthiques)

Expérience d'enseignement

J'ai eu l'opportunité de participer à des modules d'enseignement de Licence Sciences de la vie et Géosciences (L2) et Géosciences et environnement (L3) pour une charge horaire annuelle de

32h pour les années 2020/2021 et 2021/2022 (1ère et 2ème année de doctorat). Les enseignements étaient les suivants :

- **Licence 2 : Géologie quantitative**
    - TD : Norme CIPW – Pétrochimie (évaluation de travaux par groupe)
- **Licence 3 : Sédimentologie**
    - TD sur l'application de concepts sédimentologiques
    - Encadrement de la sortie terrain dans la baie du Mont St Michel (avec Pr. Hélène Howa)
- **Licence 3 : Biogéochimie environnementale**
    - Encadrement d'une sortie d'échantillonnage sur la vasière de Bourgneuf
    - Encadrement du TP de traitements d'échantillons prélevés la veille
    - TD sur le traitement des données de géochimie

Vulgarisation scientifique

- La nuit des chercheurs (Septembre 2021)
- Ma thèse en 180s (Mars 2022)
- Opération DECLICS (Décembre 2022)
    - Intervention sur la recherche scientifique et l'enseignement en faculté au lycée Joachim du Bellay, Angers

Communications scientifiques

22/09/2020 16ème journées scientifiques du CNFRA (22-23 sept 2020) La Rochelle

Oral presentation “Impact of the arctic glacier melting on benthic habitats in Kongsfjorden (Svalbard)”

***Guilhermic Corentin**, Howa Hélène, Nardelli Maria Pia, Mouret Aurélia, Baltzer Agnès*

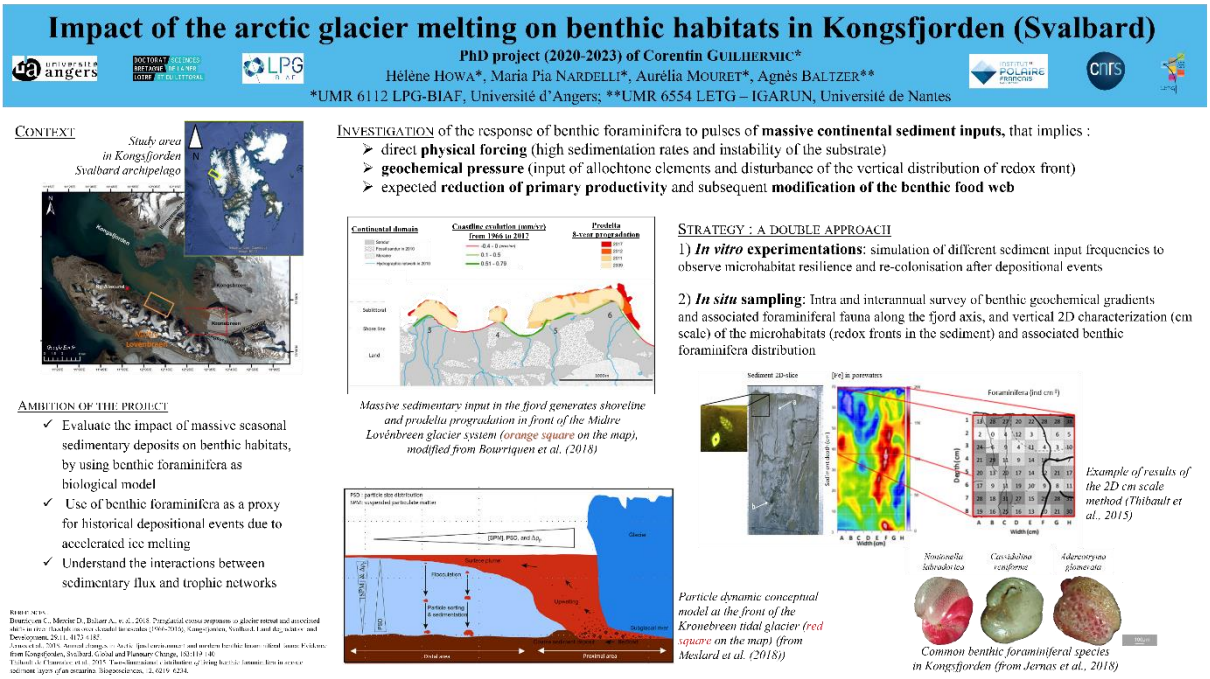

22/11/2020 Climat et impacts symposium (LSCE, en ligne)

Online poster presentation “Impact of the arctic glacier melting on benthic habitats in Kongsfjorden (Svalbard)”

***Guilhermic Corentin**, Howa Hélène, Nardelli Maria Pia, Mouret Aurélia, Baltzer Agnès*

Abstract :

Subsequent pulses of massive sediment inputs in the fjords during the melting phases represent both a physical forcing (high sedimentation rate and turbidity, substrate instability) and a biogeochemical stress (reduction of primary productivity, input of continental elements, disturbance of the vertical distribution of redox fronts) on benthic ecosystems. The aim of our project is to investigate the response of the meiobenthos, in particular of benthic foraminifera (BF) to the accelerated glacier melting in the Arctic fjord of Kongsfjorden, Svalbard.

An *in situ* approach will allow the investigation of BF ecological response to sedimentology and geochemistry of the benthic habitats, during three consecutive summers. An experimental approach will allow to test, in microcosm, the resistance and resilience of BF species and geochemical redox fronts following different *scenarii* of sediment inputs (low quantity/ high and inversely).

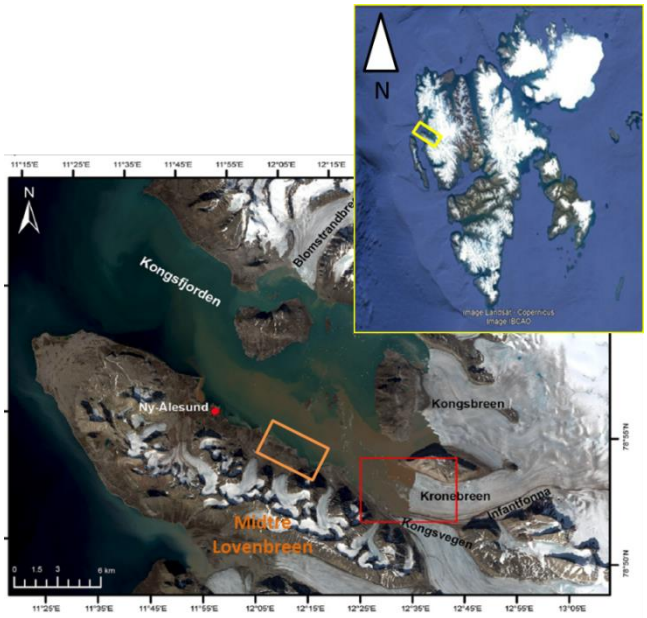

Figure 1: Zones d'étude dans le fjord (Kongsfjorden)

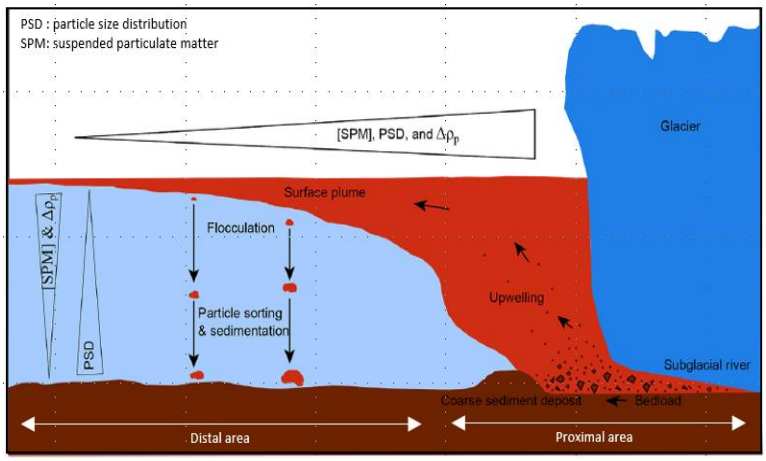

Figure 2: Forçage sédimentaire sur la géochimie de la colonne d'eau dans les fjords du Svalbard; d'après Meslard et al., 2018.

05/2022 EGU (European geosciences Union) general assembly in Vienna 23-27 May 2022
Oral presentation **"**Short-term response of benthic foraminifera to fine sediment depositional events simulated in microcosm".
Guilhermic Corentin, *Nardelli Maria Pia, Howa Hélène, Le Moigne Damien, Pusceddu Antonio, Sanchez Sophie et Mouret Aurélia*

Abstract :

An *in vitro* experiment was designed to describe how benthic foraminifera (as witness of the benthic ecosystem) reacts to "one-time high volume" vs "frequent low volume" sediment discharge, as it may occur in coastal benthic environments regularly or occasionally buried during (e.g.) river flood massive deposits, or glacier melting events in polar regions. The influence of these events on the ecology of benthic ecosystems is often neglected and the resilience of benthic foraminiferal communities is poorly known. During a 53-day long experiment in microcosm, the NE Atlantic mudflat foraminifera community, mainly

represented by *Ammonia* T6 and *Haynesina germanica* species, was confronted to two kinds of sedimentary disturbance: 1) one-time high volume (OHV) deposit, i.e. about 3 cm thick sediment is added in one time at the beginning of the experiment, and 2) frequent low volume (FLV) deposits, i.e. about 0.5 cm added each week for 4 weeks. The geochemical environment (e.g. O2 penetration in the sediment, salinity, temperature and nutrient content in the supernatant water) was monitored to follow its steady-state before and during the experiment. In the two studied cases, the foraminifera react to the disturbance by immediately moving upward to the surface within 1 day after the deposit. In the OHV treatment, a species vertical distribution in relation to the surface, comparable to the vertical distribution before the disturbance (i.e. a resilient state), is established at most 1 week after the deposit, and no effects are visible on the foraminiferal diversity after 1 month experiment (without any other sediment input). In the FLV treatment, the resilient state is already reached 1 day after a low thickness burial. This suggests that foraminifera can migrate rapidly to their preferential life position under the new sediment-water interface. However, after 4 recurrent burring events the density of *H. germanica* drastically decreases, changing in this way the foraminiferal community structure. The results of this microcosm experiment suggest that the entire foraminiferal community can migrate upward quickly enough to keep pace with at least 3 cm of abrupt burial but needs several days to reach a resilient state. Furthermore, frequent sediment deposition may affect foraminiferal biodiversity more than a massive erratic event.

26-30/06/2023 FORAMS 2023 (Perugia, Italy)

Oral presentation “Interseasonal responses of benthic foraminifera close to the Kronebreen glacier front (Kongsfjorden, Svalbard)”

***Guilhermic Corentin**, Nardelli Maria Pia, Mouret Aurélia, Pusceddu Antonio, Baltzer Agnès and Howa Hélène*

Abstract :

Arctic fjords are transitional areas between glacier-covered land and the ocean, characterised by strong environmental gradients. In addition to global changes affecting Arctic coastal environments, spatial and seasonal variabilities of physical and geochemical conditions in fjords affect benthic ecosystem, particularly living foraminiferal microhabitats. It is urgent to understand the functioning of these complex environments, to better monitor their modifications under the current global warming conditions.

Kongsfjorden (Svalbard) has entered in an intense phase of warming and ice melting, which have prevented the formation of extensive sea-ice since 2009 in winter. Therefore, the present evolution of this fjord now represents a first phase of transition from subpolar to future temperate conditions. In summer, it is characterised by high glacier melting water production resulting in freshwater spreading at the surface, associated with high turbidity close to tidewater glacier fronts, and bottom waters influenced by Atlantic water intrusions. Therefore, close to the glacier terminus, high detrital sedimentation and limited organic matter exported towards the seabed are supposed to affect both lateral and vertical foraminiferal distribution on a seasonal scale.

Two sampling campaigns were carried out in May and August 2021 to characterize seasonal environmental changes along a longitudinal transect from the Kronebreen glacier front to around 10 km far from it. Our research focused on the seasonal effect of physico-chemical gradients on foraminiferal communities, their spatial distribution, and microhabitats. Organic matter quantity and quality, sediment grain size, and physical parameters of the water masses were investigated as possible driving parameters for benthic ecosystem responses.

In May, the water column was well mixed throughout the fjord, and the environmental gradient was mainly driven by the organic matter content in the sediment, with a strong increase of biopolymeric carbon (BPC) and phytopigments from the glacier front to distal locations. In August, the water column stratification with surface turbidity induced a lowering of organic matter content in the sediment near the glacier front. In the proximal area, foraminiferal assemblages were characterised by the dominance of the pioneer species *Capsammina bowmanni* in the top sediment layers in August, and very low abundances to total absence of foraminifera in May. Food limitation and substrate instability induced by the turbid plume seem to be the major factors driving the summer foraminiferal distribution. In the distal area, foraminiferal assemblages were mainly represented by *Nonionellina labradorica* and *Adercotryma glomeratum* associated with a higher diversity in both seasons. However, in May, foraminiferal abundances were generally lower, due to food limitation. Interestingly, despite the occurrence of different bottom water masses at the two seasons, similar species compositions were observed, suggesting that the water masses do not directly influence the presence or absence of a species. However, a change in main microhabitat distribution was observed for both species, with a peak in superficial layers in summer and more infaunal behaviour in May. This change could be the response to different feeding regimes in the two

seasons and/or possibly to enhanced downward transport of foraminifera by macrofaunal bioturbation in spring.

Our results clearly show that physical and geochemical gradients induced by melting waters and sediment discharges originating from the tidewater glacier during summer are the main factors that drive foraminiferal distribution at the local (10 km) scale. This finding induces that foraminifera can be used to monitor the effects of ongoing climate change on the benthic ecosystems of Arctic fjords and have the potential to be proxies for reconstructing glacier front positions in the recent past.

06-08/09/2023 XXIII National Congress of the Italian Society of Ecology (Catania, Italy)

Poster participation "Benthic foraminiferal seasonal responses to environmental gradient variations in Kongsfjorden (Svalbard)"

*PUSCEDDU Antonio and **GUILHERMIC Corentin**, MOURET Aurélia, HOWA Hélène, BALTZER Agnès and NARDELLI Maria Pia*

Abstract :

In polar fjords, glacial meltwater and associated high sediment loads generate strong environmental gradients due to increased water column stratification and surface turbidity, which, ultimately, affect primary production. Spatial and seasonal variations in glacial inputs (from very fine silt to coarse gravel) resulting in burial of benthic ecosystems, lead to faunal biozonation and changes in sediment biogeochemistry, from tidewater glacier fronts to the outer fjord area.

To characterize the seasonal and spatial effects of environmental gradients upon benthic realms in a polar fjord, a study of living benthic foraminiferal was conducted in Kongsfjorden. During two oceanographic campaigns (May and August 2021), sediments were sampled from 4 stations along a transect from the Kronebreen glacier front to about 10 km away. Along with foraminifera diversity, abundance and vertical distribution, other environmental parameters were investigated such as sediment grain size, organic matter content and water mass distribution.

In May, the water column was well mixed throughout the fjord, and the environmental gradient was mainly driven by the organic matter content in the sediment, with a strong increase of biopolymeric carbon (BPC) and phytopigments from the glacier front to distal locations. In August, the water column stratification with surface turbidity induced a lowering of organic matter content in the sediment near the glacier front. In both seasons, we observed the same

biozonations of foraminiferal communities, with higher abundances in summer than in spring, due to higher food supply. The vertical distribution of the specimens was different in the two seasons, reflecting both biogeochemical microhabitat distribution along the transect and seasonal differences in sediment supply from the glacier.

These findings support the use of foraminifera to monitor the effects of ongoing climate change on the benthic ecosystems of Arctic fjords and to reconstruct glacier front positions in the past.

Benthic foraminiferal seasonal responses to environmental gradient variations in Kongsfjorden (Svalbard)

PUSCEDDU Antonio, GUILHERMIC Corentin, MOURET Aurélia, HOWA Hélène, BALTZER Agnès, NARDELLI Maria Pia

This work is part of Corentin Guilhermic PhD thesis performed at the UMR CNRS 6112-LPG, founded by the BEGIN project (INSU CNRS; PI: M.P. Nardelli) and Angers University (FR)

Introduction

This study investigates the seasonal and spatial effects of sediment and organic matter export towards the seabed on benthic communities, here represented by benthic foraminifera (meiofauna). It was first studied in microcosm (**Guilhermic et al., 2023**). Here are presented results from the Kongsfjorden (Svalbard, Arctic Ocean fig. 1), which is currently facing a clear warming. Nowadays, the seasonality is marked by water column mixing in winter/spring and stratification in summer. Melting of tidewater glaciers during the warm season triggers sediment-rich freshwater at the surface of the fjord and high sedimentation rates near the glacier front. In addition, the spreading of the turbid plume prevents phytoplanktonic blooms by limiting light penetration.

Guilhermic, C., Nardelli, M. P., Mouret, A., Le Moigne, D., and Howa, H.: Short-term response of benthic foraminifera to fine sediment depositional events simulated in microcosm, Biogeosciences Discussions, 1–46, https://doi.org/10.5194/bg-2023-31, 2023.

Fig. 1 Sampling sites in the Kongsfjorden Red= proximal to glacier front, green=distal

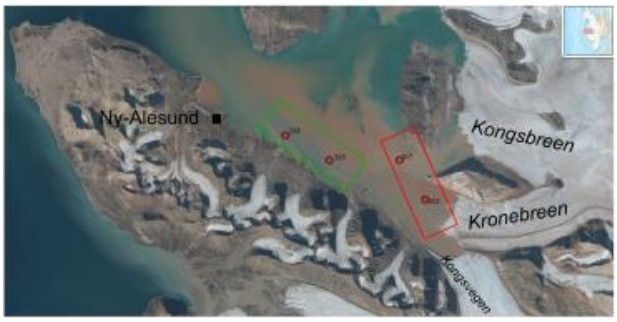

Fig. 3 Aminopeptidase vs Species richness

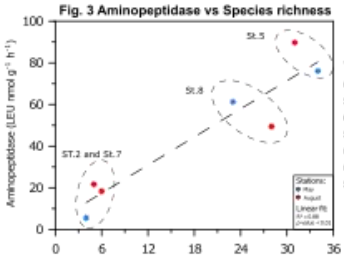

The linear relationship between the enzymatic activity (i.e. aminopeptidase) and species richness indicates **an increasing ecosystem functioning** at the distal stations (5 and 8) compared to the proximal ones (2 and 7). The highest values are observed at intermediate station 5 for both seasons.

Results and Discussion

Fig. 2 CTD data

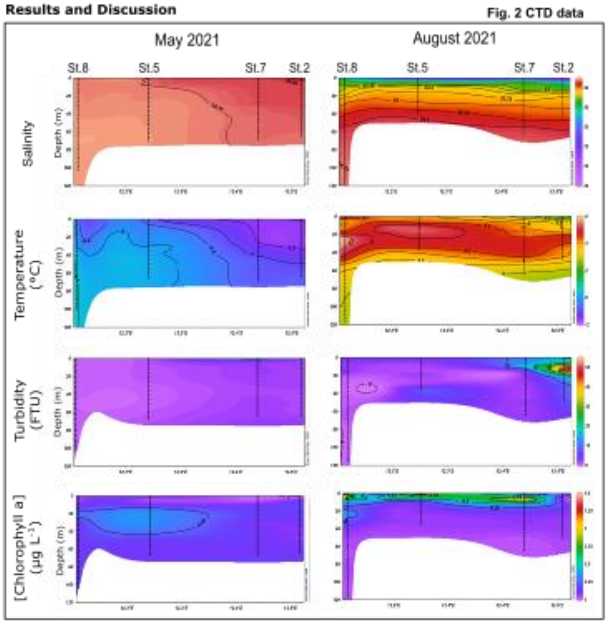

CTD data show a mixed water column **in May** with no turbidity and low chlorophyll-a concentration above St.8 and St.5. **In August**, the water stratification is enhanced by the intrusion of warmer and saltier Atlantic water at the bottom and by fresher meltwaters at the surface. At the proximal stations 2 and 7, the presence of the turbid plume is recorded and is associated to lower chl-a. Highly contrasted water column conditions in both May and August

Fig.4 Vertical distribution of main species at each station

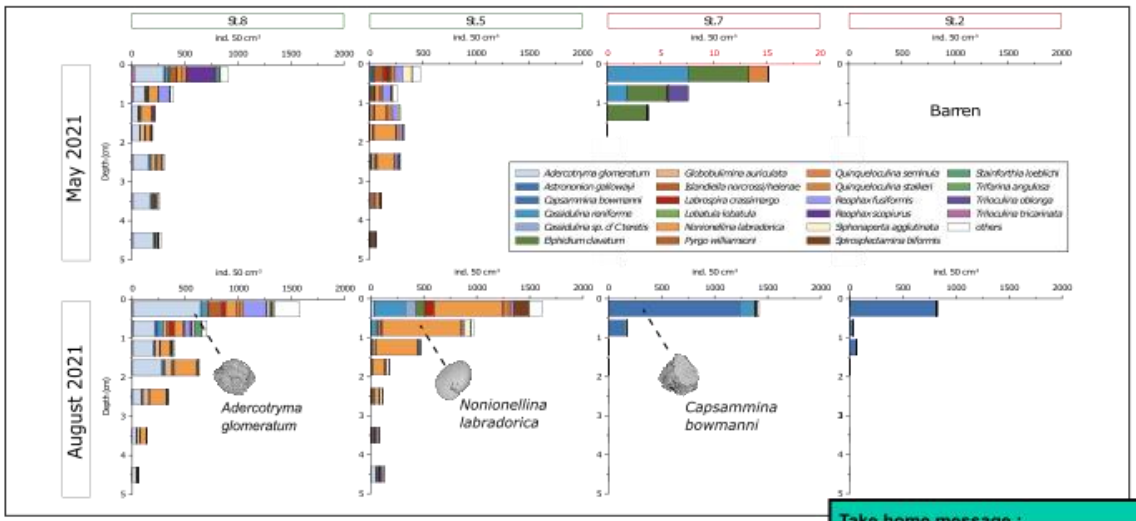

Foraminiferal assemblages observed in summer 2021 are very similar to the ones of summer 2018, described by Fossile et al. (2022), with increasing biodiversity and vertical microhabitat occurrence, moving far from the glacier front. Proximal stations show a strong dominance of the pioneer species *Capsammina bowmanni*.

Despite a much lower turbidity, during spring the two proximal stations St.7 and St.2 were almost or totally barren, most probably due to food limitation. Besides similar specific compositions among seasons, also the distal biozones show much lower abundances in spring. Some species also show a preference for deep infaunal microhabitats in spring (e.g. *N. labradorica*), maybe due to competition with other species under a poor food regime and/or to higher bioturbation by macrofauna.

The four stations show a strong community gradient that is visibly driven by physical disturbance and associated consequences on food supply.

Fossile, E., Nardelli, M. P., Howa, H., Baltzer, A., Popravski, Y., Baneschi, I., Doveri, M., and Mojtahid, M.: Influence of modern environmental gradients on foraminiferal faunas in the inner Kongsfjorden (Svalbard), Marine Micropaleontology, 173, 102117, https://doi.org/10.1016/j.marmicro.2022.102117, 2022.

Take home message :

At the scale of the fjord, the strong seasonality in sedimentary inputs must be recognised as the majord driver for the high spatial heterogeneity and consequently high regional diversity.

Benthic foraminiferal communities can be effective bio-indicators to monitor the influence of seasonal melting cycles and on-going long-term retreat of tidewater glacier induced by climate change.

Contact author:
guilhermic.corentin@gmail.com

10/2023 Svalbard Science Conference 2023 in Oslo (31/09-01/10) Session "Polar Ocean"
Poster presentation "Effect of environmental gradients generated by tidewater glacier melting on sedimentary habitats and benthic meiofauna in Kongsfjorden (Svalbard)"

***Guilhermic Corentin**, , Mouret Aurélia, Howa Hélène, Pusceddu Antonio, Baltzer Agnès and Nardelli Maria Pia*

Abstract :

In polar fjords, glacial meltwater and associated high sediment loads generate strong environmental gradients due to increased water column stratification and surface turbidity, which, ultimately, affect primary production. Spatial and seasonal variations in glacial inputs (from very fine silt to coarse gravel) resulting in burial of benthic ecosystems, lead to faunal biozonation and changes in sediment biogeochemistry, from tidewater glacier fronts to the outer fjord area.

To characterize the seasonal and spatial effects of environmental gradients upon benthic realms in a polar fjord, a study of living benthic foraminiferal was conducted in Kongsfjorden. During two oceanographic campaigns (May and August 2021), sediments were sampled from 4 stations along a transect from the Kronebreen glacier front to about 10 km away. Along with foraminifera diversity, abundance and vertical distribution, vertical redox gradients in sediments were investigated with other environmental parameters such as sediment grain size, organic matter contents and water mass distribution.

In summer, vertical distribution of oxygen, nutrients, manganese, and iron species were in a transient state in the vicinity of the glacier front whereas distal stations showed a more stable sequence. This was interpreted as the result of high sedimentation close to the glacier and higher organic matter flux in the distal area. In both seasons, we observed the same biozonations of foraminiferal communities, with higher abundances in summer than in spring, due to higher food supply. The vertical distribution of the specimens was different in the two seasons, reflecting both geochemical microhabitat distribution along the transect and seasonal differences in sediment supply from the glacier.

These findings support the use of foraminifera to monitor the effects of ongoing climate change on the benthic ecosystems of Arctic fjords and to reconstruct glacier front positions in the past.

Récompenses

-Concours photo CNRS INSU "Entre ciel et mer » 2022

Lauréat catégorie « Recherche animée »

Vidéo accélérée (timelapse) prise entre 01h30 et 07h15 AM le 27 Août 2022, du fjord dans lequel une vidange d'icebergs vers le large se produit sous un soleil se levant derrière les montagnes. Avec une orientation vers l'ouest, cette vidéo montre l'embouchure du Kongsfjorden, un fjord dans l'archipel du Svalbard étudié pour être une sentinelle du réchauffement climatique en Arctique. Notre équipe étudie l'influence de la fonte des glaciers et des apports de sédiment associés sur les écosystèmes benthiques. Plus particulièrement, nous étudions les foraminifères, des organismes unicellulaires vivant au fond des océans sur et dans le sédiment. Leur distribution horizontale et verticale sur/dans le sédiment dépend des conditions environnementales proches (géochimie, apport de nourriture). Ainsi ils sont de bons indicateurs de variations dans un milieu en transition comme le Kongsfjord.

Liens vers posts réseaux sociaux, vidéo diffusée sur youtube et site CNRS INSU

- https://www.linkedin.com/feed/update/urn:li:activity:7052683770042150912/
- https://www.insu.cnrs.fr/fr/cnrsinfo/decouvrez-les-photos-et-la-video-laureate-du-concours-entre-ciel-et-mer-de-linsu

COLLEGE VEGETAL
DOCTORAL ANIMAL, ALIMENT
PAYS DE LA LOIRE MER, ENVIRONNEMENT

université angers

Titre : Effets des instabilités sédimentaires sur les microhabitats benthiques : cas du Kongsfjorden

Mots clés : glacier, Svalbard, foraminifère, biogéochimie, perturbation, expérience

Résumé : Des évènements de dépôts sédimentaires surviennent dans les zones côtières et ont des conséquences majeures sur les écosystèmes benthiques. En Arctique, les fjords sont des environnements soumis à la fonte des glaciers et à d'importants apports sédimentaires. Avec le changement climatique actuel, les projections prévoient une augmentation de cette fonte dans le futur. Dans le Kongsfjord (Svalbard), cette décharge sédimentaire affecte fortement la productivité primaire, les faunes benthiques et la stabilité des microhabitats. Pour comprendre les effets de ces gradients environnementaux sur le compartiment benthique, cette thèse propose une approche couplant des études expérimentales et environnementales permettant de comprendre les processus de rétablissement des communautés de foraminifères benthiques et des gradients redox après des dépôts de sédiment. Des indicateurs d'enfouissement mis en évidence expérimentalement nous ont permis d'observer les effets de cette forte sédimentation estivale dans le fjord, qui peuvent être observés à la fois dans les états transitoires de la diagenèse précoce et dans les biozonations des communautés de foraminifères benthiques à l'échelle kilométrique. Les foraminifères benthiques et les stades redox dans les sédiments se sont avérés être des indicateurs pertinents pour étudier les effets interannuels de la fonte des glaciers sur les microhabitats benthiques.

Title : Effects of sediment instabilities on benthic microhabitats: case of Kongsfjorden

Keywords : glacier, Svalbard, foraminifera, biogeochemistry, disturbance, experiment

Abstract : Sediment depositional events often occur in coastal areas and have major consequences on benthic ecosystems and biogeochemistry. In the Arctic, fjords are transitional environments subjected to glacier melting and large sedimentary inputs. In a context of current climate change, projections predict an increase of this melting in the future. In Kongsfjorden (Svalbard), a gradient of turbidity highly affects primary production, benthic faunas and microhabitat stability. In order to understand the effects of these environmental gradients in this fjord on the benthic compartment, this Ph.D. proposes an experimental/environmental approach allowing to assess the recovery processes of benthic foraminifera communities and redox gradients after sediment disturbances. Experimentally highlighted burial markers allowed us to observe the effects of this strong summer sedimentation in the fjord which can be seen both in recovery states of early diagenesis processes and seasonal benthic foraminiferal community biozonations on a kilometric scale. Foraminiferal distribution and sediment redox states were proven to be relevant indicators to survey interannual effects of glacier melting on benthic microhabitats.